UNIVERSIDAD
DE LA REPÚBLICA
URUGUAY

“Diseño, síntesis y evaluación biológica de nuevos organoboranos con uso en terapia antitumoral de glioblastoma por captura neutrónica de boro (^{10}B)”

TESIS DE DOCTORADO EN QUÍMICA OCTUBRE 2019

CONFIDENCIAL

Lic. Marcos Couto
UNIVERSIDAD DE LA REPÚBLICA | PEDECIBA QUÍMICA

CONFIDENCIAL

Tesis de Doctorado en Química

Programa de posgrado:

-Facultad de Química

-PEDECIBA Química

Tutores:

***Prof. Dr. Hugo Cerecetto**, Área de Radiofarmacia, Centro de Investigaciones Nucleares,, Facultad de Ciencias, UdelaR.*

***Dr. Pablo Cabral**, Área de Radiofarmacia, Centro de Investigaciones Nucleares,, Facultad de Ciencias, UdelaR.*

***Prof. Dr. Clara Vinas**, Institut de Ciènciade Materials de Barcelona (ICMAB—CSIC), España.*

***Prof. Dr. Francesc Teixidor**, Institut de Ciència de Materials de Barcelona (ICMAB-CSIC), España.*

CONFIDENC

Grupo de Química Orgánica Medicinal, Facultad de Ciencias, UdelaR. Setiembre

CONFIDENCIAL

Dedicada a Mercedes González …

Agradecimientos

Agradezco a los Profesores Hugo Cerecetto, Pablo Cabral, Clara Viñas y Francesc Teixidor por la dirección de esta Tesis Doctoral pues sin sus consejos y recomendaciones no se hubiera podido realizar.

Agradezco a los Investigadores Dra. Fernanda García, Dr. Mauricio Cabrera, Dra. Alicia Merlino, Dr. Emiliano Trias, MSc. Susana Mendoza, Prof. Moshe Gavish, Prof. Luis Barbeito, quienes han contribuido intensamente en el desarrollo de las investigaciones abordadas en la presente Tesis.

Agradezco a todos los compañeros del Grupo de Química Orgánica Medicina (IQB), compañeros del área de Radiofarmacia (CIN) y compañeros del Institut de Ciències dels Materials de Barcelona.

Darle las gracias a todas las agencias y centroes que han brindado su apoyo para el desarrollo de la presente tesis: Universidad de la República, Facultad de Ciencias, Facultad de Química, Instituto Pasteur, PEDECIBA, ANII, CSIC, CSIC-España, ICMAB.

CONFIDENCIAL

Resumen

En la presente tesis doctoral se pretende profundizar en las respuestas a preguntas de relevancia en un tema de salud humana como es la farmacología para el tratamiento de enfermedades neoplásicas, en particular, glioblastoma multiforme (GBM). La falta de tratamientos eficientes para gliomas de alto grado, como lo es el GBM, conduce a la necesidad de la I+D en nuevas estrategias farmacológicas eficaces. En esa línea, en el terreno de la terapia oncológica se ha experimentado una rápida evolución hacia la llamada terapia dirigida a blancos moleculares (en inglés, *targeted therapy*). Esta modalidad de tratamiento utiliza fármacos que van específicamente dirigidos a dianas moleculares que han demostrado desempeñar un rol crucial en la supervivencia, proliferación o capacidad invasiva de las células tumorales. En el caso de GBM, los receptores celulares con actividad tirosina quinasa (EGFR, VEGFR, PDGFR, entre otros) son claros ejemplos de dianas prometedoras. Por otro lado, actualmente se encuentra en estudio la terapia para GBM por captura neutrónica de boro (BNCT, del inglés *Boron Neutron Capture Therapy*) técnica que involucra radioterapia *in situ*. Se basa en la inusual capacidad del nucleido ^{10}B (un isotopo estable de boro) en capturar neutrones térmicos de baja energía produciéndose partículas alfa y núcleos de litio los que depositarán la energía en la célula tumoral.

En la presente tesis se abordó la modificación estructural de compuestos con bio-actividad reconocida, los fármacos erlotinib y sunitinib, mediante hibridación molecular con entidades con alto contenido de boro, entre ellos carboranos y metalacarboranos. Se estudió la actividad biológica de los compuestos desarrollados, *in silico*, *in vitro* e *in vivo*, así como la determinación de boro intracelular con el objetivo de poder ser aplicados en procesos de BNCT.

CONFIDENCIAL

1 Tabla de Contenido

1 Tabla de Contenido 4
1.1 Abreviaturas 7
2 Introducción 8
2.1 Aspectos generales del Cáncer 8
2.1.1 Tumores cerebrales, gliomas: definición y clasificación. 8
2.2 Glioblastoma multiforme (GBM) 10
2.2.1 Clasificación de GBM y alteraciones genéticas asociadas a los gliomas 11
2.2.2 Estrategias terapéuticas para el tratamiento del GBM 12
2.2.3 Proteínas con actividad tirosina quinasa como dianas terapéuticas en GBM 16
2.3 Reseña histórica del Boro 23
2.3.1 Clústeres de boro 24
2.4 Aplicaciones de clústeres de boro en el campo de la biomedicina 30
2.4.1 Características estructurales de *closo*-carboranos y metalacarboranos. Implicancia en las propiedades “tipo medicamento” 31
2.4.2 Terapia por captura de neutrones de boro (BNCT) 32
2.4.3 *closo*-carboranos y metalacarboranos estudiados en GBM a través de BNCT. 36
3 Justificación, hipótesis y diseño metodológico 42
4 Objetivo general 44
5 Capítulo I 45
Serie derivada de erlotinib 45
Artículo I 45
5.1 Objetivos específicos 46
5.2 Resultados y Discusión 47
5.2.1 Síntesis de híbridos 47
5.2.2 Estudios de citotoxicidad sobre células tumorales y selectividad *in vitro* 54
5.2.3 Influencia de lipofilicidad en la bioactividad 56
5.3 Conclusiones 58
Serie derivada de erlotinib 59
Artículo II 59
5.4 Objetivos específicos 60
5.5 Resultados y Discusión 61
5.5.1 Estudios *in vitro* de inhibición enzimática 61
5.5.2 Estudios *in silico* de inhibición enzimática 63

CONFIDENCIAL

5.5.3 Estudio de propiedades tipo-fármaco 67
5.5.4 Determinación cualitativa de captación de boro intracelular 73
5.6 Conclusiones 74
Serie derivada de erlotinib 75
Artículo III 75
5.7 Objetivos específicos 76
5.8 Resultados y Discusión 77
5.8.1 Estudio de la capacidad citotóxica 77
5.8.2 Estudio de propiedades tipo-fármaco 79
5.8.3 Estudios *in vitro* de mutagenicidad y estudios *in vivo* de toxicidad aguda vía oral. 82
5.8.4 Formulaciones como estrategia de solubilización de entidades poco solubles. 83
5.9 Conclusiones 85
6 Capítulo II 86
Serie derivada de Sunitinib 86
Artículo IV 86
6.1 Objetivos específicos 87
6.2 Resultados y Discusión 88
6.2.1 Síntesis de intermedios e híbridos. 88
6.2.2 Evaluación biológica *in vitro* 90
6.3 Conclusiones 102
7 CAPITULO III 103
Misceláneos 103
7.1 Valoración de boro intracelular 104
7.1.1 Materiales y métodos 104
7.1.2 Resultados y discusión 105
7.2 Estudios *in vitro* e *in vivo del derivado **1** (Figura 62)* 107
7.2.1 Materiales y métodos 107
7.2.2 Resultados y discusión 110
8 Bibliografía 113
9 Anexo 125

CONFIDENCIAL

CONFIDENCIAL

1.1 Abreviaturas

CC: cromatografía en columna
CCF: cromatografía en capa fina
EGFR: Receptor del factor de crecimiento epidérmico (del inglés, epidermal growth factor receptor)
PDGFR: Receptor del factor de crecimiento plaquetario (del inglés platelet-derived growth factor receptor)
VEGF/VEGFR: factor de crecimiento de endotelio vascular/receptor del (del inglés, vascular endothelial growth factor/receptor)
RTKs: Receptores con actividad tirosina quinasa (del inglés, receptor tyrosine kinases)
EM: Espectrometría de masas.
ESI: ionización por electrospray (del inglés, electrospray ionization)
Eq: equivalentes
HMBC: Correlación de enlace múltiple heteronuclear (del inglés, heteronuclear multiple bond correlation)
COSY: espectroscopía de correlación (del inglés, *correlation spectroscopy)*
HPLC: Cromatografía líquida de alta performance (del inglés, high performance liquid chromathography)
HSQC: Correlación de enlace simple heteronuclear (del inglés, heteronuclear single quantum correlation)
IE: impacto electrónico.
MALDI-TOF-MS matrix assisted laser desorption ionization-time of flight–mass spectrometry
GBM: glioblastoma multiforme.
SNC: sistema nerviosos central
CHLCC: Comisión Honoraria de Lucha contra el Cáncer
WHO: Organización Mundial de la Salud (del inglés, World Health Organization)
BHE: barrera hematoencefálica
BCNU: carmustina
TMZ: temozolomida
BNCT: Terapia por captura neutrónica de boro
LET: Transferencia lineal de energía (del inglés, linear energy transfer)
AcOEt: acetato de etilo
ACN: acetonitrilo
CuAAC: cicloadición entre azidas y alquinos catalizada por cobre (del inglés, *catalyzed azide–alkyne cycloaddition*)
DMF: dimetilformamida
DMSO: dimetilsulfóxido
Et_3N: trietilamina
MeOH: metanol
PF: punto de fusión
SNIE: sustitución nucleofílica inducida electrofílicamente
S_EAr: Sustitución electrofílica aromática
S_N: Sustitución nucleofílica

CONFIDENCIAL

2 Introducción

2.1 Aspectos generales del Cáncer

Cáncer es un término genérico que designa un amplio grupo de patologías que tienen la potencialidad de afectar a cualquier parte del organismo. La etiología del cáncer es multifactorial cuyo factor común es un desequilibrio en la relación proliferación/muerte celular provocado por la división de células malignas que escapan a los mecanismos de control del ciclo celular, adquiriendo la capacidad de invasión y destrucción tisular[1]. Estas características de autosuficiencia hacia señales de crecimiento y resistencia a las señales apoptóticas y antiproliferativas son el resultado de sucesivos procesos de acumulación de alteraciones génicas dando lugar a la proliferación crónica. Cada tipo de cáncer difiere de forma variable en su histogénesis, morfología, evolución clínica y pronóstico[2]. Cuando existen tumores y a medida que la enfermedad progresa, los mismos adquieren la capacidad de invadir el tejido normal circundante y diseminarse a otras regiones del cuerpo a través de la sangre o la linfa, formando tumores secundarios o metástasis.

A nivel mundial millones de personas se ven afectadas por el cáncer, siendo la segunda causa de mortalidad. No obstante, en los últimos 30 años la tasa de supervivencia a 5 años de todos los cánceres combinados ha aumentado un 20 % como resultado de numerosos esfuerzos en investigación y desarrollo en diversas áreas abocadas a la detección temprana, control de factor de riesgos, concientización social de buenos hábitos, mejora en los tratamientos, ya sea con agentes quimioterápicos, de síntesis o de origen natural, o con radioterapia, así como también nuevas terapias como los inmunotratamientos a través de biofármacos, entre otras. Si bien dicha tendencia se traduce en una disminución de la mortalidad por cáncer en los últimos 20 años[3], el cáncer es considerado un problema de salud pública a nivel mundial, estimándose unos 20 millones de nuevos casos anuales para el 2025[4]. Este escenario requiere de investigación clínica y básica continua enfocada en mejorar las prácticas de prevención, diagnóstico y tratamientos de los distintos tipos de cáncer.

2.1.1 Tumores cerebrales, gliomas: definición y clasificación.

El tejido conectivo especializado del sistema nervioso central (SNC) encargado del mantenimiento, protección y nutrición de las neuronas se denomina glía. Dentro de éste se distinguen tres tipos de células: los astrocitos, los oligodendrocitos y las células del epéndimo.

CONFIDENCIAL

Los astrocitos o astroglía es la más grande de todas las células de la glía, tienen forma estrellada y se encargan de proporcionar soporte o sostén mecánico a las neuronas y fagocitar los desechos del cerebro. Los oligodendrocitos u oligodendroglía son células más pequeñas que proporcionan soporte a los axones y producen la vaina de mielina que aísla a la mayoría de los axones entre sí. Las células del epéndimo o glía ependimaria revisten el conducto central de la médula espinal y los ventrículos cerebrales[5]. Una vez el sistema nervioso haya completado su desarrollo y madurez, las neuronas pierden su capacidad de dividirse y diferenciarse, mientras que las células gliales mantienen la capacidad de proliferar a lo largo de la vida. Por ello, la mayor parte de los tumores neurológicos en adultos son de origen glial, denominándose genéricamente gliomas.

Los gliomas fueron descritos por primera vez por el patólogo alemán Rudolf Virchow y actualmente se conocen, según la *National Brain Tumors Society*, más de 120 tipos de tumores cerebrales y suponen el 2 % de todas las neoplasias siendo la segunda causa de muerte por causas neurológicas detrás de los accidentes cerebrovasculares. Constituyen uno de los tipos de cáncer con peor pronóstico, por su difícil tratamiento y su alta tasa de recidivas.

Los gliomas son clasificados por la *World Health Organization* (WHO) en base al grado de malignidad, alteraciones genéticas y características histopatológicas dentro de las que se destacan: atipia nuclear, células mitóticas, proliferación microvascular y necrosis (Figura 1)[6].

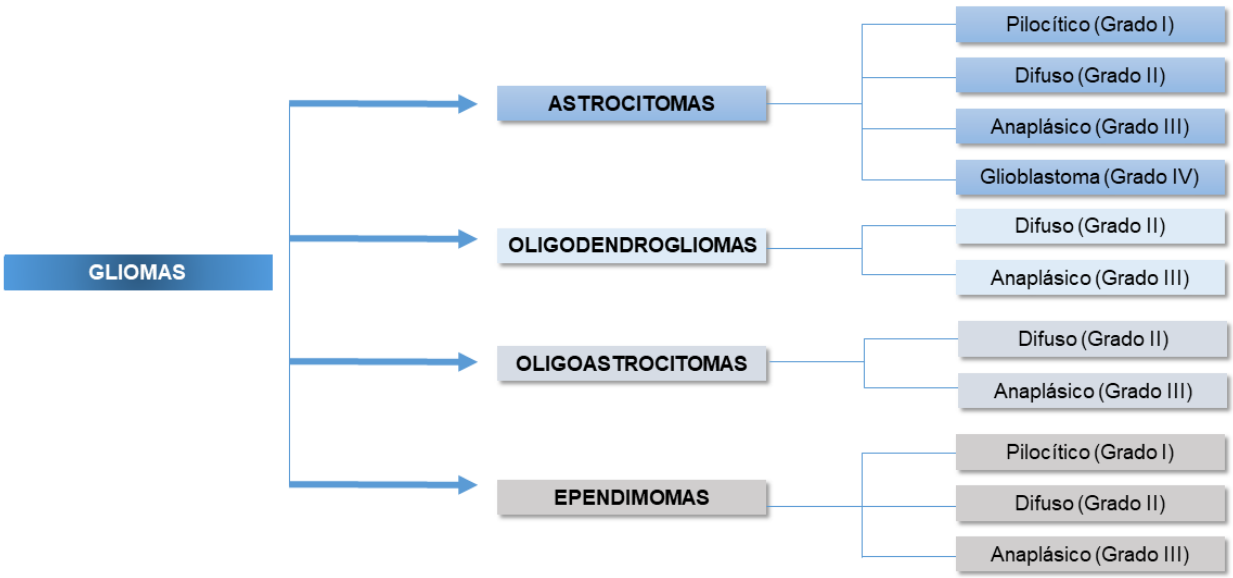


Figura 1. Clasificación de gliomas según la WHO (modificado de referencia 6).

Particularmente los gliomas astrocíticos se clasifican y describen de la siguiente manera[7]:

- **Grado I (astrocitoma pilocítico)**, son aquellas lesiones benignas que pueden ser curadas tras resección quirúrgica. Es un tumor de crecimiento lento, bien delimitado y localizado, no infiltrante y poco frecuente, que se presenta mayoritariamente en niños y adultos jóvenes. Representan un 10 % de los astrocitomas cerebrales.
- **Grado II (astrocitoma difuso)**, considerados los gliomas de bajo grado más frecuentes y pueden tener largos procesos clínicos, pero su temprana infiltración en los alrededores del cerebro los hace incurables mediante cirugía. Tienen crecimiento lento, infiltración difusa y atipia citológica. Se presentan en adultos jóvenes y tienden a proliferar hasta astrocitoma anaplásico y finalmente a glioblastoma. Representan alrededor del 35 % de los tumores astrocitarios.
- **Grado III (astrocitoma anaplásico)**, difuso, altamente infiltrante y con alta tasa proliferativa. Histológicamente caracterizado por atipia nuclear, aumento de la celularidad, anaplasia y actividad mitótica. Constituyen el 4 % de todos los tumores primarios del SNC. Mayormente aparecen en la edad adulta, generalmente diagnosticados entre los 45 y 69 años. Tiene una tendencia marcada hacia la evolución a glioblastoma con una mediana de tiempo de 2 años.
- **Grado IV (glioblastoma multiforme)**, es la variante de mayor malignidad dentro del sistema nervioso central. Provienen de una progresión de un astrocitoma anaplásico o, más frecuentemente de una mutación *de novo* sin la manifestación de un precursor maligno previo. El tamaño de las células presentes en el tumor puede ser muy variable, de pequeñas células uniformes a células gigantes de gran tamaño. Presentan características más avanzadas de tumorogenicidad, incluyendo proliferación microvascular o necrosis del tejido en pseudoempalizada, angiogénesis robusta, alta resistencia a la apoptosis y gran inestabilidad genómica. Debido a su capacidad de infiltración a otras zonas del cerebro o médula espinal y su extrema resistencia a la radio/quimioterapia, generalmente son letales, el pronóstico es de aproximadamente 14 meses de supervivencia.

2.2 Glioblastoma multiforme (GBM)

Es el tumor cerebral primario más frecuente, representa más del 51 % de los gliomas así como un 20 % de los tumores intracraneales y es la variante de mayor malignidad dentro del SNC[8]. La tasa de incidencia en Europa es de 5/100.000 adultos por año, siendo ligeramente superior

CONFIDENCIAL

en hombres (la relación hombres/mujeres es de 1,5) y con una cierta variabilidad en la incidencia de este tipo de tumor entre países y grupos étnicos[9]. En Uruguay y de acuerdo a los registros de la Comisión Honoraria de Lucha contra el Cáncer (CHLCC), en el periodo 2011-2015 se registraron un total de 807 casos de glioma de los cuales 428 casos fueron clasificados como glioblastoma.[1]

El sufijo "blastoma", hace referencia al gran contenido de células escasamente diferenciadas en este tipo de tumores mientras que el término "multiforme" denota la naturaleza heterogénea y la variada composición histológica característica de este tipo de tumor. Dicha diversidad celular incluye, tipos celulares diferenciados con morfología estrellada y expresión de marcadores tales como GFAP y S100, así como también tipos celulares indiferenciados, más pequeños y redondeados, mezclados con elementos del estroma tales como proliferación celular microvascular, astrocitos reactivos, microglía y otros infiltrados inmunitarios.

2.2.1 Clasificación de GBM y alteraciones genéticas asociadas a los gliomas

Tradicionalmente los GBM se han clasificados en base a sus características genéticas y biológicas en dos tipos: primarios o *de novo* que representan la mayoría de los GBM (90-95 % de los GBM) y secundarios. Si bien en ocasiones presentan similitudes histológicas se los considera enfermedades distintas. Involucran a grupos de personas con edades variadas, presentan diferentes velocidades de evolución de la enfermedad y tienen alteraciones genéticas y rutas de señalización distintas[10]. Los GBM primarios suelen aparecer en personas con edades avanzada, 50 años en promedio, teniendo una esperanza de vida muy corta debido a la gran malignidad y rápido crecimiento del tumor. Los GBM secundarios, que representan menos del 5-10 % de los GBM, surgen como progresión de astrocitomas de más bajo grado (astrocitoma difuso o astrocitoma anaplásico) y afectan a pacientes más jóvenes. La evolución clínica es más lenta y los pacientes tienen una supervivencia media significativamente superior, tanto por la menor edad del paciente como por el crecimiento tumoral más lento[11].
En la Figura 2 se resumen ciertas características y las alteraciones genéticas más frecuentes en los distintos gliomas astrocíticos[12].

[1] Datos otorgados por el Registro Nacional de Cáncer, CHLCC.

CONFIDENCIAL

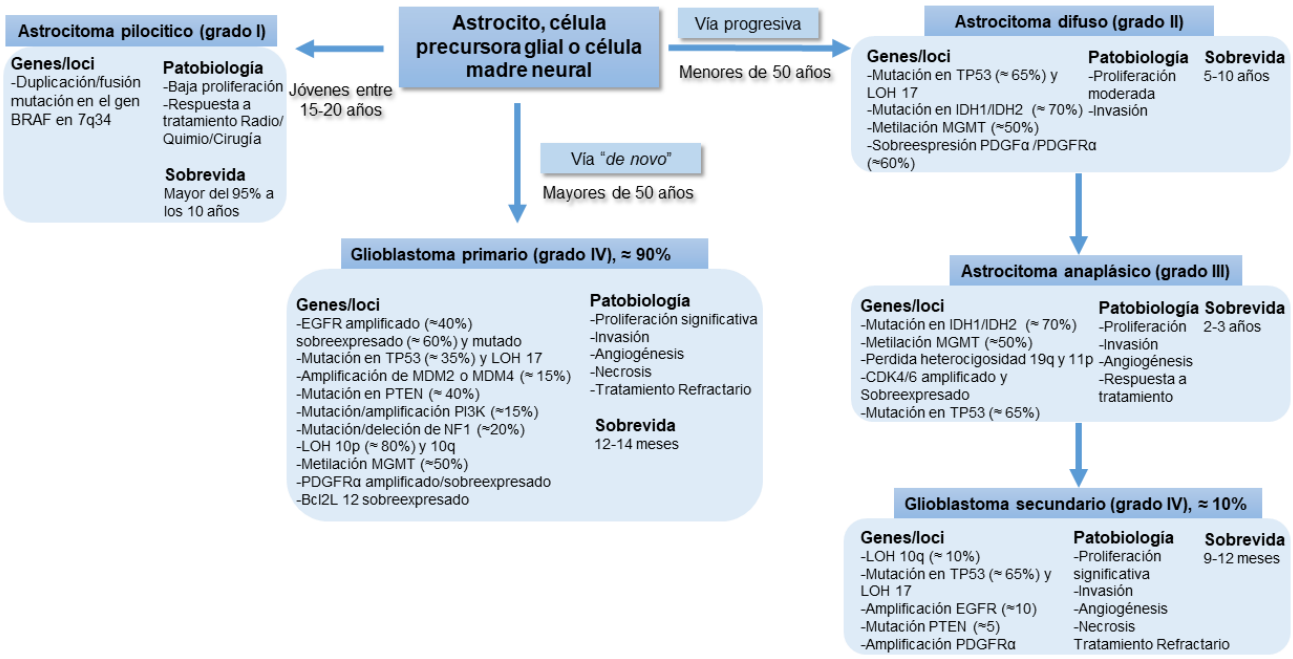


Figura 2. Mecanismo y frecuentes alteraciones génicas implicadas en la gliogénesis[7].

2.2.2 Estrategias terapéuticas para el tratamiento del GBM

Los tratamientos actualmente utilizados para GMB varían dependiendo si se trata de un glioma de diagnóstico reciente o un glioma recurrente. Aquellos pacientes que son diagnosticados por primera vez, y en la medida de que sea posible, son sometidos a cirugía con el objetivo de lograr la máxima resección tumoral preservando la función neurológica[13]. Este procedimiento permite la descompresión inmediata del cerebro de forma de mitigar el efecto de masa que genera sobre los tejidos adyacentes, aumentando, de esta forma, la efectividad de las terapias adyuvantes posteriores así como también el diagnóstico histopatológico preciso. Ciertos avances como la utilización del ácido 5-aminolevulínico (5-ALA) el cual actúa como precursor de las porfirinas y tiene la potencialidad de ser acumulado en GBM (Figura 3), han permitido la detección por fluorescencia de las células tumorales no visibles macroscópicamente (Figura 4)[14].

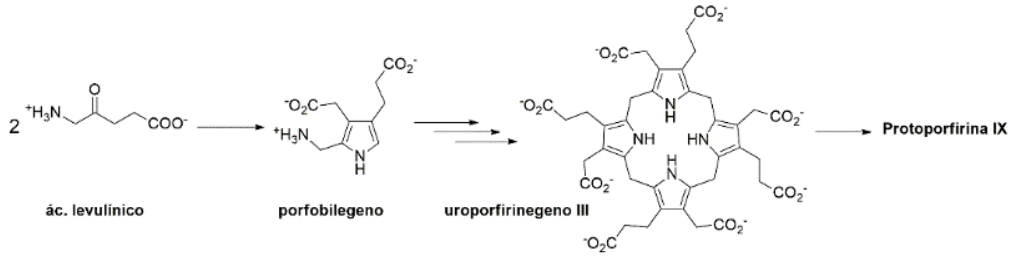


Figura 3. Resumen de la biosíntesis de porfirina a partir del ácido 5-aminolevulínico.

CONFIDENCIAL

Además, se han incorporado a la cirugía de gliomas de alto grado avances como el uso de microscopio quirúrgico, la coagulación bipolar, el aspirador ultrasónico y la neuronavegación. No obstante, la extirpación completa del tumor sigue siendo prácticamente imposible debido a la naturaleza altamente infiltrante del mismo. Por este motivo, el tratamiento de los pacientes viene acompañado por la administración de radioterapia concomitante con quimioterapia y posteriormente tratamiento adyuvante quimioterápico[15].

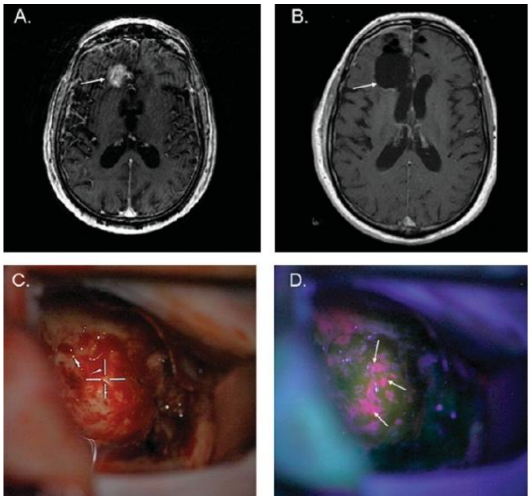


Figura 4. Resección quirúrgica guiada por fluorescencia de un GBM: A) – B) Resonancia magnética pre y postoperatoria de un paciente, mostrando las zonas de infiltración tumoral resecadas no detectadas por la MRI preoperatoria. C) – D) Visión intraoperatoria del tumor (flechas) observada con y sin fluorescencia tras la administración de 5-ALA vía oral, previo a la cirugía[14].

La radioterapia que se suele utilizar y que incrementa la supervivencia de los pacientes desde 3-4 a 12-14 meses, es la radioterapia externa fraccionada (ERBT, del inglés *external beam radiotherapy*), que consiste en irradiar durante seis semanas y utilizando una dosis total de 60 Gy en 30 fracciones de 2 Gy[16].

Como tratamientos quimioterápicos adyuvantes generalmente se utilizan carmustina (BCNU, Gliadel®) como estrategia de quimioterapia local o temozolomida (TMZ, Temodal®) como quimioterapia sistémica, ambos con buena estabilidad y capacidad de penetración de la barrera hematoencefálica (BHE o *BBB, del inglés blood-brain barrier*).

La nitrosourea BCNU es un pro-fármaco que se administra de forma intraoperatoria como polímero reabsorbible en el lecho quirúrgico tumoral (Figura 5)[17]. La BCNU fue aprobada por la FDA como tratamiento inicial en febrero de 2003 luego de constatarse que la supervivencia fue de 13,9 meses en el grupo de tratamiento versus 11,6 en el grupo de control[18].

Sintetizado en 1984 por Stevens y cols., TMZ (Figura 6) es el principal agente quimioterápico administrado vía oral que se utiliza actualmente en clínica para el tratamiento de GBM. Posee 100 % de biodisponibilidad por vía oral, y está demostrado su adecuada capacidad de penetración de la BHE donde alcanza una concentración del 25 al 30 % de los niveles plasmáticos[19]. Presenta además un buen perfil farmacocinético con rápido aclaramiento plasmático, lo que reduce la posibilidad de efectos sistémicos. Al igual que la BCNU, la TMZ actúa como pro-fármaco sufriendo en condiciones de hidrólisis, a pH neutro o alcalino, la apertura del anillo de tetrazina generando el triazeno de cadena abierta (MTIC, Figura 6).

CONFIDEN

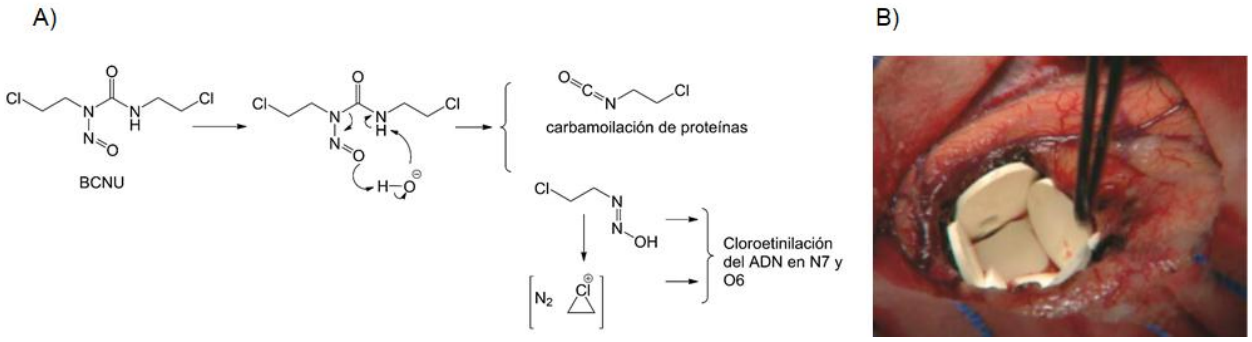


Figura 5. A) Mecanismo de activación y acción del pro-fármaco BCNU. B) Luego de la cirugía se administran en el interior del tumor hasta 8 comprimidos del polímero que liberará la BCNU[17].

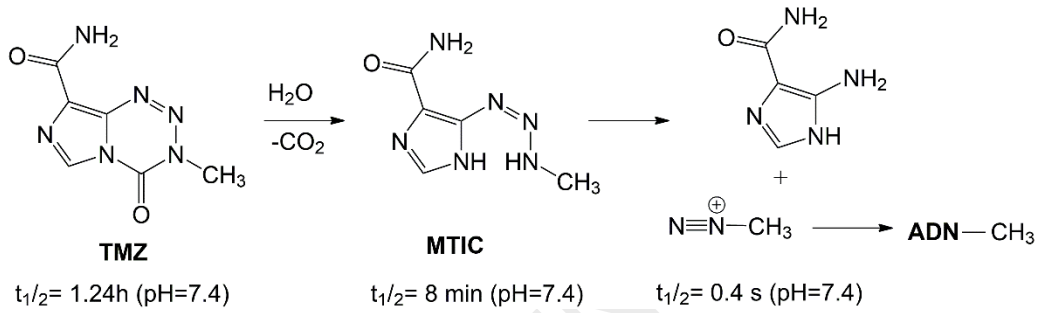


Figura 6. Esquema del mecanismo de activación del pro-fármaco TMZ.

El intermedio MTIC es capaz de transferir el grupo metilo a diferentes bases nitrogenadas del ADN. La mayoría de los grupos metilo transferidos al ADN aparecen 70 % en los sitios de guanina N^7, alrededor del 10 % en adenina N^3 y el 5 % en guanina O^6 [20,21]. Si bien esta última transformación representa un porcentaje bajo, la O^6-G metilada (O^6-MeG) es responsable del mayor efecto citotóxico de la TMZ como consecuencia del emparejamiento incorrecto o *missmatch* con una Timina (O^6-G-T) en lugar de hacerlo con su base natural. Como consecuencia de la mala reparación de las bases se generan lesiones que acabarán produciendo la rotura de la doble cadena del ADN y consecuentemente, muerte por apoptosis o autofagia de la célula.

CONFIDEN

El mecanismo más aceptado en la actualidad por el cual ciertos pacientes presentan resistencia a la TMZ, y a BCNU, es consecuencia de la expresión de la enzima de reparación del ADN MGMT (O^6-metilguanina-ADN-metiltransferasa) responsable de eliminar los grupos metilos de las lesiones O^6-MeG. Por el contrario, la metilación del promotor de MGMT silencia el gen y por ello en dichos casos se ve aumentada la citotoxicidad debido a las lesiones O^6-MeG[22]. Si bien MGMT se expresa de manera constitutiva, sus niveles de expresión son algo variable entre los distintos tipos de tumores. En tumores cerebrales se ha visto que es baja, posiblemente resultado de la metilación del promotor de MGMT[23]. En la Figura 7 se muestra la representación del mecanismo de acción de MGMT con un inhibidor clínicamente probado como lo es la O^6-bencilguanina. En el sitio activo y promovido por una catálisis básica, se genera un residuo nucleofílico a partir de la cisteína 145 quien será el responsable de cribar el enlace C-O de O^6-MeG lo que resultará en la inactivación de la proteína.

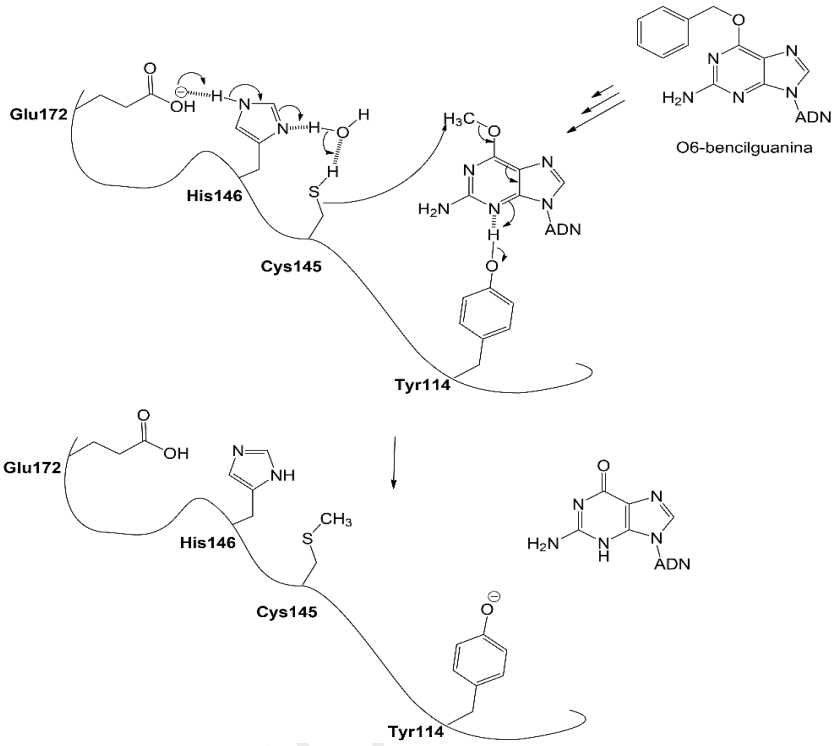


Figura 7. Mecanismo de inhibición de O^6-bencilguanina sobre MGMT.

Aquellos pacientes en los que la primera línea de tratamiento no es efectiva desarrollan un GBM recurrente de muy mal pronóstico con un tiempo aproximado de progresión al tratamiento de segunda línea de unas 10 semanas y una supervivencia total de 25-30 semanas. Son muy pocos los casos en los cuales los pacientes pueden volver a someterse a re-intervención quirúrgica o re-irradiación[24]. En referencia a los agentes quimioterápicos, se suele utilizar los agentes alquilantes antes mencionados TMZ y BCNU, que presentan una alta lipofilicidad lo que les permite atravesar la BHE. Además de estos y como consecuencia del elevado número de alteraciones moleculares presentes en los GBM, se vienen investigando diversas estrategias dirigidas específicamente a estas dianas, como ser:

- Tratamientos con inhibidores de angiogénesis, VEGF/VEGFR (*del inglés vascular endothelial growth factor/receptor*). Un ejemplo es el uso del anticuerpo monoclonal

humanizado bevacizumab (Avastin®), dirigido específicamente al VEGF secretado por las células tumorales para la formación de nuevos vasos sanguíneos[25].

- Anticuerpos contra el receptor del factor de crecimiento epidérmico (EGFR, *del inglés epidermal growth factor receptor*). Dentro de esta clase se destaca el uso de cetuximab (Erbitux®)[26] y nimotuzumab (Theraloc®)[27]. Estos anticuerpos tienen como principal objetivo bloquear la interacción receptor-ligando y la activación de las vías de señalización subyacente.
- Moléculas inhibidoras de la actividad tirosina quinasa: EGFR, PDGFR (*del inglés platelet-derived growth factor receptors*). Moléculas de bajo peso molecular que interaccionan a nivel intracelular en el dominio tirosina quinasa del EGFR impidiendo su fosforilación y, por tanto, evitando su activación[28]. Están siendo ampliamente estudiados para el tratamiento de gliomas y se desarrollarán en detalle en la siguiente sección.
- Inhibidores de la vía PI3K-Akt-mTOR (*del inglés mammalian target of rapamycin*). Ejemplos de inhibidores son sirolimus (Rapamicina), temsirolimus (CCI-779) y enzastaurin.
- Inhibidores de las HDAC (*del inglés histone deacetilase*). Comprende a moléculas de bajo peso molecular que inducen la hiperacetilación de las histonas de forma que reactivan así la expresión de ciertos genes que estaban siendo reprimidos. Un ejemplo de estos es el vorinostat (suberoyanilide, SAHA)[29]. El mismo fue aprobado por la FDA en octubre de 2006 para uso clínico en el tratamiento de linfoma de células T cutáneo y debido a su éxito actualmente se está utilizando en ensayos clínicos de otras enfermedades, entre otras el GBM, aunque con menor eficacia por el momento.

2.2.3 Proteínas con actividad tirosina quinasa como dianas terapéuticas en GBM

En conjunto con las fosfatasas, las proteínas quinasas regulan el estado de fosforilación de proteínas intracelulares, destacándose los receptores con actividad quinasa de tirosina. Debido a su rol en la transmisión de señales extracelulares hacia el interior de las células, dichas proteínas están implicadas en el desarrollo de enfermedades como el cáncer, inflamación, diabetes y enfermedades inmunológicas. Por ello en los últimos años han emergido como dianas moleculares en la terapia de dichas patologías[30]. Los principales sitios de fosforilación de estas quinasas son el grupo alcohol de la serina, treonina o de la tirosina. En la Ecuación 1 se puede observar de forma general la reacción de transferencia del grupo fosfato del ATP al grupo hidroxilo de las proteínas.

CONFIDENCIAL



Ecuación 1. Reacción general de fosfotransferencia desde el ATP a las proteínas sustrato.

2.2.3.1 Integrantes de la familia de receptores con actividad tirosina quinasa y estructura general

En la actualidad están descritas aproximadamente 20 subfamilias de receptores con actividad tirosina quinasa (RTKs, del inglés *receptor tyrosine kinases*) y son clasificadas según[31]:

- Clase I: Familia del receptor de EGF
- Clase II: Familia del receptor de Insulina
- Clase III: Familia del receptor de PDGF
- Clase IV: Familia del receptor de FGF
- Clase V: Familia del receptor de VEGF
- Clase VI: Familia del receptor de HGH
- Clase VII: Familia del receptor de Trk
- Clase VIII: Familia del receptor de AXL

De la clase I a la VI se ha visto una fuerte asociación con enfermedades oncológicas resultando por ende un campo de investigación latente para el tratamiento de dicha patología.

La mayor parte de los RTK tienen una estructura similar (Figura 8), se caracterizan por:

- un dominio transmembrana monomérico hidrofóbico compuesto por 25-28 aminoácidos que tiene un rol fundamental en la formación y estabilización de las cadenas del dímero.
- un dominio extracelular *N*-terminal glicosilado con un elevado número de enlaces disulfuro. Dicho extremo está involucrado en el proceso de dimerización de los receptores y, por consiguiente, en el reconocimiento del o los ligando/s. Esta región es característica de cada subfamilia de RTK aunque exhiben una variedad de elementos constantes, los dominios inmunoglobulinas (Ig)-*like* o factor de crecimiento epidérmico (EGF)-*like*, que son repeticiones de fibronectina tipos III o regiones ricas en cisteínas.
- una región intracelular *C*-terminal formada por los dominios catalíticos, responsable de la actividad quinasa del receptor la cual se encarga de la fosforilación del mismo.

CONFIDENCIAL

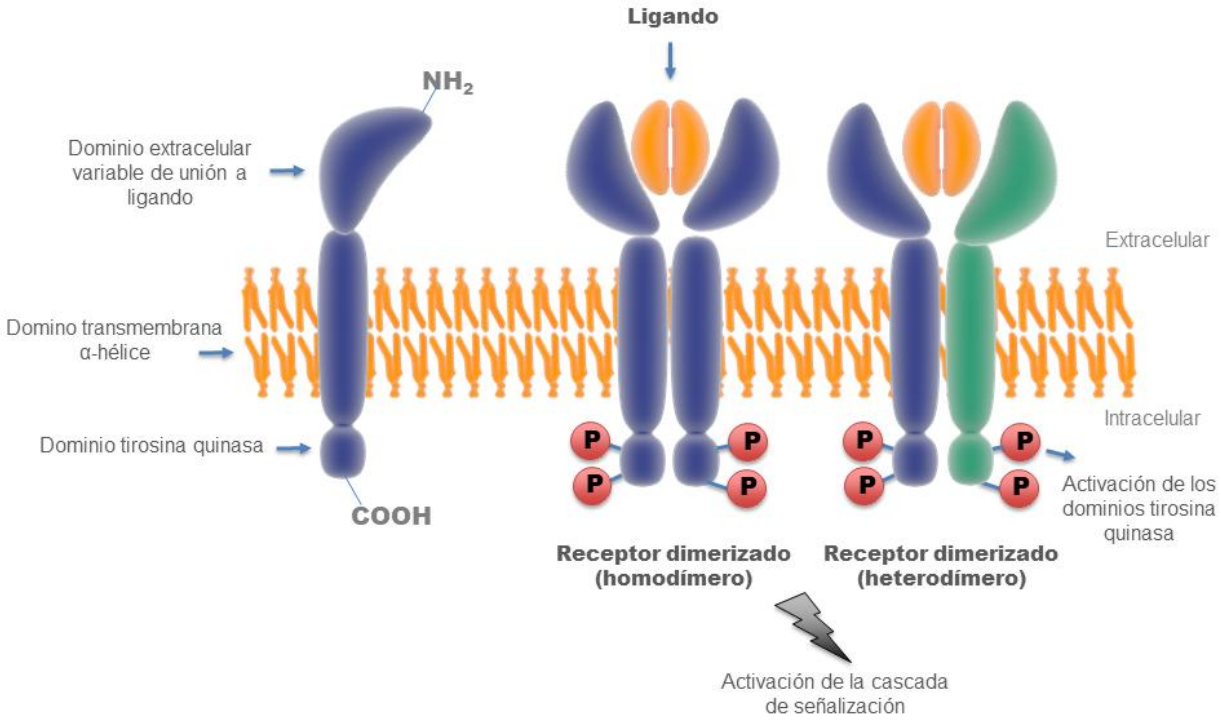


Figura 8. Organización general de los dominios moleculares que conforman los RTKs. Los RTKs se caracterizan por la dimerización de dos cadenas receptoras con un dominio extracelular N-terminal y un dominio intracelular C-terminal. El dominio extracelular está implicado en el reconocimiento de los ligandos y en la formación del proceso de dimerización de la cadena del receptor. Está compuesto de varios dominios según la clase de RTK. El dominio transmembrana está compuesto por una cadena de hélice α, que contribuye a la estabilización de las cadenas receptoras diméricas. La unión de un ligando (en naranja) a los dominios extracelulares de las cadenas receptoras refuerza la estabilización de las cadenas receptoras, que se autofosforilan a través de sus dominios de tirosina quinasa y luego se transducen en vías de señalización descendentes específicas.

2.2.3.2 EGFR como diana terapéutica en GBM

El receptor del factor de crecimiento epitelial (EGFR), también nombrado como HER-1 o c-erbB-1, integra, como se comentó en el punto anterior, junto con HER2/neu (c-erbB-2), HER3 (c-erbB-3) y HER4 (c-erbB-4) la familia de receptores quinasa clase I. EGFR es el receptor de ligandos extracelulares de la familia EGF entre las que se hallan el propio EGF, el factor de crecimiento transformante alfa (TGF-α, *del inglés transforming growth factor alpha*), anfirregulina, betacelulina, epirregulina y el factor de crecimiento epidérmico de unión a la heparina (HB-EGF, *del inglés heparin-binding EGF-like growth factor*). La unión del ligando con EGFR da como resultado una homo o heterodimerización del receptor en la superficie celular,

seguida de la internalización del receptor dimerizado. Tras la dimerización e internalización, se produce la autofosforilación de los dominios intracitoplasmáticos de tirosina quinasa en EGFR[32]. Los residuos de tirosina quinasa fosforilados sirven como sitios de unión para el reclutamiento de transductores de señal y sustratos activadores intracelulares, tales como Ras, PI3K, que luego estimulan una cascada intracelular de transducción de señales (Figura 9).

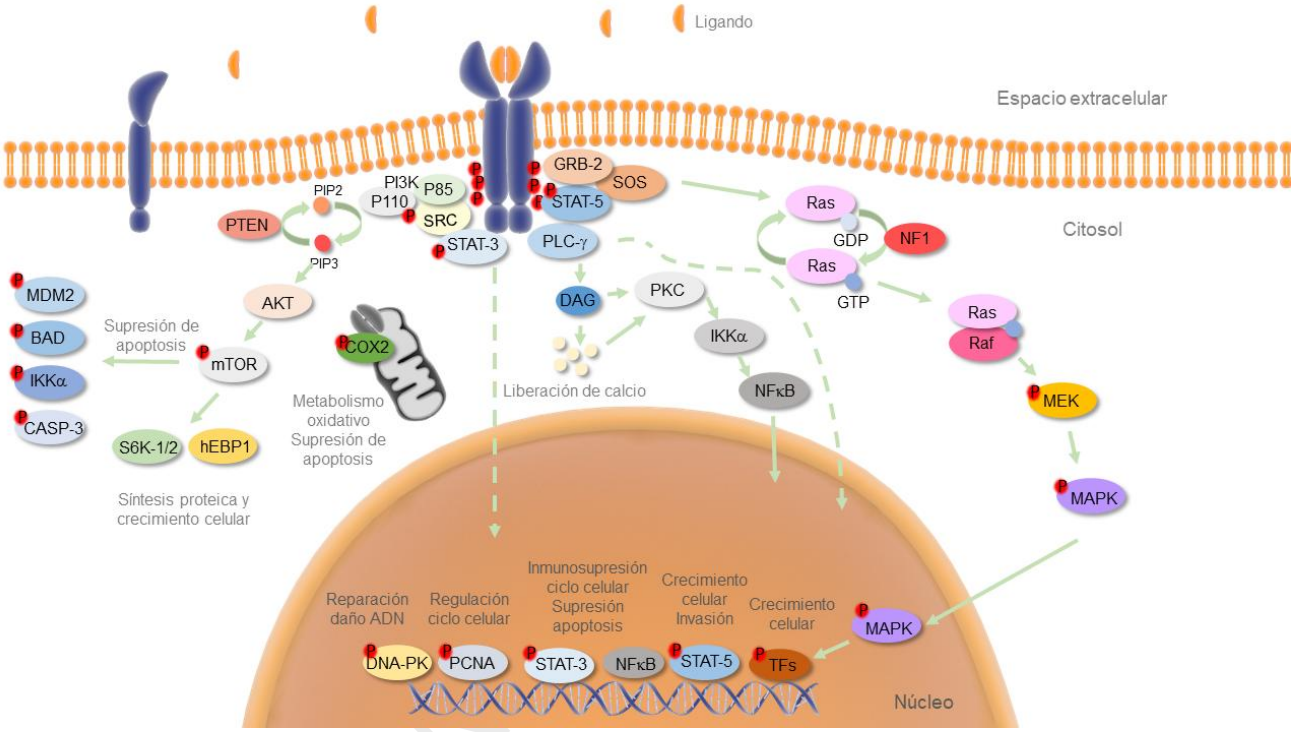


Figura 9. Vías de señalización de EGFR dependientes de la actividad tirosina quinasa del receptor. La unión de EGF al EGFR desencadena la fosforilación de varios residuos en el dominio intracelular del receptor y el reclutamiento de diversas moléculas adaptadoras capaces de activar una variedad de vías de señalización intracelulares que implican MAPK/ERK, PI3K, STAT-3, PLCγ-PKC-NFκβ y SRC, entre otros transductores de señales. Estos procesos tiene como resultado cambios en la síntesis proteica, el crecimiento celular, la supresión de la respuesta inmune y de la apoptosis así como la alteración del metabolismo celular. Además EGFR puede ser translocado al núcleo, donde tiene efecto sobre la regulación del ciclo celular y la reparación del daño al ADN.

El gen de EGFR se localiza en el cromosoma 7p12, consta de 28 exones y codifica una proteína de 170 kDa que tiene cuatro dominios funcionales: el dominio extracelular o ectodominio de unión a ligando que se encuentra subdividido en cuatro dominios (L1, L2, CR1 y CR2), el dominio transmembrana, el dominio intracelular donde se localiza la región con actividad tirosina quinasa y la región de regulación carboxilo terminal que contiene múltiples tirosinas que se fosforilan específicamente tras la unión del ligando (Figura 10).

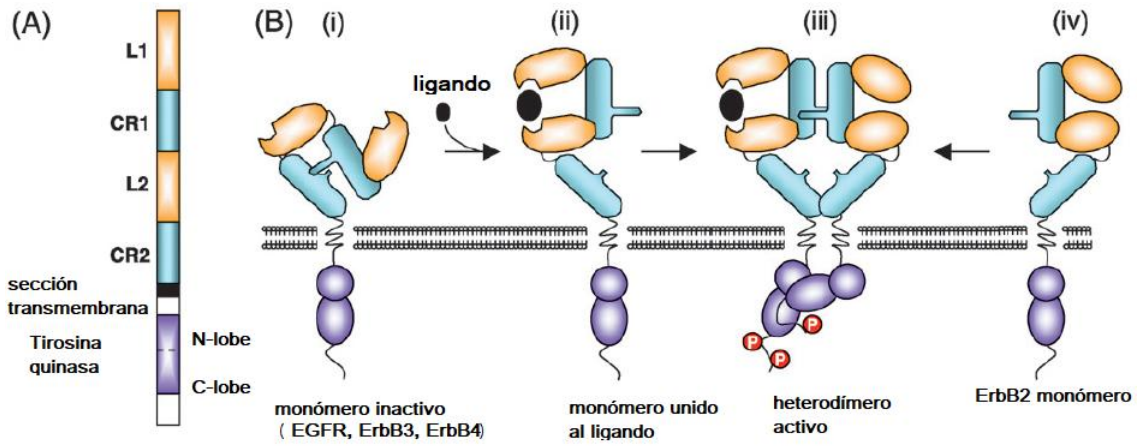


Figura 10. (A) Representación lineal de los dominios del receptor ErbB. El dominio N-terminal extracelular contiene cuatro subdominios. Los subdominios ricos en leucina L1 y L2 interactúan directamente con el ligando. El subdominio CR1 rico en cisteína contiene el bucle de dimerización responsable de la interacción receptor-receptor. Un corto dominio transmembrana y yuxtamembrana une el dominio extracelular al dominio de tirosina quinasa bilobulado y la cola C-terminal. (B) Descripción esquemática del proceso de dimerización y activación del receptor ErbB. (i) En el estado libre de ligando, EGFR, ErbB3 y ErbB4 tienen una conformación anclada estabilizada por la interacción entre CR1 y CR2. (ii) La unión del ligando entre L1 y L2 crea una conformación extendida, que expone el bucle de dimerización de CR1 permitiendo la homo y heterodimerización del receptor. (iii) La dimerización del receptor presenta la región tirosina quinasa N-lóbulo de un receptor con el C-lobe de su compañero, lo que lleva a la fosforilación de la tirosina C-terminal, creando sitios de unión de fosfotirosina para la unión de adaptadores, moléculas de señalización y proteínas reguladoras. (iv) ErbB2 es único porque está fijo en la conformación extendida Listo para interactuar con otros receptores ErbB. Adaptado de[33].

CONFIDENCIAL

Como se comentó el gen de EGFR se encuentra amplificado en un 40 % y sobreexpresado en aproximadamente 60 % de los tumores de alto grado (GBM primarios y astrocitomas de grado III)[7]. La media de edad de los pacientes que portan dicha alteración es de 62 años siendo muy poco frecuente en aquellos menores de 35 años[11]. Dentro de ese 40 % el 30 % presenta expresada la variante EGFRvIII, siendo ésta la mutación con mayor frecuencia 60-70 %[34]. EGFRvIII carece de los exones 2 al 7 correspondientes a los dominios extracelulares I y II y codifica un receptor que carece de los aminoácidos 6 a 273[35]. El efecto oncogénico de dicha variante se podría explicar por la actividad tirosina quinasa constitutiva en ausencia de ligando resultando en la activación de forma selectiva o constitutiva de las rutas que implican PI3K, Ras, JNKs (*del inglés c-Jun N-terminal kinases)*, SFKs (*del inglés Src family kinases*), uPAR (*del inglés Plasminogen activator urokinase receptor*) y NF-κB (*del inglés Nuclear factor kappa-light-chain-enhancer of activated B cells*). Otras alteraciones no tan frecuentes pero que de igual modo se asocian al crecimiento tumoral son las deleciones que originan las variantes EGFRvI a EGFRvV[36,37].

2.2.3.3 VEGF/VEGFR como diana terapéutica en GBM

La angiogénesis es reconocida como un proceso fundamental y crítico para el crecimiento de tumores sólidos y para el proceso de metástasis. En particular en GBM el aumento de la vascularización y la proliferación microvascular son rasgos histopatológicos muy importantes. Por ello, dirigir fármacos a la vasculatura tumoral del GBM resulta muchas veces una estrategia atractiva. La inducción de daños en los vasos sanguíneos del tumor o la inhibición de la angiogénesis privan a las células cancerosas de oxígeno y nutrimentos, al tiempo que evita la eliminación de productos de desecho. La hipoxia resultante, la inanición de las células tumorales y la acumulación de productos de desecho eventualmente llevan al cese del crecimiento tumoral y a la necrosis de las células cancerosas.

El VEGF, también conocido como VEGF-A e identificado por primera vez como factor de permeabilidad vascular (VPF, *vascular permeability factor*), es una glicoproteína de secreción de aproximadamente 45 kDa que cumple un rol clave en el proceso de angiogénesis. Desde su identificación, se han descrito varios miembros adicionales de la familia: VEGF-B, VEGF-C, VEGF-D y PlGF, aunque sigue siendo VEGF-A la familia con rol más protagónico. La unión de VEGF a VEGFR2 induce la dimerización del receptor y la autofosforilación, lo que estimula la supervivencia, proliferación, migración y permeabilidad de las células endoteliales (Figura 11). VEGFR2 media la supervivencia mediante la activación de PI3K, que fosforila Akt, e inhibe la activación de proteínas pro-apoptóticas. El promotor de la muerte asociado a Bcl2 (BAD) y la caspasa VEGF también induce la expresión de proteínas anti-apoptóticas, como Bcl2. La activación de PI3K / Akt también promueve la permeabilidad vascular mediante la estimulación de la generación de óxido nítrico mediada por la síntesis de óxido nítrico endotelial (eNOS).

Es sabido que el VEGF se encuentra sobreexpresado en muchos gliomas de alto grado y además esos niveles se correlacionan directamente con la vascularidad y el grado del tumor e inversamente proporcional con el pronóstico. Las células endoteliales asociadas a tumores expresan VEGFR2, creando un ciclo paracrino de activación angiogénica, lo que indica que el VEGF y sus receptores son una importante diana terapéutica. En ese sentido en los últimos años los fármacos antiangiogénicos han sido una de las estrategias terapéuticas con mayor aplicabilidad como tratamiento de segunda línea en pacientes afectos de GBM recurrente. El Bevacizumab, un anticuerpo monoclonal humano inhibidor de VEGF ha sido aprobado en 2009 por la FDA para el uso de GBM recurrente a partir de estudios de fase II con alto índice de respuestas[38]. Además pequeñas moléculas anti-VEGFR y EGFR inhibidoras de tirosina quinasa como axitinib, sunitinib, sorafenib, imatinib, erlotinib y lapatinib entre otras también se han evaluado en estudios anti-GBM (Figura 12).

CONFIDENCIAL

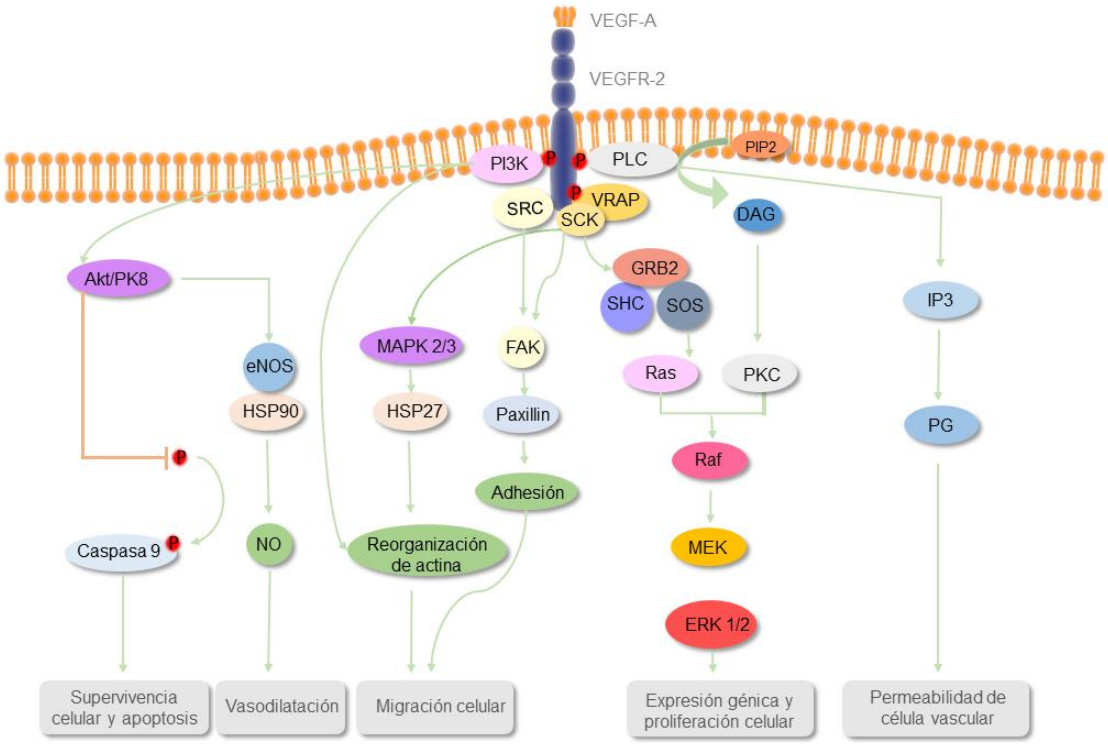


Figura 11. Representación esquemática de la vía de señalización VEGFA-VEGFR2. En células endoteliales VEGF se une a VEGFR-2 e induce la dimerización y autofosforilación de VEGFR-2. La activación de VEGFR-2 conduce a la activación de vías de señalización descendentes que repercuten en cambios en la supervivencia celular, proliferación, migración y permeabilidad de los vasos.

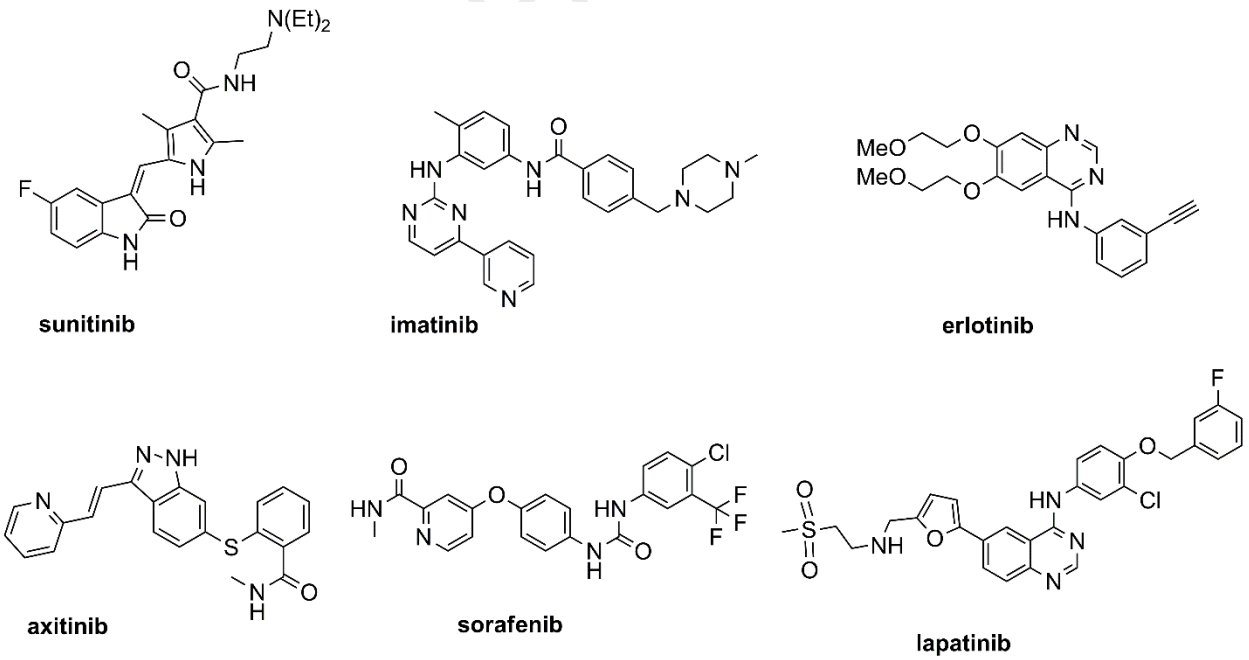


Figura 12. Inhibidores de proteínas tirosina quinasa que se han evaluado in vitro e in vivo en GBM[39].

2.3 Reseña histórica del Boro

El boro es el único elemento del grupo 13 de la tabla periódica de carácter no metálico; es considerado un elemento semi-metálico (o *metaloide).* Es capaz de formar enlaces covalentes como el carbono y el silicio, aunque con las peculiaridades que ofrece su configuración electrónica trivalente y que posee un orbital *p* vacante que da como resultado una compleja y variada química.

El boro tiene número atómico 5 y por contar con un orbital *p* vacante puede aceptar fácilmente electrones de una entidad donante, por ejemplo hidruro, para interconvertirse con facilidad entre una situación de sp^2 neutro y un estado aniónico de hibridación sp^3 (Figura 13).

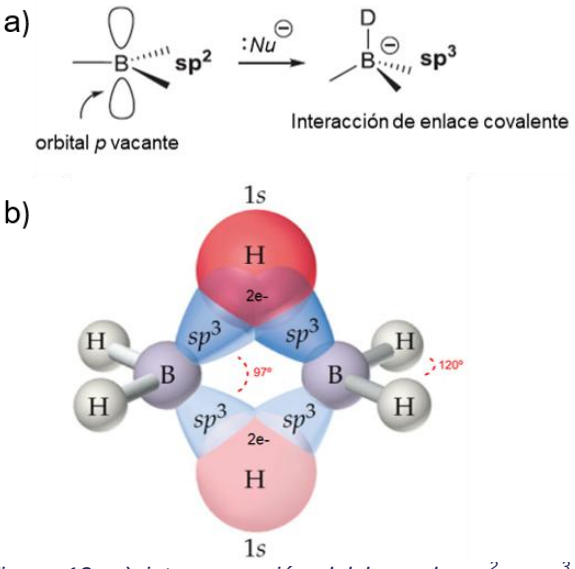


Figura 13: a) interconversión del boro de sp^2 a sp^3 por acción de dadores de electrones. b) estructura del B_2H_6 en donde se representan los dos centros B-H-B y los dos electrones compartidos en cada situación.

En la naturaleza se encuentran dos isótopos estables del boro, el ^{11}B (80.1 %) y el ^{10}B (19.9 %). Su abundancia es comparativamente pequeña en el universo (≈1 ppb) y en la corteza terrestre (≈9 ppm), donde se encuentra en forma de boratos o borosilicato, principalmente bórax, $Na_2[B_4O_5(OH)_4]$ $8H_2O$.

Los compuestos de boro se conocen desde hace aproximadamente 6000 años. Su nombre proviene del árabe *Buraq* y del persa *burah.* Desde los babilonios y pasando por los egipcios, chinos, tibetanos, romanos y árabes, los compuestos de boro se han utilizado con múltiples propósitos como soldaduras y refinación de oro y plata, materiales para la momificación y sobre todo para la fabricación de materiales duros como los borosilicatos. Las primeras investigaciones químicas relacionadas con el boro datan de 1702 cuando W. Homberg aisló ácido bórico a partir de bórax y sulfato ferroso. Sin embargo, no fue hasta 1808 cuando H. Davy, J.L. Gay-Lussac y J. Thénard aislaron por primera vez el boro con 50 % de pureza al calentar el ácido bórico con potasio metálico, aunque ninguno de ellos adjudicó tal sustancia como un nuevo elemento, algo que haría en 1824 J.J. Berzelius[40]. Finalmente, en 1911 el químico estadounidense W. Weintraub sintetizó por primera vez boro con un 99 % de pureza. En 1912 el químico alemán A. Stock preparó los primeros compuestos conteniendo únicamente átomos de hidrógeno y boro en la estructura a los que llamó boranos, iniciando así un nuevo campo de la química: la química del boro[41]. Las estructuras propuestas para todos los boranos

CONFIDE

fueron incorrectas, excepto la propuesta por W.C. Price para el diborano B_2H_6 (Figura 13)[42]. No fue hasta entrada la década del cuarenta cuando H.C. Longuet-Higgins publicó que la fórmula molecular de los hidruros de boro no podía explicarse en los términos de enlace 2e-2c ya que el número total de electrones era insuficiente [43]

Hasta el comienzo de la segunda guerra mundial este campo de la química tendría un desarrollo meramente académico. La situación cambió cuando en 1946, tanto Estados Unidos como la antigua URSS y Gran Bretaña invirtieron enormes cantidades de dinero en la síntesis de diversos boranos para su aplicación como combustible de aeronaves ("Project Hermes" y "Project Zip"), esto quedó reflejado en los simposios "From Borax to Boranes" (San Francisco, EEUU, 1958) y "Boron and Binary Boron Compounds" (Boston, EEUU, 1959)[44]. A pesar de ello no se lograron los resultados esperados, aunque las investigaciones sirvieron para establecer bases sólidas de la nueva química. Los grandes retos de principio de siglo se empezaron a resolver con la utilización de las primeras líneas de vacío, más conocidas como técnica *Schlenk* y sobretodo, con la obtención del Premio Nobel de Química en 1976 por W.N. Lipscomp en relación a sus estudios sobre la estructura de los boranos[45]. Para explicarla definió los enlaces tricéntricos (3c-2e). Posteriormente, en 1979 H.C. Brown y G.W. Wittig recibieron también el Premio Nobel de Química por el desarrollo de los compuestos de boro y fósforo, respectivamente, como reactivos importantes en el campo de la química orgánica sintética[46].

CONFIDENCIAL

2.3.1 Clústeres de boro

2.3.1.1 Boranos

Los boranos, compuestos de formula general $[B_nH_m]^{x-}$, son compuestos moleculares diamagnéticos, incoloros, blancos o amarillos, que pueden ser neutros o aniónicos y se estructuran como clústeres poliédricos de caras triangulares con vértices formados exclusivamente por unidades *-B-H*. Los clústeres con un número menor de vértices se encuentran en estado gaseoso a temperatura ambiente y, algunos de ellos, son extremadamente reactivos hasta el punto de ocasionar una combustión espontánea en el aire, pero, a medida que aumenta su peso molecular, son líquidos volátiles o sólidos, más estables térmicamente como es el caso del sistema icosaédrico *closo*-dodecaborato $[B_{12}H_{12}]^{2-}$ (Figura 14). Estos átomos de boro presentan un gran número de conectividades formando enlaces 3c-2e entre sí para compensar su deficiencia electrónica.

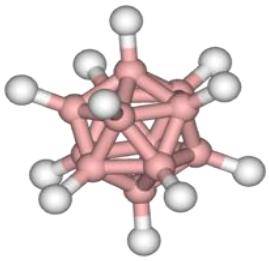


Figura 14. Representación tridimensional del ion closo-dodecaborato $[B_{12}H_{12}]^{2-}$. B= rosa; H= blanco.

2.3.1.2 Carboranos

La sustitución de uno o más vértices de boro por algún heteroátomo genera la familia de los heteroboranos. Los sistemas más estudiados por la comunidad científica a lo largo de la historia son los carboranos (o carbaboranos) en donde el átomo incorporado es un átomo de carbono[47]. La fórmula empírica de estos compuestos es:

$$[C_pB_qH_{p+q+r}]^{x-} = [(CH)_p(BH)_qH_r]^{x-}$$

En esta fórmula:

- ***p*** es el número de átomos de carbono en los vértices del clúster
- ***q*** es el número de átomos de boro
- ***r*** el número de átomos de hidrógeno pontal
- ***x*** es la carga de la molécula

Las reglas que gobiernan la estructura, el enlace y el conteo de electrones en los boranos y heteroboranos fueron estudiadas por Wade, Mingos, Williams y Rudolph, y son conocidas como "Las reglas de Wade"[48-51]. Los términos *closo*, *nido* y *arachno* (Figura 15) se usan para clasificar los clústeres poliédricos y tienen un papel doble. Por un lado, describen el tipo de clúster, si es cerrado se denomina *closo*, si es abierto debido a la eliminación de uno de los vértices -BH con sus dos electrones esqueletales se denomina *nido* y si se repite la operación eliminando otro vértice -BH se genera una estructura aún más abierta denominada *arachno*. Por otro lado, indican cuantos electrones se deslocalizan en el clúster, si el clúster tiene *n* + 1 pares de electrones es *closo*, *n* + 2 *nido* y si tiene *n* + 3 pares de electrones es *arachno*, donde *n* es el número de vértices del clúster. Dichos electrones se encuentran deslocalizados por todo el clúster y es por ello que en numerosas ocasiones se les considera compuestos con aromaticidad tridimensional[52,53]. A destacar que en la Figura 15, las líneas diagonales unen las estructuras que mantienen constante el número de electrones del clúster disminuyendo el número de vértices lo que conlleva a abrir el clúster, mientras que las líneas horizontales

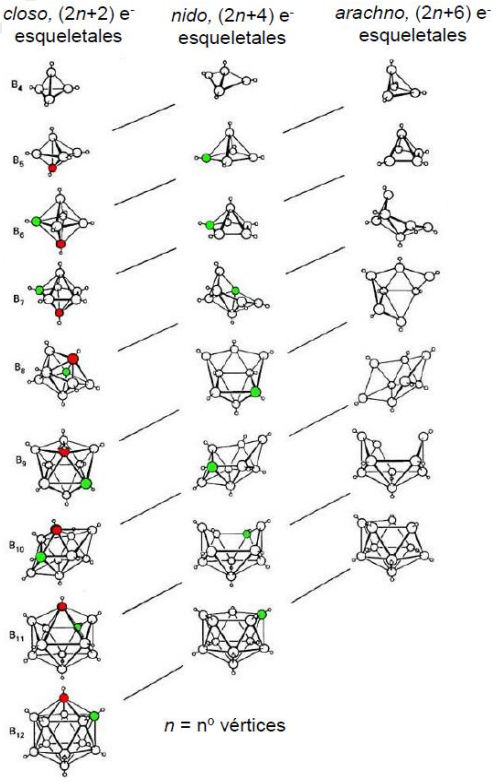


Figura 15. Relación estructural en boranos y heteroboranos.

CONFIDENCIAL

mantienen constante el número de vértices aumentando el número de electrones del clúster lo que conduce a su reducción.

La presencia de vértices conteniendo átomos de carbono en los carboranos ($C_{clúster}$-H) determina ciertas características y propiedades que hacen de ellos un campo en sí mismo dentro de la química del boro. De los 4 electrones que posee un vértice $C_{clúster}$, 3 electrones forman parte del esqueleto del clúster, mientras que el electrón restante se dispone *exo*-clúster para formar el enlace con el átomo de hidrógeno. Debido a que $C_{clúster}$-H es isoelectrónico con el grupo $[B\text{-}H]^-$, si se remplaza un vértice $[B\text{-}H]^-$ por un $C_{clúster}$-H en el sistema $[B_{12}H_{12}]^{2-}$, se obtiene el derivado monoaniónico carba-*closo*-dodecaborato $[CB_{11}H_{12}]^{1-}$. Análogamente, si se reemplazan dos vértices $[B\text{-}H]^-$ por dos grupos $C_{clúster}$-H se formará el derivado neutro $C_2B_{10}H_{12}$ comúnmente llamado carborano o dicarba-*closo*-dodecaborano. Este compuesto fue descubierto en 1950 aunque su síntesis no fue publicada hasta 1963[54]. Para la síntesis de carborano se hace reaccionar en una primera instancia el *nido*-decaborano ($B_{10}H_{14}$) con dos equivalentes de una base de Lewis (L= CH_3CN, Et_2S, Et_3N, Figura 16). El aducto formado, *arachno*-$B_{10}H_{12}L_2$, se trata posteriormente con derivados acetilénicos para dar lugar al clúster icosaedro *closo-dicarbaborano,* 1,2-$C_2B_{10}H_{12}$*,* con los dos átomos de carbonos contiguos.

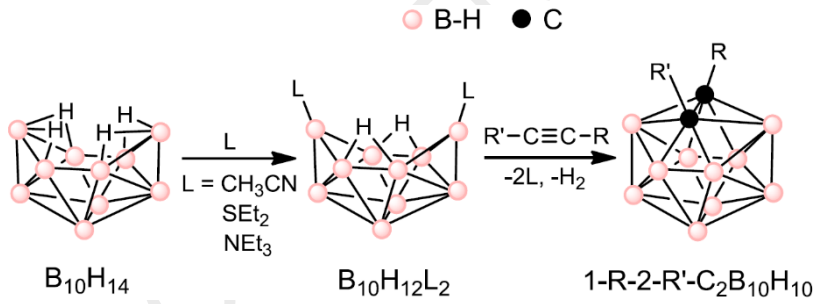


Figura 16. Síntesis del icosaedro orto-closo-carborano 1-R-2-R´-$C_2B_{10}H_{12}$ a través de un proceso de inserción alquínica.

En 1963 D. Grafstein y J. Dvkrak llevaron a cabo la preparación de los isómeros de posición *meta*- y *para*-carborano, 1,7-$C_2B_{10}H_{12}$ y 1,12-$C_2B_{10}H_{12}$ respectivamente, a través de un proceso de isomerización térmica bajo condiciones de vacío[55]. En estas condiciones se produce un reordenamiento intramolecular que da como resultado la formación irreversible del derivado 1,7-$C_2B_{10}H_{12}$ o *meta*-carborano en el cual los dos átomos de carbono están separados por un átomo de B (Figura 17). Al año siguiente se describió que al incrementar la temperatura se genera el isómero 1,12-$C_2B_{10}H_{12}$ o *para*-carborano[56]. Esta transformación no es completa ya que a las temperaturas de trabajo las especies *meta*- y *para*-carborano están en equilibrio, además de constatarse cierto grado de descomposición, por lo que para la purificación se suele utilizar cromatografía en columna sobre soporte de alúmina.

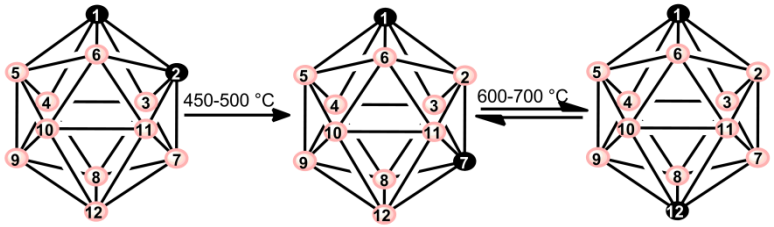


Figura 17. Isomerización térmica partiendo del isómero orto-caborano pasando por meta-carborano hasta llegar al para-carborano. Se muestra la numeración de cada uno de los vértices en las diferentes situaciones.

Un aspecto interesante de los carboranos es que los átomos que lo conforman tienen electronegatividades diferentes (2.5 para C, 2.0 para B y 2.2 para H, en la escala de Pauling) lo que determina que tanto la distribución electrónica como las propiedades fisicoquímicas y de reactividad sean diferentes dependiendo del vértice y del isómero en cuestión. En ese sentido los hidrógenos unidos a carbono, $C_{clúster}$-H, son relativamente ácidos (p*K*a (*orto*) = 22.0, p*K*a (*meta*) = 25.6, p*K*a (*para*) = 26.8) y pueden ser fácilmente extraídos generando nucleófilos[57]. Por el contrario, los hidrógenos unidos a boro, B-H, tienen carácter de hidruro y por tanto, reaccionan con electrófilos (Figura 18)[58]. Es por esto que es posible preparar de manera regioselectiva una gran variedad de derivados de los carboranos sustituidos en los carbonos o boros, sin la necesidad de recurrir a estrategias complicadas con grupos protectores.

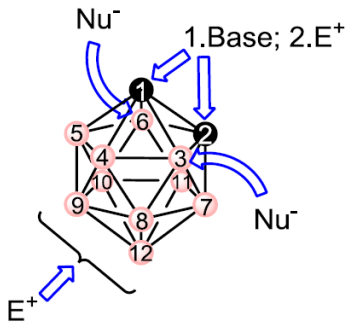


Figura 18. Numeración y reactividad de los diferentes vértices del 1,2-o-$C_2B_{10}H_{12}$ frente a bases fuertes, nucleófilos (Nu^-) y electrófilos (E^+).

Así, la funcionalización de los átomos de carbono del clúster se realiza, generalmente, a baja temperatura y usando una base fuerte, *n*-BuLi en la mayoría de los casos. El carbaboranil anión resultante es lo suficientemente nucleófilo como para reaccionar con un amplio rango de electrófilos, RX (Figura 19), por ejemplo halógenos (I_2, Br_2, Cl_2), haluros de alquilo, aldehídos, CO_2, entre otros.

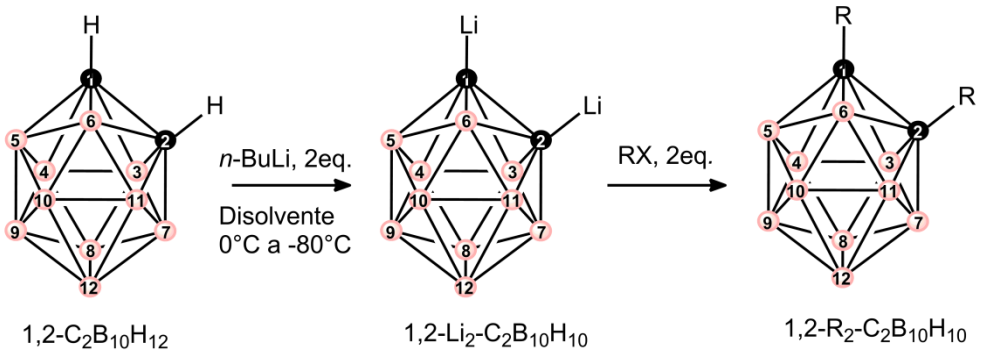


Figura 19. Reacción general se sustitución nucleofílica por parte de carbonos carbaniónicos del clúster.

En referencia a la reactividad de los vértices -BH, estará gobernada por la posición del mismo respecto a los vértices de carbono así como del isómero en cuestión. Por ejemplo los *B(3)* y *B(6),* ambos unidos a los 2 átomos de carbono en el isómero *orto*-carborano, poseen un efecto inductivo "electrón atrayente" por su baja densidad electrónica, mientras que los B que están unidos a un solo carbono prácticamente no presentan dicho efecto. Los boros en las posiciones antípodas, B(9) y B(12) en el *orto*-carborano ó B(9) y B(10) en el *meta*-carborano tienen un efecto "electro-donante". Como consecuencia de estos efectos electrónicos, cada región del clúster es susceptible de sufrir diferentes tipos de reacciones especialmente en los isómeros *orto*- y *meta*- por tratarse de sistemas asimétricos[59,60].

Otra reacción de gran relevancia en la química del *o*-carborano es la reacción de degradación parcial del clúster (comúnmente llamada decapitación del clúster) mediante el uso de bases de Lewis fuertes como alcóxidos[61-63], aminas[64-66], fosfanos[67] o fluoruros[68-72], produciendo un anión *nido*-[7,8-$C_2B_9H_{12}$]$^-$, (Figura 20). Consiste en eliminar un vértice B-H permaneciendo el hidrógeno de este grupo sobre la cara abierta en una situación de hidrógeno puente (formalmente se elimina un B^+). El hidrógeno puente (pontal) en este anión puede abstraerse mediante una base para dar lugar al dianión dicarbaluro *nido*-[7,8-$C_2B_9H_{11}$]$^{2-}$, (Figura 20)[73]. Este dianión es isoelectrónico con el anión ciclopentadienuro y por tanto, se ha utilizado ampliamente como ligando en química organometálica, un ejemplo de ello son los metallacarboranos análogos al ferroceno descrito por Hawthorne y colaboradores (ver siguiente sección).

CONFIDENCIAL

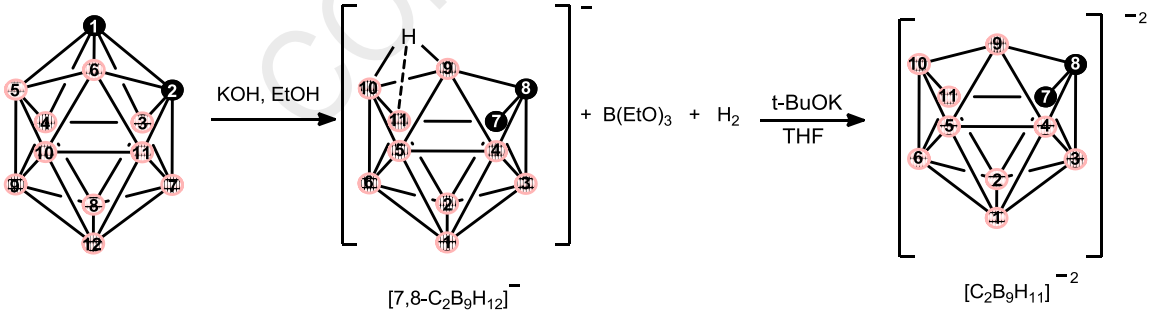


Figura 20. Degradación parcial del sistema o-carborano y formación del dianión dicarbaluro. El mayor carácter electronegativo de los $C_{clúster}$, respeto a los átomos de B, provoca una polarización de los enlaces $C_{clúster}$–B, dejando una mayor densidad de carga positiva sobre los dos núcleos de B unidos simultáneamente a los dos $C_{clúster}$ (posiciones 3 y 6). La numeración de los vértices del nido cambia respecto al closo (I.U.P.A.C).

2.3.1.3 Metalacarboranos

En 1965 el grupo de investigación del Prof. M. F. Hawthorne describió por primera vez lo que hoy se conoce como metalacarborano, un tipo de complejo "*sandwich*" aniónico, en donde dos ligandos dicarbaluro complejan un metal de transición o lantánido. El primero en describirse fue con el catión hierro (Fe^{3+}) conocido como ferrabisdicarbaluro o *FESANE* $[3,3´\text{-}Fe(1,2\text{-}C_2B_9H_{11})_2]^-$, y poco tiempo después se publicó el análogo pero con cobalto (Co^{3+}) conocido como cobaltabisdicarbaluro o *COSANE* $[3,3´\text{-}Co(1,2\text{-}C_2B_9H_{11})_2]^-$ [74,75]. El método más utilizado para la preparación de dicha entidades es haciendo reaccionar la especie *o*-carborano con dos equivalentes de una base fuerte, bajo atmósfera inerte (N_2 o Ar) y en condiciones anhidras, para obtener el dicarbaluro correspondiente. Seguidamente se coloca las sales adecuadas ($CoCl_2$ o $FeCl_2$, en el caso de *COSANE* y *FESANE*, respectivamente) para obtener el complejo sándwich dicarbaluro en cuestión (Figura 21).

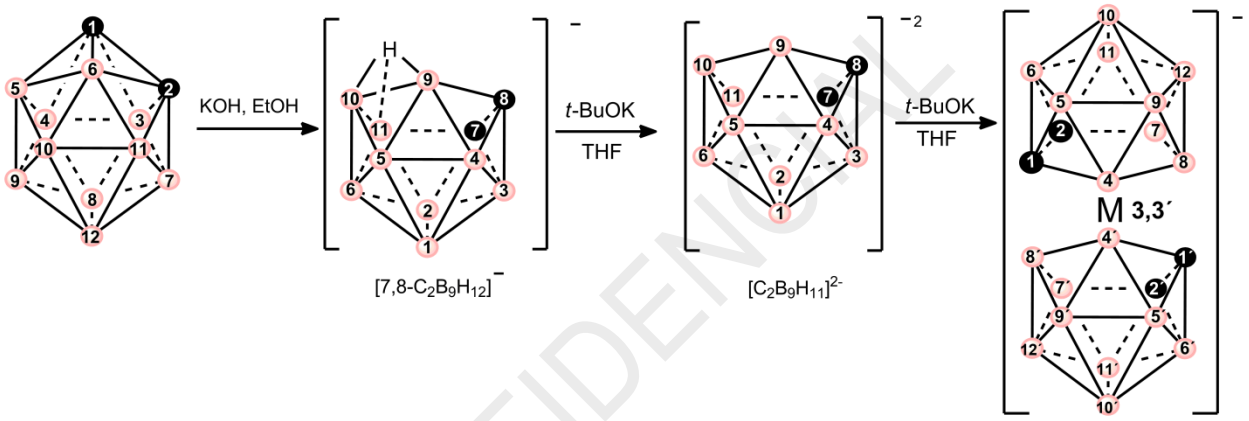


Figura 21. Síntesis de COSANE (M= Co(III)) y FESANE (M= Fe(III)) y numeración de los vértices del clúster.

En la presente tesis doctoral se hará referencia específicamente al metalacarborano *COSANE* que fue el complejo con el que se trabajó. Dicho anión contiene un átomo de cobalto central en estado de oxidación +3 coordinado mediante enlaces π (y cierta componente σ) a dos ligandos dicarbaluro. Cada ligando dicarbaluro posee dos cargas negativas por tanto el complejo tiene una carga neta negativa que se encuentra deslocalizada por todo el volumen del complejo, por esto se dice que es un anión electroactivo de baja densidad de carga. Desde hace ya varios años, el estudio del comportamiento y propiedades electroquímicas de los metalacarboranos se ha expandido por varias disciplinas como ser la química de polímeros[76], de nuevos materiales[77], así como también en áreas relacionada a la química médica[78,79].

Al igual que se describió para las entidades closo-*orto* y closo-*meta*-carborano, en los metalacarboranos la reactividad entre los vértices $C_{clúster}$-H y B-H también será diferente, y en este último también dependerá de la densidad electrónica de los B-H determinada por el posicionamiento que ocupen en el clúster[80]. Este anión presenta dos puntos diferentes de

CONFIDENCIAL

reactividad, los vértices $C_{clúster}$-H y los B-H[81]. Las sustituciones directas en los átomos de boro han sido mucho más estudiadas que las sustituciones en átomos de carbono y existe relativa facilidad para funcionalizar los clústeres en los átomos B(8) y B(8´). Una de las reacciones más estudiadas es la Sustitución Nucleofílica Inducida Electrofílicamente (EINS *del inglés electrophile-induced nucleophilic substitution*). En ésta se aprovecha el carácter de "hidruro" que presentan los hidrógenos B-H, en especial en aquellos vértices en donde la densidad electrónica es mayor; siendo el orden B(8,8´) > B(9,9´;12,12´) > B(10,10´). Como consecuencia de esto, en presencia de ácidos fuertes (o electrófilos) dichos vértices reaccionan produciéndose eliminación y dejando vacante el B(8) o B(8´) que reaccionará *in situ* con nucleófilos (Figura 22).

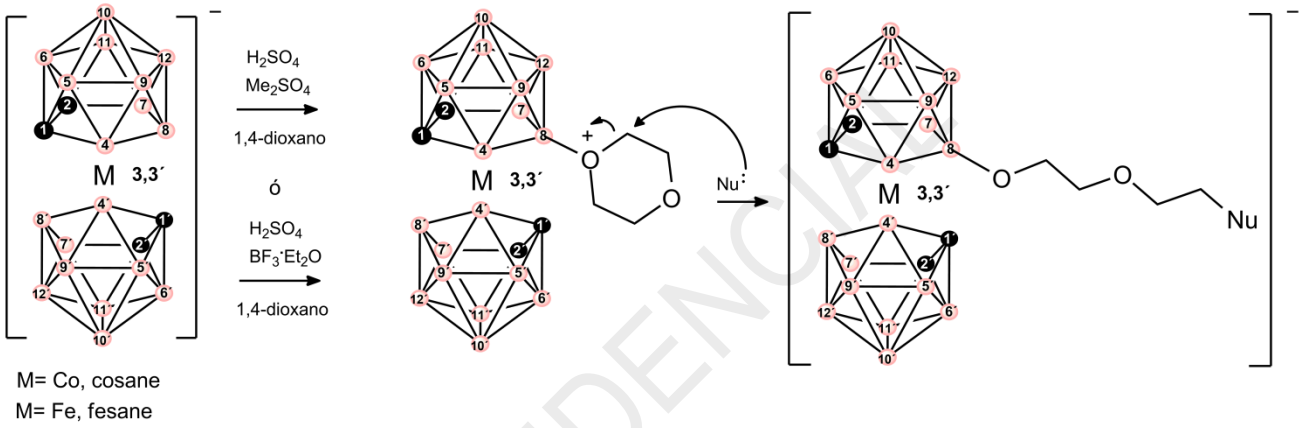


Figura 22. Preparación de las entidades zwitterónicas COSANE-dioxonio o FESANE-dioxonio y posterior funcionalización con nucleófilos mediante reacción de apertura de anillo.

CONFIDENCIAL

2.4 Aplicaciones de clústeres de boro en el campo de la biomedicina

Ya desde su origen, el descubrimiento de fármacos y la química medicinal en general estuvieron fuertemente gobernada por la química orgánica. Así, la mayoría de los fármacos comercializados son moléculas puramente orgánicas de origen natural (o de semi-síntesis) o resultado de procesos de síntesis total. Los átomos a la derecha del carbono en la tabla periódica como nitrógeno, oxígeno y halógenos, ya se han incorporado a una variedad de productos farmacéuticos. Por el contrario, el átomo vecino de la izquierda, el boro, es casi un elemento desconocido en los fármacos comerciales.

El descubrimiento de los boranos poliédricos y las posteriores síntesis de carboranos y metalacarboranos crearon la base para un nuevo y emocionante campo de la química medicinal que aprovecha las propiedades de los compuestos de boro que no contienen uno sino varios átomos de boro en su estructura.

2.4.1 Características estructurales de *closo*-carboranos y metalacarboranos. Implicancia en las propiedades "tipo medicamento".

Entre las propiedades más destacadas y ampliamente exploradas de los carboranos y metalacarboranos en el campo de la química medicinal se pueden destacar:

- la geometría y la naturaleza deficiente en electrones de los átomos de boro, que generan un fuerte carácter hidruro en la superficie -BH. Ambas características influyen en las interacciones intermoleculares con dianas biológicas porque hacen que los grupos -B sean extremadamente hidrófobos;
- tanto la farmacocinética como la biodisponibilidad pueden modularse de acuerdo con el clúster de boro seleccionado, por lo que la hidrofilicidad y la lipofilicidad, o ambas, podrían ajustarse dependiendo la diana (Figura 23);
- la arquitectura globular y la geometría rígida permiten la construcción molecular en tres dimensiones mejorando el acoplamiento, o no, con los blancos moleculares;
- el alto contenido de boro por molécula y la estabilidad al catabolismo son criterios importantes para el desarrollo de agentes para la terapia por captura neutrónica de boro (BNCT, *del inglés boron neutrón capture therapy*) (ver próxima sección);
- la química bien establecida que hace que los clústeres de boro sean sintones atractivos para construir nuevos quimiotipos con aplicabilidad en el campo de la biomedicina.

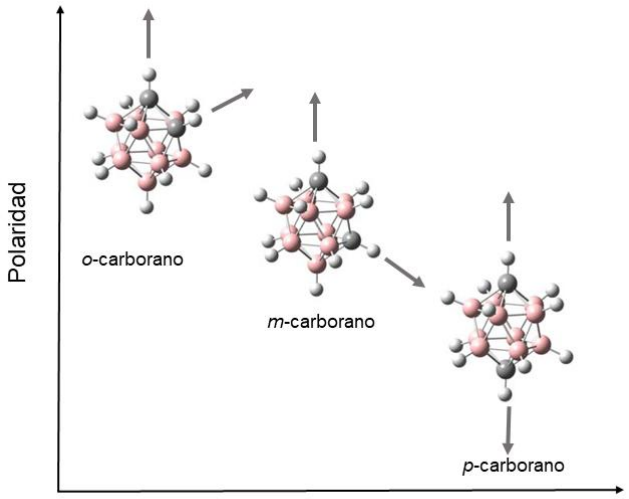


Figura 23. Efecto del momento dipolar sobre la hidrofobicidad de los carboranos.

Una característica destacable de los carboranos es que tienen aproximadamente el mismo volumen molecular que el sistema adamantano, alrededor de un 40 % más grande que el volumen de rotación de un anillo fenilo[82], pero con la salvedad de presentar mayor hidrofobicidad y mayor área de superficie lo que podría potencialmente incrementar las interacciones de baja energía con regiones apolares de proteínas (Figura 24).

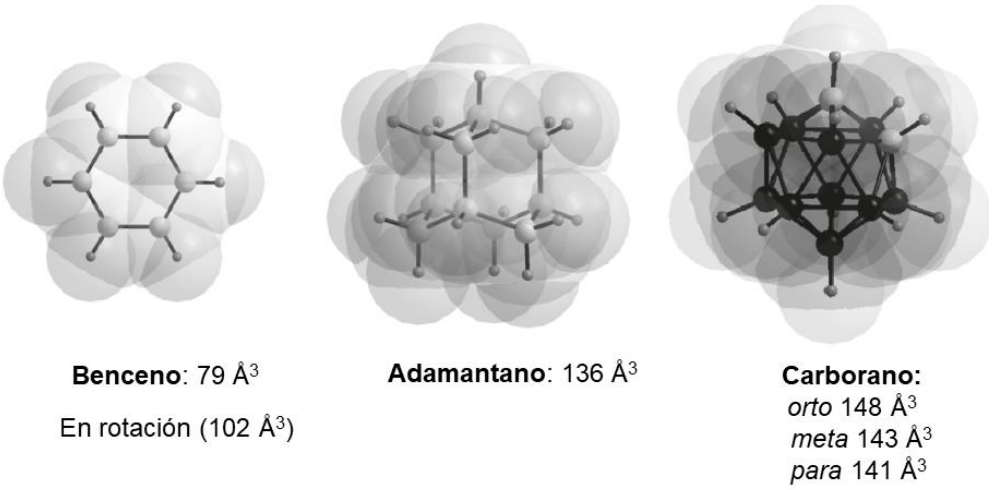


Figura 24. Visualización gráfica de los volúmenes de van der Waals de benceno, adamantano y orto-carborano basados en el programa DIAMOND (C y H = gris, B = negro). Los cálculos se basan en el programa PLATON con el uso de datos de estructura cristalina depositados. Imagen extraída de [57]. Copyright (2011) American Chemical Society.

CONFIDENCIAL

Por otro lado, como resultado de la electronegatividad de los átomos de hidrógenos en la superficie de los clústeres de boro, los vértices B-H tienden a formar enlaces de hidrógeno (B-H···X) y de di-hidrógeno (B-H···H-X). Estos enlaces también conocido como interacciones protón-hidruro, generalmente se establecen entre un átomo de hidrógeno con densidad electropositiva (H-X, siendo X un elemento con electronegatividad mayor a 2.2) y un hidrógeno con carácter de hidruro como entidad receptora del enlace de hidrógeno. El carácter de hidruro de los vértices B-H depende de la posición del vértice B-H y del isómero en cuestión. Se han observado experimentalmente enlaces de di-hidrógeno en estructuras cristalinas de pequeñas moléculas[83,84] y también, a través de cálculos teóricos, en el sitio activo de enzimas lo que ha permitido explicar la bio-respuesta generada por tales motivos estructurales.

2.4.2 Terapia por captura de neutrones de boro (BNCT)

Dentro de las aplicaciones biomédicas de los clústeres de boro, sin lugar a dudas la aplicación más destacada es en la terapia por captura neutrónica de boro (BNCT).

La BNCT se define como una modalidad de tratamiento binaria que contempla, por un lado, entidades químicas portadoras de boro y por otro, una fuente de irradiación externa utilizando neutrones de una determinada energía dependiendo de la localización tumoral. Estas dos componentes, por separado, son relativamente inocuas para las células normales y pueden ser manipuladas de forma independiente, pero, cuando son combinadas, generan un efecto letal en el tejido tumoral con escaso daño al tejido normal[85]. Este concepto de terapia por captura

neutrónica de boro fue propuesto por G. Locher en 1936[86] después de los descubrimientos de los neutrones por J. Chadwick de la Universidad de Cambridge, en 1932, y el trabajo de M. Goldhaber relacionado con la inusual capacidad del nucleido ^{10}B, un isótopo estable de boro, en capturar neutrones térmicos de baja energía (en la clasificación generalmente aceptada en BNCT se consideran neutrones térmicos los que tienen menos de 0.5 eV de energía)[87,88]. La peculiaridad de la reacción nuclear que sufre el ^{10}B durante la captura de neutrones [$^{10}B(n,\alpha)^{7}Li$] (Figura 25) es que se produce el nucleido boro 11 excitado ($^{11}B^*$) que decae rápidamente, en el orden de los picos segundos, generando por un lado una partícula α ($^{4}He^{2+}$) y por otro y en dirección opuesta un núcleo de litio ($^{7}Li^{3+}$), ambos con alta transferencia lineal de energía (LET, *del inglés linear energy transfer*). El 94 % de los casos el Li queda en un estado excitado, por lo que regresa a su estado fundamental tras la emisión de un rayo gamma, mientras que en el 6 % restante el Li es emitido en su estado fundamental (Ecuación 2). La LET será depositada en un rango de 5 a 9 micrones, que se corresponde con el diámetro celular. Por lo que la energía nuclear liberada, tras la captura neutrónica por parte del boro, ocurre dentro de la célula donde se encuentra confinado el B[89].

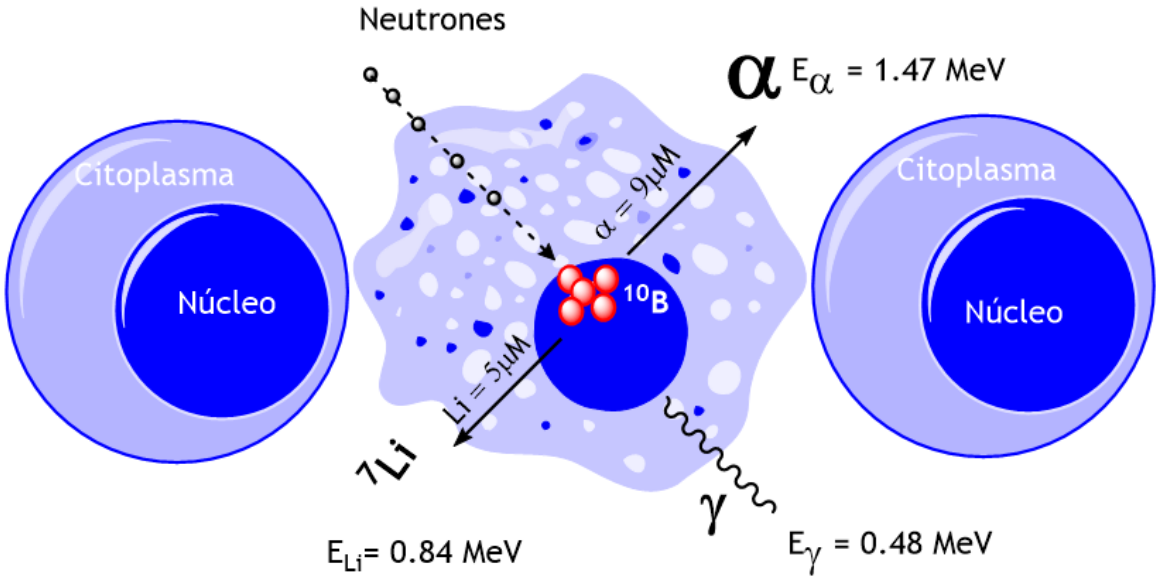
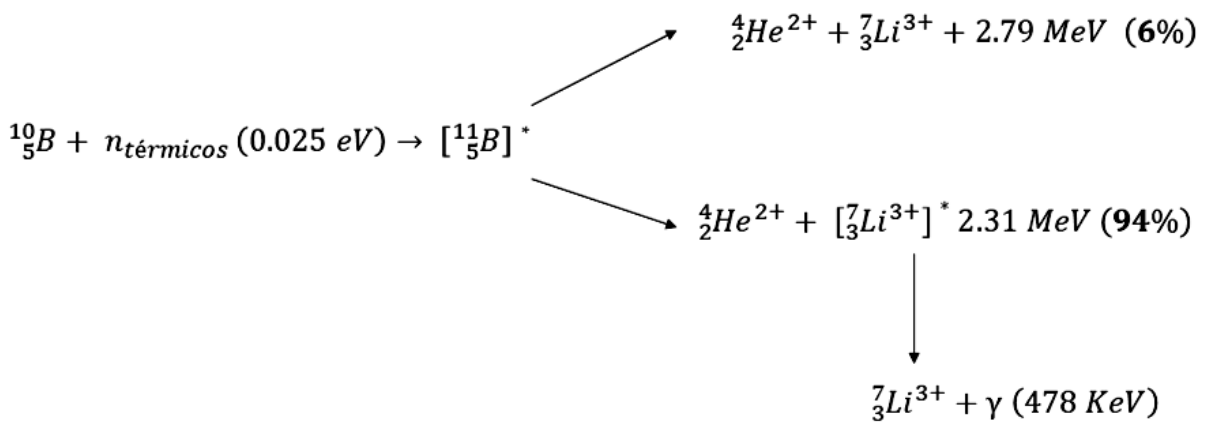


Figura 25. Secuencia de eventos para la reacción nuclear del ^{10}B y neutrones térmicos.



Ecuación 2. Las dos reacciones paralelas de fisión nuclear que ocurren al capturar un neutrón lento (térmico) por un núcleo ^{10}B.

Las partículas alfa emitidas tras el decaimiento del $^{11}B^{*}$, tienen la potencialidad de generar ruptura en la doble hebra de ADN resultando en aberraciones cromosómicas y deterioro de la integridad reproductiva de la célula.

La idea de usar radiaciones con alta LET en el tratamiento del cáncer se viene empleando desde hace mucho tiempo y está basada en un concepto simple: a igual dosis física, las radiaciones con alto LET producirán un mayor daño en las células blanco (este es el concepto de Eficacia Biológica Relativa o RBE, *del inglés relative biological effectiveness*). Si bien existen diferentes nucleídos que presentan una gran propensión a capturar neutrones de bajas energías o neutrones térmicos, como ser: ^{3}He, ^{6}Li, ^{113}Cd, ^{157}Gd y ^{235}U, entre otros, el ^{10}B es uno de los más atractivos debido, entre otras, a las siguientes razones:

- Mínima toxicidad, no radiactivo y está fácilmente disponible, constituyendo aproximadamente el 20 % del boro en la naturaleza
- Las partículas emitidas por la reacción de captura [$^{10}B(n,\alpha)^{7}Li$] son mayoritariamente de alto LET
- El alcance de las partículas de alto LET es de aproximadamente el diámetro de una célula
- Puede ser incorporado en una gran cantidad de estructuras químicas diferentes, debido a las uniones estables que se producen entre los átomos de boro y otros elementos como el carbono, oxígeno y nitrógeno

Una de las propiedades más importantes que posee el nucleido ^{10}B es su elevada sección eficaz (σ_{th}, área efectiva para la colisión) para la captura de neutrones térmicos, σ_{th} = 3838 barns, que es casi 4000 veces mayor que la del nitrógeno, 10000 veces mayor que el hidrógeno y un millón de veces superior a la del carbono y el oxígeno. Esto hace posible que

CONFIDENCIAL

las reacciones nucleares de neutrones térmicos con estos tres átomos, que son siempre abundantes en toda la materia orgánica, prácticamente carezcan de importancia frente a la captura de estas partículas por parte del ^{10}B[90,91]. De esta manera resultaría posible producir una destrucción selectiva de tejido tumoral siempre que fuera posible enriquecer esos tejidos en ^{10}B.

En base a este concepto en los comienzos de 1950 científicos del Brookhaven National Laboratory en colaboración con investigadores del Massachusetts General Hospital y el Massachusetts Institute of Technology (MIT) comenzaron estudios de tratamiento con 10 pacientes con glioblastoma utilizando como entidad portadora de boro al bórax (tetraborato disódico decahidratado, $Na_2B_4O_7 \cdot 10H_2O$, Figura 26) pero los resultados no fueron los esperados. Si bien no hubo efectos secundarios graves propios de la BNCT en los pacientes, las grandes dosis de bórax (enriquecido con ^{10}B), infundiendo 200 mg/kg, repercutieron en leves síntomas de toxicidad[92,93].

Para mejorar esto, se desarrolló un segundo enfoque que incluyó nueve pacientes con glioma pero ahora tratados con un compuesto menos tóxico, el pentaborato de sodio (NaB_5O_8; Figura 26) en combinación con *D*-glucosa. A diferencia de la primera, se utilizó una dosis más alta de ^{10}B, y se aplicó una mayor fluidez de neutrones térmicos incidentes[94]. Desafortunadamente, nuevamente se observaron efectos secundarios graves, como la radiodermatosis del cuero cabelludo y ulceraciones profundas[95]. Simultáneamente, en 1963, Sweet y colaboradores, del MIT, trataron a 18 pacientes con decahidrodecaborato disodico, enriquecido en ^{10}B ($Na_2B_{10}H_{10}$; Figura 26)[96]. Dicha entidad fue considerada en una primera instancia menos tóxica y además con la ventaja de depositar más átomos de boro por célula. Lamentablemente tras el tratamiento por BNCT se observó en pacientes necrosis cerebrales[97]. Debido a estos eventos decepcionantes en 1961 EEUU detuvo el progreso de la investigación sobre la BNCT.

Por otra parte, en 1968 en el Hitachi training reactor, el neurocirujano japonés Hiroshi Hatanaka, quien en años anteriores había trabajado con Sweet en Boston, comenzó a tratar pacientes con gliomas malignos de alto grado con mercaptoundecahidro-*closo*-dodecaborato disódico ($Na_2B_{12}H_{11}SH$, denominado BSH; Figura 26) que había sido sintetizado por Soloway originalmente en 1967. Los resultados descritos por Hatanaka y sus colaboradores fueron extraordinarios, con una tasa de supervivencia de 5 años del 58 %[98,99].

Sin embargo, BSH no ha colmado todas las expectativas, como agente para uso en BNCT, especialmente para la acumulación inespecífica del agente.

CONFIDENCIAL

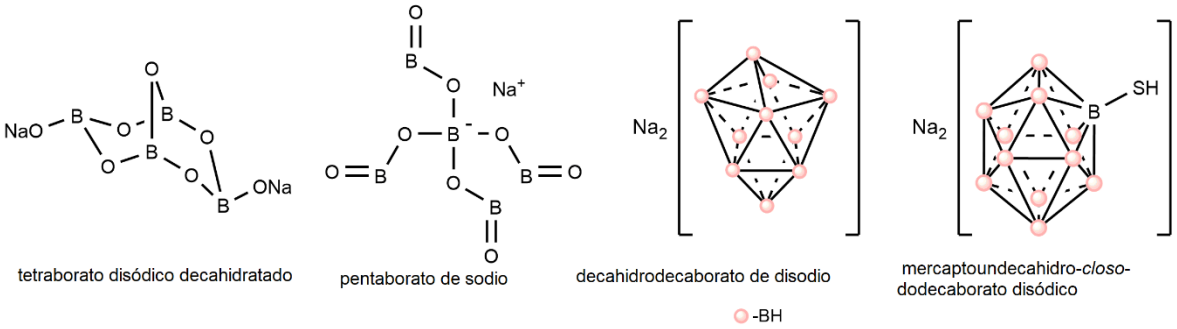


Figura 26. Entidades químicas conteniendo alto contenido de boro para su uso en BNCT.

2.4.3 *closo*-carboranos y metalacarboranos estudiados en GBM a través de BNCT.

En las últimas décadas, los carbohidratos han sido ampliamente estudiados como moldes para el desarrollo de fármacos antitumorales debido a su baja toxicidad, alta solubilidad en agua, aumento de la tasa de glicólisis en las células cancerosas y no menos importante, alta expresión de sus receptores en la superficie de la célula tumoral (específicamente en las células endoteliales que recubren los capilares del cerebro que forman las barreras cerebrales, lo que resulta en una óptima penetración de BHE). De acuerdo con esto y para mejorar la captación de boro, con el fin de utilizarse en BNCT, se han elegido inicialmente un conjunto de carbohidratos como la ribosa, manosa, maltosa y galactosa para generar plataformas de entrega de boro basadas en carbohidratos con la finalidad de tener, una vez internalizado el compuesto, un tratamiento por captura neutrónica de boro exitoso. Desde la primera descripción por parte del grupo de Hawthorne, se han realizado numerosos trabajos sobre la síntesis y evaluación biológica de los conjugados de carbohidratos a sistemas *closo*-carboranos[100]. Tietze y sus colaboradores desarrollaron y evaluaron *in vitro* e *in vivo*, contra las células de glioma de rata (C6) y la línea celular de melanoma (B16), una serie de *closo*-carborano-glicósidos que incluyen glucósido, lactósido y maltósido (Figura 27, estructuras **1**-**3**). Aunque en los ensayos *in vitro* observaron un efecto citotóxico significativo para todos los derivados, además de presentar una captación celular óptima en la línea celular de glioma C6, siendo el maltosido **3** el derivado que presentó la mayor captación (65,7 ppm a las 12 h), el comportamiento *in vivo* en un modelo de rata portando un tumor cerebral, reveló que la concentración de todos los carbohidratos unidos a los sistemas carboranilos se encontraba con niveles en sangre que eran inaceptablemente altos para su uso en BNCT[101,102]. Para superar este inconveniente, Tietze y Yamamoto diseñaron un nuevo tipo de derivados mixtos de bisglicosido de carboranilo pensando en que actúen como pro-fármacos (**4**-**7**; Figura 27)[103]. Inicialmente, no se esperaba una captación selectiva de estos compuestos debido a que los restos de azúcares hidrofílicos a ambos extremos del carborano impedirían la internalización

CONFIDENCIAL

celular. Los autores demostraron que la activación del pro-fármaco podría realizarse utilizando anticuerpos monoclonales conjugados a glicohidrolasas, que se unen a antígenos asociados a tumores, a través de la escisión del enlace glucosídico con liberación concomitante del resto carboranilo en la superficie de la célula tumoral.

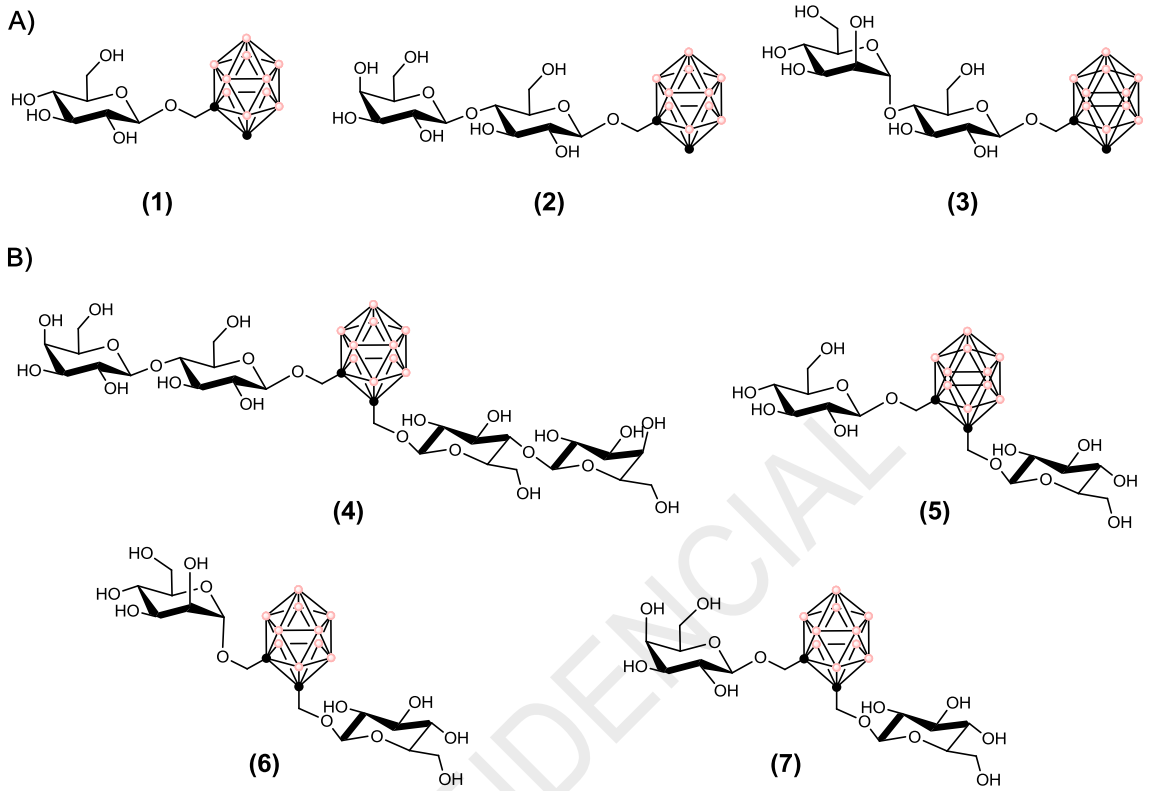


Figura 27. A) El compuesto 1 corresponde al derivado de carboranilo de D-glucosa, y los compuestos 2 y 3 son derivados de lactosa y maltosa, respectivamente. (B) orto-carboranil-bisglicosidos 4–7 que contienen lactosa, glucosa, manosa y galactosa en sus estructuras.

Otro enfoque que se ha venido estudiando en los últimos años como estrategia para mejorar la captación de compuestos con alto contenido en boro por las células de glioma es a través del uso de nucleosidos y nucleótidos (purinas, pirimidinas, timidinas). Esta estrategia se basa en el hecho de que las células tumorales tienen una mayor actividad metabólica y un mayor requerimiento de precursores de ADN y ARN[104]. Aunque en los últimos años se han abordado varias estrategias, el enfoque principal ha estado en los análogos de timidina sustituidos con el grupo *o*-carborano en las posiciones *N*-3 (**8** y **9**, conocidos como 3CTAs; Figura 28). Ambos análogos son sustratos potenciales para la enzimas timidina quinasa 1 humana (hTK1), una desoxinucleósido quinasa citosólica de la vía de recuperación de la síntesis de ADN que se encuentra predominantemente en células cancerosas en proliferación. La acumulación selectiva y la retención de 3CTAs en células tumorales a través de un mecanismo conocido como atrapamiento mediado por quinasas hacen que estas moléculas sean posibles agentes de administración en glioblastomas para su potencial aplicación a través de BNCT[105-107].

CONFIDENCIAL

Barth y sus colaboradores evaluaron el derivado **9** enriquecido con ^{10}B, utilizando el modelo RG2 como modelo *in vivo* de tumor cerebral[108]. Demostraron que el derivado **9** entrega eficazmente átomos de boro en las células tumorales positivas para TK1, lo que permitió la reducción del tumor en ratones *nude* después de aplicar la BNCT. Además, sobre la base de estos resultados favorables, los estudios de BNCT realizados en el modelo de rata RG2 condujeron a un aumento en la vida útil ILS 2,4 × (ILS, *del inglés increase in life span*) en comparación con el L-BPA, ácido borónico en estudios clínicos, como terapia de control.

Sin embargo, el porcentaje más alto de ILS (122 %) se observó en ratas portadoras de gliomas RG2 que recibieron la combinación del derivado **9** y L-BPA, y esto se correlacionó con el hecho de que el tumor en estos animales recibió las dosis más altas de radiación física. Estos estudios biológicos revelaron claramente el potencial terapéutico del derivado **9**, aunque aparecieron algunos problemas y limitaciones. Entre estos, el derivado **9** mostró problemas claros de solubilidad en condiciones fisiológicas, posiblemente debido a la presencia del núcleo hidrófobo de carborano y la ausencia de un grupo funcional que pueda ionizarse[108].

Otros quimiotipos de boro que también que se han evaluado son los derivados de los metalacarboranos ferrabisdicarbaluro y cobaltabisdicarbaluro (**10**-**12**, Figura 28)[109]. No obstante a la fecha aún no se han descrito investigaciones en líneas de glioma de alto grado.

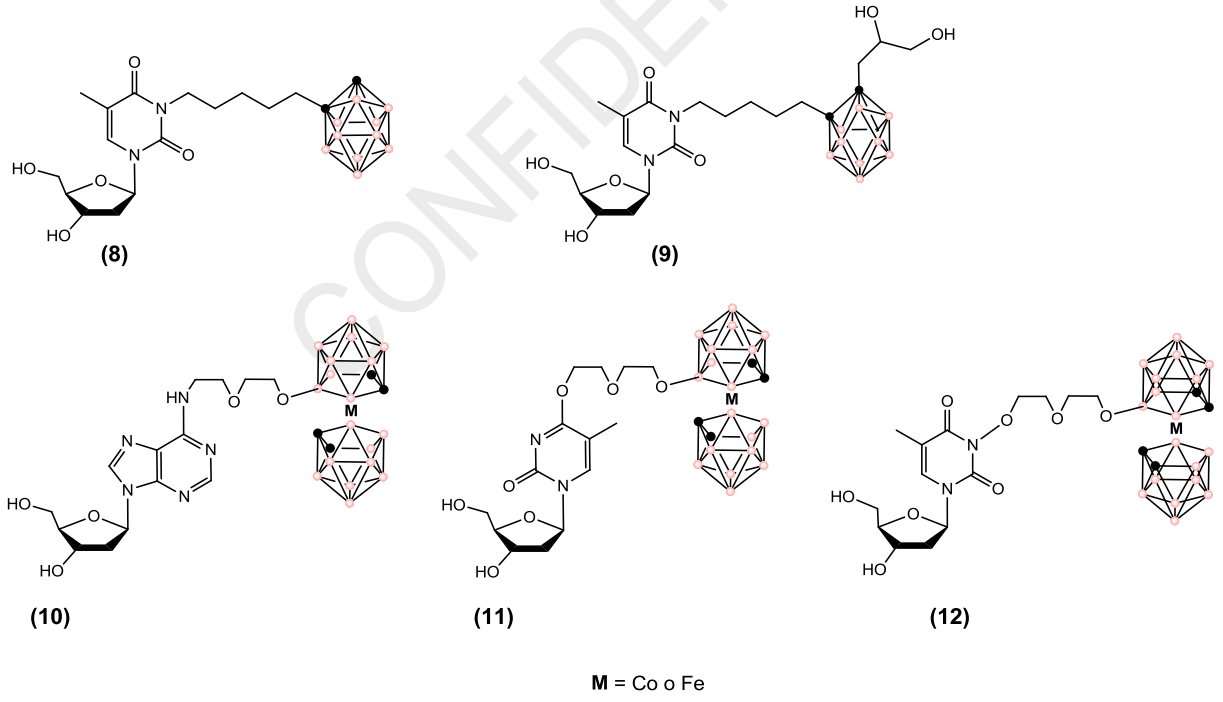
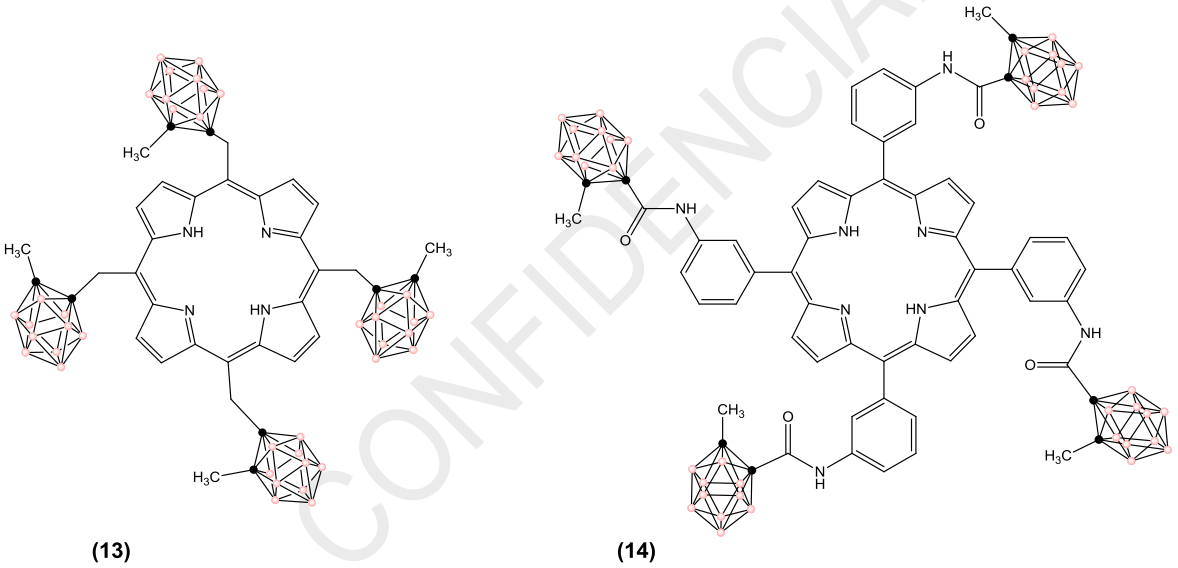


Figura 28. Estructura química de los principales nucleósidos derivatizados con carborano y metalacarborano.

Desde la primera descripción por Haushalter y Rudolph en 1978 la potencial aplicación en biomedicina de varios colorantes fluorescentes incluidos las porfirinas y ciertos macrocíclicos

CONFIDENCIAL

relacionados, conteniendo entidades portadoras de boro en su estructura, ha sido altamente explorado y examinado por varias razones (**13** y **14**; Figura 29)[110,111], entre ellas: (a) capacidad de acumulación selectiva en células tumorales y en alta concentración, (b) capacidad de retención dentro de los tumores, (c) citotoxicidad baja en oscuridad, (d) capacidad para unirse al ADN debido a su estructura aromática plana, y (e) gran capacidad de fluorescencia, permitiendo así el diagnóstico de tumores y facilitando la planificación del tratamiento. Sin embargo, sin duda, la característica más explotada de estas moléculas es la capacidad de actuar en la terapia fotodinámica (PDT, *del inglés photodynamic therapy*). La PDT combina un fotosensibilizador (porfirina), luz y oxígeno tisular para generar especies reactivas de oxígeno, incluido el oxígeno singulete, que desencadenan posteriormente mecanismos de muerte celular por necrosis o apoptosis. La combinación de esta terapia con la BNCT ha sido de particular interés para controlar la recurrencia local de gliomas de alto grado como el GBM, ya que tienen diferentes mecanismos de muerte y, por lo tanto, aumentan el efecto terapéutico.



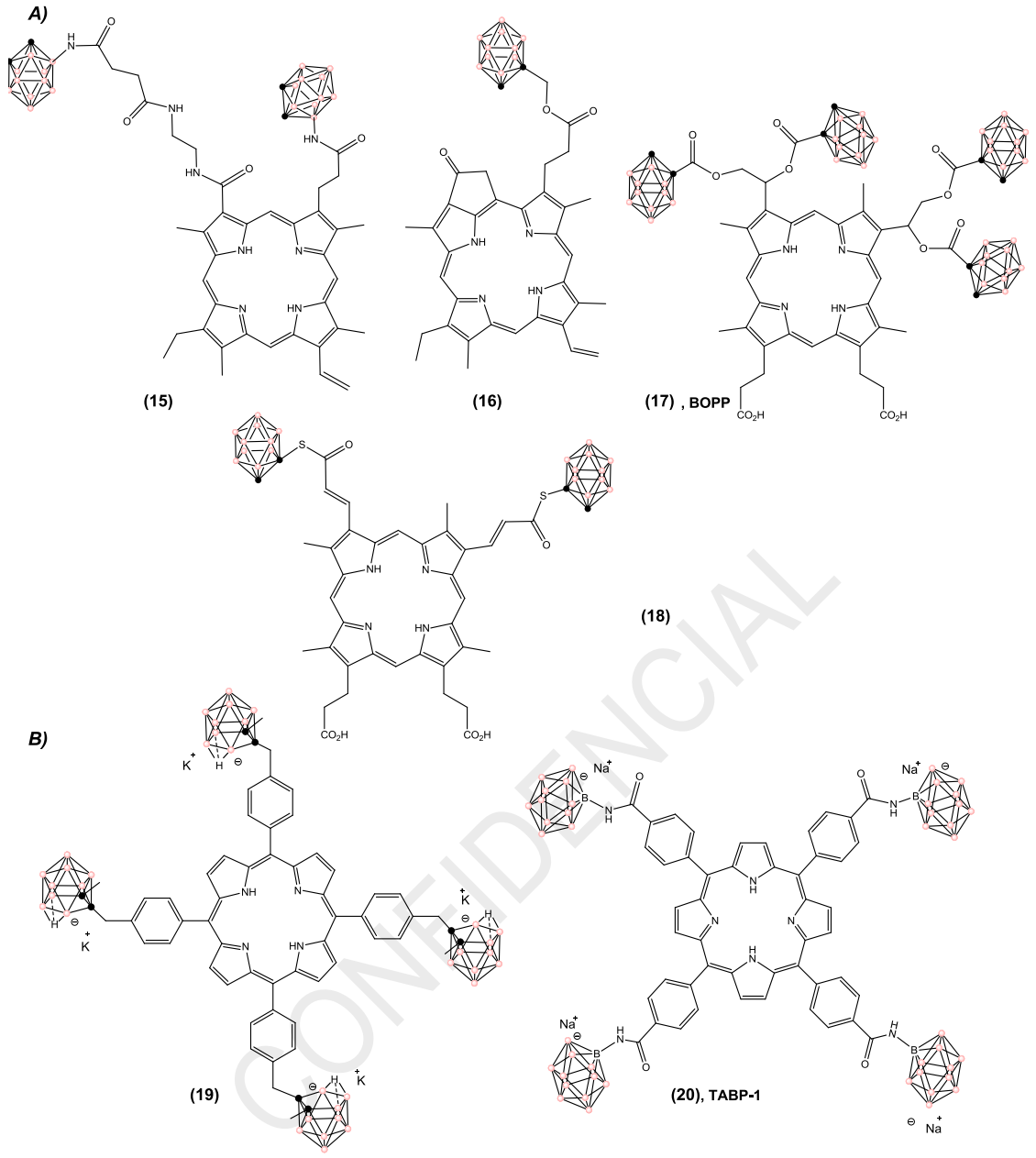
CONFIDENCIAL

Figura 29. Primeras porfirinas que contienen boro desarrolladas por Haushalter y Rudolph[110] para la aplicación en catálisis.

En los últimos años, una gran cantidad de porfirinas naturales que contienen estructuras portadoras de boro han sido sintetizadas y evaluadas tanto en modelos celulares como en modelos animales (**15**-**18**; Figura 30)[112]. Hasta la fecha, el éster **17** conocido como BOPP, fue el único compuesto que se utilizó en un estudio clínico de fase I contra GBM[113,114]. Los estudios farmacológicos mostraron su capacidad para incorporarse selectivamente en células tumorales, en modelos de xenoinjerto de glioma, en relación con las células cerebrales normales circundantes (relación tumor:cerebro cercana a 400) y situada preferentemente en las

mitocondrias de células tumorales. Sin embargo, estos resultados no pudieron ser replicados en humanos. El éxito terapéutico del derivado **17** se interrumpió en un ensayo clínico de fase I por varias razones: (a) en pacientes con GBM **17** no era capaz de entregar la cantidad terapéutica suficiente de boro como para tener éxito en BNCT; (b) se observó trombocitopenia en pacientes debido al efecto tóxico sobre las plaquetas del derivado **17** o sus metabolitos (probablemente del producto de hidrólisis del éster); y (c) el comportamiento farmacocinético del derivado **17** en humanos se caracterizó por una fase de eliminación prolongada, que dio lugar a metabolitos potencialmente tóxicos y fotosensibilidad cutánea[115]. Para superar estos problemas, varios investigadores diseñaron y sintetizaron porfirinas con alto contenido en boro y solubles en medios acuosos. En este sentido, Vicente y sus colaboradores describieron las porfirinas conjugadas a *nido*-carborano (por ejemplo compuesto **19**; Figura 30). Estos derivados anfifílicos mostraron una muy baja toxicidad, fueron bien captados por las líneas celulares 9L y U-373MG tanto en el tiempo como en la concentración, y se localizaron preferentemente en los lisosomas celulares[116]. Por otro lado, Deen y sus colaboradores desarrollaron la porfirina iónica poliborada **20**, conocida como TABP-1, que se dosificó mediante administración mejorada por convección (CED, *del inglés convection-enhanced deliver*) a ratas *nude* con implante intracerebral de la línea celular de glioblastoma humano U-87MG[117]. En contraste con la difusión, la CED utiliza un gradiente de presión establecido en la punta de un catéter de infusión para establecer el flujo en masa y distribuir el fármaco y el disolvente en todo el espacio extracelular. Esto demostró a diferencia de la administración sistémica, una alta concentración de boro en el tumor y en la sangre.

CONFIDENCIAL



CONFIDENCIAL

Figura 30. (A) Estructuras de algunas porfirinas relevantes con alto contenido en boro. (B) Derivados porfirina conjugados a diferentes clústeres de boro que le aportan buena solubilidad en agua.

3 Justificación, hipótesis y diseño metodológico

En esta tesis doctoral se pretende profundizar en las respuestas a preguntas de relevancia en un tema de salud humana como es la farmacología para el tratamiento de enfermedades neoplásicas, en particular, glioblastoma multiforme (GBM). La falta de tratamientos eficientes para gliomas de alto grado, como lo es el GBM, conduce a la necesidad de la I+D en nuevas estrategias farmacológicas eficaces. En esa línea, en el terreno de la terapia oncológica se ha experimentado una rápida evolución hacia la llamada terapia dirigida frente a dianas (*del inglés targeted therapy*). Esta modalidad de tratamiento utiliza fármacos que van específicamente dirigidos frente a dianas moleculares concretas que han demostrado desempeñar un rol crucial en la supervivencia, proliferación o capacidad invasiva de las células tumorales. En el caso de GBM, los receptores celulares con actividad tirosina quinasa (EGFR, VEGFR y PDGFR, entre otros) son claros ejemplos de dianas prometedoras. No obstante, en la actualidad y en particular los fármacos utilizados como inhibidores de la actividad tirosina quinasa del EGFR, VEGFR y PDGFR han generado escasos resultados en ensayos clínicos sin que exista, en muchos casos, una clara explicación para la resistencia a dicha terapia. En la actualidad, la generación de nuevos compuestos con capacidad inhibitoria de receptores con actividad tirosina quinasa está siendo ampliamente explorada por la comunidad científica abocada al estudio de gliomas de alto grado.

Por otro lado, las entidades químicas portadoras del nucleído estable ^{10}B que una vez distribuidas selectivamente en el organismo puedan ser capaces de generar radiaciones ionizantes dañinas, por acción de una fuente externa de neutrones (*BNCT*), vienen siendo profundamente estudiadas en su aplicabilidad en terapia de GBM.

Ciertos procesos fisiopatológicos requieren del uso de fármacos cuya estructura es tal que el agente posee más de un mecanismo de acción, actuando sobre dos bio-receptores, en dos etapas bioquímicas diferentes o iguales, o teniendo dos mecanismos de acción. Este tipo de agentes es conocido como fármacos híbridos. Los fármacos híbridos poseen la ventaja, frente al uso conjunto de más de un medicamento, que durante la etapa de I+D los estudios de biodisponibilidad, estabilidad, incompatibilidades entre fármacos, son completados en forma eficiente por tratarse de una estructura química única. Mientras que, en la multi-terapia durante el tratamiento terapéutico surgen problemas, por ejemplo incompatibilidades medicamentosas, ajustes de posologías según las farmacocinéticas individuales, etc, por tratarse de más de una entidad química que debe ser suministrada.

CONFIDENCIAL

En la presente tesis se utilizará este concepto, fármacos híbridos, para el desarrollo de agentes que posean *per se* actividad frente al blanco oncológico elegido (GBM), en particular dirigidos específicamente hacia receptores oncogénicos con actividad tirosina quinasa y además posean un fragmento estructural portador de ^{10}B capaz de capturar neutrones de baja energía produciendo ^{11}B-metaestable cuyo decaimiento produzca las partículas que aporten el componente de radioterapia.

CONFIDENCIAL

4 Objetivo general

Los objetivos generales de la presente tesis doctoral se encuentran divididos en tres bloques:

1. Diseño, síntesis y caracterización fisicoquímica de nuevas entidades químicas híbridas conteniendo por un lado fragmentos de alto contenido en boro, entre ellos se destacan los sistemas *closo*-orto/meta-carborano, metalacarboranos y dodecaboratos y, por otro, farmacóforos con actividad inhibitoria de dominios tirosina quinasa, utilizando como moldes estructurales los fármacos erlotinib y sunitinib.
2. Caracterización biológica *in vitro*, *in silico* e *in vivo* de las entidades desarrolladas.
3. Estudios teóricos y experimentales de propiedades “tipo-fármaco”, entre ellas estabilidad química y biológica; capacidad de penetración de la BHE, acumulación de boro intracelular, entre otras.

CONFIDENCIAL

5 Capítulo I

Serie derivada de erlotinib

Artículo I.

CHEMISTRY
A European Journal

ChemPubSoc Europe

Communication

Small-Molecule Kinase-Inhibitors-Loaded Boron Cluster as Hybrid Agents for Glioma-Cell-Targeting Therapy

Marcos Couto, Ignacio Mastandrea, Dr. Mauricio Cabrera, Dr. Pablo Cabral, Prof. Dr. Francesc Teixidor, Dr. Hugo Cerecetto ✉, Prof. Dr. Clara Viñas ✉

CONFID

5.1 Objetivos específicos

1- Preparación y caracterización fisicoquímica de precursores *closo*-carborano, *closo*-dodecaborato y derivados del sistema metalacarborano COSANE.
2- Conjugación de los precursores obtenidos en el punto 1 con el inhibidor erlotinib para generar los productos híbridos. Caracterización fisicoquímica.
3- Evaluación biológica *in vitro* de los productos desarrollados en el punto 2 en línea celular de glioma C6 y en células normales; en cultivo primario mixto derivado de neonatos de ratón conteniendo distintos tipos celulares: atrocitos, microglia y macrófagos.
4- Estudios de relación estructura-actividad.

CONFIDENCIAL

5.2 Resultados y Discusión.

5.2.1 Síntesis de híbridos

Como se menciona previamente, los sistemas *closo*-1,2-$R_2C_2B_{10}H_{10}$ (*orto*-carborano, Figura 31) pueden ser preparados a través de reacciones de inserción alquínica, en la que se utiliza al decaborano $B_{10}H_{14}$ como sustrato de partida y un alquino en un disolvente orgánico adecuado. Por lo que, inicialmente se decide incorporar el inhibidor de EGFR erlotinib al clúster $B_{10}H_{14}$, a través del extremo alquino que posee este fármaco en su estructura. Para ello, se ensayaron diferentes metodologías de síntesis según lo descrito en la literatura para este tipo de reacciones (Figura 32)[118,119]. Sin embargo, en ninguna de las condiciones ensayadas, fue posible obtener el producto de interés.

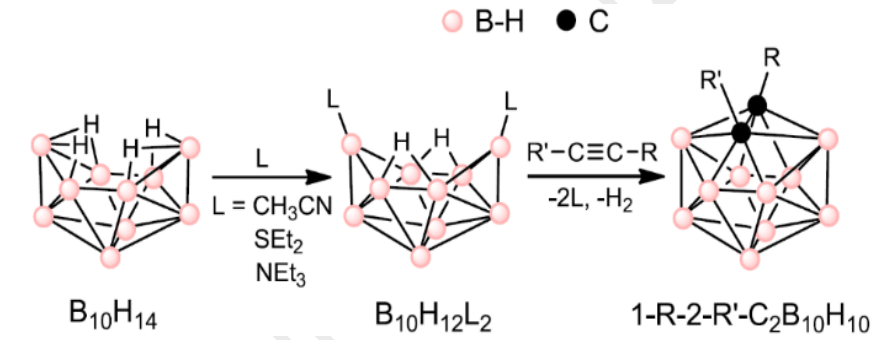


Figura 31. Inserción de alquinos para generar sistemas closo-orto-carboranos sustituidos.

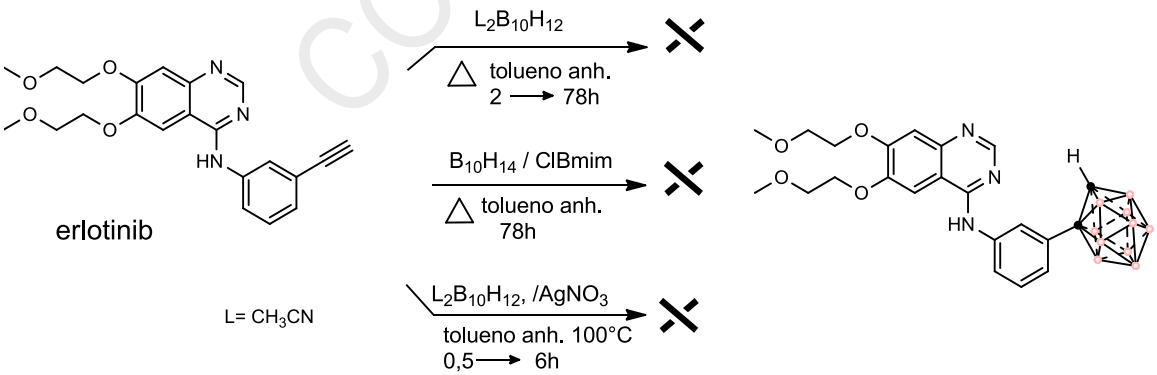


Figura 32. Condiciones de reacción estudiadas para la inserción alquínica entre erlotinib y el sustrato decaborano.

Posiblemente y en base a lo descrito en literatura[120], la no generación del producto de interés esté asociado a la "competencia" de la base de Lewis acetonitrilo "ligando L", con los pares de electrones libres de los nitrógenos del erlotinib generando mezclas complejas de aductos que imposibilitan la promoción de dicha reacción.

En base a esto, se planteó un re-diseño y síntesis de nuevas moléculas híbridas. La primera aproximación consistió en preparar derivados del clúster carborano portando en su estructura el agrupamiento azida que permita modificaciones posteriores. De esta forma, teniendo en cuenta la reactividad *per se* de los alquinos terminales, se generó en una etapa posterior a través de una reacción de cicloadición 1,3-dipolar, "*click reaction*", los correspondientes híbridos **5**, **6**, **11** y **12** con buenos rendimientos 69-78 % (Figura 33). Los intermedios **3**, **4**, **9** y **10** fueron seleccionados como forma de introducir quimiodiverisdad en los productos finales, isómeros metil y desmetil de *orto*- y *meta*-carboranos[121]. El segundo abordaje involucró la transformación del agrupamiento etinilo de erlotinib en un conector tipo benciletinil (Figura 33) vía un proceso de *Sonogashira "cross-coupling"* generando así los compuestos **15**, **16**, **19** y **20** con rendimientos moderados 35-49 %. Nuevamente los intermedios iodofenil **13**, **14**, **17** y **18** se prepararon como forma de introducir quimiodiverisdad en los híbridos resultantes.

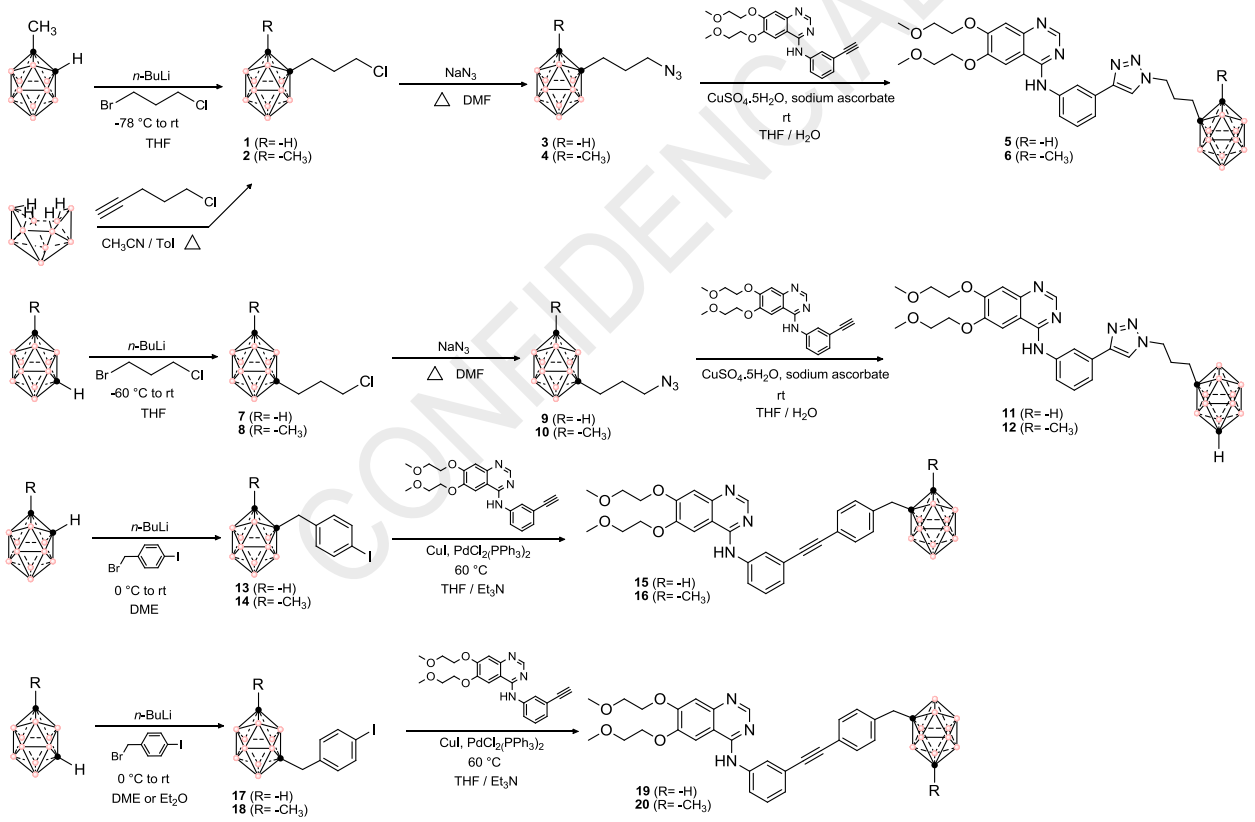


Figura 33. Síntesis de intermedios e híbridos closo-carboranilquinazolina.

Otro *clúster* de boro seleccionado en esta etapa para ser conjugado al erlotinib es el metalacarborano COSANE (cobalto-bis(dicarbaluro)[3,3'-Co(1,2-$C_2B_9H_{11})_2]^-$. Éste fue preparado de acuerdo a lo descrito en la literatura[122] (Figura 34). A modo de resumen, una de las vías para derivatizar el complejo [3,3'-Co(1,2-$C^2B^9H^{11})_2]^-$ en los vértices *B-H* es a través de una

sustitución nucleofílica inducida electrofílicamente (SNIE). En ésta se aprovecha que el vértice *B(8)* sustenta un hidrógeno con carácter de hidruro y por tanto la reacción con especies ácidas resultará en la abstracción del mencionado hidrógeno quedando así una posición electrofílica vacante que será ocupada luego por una especie nucleofílica. De esta forma se sintetizó el zwitterión formado por dicho complejo y la molécula de dioxano (**21**). Luego se realizó la apertura del anillo a través de una sustitución nucleofílica utilizando como entidad el nucleófilo azida (N_3^-), obteniéndose el compuesto (**22**). El híbrido **23** se genera con muy buen rendimiento, 79 %, tras la reacción de cicloadición.

Por otro lado y continuando con el desarrollo sintético de las entidades híbridas erlotinib-clúster de boro, se decide utilizar el anión *closo*-dodecaborato de sodio $[B_{12}H_{12}]^{2-}$ Na^{2+}, un clúster de boro que no contiene átomos de carbono en su estructura y que además presenta, según lo descrito en la literatura, una alta estabilidad metabólica. Inicialmente fue intercambiado el catión sodio por el catión tetrabutilamonio mediante precipitación diferencial de éste último. En la Figura 34 se presenta la estrategia utilizada para el acople con erlotinib[123]. Nuevamente el rendimiento tras la reacción de cicloadición fue muy bueno, 71 %.

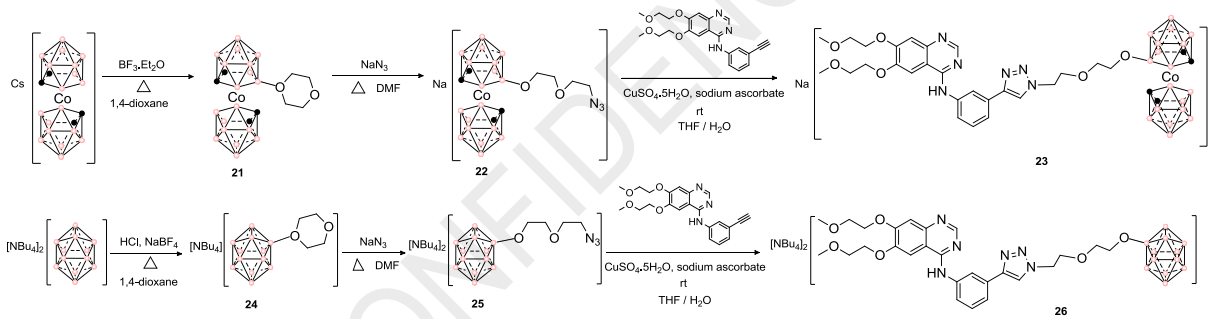


*Figura 34. Síntesis de entidades aniónicas híbridas **23** y **26**.*

Finalmente, con el objetivo de analizar la relevancia en la bio-actividad del fragmento carbaboranil en el híbrido resultante, se decidió sintetizar las análogos híbridos fenil- y adamantinil-anilinoquinazolina (**28** y **29**, respectivamente), los cuales son considerados unidades bioisostéricas de los clústeres de boro[124,125], Figura 35.

CONFIDENCIAL

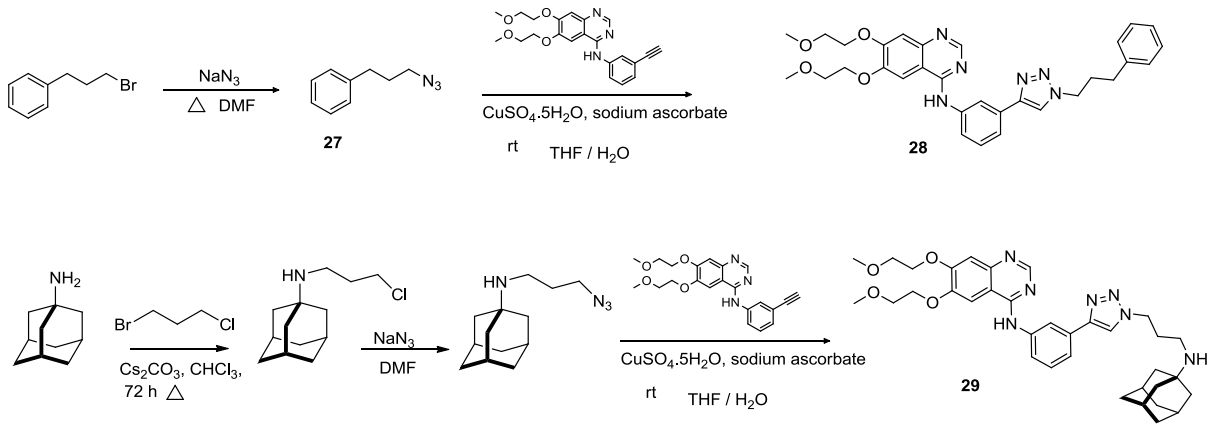


*Figura 35. Síntesis de bioisósteros **28** y **29**.*

Caracterización a través de RMN de ^{11}B y ^{1}H y espectrometría de masas

Todos los compuestos preparados se caracterizaron mediante espectroscopia de RMN de ^{1}H, ^{11}B y ^{13}C, así como espectrometría de masas mediante impacto electrónico y análisis elemental. También ha sido posible para los derivados **23** y **26** obtener los espectros de masas a través de MALDI-TOF y para el resto de las entidades híbridas a través de espectrometría de masas por impacto electrónico (artículo I, material suplementario). Para todos los derivados sólidos se ha determinado su punto de fusión (artículo I, material suplementario).

A modo de ejemplo se analizará la caracterización a través de RMN de ^{11}B y ^{1}H del compuesto **11**.

Existes dos isótopos estables de Boro, ^{10}B y ^{11}B, cuyas abundancias isotópicas naturales son 19.9 % y 80.1 % respectivamente (Tabla 1). Debido a que ambos isótopos poseen momentos magnéticos, ambos exhiben también absorciones características en RMN. Sin embargo el isótopo ^{11}B ha sido el más utilizado, esto puede explicarse por varias razones:

- las señales espectroscópicas son de mayor intensidad que las presentadas por el ^{10}B, debido a una mayor abundancia isotópica;
- ^{11}B posee un momento magnético nuclear mayor que el ^{10}B, 2.688 y 1.80 respectivamente lo que resulta en una mayor relación señal/ruido;
- el spin nuclear (*I*) en unidades de $h/2\pi$ para el ^{11}B es de 3/2 mientras que para el ^{10}B es de 3, resultando en un mayor momento cuadrupolar nuclear para el ^{10}B dando señales más anchas en el espectro de RMN respecto del ^{11}B.

CONFIDENCIAL

Tabla 1. Propiedades nucleares de los nucleídos ^{10}B y ^{11}B

Propiedades	^{10}B	^{11}B
Masa atómica relativa ($^{12}C = 12$)	10.012939	11.009305
(%) Abundancia isotópica natural	19.6	81.4
Espin nuclear (*I*)	3	3/2
Momento magnético[a]	1.80063	2.68857
Frecuencia de Larmor[b]	4.575	13.660
Momento cuadripolar eléctrico[c]	0.0740	0.0355
Señales de B (ppm) en $BF_3.OEt_2$[d]	0	0
Rango de desplazamiento químico (ppm)	-120 a 90	-120 a 90

[a] En unidades de magnetón nuclear, I = 5.0505 x 10^{-27} A m^2. [b] En MHz a 10^4 gauss. En unidades de e x 10^{-28} cm^2, "e" es la carga del electrón. [d] En $CDCl_3$ al 15% v/v.

En todos los productos intermedios que involucre entidades icosaédricas de boro así como en las entidades híbridas objeto de la presente tesis, aparece una banda de gran amplitud en el rango 1.0 a 3.5 ppm correspondiente a los protones B-H del clúster, cuya forma es consecuencia del acoplamiento entre el núcleo de ^1H con los núcleos ^{10}B y ^{11}B (Figura 36, izquierda). Ésta señal, sumada a la señal en 8.1 ppm del protón triazólico (en el caso particular de la síntesis de **11**) son consideradas las "señales huella" en el espectro que dan indicio de la promoción de dicha reacción. No obstante, otras señales como la del hidrógeno *exo*-cluster $C_{clúster}$-H en 2.9 ppm con multiplicidad singulete y con área relativa de integración de 1, son de gran utilidad para la rápida identificación del producto final.

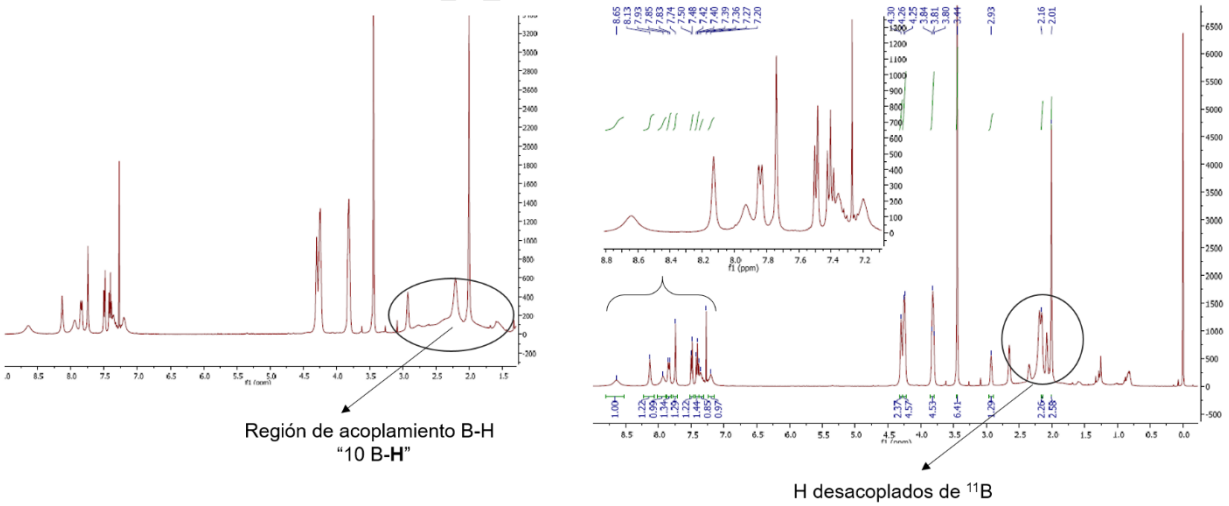


*Figura 36. Izquierda, ^1H-RMN de compuesto **11** en $CDCl_3$; Derecha, $^1H\{^{11}B\}$-RMN de compuesto **11** en $CDCl_3$.*

En relación a la espectroscopia de RMN de ^{11}B, el núcleo de boro percibe dos campos magnéticos debido al momento de spin (I) ½ del ^1H resultando en una señal con multiplicidad de tipo doblete (simétrica, acoplamiento B-H) en el espectro (Figura 37, ^{11}B-RMN). Por otro lado, las señales observadas en la RMN de ^{11}B son consistentes con un sistema *closo*-

carborano mono-sustituído resultando en 4 resonancias entre δ -4 y -16 para 10 átomos de boro en una relación 1:5:2:2 y con constantes de acoplamiento ^{11}B-^{1}H entre 164 y 190 Hz.

Los desplazamientos químicos de cada ^{11}B en los clúster de boro no se corresponden generalmente con las densidades electrónicas presentes en los vértices individuales de los compuestos orgánicos, debido al efecto antipodal y efecto vecino que influyen en su anisotropía electrónica[126,127]. Por lo tanto, los átomos de boro que están más cerca de los átomos de carbono están más protegidos que los que están más alejados de los carbonos. Asimismo, la adición de sustituyentes cambia la simetría y la densidad electrónica de los sistemas *closo*-carborano resultando en cambios en los desplazamientos químicos. Teniendo en cuenta estos aspectos es que se asignan todas las señales de BH como se muestra en la Figura 37. Además de esto, puede apreciarse que las señales son más anchas respecto a las del ^{1}H-RMN, esto se debe al momento cuadrupolar del ^{11}B (s= 3/2) con efecto en los tiempos de relajación los que están directamente relacionados con el ancho de las señales.

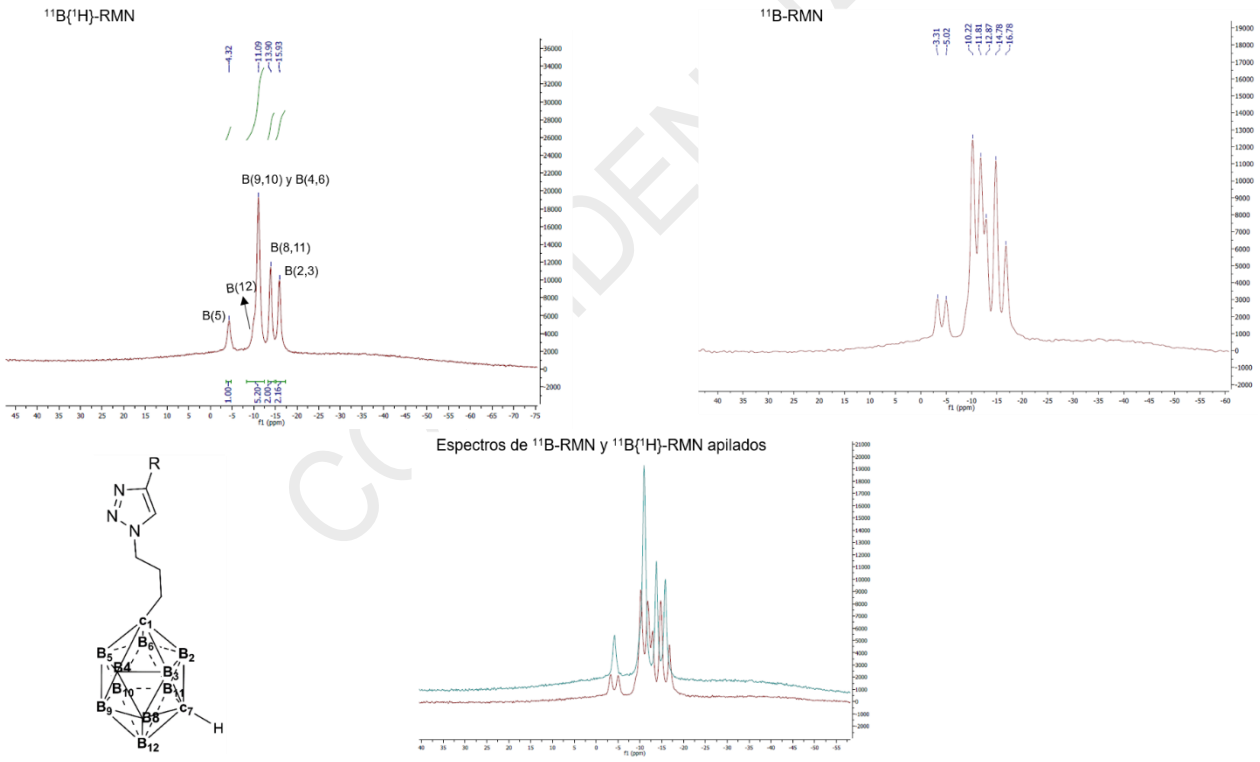


*Figura 37. ^{11}B y $^{11}B\{^{1}H\}$-RMN del derivado **11**. Se muestra la integración, desplazamiento químico y asignación de cada vértice de boro.*

La preparación de la entidad **23** involucra varias etapas y, como se comentó anteriormente, se siguieron las condiciones descritas en la bibliografía para la preparación de los intermedios **21** y **22**. A modo de ejemplo, el seguimiento de la reacción para la obtención de **22**, que involucra la apertura del heterociclo de dioxonio en presencia de azida de sodio, se siguió mediante

$^{11}B\{^{1}H\}$-RMN, debido al cambio que se produce en la distribución de las resonancias de los átomos de boro en la entidad precursora **21**, a medida que avanza la reacción, y además, por el desplazamiento químico producido por el vértice *B(8)-O,* al generarse la apertura del anillo de dioxonio y alterar su entorno electrónico (Figura 38).

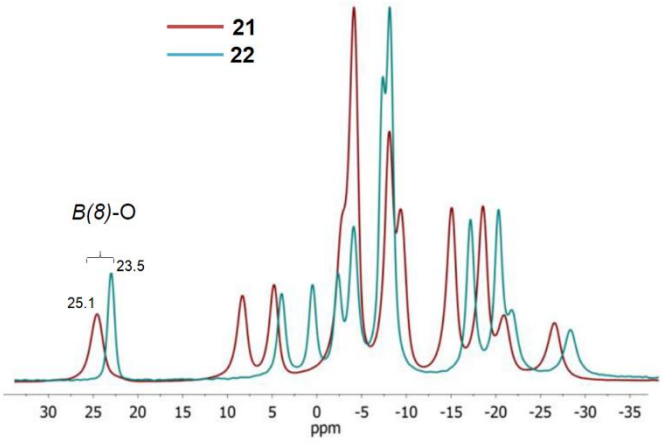


*Figura 38. $^{11}B\{^{1}H\}$-RMN de la entidad **21** y del producto **22** tras la apertura con la sal de azida.*

El compuesto **23**, sintetizado a través de un proceso de *click chemistry,* fue caracterizado utilizando varias técnicas (artículo I, material suplementario). En ese sentido cabe mencionar el uso de la espectrometría de MALDI-TOF-MS mediante la cual se observa el ión molecular que se corresponde con el pico de mayor intensidad (Figura 39). El pico molecular muestra la distribución isotópica típica del boro y con separación entre los picos de 1 unidad m/z, lo que indica que se trata de un compuesto monoaniónico.

CONFIDENCIAL

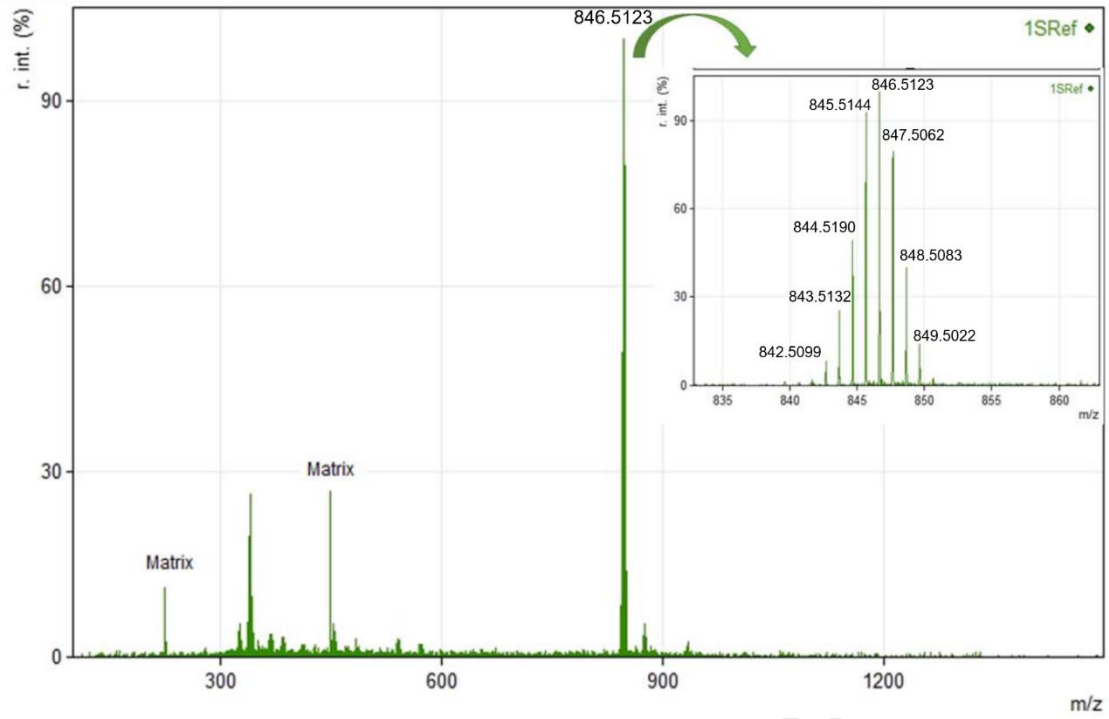


Figura 39. Espectro de MLADI-TOF-MS y ampliación del pico asociado con el ión molecular 846.51 m/z.

5.2.2 Estudios de citotoxicidad sobre células tumorales y selectividad *in vitro*

Siguiendo metodologías experimentales previamente establecidas por nuestro grupo de investigación[128], se procedió a cribar *in vitro* los compuestos híbridos desarrollados. Para ello se seleccionaron células tumorales gliales, específicamente la línea C6 (ATCC, CCL-107), derivada de glioma de rata, como forma de evaluar la citotoxicidad. La misma se analizó mediante el ensayo colorimétrico de Sulforrodomina B. A su vez se demostró, mediante un ensayo de inmunohistoquímica, que la línea C6 presenta sobreexpresión del receptor EGFR (artículo I, material suplementario, Figura S1).

Los resultados de citotoxicidad en las células de glioma revelaron que algunos compuestos que contienen boro poseen un efecto citotóxico dependiente de la concentración (Tabla 2) y además un mejor perfil de bio-respuesta, cuando se los compara con el fármaco de partida erlotinib. Por ejemplo, los derivados **5** y **11** fueron los más activos, siendo **11** al menos 3,3 veces más activos que erlotinib. Además, **23** fue al menos 2,3 veces más activo que el compuesto original. Por otro lado, todos los derivados pertenecientes a la serie que contiene el conector benciletinil (**15**, **16**, **19**, **20**), así como el compuesto dianiónico **26**, fueron inactivos a las dosis ensayadas. Cabe destacar que el compuesto **28** y el **29** no mostraron actividad relevante a las dosis ensayadas, como sus carbaboranil bioisosteros **5** y **11**.

CONFIDENCIAL

Por otro lado, con el objetivo de estudiar la selectividad hacia células tumorales, se realizó para los compuestos más activos **5**, **11** y **23** estudios de citotoxicidad sobre un cultivo primario mixto de células gliales (Tabla 2). Claramente, los resultados mostraron que estos compuestos son al menos 2,3 veces más citotóxicos para las células de glioma que para las células gliales normales.

Otro aspecto interesante a mencionar dentro de la serie *closo*-carbaboranilquinazolina es la relación entre la estructura y la actividad que se observa al comparar las actividades de los pares de compuestos **5** y **6** ó **11** y **12** (Figura 40). Por un lado, la sustitución de un metilo por hidrógeno, en la posición *orto* o *meta*, es decir, los compuestos **6** y **12**, produce una disminución de la citotoxicidad en las células de glioma. Además, cabe destacar que esta relación fue independiente del conector utilizado entre el grupo quinazolinilo y carbaboranilo. La serie conteniendo el conector benciletinil, es decir, **15**, **16**, **19** y **20**, mostró la misma tendencia pero con valores de citotoxicidad ligeramente más bajos (Figura 40). Por otro lado e indiferentemente del tipo de conector, cuando se compara los isómeros *orto* y *meta*, es decir, el par de isómeros **5** y **11** ó isómeros **6** y **12** (Figura 40), los compuestos *meta*-carboranilo fueron más activos que los análogos *orto*.

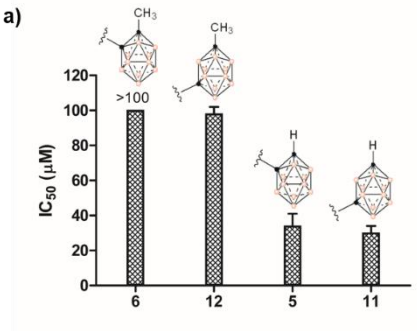
CONFIDENCIAL

Tabla 2. Efecto de los híbridos sobre la línea celular de glioma C6, e índice de selectividad en un cultivo primario mixto de células gliales.

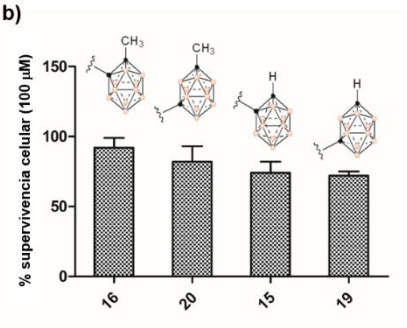
Compuesto	IC_{50},C6 (μM)[a]	Compuesto	IC_{50},mixto (μM)[b,c]	IS[d]
5	34 ± 7	**5**	> 100	> 2.9
6	> 100	**11**	> 100	> 3.3
11	30 ± 4	**23**	> 100	> 2.3
12	99 ± 4	**Erlotinib**	> 100	-
15	> 100			
16	> 100			
19	> 100			
20	> 100			
23	44 ± 6			
26	> 100			
28	79 ± 4			
29	>100			
Erlotinib	> 100			

[a] Las concentraciones para inhibir el crecimiento al 50% fueron determinadas a través de curvas dosis respuesta (triplicado). [b] Las concentraciones para inhibir el crecimiento al 50% del cultivo primario mixto de células gliales fueron determinadas a través de curvas dosis respuesta (triplicado) [c] Dosis superiores a 100 μM no fueron evaluadas por baja solubilidad. [d] IS: Índice de Selectividad, definido como $IC_{50,mixto}/IC_{50,C6}$.

a)



b)



c)

Compuesto	% supervivencia celular (100 μM)
15	74
16	92
19	72
20	82

Figura 40. a) Relación de estructura-actividad para los derivados metil-, desmetil- y orto-, meta-isómeros de la serie que contiene el conector propiltriazol. b) Relación de estructura-actividad para los derivados metil-, desmetil- y orto-, meta-isómeros de la serie que contiene el conector benciletinil. c) % de supervivencia en línea celular C6 de los derivados de la serie que contiene el conector benciletinil.

5.2.3 Influencia de lipofilicidad en la bioactividad

Otro estudio de relación estructura-actividad que se lleva a cabo es la relación con la lipofilia. Para cada uno de los derivados híbridos preparados se pretendió explorar si las bioactividades observadas tenían o no relación con dicha propiedad. En este sentido, las lipofilicidades se determinaron en términos de R_M, siendo R_f la relación de frente obtenida en fase estacionaria C18 y fase móvil acuosa.

$$R_M = \log [(1/R_f)-1]$$

Como era de esperarse, los compuestos con valores de hidrofilicidad más altos, **26** y erlotinib, o los compuestos con las lipofilicidades más altas, **15**, **16**, **19** y **20**, fueron inactivos (ver Tabla 3).

Cuando los valores de R_M se graficaron frente a los valores de IC_{50} obtenidos para C6, se observa una curva con tendencia cuadrática. Cuando se consideraron los compuestos pertenecientes a la serie conteniendo el conector [1,2,3]triazolilpropil es decir, los derivados **5**, **6**, **11**, **12**, **23**, **26**, y además el erlotinib, se obtuvo una curva cuadrática (r^2 aj. 0.9815, Figura 41). Este tipo de comportamiento, con un valor óptimo de lipofilicidad, es típico de compuestos que interactúan con una biomolécula[129]. Como era de esperarse, el derivado bioisostérico fenil-triazol **28** no se ajustó a esta relación, quedando por fuera de la tendencia, comúnmente designado como *outlier*.

CONFIDENCIAL

Tabla 3. Valores del descriptor R_M

Compuesto	R_M[a]
5	0.738
6	0.857
11	0.766
12	0.966
15	1.420
16	1.370
19	1.440
20	1.320
23	0.150
26	-0.857
28	0.209
Erlotinib	-0.209

[a] Coeficientes determinados en CCF de fase reversa en metanol:buffer fosfato salino (pH 7.4, 0.01M.

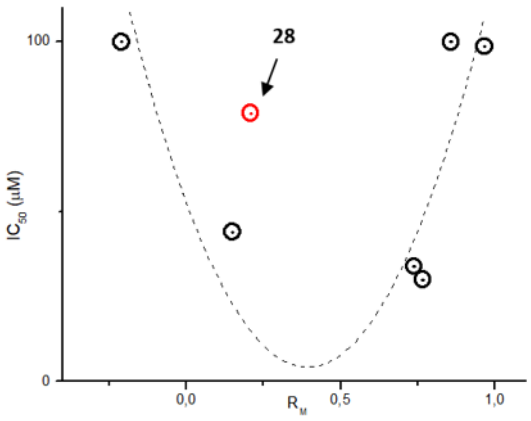


Figura 41. Relación entre IC_{50} y lipofilicidad (R_M) para derivados con conector [1,2,3]triazolilpropil.

CONFIDENCIAL

5.3 Conclusiones

En el presente trabajo se prepararon y caracterizaron nuevos agentes híbridos conteniendo por un lado el farmacóforo 4-anilinoquinazolina y por otro clústeres icosaédricos de boro. Los mismos se evaluaron en relación a su citotoxicidad *in vitro* hacia células de glioma C6 que sobreexpresan EGFR. Además, se estudió su selectividad hacia células normales del sistema nervioso central. Se determinó la lipofilicidad de los híbridos y se observó una clara relación de la bioactividad con dicha propiedad. Los resultados generales mostraron que los híbridos preparados son potenciales agentes antitumorales con posible doble acción, con capacidad inhibitoria en células que presentan alta expresión de EGFR y eventualmente con potencial aplicación a través de procesos de BNCT, si bien este aspecto no fue abordado en el presente trabajo.

CONFIDENCIAL

Serie derivada de erlotinib

Artículo II.

CHEMISTRY
A European Journal

ChemPubSoc Europe

Communication

Discovery of Potent EGFR Inhibitors through the Incorporation of a 3D-Aromatic-Boron-Rich-Cluster into the 4-Anilinoquinazoline Scaffold: Potential Drugs for Glioma Treatment

Marcos Couto, María Fernanda García, Catalina Alamón, Prof. Mauricio Cabrera, Prof. Pablo Cabral, Prof. Alicia Merlino, Prof. Francesc Teixidor, Prof. Hugo Cerecetto ✉, Prof. Clara Viñas ✉

CONFI

5.4 Objetivos específicos

1- Estudio del mecanismo de acción de los derivados híbridos generados (Capítulo I), mediante estudios *in vitro* e *in silico* de inhibición enzimática.
2- Estudio de propiedades tipo-fármaco. Estabilidad química (en disoluciones acuosas a distintos pH) y biológica (frente a fracción citosólica y microsomal hepática).
3- Capacidad de penetración de la BHE: aproximaciones teóricas y experimentales.
4- Determinación cualitativa de la captación celular de boro.

CONFIDENCIAL

5.5 Resultados y Discusión

5.5.1 Estudios *in vitro* de inhibición enzimática

Como se comentó, los receptores oncogénicos con dominios tirosina quinasa, entre los que se encuentra el EGFR, están sobreexpresados, amplificados y en ciertas ocasiones mutados en glioblastoma multiforme por lo que los mismos se consideraron como dianas moleculares para la búsqueda de nuevos fármacos.

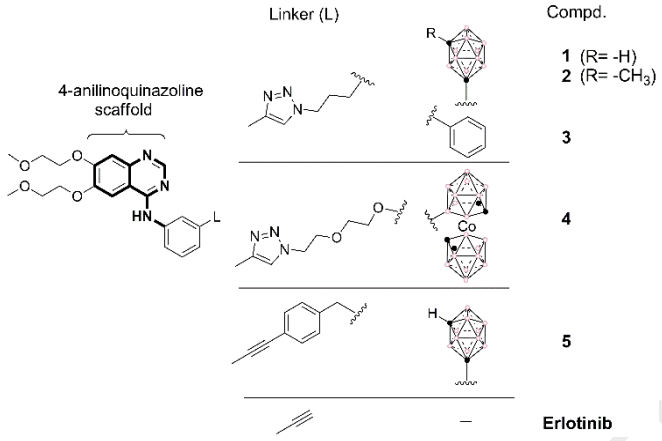
Los resultados obtenidos en el apartado anterior (Capítulo I, Artículo I) en líneas celulares con sobreexpresión de EGFR motivaron a continuar explorando la interacción de los compuestos desarrollados con el EGFR. Por tal motivo, se procedió a evaluar la inhibición enzimática sobre EGFR en su forma salvaje ($EGFR_{WT}$) y sobre la variante mutada EGFR T790M. La variante EGFR T790M se seleccionó debido a que es una forma mutada que se observa frecuentemente en distintos tipos de cánceres y está asociada con la resistencia a la terapia con erlotinib[130.] Las mediciones de inhibición enzimática sobre $EGFR_{WT}$ y la variante mutada EGFR T790M se realizaron en un ensayo libre de células (utilizando el sistema ADP-GloTM kinase Assay y EGFR Kinase Enzyme System, Artículo II, material sumplementario, Figura S1 y S2).

La incorporación de sistemas *closo*-carbaboranilo (compuestos **1**, **2** y **5**) y cobaltabisdicarbaluro (derivado **4**) en el fragmento 4-anilinoquinazolina produjo, sobre $EGFR_{WT}$, valores de IC_{50} en el rango nanomolar (Tabla 4). Interesantemente, la inhibición de $EGFR_{WT}$ para los híbridos carboranil-anilinoquinazolina mostró la misma tendencia que en los ensayos de citotoxicidad antes descritos sobre la línea celular de glioma C6 la cual sobreexpresa EGFR (Figura 42). Nuevamente el derivado **1** fue el inhibidor más potente con un valor de IC_{50} de 2.3 nm sobre $EGFR_{WT}$, 10 veces más activo que el compuesto padre erlotinib. Entre los derivados *closo*-carbaboranilo (**1**, **2** y **5**), la presencia de un conector rígido como es el caso del fragmento benciletinil en el derivado **5** dio lugar a una marcada pérdida de actividad, siendo 224 veces menos activo que **1**, que porta un conector [1,2,3]triazolilo. En el mismo sentido, la incorporación de un grupo metilo en el clúster, derivado **2**, condujo a una pérdida de actividad inhibitoria de 136 veces respecto al derivado **1**. Como resultado de combinar en el derivado **1**, las propiedades de un sistema aromático-2D (como es el caso del derivado **3**) y las propiedades de un grupo hidrofóbico no aromático-3D (como es el caso del derivado **29** del apartado anterior, referenciado como **6** en el presente apartado, que porta un sistema

CONFIDENCIAL

adamantilo como bioisóstero 3D del sistema carboranilo) se obtuvo un potente inhibidor de $EGFR_{WT}$ (comparar **1** con los derivados **3** o **6**).

Por otro lado se indagó la capacidad inhibitoria sobre la variante mutada EGFR T790M. Como era de esperar erlotinib fue incapaz de inhibir la enzima a las concentraciones ensayadas mientras que el derivado **1** mostró una buena capacidad inhibitoria con un valor de IC_{50} de 1125 nm, resaltando el potencial terapéutico de este nuevo compuesto (Tabla 4).



Compuesto	IC_{50},C6 (μM)[a]	IS[d]
1	30 ± 4	> 3.3
2	99 ± 4	ND
3	79 ± 4	ND
4	44 ± 6	> 2.3
5	> 100	ND
Erlotinib	> 100	ND

[a] Las concentraciones para inhibir el crecimiento al 50 % fueron determinadas a través de curvas dosis respuesta (triplicado). [d] IS: Índice de Selectividad, definido como $IC_{50,mixto}/IC_{50,C6}$.

Figura 42. Derivados seleccionados para estudiar la inhibición in vitro sobre EGFR.

Tabla 4. Inhibición de la actividad tirosina quinasa de la enzima $EGFR_{WT}$ y $EGFR_{T790M}$

Compuesto[a]	IC_{50}, $EGFR_{WT}$ (nM)[b]	IC_{50}, $EGFR_{T790M}$ (nM)[b]	Intervalo de Confianza[d]
1	2.3	1125	0.9 – 6.2
4	296.3	ND	155.7 – 564.2
2	312.2	ND	200.3 – 487.6
5	517.2	ND	320.0 – 836.0
3	2340.0	ND	1215 – 4506.0
6	974.4	ND	600.7 – 1581.0
Erlotinib	22.9	Inactivo[c]	14.1 – 37.2

[a] Los compuestos están ordenados de acuerdo con la actividad *in vitro* frente a la línea celular C6. [b] Las concentraciones son las requeridas para inhibir un 50 % la fosforilación del sustrato poli(Glu:Tyr), determinados por triplicado a partir de curvas dosis respuesta y expresadas como el promedio y su intervalo de confianza. [c] No se observó inhibición a ninguna de las dosis evaluadas. [d] Intervalos de confianza asociados a la medida sobre $EGFR_{WT}$.

CONFIDENCIAL

5.5.2 Estudios *in silico* de inhibición enzimática

Para un mejor entendimiento de la interacción establecida entre los híbridos desarrollados y el receptor de EGF, se exploró *in silico* a través de modelado molecular (*docking*) el modo de unión de los híbridos **1**, **2** y **3** y el bioisóstero **6** empleando para esto el conjunto de programas AutoDock4.2 y Gaussian 09 (Artículo II, material suplementario).

El inhibidor reversible de tirosina quinasa erlotinib, se posiciona perfectamente en el sitio de unión del ATP y compite con éste inhibiendo la autofosforilación de EGFR y la señalización cascada abajo (Figura 43).

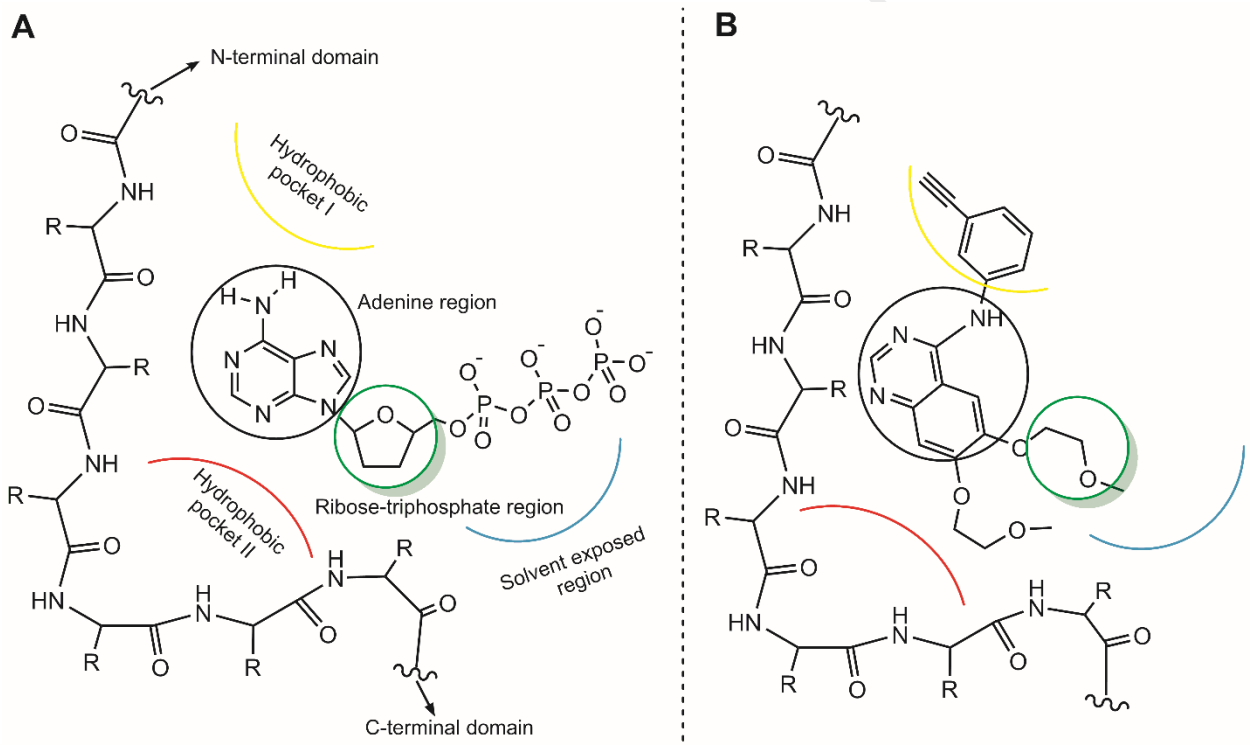


Figura 43. A) Principales interacciones del ATP en su sitio de unión. B) Representación de la disposición adoptada por el inhibidor de tirosina quinasa erlotinib en su sitio de acción.

Como se puede observar en la Figura 44B, todos los híbridos estudiados son capaces de interaccionar con el sitio catalítico de la enzima. En principio, los resultados experimentales podrían explicarse a través de la incorporación del agrupamiento carbaboranilo en la estructura de 4-anilinoquinazolina. Es sabido que el agrupamiento carborano puede interactuar a través de enlaces de di-hidrógeno no clásico como ser B-H---H-X (X= N, C, O y S), también llamados enlaces protón-hidruro debido a la electropositividad de los átomos de boro en el clúster de

carborano. Además, pueden establecer enlaces por puente de H, y enlaces de hidrógeno de tipo B-H---π y C-H---π.

El compuesto **1**, que fuese el derivado más activo en los experimentos *in vitro*, tanto en células como sobre la bio-molécula EGFR aisalada, se posiciona perfectamente en la hendidura catalítica Figura 45A. En el bucle (*loop)* de unión a ATP el fragmento 3-[1,2,3]triazolil-4-fenilo establece interacciones hidrofóbicas con los residuos Leu718 y Val726 mientras que el grupo carborano forma enlaces de hidrógeno con Glu762 presente α-hélice C y el residuo Asp855 del motivo DFG (Asp855-Phe856-Gly857). Además, se establecen interacciones por enlace de di-hidrógeno con Thr854 y Asp855 (Tabla 5). El derivado **2**, que exhibió un valor de IC_{50} 135 veces mayor que **1**, adopta un modo de unión algo diferente posicionando la porción 4-anilinoquinazolina hacia fuera de la hendidura catalítica Figura 44 y 45B. Sin embargo, la actividad moderada de este compuesto puede explicarse como resultado de las interacciones de hidrógeno y di-hidrógeno establecidas entre el clúster y los residuos Asp837 y Asn842 en el *loop* catalítico y además al enlace de hidrógeno establecido con el residuo Asp855 del motivo DFG (Figura 45B). Por otra parte, el derivado **6**, portando un agrupamiento adamantilo en su estructura en lugar de un clúster de boro, adoptó una disposición similar a la del compuesto **1**, extendiéndose a lo largo de la hendidura catalítica (Figura 45C). Sin embargo, el compuesto **6** muestra un valor de IC_{50} 400 veces mayor, lo que podría estar destacando la importancia de las interacciones adicionales que permite establecer el fragmento carborano y que por ende resultan en una mayor capacidad inhibitoria sobre $EGFR_{WT}$. De hecho **6** no logra posicionarse de forma tal que pueda entrar en contacto con residuos relevantes involucrados en la catálisis. Entre los híbridos analizados, el derivado **3** quien presentase la menor capacidad inhibitoria de EGFR, se posiciona en el surco catalítico (Figura 45C). Si bien el grupo fenilo se localiza entre el *loop* catalítico y el *loop* de unión a ATP, la molécula, al igual que el derivado **6**, no posee la capacidad de establecer interacciones por enlace de hidrógeno ni tampoco interacciones hidrofóbicas relevantes con ningún residuo en la superficie de la hendidura catalítica. Esto podría explicar, al menos en parte, su bajo poder inhibitorio, realzando nuevamente la hipótesis del trabajo, en la cual la sustitución del grupo fenilo en el esqueleto de 4-anilinoquinazolina por un sistema con aromaticidad tridimensional resulta ser una estrategia eficaz en la búsqueda de mejores inhibidores de EGFR.

CONFIDENCIAL

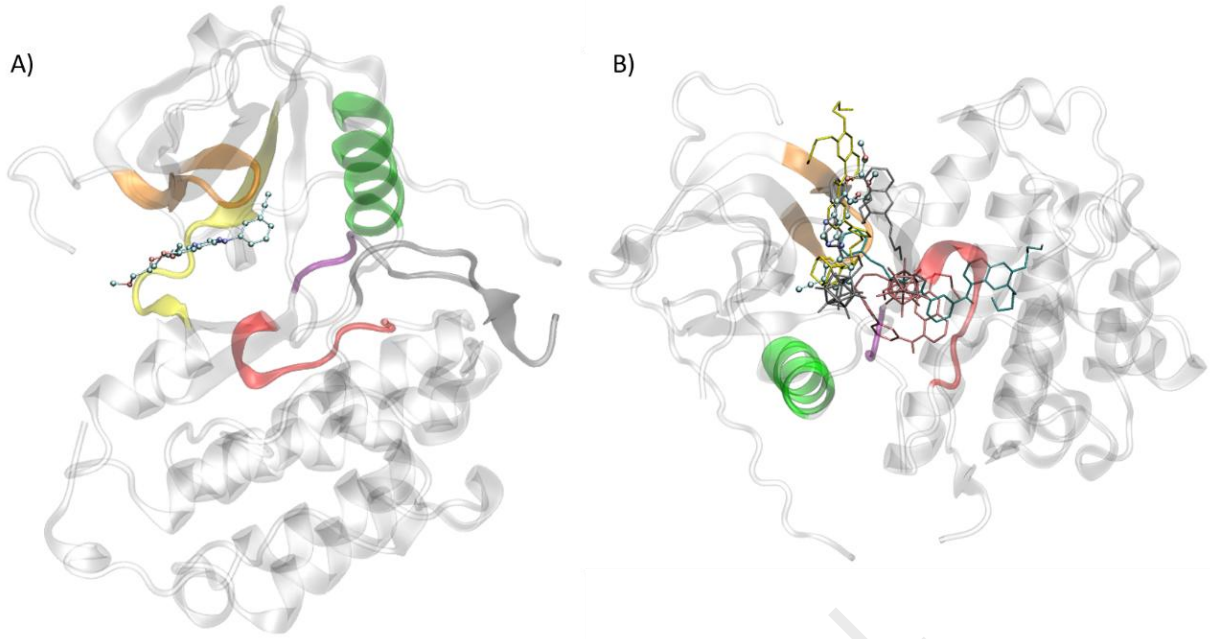


*Figura 44. Disposición y modo de unión de ligandos en el dominio tirosina quinasa de EGFR mediante cálculos de docking. En A) erlotinib. B) Comparación del modo de unión de compuesto **1** (gris), compuesto **2** (rosa), compuesto **3** (celeste), compuesto **6** (amarillo) y erlotinib (esferas y varillas). Los elementos estructurales de EGFR se resaltan de la siguiente manera, naranja: bucle de unión a ATP (residuos 718 a 726), verde: α-hélice C (residuos 756 a 768), amarillo: región bisagra (residuos 788 a 797), rojo: bucle catalítico (residuos 836) a 842), púrpura: motivo DFG (residuos 855 a 857), gris: bucle de activación (residuos 855 a 876).*

CONFIDENCIAL

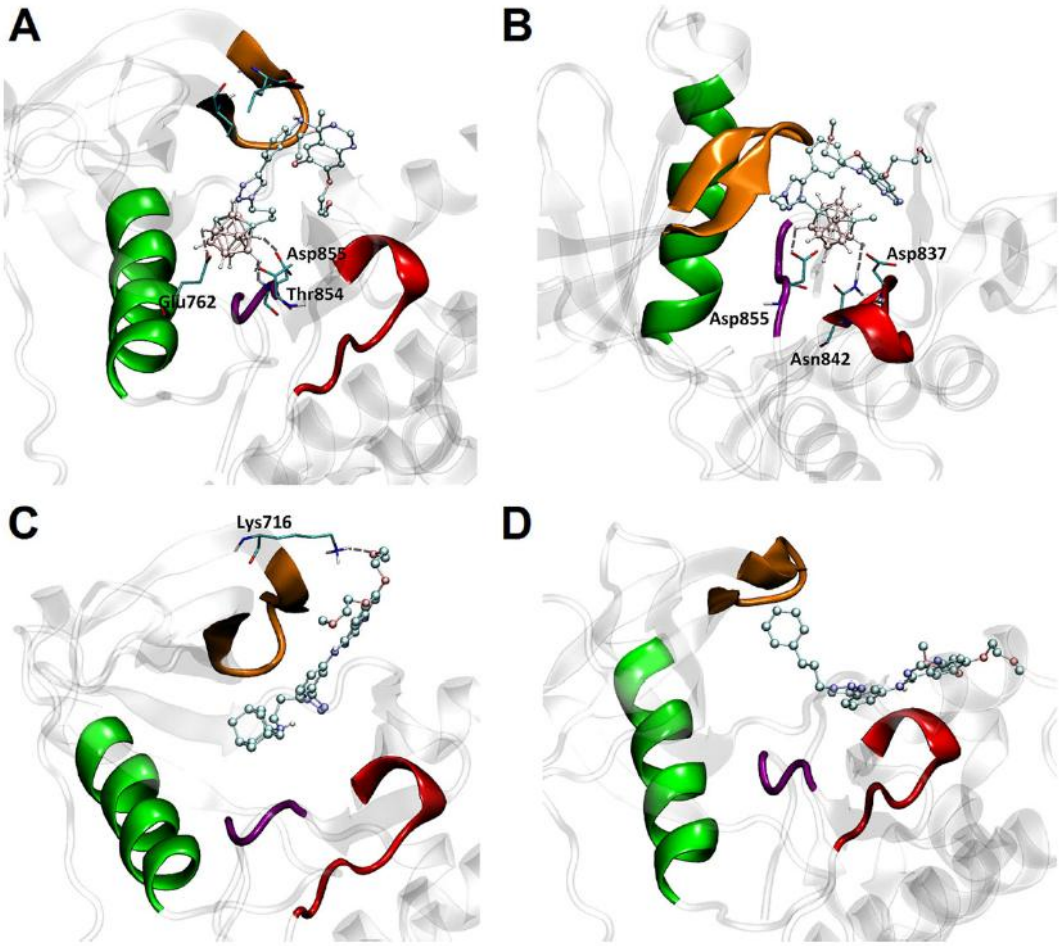


*Figura 45. Predicción mediante cálculos de docking del modo de unión a EGFR de los híbridos **1** (A), **2** (B), **6** (C) y **3** (D). Los híbridos se muestran en representaciones de esferas y varillas y los aminoácidos relevantes en representaciones de cintas. Naranja: bucle de unión a ATP, verde: α-hélice C, púrpura: motivo DFG, rojo: bucle catalítico.*

Tabla 5. Distancia entre los hidrógenos y los átomos en cuestión en los enlaces de hidrogeno y de dihidrógeno en los complejos híbrido-EGFR.

Compuesto	Enlace de Hidrógeno	Enlace de dihidrógeno	Distancia (A)
1	Bx-H···Glu762@OE2	-	2.07
	Bx-H···Asp855@OD2	-	1.89
	-	Bx-H···Thr854@OH	0.92
	-	Bx-H···Asp855@NH	1.34
2	Bx-H···Asp837@OD2	-	2.05
	Bx-H···Asp855@OD2	-	1.95
	H3CO···Lys716@NZ		2.04
		Bx-H···Asn842@HD2	1.85
6	-	-	-

5.5.3 Estudio de propiedades tipo-fármaco.

5.5.3.1 Estudios de estabilidad

El primer estudio se realizó para conocer el comportamiento de los compuestos **1** y **4** en disoluciones acuosas de distintos pHs, simulando diferentes desafíos a los que se puede enfrentar el agente híbrido en el organismo del paciente. Tanto el compuesto **1** como el **4** fueron estables a todos los pHs evaluados, del mismo modo el fármaco padre, erlotinib (Figura 46, 47, y 48, respectivamente).

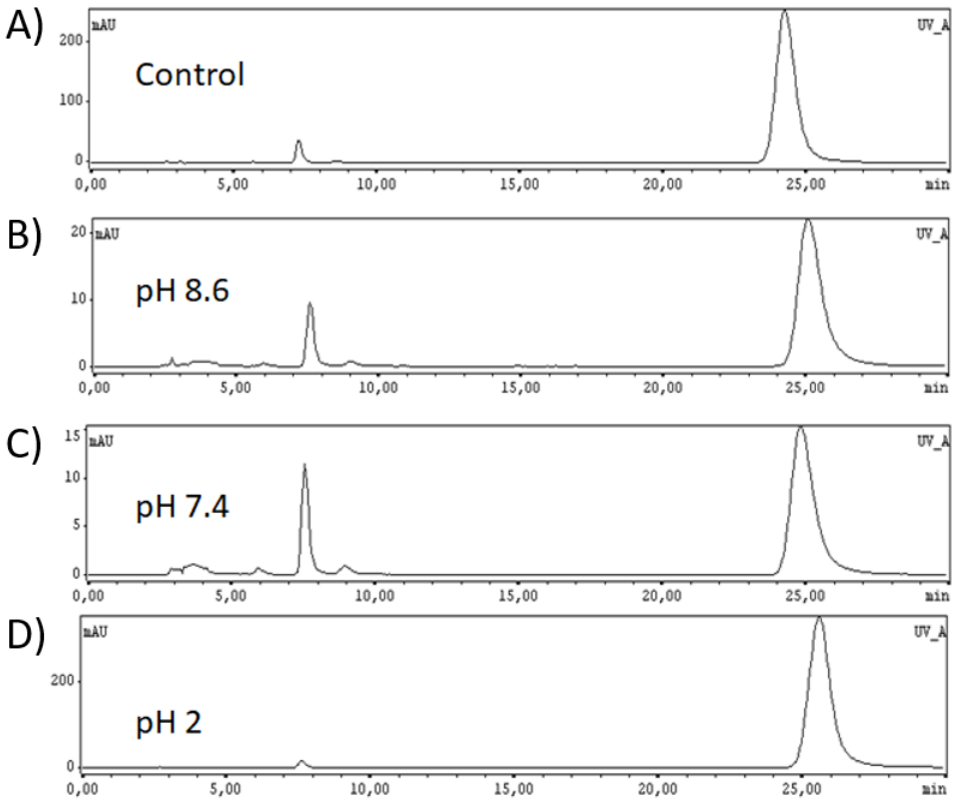


*Figura 46. HPLC de fase reversa de estudios de estabilidad de **1** en disoluciones acuosas a distintos pHs. La solución stock fue preparada en DMSO e incubada a 37 °C durante 24 h en distintas disoluciones acuosas. En A sin incubación; en B incubación en buffer Tris.HCl pH 8.6; en C incubación en buffer fosfato pH 7.4; en D incubación en buffer KCl.HCl, pH 2. Detección UV a λ= 340 nm.*

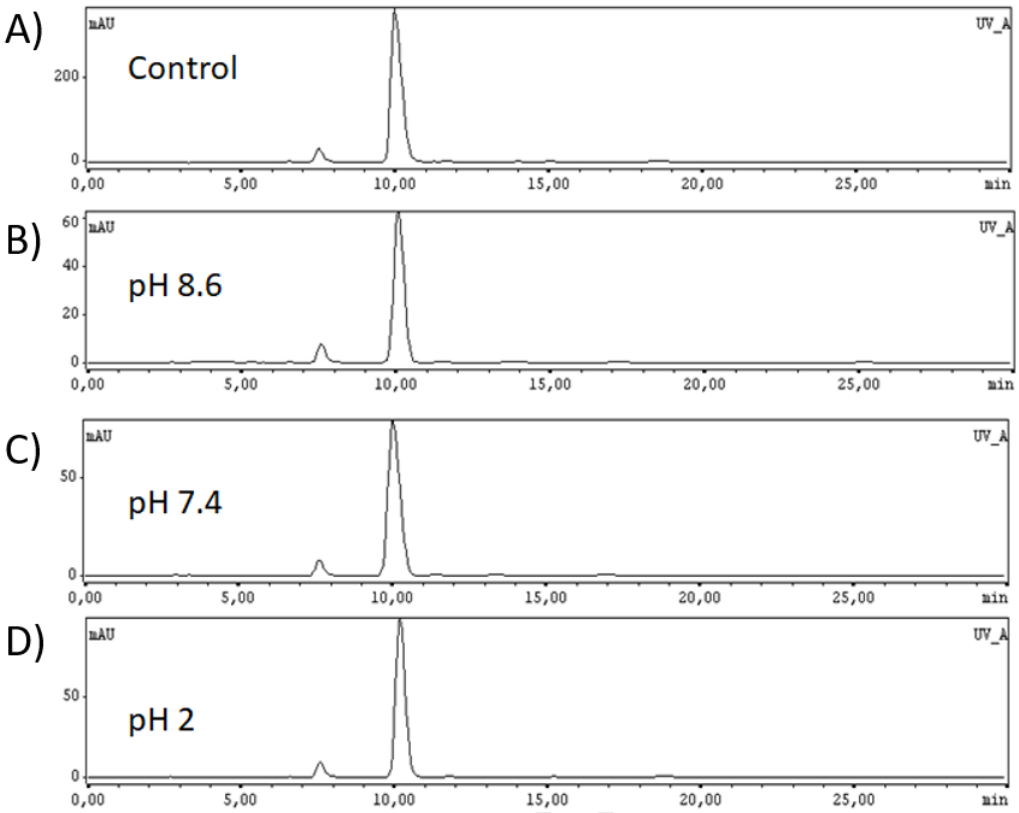


*Figura 47. HPLC de fase reversa de estudios de estabilidad de **4** en disoluciones acuosas a distintos pHs. La solución stock fue preparada en DMSO e incubada a 37 °C durante 24 h en distintas disoluciones acuosas. En A sin incubación; en B incubación en buffer Tris.HCl pH 8.6; en C incubación en buffer fosfato pH 7.4; en D incubación en buffer KCl.HCl, pH 2. Detección UV a λ= 340 nm.*

CONFIDENCIAL

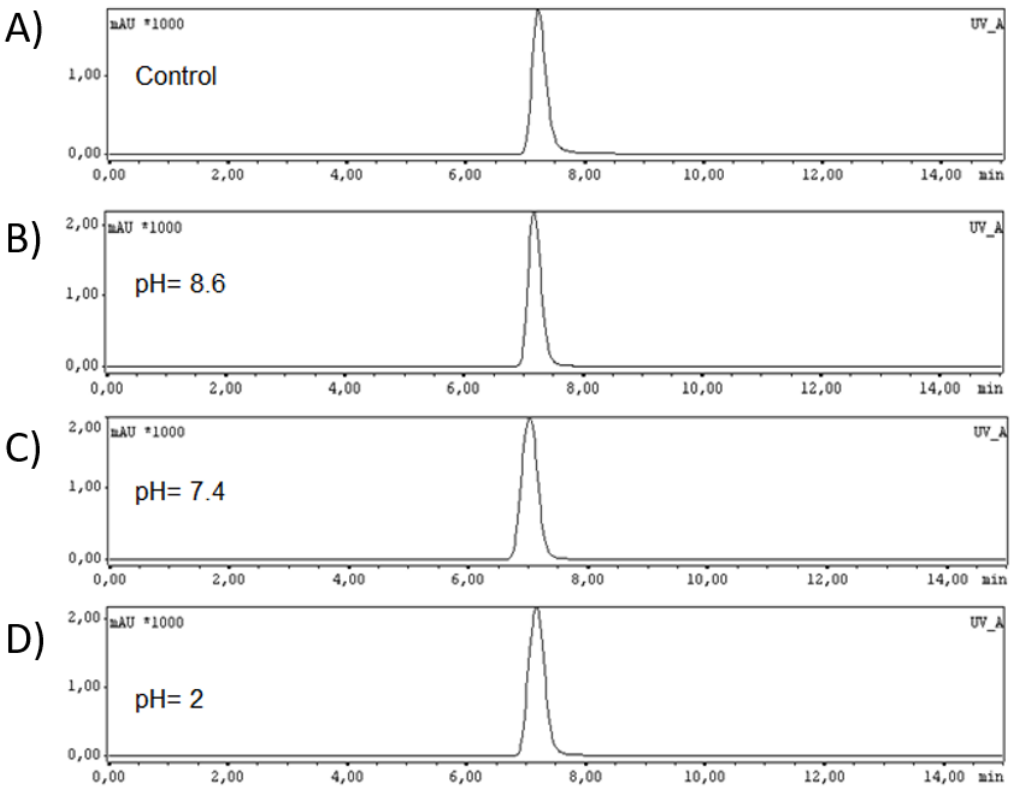


Figura 48. HPLC de fase reversa de estudios de estabilidad de erlotinib en disoluciones acuosas a distintos pHs. La solución stock fue preparada en DMSO e incubada a 37 °C durante 24 h en distintas disoluciones acuosas. En A sin incubación; en B incubación en buffer Tris.HCl pH 8.6; en C incubación en buffer fosfato pH 7.4; en D incubación en buffer KCl.HCl, pH 2. Detección UV a λ= 340 nm.

Por otro lado, se estudió la estabilidad de dichos derivados frente a desafíos biológicos, en presencia de fracciones citosólicas (Figura 49) y microsomales (Figura 50) de hepatocitos de rata. Los resultados revelaron que el derivado **1** fue estable en ambas condiciones mientras que **4** y erlotinib presentaron metabolización total y parcial, respectivamente, al cabo de 30 minutos (Artículo II, Material Suplementario, sección 2.5). En la Tabla 6 se resumen los resultados de estabilidad en las condiciones ensayadas para los compuestos estudiados.

CONFIDENCIAL

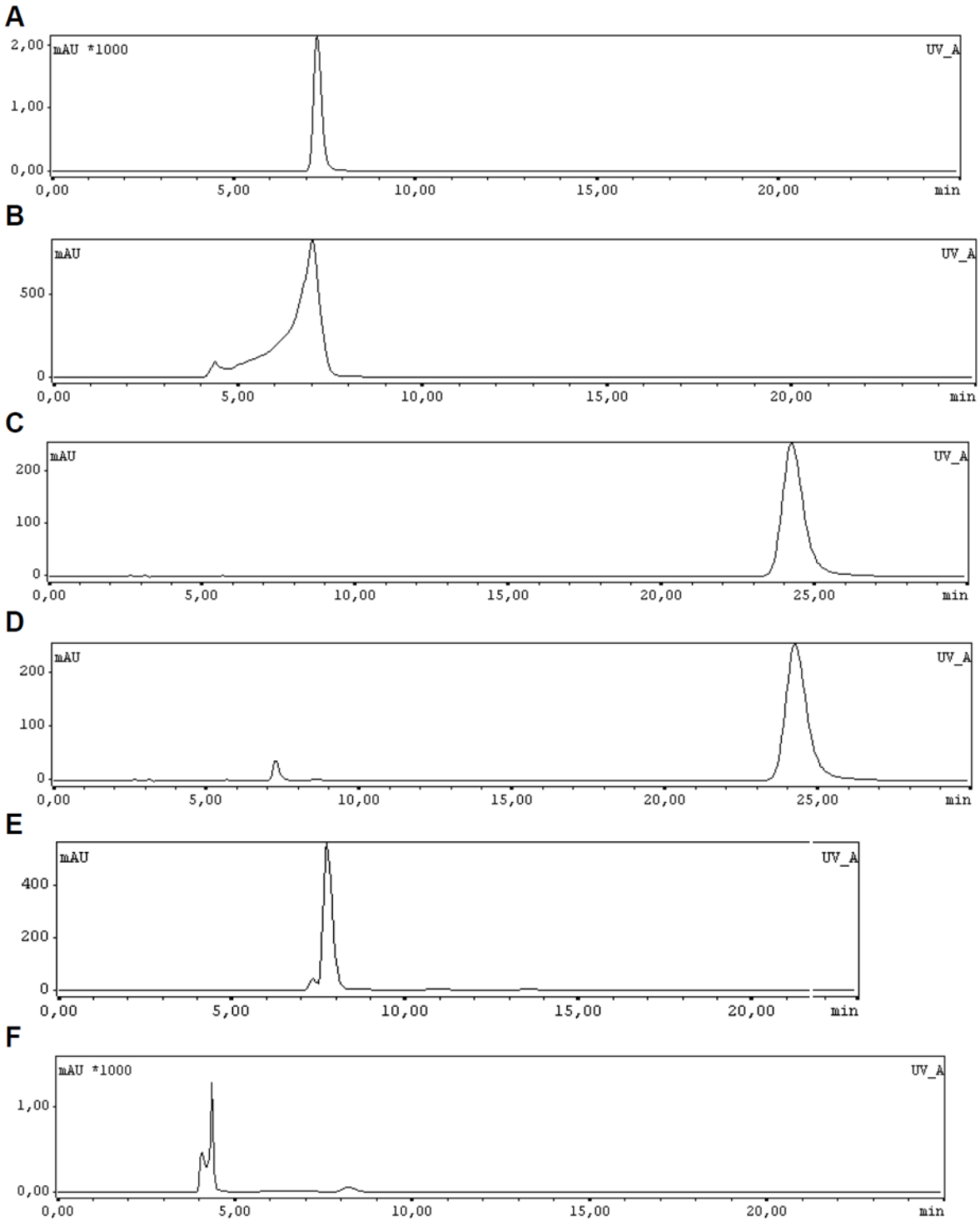


*Figura 49. HPLC de fase reversa de estudios de estabilidad de los compuestos estudiados frente a fracción citosólica hepática. Los compuestos fueron incubados a 37 °C durante 30 min. En A y B, erlotinib sin y con incubación, respectivamente; C y D, híbrido **1** sin y con incubación, respectivamente; E y F, híbrido **4** sin y con incubación, respectivamente.*

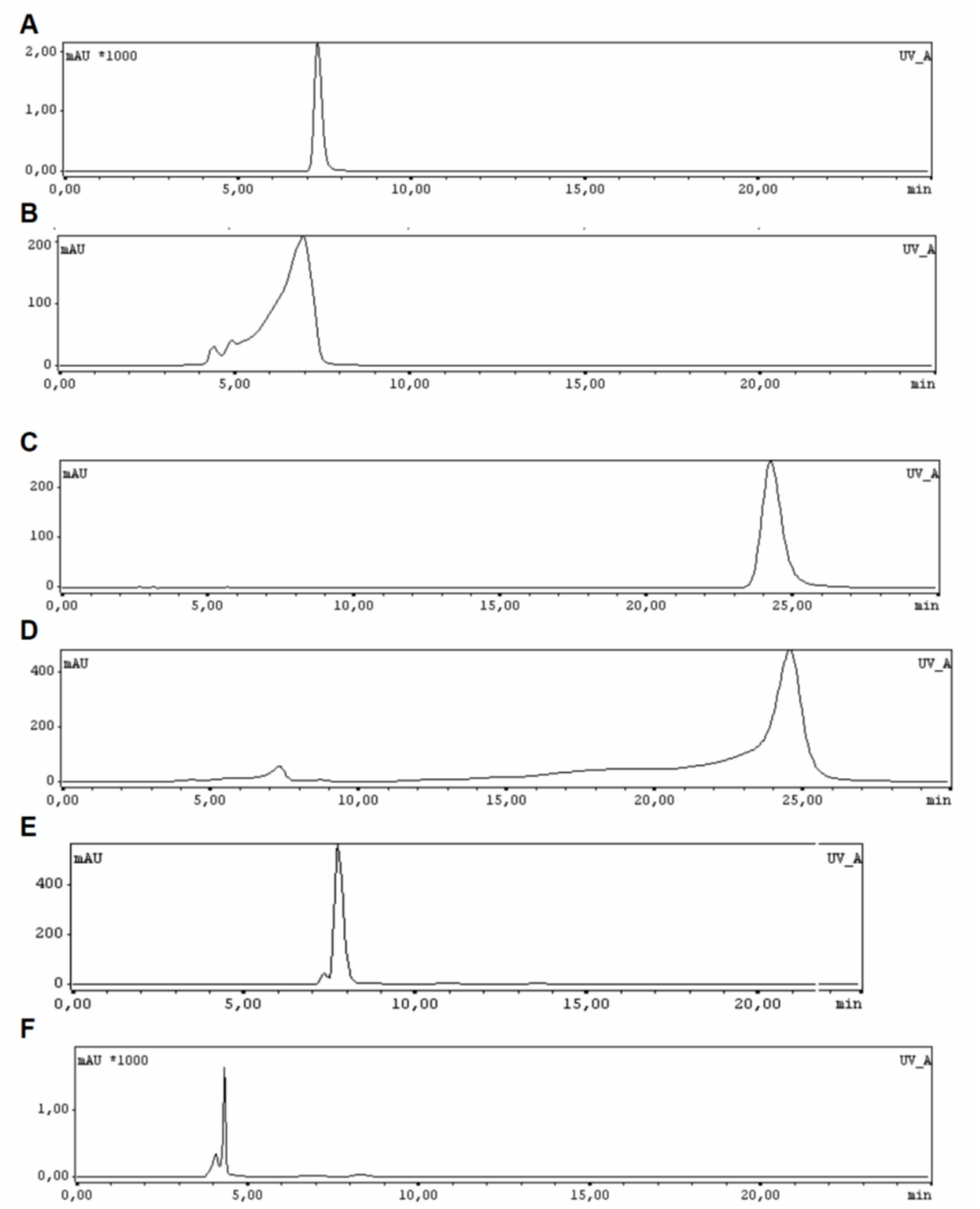


*Figura 50. HPLC de fase reversa de estudios de estabilidad de los compuestos estudiados frente a fracción microsomal hepática. Los compuestos fueron incubados a 37 °C durante 30 min. En A y B, erlotinib sin y con incubación, respectivamente; C y D, híbrido **1** sin y con incubación, respectivamente; E y F, híbrido **4** sin y con incubación, respectivamente.*

Tabla 6. Resumen de los estudios de estabilidad de los compuestos estudiados.

Compuesto	**Estabilidad**				
	2.0[a]	**7.4**[a]	**8.6**[a]	**Fracción citosólica**[b]	**Fracción microsomal**[b]
1	estable	estable	estable	No metaboliza	No metaboliza
4	estable	estable	estable	Metabolización total	Metabolización total
Erlotinib	estable	estable	estable	Metabolización parcial	Metabolización parcial

[a] Estabilidad a 37 °C durante 24 h. [b] Estabilidad a 37 °C durante 30 min.

5.5.3.2 Estudios para indagar la potencialidad de atravesar la BHE

La BHE es una estructura compleja formada mayoritariamente por células epiteliales y gliales que tienen como función principal proteger el SNC restringiendo el pasaje de sustancias tóxicas pero permitiendo el pasaje de metabolitos necesarios para el correcto funcionamiento de dicho órgano. Si bien en los gliomas de alto grado, como lo es el GBM, las uniones estrechas entre las células endoteliales que forman la BHE están altamente alteradas, se decidió, para los derivados **1**, **4** y erlotitnib, realizar estudios experimentales y teóricos con el objetivo de estudiar la capacidad de estos de atravesar de forma pasiva la BHE (Tabla 7). En ese sentido, se utilizó como modelo fisicoquímico experimental, el método del ΔLog*P* el cual se basa en estimar la contribución de los enlaces de hidrógeno[131,132]. Para ello, se determina el coeficiente de partición *n*-octanol/PBS y el coeficiente de partición ciclohexano/PBS, obteniéndose el parámetro de interés según:

$$\Delta \text{Log}P = \log P \text{ (}n\text{-octanol/PBS)} - \log P \text{ (ciclohexano/PBS)}$$

El fundamento del uso de este parámetro para predecir la capacidad de un compuesto de atravesar la BHE, se basa en que el *n*-octanol es capaz de establecer enlaces de hidrógeno con el fármaco, mientras que el ciclohexano no, simulando un contexto totalmente hidrofóbico como lo sería en el interior de una membrana celular. Se establece que si un compuesto presenta un valor de ΔLog*P* menor a 2, es probable que este atraviese la BHE.

Por otro lado, el cálculo teórico de la capacidad de atravesar la BHE se realizó utilizando el programa http://lmmd.ecust.edu.cn:8000/predict/ (Artículo II y Material Suplementario). Los resultados obtenidos por ambas metodologías revelan que el derivado **1** podría ser capaz de atravesar la BHE y de esta forma alcanzar el órgano objetivo, el cerebro.

CONFIDENCIAL

Tabla 7. Capacidad de atravesar barrera hematoencefálica mediante método de ∆log P *y teórico.*

Compuesto	Capacidad de atravesar barrera hematoencefálica	
	∆log *P* [a]	**Teórico** [b]
1	1.49 ± 0.15	+ BHE
4	4.05 ± 0.30	- BHE
Erlotinib	3.32 ± 0.30	+ BHE
Diazepan	0.0008 ± 0.002	-

[a] Los valores de ∆log *P* fueron determinados mediante HPLC. ΔLog*P* = log *P* (*n*-octanol/PBS) - log *P* (ciclohexano/PBS). [b] Calculado de acuerdo a http://lmmd.ecust.edu.cn:8000/predict/; (+) atraviesa BHE, (-) no atraviesa BHE.

5.5.4 Determinación cualitativa de captación de boro intracelular

Pensando en una potencial aplicación del derivado **1** a través de un proceso de terapia por captura neutrónica de boro, es que se decidió determinar, de manera cualitativa mediante XPS de alta resolución, la presencia de boro intracelular en células C6 derivada de rata. Como se puede observar en la Figura 51, la presencia de una señal a 189 eV en el espectro de XPS, es característica del enlace B-B[133], confirmando así la incorporación del derivado **1** en la línea C6 previamente tratadas con **1**.

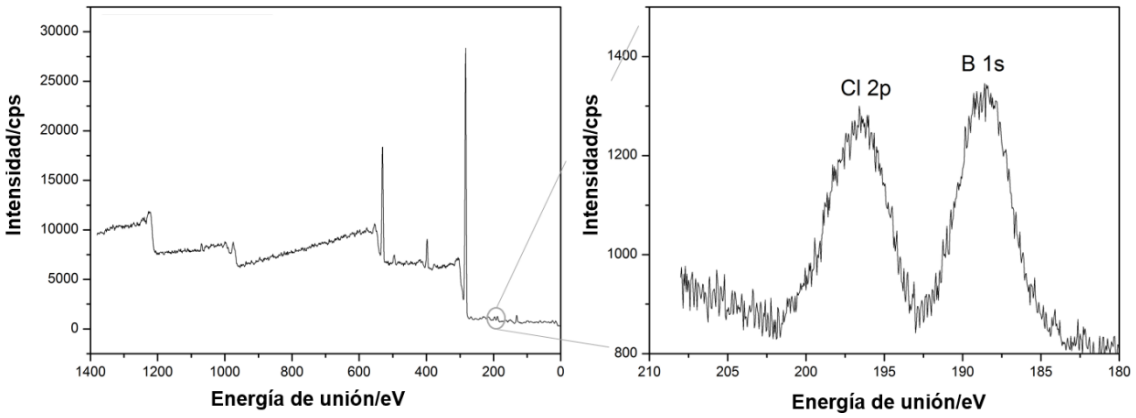


*Figura 51. Espectro de fotoelectrón de rayos X del cultivo de células C6 tratadas con el híbrido **1**. Las señales de Cl y B-B características se señalan en la región del espectro ampliada (Derecha).*

5.6 Conclusiones

Se demostró que el derivado **1** actúa como inhibidor de EGFR tanto de la forma salvaje como la mutada, aunque con diferente potencia. Por otro lado, se confirmó de manera cualitativa la presencia de boro intracelular, en C6, lo que determina que no sólo es capaz de interaccionar con el blanco molecular EGFR, sino que también es capaz de acumularse en la línea celular maligna. Esto convierte a **1** en un potencial compuesto líder con acción antitumoral dual, a través de receptores con actividad tirosina quinasa y para su aplicación en terapia por captura neutrónica de boro. En ese mismo sentido, las propiedades fisicoquímicas estudiadas también revelaron que el híbrido **1** podría ser un promisorio agente antitumoral de glioma.

CONFIDENCIAL

Serie derivada de erlotinib

Artículo III.

Research Article

For reprint orders, please contact: reprints@future-science.com

Future Medicinal Chemistry

Carboranylanilinoquinazoline EGFR-inhibitors: toward 'lead-to-candidate' stage in the drug-development pipeline

Marcos Couto[1], Catalina Alamón[1], Carina Sánchez[1], Belén Dávila[1], Marcelo Fernández[2], Nicole Lecot[1,3], Pablo Cabral[4], Francesc Teixidor[5], Clara Viñas[5] & Hugo Cerecetto*[,1,4]

CONFIDENC

5.7 Objetivos específicos

1- Estudio de la capacidad citotóxica por parte de los compuestos derivados de erlotinib en líneas celulares no ensayadas previamente y que poseen elevada expresión de EGFR.
2- Predicción a través de estudio teórico de propiedades tipo-fármaco.
3- Estudios *in vitro* de mutagenicidad para el compuesto líder.
4- Estudios *in vivo* de toxicidad aguda vía oral para el compuesto líder.
5- Preparación de distintas formulaciones como estrategia de solubilización de entidades poco solubles.

CONFIDENCIAL

5.8 Resultados y Discusión

5.8.1 Estudio de la capacidad citotóxica

Con el objetivo de seguir analizando el potencial de los agentes híbridos previamente desarrollados (Figura 52), se realizaron ensayos de citotoxicidad utilizando diferentes líneas celulares humanas que expresen EGFR. Por un lado, se realizó el estudio sobre la línea celular U87 MG (HTB-14 ™, ATCC®), células derivadas de gliomas malignos de *Homo sapiens* y que sobreexpresan EGFR. Por otro lado, también se incluyó HT-29 (HTB-38 ™, ATCC®), células derivadas de adenocarcinoma colorrectal de *Homo sapiens* y que poseen sobreexpresión de EGFR[134]. Esta última se incluyó como forma de evaluar una potencial estrategia de BNCT en otra patología tumoral.

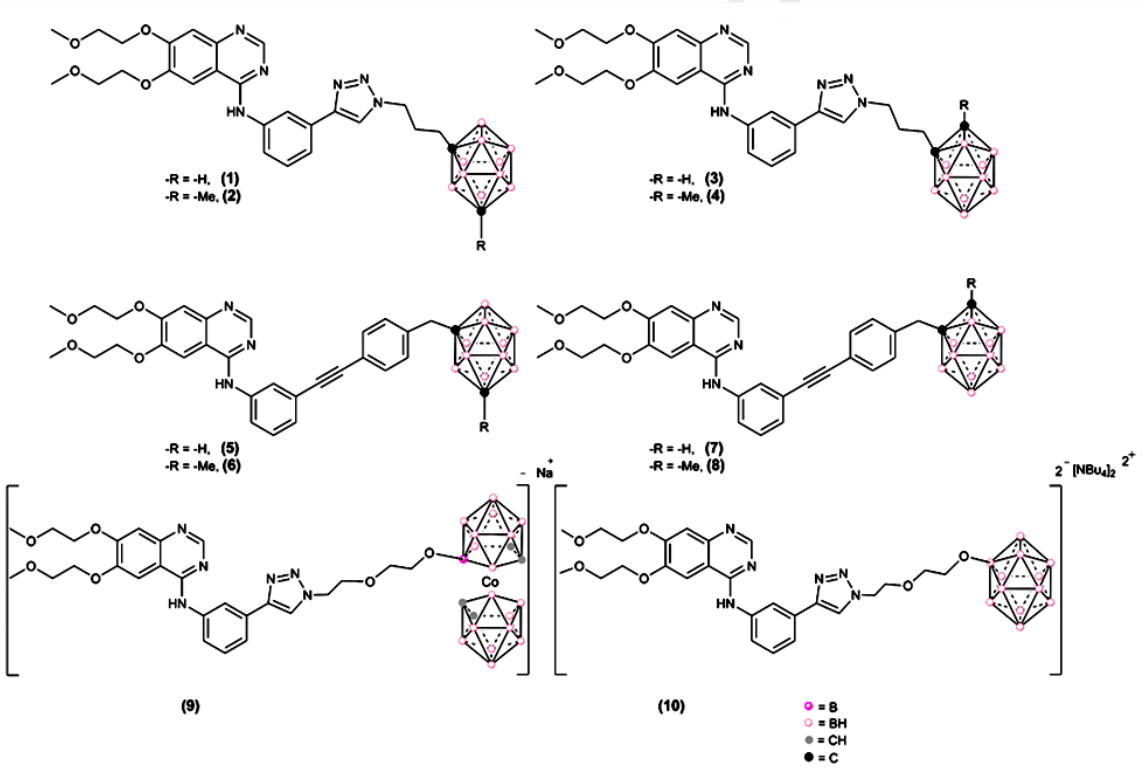


Figura 52. Derivados híbridos previamente desarrollados y seleccionados para su evaluación biológica

De la misma forma que sobre la línea celular C6, derivada de glioma de rata, los derivados **1**-**3** y **9** portando un conector [1,2,3]triazolilpropil, fueron los que presentaron mayor citotoxicidad, por ende los más activos en ambos sistemas celulares (Tabla 8). Por otro lado los derivados conteniendo el sistema benciletinil como conector, derivados **5**-**8**, fueron los menos activos.

Adicionalmente, se observó que tanto el isómero en cuestión como el patrón de sustitución en los carbonos del clúster adquieren un rol clave en la respuesta observada. Así, sobre la línea HT-29, los isómeros *meta*-carboranilo derivados **1** y **2**, fueron más activos que su isómero *orto*-carboranilo, compuestos **3** y **4** (Tabla 8). Esto podría deberse principalmente a la diferencia de los momentos dipolares y a la hidrofobicidad del fragmento *closo*-carboranilo, que depende en gran medida de la disposición relativa de los átomos de carbono en el icosaedro. La hidrofobicidad en el sistema *closo*-carboranilo aumenta en el siguiente orden: *orto* < *meta* < *para*. Por otro lado, la sustitución, en la posición *orto* o *meta*, es decir, los híbridos **2** y **4**, produjo una disminución de la citotoxicidad en células tumorales HT-29, en comparación con los análogos no sustituidos, **1** y **3**. Es interesante resaltar que el efecto que ejercen estas características estructurales que "decoran" el sistema de anilinoquinazolina también fue observado previamente en la línea celular C6 de glioma. Entre los derivados iónicos, el compuesto **9** fue el más activo en ambas líneas celulares que sobreexpresan EGFR. Sin embargo, a pesar de la actividad mostrada y el hecho de que puede depositar el doble de átomos de boro por molécula, no se realizaron ensayos adicionales debido al perfil de estabilidad y los parámetros de penetración de la BHE desfavorables, previamente descritos.

CONFIDENCIAL

Tabla 8. Actividad in vitro de los híbridos carboranil-anilinoquinazolina en líneas celular de glioma y cáncer colorrectal humanas

Compuesto	IC_{50}, U87 MG (μM)[a]	IC_{50}, HT-29 (μM)[a]
1	70.0	25.0
2	No evaluado	45.0
3	49.0	100.0
4	No evaluado	>100.0[b]
5	No evaluado	100.0
6	No evaluado	100.0
7	No evaluado	100.0
8	>100.0[b]	100.0
9	23.0	25.0
10	No evaluado	100.0
Erl	63	>100.0[b]

[a] Las concentraciones son las requeridas para inhibir el crecimiento celular en un 50 %. Valores determinados por triplicado a partir de curvas dosis respuesta y expresadas como el promedio. [b] Dosis superiores a 100 μM no fueron evaluados por baja solubilidad.

5.8.2 Estudio de propiedades tipo-fármaco

5.8.2.1 Predicción a través de estudios teóricos

En la etapa inicial del desarrollo del fármaco, el conocimiento de las propiedades de absorción, distribución, metabolismo, excreción y toxicidad (ADMETox) es relevante para la selección de posibles fármacos candidatos. En este mismo sentido, las predicciones teóricas de dichas propiedades podrían proporcionar ventajas claras y convincentes en la toma de decisiones para la correcta selección de moléculas a ser consideradas como candidatos a fármacos y a ser sometidas en estudios posteriores. En este trabajo se determinaron ciertos predictores farmacológicos para algunos de los híbridos previamente descritos mediante el kit de herramientas admetQSAR. Específicamente, el enfoque estuvo dirigido sobre la absorción intestinal humana (AIH)[135], la permeabilidad de Caco-2[136], la inhibición de la glicoproteína P (P-gp)[137,138], la inhibición del transportador de cationes orgánicos renales (OCT2)[139], la capacidad de ser un sustrato de CYP450[140], la inhibición del gen hERG (human ether-a-go-go-related gene)[141,142] y efectos carcinógenos[143]. Los compuestos **1**-**4**, **8** y **9** se compararon con el fármaco original erlotinib. Por otro lado, se determinó la solubilidad en medio acuoso (LogS)[144] debido a los problemas de solubilidad observados en los ensayos *in vitro*. Finalmente, utilizando el $LogD_{7.4}$ descrito anteriormente[145], se analizó el ajuste a las "regla de los cinco" de Lipinski y se determinó la afinidad de unión a EGFR a través del descriptor de eficiencia del ligando lipófilo[146] (ELL = pIC_{50} - LogD) para los derivados más promisorios, es decir, **1 9** y erlotinib.

Como se comentó anteriormente, uno de los desafíos más importantes al que se enfrenta un fármaco que será administrado vía oral es la absorción de la barrera epitelial a nivel del tracto gastrointestinal. En ese sentido, para la mayoría de los derivados el parámetro AIH predicho resultó en un valor positivo, indicando que podrían ser adsorbidos por el torrente sanguíneo (Tabla 9). Sin embargo, la permeabilidad a través de Caco-2 fue inferior a 8×10^{-6} cm/s para todos los híbridos analizados, sin encontrar diferencias según el tipo de subestructuras (Tabla 9). Este aspecto debe ser considerado en el momento de seleccionar la vía de administración del medicamento.

El transporte de fármacos mediado por P-gp, una familia de proteínas de unión a ATP, es otro de los parámetros ampliamente estudiados en las etapas iniciales del descubrimiento de fármacos. Estas proteínas están ampliamente distribuidas y expresadas en muchos órganos humanos; funcionan como bombas de eflujo en diferentes tejidos, entre ellos, epitelio intestinal, hepatocitos, células tubulares proximales renales, glándulas suprarrenales y capilares endoteliales del cerebro. Además, se ha demostrado que la sobreexpresión de P-gp genera fenotipos resistentes en varios tumores. De acuerdo con la predicción, todos los híbridos fueron

CONFIDENCIAL

sustrato potencial de la glicoproteína P sin capacidad de inhibición de esta (Tabla 9). Sin embargo, los derivados **2** y **4**, sustituidos con metilo y que pertenecen a derivados conteniendo el conector [1,2,3]triazolilpropil, al igual que erlotinib, se predijeron como inhibidores con uno de los métodos y podrían considerarse como una forma eficaz de sensibilizar la resistencia a los fármacos en la quimioterapia del cáncer (Tabla 9).

Tabla 9. Propiedades tipo-fármaco de los derivados estudiados.

Nº	Absorción				Metabolización	Toxicidad		LogS[h]	$LogD_{7.4}$[i]	"5 Reglas"	ELL[k]
	AIH[a]	Caco-2[b]	P-gp inh[c]	OCT2 inh[d]	CYP-subs[e]	hERG[f]	Carc[g]			n viol[j]	
1	(+)	(-)	(-)	(-)	CYP450 3A4	w-in[108] in[112]	(-)	-3.13	3.10	1[l]	5.54
2	(+)	(-)	(+)[137] (-)[138]	(-)	CYP450 3A4	w-in[141] in[142]	(-)	-3.23	-	1[l]	-
3	(+)	(-)	(-)	(-)	CYP450 3A4	w-in[141] in[142]	(-)	-3.13	-	1[l]	-
4	(+)	(-)	(+)[137] (-)[138]	(-)	CYP450 3A4	w-in[141] in[142]	(-)	-3.23	-	1[l]	-
8	(-)	(-)	(-)	(-)	CYP450 3A4	w-in[141] in[142]	(-)	-3.29	-	1[l]	-
9	(+)	(-)	(-)	(-)	CYP450 3A4	w-in[141] in[142]	(-)	-3.13	3.10	2[m]	4.02
Erl	(+)	(+)	(+)[137] (-)[138]	(-)	CYP450 3A4	w-in[141] sin[142]	(-)	-3.23	-	0	5.19

[a] Absorción intestinal humana; compuestos con AIH menor de 30 % se indican con (-), de otra forma se indican como (+)[135]. [b] Permeabilidad en Caco-2; compuestos con valor de permeabilidad alta ≥ 8×10^{-6} cm/s se indican como (+), de otra forma se indican como permeabilidad moderada o baja (-)[136]. [c] Inhibición glicoproteína-P; sin inhibición se indica (-) de otra forma se indica (+)[137,138]. [d] Inhibición del transportador renal de cationes orgánicos (OCT2); sin inhibición se indica (-), de otra forma se indica (+)[139]. [e] Sustrato de las tres isoenzimas de Cytocromo P450 (CYP450 2C9, CYP450 2D6, and CYP450 3A4); se indica la isoforma de CYP para la cual el compuesto es un potencial sustrato[140]. [f] Canal de potasio del gen relacionado con el éter-a-go-go (hERG) humano; según el grado de inhibición se indica como "sin", débil "w-in" e inhibidor "in" [141,142]. [g] Potencial carcinógeno; no carcinógeno se indica como (-)[143]. [h] Solubilidad en agua[144]. [i] Coeficiente de distribución a pH 7.4[145]. [j] Número de violaciones de las "5 reglas" Lipinski; [k] Eficiencia Lipofílica del ligando (pIC_{50} – $LogD_{7.4}$)[146]; [l] Masa molecular superior de 500 Da; [m] Masa molecular superior de 500 Da y aceptor de enlace de H mayor a 10.

En referencia a los procesos de eliminación de fármacos, los riñones desempeñan un papel clave en la eliminación de fármacos catiónicos. El transportador de cationes orgánicos de tipo 2 (OCT2) está involucrado en el paso inicial de la secreción renal en el túbulo proximal en el riñón. Varios medicamentos se han clasificado como sustrato o inhibidor de OCT2, lo que conduce a posibles interacciones entre medicamentos. Debido a la presencia de un sistema susceptible a la protonación como es el fragmento anilinoquinazolina en los compuestos estudiados, se evaluó el potencial de inhibición de OCT2. En ese sentido todos los híbridos y erlotinib se predijeron como inhibidores de la OCT2, lo que indica la posible ausencia de problemas de interacciones medicamentosas a nivel renal.

CONFIDENCIAL

En referencia a los procesos de metabolización, se analizó los híbridos como sustrato de las isoenzimas del citocromo P450 (CYP). Hoy en día, la metabolización por la superfamilia de CYP, junto con la P-gp, es la principal causa de reacciones adversas a los medicamentos que llevan a retirar los productos del mercado. En humanos, erlotinib es metabolizado en el hígado por los citocromos hepáticos, principalmente por CYP3A4 y en menor medida por CYP1A2. También contribuye potencialmente al aclaramiento metabólico de erlotinib, el metabolismo extrahepático por CYP3A4 en el intestino, CYP1A1 en pulmones y CYP1B1 en tejido tumoral. Los híbridos **1**-**4**, **8** y **9**, como erlotinib, se clasificaron como sustrato del CYP450 3A4, por lo que este aspecto debe considerarse cuando se seleccione la vía de administración.

Por otro lado, se estimó la capacidad que poseen los derivados de inhibir hERG y también como carcinógenos. En este sentido y de acuerdo a los métodos de predicción utilizados, los híbridos se clasificaron como inhibidores o inhibidores débiles de hERG mientras que el erlotinib fue predicho como no inhibidor por el método de Wang. Sin embargo, experimentalmente erlotinib se identificó como un inhibidor débil de hERG en comparación con otros inhibidores de tirosina quinasa. Por otro lado, los efectos carcinógenos se descartaron según la clasificación de Lagunin y colaboradores[143].

Otros propiedades predichas fueron mutagenicidad, frente a *Salmonella typhimurium y* la dosis letal 50 (DL_{50}), que es la toxicidad aguda en ratas por exposición oral. Los parámetros obtenidos para la mutagenicidad predicen que todos los derivados son no mutagénicos al igual que erlotinib. Adicionalmente la DL_{50} resultó ser mayor de 2000 mg/kg de peso corporal para todos los híbridos, y erlotinib[147], indicando ausencia de citotoxicidad.

Otro de los parámetros que se determinó es el LogS y la “regla de los cinco” de Lipinski, ambos se encuentran entre los filtros de propiedades farmacológicas más comunes en el proceso de desarrollo de un fármaco. Por esta razón, se predijo el LogS para todos los derivados obteniéndose valores en un rango adecuado pensando en compuestos candidatos a fármacos[148]. Específicamente, los híbridos **1** y **3** son más solubles en agua que erlotinib, lo que sugiere que podrían administrarse por vía oral o intravenosa. Como era de suponerse, se observaron variaciones en los valores de LogS debido a diferentes características estructurales, por ejemplo, el sustituyente metilo o el conector benciletinil, reduce la solubilidad en agua de los compuestos que portan estos agrupamientos (Tabla 9). En referencia a la "regla de cinco", a diferencia de erlotinib, los híbridos **1**-**4**, **8** y **9** poseen un masa molecular superior a 500 Da. Además, el híbrido **9** tiene un número de aceptadores de enlaces de hidrógeno, según la definición de Lipinski, superior a 10.

Finalmente, se determinó el descriptor ELL (Eficiencia Lipofílica del ligando) utilizando valores de $LogD_{7.4}$ previamente descritos para los derivados **1**, **9** y erlotinib[145]. El ELL es un índice

CONFIDENCIAL

simple pero relevante (ELL = pIC_{50} - $LogD_{7.4}$) que combina la potencia *in vitro* y la lipofilicidad. Estima la eficacia de una interacción de unión con respecto a la magnitud de las propiedades físicas del ligando siendo un valor ideal de LEE entre 5-7 unidades para un candidato a fármaco optimizado[149]. Entre los compuestos evaluados, se destacó el derivado **1**, con mejor comportamiento que el fármaco padre erlotinib y el híbrido **9**.

5.8.3 Estudios *in vitro* de mutagenicidad y estudios *in vivo* de toxicidad aguda vía oral.

Con la finalidad de obtener mayor información sobre la potencialidad del híbrido **1** como candidato a fármaco, se llevaron a cabo estudios experimentales relacionados con la toxicidad. Se centró la atención en algunos de las recomendaciones de la O.E.C.D, específicamente se exploró la genotoxicidad *in vitro* (mutagenicidad) a través de test de Ames y la toxicidad aguda vía oral (DL_{50}) a través de un ensayo *in vivo*. El estudio de la aparición de revertantes de bacterias Salmonella thyphimurium His^- (test de Ames) frente a la administración de un compuesto permite determinar la capacidad mutagénica del mismo. En esa sentido, el híbrido **1** resultó ser no mutagénico, tanto en presencia (10% mezcla S9) como ausencia de activación metabólica S9 (0% mezcla S9) (Figura 53) ya que no se observó dosis-respuesta en un amplio rango de dosis evaluadas y además en todos los casos el número de colonias revertantes fue dos veces inferior a los valores naturalmente producidos por el vehículo control (Figura 53). La dosis máxima se determinó de acuerdo a la solubilidad de cada compuesto y teniendo en cuenta que no fuese tóxico para las bacterias. En cada ensayo se incluyó un control negativo (DMSO) y un control positivo en el cual las bacterias se cultivaron en presencia del mutágeno 4-nitro-o-fenilendiamina (NPD, sin activación metabólica) o 2-aminofluoreno (2-AF, con activación metabólica).

En referencia a la toxicidad oral *in vivo*, se aplicó la "prueba límite" recomendada por O.E.C.D.[150]. La Tabla 10 resume los resultados de los análisis realizados que muestran el perfil de seguridad del híbrido **1**.

Además, los resultados experimentales observados para ambas propiedades para el híbrido **1** son concordantes con los parámetros predichos, lo que convierte a este derivado como un potencial candidato para estudios adicionales.

CONFIDENCIAL

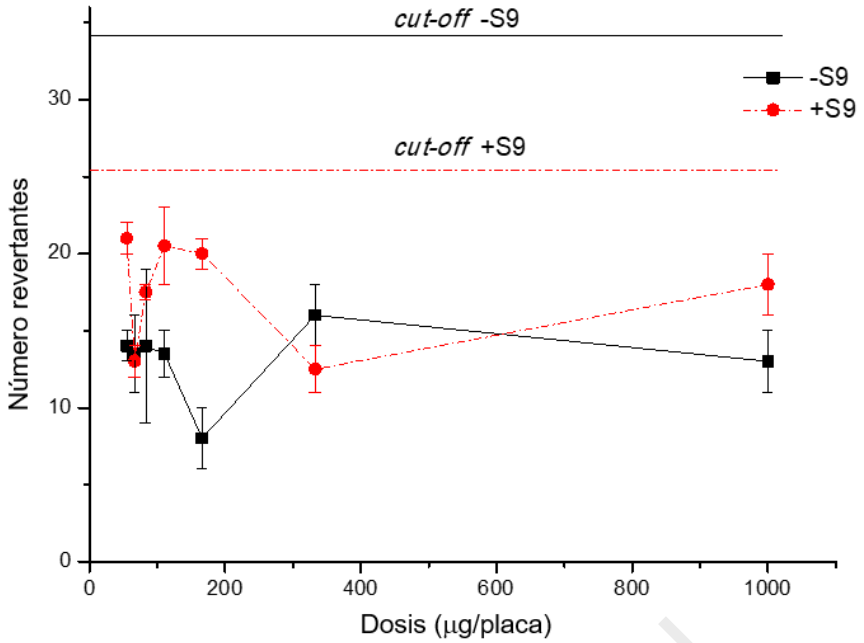


*Figura 53. Número de revertantes en Salmonella typhimurium cepa TA98 para el híbrido **1** a diferentes dosis, con (+S9) y sin (-S9) activación metabólica. El "cut-off" se define como el doble de revertantes naturales producidas por el vehículo control (DMSO).*

*Tabla 10. Toxicidad oral aguda para híbrido **1**.*

Vía de administración	Vehículo	DL_{50} (mg/kg bw)	Test de Irwin[a,b]	Observación de necropsias[c]
Oral	solución salina:Tween 80 (4:1)[d]	> 2000	(+)	(-)

[a] De acuerdo con [151]. [b] El test fue realizado a 0.5, 1.5, 3, 5, 12, 24, 48, and 72 h luego de la administración de la dosis. Si todos los parámetros analizados fueron similares al tratamiento con disolución salina se indica como (+), de otra forma se indica como (-). [c] (-) denota ausencia de alteraciones o presencia de adherencias en los órganos estudiados. [d] DMSO (4 %) fue añadido para la completa solubilización de **1**.

CONFIDENCIAL

5.8.4 Formulaciones como estrategia de solubilización de entidades poco solubles.

Debido a que algunos de los derivados híbridos presentaron notorios problemas de solubilidad en los ensayos *in vitro*, por ejemplo el derivado **8** así como también el erlotinib (ver arriba nota de Tabla 10) se decidió analizar diferentes estrategias de formulación, entre ellas micelas poliméricas (PM) y liposomas, con el objetivo de mejorar los perfiles de solubilización[152]. Como primera aproximación se ensayaron sistemas poliméricos, combinando para ello los co-polímeros del bloque Plurónico, Pluronic® F127 (hidrófilo) y L121 (hidrófobo) o los hidrofílicos Pluronic® F127 y Tetronic® T1307[153,154]. En primer lugar, para estudiar estas PM, se seleccionó el híbrido insoluble **8** y se cargó en el sistema F127/L121 generando una formulación con un tamaño de partícula homogéneo y adecuado (Tabla 11). Sin embargo, de manera similar a lo descrito para con otras líneas celulares[155], la citotoxicidad *per ser* de las

micelas F127/L121 determinó no seguir trabajando con este sistema en los siguientes ensayos. A raíz de esto, se procedió a cargar el híbrido **8** en el sistema PM F127/T1307. Interesantemente, el resultado confirmó que la falta de citotoxicidad por parte de **8** no está relacionada con la pobre solubilidad en agua de dicho compuesto (Tabla 12) pudiendo adjudicar dicho comportamiento al mero hecho estructural de la entidad química.

Para el híbrido **1** y erlotinib, se ensayó directamente la formulación MP F127/T1307. Esta formulación mejoró la bioactividad de erlotinib contra las células U87 MG (Tabla 11), mostrando un incremento en la solubilidad en el medio en donde se realizó el bioensayo. Por otro lado la nanovehiculización de **1** produjo dos poblaciones de partículas que resultaron tener cierto grado de polidispersión (Tabla 11) y con potenciales zeta ligeramente negativos. Asimismo, no se observaron diferencias significativas en la bioactividad en los sistemas biológicos evaluados (Tabla 12).

Cuando se utilizaron liposomas como vehículo, la formulación obtenida para el híbrido **1** presentó baja polidispersión (Tabla 11) del mismo modo que para el erlotinib. Esta formulación mejoró la actividad de **1** en ambas líneas celulares y, para erlotinib, como en el caso de los sistemas PM, la citotoxicidad contra las células de glioblastoma U87 MG aumentó (Tabla 11).

*Tabla 11. Caracterización de las formulaciones realizadas para los híbridos **1** y **8**.*

Nano-vehículo	Compuesto[a]	T (K)	Pico 1		Pico 2		IPD[c]
			D_h (nm)[b]	%	D_h (nm)[b]	%	
F127/L121	-	298	44 2.3±18.7	100	-	-	0.252±0.029
		310	340.3±6.3		-	-	0.172±0.012
	8	298	359.5±14.2		-	-	0.234±0.020
		310	322.1±4.0		-	-	0.207±0.006
F127/T1307	-	298	57.38±1.83	70.3±0.9	1537±263	29.7±2.3	0.530±0.028
	1		57.10±1.83	14.8±2.6	1346±253	86.2±9.3	0.865±0.292
Liposoma	-	298	261.8±14.1		-	-	0.490±0.034
	1	298	321.6±0.3	100	-	-	0.280±0.009
		310	323.4±4.5		-	-	0.269±0.002

[a] Concentración de 1mg/mL; [b] Tamaño de partícula; [c] Índice de polidispersión

Tabla 12. Estudios de citotoxicidad para las formulaciones realizadas en líneas celulares C6 y U87 MG.

Compuesto	**Sin vehículo**		**F127/T1307**		**Liposoma**	
	$IC_{50,C6}$[a,b]	$IC_{50,U87\ MG}$[a,c]	$IC_{50,C6}$[a]	$IC_{50,U87\ MG}$[a]	$IC_{50,C6}$[a]	$IC_{50,U87\ MG}$[a]
1	30.0	70.0	7.0	>100.0	14.0	< 6.25[d]
8	>100.0[e]	>100.0[f]	>100.0[e]	NE[g]	NE	NE
Erl	>100.0[f]	63	>100.0[e]	NE	>100.0[e]	17.0

[a] Las concentraciones son las requeridas para inhibir el crecimiento celular en un 50 % (μM). Valores determinados por triplicado a partir de curvas dosis respuesta y expresadas como el promedio. [b] Extraído de tabla 2[155]. [c] Extraído de tabla 8. [d] Dosis mínimas evaluadas. [e] Dosis máximas evaluadas. [f] Dosis superiores a 100 μM no fueron evaluadas por problemas de solubilidad. [g] NE, no estudiado

CONFIDENCIAL

5.9 Conclusiones

Previamente se demostró que el derivado **1** posee capacidad de inhibir la forma salvaje de EGFR en el rango nanomolar. Esto, conjuntamente con los excelentes resultados de citotoxicidad *in vitro* sobre diferentes líneas celulares de mamíferos que también sobreexpresan EGFR, abre la posibilidad de nuevas dianas para las aplicaciones mediante BNCT. Además el híbrido **1** cumple con muchas propiedades farmacológicas favorables entre las que se destacan, la ausencia de toxicidad, la adecuada solubilidad en agua y la eficiencia del ligando lipófilo (LLE). En referencia a esto, **1** ha sido el ligando más eficiente dentro de los derivados estudiados y también en base a lo descrito en la literatura para otros inhibidores de EGFR[156]. Por otro lado y en base a los estudios predictivos relacionado con la permeabilidad de Caco-2, se reveló que el derivado **1** podría presentar ciertos problemas de absorción cuando es administrado vía oral. Además, debido a la falta de inhibición de P-gp podría esperarse cierto grado de resistencia a fármacos, algo que podría minimizarse con las formulaciones analizadas[157,158]. Por último algo altamente relevante es que el derivado **1** cumple con los requisitos iniciales de la O.E.C.D. en relación a la ausencia de mutagenicidad y baja toxicidad oral aguda.

CONFIDENCIAL

6 Capítulo II

Serie derivada de Sunitinib

Artículo IV.

(MANUSCRITO EN PREPARACIÓN)

CONFIDENCIAL

6.1 Objetivos específicos

1- Conjugación de precursores de *closo*-carborano y metalacarborano COSANE con el inhibidor sunitinib y caracterización fisicoquímica.
2- Evaluación biológica *in vitro* de los productos desarrollados en el punto 1 sobre líneas celulares, U87 MG, C6 y HT-29.
3- Estudio de selectividad sobre células normales.
4- Estudio de la capacidad inhibitoria sobre un panel de tirosina quinasas del híbrido más relevante.
5- Estudio de citotoxicidad *in vitro* en co-cultivo celular y estudio del tipo de muerte asociada.
6- Estudios teóricos y experimentales de propiedades “tipo-fármaco” del híbrido más relevante.
7- Estudios de mutagenicidad del híbrido más relevante.
8- Estudios de capacidad de atravesar la BHE del híbrido más relevante.
9- Estudios *in vivo* en ratones inmunosuprimidos portando tumores derivados de U87 MG del híbrido más relevante.
10- Prueba de concepto *in vitro* de politerapia temozolomida-híbrido más relevante.

CONFIDENCIAL

6.2 Resultados y Discusión.

6.2.1 Síntesis de intermedios e híbridos.

Inicialmente el inhibidor de tirosina quinasa sunitinib fue regio-selectivamente modificado a través de la incorporación de un fragmento propargilo a nivel del nitrógeno del heterociclo oxo-indol. Esta modificación permitió en una etapa posterior realizar la incorporación de los diferentes clústeres de boro a través de dos procesos: por un lado cicloadición 1-3 dipolar (*click reaction*) y por otro, reacción de *cross-coupling* Sonogashira (Figura 54).

Si bien está establecido en la literatura que el agrupamiento oxo-indol desempeña un rol clave en los procesos de unión a proteína[159,160], de acuerdo a la experiencia previa con los híbridos erlotinib-carborano, los clústeres de boro podrían establecer interacciones adicionales y en ciertas circunstancias, beneficiosas con las biomoléculas diana. Entre éstas, se destacan las interacciones especiales como los enlaces de di-hidrógeno no clásicos BH ⋯ HX (X = N, C, O y S), interacciones por puente de hidrógeno y enlaces de hidrógeno BH ⋯ π y CH ⋯ π. La primera aproximación consistió en preparar derivados del clúster carborano portando en su estructura el agrupamiento azida (intermedios **C**, **D**, **H** y **G,** Figura 54). De esta forma, se generó en una etapa posterior a través de una reacción de cicloadición 1,3-dipolar, "*click reaction*", los correspondientes híbridos **1**, **2**, **3**, y **4** (Figura 54) con buenos rendimientos (artículo IV, Material Suplementario). Los intermedios **K**, **L**, **M** y **N** portando un fragmento iodobencil-carborano, en sus variantes R= -H, -Me así como *orto*- y *meta*-isómeros, fueron preparados como forma de introducir quimiodiversidad en los híbridos resultantes y así poder extraer información relacionada con la estructura-bioactividad. De esta forma se generó vía *Sonogashira cross-coupling* los compuestos **6**, **7**, **8**, y **9** (Figura 54) con rendimientos moderados (artículo IV, Material Suplementario). Otro *clúster* de alto contenido de boro seleccionado en esta etapa para ser conjugado al sunitinib es el metalacarborano COSANE, **5**. Éste fue preparado de acuerdo a lo descrito en la literatura[122] (Figura 54). El híbrido **5** se generó con muy buen rendimiento (artículo IV, Material Suplementario) tras la reacción de cicloadición.

Todos los compuestos preparados se caracterizaron mediante espectroscopia de RMN de ^{1}H, ^{11}B y ^{13}C, así como espectrometría de masas mediante impacto electrónico y análisis elemental (artículo IV, Material Suplementario).

CONFIDENCIAL

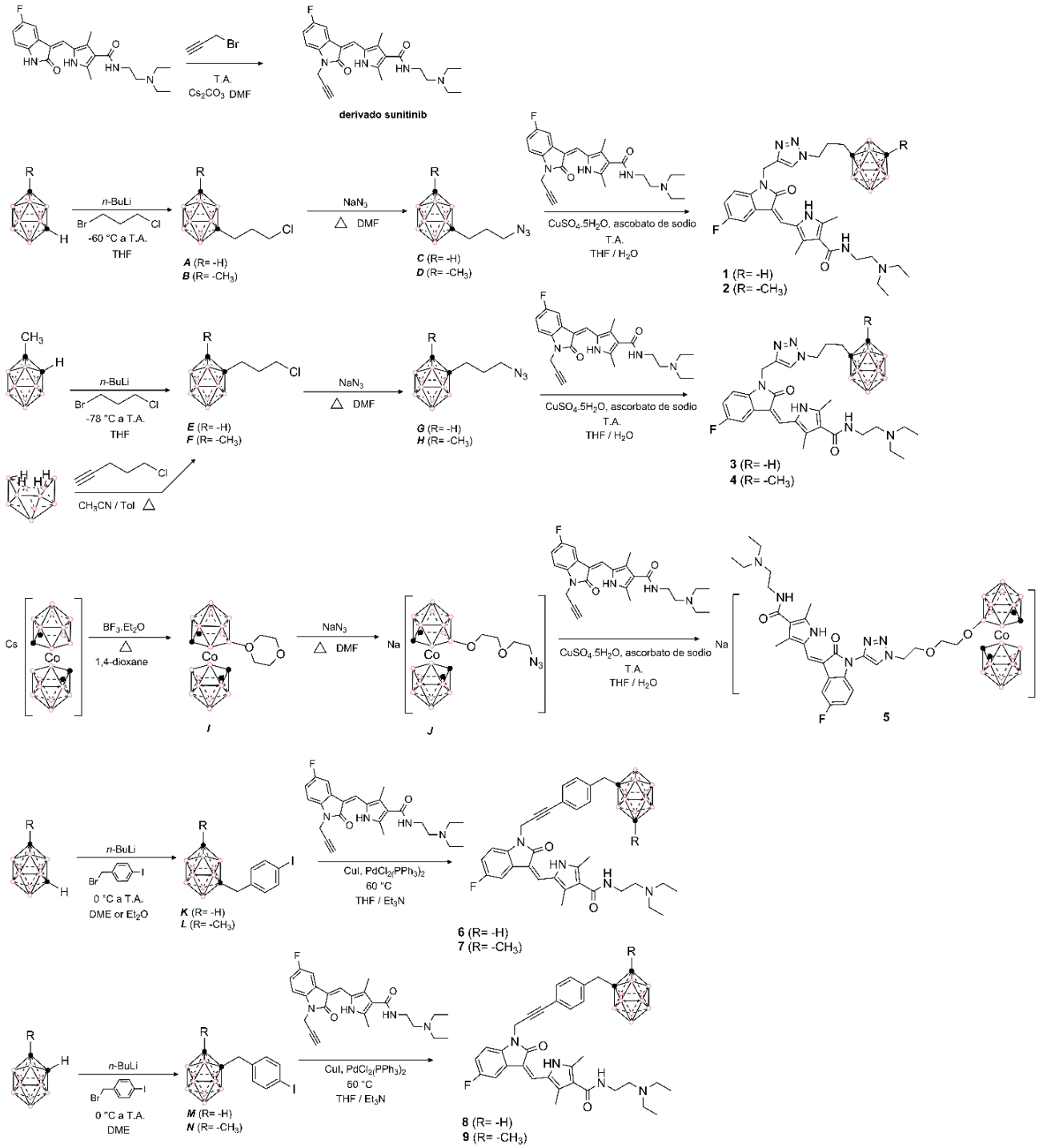


*Figura 54. Procedimientos sintéticos para la preparación de las entidades híbridas **1**-**9**.*

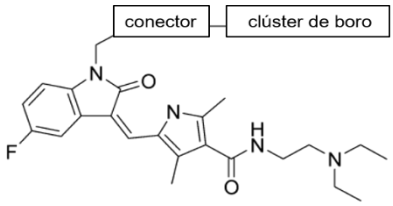
6.2.2 Evaluación biológica *in vitro*.

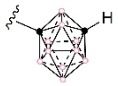
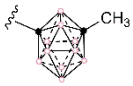
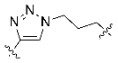
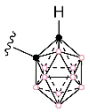
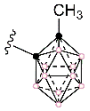
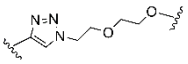
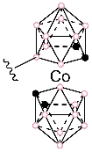
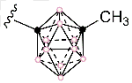
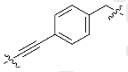
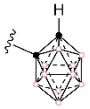
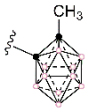
6.2.2.1 Estudios de citotoxicidad sobre cultivos celulares U87 MG, C6 y HT-29.

Los compuestos sintetizados se evaluaron *in vitro* en una primera instancia en las líneas celulares de glioma U87 MG (línea celular humana) y C6 (línea celular murina). Los derivados **1**, **2** y **4**, que portan el sistema [1,2,3]triazolilpropil como conector, se identificaron como los agentes anti-glioblastoma más promisorios (Tabla 13). Además, los compuestos **1**, **2** y **4** también mostraron ser potentes inhibidores del crecimiento de las líneas celulares HT-29 (Tabla 13), una línea celular tumoral humana que sobreexpresa proteínas con actividad tirosina quinasa[134]. Al igual que se observó para los híbridos pertenecientes a la serie erlotinib-carborano, los resultados biológicos más promisorios para la familia actual de compuestos se observan cuando el conector es el sistema [1,2,3]triazolilpropil (Tabla 13). Por otro lado, aquellos derivados con el conector benciletinil mostraron actividad inferior o nula. Este comportamiento podría atribuirse a la diferencia que existe entre las lipofilia (expresado como R_M, Figura 55), siendo el compuesto **1** el derivado que presentó el mejor valor (mínimo de la cuadrática) para un conjunto de compuestos estudiados en las tres líneas celulares en cuestión. Al igual que para la serie de erlotinib, dentro de la serie de derivados que portan el conector [1,2,3]triazolilpropil, el sistema 1,7-dicarba-*closo*-dodecarboran-1-ilo, por ejemplo el derivado **1**, resultó ser el mejor inhibidor celular en las tres líneas tumorales estudiadas. Sin embargo, a diferencia de los resultados anteriores, el derivado que porta el sistema metalacarborano COSANE, **5**, no resultó activo en las condiciones analizadas. Asimismo, el compuesto **1**, además de ser un mejor inhibidor del crecimiento celular que los inhibidores del receptor de tirosina quinasa erlotinib y lapatinib (Lap), fue al menos cuatro veces más activo contra las células de glioblastoma U87 MG que el compuesto original sunitinib (Tabla 13) y 12 veces más activo contra U87 MG que el agente alquilante temozolomida (Tmz), agente terapéutico de referencia en GBM[161].

CONFIDENCIAL

*Tabla13. Estructuras y actividad in vitro de los compuestos **1**-**9** expresada como IC_{50} (μM) o el porcentaje de supervivencia celular a 100 μM frente a células C6, U87 MG y HT-29.*



Compuesto	Conector	Clúster de boro	$IC_{50,C6}$ (μM)[a]	$IC_{50,U87MG}$ (μM)[a]	$IC_{50,HT-29}$ (μM) [a,b]
1			**6.9 ± 0.5**	**8.0 ± 0.3**	**< 6.25 (0.45 ± 0.04 %)**
2			**5.2 ± 0.5**	**8.0 ± 0.4**	**< 6.25 (0.79 ± 0.01 %)**
3			**78.3 ± 0.8**	**> 100 (95 ± 5 %)**	**> 100 (34 ± 5 %)**
4			**4.4 ± 0.5**	**8.0 ± 0.5**	**< 6.25 (0.63 ± 0.03 %)**
5[b]			**> 100 (100 ± 5 %)**	**> 100 (100 ± 4 %)**	**100 ± 5**
6			**> 100 (65 ± 5 %)**	**> 100 (100 ± 5 %)**	**45 ± 4**
7			**> 100 (100 ± 5 %)**	**> 100 (64 ± 4 %)**	**40 ± 6**
8			**80 ± 4**	**> 100 (100 ± 5 %)**	**> 100 (40 ± 5 %)**
9			**30 ± 5**	**> 100 (94 ± 6 %)**	**94 ± 7**
Sun	-	-	**36 ± 10**	**32 ± 4**	**6.25 ± 0.04**
A[d]	-	-	**30 ± 5**	**70 ± 5**	**25.0 ± 5.0**
Erl	-	-	**> 100**	**63 ± 5**	**> 100**[d]
gLap	-	-	**54 ± 14**	**> 100 (89 ± 5 %)**	**6.25 ± 0.05**
Tmz	-	-	***ns***[c]	**> 100**	**-**

[a] Valores en paréntesis refieren al porcentaje de supervivencia celualr a 100 μM. [b] Como sal de sodio. [c] No estudiado. [d] **A** refiere al derivado **1** de la serie del erlotinib (Figura 42 y 52).

CONFIDENCIAL

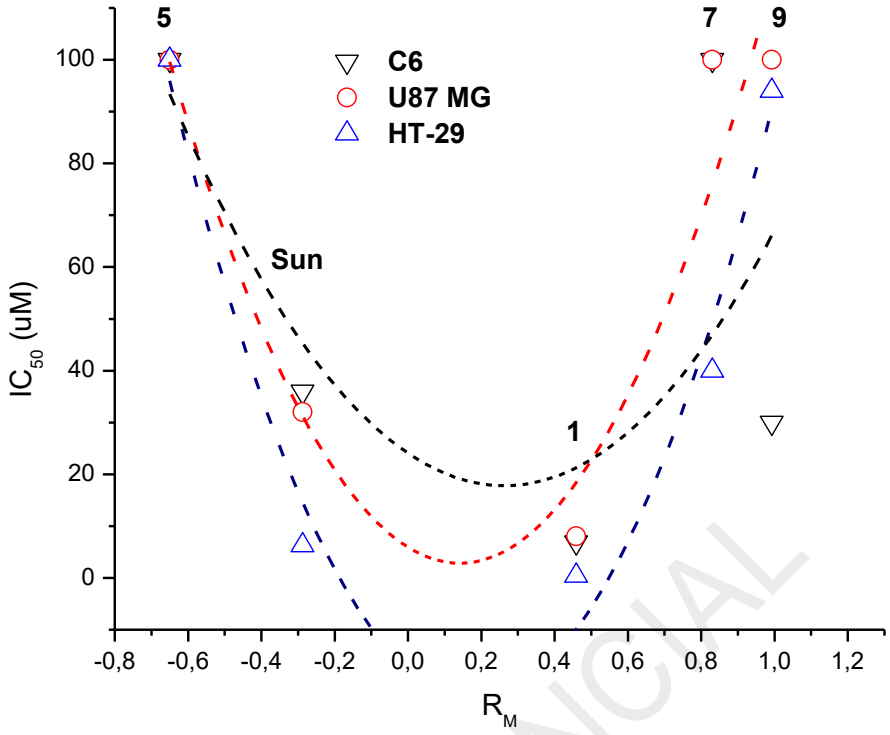


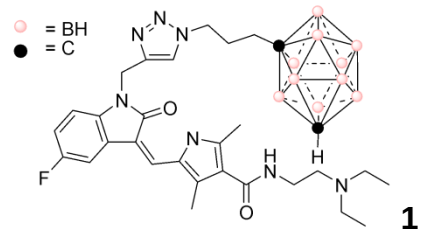
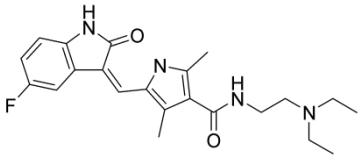
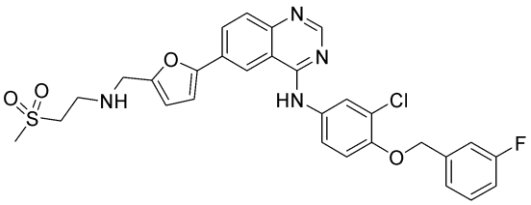
*Figura 55. Relación IC_{50} y lipofilicidad (expresada en términos de RM) para el derivado **5, 1, 7, 9 y sunitinib.***

CONFIDENCIAL

6.2.2.2 Estudios de selectividad frente a células normales.

Por otro lado, el compuesto **1** se evaluó frente a células gliales normales, astrocitos, (Tabla 14), para determinar si este compuesto destruía selectivamente las células tumorales, sin tener efectos citotóxicos en las células cerebrales normales. Los resultados mostraron que el compuesto **1**, independientemente de no mostrar selectividad para las líneas celulares de glioma C6 y U87 MG en relación a las células normales astrocíticas, resultó poseer el mismo o mejor índice de selectividad en comparación con el compuesto de partida sunitinib y con otro fármaco utilizado como inhibidor de proteína tirosina quinasa como lo es el lapatinib (Tabla 14). Además, a diferencia del lapatinib el compuesto **1** y el sunitinib, mostraron valores de IC_{50} similar tanto en las células normales como en las líneas celulares tumorales.

Tabla 14. Actividad biológica in vitro de compuestos estudiados contra astrocitos.

Compuesto	$IC_{50,astrocitos}$ (μM)[a]	Índice de selectividad	
		C6	U87 MG
 **1**	**4.7 ± 0.6**	**0.7**	**0.6**
 **Sun**	**20 ± 4**	**0.6**	**0.6**
 **Lap**	**8 ± 3**	**0.15**	**< 0.08**

[a] Las concentraciones para inhibir el crecimiento al 50 % fueron determinadas a través de curvas dosis respuesta y se representan como la media ± s.d. Todos los experimentos fueron repetidos al menos tres veces.

CONFIDENCIAL

6.2.2.3 Estudios de mecanismo de acción

Con el fin de indagar la capacidad de inhibición de proteínas con actividad tirosina quinasa para el compuesto más relevante, derivado **1**, se realizó un ensayo cuantitativo de unión competitiva a 10 μM, a través de cribado masivo "high-throughput" contra un panel de 460 quinasas humanas y ciertas variantes mutantes relevantes (KINOMEscan®). El derivado **1** presentó una gran actividad contra 33 de los 460 dianas analizados (Figura 56a y Tabla S3 en Material Suplementario, artículo IV), con un índice "score" de selectividad "*S(35)*", de 0.047 (Tabla 14). Dicho score se calcula dividiendo el número de quinasas a las que se unen los compuestos por el número total de quinasas distintas analizadas, excluyendo las variantes mutantes. Al igual que sunitinib, el híbrido **1** mostró propiedades de inhibición frente a FLT3, PDGFR-α y -β, KIT, CSF1R y VEGFR2. El compuesto **1** se identificó como un inhibidor de múltiples tirosina quinasas, pero a diferencia de sunitinib (Figura 56b) es selectivo contra algunos sistemas biológicos específicos. Específicamente, la mejor capacidad de inhibición del compuesto **1** fue contra la mutación de duplicación en tándem interna FLT3 del residuo gatekeeper F691 (FLT3-ITD, F691L) involucrado, entre otros, en la leucemia mieloide aguda[162]. En segundo lugar, **1** inhibió en muy buen nivel PDGFR-β y las mutaciones que ocurren en el exón 11 del gen KIT

que codifica el dominio yuxtamembrana (V559D y L576P) involucrado, entre otros, en tumores del estroma gastrointestinal[163].

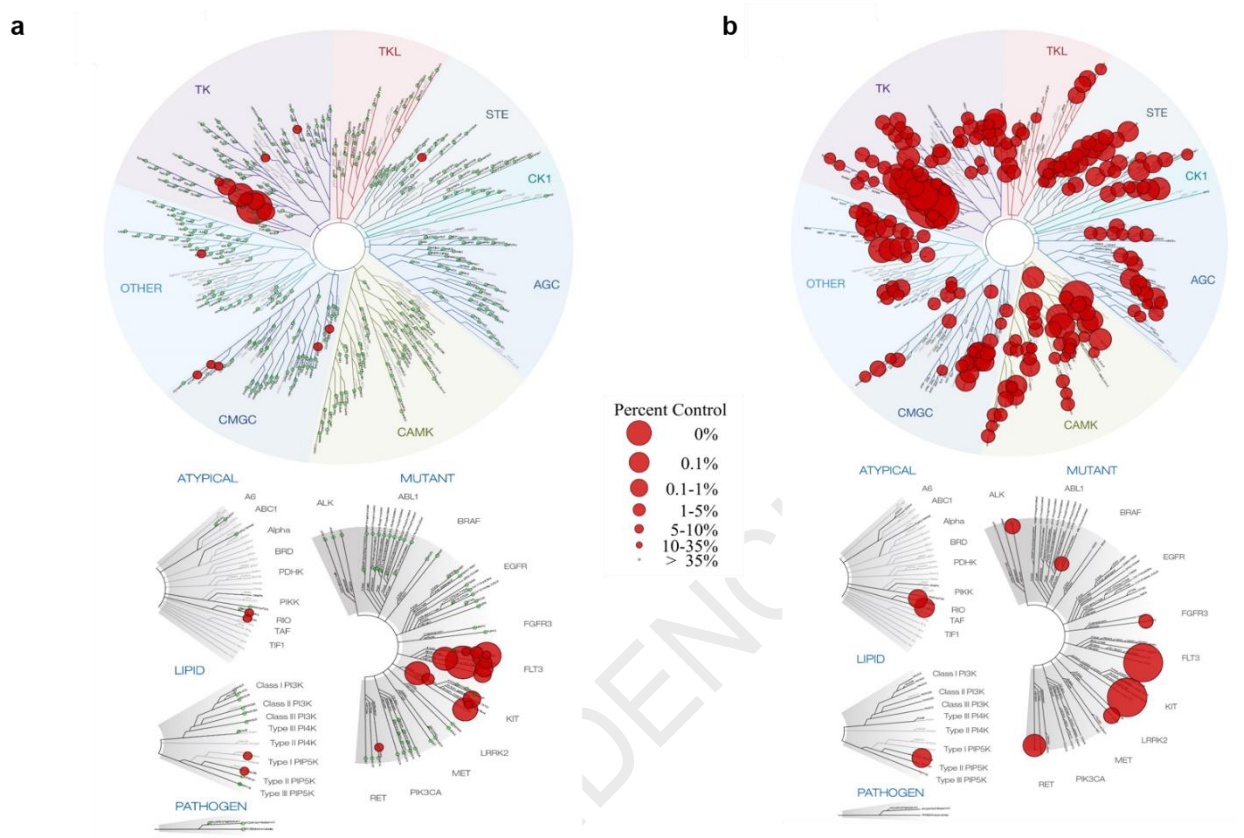


*Figura 56. Perfil de selectividad del compuesto **1** (a) y sunitinib (b) contra 460 proteínas humanas con actividad quinasas. Las afinidades de unión relativas se indican mediante círculos rojos en el árbol filogenético de kinoma para enzimas de tipo salvaje (arriba) y variantes atípicas / mutantes / lipo / patógenas (abajo). El tamaño de los círculos rojos es proporcional a la fuerza de la unión, los círculos más grandes indican una mayor afinidad. Imagen generada con la herramienta de software TREEspot™ y reimpresa con permiso de KINOMEscan®, una división de DiscoveRx Corporation, © DISCOVERX CORPORATION 2010.*

*Tabla 14. Índices de selectividad para el derivado **1** evaluado a 10 µM.*

Tipo de Índice de selectividad	Número de Hits	Número de kinasas no-mutante	Índice de selectividad
S(35)	19	403	0.047
S(10)	6	403	0.015
S(1)	2	403	0.005

6.2.2.4 Estudios de citotoxicidad in vitro en co-cultivo celular y del tipo de muerte celular asociada.

Con el objetivo de indagar el comportamiento del derivado **1,** y también del compuesto "padre" sunitinib, en condiciones similares a las del microambiente tumoral, la línea celular U87 MG se co-cultivó con astrocitos. Ambas entidades se incubaron a las dosis de IC_{50} durante 24 horas (artículo IV, Material Suplementario). Como se puede observar en las imágenes generadas a través de microscopía confocal (Figura 57), se revelaron perfiles notoriamente diferentes en cada uno de los experimentos ensayados. Por un lado, el cultivo sometido a la sonda PKH26, marcador fluorescente de membrana (intercalante) en U87 MG, mostró la disminución de dicha población tras el tratamiento con el derivado **1**, en comparación con las condiciones de cultivo control, es decir células sin tratamiento. Por otro lado con la sonda fluorescente M2, la cual se utiliza para el marcaje de membrana de astrocitos se observó un hecho negativo, ya que el compuesto **1** fue capaz de abolir la presencia de los mismos, presentes en altos porcentajes en el control, mientras que sunitinib presentó un comportamiento intermedio. De forma similar, según la sonda fluorescente GFAP, la cual da indicios de la activación de astroglia, se observó que la población de astrocitos asociados a tumores, presentes en el control y principalmente en el sistema incubado con sunitinib, no estaba presente en el co-cultivo tratado con el compuesto **1**. Además, al comparar la tinción GFAP de las células tratadas con sunitinib y las células de control, fue posible observar que sunitinb hizo que la población astrocitica se activara, como lo indica el aumento de la señal GFAP. Finalmente, la tinción de los núcleos mediante DAPI mostró una notoria condensación de cromatina en el tratamiento con sunitinib y de forma similar para el compuesto **1**, lo que podría estar asociado con el inicio del proceso de apoptosis.

CONFIDENCIAL

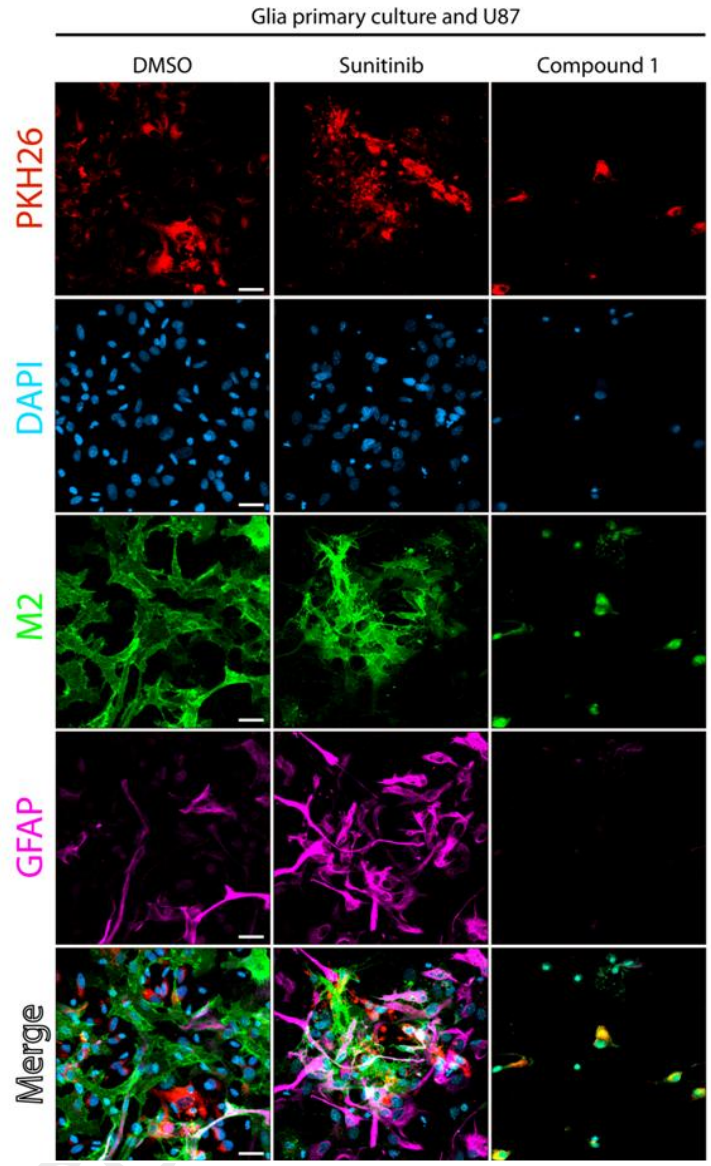


*Figura 57. Microscopias de fluorescencia de astrocitos co-cultivados con U87 MG y tratados con sunitinib, **1** o con DMSO como control durante 24 h. Las sondas utilizadas: PKH26 marcador de la membrana celular U87-MG, DAPI marcador de núcleo, M2 marcador de la membrana celular de astrocitos y GFAP marcador de activación de astrocitos,*

Seguidamente se abordó el estudio del mecanismo de muerte celular inducido por el compuesto **1** sobre la línea U87 MG. Para ello se realizaron ensayos de citometría de flujo para determinar la vía de muerte de las células U87-MG tras el tratamiento con dicho compuesto. Nuevamente, con el objetivo de simular las condiciones de microambiente tumoral en desarrollo, U87 MG se co-cultivó con una población de astrocitos. Estas células co-cultivadas se incubaron con **1**, sunitinib o DMSO (control), de forma independiente y a las correspondientes dosis de IC_{50} en U87 MG (Material Suplementario, artículo IV). Los ensayos experimentales de citometría mostraron que tanto para el compuesto **1** como el sunitinib, se produjo la muerte celular de la línea U87 MG principalmente a través de apoptosis (Figura 58).

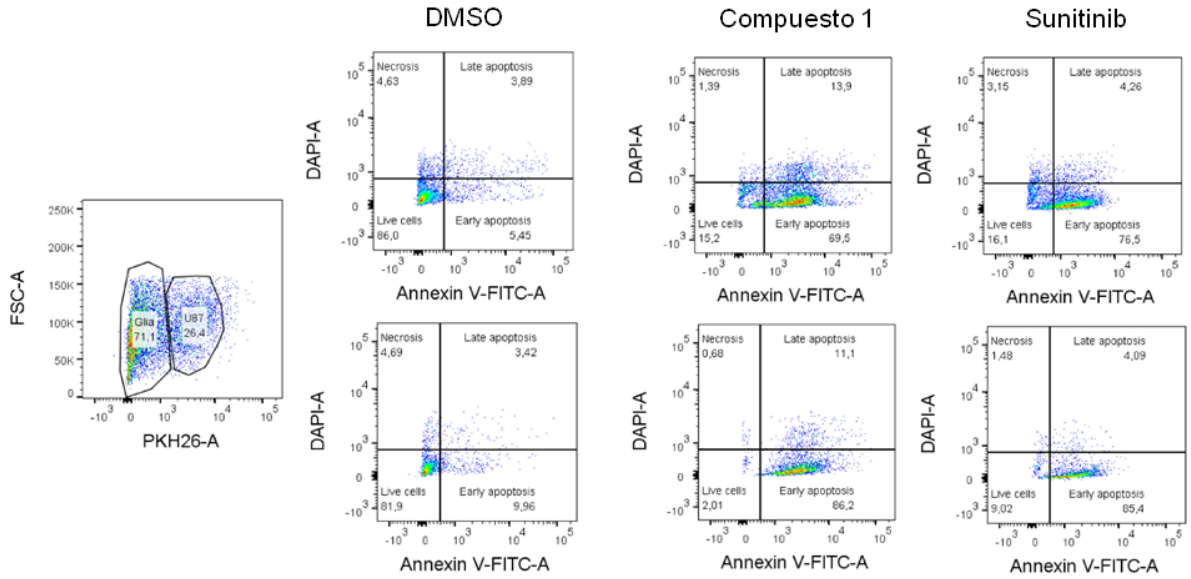


*Figura 58. Resultados de citrometría de flujo de astrocitos co-cultivados con U87 MG y tratados durante 24h con sunitinib, **1** o con DMSO como control.*

Adicionalmente, se midió el colapso del potencial de membrana mitocondrial, ΔΨm, asociado a los procesos apoptóticos[164]. Los resultados obtenidos concuerdan con lo observado mediante citometría de flujo, indicando que las células U87 MG mueren a través de un mecanismo apoptótico cuando se tratan con el compuesto **1** o sunitinib (Figura 59).

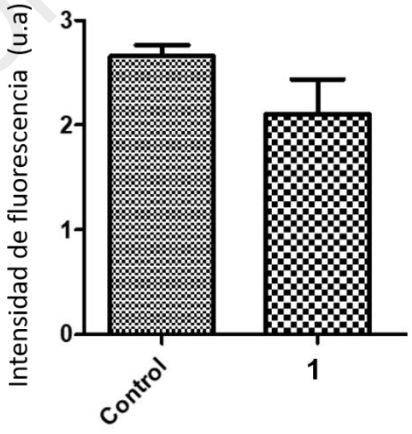


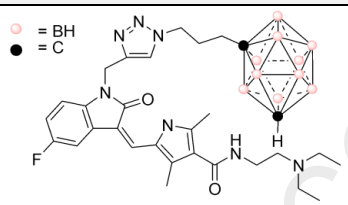
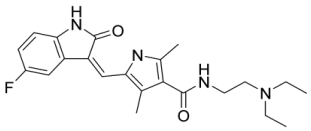
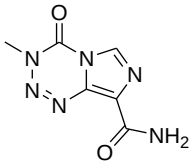
*Figura 59. Colapso del potencial de membrana mitocondrial ($\Delta\Psi m$) para el compuesto **1**.*

CONFIDENCIAL

6.2.2.5 Estudios teóricos y experimentales de propiedades "tipo-fármaco".

Inicialmente se predijeron ciertas propiedades tipo-fármaco relevantes en el desarrollo de medicamentos[165] (Tabla 15) tanto para el derivado **1** como para el sunitnib y la temozolomida. Por un lado, **1** mostró ausencia de toxicidad y una adecuada solubilidad en agua (LogS). Por otro lado, el compuesto **1** también demostró ser no mutagénico (Tabla 15) en estudios experimentales llevados a cabo en nuestro laboratorio (Tabla 16), otra característica deseable a la hora de pensar en una potencial traslación a ensayos preclínicos[150]. Asimismo, como se diseñaron los compuestos pensando en ser aplicados en un modelo *in vivo* de GBM, es importante determinar si el derivado más promisorio, **1**, es capaz de atravesar la BHE para poder llegar al cerebro, que es donde se desarrollará el tumor, y así poder ejercer su acción terapéutica. Para evaluar esto se utilizó, en este caso, un modelo *in vitro* de BHE de no contacto[166]. La resistencia eléctrica de las células endoteliales se midió antes y después del tratamiento para garantizar la integridad del BHE (Material Suplementario, artículo IV). De acuerdo con los resultados de cuantificación generados a través de HPLC, se constató que el derivado **1** atravesó la BHE en una relación 3:1 (Tabla 16).

*Tabla 15. Propiedades "tipo-fármaco" del compuesto **1**, Sun y Tmz*

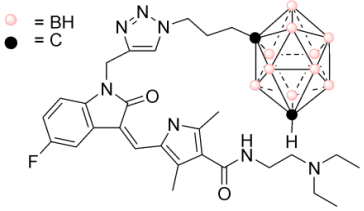
Compuesto	AIH[a]	Localización subcelular	CYP-subs[b]	hERG[c]	Carc[d]	LD_{50}[e]	LogS[f]	Regla 5, n viol[g]
 **1**	(+)	Mit[h]	3A4	w-in	(-)	2.69	-3.48	1[i]
 **Sun**	(+)	Mit	3A4	w-in	(-)	2.66	-3.24	0
 **Tmz**	(+)	Mit	-	w-in	(-)	2.53	-1.63	0

[a] Absorción intestinal humana; compuestos con AIH menor de 30 % se indican con (-), de otra forma se indican como (+)[135]. [e] Sustrato de las tres isoenzimas de Cytocromo P450 (CYP450 2C9, CYP450 2D6, and CYP450 3A4); se indica la isoforma de CYP para la cual el compuesto es un potencial sustrato[140]. [c] Canal de potasio del gen relacionado con el éter-a-go-go (hERG) humano; según el grado de inhibición se indica como "sin", débil "w-in" e inhibidor "in" [141,142]. [d] Potencial carcinógeno; no carcinógeno se indica como (-)[143]. [e] Eficiencia Lipofílica del

CONFIDENCIAL

ligando (pIC_{50} – $LogD_{7.4}$)[146]. [f] Solubilidad en agua [148]. [g] Numero de violaciones de Lipinski "5 reglas".

*Tabla 16. Test de Ames y permeabilidad de BHE para el compuesto **1**.*

	Test de Ames			BHE	
		TA98	TA100		
 **1**	**dosis (µg/placa)**	**Número de colonias revertantes**		Concentración de **1** en el medio de ensayo antes y después del BHE determinado por HPLC. De acuerdo con los resultados, el compuesto tiene la capacidad de atravesar dicha barrera.	
	0.45	12 ± 1	67±3		
	0.15	9 ±1	56±3		
	0.05	7.5 ± 1.5	46.5±1.5		
	0.016	6 ±1	37±6		
	0.005	8± 1	29.5±0.5		
	0	11.6 ± 2.05	95.6±5.7		
	Control positivo	294.6 ± 11.1	704.3±6.3	Antes de la BHE	[**1**] = 15 µM
	matagenicidad	(-)	(-)	Después de la BHE	[**1**] = 48 µM

CONFIDENCIAL

6.2.2.6 Estudios in vivo en ratones inmunosuprimidos portando tumores derivados de U87 MG

Para determinar la actividad anti-glioblastoma *in vivo* de **1** se utilizaron ratones inmunosuprimidos portando tumor derivado de la línea humana U87 MG[167]. El compuesto **1** se administró vía intraperitoneal a una dosis de 1 mg/kg/día tres veces a la semana (artículo IV, Material Suplementario). En este ensayo, se usó Tmz como fármaco terapéutico de referencia administrado en las mismas condiciones a 4 mg/kg/día. Los resultados generados en el experimento relevaron que tras someter al set de ratones con **1** se produjo un notorio enlentecimiento en el crecimiento del tamaño del GBM en comparación con los animales no tratados (Figura 60 A). Este comportamiento fue capaz de visualizarse a través de quimioluminiscencia (Figura 60 A y B). Además, el compuesto **1**, a una dosis cuatro veces menor que la dosis suministrada con Tmz y en las mismas condiciones, prolongó significativamente la supervivencia de ratones enfermos, con una media de tiempo de supervivencia de 45 días (Figura 60D). El grupos de ratones tratados con Tmz y el grupo control (grupo que no recibió tratamiento) presentaron valores de tiempo de supervivencia media de 23 y 25 días, respectivamente.

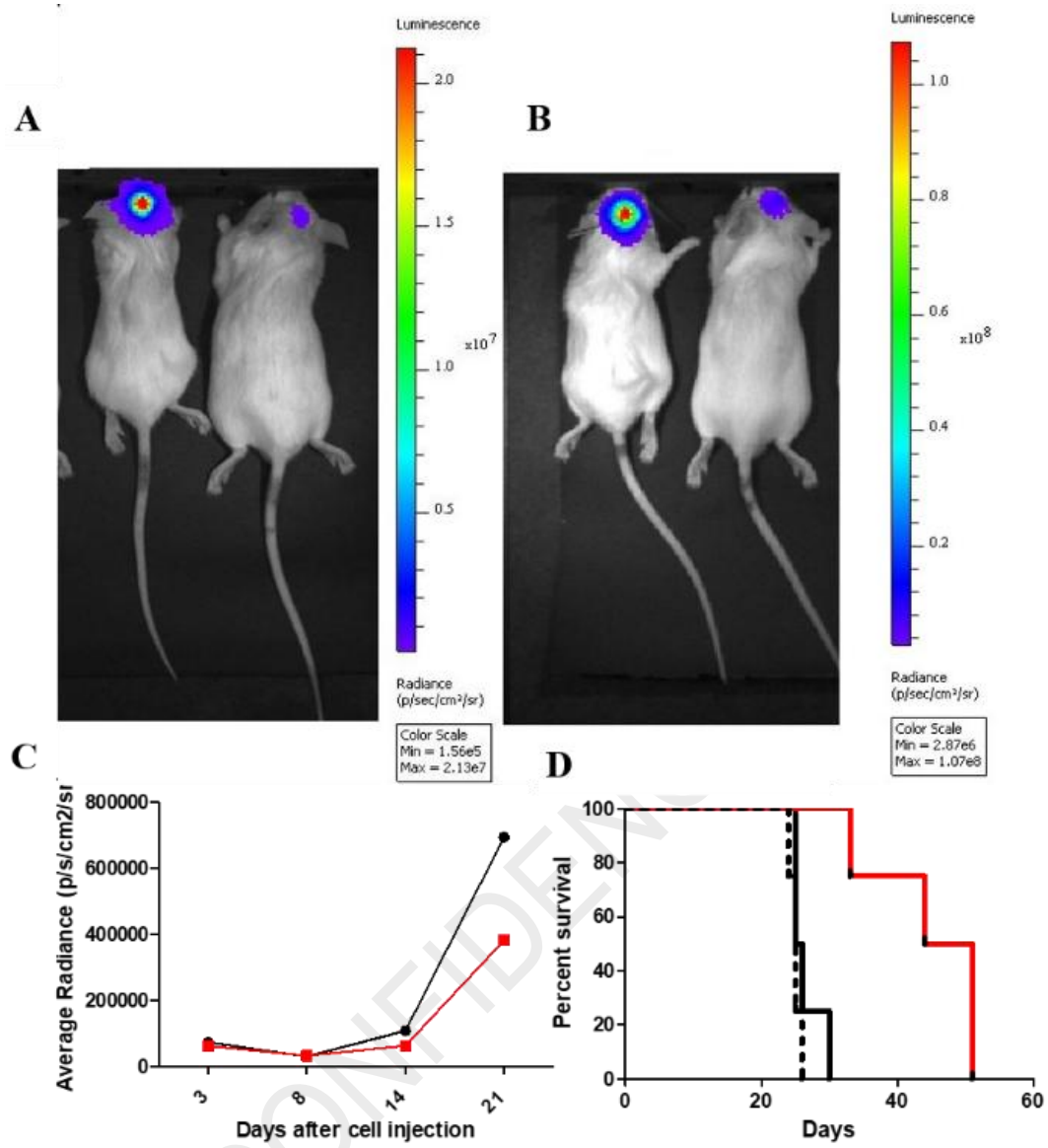


*Figura 60. (A y B) Imágenes seleccionadas representativas de la evolución del crecimiento del tumor de GBM inducido con células U87 MG (información detallada en artículo IV, material suplementario).(A) corresponde al día 14 y (B) al día 21 luego de la inoculación de las células. En cada caso a la izquierda se encuentra el animal control sin tratamiento y a la derecha tratado con compuesto **1** C) Evolución semanal del tamaño tumoral del GBM. En la semana se pone punto final al experimento por el deceso de los animales control.(D) Curva de supervivencia de Kaplan-Meier en ratones portadores de GBM. En negro: animales sin tratamiento; punteado: animales tratados con Tmz; rojo: animales tratados con compuesto **1**.*

6.2.2.7 Prueba de concepto in vitro de politerapia

Hoy en día, el uso de la terapia utilizando estrategias que combinan dos o más fármacos (quimioterapia poli-terapéutica) con diferente modo de acción o mecanismo de muerte celular, está siendo ampliamente explorado, tanto en oncología como en otras patologías. Es así que se decidió realizar una primera aproximación *in vitro* sobre la línea celular U87 MG combinando el derivado **1** con el agente de referencia utilizado en GBM como lo es la Tmz, trabajando con

cada compuesto a la dosis de IC_{25} como primera aproximación experimental (Figura 61). Los resultados obtenidos mostraron un excelente perfil biológico, denotando la potencialidad de esta modalidad de terapia para ser trasladado a ensayos *in vivo*. Previo a realizarse dicha aproximación experimental, sería conveniente proceder con los análisis isobolográficos de la combinación de ambas entidades químicas para determinar el tipo de proceso, aditividad, sinergismo o antagonismo y a su vez encontrar la dosis adecuadas para trasladar el experimento *in vitro* al ensayo *in vivo*.

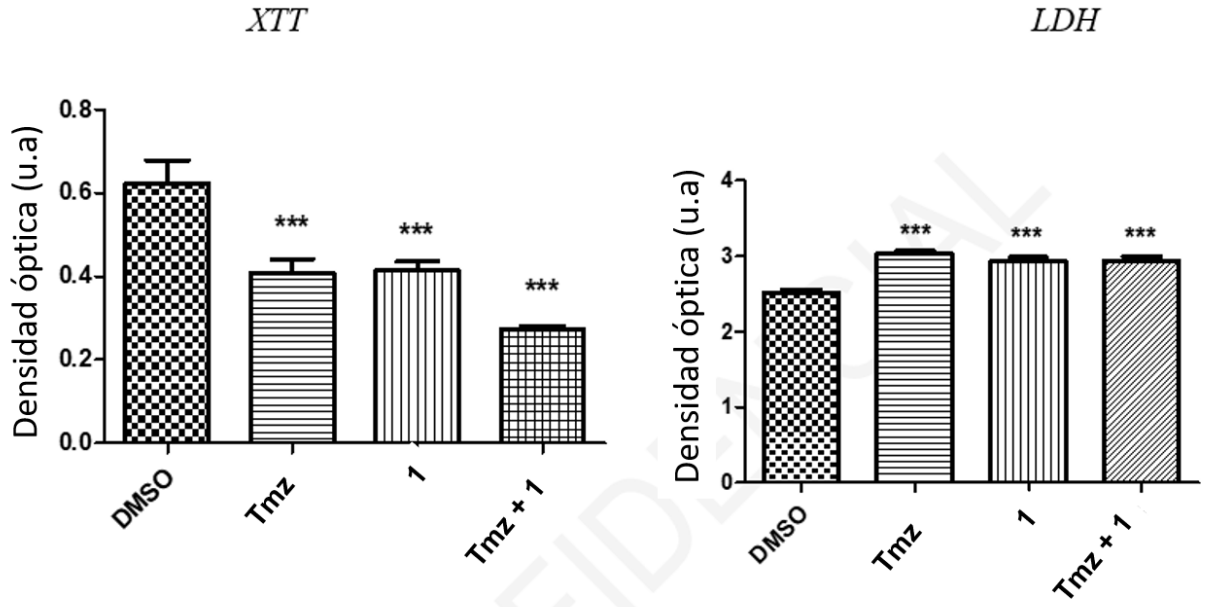


*Figura 61. Ensayos in vitro de tratamientos combinados en células U87 MG. Cuando se combinaron cada agente se analizó a sus dosis de IC_{25} y cuando se administraron solos se trabajó a sus dosis de IC_{50}. El metabolismo celular se midió usando el kit de ensayo colorimétrico de viabilidad celular a través de XTT. Medición de citotoxicidad celular por actividad enzimática LDH. ANOVA unidireccional en comparación con DMSO (*** p <0.0001)*

6.3 Conclusiones

En este trabajó se sintetizó y caracterizó fisicoquímicamente nueve nuevos derivados híbridos conteniendo por un lado la sub-estructura farmacofórica de sunitnib y por otro lado funcionalidades derivadas de clústeres de boro. Los nuevos compuestos fueron evaluados *in vitro* contra las células U87-MG, C6 y HT-29 mediante el ensayo colorimétrico de sulforrodamina B y XTT. Entre los compuestos evaluados, el compuesto **1**, además de ser uno de los compuestos más activos *in vitro*, presentó otras características interesantes que hicieron de él un buen candidato para pasar a ensayos biológicos en un modelo *in vivo*. Además, a través del test de Ames se demostró que el compuesto **1** resultó ser no mutagénico. Por otro lado, el compuesto **1** fue capaz de atravesar la barrera hematoencefálica, un aspecto relevante en el diseño de fármacos con capacidad de actuar en el sistema nervioso central. Los experimentos de citometría de flujo revelaron que el compuesto **1**, en condiciones de co-cultivo celular, produce la muerte celular vía un mecanismo de apoptosis, siendo esto un aspecto altamente relevante pensando en que estos compuestos puedan tener potencial acción terapéutica dual, dirigido a proteínas con actividad tirosina quinasa y mediante procesos de BNCT. Con el objetivo de elucidar las principales vías de acción del derivado **1** se realizó un ensayo de cribado masivo sobre 460 proteínas humanas con actividad tirosina quinasa encontrando que **1** tienen actividad frente a 33 de estas proteínas, teniendo como principales dianas a FLT3, PDGFR-α and -β, KIT, CSF1R and VEGFR2. Finalmente, el ensayo *in vivo* evidenció el espectacular comportamiento antitumoral de **1.** En comparación con los animales no tratados o tratados con temozolomida, **1** duplicó el tiempo de supervivencia media de los ratones, de 25 ó 23 a 45 días respectivamente. Lo que resultó en un aumento del 70 u 89% del tiempo de supervivencia de los ratones, a partir de 30 ó 27 a 51 días, y un aumento del 32 ó 43% del tiempo sin muertes de ratones, de 25 ó 23 a 33 días respectivamente.

CONFIDENCIAL

7 CAPITULO III

Misceláneos

En el siguiente apartado se presentan resultados preliminares de diferentes abordajes experimentales que se están llevando a cabo en la actualidad y que aún no han sido publicados.

CONFIDENCIAL

7.1 Valoración de boro intracelular

La aplicabilidad de los compuestos desarrollado en la presente tesis doctoral en el campo de la terapia por captura neutrónica de boro dependerá en parte de la capacidad de acumulación de éstos en las diferentes líneas celulares ensayadas. Las técnicas más utilizadas para la medición de boro son: el análisis por activación neutrónica de radiación gamma instantánea o prompt gamma (PGNAA), espectrometría de emisión óptica por plasma inductivo de argón (ICP-OES / AES), espectrometría de masas por plasma inductivo de argón (ICP-MS), espectrometría alfa y la espectroscopía de fotoelectrones de rayos X de alta resolución (XPS-HR).

7.1.1 Materiales y métodos

7.1.1.1 Medición de boro por ICP-AES

CONFIDENCIAL

El contenido de boro fue medido en cada una de las muestras y en cada línea celular por el método de ICP-AES. El instrumento utilizado fue un ICP optima 3100 XL UV, axial (Perkin Elmer). En ese equipo la muestra ingresa como un flujo de líquido que es convertido en aerosol a través de un proceso denominado nebulización. Este aerosol es transportado al interior del equipo donde es atomizado y/o ionizado por el plasma, emitiendo una energía característica. Esta energía pasa luego por un policromador que separa la radiación en componentes de distintas longitudes de onda. Luego la radiación de interés se transforma en una señal electrónica que es expresada como una medida de concentración del elemento analizado. Para determinar la cantidad de elemento presente en la muestra es necesario realizar una curva de calibración utilizando soluciones estándar de concentración conocida y midiendo en el ICP la intensidad de emisión característica de la señal para el elemento a determinar. Para realizar el análisis de boro en las células se estudiaron 4 líneas atómicas: 249.772 nm, 249.677 nm, 208.957 nm y 208.889 nm. La segunda línea fue la seleccionada para realizar los cálculos correspondientes por no tener interferencia con el Fe. Cada día en que se midió boro se preparó una curva de calibración utilizando un estándar acuoso de ácido bórico (5000 µgB/mL Merck). El límite de detección en células fue de 4 ppb.

Todos los compuestos en estado sólido fueron disueltos en DMSO a una concentración madre de 1 mM. Una vez conocidas las dosis a usar de cada compuesto se realizaron diluciones 1/10 de las madres, quedando 100 µM. A esta última dilución, por ejemplo para el compuesto **2** (Figura 62) se realizó una nueva dilución 1/10, quedando 10 µM, la cual fue usada para los

experimentos de captación. Una vez agregado los compuestos, se agrega un volumen de medio de cultivo suplementado con 10 % de SFB hasta un volumen final de 500 µL. Así se incuba en estufa a 37 ºC en atmósfera de CO_2 al 5 % a 1, 2 y 4 horas (en algunos casos 6, 24 y 48 horas) cada placa.

Finalizado cada tiempo de incubación, se elimina el sobrenadante, se lava 2 veces con PBS 1x frío (4 ºC), se elimina el sobrenadante y se agregan 500 µL de ácido fórmico para digerir las células. Una vez completado este proceso el sobrenadante se divide en 2 alícuotas iguales de 250 µL. Una de ellas se coloca en tubo eppendorff para medición de B por ICP-AES y la otra se deja en estufa hasta su evaporación, luego se resuspende con NaOH 0.3 N para medir proteínas por el método de Lowry.

7.1.1.2 Determinación de proteínas mediante la técnica de Lowry

Cada una de las muestras resuspendidas en ácido fórmico fue evaporada en estufa a 37 °C y luego resuspendida en NaOH 0.3 N para la determinación de proteínas por el método descrito por Lowry (Lowry O.H., 1951). Luego una alícuota de 100 µL de la muestra se le agregó 1 mL de la disolución A (2 % $NaCO_3$ en 0.1 N NaOH; 2 % Na-K tartrato; 1 % $CuSO_4$), se la agitó y se la dejó en reposo durante 10 minutos. A continuación a cada una de las muestras se le agregó 200 µL de una mezcla de Folin (Folin y H_2O bidestilada, en una relación de 2:1). Cada día de medida se realizó una curva de calibración con albúmina (1 mg/mL). Se midió en espectrofotómetro la absorbancia a 720 nm.

CONFIDENCIAL

7.1.2 Resultados y discusión

Tras incubar los compuestos **1**, **2** y BPA éste enriquecido en ^{10}B (Figura 62) a distintos tiempos y a dosis sub-leales, por debajo de la IC_{50}, se obtuvieron resultados muy interesantes. En primer lugar, ambos compuestos presentan a todos los tiempos una marcada captación por ambas líneas celulares (Figura 63). El compuesto **2** presenta, a todas las horas, un perfil de captación mayor que el compuesto **1** y a su vez mucho mayor que el control (PA) no encontrándose efectos citotóxicos a las dosis y tiempos ensayados (Figura 63). Estas observaciones en los experimentos de captación permiten pensar en una potencial aplicación de ambos derivados mediante procesos de BNCT en combinación con la terapia dirigida a proteínas tirosina quinasa.

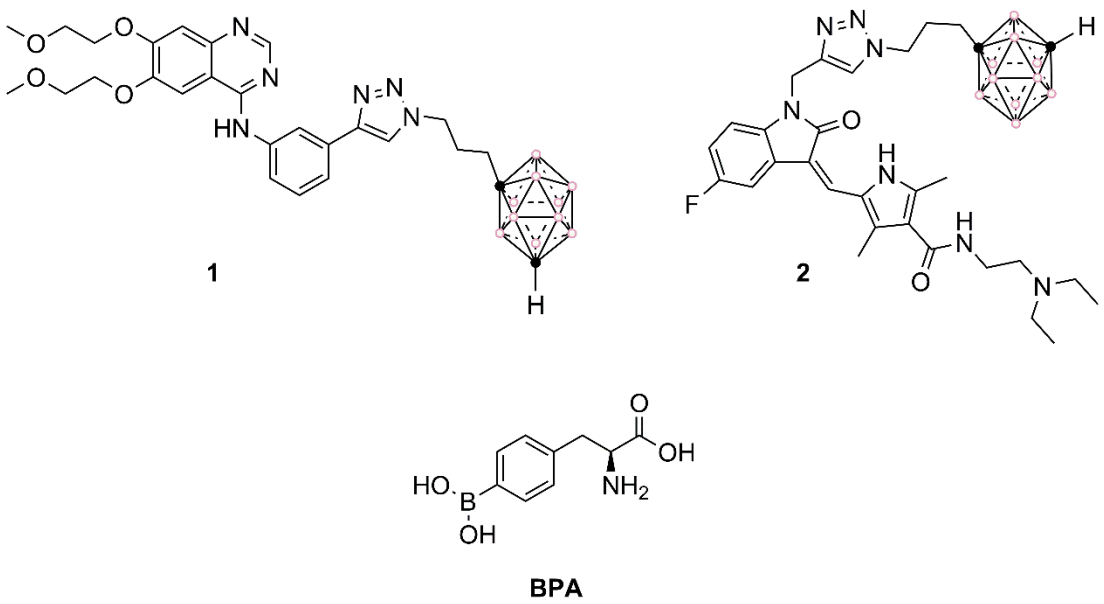
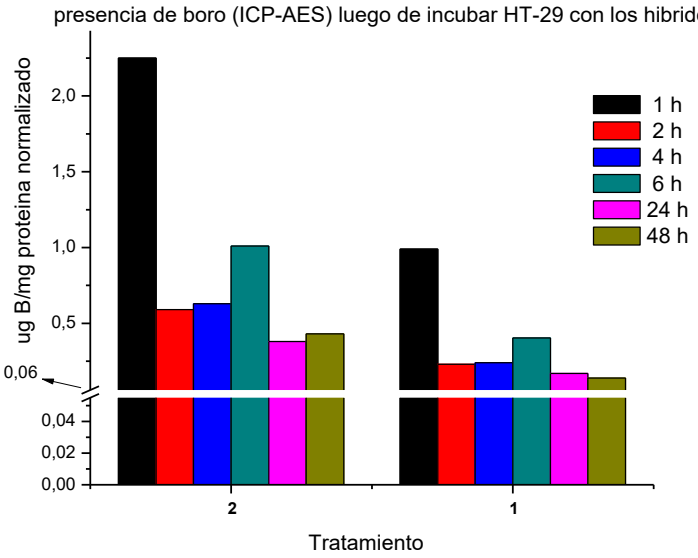
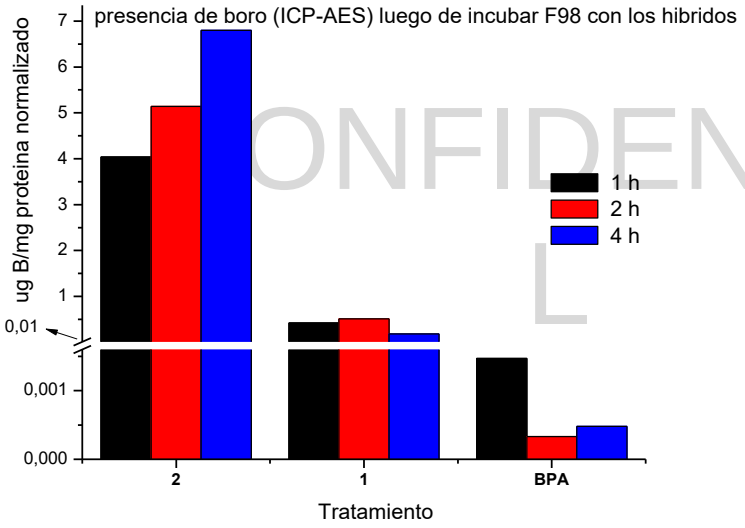


Figura 62. Compuestos seleccionados para ser evaluados en las líneas celulares HT-29 y F98

CONFIDENCIAL





ONFIDENCIA
L

*Figura 63. Captación intracelular en líneas celulares HT-29y F98 para los derivados **2**, **1** y **BPA** (enriquecido en ^{10}B).*

7.2 Estudios *in vitro* e *in vivo del derivado **1** (Figura 62)*

7.2.1 Materiales y métodos

7.2.1.1 Estudios de citotoxicidad in vitro en co-cultivo celular

Para la realización de la microscopía confocal se realizó un co-cultivo de astrocitos y células U87 MG. Para ello 3 × 10^4 astrocitos fueron sembradas en placas p35, permitiendo su

crecimiento hasta un 80 % de confluencia. Seguidamente 5 × 10^4 células U87 MG, marcadas con la sonda fluorescente PKH26, se sembraron en una placa p35 conteniendo un cultivo primario de astrocitos. Luego de 48 h placas p60 fueron tratadas con el compuesto **1** durante 24 h a la dosis de IC_{50}. Como control negativo una placa se trató con DMSO. Luego del periodo de incubación los co-cultivos se fijaron con paraformaldehído a 4°C por 20 min, seguido de dos lavados con PBS. Las células se permeabilizaron por 10 min a temperatura ambiente con 0.1 % de Tritón X-100 en PBS, se lavaron con PBS y se bloquearon con 5 % BSA-PBS por 1 h a temperatura ambiente. Como control negativo se utilizó una placa p60 tratada con DMSO 1 %. Finalmente, las placas fueron incubadas a 4 °C durante toda la noche con una disolución de 1 % BSA en PBS conteniendo los anticuerpos primarios y DAPI (1:1000). Luego de los lavados las células fueron incubadas con los anticuerpos secundarios (1:500) durante 2 h a temperatura ambiente. Para la inmunofluorescencia se utilizaron como anticuerpos primarios el monoclonal de ratón anti-GFAP (1:400, Sigma) y monoclonal de rata anti-M2 (1:50); y los respectivos anticuerpos secundarios conjugados a AlexaFluor 633 (Invitrogen) y AlexaFluor 488 (Invitrogen). Los anticuerpos fueron detectados por microscopía confocal con un microscopio Olympus FV300.

CONFIDENCIA

7.2.1.2 Animales

Todos los protocolos para la experimentación con animales se llevaron a cabo de acuerdo con los procedimientos de experimentación aprobados por la Comisión Ética del Instituto Tecnológico Technion de Israel (Número de protocolo IL-143-10-17 Technion). Todos los protocolos experimentales con animales siguieron los principios de la Declaración de Helsinki. Los animales se alojaron en jaulas de malla de alambre a 20 ± 2 ^oC con ciclos artificiales de luz-oscuridad de 12 h. Los animales se alimentaron con una dieta estándar de pellets y agua y se usaron después de un mínimo de 5 días de aclimatación a las condiciones de alojamiento.

7.2.1.3 Cultivo celular

Las células U87 MG de glioblastoma se cultivaron en un medio completo, MEM-Eagle con suero fetal bovino (9 %), glutamina (2 %) y gentamicina (0.05 %) (Biological Industries, Beit Ha'emek, Israel). Las células se descongelaron y crecen durante tres días, tras un pasaje las mismas se dejaron crecer durante 4 días más hasta la inoculación.

7.2.1.4 Cirugía estereotáctica: inoculación celular en el cerebro.

Los ratones se anestesiaron por inhalación de isoflurano o por inyección con una mezcla de ketamina-xilacina en solución salina fisiológica (ketamina 1 mg / mL: xilacina 20 mg / mL). Para

mantener la humedad ocular adecuada durante el procedimiento, se debe aplicó ungüento para los ojos. Con un bisturí estéril, se realiza una incisión sagital sobre el hueso parieto-occipital, de aproximadamente 1 cm de largo. Luego se limpia la superficie expuesta del cráneo. Con la cirugía estereotáctica se marcan las coordenadas donde se inyectaron las células (1.5 mm hacia la derecha y 1.5 mm hacia atrás del bregma). Se inyectó un volumen de 3 µL que contiene 2.5-3.0 × 10^5 células U87 MG en una profundidad del cráneo de 2.5 mm. Después de la inyección celular, esperó 4 minutos hasta sacar la jeringa.

7.2.1.5 Tratamientos en ratones inmunosuprimidos portando tumores derivados de U87 MG

Los experimentos se llevaron a cabo en 7-8 ratones hembra BALB / c débiles (17.6-18.0 g de peso corporal, pc) criados en condiciones específicas libres de patógenos. Al final de los experimentos, se anestesiaron con isoflurano y se sacrificaron por dislocación cervical.

El tratamiento se inició cuando los tumores comenzaron a desarrollarse según las imágenes de bioluminiscencia. Se definieron tres grupos de tratamiento (n=6): i) compuesto **1**, disuelto en disolución salina fisiológica estéril: Tween 80 (4:1, v/v), administrado a 1 mg / kg de pc ip; ii) administración en la formulación liposómica: 30% fosfatidilcolina, 40% colesterol, 10% ácido fosfatídico, 0.5% péptido, compuesto agregado al 1%; iii) Tmz, disuelto en disolución salina fisiológica estéril: Tween 80 (4:1, v/v), administrado a 4 mg / kg de pc ip; iv) control negativo (vehículo, disolución salina fisiológica estéril: Tween 80 (4: 1, v / v)). Días de tratamientos: 5, 7, 9, 12, 14 y 16. Los volúmenes tumorales se determinaron mediante imágenes de bioluminiscencia semanalmente.

CONFIDENCIAL

7.2.1.6 Imágenes

Imágenes de bioluminiscencia se adquirieron con el sistema de imágenes LUMINA X5. Las mismas se basaron en la oxidación de la luciferina [ácido *d*-(-)-2-(6-hidroxi-2-benzotiazolil)-tiazol-4-carboxílico] en presencia de oxígeno y adenosina trifosfato. Esta reacción es catalizada por la enzima luciferasa, que convierte la energía química en fotones con la emisión resultante de luz. La luciferasa está presente sólo en las células cancerosas inoculadas, ya que fueron transfectadas previamente con un plásmido que codifica la enzima. El monitoreo de bioluminiscencia se realizó una vez a la semana, comenzando dos días después de la inyección celular hasta la muerte de los ratones. Después de la administración de luciferina (sal de potasio de *d*-luciferina, 150 mg/kg) mediante inyección ip, los ratones se anestesiaron con isoflurano. Las mediciones se tomaron cada un minuto hasta 24 minutos después de la inyección de luciferina. Las regiones de interés que abarcan el área intracraneal de la señal se definen utilizando el software Living Image, y se registraron los fotones/s/radian/cm^2.

7.2.2 Resultados y discusión

7.2.2.1 Estudios de citotoxicidad in vitro en co-cultivo celular

Del mismo modo que con el derivado más activo perteneciente a la serie del sunitinib (derivado **2**, Figura 62), se procedió con el derivado **1** (Figura 62) perteneciente a la serie del erlotinib. Con el objetivo de indagar el comportamiento del derivado **1** en condiciones similares a las del microambiente tumoral, la línea celular U87 MG se co-cultivó con astrocitos. Ambas entidades se incubaron a las dosis de IC_{50} durante 24 y 48 horas. Como se puede observar en las imágenes generadas a través de microscopía confocal (Figura 64), se revelaron perfiles notoriamente diferentes en cada uno de los experimentos ensayados. Por un lado, el cultivo sometido a la sonda PKH26, marcador fluorescente de membrana en U87 MG, mostró la disminución de dicha población tras el tratamiento con el derivado **1** mayoritariamente a 48 horas, en comparación con las condiciones de cultivo control, es decir células sin tratamiento. Por otro lado, con la sonda fluorescente M2 (utilizada para el marcaje de membrana de astrocitos), se observó que el compuesto **1** fue capaz de mantener inalterada dicha población tanto a 24 como a 48 horas, denotando la potencial aplicabilidad de dicho compuesto resultado de su clara selectividad por la población de células tumorales. De forma similar, según la sonda fluorescente GFAP, la cual da indicios de la activación de astroglia, se observó que la población de astrocitos asociados a tumores, presentes en el control, no sufrió alteraciones apreciables luego del tratamiento durante 24 y 48 horas con el compuesto **1**, nuevamente realzando la selectividad hacia el tejido maligno por parte de la entidad. Finalmente, la tinción de los núcleos mediante DAPI mostró cierto grado de condensación de cromatina lo que, como se comentó anteriormente, podría estar asociado con el inicio de la apoptosis.

CONFIDENCIAL

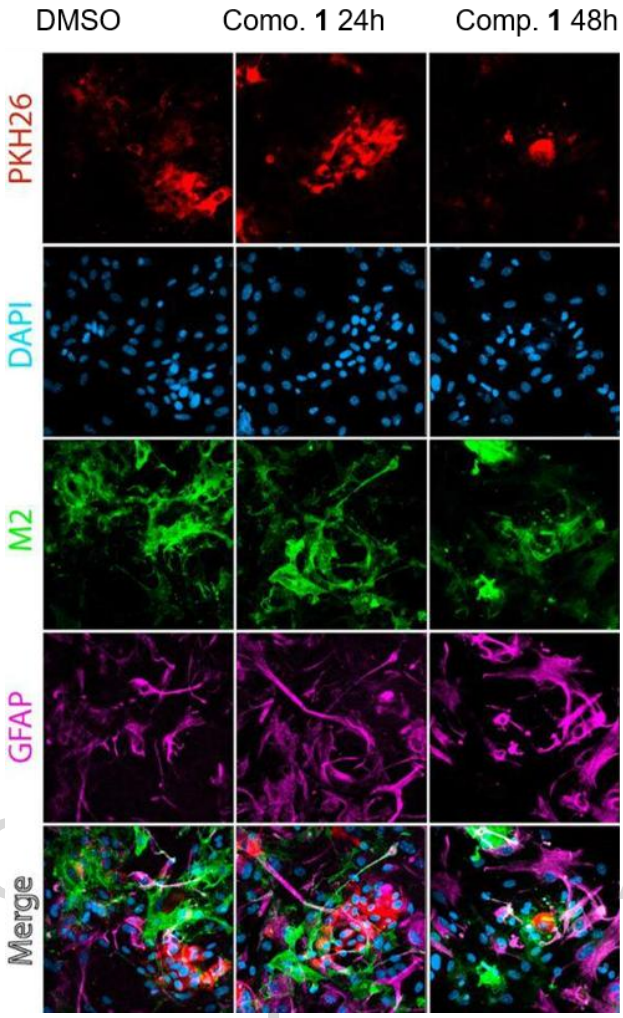


*Figura 64. Microscopias de fluorescencia de astrocitos co-cultivados con U87 MG y tratados con **1** o con DMSO como control durante 24 y 48 h. Las sondas utilizadas: PKH26 marcador de la membrana celular U87-MG, DAPI marcador de núcleo, M2 marcador de la membrana celular de astrocitos y GFAP marcador de activación de astrocitos*

7.2.2.2 Estudios in vivo en ratones inmunosuprimidos portando tumores derivados de U87 MG

El derivado híbrido **1** (Figura 62), proveniente de la serie del erlotinib, se administró a la misma dosis que el Tmz, a 4 mg/kg (previamente fue realizado el ensayo de toxicidad oral *in vivo* "up and down", capítulo I, artículo III). Como se puede observar en el gráfico de sobrevida (Figura 64), el tratamiento con **1** en su forma libre y vehiculizado con liposomas, prolongó la sobrevida de los ratones en comparación con el grupo control en 1.5 y 2.2 veces respectivamente, pasando de 25 a 38 y 55 días respectivamente. En relación a la permanecía de animales sin morir se puede observar que, para el derivado **1** en su forma libre asciende de 25 días a 38 días mientras que en el caso de **1** con liposoma aumenta de 25 a 49 días. Asimismo, el seguimiento de la evolución de la enfermedad a través de quimioluminiscencia permite observar un claro enlentecimiento en el crecimiento del tumor, especialmente en aquellos

ratones que fueron tratados con el derivado **1** encapsulado en liposomas. Estos resultados alentadores, conjuntamente con los resultados favorables de captación celular tanto en HT-29 como F98, abren la posibilidad de, en un futuro, diseñar experimentos de BNCT, *in vitro* en una primera instancia, para luego abordar los experimentos de BNCT *in vivo*.

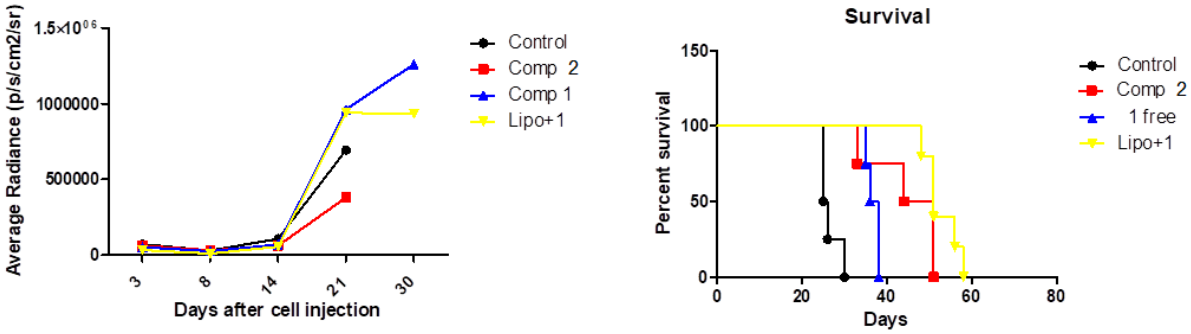


*Figura 65. Izquierda: evolución del tamaño del GBM; derecha: curva de sobrevida. Se incluye también en el gráfico el compuesto **2** derivado de la serie del sunitinib (Figura 62).*

CONFIDENCIAL

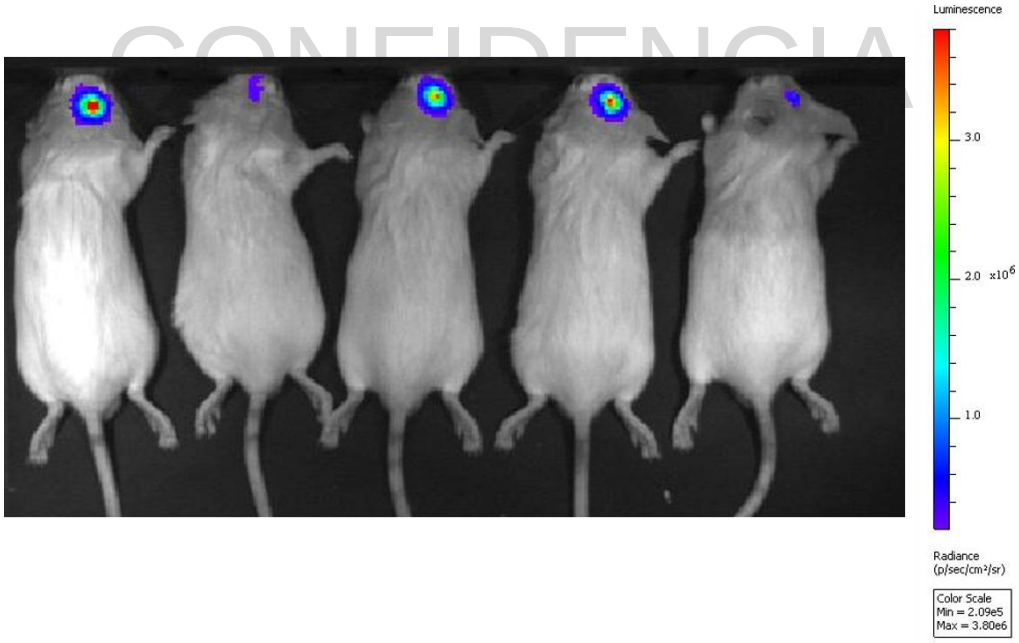


*Figura 66. Imagen representativa de la evolución del crecimiento del tumor de GBM inducido con células U87 MG. Se corresponde al día 21 luego de la inoculación de las células. De izquierda a derecha: Control; Liposoma-**1**; **1**-libre; **1**-libre; Liposoma-**1**.*

8 Bibliografía

1. Bunz, F. Principles of Cancer Genetics. (Springer Netherlands, 2008).
2. Hanahan, D. & Weinberg, R. A. Hallmarks of Cancer: The Next Generation. Cell 144, 646–674 (2011).
3. Etzioni, R. *et al*. The Case for Early Detection. Nat. Rev. Cancer 3, 243–252 (2003).
4. Ferlay, J. *et al*. Cancer Incidence and Mortality Worldwide: Sources, Methods and Major Patterns in GLOBOCAN 2012. Int. J. Cancer 136, E359–E386 (2015).
5. Zhu, Y. & Parada, L. F. The Molecular and Genetic Basis of Neurological Tumours. Nat. Rev. Cancer 2, 616–626 (2002).
6. Louis, D. N. *et al*. The 2007 WHO Classification of Tumours of the Central Nervous System. Acta Neuropathol. 114, 97–109 (2007).
7. Furnari, F. B. *et al*. Malignant Astrocytic Glioma: Genetics, Biology, and Paths to Treatment. Genes Dev. 21, 2683–2710 (2007).
8. Wen, P. Y. & Kesari, S. Malignant Gliomas in Adults. N. Engl. J. Med. 359, 492–507 (2008).
9. Lisak, R. P., Truong, D. D., Carroll, W. M. & Bhidayasiri, R. International Neurology, 2nd Edition. (Wiley-Blackwell, 2016).
10. Kanu, O. O. *et al*. Glioblastoma Multiforme Oncogenomics and Signaling Pathways. Clin. Med. Oncol. 3, 39–52 (2009).
11. Ohgaki, H. & Kleihues, P. Genetic Pathways to Primary and Secondary Glioblastoma. Am. J. Pathol. 170, 1445–1453 (2007).
12. Riemenschneider, M. J., Jeuken, J. W. M., Wesseling, P. & Reifenberger, G. Molecular Diagnostics of Gliomas: State of the Art. Acta Neuropathol. 120, 567–584 (2010).
13. Lacroix, M. *et al*. A Multivariate Analysis of 416 Patients with Glioblastoma Multiforme: Prognosis, Extent of Resection, and Survival. J. Neurosurg. 190–198 (2001).
14. Van Meir, E. G. *et al*. Exciting New Advances in Neuro-Oncology: The Avenue to a Cure for Malignant Glioma. CA. Cancer J. Clin. 60, 166–193 (2010).
15. Stupp, R. *et al*. Radiotherapy plus Concomitant and Adjuvant Temozolomide for Glioblastoma. N. Engl. J. Med. 352, 987–996 (2005).
16. Walker, M. D., Strike, T. A. & Sheline, G. E. An Analysis of Dose-effect Relationship in the Radiotherapy of Malignant Gliomas. Int. J. Radiat. Oncol. Biol. Phys. 5, 1725–1731 (1979).
17. Lesniak, M. S. & Brem, H. Targeted Therapy for Brain Tumours. Nat. Rev. Drug Discov. 3, 499–508 (2004).

CONFIDENCIAL

18. Westphal, M. *et al*. A Phase 3 Trial of Local Chemotherapy with Biodegradable Carmustine (BCNU) Wafers (Gliadel wafers) in Patients with Primary Malignant Glioma. Neuro. Oncol. 5, 79–88 (2003).
19. Spiro, T. P. *et al*. Temozolomide: the Effect of Once- and Twice-a-day Dosing on Tumor Tissue Levels of the DNA Repair Protein *O*(6)-Alkylguanine-DNA-alkyltransferase. Clin. Cancer Res. 7, 2309–2317 (2001).
20. Zhang, J., Stevens, M. F. G. & Bradshaw, T. D. Temozolomide: Mechanisms of Action, Repair and Resistance. Curr. Mol. Pharmacol. 5, 102–114 (2012).
21. Denny, B. J., Wheelhouse, R. T., Stevens, M. F., Tsang, L. L. & Slack, J. A. NMR and Molecular Modeling Investigation of the Mechanism of Activation of the Antitumor Drug Temozolomide and its Interaction with DNA. Biochemistry 33, 9045–9051 (1994).
22. Hegi, M. E. *et al*. MGMT Gene Silencing and Benefit from Temozolomide in Glioblastoma. N. Engl. J. Med. 352, 997–1003 (2005).
23. Esteller, M., Hamilton, S. R., Burger, P. C., Baylin, S. B. & Herman, J. G. Inactivation of the DNA Repair Gene O6-Methylguanine-DNA Methyltransferase by Promoter Hypermethylation is a Common Event in Primary Human Neoplasia. Cancer Res. 59, 793–797 (1999).
24. Wong, E. T. *et al*. Outcomes and Prognostic Factors in Recurrent Glioma Patients Enrolled Onto Phase II Clinical Trials. J. Clin. Oncol. 17, 2572–2572 (1999).
25. Beal, K., Abrey, L. E. & Gutin, P. H. Antiangiogenic Agents in the Treatment of Recurrent or Newly Diagnosed Glioblastoma: Analysis of Single-agent and Combined Modality Approaches. Radiat. Oncol. 6, 2 (2011).
26. Combs, S. E. *et al*. Treatment of Primary Glioblastoma Multiforme with Cetuximab, Radiotherapy and Temozolomide (GERT) – Phase I/II Ttrial: Study Protocol. BMC Cancer 6, 133 (2006).
27. Ramos, T. C. *et al*. Treatment of High-grade Glioma Patients with the Humanized Anti-epidermal Growth Factor Receptor (EGFR) Antibody h-R3: Report from a Phase I/II Trial. Cancer Biol. Ther. 5, 375–379 (2006).
28. Karpel-Massler, G., Schmidt, U., Unterberg, A. & Halatsch, M.-E. Therapeutic Inhibition of the Epidermal Growth Factor Receptor in High-Grade Gliomas: Where Do We Stand? Mol. Cancer Res. 7, 1000–1012 (2009).
29. Lee, J.-H., Choy, M. L., Ngo, L., Foster, S. S. & Marks, P. A. Histone Deacetylase Inhibitor Induces DNA Damage, which Normal but not Transformed Cells can Repair. Proc. Natl. Acad. Sci. 107, 14639–14644 (2010).
30. Hunter, T. The Croonian Lecture 1997. The Phosphorylation of Proteins on Tyrosine: Its Role in Cell Growth and Disease. Philos. Trans. R. Soc. London. Ser. B Biol. Sci. 353, 583–605 (1998).

CONFIDENCIAL

31. Ségaliny, A. I., Tellez-Gabriel, M., Heymann, M.-F. & Heymann, D. Receptor Tyrosine Kinases: Characterization, Mechanism of Action and Therapeutic Interests for Bone Cancers. J. Bone Oncol. 4, 1–12 (2015).
32. Franklin, W. A., Veve, R., Hirsch, F. R., Helfrich, B. A. & Bunn, P. A. Epidermal Ggrowth Factor Receptor Family in Lung Cancer and Premalignancy. Semin. Oncol. 29, 3–14 (2002).
33. Wieduwilt, M. J. & Moasser, M. M. The Epidermal Growth Factor Receptor Family: Biology Driving Targeted Therapeutics. Cell. Mol. Life Sci. 65, 1566–1584 (2008).
34. Xu, H. et al. Epidermal Growth Factor Receptor in Glioblastoma. Oncol. Lett. 14, 512–516 (2017).
35. Gan, H. K., Kaye, A. H. & Luwor, R. B. The EGFRvIII Variant in Glioblastoma Multiforme. J. Clin. Neurosci. 16, 748–754 (2009).
36. Endres, N. F., Engel, K., Das, R., Kovacs, E. & Kuriyan, J. Regulation of the Catalytic Activity of the EGF Receptor. Curr. Opin. Struct. Biol. 21, 777–784 (2011).
37. Zawrocki, A. & Biernat, W. Epidermal Growth Factor Receptor in Glioblastoma. Folia Neuropathol. 43, 123–132 (2005).
38. Kreisl, T. N. *et al*. Phase II Trial of Single-Agent Bevacizumab Followed by Bevacizumab Plus Irinotecan at Tumor Progression in Recurrent Glioblastoma. J. Clin. Oncol. 27, 740–745 (2009).
39. De Witt Hamer, P. C. Small molecule kinase inhibitors in glioblastoma: a systematic review of clinical studies. Neuro. Oncol. 12, 304–316 (2010).
40. Berzelius, J. Untersuchungen über die Flussspathsäure und deren merkwürdigsten Verbindungen. Ann. Phys. 78, 113 (1824).
41. Stock, A. Hydrides of Boron and Silicon. Phys. Chem. 38, 714–715 (1934).
42. Price, W. C. The Structure of Diborane. J. Chem. Phys. 15, 614–614 (1947).
43. Longuet-Higgins, H. C. & Bell, R. P. 64. The Structure of the Boron Hydrides. J. Chem. Soc. 250 (1943).
44. Borax to Boranes. 32, (American Chemical Society, 1961). doi:10.1021/ba-1961-0032
45. Lipscomb, W. N. The Nobel Prize in Chemistry 1976. Available at: https://www.nobelprize.org/prizes/chemistry/1976/press-release/.
46. Georg Wittig, H. C. B. The Nobel Prize in Chemistry 1979. Available at: https://www.nobelprize.org/prizes/chemistry/1979/summary/.
47. Grimes, R. N. Chapter 2: Structures and Bonding page 1058, in Carboranes 3rd edition (Academic Press, 2016).
48. Williams, R. E. Carboranes and Boranes; Polyhedra and Polyhedral Fragments. Inorg. Chem. 10, 210–214 (1971).

CONFIDENCIAL

49. Wade, K. The Structural Significance of the Number of Skeletal Bonding Electron-pairs in Carboranes, the Higher Boranes and Borane Anions, and various Transition-metal Carbonyl Cluster Compounds. J. Chem. Soc., Chem. Commun. 792 (1971).
50. Mingos, D. M. P. A General Theory for Cluster and Ring Compounds of the Main Group and Transition Elements. Nat. Phys. Sci. 236, 99–102 (1972).
51. Rudolph, R. W. Boranes and heteroboranes: a paradigm for the electron requirements of clusters? Acc. Chem Res. 9, 446–452 (1976).
52. Schleyer, P. von R. & Najafian, K. Stability and Three-Dimensional Aromaticity of closo - Monocarbaborane Anions, CB n - 1 H n - , and closo -Dicarboranes, C 2 B n - 2 H n. Inorg. Chem. 37, 3454–3470 (1998).
53. Poater, J., Solà, M., Viñas, C. & Teixidor, F. π Aromaticity and Three-Dimensional Aromaticity: Two sides of the Same Coin? Angew. Chemie Int. Ed. 53, 12191–12195 (2014).
54. Fein, M. M. *et al*. Carboranes. II. The Preparation of 1- and 1,2-Substituted Carboranes. Inorg. Chem. 2, 1115–1119 (1963).
55. Grafstein, D. & Dvorak, J. Neocarboranes, a New Family of Stable Organoboranes Isomeric with the Carboranes. Inorg. Chem. 2, 1128–1133 (1963).
56. Papetti, S. & Heying, T. L. p -Carborane [1,12-Dicarbaclovododecaborane(12)]. J. Am. Chem. Soc. 86, 2295–2295 (1964).
57. Hermansson, K., Wójcik, M. & Sjöberg, S. o- , m- , and p -Carboranes and Their Anions: Ab Initio Calculations of Structures, Electron Affinities, and Acidities. Inorg. Chem. 38, 6039–6048 (1999).
58. Bregadze, V. I. Dicarba-closo-dodecaboranes $C_2B_{10}H_{12}$ and their Derivatives. Chem. Rev. 92, 209–223 (1992).
59. Puga, A.V. *et al*. From Mono- to Poly-Substituted Frameworks: Away of Tuning the Acidic Character of C_cH in *o*-Carborane Derivatives. Chem. Eur. J. 15, 9755–9763 (2009).
60. Olid, D., Núñez, R., Viñas, C., and Teixidor, F. Methods to produce B–C, B–P, B–N and B–S bonds in boron clusters. Chem. Soc. Rev. 42, 3318–3336 (2013).
61. Hawthorne, M. F. *et al*. Preparation and Characterization of the (3)-1,2- and (3)-1,7-Dicarbadodecahydroundecaborate(-1) Ions. J. Am. Chem. Soc. 90, 862–868 (1968).
62. Wiesboeck, R. A.; Hawthorne, M. F. Dicarbaundecaborane(13) and Derivatives. J. Am. Chem. Soc. 1964, 86, 1642-1643.
63. Garret, P. M., Tebbe, F. N. & Hawthorne, M. F. The Thermal Isomerization of C-Phenyldicarbaundecaborate. J. Am. Chem. Soc. 86, 5016–5017 (1964).
64. Zakharkin, L. I. & Kalinin, V. N. On the Reaction of Amines with Barenes. Tetrahedron Lett. 6, 407–409 (1965).

CONFIDENCIAL

65. Zakharkin, L. I. & Kirillova, V. S. Cleavage of o-carboranes to (3)-l,2-Dicarbaundecarborates by Amines. Russ. Chem. Bull. 24, 2484–2486 (1975).
66. Taoda, Y.; *et al*. Identification of an Intermediate in the Deboronation of ortho-carborane: an Adduct of ortho-carborane with Two Nucleophiles on One Boron Atom. Chem. Commun. 2049-2051 (2008).
67. Davidson, M. G. *et al*. Deboronation of Ortho-carborane by an Iminophosphorane: Crystal Structures of the Novel Carborane Adduct Nido-$C_2B_{10}H_{12}{\cdot}HNP(NMe_2)_3$ and the Norenium salt $[(Me_2N)_3PNHBNP(NMe_2)_3]_2O^{2+}(C_2B_9H_{12}^-)_2$. Chem. Comm. 1649–1650 (1999).
68. Fox, M. A.; Gill, W. R.; Herbertson, P. L.; MacBride, J. A. H.; Wade, K. Deboronation of c-substituted ortho- and meta-closo-carboranes using "wet" fluoride ion solutions. Polyhedron. 1996, 16, 565-571.
69. Fox, M. A., MacBride, J. A. H. & Wade, K. Fluoride-ion Deboronation of p-fluorophenyl-ortho- and -meta-carboranes. NMR Evidence for the New Fluoroborate, $HOBHF_2^-$. Polyhedron. 16, 2499–2507 (1997).
70. Fox, M. A. & Wade, K. Cage-fluorination During Deboronation of meta-carboranes. Polyhedron. 16, 2517–2525 (1997).
71. Yoo, J., Hwang, J. W. & Do, Y. Facile and Mild Deboronation of o-Carboranes Using Cesium Fluoride. Inorg. Chem. 40, 568-570 (2001).
72. Davidson, M. G. et al. Deboronation of ortho-Carborane by an Iminophosphorane: Crystal Structures of the Novel Carborane Adduct nido-$C_2B_{10}H_{12}{\cdot}HNP(NMe_2)_3$ and the borenium salt $[(Me_2N)_3PNHBNP(NMe_2)_3]_2O^{2+}(C_2B_9H_{12}^-)_2$. Chem. Comm. 1649–1650 (1999).
73. Hawthorne, M. F., Young D. C. & P. A. Wegner, J. Carbametallic Boron Hydride Derivatives. I. Apparent Analogs of Ferrocene and Ferricinium Ion. Am. Chem. Soc. 87, 1818–1819 (1965).
74. Hawthorne, M. F., Young, D. C. & Wegner, P. A. Carbametallic Boron Hydride Derivatives. I. Apparent Analogs of Ferrocene and Ferricinium Ion. J. Am. Chem. Soc. 87, 1818–1819 (1965).
75. Viñas, C., *et al*. Synthesis of Cobaltabis(dicarbollyl) Complexes Incorporating Exocluster SR Substituents and the Improved Synthesis of [3,3‘-Co(1-R-2-R‘-1,2-C2B9H9)2]-Derivatives. Inorg. Chem. 36, 2482–2486 (1997).
76. Núñez, R., Romero, I., Teixidor, F. & Viñas, C. Icosahedral Boron Clusters: a Perfect Tool for the Enhancement of Polymer Features. Chem. Soc. Rev. 45, 5147-5173 (2016).
77. Núñez, R., Tarrés, M., Ferrer-Ugalde, A., Fabrizi de Biani. F. & Teixidor. F. Electrochemistry and Photoluminescence of Icosahedral Carboranes, Boranes, Metallacarboranes, and Their Derivatives, Chem. Rev. 116, 14307−14378 (2016).

CONFIDENCIAL

78. Viñas, C & Hey-Hawkins, E. Boron-Based Compounds: Potential and Emerging Applications in Medicine. (John Wiley & Sons, 2018).
79. Hosmane, N.S & Eagling, R. Handbook of Boron Chemistry in Organometallics, Catalysis, Materials and Medicine. (World Science Publishers, 2018).
80. Farràs, P. *et al*. Metallacarboranes and Their Interactions: Theoretical Insights and Their Applicability. Chem. Soc. Rev. 41, 3445 (2012).
81. Sivaev, I. B. & Bregadze, V. I. Chemistry of Cobalt Bis(dicarbollides). A Review. Collect. Czechoslov. Chem. Commun. 64, 783–805 (1999).
82. Scholz, M. & Hey-Hawkins, E. Carbaboranes as Pharmacophores: Properties, Synthesis, and Application Strategies. Chem. Rev. 111, 7035–7062 (2011).
83. Fox, M.A. & Hughes, A.K. Coord. Chem. Rev. 248, 457–476 (2004).
84. Puga, A.V., Teixidor, F. Sillanpää, R., Kivekäs, R. & Viñas, C. Iodinated ortho-Carboranes as Versatile Building Blocks to Design Intermolecular Interactions in Crystal Lattices. Chem. Eur. J. 15, 9764 – 9772 (2009).
85. Hopewell, J. W., Morris, G. M., Schwint, A. & Coderre, J. A. The Radiobiological Principles of Boron Neutron Capture Therapy: A Critical Review. Appl. Radiat. Isot. 69, 1756–1759 (2011).
86. Locher, G. Biological Effects and Therapeutic Possibilities of Neutrons. Am. J. Roentgenol. Radium Ther. 36, 1–13 (1936).
87. Coderre, J. A. & Morris, G. M. The Radiation Biology of Boron Neutron Capture Therapy. Radiat. Res. 151, 1–18 (1999).
88. Pozzi, E. *et al*. Dosimetry and Radiobiology at the New RA-3 Reactor Boron Neutron Capture Therapy (BNCT) Facility: Application to the Treatment of Experimental Oral Cancer. Appl. Radiat. Isot. 67, S309–S312 (2009).
89. Byvaltsev, V., Kanygin, V., Belykh, E. & Taskaev, S. Prospects in Boron Neutron Capture Therapy of Brain Tumors. World Neurosurg. 78, 8–9 (2012).
90. Barth, R. F., Soloway, A. H. & Brugger, R. M. Boron Neutron Capture Therapy of Brain Tumors: Past History, Current Status, and Future Potential. Cancer Invest. 14, 534–550 (1996).
91. Soloway, A. H. *et al*. The Chemistry of Neutron Capture Therapy. Chem. Rev. 98, 1515–1562 (1998).
92. Sweet, W. H. The Uses of Nuclear Disintegration in the Diagnosis and Treatment of Brain Tumor. N. Engl. J. Med. 245, 875–878 (1951).
93. Javid, M., Brownell, G. L. & Sweet, W. H. The Possible use of Neutron capturing Isotopes such as Boron10 in the Treatment of Neoplasms. II. Computation of the Radiation Energies and Estimates of Effects in Normal and Neoplastic Brain. J. Clin. Invest. 31, 604–610 (1952).

CONFIDENCIAL

94. Farr, L. E., Robertson, J. S., Stickley, E. E., Bagnall, H. J., Easterday, O. D. K. W. Recent Advances in Neutron Capture Therapy. Proceedings of the Second United Nations International Conference on the Peaceful Uses of Atomic Energy 451–456 (1958).
95. Archambeau, J. O. The Effect of Increasing Exposures of the 10 B(n,α) 7 Li Reaction on the Skin of Man. Radiology 94, 179–187 (1970).
96. Sweet, W. H., Soloway, A. H. & Brownell, G. L. Boron-Slow Neutron Capture Therapy of Gliomas. Acta Radiol. Ther. Phys. Biol. 1, 114–121 (1963).
97. Asbury, A. K., Ojemann, R. G., NielsenI, S. L. & Sweet, W. H. Neuropathologic Study of Fourteen cases of Malignant Brain Tumor Treated by Boron-10 Slow Neutron Capture Radiation. J. Neuropathol. Exp. Neurol. 31, 278–303 (1972).
98. Hatanaka H. Boron-neutron Capture Therapy for Tumors, in Glioma Principles and Practice in Neuro-Oncology. (Springer-Verlag Berlin Heidelberg, 1986).
99. Hatanaka, H., Sweet, W. H., Sano, K. & Ellis, F. The Present Status of Boron-neutron Capture Therapy for Tumors. Pure Appl. Chem. 63, 373–374 (1991).
100. Maurer, J. L., Serino, A. J. & Hawthrone, M. F. Hydrophilically Augmented Glycosyl Carborane Derivatives for Incorporation in Antibody Conjugation Reagents. Organometallics 7, 2519–2524 (1988).
101. Tietze, L. F. & Bothe, U. Ortho-Carboranyl Glycosides of Glucose, Mannose, Maltose and Lactose for Cancer Treatment by Boron Neutron-Capture Therapy. Chem. - A Eur. J. 4, 1179–1183 (1998).
102. Tietze, L. F., Bothe, U. & Schuberth, I. Preparation of a New Carboranyl Lactoside for the Treatment of Cancer by Boron Neutron Capture Therapy: Synthesis and Toxicity of Fluoro Carboranyl Glycosides for in vivo ^{19}F-NMR Spectroscopy. Chem. - A Eur. J. 6, 836–842 (2000).
103. Tietze, L. F. *et al*. Carboranyl Bisglycosides for the Treatment of Cancer by Boron Neutron Capture Therapy. ChemBioChem 2, 326–334 (2001).
104. Tjarks, W. The Use of Boron Clusters in the Rational Design of Boronated Nucleosides for Neutron Capture Therapy of Cancer. J. Organomet. Chem. 614–615, 37–47 (2000).
105. Byun, Y. *et al*. Preparation and Biological Evaluation of 10 B-Enriched 3-[5-{2-(2,3-Dihydroxyprop-1-yl)- o -carboran-1-yl}pentan-1-yl]thymidine (N5-2OH), a New Boron Delivery Agent for Boron Neutron Capture Therapy of Brain Tumors. J. Med. Chem. 49, 5513–5523 (2006).
106. Barth, R. F. *et al*. Boron-Containing Nucleosides as Potential Delivery Agents for Neutron Capture Therapy of Brain Tumors. Cancer Res. 64, 6287–6295 (2004).

CONFIDENCIAL

107. Al-Madhoun, A. S., Johnsamuel, J., Barth, R. F., Tjarks, W. & Eriksson, S. Evaluation of Human Thymidine Kinase 1 Substrates as New Candidates for Boron Neutron Capture Therapy. Cancer Res. 64, 6280–6286 (2004).

108. Barth, R. F. *et al*. Thymidine Kinase 1 as a Molecular Target for Boron Neutron Capture Therapy of Brain Tumors. Proc. Natl. Acad. Sci. 105, 17493–17497 (2008).

109. Leśnikowski, Z. J. *et al*. Towards New Boron Carriers for Boron Neutron Capture Therapy: Metallacarboranes and their Nucleoside Conjugates. Bioorg. Med. Chem. 13, 4168–4175 (2005).

110. Haushalter, R. C. & Rudolph, R. W. meso-Tetracarboranylporphyrins. J. Am. Chem. Soc. 100, 4628–4629 (1978).

111. Haushalter, R. C., Butler, W. M. & Rudolph, R. W. The Preparation and Characterization of Several meso-Tetracarboranylporphyrins. J. Am. Chem. Soc. 103, 2620–2627 (1981).

112. Renner, M., Miura, M., Easson, M. & Vicente, M. Recent Progress in the Syntheses and Biological Evaluation of Boronated Porphyrins for Boron Neutron-Capture Therapy. Anticancer. Agents Med. Chem. 6, 145–157 (2006).

113. Kahl, S. B. & Koo, M.-S. Synthesis of Tetrakis-carborane-carboxylate Esters of 2,4-Bis-(α,β-dihydroxyethyl)-deuteroporphyrin IX. J. Chem. Soc., Chem. Commun. 1769–1771 (1990).

114. Hill, J. S. *et al*. Selective Tumor Uptake of a Boronated Porphyrin in an Animal Model of Cerebral Glioma. Proc. Natl. Acad. Sci. 89, 1785–1789 (1992).

115. Rosenthal, M. A. *et al*. Phase I and Pharmacokinetic Study of Photodynamic Therapy for High-Grade Gliomas Using a Novel Boronated Porphyrin. J. Clin. Oncol. 19, 519–524 (2001).

116. Vicente, M. G. H., Edwards, B. F., Shetty, S. J., Hou, Y. & Boggan, J. E. Syntheses and Preliminary Biological Studies of Four meso-Tetra[(nido-carboranylmethyl)phenyl]porphyrins. Bioorg. Med. Chem. 10, 481–492 (2002).

117. Ozawa, T. *et al*. In Vivo Evaluation of the Boronated Porphyrin TABP-1 in U-87 MG Intracerebral Human Glioblastoma Xenografts. Mol. Pharm. 1, 368–374 (2004).

118. Sneddon. L.G, *et al*. Polyborane Reactions in Ionic Liquids. Pure. Appl. Chem. 78, 1349-1355 (2006).

119. Valliant, J.F. *et al*. High Yielding Preparation of Dicarba-closo-dodecaboranes Using a Silver(I) Mediated Dehydrogenative Alkyne-insertion Reaction. Inorg. Chem. 52, 8743−8749 (2013).

120. Bould, J. *et al*. Borane reaction chemistry. Alkyne insertion reactions into boron-containing clusters. Products from the thermolysis of [6,9-(2-HC≡C–C_5H_4N)2-arachno-$B_{10}H_{12}$]. Dalton Trans. 12, 1552–1563 (2008).

CONFIDENCIAL

121. a) Li, Y., Kusari, U., Patrick J.C., Bradley, M.G., & Sneddon L.G. Polyborane reactions in ionic liquids. Pure App. Chem. 78, 1349-1355 (2006); b) Toppino, A., Genady., A.R, El-Zaira, M., Mostofian, F., Kent, J & Vaillant. High Yielding Preparation of Dicarba-closo-dodecaboranes Using a Silver(I) Mediated Dehydrogenative Alkyne-Insertion Reaction. J. Inorg. Chem. 52, 8743−8749 (2013). c) El compuesto **2** fue preparado utilizando la metodología descrita por Teixidor, F., Gómez, S., Lamrani, M. & Viñas, C. Mixed Cobaltacarboranes Incorporating η5-Pyrrolyl and Dicarbollide Ligands. Synthetic Routes, Structures, and Mechanistic Implications. Organometallics. 16, 1278-1283. (1997); d) El compuesto **3** fue preparado utilizando la metodología descrita por Matuszewski, M., Kiliszek, A., Rypniewski, W., Lesnikowski, Z.J. & Olejniczak, A.B. Nucleoside bearing boron clusters and their phosphoramidites – building blocks for modified oligonucleotide synthesis. New J. Chem. 39, 1202–1221 (2015); e) El compuesto **4** fue preparado utilizando la metodología por Satapathy, R. *et al*. New classes of carborane-appended 5-thio-D-glucopyranose derivatives. Dalton Trans. 41, 8982–8988 (2012)

122. Bregadze, V. I. *et al*. Novel types of boronated chlorin e_6 conjugates via 'click chemistry. Appl. Organometal. Chem. 23, 370–374 (2009).

123. Orlova, A. V. *et al*. Synthesis of Novel Derivatives of Closo-dodecaborate Anion With Azido Group at the Terminal Position of the Spacer. Appl. Organometal. Chem. 21, 98–100 (2007).

124. Armstrong, A. F. & Valliant, J. F. The Bioinorganic and Medicinal Chemistry of Carboranes: From New Drug Discovery to Molecular Imaging and Therapy. Dalton Trans. 4240–4251 (2007).

125. Hermanek, S. NMR As a Tool for Elucidation of Structures and Estimation of Electron Distribution in Boranes and Their Derivatives. Inorg. Chim. Acta. 289, 20–40 (1999).

126. Hawthorne, M. F. & Pushechnikov, A. Polyhedral Borane Derivatives: Unique and Versatile Structural Motifs. Pure Appl. Chem. 84, 2279–2288 (2012).

127. Viñas, C. *et al*. Are Halocarboranes Suitable for Substitution Reactions? The Case for 3-I-1,2-closo-$C_2B_{10}H_{11}$: Molecular Orbital Calculations, Aryldehalogenation Reactions, B-11 NMR Interpretation of Closo-carboranes, and Molecular Structures of 1-Ph-3-Br-1,2-closo-$C_2B_{10}H_{10}$ and 3-Ph-1,2-closo-$C_2B_{10}H_{11}$. Inorg. Chem. 40, 66555–6562 (2001).

128. Cabrera, M., *et al*. Synthetic Chalcones, Flavanones, and Flavones as Antitumoral Agents: Biological Evaluation and Structure-activity Relationships. Bioorg. Med. Chem. 15, 3356–3367 (2007).

CONFIDENCIAL

129. Hansch, C. & Leo, A. The Hydrophobic Parameter: Measurement and Calculation, Exploring QSAR, Fundamentals and Applications in Chemistry and Biology. (American Chemical Society, 1995).

130. Sequist L.V. *et al*. Genotypic and Histological Evolution of Lung Cancers Acquiring Resistance to EGFR Inhibitors. Sci. Transl. Med. 3, 75ra26 (2011).

131. Young, R.C. *et al*. Development of a New Physicochemical Model for Brain Penetration and its Application to the Design of Centrally Acting H2 Receptor Histamine Antagonists, J. Med. Chem. 31, 656–671 (1988).

132. Di, L. & Kerns, E. Drug-like Properties: Concepts, Structure Design and Methods from ADME to Toxicity Optimization, (Academic Press, 1st Ed., 2008).

133. Lu, X., Liu, W., Ouyang, J. & Tian, J. Distinct Surface Hydration Behaviors of Boron-rich Boride Thin Film Coatings. Appl. Surf. Sci. 311, 749–752 (2014).

134. Cheng, C.C. *et al*. STAT3 Exacerbates Survival of Cancer Stem-like Tumor Spheres in EGFR-Positive Colorectal Cancers: RNAseq Analysis and Therapeutic Screening. J. Biomed. Sci. 25, 60 (2018).

135. Shen, J., Cheng, F., Xu, Y., Li, W. & Tang, Y. Estimation of ADME properties with substructure pattern recognition. J. Chem. Inf. Model. 50, 1034–1041 (2010).

136. Pham-The, H. *et al*. In Silico prediction of Caco-2 cell permeability by a classification QSAR approach. Mol. Inf. 30, 376–385 (2011).

137. Chen, L., Li, Y., Zhao, Q., Peng, H. & Hou, T. ADME evaluation in drug discovery. 10. Predictions of P-glycoprotein inhibitors using recursive partitioning and naive Bayesian classification techniques. Mol. Pharm. 8, 889–900 (2011).

138. Broccatelli, F. *et al*. A novel approach for predicting P-glycoprotein (ABCB1) inhibition using molecular interaction fields. J. Med. Chem. 54, 1740–1751 (2011).

139. Kido, Y., Matsson, P. & Giacomini, K. M. Profiling of a Prescription Drug Library for Potential Renal Drug-drug Interactions Mediated by the Organic Cation Transporter 2. J. Med. Chem. 54, 4548–4558 (2011).

140. Carbon-Mangels, M. & Hutter, M. C. Selecting relevant descriptors for classification by Bayesian estimates: A comparison with decision trees and support vector machines approaches for disparate data sets. Mol. Inf. 30, 885–895 (2011).

141. Marchese Robinson, R. L., Glen, R. C. & Mitchell, J. B. O. Development and Comparison of hERG Blocker Classifiers: Assessment on Different Datasets Yields Markedly Different Results. Mol. Inf. 30, 443–458 (2011).

142. Wang, S. *et al*. ADMET Evaluation in Drug Discovery. 12. Development of Binary Classification Models for Prediction of hERG Potassium Channel Blockage. Mol. Pharm. 9, 996–1010 (2012).

CONFIDENCIAL

143. Lagunin. A. *et al*. Computer-aided prediction of rodent carcinogenicity by PASS and CISOC-PSCT. QSAR Comb. Sci. 28, 806–810 (2009).

144. Hou, T. J., Xia, K., Zhang, W. & Xu, X. J. ADME Evaluation in Drug Discovery. 4. Prediction of Aqueous Solubility Based on Atom Contribuition Approach. J. Chem. Inf. Comput. Sci. 44, 266-275 (2004).

145. Couto, M. *et al*. Discovery of Potent EGFR Inhibitors Through the Incorporation of a 3D Aromatic-boron-rich-cluster Into the 4-anilinoquinazoline Scaffold: Potential Drugs for Glioma Treatment. Chem. Eur. J. 24, 3122–3126 (2018).

146. Murray, C. W. *et al*. Validity of ligand efficiency metrics. ACS Med. Chem. Lett. 5, 616–618 (2014).

147. Zhu, H. *et al*. Quantitative structure-activity relationship modeling of rat acute toxicity by oral exposure. Chem. Res. Toxicol. 22, 1913–1921 (2009).

148. Wang, J. *et al*. Development of reliable aqueous solubility models and their application in druglike analysis. J. Chem. Inf. Model. 47, 1395-1404 (2007).

149. Leeson PD, Springthorpe B. The influence of drug-like concepts on decision-making in medicinal chemistry. Nat. Rev. Drug Discov. 6, 881-890 (2007).

150. OECD, Test No. 423: Acute Oral toxicity - Acute Toxic Class Method, OECD Guidelines for the Testing of Chemicals, Section 4. (OECD Publishing, Paris, 2002) https://doi.org/10.1787/9789264071001-en.

151. Irwin S. Comprehensive observational assessment: Ia. A systematic, quantitative procedure for assessing the behavioral and physiologic state of the mouse. Psychopharmacology (Springer-Verlag, 1968).

152. Bruce. L. & Bruce I. Polymer-based anti-cancer agents. WO 2007/123468 A1 (2007)

153. Oh, K. T., Bronich, T. K. & Kabanov, A. V. Micellar formulations for drug delivery based on mixtures of hydrophobic and hydrophilic Pluronic® block copolymers. J. Control. Release 94, 411-422 (2004).

154. Wei, Z., Hao, J., Yuan, S. *et al*. Paclitaxel-loaded Pluronic P123/F127 mixed polymeric micelles: Formulation, optimization and in vitro characterization. Int. J. Pharm. 376, 176-185 (2009).

155. Couto, M. *et al*. Small-molecule kinase-inhibitors-loaded boron cluster as hybrid 463 agents for glioma-cell-targeting therapy. Chem. Eur. J. 23, 9233–9238 (2017).

156. Hu, J. *et al*. Discovery of selective EGFR modulator to inhibit L858R/T790M double mutants bearing a N-9-diphenyl-9H-purin-2-amine scaffold. Bioorg. Med. Chem. 26, 1810–1822 (2018).

CONFIDENCIAL

157. Guan, Y. *et al*. Effect of pluronic P123 and F127 block copolymer on P-glycoprotein transport and CYP3 A metabolism. Arch. Pharmacol. Res. 34, 1719–1728 (2011).

158. Patra, A. *et al*. Formulation and evaluation of mixed polymeric micelles of quercetin for treatment of breast, ovarian, and multidrug resistant cancers. Int. J. Nanomed. 13, 2869–2881 (2018).

159. Laird, A. D. *et al*. SU6668 is a potent antiangiogenic and antitumor agent that induces regression of established tumors. Cancer Res. 60, 4152–4160 (2000).

160. Sun, L. *et al*. Discovery of 5-[5-fluoro-2-oxo-1,2- dihydroindol-(3Z)-ylidenemethyl]-2,4- dimethyl-1H-pyrrole-3-carboxylic acid (2-diethylaminoethyl)amide, a novel tyrosine kinase inhibitor targeting vascular endothelial and platelet-derived growth factor receptor tyrosine kinase. J. Med. Chem. 46, 1116–1119 (2003).

161. Stupp, R. *et al*. Radiotherapy plus concomitant and adjuvant temozolomide for glioblastoma. N Engl J Med. 352, 987–96 (2005).

162. Gilliland, D. G., Griffin, J. D. The roles of FLT3 in hematopoiesis and leukemia. Blood. 100, 1532-1542 (2002).

163. Heinrich, M. C. Kinase mutations and imatinib response in patients with metastatic gastrointestinal stromal tumor. J. Clin. Oncol. 21, 4342-4349 (2003).

164. Lago, J., Santaclara, F., Vieites, J. M. & Cabado, A. G. Collapse of mitochondrial membrane potential and caspases activation are early events in okadaic acid-treated Caco-2 cells. Toxicon. 46, 579-86 (2005).

165. Cheng, F. AdmetSAR: a comprehensive source and free tool for assessment of chemical ADMET properties. J. Chem. Inf. Model. 52, 3099-105 (2012).

166. Malina, K.; Cooper, I.; Teichberg, V. Closing the gap between the in-vivo and in-vitro blood–brain barrier tightness. Brain Research. 1284, 12-21 (2009).

167. Vainshtein, A. *et al*. Quinazoline-based tricyclic compounds that regulate programmed cell death, induce neuronal differentiation, and are curative in animal models for excitotoxicity and hereditary brain disease. Cell. Death. Discov. 1, 15027 (2015).

CONFIDENCIAL

9 Anexo

CONFIDENCIAL

ChemPubSoc Europe

DOI: 10.1002/chem.201701965

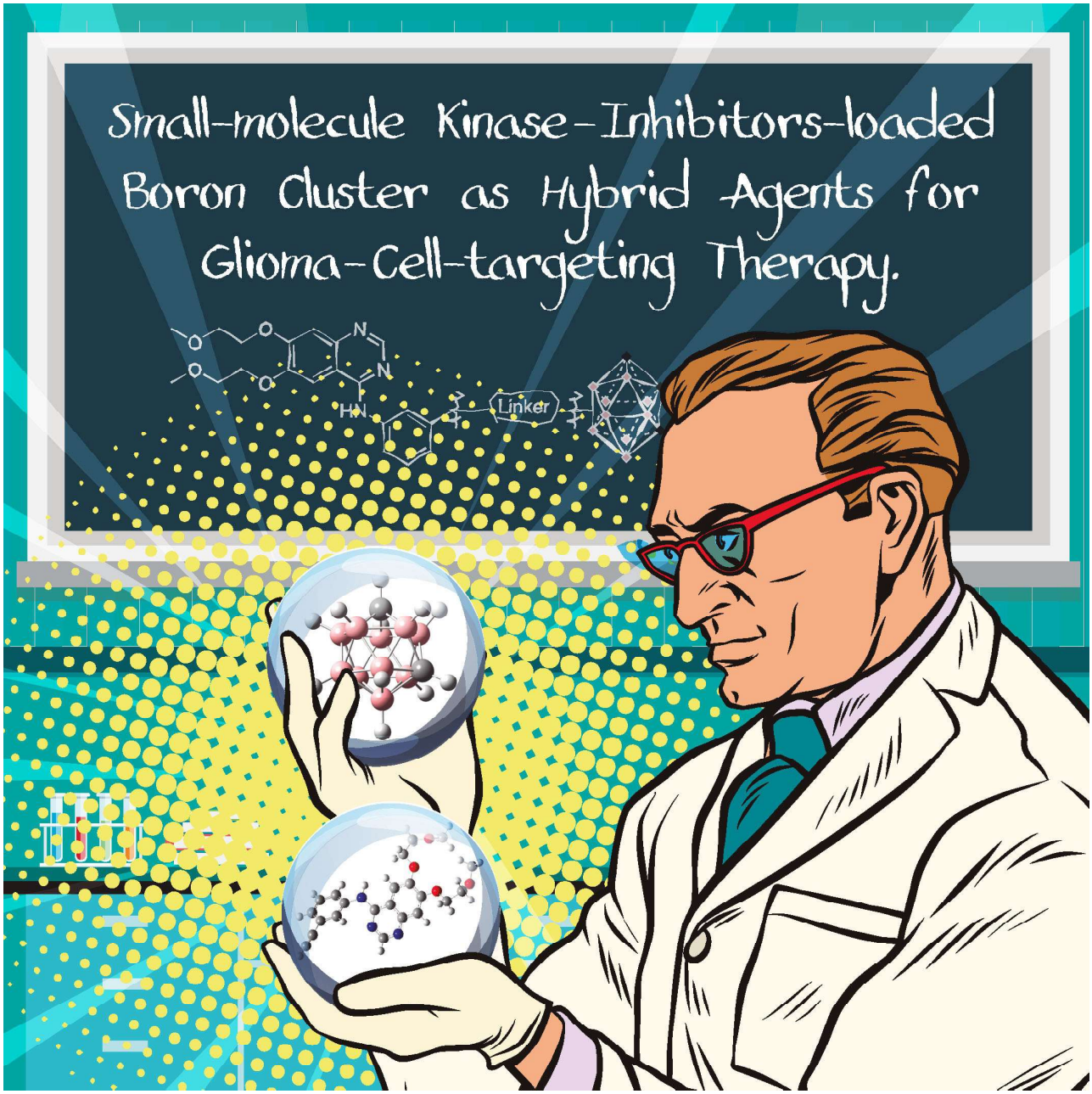
CHEMISTRY
A European Journal
Communication

Synthetic Methods | *Hot Paper*

Small-Molecule Kinase-Inhibitors-Loaded Boron Cluster as Hybrid Agents for Glioma-Cell-Targeting Therapy

Marcos Couto,[a, b, c] Ignacio Mastandrea,[d, e] Mauricio Cabrera,[d] Pablo Cabral,[c] Francesc Teixidor,[b] Hugo Cerecetto,*[a, c] and Clara Viñas*[b]

Dedicated to Prof. Evamarie Hey-Hawkins for her contributions to the chemistry of boron and phosphorus on the occasion of her 60th birthday



© 2017 Wiley-VCH Verlag GmbH & Co. KGaA, Weinheim

Abstract: The reported new anilinoquinazoline-icosahedral borane hybrids have been evaluated as glioma targeting for potential use in cancer therapy. Their *anti*-glioma activity depends on hybrids' lipophilicity; the most powerful compound against glioma cells, a 1,7-*closo*-derivative, displayed at least 3.3 times higher activity than the parent drug erlotinib. According to the cytotoxic effects on normal glia cells, the hybrids were selective for epidermal growth factor receptor (EGFR)-overexpressed tumor cells. These boron carriers could be used to enrich glioma cancer cells with boron for cancer therapy.

Glioblastoma multiforme (GBM) is the most common primary central nervous system tumor in USA and Europe: World Health Organization (WHO) reported more than 50% of diagnosed gliomas corresponded to grade IV ones, the most malignant form.[1] The etiology and the predisposing factors of GBM are still poorly understood being the exposure to ionizing radiation, such as children irradiated for leukemia, one of the few proven environmental risk factor.[2] Despite GBM being a genetically heterogeneous tumor, there has been some common molecular characteristic described, such as the loss of heterozygosity on chromosome 10,[3] and the amplification of epidermal growth factor receptor (EGFR) gene on chromosome 7, often in the form of double minutes.[4] EGFR overexpression is more common in primary GBM (40–60%) than in secondary ones (less than 10%). EGFR, also known as erb-B1 or Her-1, is a member of ErbB family of transmembrane tyrosine kinase receptor (TKR)[5] involved in enhancing growth, proliferation, migration, tumor neovascularization, and resistance to chemotherapies.[6] The GBM standard treatment is surgical resection of the tumor followed by a combination of radiation and chemotherapy to kill any remaining tumor cells infiltrated in the brain parenchyma.[7a] However, the current therapeutic success is still limited.[7b] For this reason, new chemotherapies (antiangiogenic, immune and gene therapies, drugs to overcome resistance, radiation-enhancement, targeted-molecular therapies,[7c,d] and boron neutron capture therapy (BNCT)) are under investigation. EGFR and other TKRs are among the most studied pathways for the development of new targeted molecular agents. In this sense, small molecules porting the 4-anilinoquinazoline pharmacophore have been described as TKRs-inhibitors.[8] The 4-anilinoquinazoline TKRs-inhibitors, such as erlotinib (approved for clinical treatment as Tarceva, Figure 1),[9]

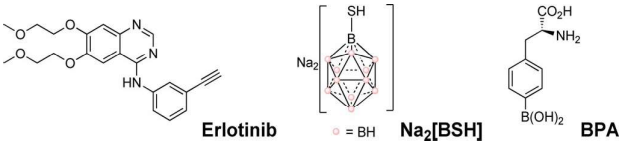


Figure 1. TKRs inhibitor and boronated agents used for clinical treatment of GBM.

competitively binds to the ATP binding site of the protein kinases intracellularly located in the transmembrane receptor.[10] On the other hand, BNCT relies upon the production of the high linear energy transfer particles ($^4He^{2+}$ and $^7Li^{3+}$) formed by the capture of thermal neutrons by a non-radioactive drug that contains in its structure ^{10}B isotopes.[11] Due to these particles having a linear path trajectory similar to the diameter of a cell, the BNCT damage is selectively confined in the tumor when the drug is selectively delivered in its cells. The current BNCT boronated clinical agents for GBM are BPA (*p*-boronophenylalanine) and BSH (mercaptoundecahydro-*closo*-dodecaborate; Figure 1). Nevertheless, none of them selectively target tumor cells, which results in cytotoxicity and limits their application.[12] Recently, TK inhibitors incorporating a single boron atom, as boronic acid moiety, have been exploited as boron-containing drug targeting within glioma cells,[13] though their BNCT applications could be limited due to the low concentration of boron in the cells. Contrarily, the incorporation of the anionic dodecaborate cage present in BSH contributes with twelve boron atoms per molecule. In this sense, the use of neutral *closo*-carborane (1,2-*closo*-$C_2B_{10}H_{11}$, 1,7-*closo*-$C_2B_{10}H_{11}$) and anionic *closo*-borane ($[B_{12}H_{12}]^{2-}$) and cobaltabisdicarbollide ($[3,3'\text{-}Co(1,2\text{-}C_2B_9H_{11}]^-$) moieties may offer distinct advantages in BNCT medicinal chemistry, that is, are inert to metabolic degradation, which increases their bioavailability, promote hydrophobic interactions with biological moleculles, which are possible drug targets, and could be incorporated to organic framework.[11,14]

Herein, we describe the development of new hybrid molecules with potential dual action (drug-radiotherapy combinations) to result in significant clinical benefits. For this purpose, the synthesis of new boron-containing quinazolines has been achieved, and their in vitro activities toward glioma cells were assessed (Figure 2). These new compounds combine the 4-anilinoquinazolinyl moiety that possesses the capability to interact intracellularly with EGFR, with the icosahedral boron clusters, as the source of boron. Moreover, the different icosahedral boron clusters that have different lipophilicity could pro-

[a] *M. Couto, Dr. H. Cerecetto*
Grupo de Química Medicinal, Laboratorio de Química Orgánica
Facultad de Ciencias, Universidad de la República
Iguá 4225, 11400 Montevideo (Uruguay)
E-mail: hcerecetto@cin.edu.uy

[b] *M. Couto, Prof. Dr. F. Teixidor, Prof. Dr. C. Viñas*
Institut de Ciències dels Materials de Barcelona
ICMAB-CSIC Campus UAB, 08193 Bellaterra (Spain)
E-mail: clara@icmab.es

[c] *M. Couto, Dr. P. Cabral, Dr. H. Cerecetto*
Área de Radiofarmacia
Centro de Investigaciones Nucleares Facultad de Ciencias
Universidad de la República Mataojo 2055, 11400 Montevideo (Uruguay)

[d] *I. Mastandrea, Dr. M. Cabrera*
Centro Universitario Paysandú. CenUR Litoral Norte
Universidad de la República. 60000 Paysandú (Uruguay)

[e] *I. Mastandrea*
Instituto de Investigaciones Biológicas Clemente Estable
11600 Montevideo (Uruguay)

Supporting information and the ORCID identification number(s) for the author(s) of this article can be found under https://doi.org/10.1002/chem.201701965.

© 2017 Wiley-VCH Verlag GmbH & Co. KGaA, Weinheim

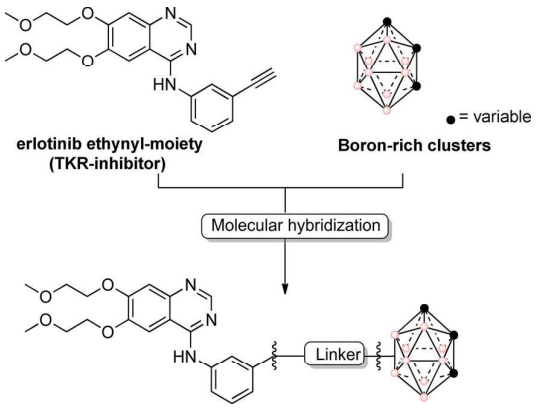


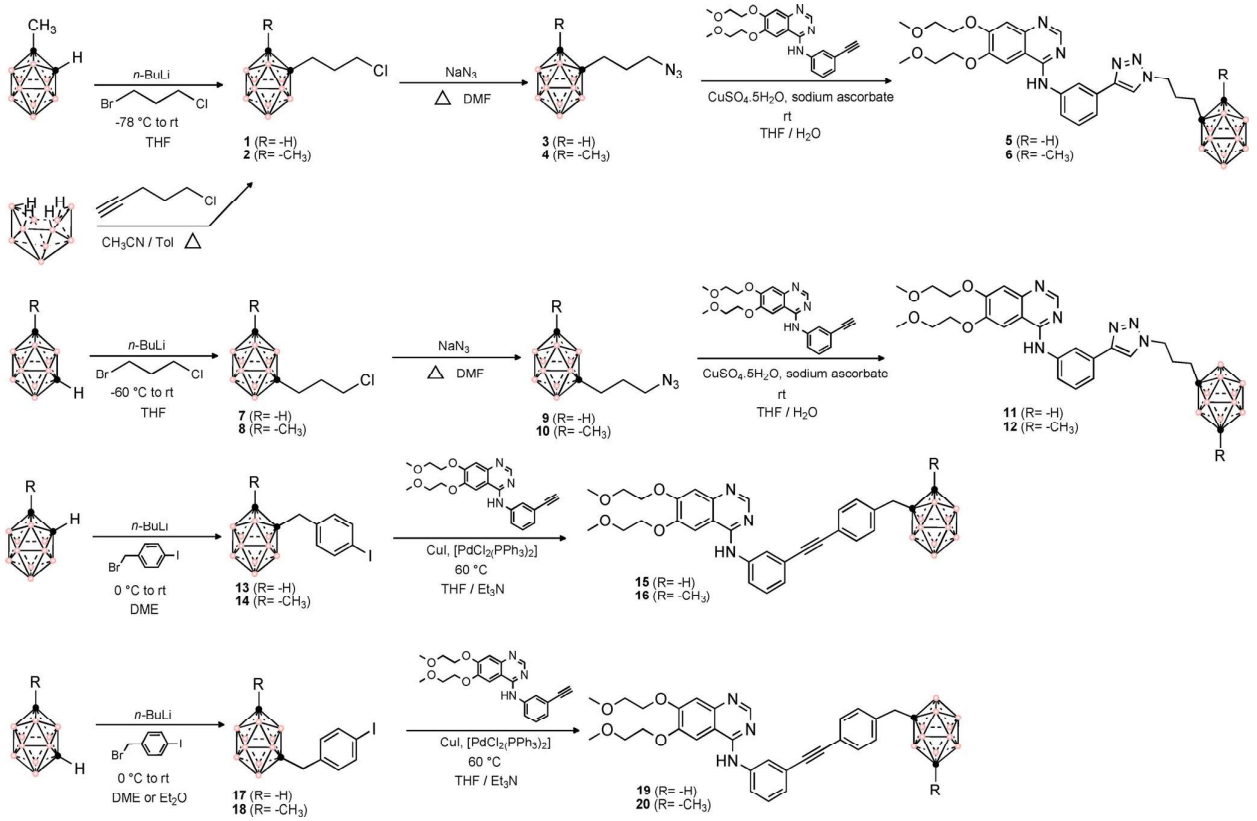
Figure 2. General design of the hybrid agents.

vide different bioactivity to the boron-containing anilinoquinazoline derivatives.[10,15]

To enhance the interaction between the quinazoline derivatives and the EGFR, by increasing lipophilicity,[10,15] we selected the erlotinib ethynyl moiety as synthon of structural modifications. The direct reaction between ethynyl/erlotinib and decaborane via decaborane/acetonitrile adduct formation followed by alkyne insertion was first attempted. However, the coordination capability of the nitrogen from the quinazoline produced a complex mixture, but not the desired compounds, as has been previously reported for the synthesis of 1-(C_5H_4N)-1,2-*closo*-$C_2B_{10}H_{11}$.[16] Consequently, the ethynyl moiety was used as connector to design several families with a linker between TKR-interacting group and the icosahedral boron cluster. Scheme 1 shows the synthesis of the new anilinoquinazoline/icosahedralborane cluster hybrids. The first approach consisted in the use of [1,2,3]triazolylpropyl connector generated by 1,3-dipolar cycloaddition,[17] in the presence of $CuSO_4 \cdot 5H_2O$ and sodium ascorbate, giving hybrids **5**, **6**, **11**, and **12** in good yield (69–78% after purification). The intermediate carboranylazides (**3**,[18a] **4**,[18b] **9**, and **10**) were selected to introduce chemodiversity to the final compounds, that is, un-substituted and methyl-substituted 1,2- and 1,7-*closo*-carboranyl frameworks. The second approach involved the transformation of ethynyl-erlotinib group into an erlotinib-ethynylbenzyl connector (Scheme 1), via Sonogashira cross-coupling in presence of CuI and $[PdCl_2(PPh_3)_2]$, generating compounds **15**, **16**, **19**, and **20** in 35–49% yield, after purification. Again, the iodophenyl intermediates (**13**, **14**, **17**, and **18**) introduced chemodiversity.

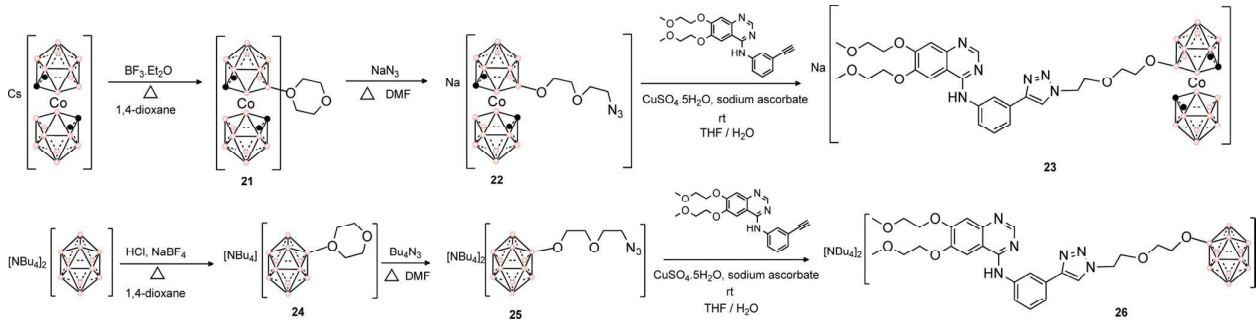
The anionic boron-containing [1,2,3]triazole derivatives **23** and **26** were obtained in 79 and 71%, respectively, after purification via 1,3-dipolar cycloaddition between ethynyl-erlotinib and azides **22**[19a] and **25**[19b] (Scheme 2).

Finally, we focused on the confirmation of the relevance of carboranyl moiety in the displayed bioactivity. For that, and according to the bioisosterism proposed by Armstrong and Valliant,[14b,20] we prepared the phenyl analogue, **28** (Scheme 3), of

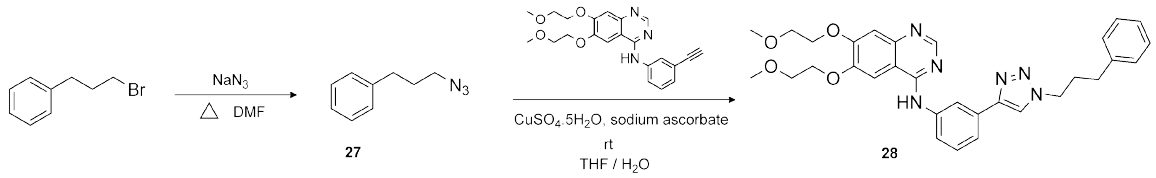


Scheme 1. Synthesis of *closo*-carboranylquinazoline.

© 2017 Wiley-VCH Verlag GmbH & Co. KGaA, Weinheim



Scheme 2. Synthesis of anionic cobaltabisdicarbollidequinazoline (**23**) and dodecaboranylquinazoline (**26**).



Scheme 3. Synthesis of bioisoster **28**.

the two most active derivatives, that is, **5** and **11** (see below). Compounds were characterized by multinuclear NMR and FT-IR spectroscopic techniques, mass spectrometry, and elemental analysis (see the Supporting Information).

The cytotoxicity of anilinoquinazoline carboranyl and dodecaboranyl derivatives was evaluated by conducting sulforhodamine B assays on C6 cells from rat glioma.[21] It has been demonstrated that this kind of cells overexpress of EGFR21f (see own results, the Supporting Information, Figure S1), even in brain tumors derived from C6 cultures. The results revealed that some boron-containing compounds had a concentration dependent cytotoxic effect on glioma cells (Table 1). Good to excellent biological results were obtained for some boron-containing derivatives when they were compared with the parent erlotinib. Compounds **5** and **11** were the most active being **11** at least 3.3 times more active than erlotinib. Additionally, **23** was at least 2.3 times more active than the parent compound. On the other hand, all the derivatives belonging to ethynylbenzyl-connector series (**15**, **16**, **19**, **20**), as well as the dianionic compound **26**, were inactive at the assayed doses. To emphasize that phenyl-analogue **28** was not as active as its bioisosters (**5** and **11**).

Table 1. Effect of the hybrids on C6 glioma cells; lipophilicity values (determined in terms of R_M) and the most active hybrids (**5**, **11**, and **23**) on a mix of primary glial cells.

Compd	IC_{50},C6 [μM][a]	R_M	Compd	IC_{50},mix [μM][b,c]	SI[d]
5	34±7	0.738	**5**	>100	>2.9
6	>100	0.857	**11**	>100	>3.3
11	30±4	0.766	**23**	>100	>2.3
12	99±4	0.966	**Erlotinib**	>100	–
15	>100	1.420			
16	>100	1.370			
19	>100	1.440			
20	>100	1.320			
23	44±6	0.150			
26	>100	−0.857			
28	79±4	0.209			
Erlotinib	>100	−0.209			

[a] Compound concentrations required to inhibit the C6 growth by 50% were determined from dose-response plots. Assays were run in triplicate. [b] Compound concentrations required to inhibit mix of primary glial cell culture growth by 50%. Assays were run in triplicate. [c] Higher doses than 100 μM could not be evaluated due to solubility problems. [d] SI: Selectivity index, defined as $IC_{50,\text{mix of primary glial cells}}/IC_{50,\text{C6 cells}}$.

To find out the selectivity toward tumor cells, cytotoxicity values of the most active compounds (**5**, **11**, and **23**) and parent erlotinib were evaluated on a mixed primary glial cell culture, and these results were compared with C6 cells (Table 1 and the Supporting Information). Clearly, the results showed that these compounds were at least 2.3 times more cytotoxic for gliomas than for the normal glial cells.

Interesting, structure–activity relationship has been assumed for the *closo*-carboranylquinazoline series. On one hand, the methyl substitution, in the *ortho* or the *meta* position, that is, compounds **6** and **12**, produced a decrease of the cytotoxicity on glioma cells (compare activities of pair of compounds **5** and **6**, and **11** and **12**, see the Supporting Information, Figure S2). This relationship was independent of the linker used between quinazolinyl and carboranyl cluster showing ethynylbenzyl connector derivatives, that is, **15**, **16**, **19**, and **20**, the same tendency but slightly lower values (see the Supporting Information, Figure S3). On the other hand, when we compared the *ortho* and *meta* isomers, that is, couple of isomers **5** and **11** or isomers **6** and **12** (see the Supporting Information, Figure S2), *meta*-carboranyl compounds were more active than the *ortho* analogues. The influence of the lipophilicity was studied to explain the observed bioactivities. In this sense, lipophilicities were determined in terms of R_M.[22] As can be seen

© 2017 Wiley-VCH Verlag GmbH & Co. KGaA, Weinheim

from Table 1, compounds with the highest hydrophilicities, **26** and the parent erlotinib, or compounds with the highest lipophilicities, **15**, **16**, **19**, and **20**, were inactive. When the R_M values were plotted versus the IC_{50} against C6 cells, quadratic curve was obtained, although the results were not statistically robust. When only the structural related compounds were considered, that is, triazole-connector derivatives **5**, **6**, **11**, **12**, **23**, **26**, and erlotinib, a statistic quadratic fitted curve was obtained (r^2_{adj} 0.9815, Figure 3). This kind of behavior, with an optimum lipophilicity, is typical of compounds that interact with a biomolecule.[23] As one could expect, the phenyl triazole derivative **28** did not fit to this relationship, it was an outlier (Figure 3).

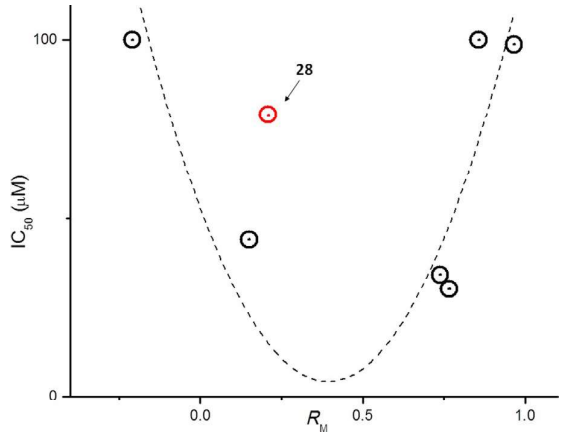


Figure 3. Relationship between IC_{50} and lipophilicity (expressed as R_M).

In conclusion, new anilinoquinazoline/icosahedralborane hybrids have been synthesized, and the in vitro cytotoxic effects toward EGFR-overexpressing C6 glioma cells were evaluated. The overall results showed that the hybrids are highly promising antitumor agents with dual action, targeting EGFR and for potential BNCT application.

Acknowledgements

We thank the Comisión Sectorial de Investigación Científica-Universidad de la República (UdelaR, Uruguay) and "Convenio CSIC (Spain)-UdelaR (Uruguay)" for financial support, and the Agencia Nacional de Investigación e Innovación (ANII, Uruguay) for providing M.C. with a fellowship (POS-NAC-2015-1-110068). This work has been supported by the Spanish Ministerio de Economía *y* Competitividad CTQ2013-44670-R and the Generalitat de Catalunya (2014/SGR/149).

Conflict of interest

The authors declare no conflict of interest.

Keywords: carboranes · cross-coupling · cycloaddition · glioblastoma multiforme · synthetic methods

[1] K. Messaoudi, A. Clavreul, F. Lagarce, *Drug Discovery Today* **2015**, *20*, 899–905.
[2] J. L. Fisher, J. A. Schwartzbaum, M. Wrensch, J. L. Wiemels, *Neurol. Clin.* **2007**, *25*, 867–890.
[3] a) B. K. Rasheed, R. E. McLendon, H. S. Friedman, A. H. Friedman, H. E. Fuchs, D. D. Bigner, S. H. Bigner, *Oncogene* **1995**, *10*, 2243–2246; b) A. E. Pegg, *Mutat. Res.* **2000**, *462*, 83–100.
[4] a) H. Ohgaki, P. Kleihues, *Am. J. Pathol.* **2007**, *170*, 1445–1453; b) I. Crespo, A. L. Vital, M. Gonzalez-Tablas, M. C. Patino, A. Otero, M. C. Lopes, C. de Oliveira, P. Domingues, A. Orfao, M. D. Tabernero, *Am. J. Pathol.* **2015**, *185*, 1820–1833.
[5] a) J. J. Laskin, A. B. Sandier, *Cancer Treat. Rev.* **2004**, *30*, 1–17; b) M. E. Halatsch, U. Schmidt, J. Behnke-Mursch, A. Unterberg, C. R. Wirtz, *Cancer Treat. Rev.* **2006**, *32*, 74–89.
[6] M. Yan, B. A. Parker, R. Schwab, R. Kurzrock, *Cancer Treat. Rev.* **2014**, *40*, 770–780.
[7] a) R. Stupp, W. P. Mason, M. J. van den Bent, M. Weller, B. Fisher, M. J. Taphoorn, K. Belanger, A. A. Brandes, C. Marosi, U. Bogdahn, J. Curschmann, R. C. Janzer, S. K. Ludwin, T. Gorlia, A. Allgeier, D. Lacombe, J. G. Cairncross, E. Eisenhauer, R. O. Mirimanoff, *N. Engl. J. Med.* **2005**, *352*, 987–996; b) Q. T. Ostrom, H. Gittleman, P. M. de Blank, J. L. Finlay, J. G. Gurney, R. McKean-Cowdin, D. S. Stearns, J. E. Wolff, M. Liu, Y. Wolinsky, C. Kruchko, J. S. Barnholtz-Sloan, *Neuro Oncol.* **2016**, *18 Suppl 1*, i1-i50; c) A. S. Chi, P. Y. Wen, *Expert Opin. Ther. Targets* **2007**, *11*, 473–496; d) S. Sathornsumetee, D. A. Reardon, A. Desjardins, J. A. Quinn, J. J. Vredenburgh, J. N. Rich, *Cancer* **2007**, *110*, 13–24.
[8] D. W. Fry, A. J. Kraker, A. McMichael, L. A. Ambroso, J. M. Nelson, W. R. Leopold, R. W. Connors, A. J. Bridges, *Science* **1994**, *265*, 1093–1095.
[9] D. R. Duckett, M. D. Cameron, *Expert Opin. Drug Metab. Toxicol.* **2010**, *6*, 1175–1193.
[10] J. Stamos, M. X. Sliwkowski, C. Eigenbrot, *J. Biol. Chem.* **2002**, *277*, 46265–46272.
[11] a) R. F. Barth, A. H. Soloway, R. G. Fairchild, R. M. Brugger, *Cancer* **1992**, *70*, 2995–3007; b) M. F. Hawthorne, *Angew. Chem. Int. Ed. Engl.* **1993**, *32*, 950–986; c) G. Calabrese, J. J. Nesnas, E. Barbu, D. Fatouros, J. Tsibouklis, *Drug Discovery Today* **2012**, *17*, 153–159; d) E. Justus, D. Awad, M. Hohnholt, T. Schaffran, K. Edwards, G. Karlsson, L. Damian, D. Gabel, *Bioconjugate Chem.* **2007**, *18*, 1287–1293; e) E. M. Heber, M. F. Hawthorne, P. J. Kueffer, M. A. Garabalino, S. I. Thorp, E. C. C. Pozzi, A. M. Hughes, C. A. Maitz, S. S. Jalisatgi, D. W. Nigg, P. Curotto, V. A. Trivillin, A. E. Schwint, *Proc. Natl. Acad. Sci. USA* **2014**, *111*, 16077–16081; f) S. Xuan, N. Zhao, Z. H. Zhou, F. R. Fronczek, M. G. H. Vincente, *J. Med. Chem.* **2016**, *59*, 2109–2117; g) *Neutron Capture Therapy: Principles and Applications* (Eds.: W. A. G. Sauerwein, A. Wittig, R. Moss, Y. Nakagawa), Springer, Heidelberg, **2012**.
[12] N. S. Hosmane in *Boron Science: New Technologies and Applications*, CRC Press, Boca Raton, **2012**.
[13] a) T. Asano, H. Nakamura, Y. Uehara, Y. Yamamoto, *ChemBioChem* **2004**, *5*, 483–490; b) H. S. Ban, T. Usui, W. Nabeyama, H. Morita, K. Fukuzawa, H. Nakamura, *Org. Biomol. Chem.* **2009**, *7*, 4415–4427; c) H. Nakamura, R. Horikoshi, T. Usui, H. S. Ban, *MedChemComm* **2010**, *1*, 282–286.
[14] a) A. H. Soloway, W. Tjarks, B. A. Barnum, F. G. Rong, R. F. Barth, I. M. Codogni, J. G. Wilson, *Chem. Rev.* **1998**, *98*, 1515–1562; b) A. F. Armstrong, J. F. Valliant, *Dalton Trans.* **2007**, 4240–4251; c) F. Issa, M. Kassiou, L. M. Rendina, *Chem. Rev.* **2011**, *111*, 5701–5722; d) M. Scholz, E. Hey-Hawkins, *Chem. Rev.* **2011**, *111*, 7035–7062; e) A. F. F. da Silva, R. S. G. R. Seixas, A. M. S. Silva, J. Coimbra, A. C. Fernandes, J. P. Santos, A. Matos, J. Rino, I. Santos, F. Marques, *Org. Biomol. Chem.* **2014**, *12*, 5201–5211.
[15] a) M. Tarrés, E. Canetta, E. Paul, J. Forbes, K. Azzouni, C. Viñas, F. Teixidor, A. J. Harwood, *Sci. Rep.* **2014**, *5*, 7804; b) H. S. Ban, H. Nakamura, *Chem. Commun.* **2015**, *51*, 616–635.
[16] J. Bould, A. Laromaine, N. J. Bullen, C. Viñas, M. Thornton-Pett, R. Sillanpää, R. Kivekäs, J. D. Kennedy, F. Teixidor, *Dalton Trans.* **2008**, 1552–1563.
[17] a) S. Fernández, J. Giglio, A. M. Rey, H. Cerecetto, *Bioorg. Med. Chem.* **2012**, *20*, 4040–4048; b) F. Teixidor, R. S. Pepiol, M. Lupu, C. Viñas, *Chem. Eur. J.* **2015**, *21*, 12778–12786.
[18] a) Compound **3** was reported by using another synthetic reaction by M. Matuszewski, A. Kiliszek, W. Rypniewski, Z. J. Lesnikowski, A. B. Olejniczak, *New J. Chem.* **2015**, *39*, 1202–1221; b) Compound **4** was reported by using another synthetic reaction by R. Satapathy, B. P. Dash, B. P.

© 2017 Wiley-VCH Verlag GmbH & Co. KGaA, Weinheim

Bode, E. A. Byczynski, S. N. Hosmane, S. Buxa, N. S. Hosmane, *Dalton Trans.* **2012**, *41*, 8982 – 8988.

[19] a) V. I. Bregadze, A. A. Semioshkin, J. N. Las'kova, M. Y. Berzina, I. A. Lobanova, I. B. Sivaev, M. A. Grin, R. A. Titeev, D. I. Brittal, O. V. Ulybina, A. V. Chestnova, A. A. Ignatova, A. V. Feofanov, A. F. Mironov, *Appl. Organomet. Chem.* **2009**, *23*, 370 – 374; b) A. V. Orlova, N. N. Kondakov, B. G. Kimel, L. O. Kononov, E. G. Kononova, I. B. Sivaev, V. I. Bregadze, *Appl. Organomet. Chem.* **2007**, *21*, 98 – 100.

[20] M. F. Hawthorne, A. Pushechnikov, *Pure Appl. Chem.* **2012**, *84*, 2279 – 2288.

[21] a) P. Skehan, R. Storeng, D. Scudiero, A. Monks, J. M. Mahon, D. Vistica, J. T. Warren, H. Bokesch, S. Kenney, M. R. Boyd, *J. Natl. Cancer. Inst.* **1990**, *82*, 1107 – 1112; b) S. Kumar, M. A. Kahn, L. Dinh, J. de Vellis, *J. Neurosci. Res.* **1998**, *54*, 754 – 765; c) R. F. Barth, B. Kaur, *J. Neuro-Oncol.* **2009**, *94*, 299 – 312; d) X. Z. Dong, C. L. Huang, B. Y. Yu, Y. Hu, L. H. Mu, P. Liu, *Phytomedicine* **2014**, *21*, 1178 – 1188; e) C.-S. Xu, Z.-F. Wang, L.-M. Dai, S.-H. Chu, L.-L. Gong, M.-H. Yang, Z.-Q. Li, *J. Transl. Med.* **2014**, *12*, 148; f) M. A. Shevtsov, B. P. Nikolaev, L. Y. Yakovleva, Y. Y. Marchenko, A. V. Dobrodumov, A. L. Mikhrina, M. G. Martynova, O. A. Bystrova, I. V. Yakovenko, A. M. Ischenko, *Int. J. Nanomed.* **2014**, *9*, 273 – 287; g) V. Thiyagarajan, M. J. Tsai, C. F. Weng, *PLoS One* **2015**, *10*, e0141285.

[22] a) In reversed-phase thin-layer chromatography (RP-TLC), $R_M = \log(1/R_F - 1)$ and R_F is defined as the ratio between the migration distances of compound and the mobile phase. b) A. Tsantili-Kakoulidou, A. Antoniadou-Vyza, *Prog. Clin. Biol. Res.* **1989**, *291*, 71 – 74; c) H. Cerecetto, R. Di Maio, M. González, M. Risso, P. Saenz, G. Seoane, A. Denicola, G. Peluffo, C. Quijano, C. Olea-Azar, *J. Med. Chem.* **1999**, *42*, 1941 – 1950.

[23] C. Hansch, A. Leo in *The Hydrophobic Parameter: Measurement and Calculation, Exploring QSAR, Fundamentals and Applications in Chemistry and Biology*, American Chemical Society, Washington, **1995**, pp. 97 – 124.

Manuscript received: May 2, 2017
Accepted manuscript online: June 12, 2017
Version of record online: July 3, 2017

© 2017 Wiley-VCH Verlag GmbH & Co. KGaA, Weinheim

View publication stats

CHEMISTRY
A European Journal

Supporting Information

Small-Molecule Kinase-Inhibitors-Loaded Boron Cluster as Hybrid Agents for Glioma-Cell-Targeting Therapy

Marcos Couto,[a, b, c] Ignacio Mastandrea,[d, e] Mauricio Cabrera,[d] Pablo Cabral,[c] Francesc Teixidor,[b] Hugo Cerecetto,*[a, c] and Clara Viñas*[b]

chem_201701965_sm_miscellaneous_information.pdf

SUPPORTING INFORMATION

	Page
Experimental Section	2
1. Synthesis	2
2. Biology	12
3. R_M determination	13
Fig. S1 Immunofluorescence image of the C6 cells stained by anti-EGFR antibodies (red). Nuclei were stained with DAPI (blue).	14
Fig. S2 Structure-activity relationship. IC_{50}s for methyl- and de-methyl-derivatives and *ortho*- and *meta*-isomers belonging to the triazole-linker series.	15
Fig. S3 Structure-activity relationship. (a) *In vitro* C6 percentage of survival of derivatives belonging to ethynylbenzyl-linker series. (b) Relationship of percentage of cell survival and structure of derivatives belonging to the ethynylbenzyl-linker series.	16
Fig. S4 Spectra of **1**.	17
Fig. S5 Spectra of **3**.	18
Fig. S6 Spectra of **4**.	19
Fig. S7 Spectra of **5**.	20
Fig. S8 Spectra of **6**.	21
Fig. S9 Spectra of **7**.	22
Fig. S10 Spectra of **8**.	23
Fig. S11 Spectra of **9**.	24
Fig. S12 Spectra of **10**.	25
Fig. S13 Spectra of **11**.	26
Fig. S14 Spectra of **12**.	27
Fig. S15 Spectra of **13**.	28
Fig. S16 Spectra of **15**.	29
Fig. S17 Spectra of **16**.	30
Fig. S18 Spectra of **17**.	31
Fig. S19 Spectra of **18**.	32
Fig. S20 Spectra of **19**.	33
Fig. S21 Spectra of **20**.	34
Fig. S22 Spectra of **23**.	35
Fig. S23 Spectra of **26**.	37
Fig. S24 Spectra of **27**.	39
Fig. S25 Spectra of **28**.	40
References	41

Experimental Section

1. Synthesis

Instrumentation: Melting points were measured on an Electrothermal 9100 apparatus and are uncorrected. Elemental analyses were performed using a Carlo Erba Model EA1108 elemental analyzer instrument. All NMR spectra were recorded on a Bruker ARX-300 spectrometer equipped with the appropriate decoupling accessories. The ^{1}H (300.13 MHz); $^{11}B\{^{1}H\}$, ^{11}B (96.29 MHz); and $^{13}C\{^{1}H\}$ (75.47 MHz) NMR spectra were recorded in $CDCl_3$ or CD_3COCD_3 at 298 K. Chemical shifts are reported in units of parts per million (ppm) downfield from the reference, and all coupling constants are reported in Hertz (Hz). Multiplicity is abbreviated as: s is the singlet, d is the doublet, dd is the doublet of doublet, dt is doublet of triplets, dq is doublet of quartets, t is the triplet, m is the multiplet, and bs is the broad singlet. MS were performed at a Shimadzu QP-2010 spectrometer at 70 eV ionizing voltage. Mass spectra are presented as *m/z* (% rel int.). MALDI-TOF mass spectra were recorded in the negative-ion mode using a Bruker Biflex MALDI-TOF (N_2 laser; λ_{exc}= 337 nm; 0.5 ns pulses); voltage ion source 20.00 KV (Uis1) and 17.50 KV (Uis2)). UV measurements were performed on spectrofluorometer Varioskan flash, Thermo ® at 298 K and using 1.0 cm cuvettes.

Materials and methods: Most reactions were performed under an atmosphere of dinitrogen by employing standard Schlenk techniques. Analytical thin-layer chromatography (TLC) was carried out on pre-coated plates with silica gel 60 on aluminium foil F254 (Merck). Compounds were visualized by use of UV light (254 nm) or by a 0.5 % acidic solution of $PdCl_2$ in HCl/Methanol by heat gun for boron containing derivatives.

Chemicals were reagent grade and were used as received from commercial suppliers. 1,2-*closo*-$C_2B_{10}H_{12}$, and 1,7-*closo*-$C_2B_{10}H_{12}$, were obtained from Katchem. 1-(3-chloropropyl)-2-methyl-1,2-dicarba-*closo*-dodecaborane, (**2**),[1] 1-(4-iodophenylmethyl)-2-methyl-1,2-dicarba-*closo*-dodecaborane, (**14**),[2] 8-dioxane-3,3'-cobaltabis(1,2-dicarbollide), (**21**),[3] Sodium salt of 8-(5-azido-3-oxa-pentyloxy)-3,3'-cobaltabisdicarbollide, (**22**),[4] [1-dioxane-*closo*-dodecaboranyl]$^-$ (**24**),[5] and [1-(5-azido-3-oxa-pentyloxy)-*closo*-dodecaboranyl]$^-$ (**25**)[6] were synthesised as reported at the literature.

Synthesis and characterization of compound 1-(3-chloropropyl)-1,2-dicarba-*closo*-dodecaborane (1).

A 10-mL round-bottom flask equipped with a condenser and a magnetic stirring bar was charged with decaborane (523 mg, 4.27 mmol) and dry acetonitrile (3.5 mL) and were heated at reflux for 2 h. To the resultant light yellow solution, 5-chloro-1-pentyne (527 mg, 5.13 mmol) in 3 mL of dry toluene, was added dropwise. The reaction mixture was heated at reflux for 6 h. After that, the solvent was removed under reduced pressure leaving an orange-brown oil. The residue was dissolved in Et_2O (2 mL) and transferred to a micro-sublimator. After the removal of the solvent, sublimation was continued under reduced pressure for 18 h at 90 °C to give the white oil **1** (564 mg, 60%).

$^{1}H\{^{11}B\}$-NMR (300.13 MHz, $CDCl_3$) δ: 3.60 (bs, 1H, -B-C_c-**H**), 3.53 (t, $J_{H,H}$= 6.0 Hz, 2H, -C**H**$_2$Cl), 2.44-2.38 (m, 2H, -C**H**$_2$CH$_2$Cl), 2.03-1.93 (m, 2H, -B-C_c-C**H**$_2$). $^{13}C\{^{1}H\}$-NMR (75.47 MHz, $CDCl_3$) δ: 74.1, 61.6, 43.3, 35.5, 31.8. $^{11}B\{^{1}H\}$-NMR (96.29 MHz, $CDCl_3$) δ: -2.43 (1B), -5.88 (1B), -9.46 (2B), -12.15 (4B), -13.19 (2B).

Synthesis and characterization of compound 1-(3-azidopropyl)-1,2-dicarba-*closo*-dodecaborane (3).

A 10-mL round-bottom flask equipped with a condenser and a magnetic stirring bar was charged with **1** (180 mg, 0.82 mmol) and sodium azide (106 mg, 1.6 mmol) and were heated at reflux in dry DMF (3 mL) for 9 h. The clear, colorless solution was evaporated under reduced pressure to dryness and the residue was suspended in CH_2Cl_2 (6 mL) and washed with 6 mL of water. Two extractions of the water were performed with CH_2Cl_2 (2 × 10 mL).The organic layers were dried over $MgSO_4$, filtered, and evaporated *in vacuo* to dryness. The product was purified by preparative TLC and 100 % Et_2O as eluent. The product was obtained following extraction of the silica with acetone and evaporation under reduced pressure to yield a colorless oil (181 mg, 97 %).[7]
$^{1}H\{^{11}B\}$-NMR (300.13 MHz, $CDCl_3$) δ: 3.59 (bs, 1H, -B-C_c-**H**), 3.34 (t, $J_{H,H}$= 6.0 Hz, 2H, -C**H**$_2$$N_3$), 2.35-2.29 (m, 2H, -C**H**$_2$$CH_2N_3$), 1.83-1.73 (m, 2H, -B-$C_c$-C**H**$_2$). $^{13}C\{^{1}H\}$-NMR (75.47 MHz, $CDCl_3$) δ: 74.0, 61.5, 43.2, 35.4, 31.7. $^{11}B\{^{1}H\}$-NMR (96.29 MHz, $CDCl_3$) δ: -2.51 (1B), -5.95 (1B), -9.52 (2B), -12.16 (4B), -13.31 (2B).

Synthesis and characterization 1-(3-azidopropyl)-2-methyl-1,2-dicarba-*closo*-dodecaborane (4).

A 25-mL round-bottom flask equipped with a condenser and a magnetic stirring bar was charged with 1-(3-chloropropyl)-1,2-dicarba-*closo*-dodecaborane **2** (200 mg, 0.85 mmol) and sodium azide (410 mg, 6.30 mmol) and were heated at reflux in dry DMF (5 mL) for 5 h. The clear, colorless solution was evaporated under reduced pressure to dryness and the residue was suspended in CH_2Cl_2 (10 mL) and washed with 8 mL of water. Two extractions of the water were performed with CH_2Cl_2 (2 × 10 mL).The organic layers were dried over $MgSO_4$, filtered, and evaporated *in vacuo* to dryness. The product was purified by preparative TLC and 100 % dichloromethane as eluent. The product was obtained following extraction of the silica with 10 % methanol in dichloromethane and evaporation under reduced pressure to yield a colorless oil (198 mg, 96 %).[8]

$^{1}H\{^{11}B\}$-NMR (300.13 MHz, $CDCl_3$) δ: 3.39 (t, $J_{H,H}$= 7.8 Hz, 2H, -C**H**$_2$$N_3$), 2.32-2.22 (m, 2H, -C**H**$_2$$CH_2N_3$), 2.04 (s, 3H, -$C_c$-C**H**$_3$), 1.90-1,83 (m, 2H, -B-$C_c$-C**H**$_2$). $^{13}C\{^{1}H\}$-NMR (75.47 MHz, $CDCl_3$) δ: 78.2, 74.8, 50.5, 32.5, 28.9, 23.1. $^{11}B\{^{1}H\}$-NMR (96.29 MHz, $CDCl_3$) δ: -4.45 (1B), -5.84 (1B), -10.0 (4B), -10.8 (4B).

Synthesis and characterization of compound 4-{3-{1-[3-(1,2-dicarba-*closo*-dodecaboran-1-yl)propyl]-1*H*-[1,2,3]triazol-4-yl}phenyl}amino-6,7-bis(2-methyloxyethyloxy)quinazoline (5).

A 10-mL round-bottom flask equipped with a magnetic stirring bar was charged with Erlotinib (1.1 equiv., 215 mg, 0.54 mmol) dissolved in THF:H_2O (3 mL, 1:1 v/v). Then, sodium ascorbate (15 mg, 15 mol %), $CuSO_4.5H_2O$ (13 mg, 10 mol %) and **3** (1 equiv., 121 mg, 0.49 mmol) were added. The mixture was left at room temperature for 15 h. After that, a heavy white precipitate formed, which it was filtered. The filtrate was poured into CH_2Cl_2 (15 mL) and washed with water (3 × 5 mL). The organic layer was dried over $MgSO_4$ and evaporated *in vacuo* to dryness. The product was purified by preparative TLC and CH_2Cl_2:MeOH (97:3) as eluent. The product was obtained following extraction of the silica with CH_2Cl_2:MeOH and evaporation under reduced pressure to yield a white solid (236 mg, 78 %), mp: 134-138 ºC.

$^{1}H\{^{11}B\}$-NMR (300.13 MHz, CD_3COCD_3) δ: 8.93 (s, 1H, pyrimidine-**H**), 8.56 (bs, 1H, -N**H**), 8.32 (s, 2H, Ar-**H**; triazole-**H**), 7.87 (d, $J_{H,H}$= 8.2 Hz, 1H, Ar-**H**), 7.79 (s,1H, Ar-**H**), 7.52 (d, $J_{H,H}$= 7.6 Hz, 1H, Ar-**H**), 7.37 (t, $J_{H,H}$= 7.9 Hz, 1H, Ar-**H**), 7.28 (bs, 1H, Ar-**H**), 4.66 (bs, 1H, -B-C_c-**H**), 4.48 (t, $J_{H,H}$= 6.7 Hz, 2H, -C**H**$_2$-triazole), 4.28-4.18 (m, 4H, (-C**H**$_2$-OAr)$_2$), 3.86-3.68 (m, 4H, (H_3CO-C**H**$_2$-)$_2$), 3.37 (s, 3H, **H**$_3$C-O-), 3.36 (s, 3H, **H**$_3$C-O-), 2.48-2.42 (m, 2H, triazole-CH_2-C**H**$_2$-), 2.03-2.00 (m, 2H, -C_c-C**H**$_2$-). $^{13}C\{^{1}H\}$-NMR (75.47 MHz, CD_3COCD_3) δ: 156.1, 154.1, 154.1, 149.2, 147.1, 140.4, 131.6, 129.6, 128.9, 121.2, 120.7, 120.3, 118.6, 112.7, 110.4, 103.3, 75.4, 70.6, 70.5, 68.8, 68.5, 62.7, 58.3, 48.9, 48.8, 34.4, 30.5. $^{11}B\{^{1}H\}$-NMR (96.29 MHz, CD_3COCD_3) δ: 2.03 (1B), -1.12 (1B), -4.74 (2B), -6.76 (4B), -8.02 (2B). *m/z* (EI): 620 ($M^{+\cdot}$, 100). Anal. Calcd. for $C_{27}H_{40}B_{10}N_6O_4$: C, 52.24; H, 6.50; N, 13.54. Found: C, 52.29; H, 6.47, N, 13.21.

Synthesis and characterization of compound 4-{3-{1-[3-(2-methyl-1,2-dicarba-*closo*-dodecaboran-1-yl)propyl]-1*H*-[1,2,3]triazol-4-yl}phenyl}amino-6,7-bis(2-methyloxyethyloxy)quinazoline (6).

A 10-mL round-bottom flask equipped with a magnetic stirring bar was charged with Erlotinib (1.1 equiv., 103 mg, 0.26 mmol) dissolved in THF:H_2O (2 mL, 1:1 v/v). Then, sodium ascorbate (6.8 mg, 15 mol %), $CuSO_4.5H_2O$ (5.8 mg, 10 mol %) and **4** (1 equiv., 60 mg, 0.23 mmol) were added. The mixture was left at room temperature for 16 h. After that, the mixture was quenched by evaporation of the solvent. The crude was dissolved in CH_2Cl_2 (15 mL) and washed with water (3 × 5 mL). The organic layer was dried over $MgSO_4$ and evaporated *in vacuo* to dryness. The product was purified by preparative TLC and CH_2Cl_2:MeOH (97:3) as eluent. The product was obtained following extraction of the silica with CH_2Cl_2 and evaporation under reduced pressure to yield a yellow solid (105 mg, 72 %), mp: 85-88 °C.

$^{1}H\{^{11}B\}$-NMR (300.13 MHz, $CDCl_3$) δ: 8.65 (s, 1H, pyrimidine-**H**), 8.16 (s, 1H, triazole-**H**), 7.84 (m, 2H, -N**H**; Ar-**H**), 7.80 (s, 1H, Ar-**H**), 7.53 (d, $J_{H\text{-}H}$= 8.1 Hz, 1H, Ar-**H**), 7.43 (t, $J_{H\text{-}H}$= 7.9 Hz, 1H, Ar-**H**), 7.30 (s, 1H, Ar-**H**), 7.23 (s, 1H, Ar-**H**), 4.34 (t, $J_{H,H}$= 5 Hz, 2H, -C**H**$_2$-triazole), 4.26 (t, $J_{H,H}$= 4.8 Hz, 4H, (-C**H**$_2$-OAr)$_2$), 3.85-3.82 (m, 4H, (H_3CO-C**H**$_2$-)$_2$), 3.46 (s, 6H, (**H**$_3$C-O-)$_2$), 2.26 (bs, 4H, triazole-CH_2-C**H**$_2$-C**H**$_2$-C_c-), 1.95 (s, 3H, -C_c-C**H**$_3$). $^{13}C\{^{1}H\}$-NMR (75.47 MHz, $CDCl_3$) δ: 156.4, 154.6, 153.6, 149.0, 147.9, 147.5, 139.5, 131.0, 129.6, 121.6, 121.2, 119.9, 118.8, 109.3, 108.8, 102.6, 79.5, 75.0, 71.0, 70.5, 69.2, 68.4, 63.1, 59.3, 49.3, 32.1, 29.9, 23.1. $^{11}B\{^{1}H\}$-NMR (96.29 MHz, $CDCl_3$) δ: -4.47 (1B), -5.81 (1B), -10.51 (8B). *m/z* (EI): m/z calcd.: 634.43. Found: 634.66 ($M^{+\cdot}$, 100). Anal. Calcd. for $C_{28}H_{42}B_{10}N_6O_4$: C, 52.98; H, 6.67; N, 13.24. Found: C, 52.87; H, 6.54; N, 13.41.

Synthesis and characterization of compound 1-(3-chloropropyl)-1,7-dicarba-*closo*-dodecaborane (7).

Under dinitrogen, *n*-butyllithium (1 equiv., 3.2 mL, 1.6 mol/L in hexane) was added dropwise to a solution of 1,7-dicarba-*closo*-dodecaborane (700 mg, 4.86 mmol) in dry THF (11 mL) at 0 °C. The mixture was kept at low temperature with stirring for 18 min. After that, the mixture was left at room temperature for 2 h. The solution was cooled to -60 °C for 1 h, and an equimolar solution of 1-bromo-3-chloropropane in THF (5 mL) was added dropwise. The mixture was kept at -60 °C for 18 min. The mixture was left at room temperature for 24 h. After that, the mixture was quenched with aqueous solution of NH_4Cl (satd.) (30 mL), transferred to a separating funnel and extracted with Et_2O (3 × 15 mL). The organic layers were dried over $MgSO_4$, filtered, and evaporated *in vacuo* to dryness. The product was

purified by preparative TLC and *n*-Hexane:Et_2O (85:15) as eluent. The product was obtained following extraction of the silica with acetone and evaporation under reduced pressure to yield a light yellow oil (717 mg, 67 %).

$^1H\{^{11}B\}$-NMR (300.13 MHz, $CDCl_3$) δ: 3.47 (t, $J_{H,H}$= 6.0 Hz, 2H, -C**H**$_2$Cl), 2.94 (bs, 1H, -B-C_c-**H**), , 2.13-2.09 (m, 2H, -C**H**$_2$$CH_2$Cl), 1.90-1.82 (m, 2H, -B-C_c-C**H**$_2$). $^{13}C\{^1H\}$-NMR (75.47 MHz, $CDCl_3$) δ: 75.0, 55.0, 43.8, 34.1, 32.5. $^{11}B\{^1H\}$-NMR (96.29 MHz, $CDCl_3$) δ: -4.4 (1B), -11.08 (5B), -13.81 (2B), -15.6 (2B).

Synthesis and characterization of compound 1-(3-chloropropyl)-7-methyl-1,7-dicarba-*closo*-dodecaborane (8).

Under dinitrogen, *n*-butyllithium (1 equiv., 0.79 mL, 1.6 mol/L in hexane) was added dropwise to a solution of 1-methyl-1,7-dicarba-*closo*-dodecaborane (200 mg, 1.26 mmol) in dry THF (6 mL) at 0 °C. The mixture was kept at low temperature with stirring for 1 h. Subsequently, 1-bromo-3-chloropropane (1 equiv., 0.12 mL) was added. After the addition, the mixture was left at room temperature for 24 h. After that, the mixture was quenched with H_2O (20 mL), transferred to a separating funnel and extracted with Et_2O (3 × 10 mL). The organic layers were dried over $MgSO_4$, filtered, and evaporated *in vacuo* to dryness. The product was purified by preparative TLC and *n*-Hexane:Et_2O (90:10) as eluent. The product was obtained following extraction of the silica with acetone and evaporation under reduced pressure to yield a colorless oil (277 mg, 94 %).

$^1H\{^{11}B\}$-NMR (300.13 MHz, $CDCl_3$) δ: 3.47 (t, $J_{H,H}$= 7.8 Hz, 2H, -C**H**$_2$Cl), 2.18-2.10 (m, 2H, -C**H**$_2$$CH_2$Cl), 1.89-1.82 (m, 2H, -B-C_c-C**H**$_2$), 1.72 (s, 3H, -C_c-C**H**$_3$). $^{13}C\{^1H\}$-NMR (75.47 MHz, $CDCl_3$) δ: 75.5, 70.7, 43.7, 34.1, 32.5, 24.5. $^{11}B\{^1H\}$-NMR (96.29 MHz, $CDCl_3$) δ: -6.66 (1B), -8.55 (1B), -10.85 (6B), -13.17 (2B).

Synthesis and characterization of compound 1-(3-azidopropyl)-1,7-dicarba-*closo*-dodecaborane (9).

A 10-mL round-bottom flask equipped with a condenser and a magnetic stirring bar was charged with **7** (191 mg, 0.87 mmol) and sodium azide (419 mg, 6.4 mmol) and were heated at reflux in dry DMF (4 mL) for 10h. The clear, colorless solution was evaporated under reduced pressure to dryness and the residue was suspended in toluene (8 mL) and washed with 6 mL of water. Two extractions of the water were performed with CH_2Cl_2 (2 × 10 mL).The organic layers were dried over $MgSO_4$, filtered, and evaporated *in vacuo* to dryness. The product was purified by preparative TLC and 100 % Et_2O as eluent. The product was obtained following extraction of the silica with acetone and evaporation under reduced pressure to yield a colorless oil (194 mg, 98 %).
$^1H\{^{11}B\}$-NMR (300.13 MHz, $CDCl_3$) δ: 3.60 (bs, 1H, -B-C_c-**H**), 3.53 (t, $J_{H,H}$= 6.0 Hz, 2H, -C**H**$_2$$N_3$), 2.44-2.38 (m, 2H, -C**H**$_2$$CH_2N_3$), 2.03-1.94 (m, 2H, -B-$C_c$-C**H**$_2$). $^{13}C\{^1H\}$-NMR (75.47 MHz, $CDCl_3$) δ: 74.1, 61.6, 43.3, 35.5, 31.8. $^{11}B\{^1H\}$-NMR (96.29 MHz, $CDCl_3$) δ: -2.42 (1B), -5.85 (5B), -9.44 (2B), -12.10 (4B), -13.22 (2B).

Synthesis and characterization of compound 1-(3-azidopropyl)-7-methyl-1,7-dicarba-*closo*-dodecaborane (10).

A 10-mL round-bottom flask equipped with a condenser and a magnetic stirring bar was charged with **8** (180 mg, 0.76 mmol) and sodium azide (373 mg, 5.7 mmol) and were heated

at reflux in dry DMF (4 mL) for 8 h. The clear, colorless solution was evaporated under reduced pressure to dryness and the residue was suspended in CH_2Cl_2 (8 mL) and washed with 6 mL of water. Two extractions of the water were performed with CH_2Cl_2 (2 × 10 mL).The organic layers were dried over $MgSO_4$, filtered, and evaporated *in vacuo* to dryness. The product was purified by preparative TLC and 100 % Et_2O as eluent. The product was obtained following extraction of the silica with acetone and evaporation under reduced pressure to yield a colorless oil (176 mg, 96 %).

$^1H\{^{11}B\}$-NMR (300.13 MHz, $CDCl_3$) δ: 3.25 (t, $J_{H,H}$= 6.5 Hz, 2H, -C**H**$_2$N$_3$), 2.06-2.00 (m, 2H, -C**H**$_2$CH$_2$N$_3$), 1.72 (s, 3H, -C$_c$-C**H**$_3$), 1.69-1.61 (m, 2H, -B-C$_c$-C**H**$_2$). $^{13}C\{^1H\}$-NMR (75.47 MHz, $CDCl_3$) δ: 75.6, 70.6, 50.6, 33.9, 29.1, 24.5. $^{11}B\{^1H\}$-NMR (96.29 MHz, $CDCl_3$) δ: -6.62 (1B), -8.51 (1B), -10.79 (6B), -13.17 (2B).

Synthesis and characterization of compound 4-{3-{1-[3-(1,7-dicarba-*closo*-dodecaboran-1-yl)propyl]-1*H*-[1,2,3]triazol-4-yl}phenyl}amino-6,7-bis(2-methyloxyethyloxy)quinazoline (11).

A 10-mL round-bottom flask equipped with a magnetic stirring bar was charged with Erlotinib (1.1 equiv., 230 mg, 0.58 mmol) dissolved in THF:H_2O (4 mL, 1:1 v/v). Then, sodium ascorbate (15 mg, 15 mol %), $CuSO_4.5H_2O$ (13 mg, 10 mol %) and **9** (1 equiv., 118 mg, 0.52 mmol) were added. The mixture was left at room temperature for 24 h. After that, a heavy white precipitate formed, which it was filtered. The filtrate was poured into CH_2Cl_2 (15 mL) and washed with water (3 × 5 mL). The organic layer was dried over $MgSO_4$ and evaporated *in vacuo* to dryness. The product was purified by preparative TLC and CH_2Cl_2:MeOH (97:3) as eluent. The product was obtained following extraction of the silica with CH_2Cl_2:MeOH and evaporation under reduced pressure to yield a white solid (229 mg, 71 %), mp: 101-104 °C.

$^1H\{^{11}B\}$-NMR (300.13 MHz, $CDCl_3$) δ: 8.65 (bs, 1H, pyrimidine-**H**), 8.13 (s, 1H, triazole-**H**), 7.93 (bs, 1H, -N**H**), 7.84 (d, $J_{H,H}$= 7.8 Hz, 1H, Ar-**H**), 7.74 (s,1H, Ar-**H**), 7.49 (d, $J_{H,H}$= 7.6 Hz, 1H, Ar-**H**), 7.40 (t, $J_{H,H}$= 7.8 Hz, 1H, Ar-**H**), 7.36 (bs, 1H, Ar-**H**), 7.20 (bs, 1H, Ar-**H**), 4.30 (bs, 2H, -C**H**$_2$-triazole), 4.26-4.24 (m, 4H, (-C**H**$_2$-OAr)$_2$), 3.84-3.80 (m, 4H, (H$_3$CO-C**H**$_2$-)$_2$), 3.44 (s, 6H, (**H**$_3$C-O-)$_2$), 2.93 (bs, 1H, -B-C$_c$-**H**), 2.16 (bs, 2H, triazole-CH$_2$-C**H**$_2$-), 2.01 (bs, 2H, -C$_c$-C**H**$_2$-). $^{13}C\{^1H\}$-NMR (75.47 MHz, CDCl3) δ: 156.7, 154.1, 153.4, 148.5, 147.6, 139.6, 130.8, 129.4, 122.5, 121.9, 121.1, 119.9, 119.0, 109.4, 108.1, 102.5, 77.3, 74.6, 70.7, 70.3, 68.6, 68.1, 59.1, 55.1, 49.4, 33.5, 30.3. $^{11}B\{^1H\}$-NMR (96.29 MHz, $CDCl_3$) δ: -4.32 (1B), -10.83 (5B), -13.58 (2B), -15.42 (2B). *m/z* (EI): m/z calcd.: 621.41. Found: 620.91 ($M^{+\cdot}$, 100). Anal. Calcd. for $C_{27}H_{40}B_{10}N_6O_4$: C, 52.24; H, 6.50; N, 13.54. Found: C, 52.51; H, 6.48, N, 13.71.

Synthesis and characterization of compound 4-{3-{1-[3-(7-methyl-1,7-dicarba-*closo*-dodecaboran-1-yl)propyl]-1*H*-[1,2,3]triazol-4-yl}phenyl}amino-6,7-bis(2-methyloxyethyloxy)quinazoline (12).

A 10-mL round-bottom flask equipped with a magnetic stirring bar was charged with Erlotinib (1.1 equiv., 219 mg, 0.55 mmol) dissolved in THF:H_2O (3 mL, 1:1 v/v). Then, sodium ascorbate (15 mg, 15 mol %), $CuSO_4.5H_2O$ (13 mg, 10 mol %) and **10** (1 equiv., 121 mg, 0.50 mmol) were added. The mixture was left at room temperature for 18 h. After that, a heavy yellow precipitate formed, which it was filtered. The filtrate was poured into CH_2Cl_2 (15 mL) and washed with water (3 × 5 mL). The organic layer was dried over $MgSO_4$ and evaporated *in vacuo* to dryness. The product was purified by preparative TLC and CH_2Cl_2:MeOH (96:4)

as eluent. The product was obtained following extraction of the silica with CH_2Cl_2:MeOH and evaporation under reduced pressure to yield a yellow solid (219 mg, 69 %), mp: 93-96 °C.

$^1H\{^{11}B\}$-NMR (300.13 MHz, $CDCl_3$) δ: 8.63 (bs, 1H, pyrimidine-**H**), 8.12 (s, 1H, triazole-**H**), 8.02 (s, 1H, -N**H**), 7.84-7.79 (m, 1H, Ar-**H**), 7.73 (s,1H, Ar-**H**), 7.48 (d, $J_{H,H}$= 7.4 Hz, 1H, Ar-**H**), 7.38 (m, 2H- Ar-**H**), 7.18 (bs, 1H, Ar-**H**), 4.27 (bs, 2H, -C**H**$_2$-triazole), 4.22 (t, $J_{H,H}$= 4.5 Hz, 4H, (-C**H**$_2$-OAr)$_2$), 3.80-3.77 (m, 4H, (H_3CO-C**H**$_2$-)$_2$), 3.42 (s, 6H, (**H**$_3$C-O-)$_2$), 2.16 (s, 2H, triazole-CH_2-C**H**$_2$-), 1.99 (s, 2H, -C_c-C**H**$_2$-), 1.67 (s, 3H, -C_c-C**H**$_3$). $^{13}C\{^1H\}$-NMR (75.47 MHz, $CDCl_3$) δ: 162.6, 156.5, 154.5, 153.5, 148.9, 147.7, 139.6, 131.1, 129.4, 121.6, 121.1, 119.8, 118.9, 109.4, 108.7, 102.7, 75.0, 70.9 (2C), 70.4, 69.1, 68.3, 59.2, 49.4, 45.0, 33.6, 30.3, 24.4.$^{11}B\{^1H\}$-NMR (96.29 MHz, $CDCl_3$) δ: -6.83 (1B), -8.66 (1B), -10.77 (6B), -13.13 (2B). *m/z* (EI): m/z calcd.: 634.43. Found: 634.20 ($M^{+\cdot}$, 100). Anal. Calcd. for $C_{28}H_{42}B_{10}N_6O_4$: C, 52.98; H, 6.67; N, 13.24. Found: C, 52.74; H, 6.77; N, 13.53.

Synthesis and characterization of compound 1-(4-iodophenylmethyl)-1,2-dicarba-*closo*-dodecaborane (13).

Under dinitrogen, *n*-butyllithium (1 equiv., 1.3 mL, 1.6 mol/L in hexane) was added dropwise to a solution of 1,2-dicarba-*closo*-dodecaborane (300 mg, 2.10 mmol) in dry DME (8 mL) at 0 °C. The resulting mixture was kept at low temperature with stirring for 45 min. Subsequently, an equimolar solution of 4-(bromomethyl)iodobenzene (618 mg, 2.10 mmol) in dry DME (2.5 mL) was added dropwise. The reaction mixture was heated at reflux for 12 h. After that, the mixture was quenched with H_2O (20 mL), transferred to a separating funnel and extracted with Et_2O (3 × 15 mL). The organic layers were dried over $MgSO_4$, filtered, and evaporated *in vacuo* to dryness. The product was purified by column chromatography SiO_2 and *n*-Hexane:Et_2O (97:3) as eluent to give title compound as colorless oil (363 mg, 48 %).

$^1H\{^{11}B\}$-NMR (300.13 MHz, $CDCl_3$) δ: 7.72 (d, J_{H-H}= 8.2 Hz, 2H, Ar-**H**), 6.91 (d, J_{H-H}= 8.1 Hz, 2H, Ar-**H**), 3.48 (s, 2H, -C**H**$_2$Ph), 3.28 (bs, 1H, -B-C_c-**H**). $^{13}C\{^1H\}$- NMR (75.47 MHz, $CDCl_3$) δ: 138.2 (2C), 133.9, 131.7 (2C), 94.4, 73.8, 59.4, 43.1. $^{11}B\{^1H\}$-NMR (96.29 MHz, $CDCl_3$) δ: -2.42 (1B), -5.85 (5B), -9.44 (2B), -12.10 (4B), -13.22 (2B).

Synthesis and characterization of compound 4-{3-{2-[4-(1,2-dicarba-*closo*-dodecaboran-1-ylmethyl)phenyl]ethynyl}phenyl}amino-6,7-bis(2-methyloxyethyloxy)quinazoline (15).

To a 10-mL oven-dried round bottom flask equipped with a magnetic stirring bar was charged under dinitrogen with **13** (1 equiv., 45 mg, 0.13 mmol), CuI (2.5 mg, 10 mol %), $PdCl_2(PPh_3)_2$ (7.2 mg, 8 mol %) and Erlotinib (1.1 equiv. 57 mg, 0.14 mmol). A dry solvent system of THF:Et_3N (3 mL, 3:1, v/v) was well-degassed under dinitrogen for 45 min prior to addition to the reaction mixture. After heating at 60 °C for 8 h, the solution was filtered through a small pad of celite and washed with methanol (10 mL). The solution was concentrated *in vacuo* and the crude was dissolved in CH_2Cl_2 (10 mL) and washed with brine (2 × 5 mL). The organic layer was dried over $MgSO_4$ and evaporated *in vacuo* to dryness. The product was purified by preparative TLC and CH_2Cl_2:MeOH (97:3) as eluent. The product was obtained following extraction of the silica with CH_2Cl_2:MeOH and evaporation under reduced pressure to yield a yellow solid (33 mg, 41 %), mp: 137-139 °C.

$^1H\{^{11}B\}$-NMR (300.13 MHz, $CDCl_3$) δ: 8.69 (s, 1H, pyrimidine-**H**), 7.95 (s, 1H, -N**H**), 7.73 (d, $J_{H,H}$= 8.0 Hz, 1H, Ar-**H**), 7.55 (d, $J_{H,H}$= 7.6 Hz, 2H, Ar-**H**, Ar-**H**), 7.44-7.37 (m, 1H, Ar-**H**), 7.34-

7.31 (m, 2H, Ar-**H**), 7.26-7.24 (m, 2H, Ar-**H**), 7.15 (d, $J_{H,H}$= 7.9 Hz, 2H, Ar-**H**), 4.32 (m, 4H, (-C**H**$_2$-OAr)$_2$), 3.84 (m, 4H, (H_3CO-C**H**$_2$-)$_2$), 3.55 (s, 2H, -Ph-C**H**$_2$-C_c-), 3.50-3.48 (m, 6H, (**H**$_3$C-O-)$_2$), 3.28 (bs, 1H, -B-C_c-**H**). $^{13}C\{^1H\}$-NMR (75.47 MHz, $CDCl_3$) δ: 156.2, 153.8, 153.6, 149.1, 147.7, 138.8, 134.3, 132.2 (2C), 129.9 (2C), 129.2, 127.4, 124.4, 123.7, 122.6, 121.8, 109.4, 109.1, 102.7, 90.4, 90.2, 74.1, 71.1, 70.5, 69.6, 68.4, 59.5, 59.3, 43.4, 29.7. $^{11}B\{^1H\}$-NMR (96.29 MHz, $CDCl_3$) δ: -2.23 (1B), -5.37 (1B), -8.88 (3B), -10.6 (2B), -12.80 (3B). *m/z* (EI): m/z calcd.: 625.39. Found: 625.32 ($M^{+\cdot}$, 100). Anal. Calcd. for $C_{31}H_{39}B_{10}N_3O_4$: C, 59.50; H, 6.28; N, 6.72. Found: C, 59.85; H, 6.44, N, 6.51.

Synthesis and characterization of compound 4-{3-{2-[4-(2-methyl-1,2-dicarba-*closo*-dodecaboran-1-ylmethyl)phenyl]ethynyl}phenyl}amino-6,7-bis(2-methyloxyethyloxy)quinazoline (16).

To a 10-mL oven-dried round bottom flask equipped with a magnetic stirring bar was charged under dinitrogen with **14** (1 equiv., 55 mg, 0.15 mmol), CuI (2.9 mg, 10 mol %), $PdCl_2(PPh_3)_2$ (8.3 mg, 8 mol %) and Erlotinib (1.1 equiv. 64 mg, 0.16 mmol). A dry solvent system of THF:Et_3N (3 mL, 3:1, v/v) was well-degassed under dinitrogen for 45 min prior to addition to the reaction mixture. After heating at 60 °C for 10 h, the solution was filtered through a small pad of celite and washed with methanol (10 mL). The solution was concentrated *in vacuo* and the crude was dissolved in CH_2Cl_2 (10 mL) and washed with brine (2 × 5 mL). The organic layer was dried over $MgSO_4$ and evaporated *in vacuo* to dryness. The product was purified by preparative TLC and CH_2Cl_2:MeOH (98:2) as eluent. The product was obtained following extraction of the silica with CH_2Cl_2:MeOH and evaporation under reduced pressure to yield an orange solid (47 mg, 49 %), mp: 134-137 °C.

$^1H\{^{11}B\}$-NMR (300.13 MHz, $CDCl_3$) δ: 8.69 (s, 1H, pyrimidine-**H**), 7.93 (s, 1H, -N**H**), 7.75 (d, $J_{H,H}$= 7.8 Hz, 1H, Ar-**H**), 7.53 (d, $J_{H,H}$= 8.1 Hz, 2H, Ar-**H**; 1H, Ar-**H**), 7.42-7.35 (m, 1H, Ar-**H**), 7.31 (d, $J_{H,H}$= 7.7 Hz, 1H, Ar-**H**), 7.26 (bs, 2H, Ar-**H**), 7.19 (d, $J_{H,H}$= 8.1 Hz, 2H, Ar-**H**), 4.28 (m, 4H, (-C**H**$_2$-OAr)$_2$), 3.84 (m, 4H, (H_3CO-C**H**$_2$-)$_2$), 3.48 (s, 6H, (**H**$_3$C-O-)$_2$), 3.46 (s, 2H, -Ph-C**H**$_2$-C_c-), 2.18 (s, 3H, -C_c-C**H**$_3$). $^{13}C\{^1H\}$-NMR (75.47 MHz, $CDCl_3$) δ: 156.3, 154.7, 153.7, 149.0, 147.5, 138.9, 135.1, 131.8 (2C), 130.4 (2C), 129.1, 127.3, 124.5, 123.8, 123.1, 121.9, 109.2, 108.9, 102.7, 90.1, 89.0, 78.6, 74.8, 71.0, 70.5, 69.4, 68.4, 59.3, 41.1, 30.9, 23.7. $^{11}B\{^1H\}$-NMR (96.29 MHz, $CDCl_3$) δ: -4.22 (1B), -5.79 (1B), -10.46 (8B). *m/z* (EI): m/z calcd.: 640.41. Found: 639.91 ($M^{+\cdot}$, 100). Anal. Calcd. for $C_{32}H_{41}B_{10}N_3O_4$: C, 60.07; H, 6.46; N, 6.57. Found: C, 60.37; H, 6.29, N, 6.66.

Synthesis and characterization of compound 1-(4-iodophenylmethyl)-1,7-dicarba-*closo*-dodecaborane (17).

Under dinitrogen, *n*-butyllithium (1 equiv., 0.87 mL, 1.6 mol/L in hexane) was added dropwise to a solution of 1,7-dicarba-*closo*-dodecaborane (200 mg, 1.39 mmol) in dry Et_2O (8 mL) at 0 °C. The resulting mixture was kept at low temperature with stirring for 45 min. Subsequently, an equimolar solution of 4-(bromomethyl)iodobenzene (413 mg, 1.39 mmol) in dry Et_2O (2.5 mL) was added dropwise. The reaction mixture was heated at reflux for 18 h. After that, the mixture was quenched with H_2O (10 mL), transferred to a separating funnel and extracted with Et_2O (3 × 8 mL). The organic layers were dried over $MgSO_4$, filtered, and evaporated *in vacuo* to dryness. The product was purified by preparative TLC and *n*-Hexane:CH_2Cl_2 (90:10) as eluent. The product was obtained following extraction of the silica with acetone and evaporation under reduced pressure to yield a light yellow oil (230 mg, 46 %).

$^{1}H\{^{11}B\}$-NMR (300.13 MHz, $CDCl_3$) δ: 7.67 (d, $J_{H\text{-}H}$= 6.9 Hz, 2H, Ar-**H**), 6.87 (d, $J_{H\text{-}H}$= 7.1 Hz, 2H, Ar-**H**), 3.17 (s, 2H, -C**H**$_2$Ph), 2.90 (bs, 1H, -B-C$_c$-**H**). $^{13}C\{^{1}H\}$- NMR (75.47 MHz, $CDCl_3$) δ: 137.6 (2C), 136.5, 131.8 (2C), 93.3, 75.7, 55.2, 42.4. $^{11}B\{^{1}H\}$-NMR (96.29 MHz, $CDCl_3$) δ: -2.91 (1B), -9.68 (5B), -12.47 (2B), -14.52 (2B).

Synthesis and characterization of compound 1-(4-iodophenylmethyl)-7-methyl-1,7-dicarba-*closo*-dodecaborane (18).

Under dinitrogen, *n*-butyllithium (1 equiv., 0.53 mL, 1.6 mol/L in hexane) was added dropwise to a solution of 1-methyl-1,7-dicarba-*closo*-dodecaborane (133 mg, 0.84 mmol) in dry DME (5 mL) at 0 °C. The resulting mixture was kept at low temperature with stirring for 2 h. Subsequently, an equimolar solution of 4-(bromomethyl)iodobenzene (250 mg, 0.84 mmol) in dry DME (2 mL) was added dropwise. After the addition, the mixture was left at room temperature for 24 h. After that, the mixture was quenched with H_2O (10 mL), transferred to a separating funnel and extracted with Et_2O (3 × 8 mL). The organic layers were dried over $MgSO_4$, filtered, and evaporated *in vacuo* to dryness. The product was purified by preparative TLC and *n*-Hexane:CH_2Cl_2 (85:15) as eluent. The product was obtained following extraction of the silica with acetone and evaporation under reduced pressure to yield a colorless oil (229 mg, 73 %).

$^{1}H\{^{11}B\}$-NMR (300.13 MHz, $CDCl_3$) δ: 7.67 (d, $J_{H\text{-}H}$= 8.1 Hz, 2H, Ar-**H**), 6.87 (d, $J_{H\text{-}H}$= 8.1 Hz, 2H, Ar-**H**), 3.15 (s, 2H, -C**H**$_2$Ph), 1.66 (s, 2H, -C$_c$-C**H**$_3$). $^{13}C\{^{1}H\}$-NMR (75.47 MHz, $CDCl_3$) δ: 137.6 (2C), 136.5, 131.8 (2C), 93.3, 76.0, 70.9, 42.4, 24.6. $^{11}B\{^{1}H\}$-NMR (96.29 MHz, $CDCl_3$) δ: -6.51 (1B), -8.33 (1B), -10.77 (5B), -13.42 (2B).

Synthesis and characterization of compound 4-{3-{2-[4-(1,7-dicarba-*closo*-dodecaboran-1-ylmethyl)phenyl]ethynyl}phenyl}amino-6,7-bis(2-methyloxyethyloxy)quinazoline (19).

To a 10-mL oven-dried round bottom flask equipped with a magnetic stirring bar was charged under dinitrogen with **17** (1 equiv., 89 mg, 0.25 mmol), CuI (4.8 mg, 10 mol %), $PdCl_2(PPh_3)_2$ (14 mg, 8 mol %) and Erlotinib (1.1 equiv. 109 mg, 0.14 mmol). A dry solvent system of THF:Et_3N (3.5 mL, 3:1, v/v) was well-degassed under dinitrogen for 45 min prior to addition to the reaction mixture. After heating at 60 °C for 12 h, the solution was filtered through a small pad of celite and washed with methanol (10 mL). The solution was concentrated *in vacuo* and the crude was dissolved in CH_2Cl_2 (10 mL) and washed with brine (2 × 10 mL). The organic layer was dried over $MgSO_4$ and evaporated *in vacuo* to dryness. The product was purified by preparative TLC and CH_2Cl_2:MeOH (95:5) as eluent. The product was obtained following extraction of the silica with CH_2Cl_2:MeOH and evaporation under reduced pressure to yield a yellow solid (55 mg, 35 %), mp: 106-109 °C.

$^{1}H\{^{11}B\}$-NMR (300.13 MHz, $CDCl_3$) δ: 8.70 (s, 1H, pyrimidine-**H**), 7.90 (s, 1H, -N**H**), 7.78 (bs, 1H, -Ar-**H**), 7.73 (d, $J_{H,H}$= 7.4 Hz, 1H, Ar-**H**), 7.48 (d, $J_{H,H}$= 8.1 Hz, 2H, Ar-**H**), 7.38-7.28 (m, 4H, Ar-**H**), 7.09 (d, $J_{H,H}$= 8.1 Hz, 2H, Ar-**H**), 4.26-4.23 (m, 2H, -C**H**$_2$-OAr), 4.19 (bs, 2H, -C**H**$_2$-OAr), 3.81-3.77 (m, 4H, (H_3CO-C**H**$_2$-)$_2$), 3.44 (s, 3H, **H**$_3$C-O-), 3.42 (s, 3H, **H**$_3$C-O-), 3.22 (s, 2H, -Ph-C**H**$_2$-C$_c$-), 2.89 (bs, 1H, -B-C$_c$-**H**). $^{13}C\{^{1}H\}$-NMR (75.47 MHz, $CDCl_3$) δ: 156.3, 154.8, 153.8, 149.1, 147.6, 139.0, 135.2, 131.9 (2C), 130.5 (2C), 129.1, 127.4, 124.6, 123.9, 123.2, 122.0, 109.2, 109.0, 102.8, 90.1, 89.0, 74.9, 71.1, 70.5, 69.5, 68.5, 59.8, 59.4, 41.2, 23.8. $^{11}B\{^{1}H\}$-NMR (96.29 MHz, $CDCl_3$) δ: -4.09 (1B), -10.9 (5B), -13.73 (2B), -15.72 (2B). *m/z* (EI):

m/z calcd.: 625.39. Found: 625.11 ($M^{+\cdot}$, 100). Anal. Calcd. for $C_{31}H_{39}B_{10}N_3O_4$: C, 59.50; H, 6.28; N, 6.72. Found: C, 59.21; H, 6.49, N, 6.59.

Synthesis and characterization of compound 4-{3-{2-[4-(7-methyl-1,7-dicarba-*closo*-dodecaboran-1-ylmethyl)phenyl]ethynyl}phenyl}amino-6,7-bis(2-methyloxyethyloxy)quinazoline (20).

To a 10-mL oven-dried round bottom flask equipped with a magnetic stirring bar was charged under dinitrogen with **18** (1 equiv., 60 mg, 0.16 mmol), CuI (3.0 mg, 10 mol %), $PdCl_2(PPh_3)_2$ (9.0 mg, 8 mol %) and Erlotinib (1.1 equiv. 70 mg, 0.18 mmol). A dry solvent system of THF:Et_3N (3.0 mL, 3:1, v/v) was well-degassed under dinitrogen for 45 min prior to addition to the reaction mixture. After heating at 60 °C for 8 h, the solution was filtered through a small pad of celite and washed with methanol (10 mL). The solution was concentrated *in vacuo* and the crude was dissolved in CH_2Cl_2 (10 mL) and washed with brine (10 mL). The organic layer was dried over $MgSO_4$ and evaporated *in vacuo* to dryness. The product was purified by preparative TLC and CH_2Cl_2:MeOH (97:3) as eluent. The product was obtained following extraction of the silica with CH_2Cl_2:MeOH and evaporation under reduced pressure to yield a yellow solid (45 mg, 44 %), mp: 110-112 °C.

$^1H\{^{11}B\}$-NMR (300.13 MHz, $CDCl_3$) δ: 8.69 (bs, 1H, pyrimidine-**H**), 7.93 (s, 1H, -N**H**), 7.74 (d, $J_{H,H}$= 7.9 Hz, 1H, -Ar-**H**), 7.51 (d, $J_{H,H}$= 7.9 Hz, 3H, Ar-**H**), 7.39 (t, $J_{H,H}$= 7.8 Hz, 1H, Ar-**H**), 7.32 (d, $J_{H,H}$= 7.6 Hz, 1H, Ar-**H**), 7.27-7.21 (m, 2H, Ar-**H**), 7.11 (d, $J_{H,H}$= 7.9 Hz, 1H, -Ar-**H**), 4.28-4.26 (m, 4H, (-C**H**$_2$-OAr)$_2$), 3.84 (bs, 4H, (H_3CO-C**H**$_2$-)$_2$), 3.48 (s, 3H, **H**$_3$C-O-), 3.47 (s, 3H, **H**$_3$C-O-), 3.21 (s, 2H, -Ph-C**H**$_2$-C_c-), 1.66 (s, 3H, -C_c-C**H**$_3$). $^{13}C\{^1H\}$-NMR (75.47 MHz, $CDCl_3$) δ: 156.4, 154.6, 153.7, 148.9, 147.6, 139.0, 137.2, 131.7 (2C), 129.9 (2C), 129.0, 127.3, 124.5, 123.9, 122.5, 121.8, 109.2, 108.9, 102.8, 89.7, 89.2, 75.8, 71.0 (2C), 70.4, 69.3, 68.3, 59.2, 42.8, 29.7, 24.5. $^{11}B\{^1H\}$-NMR (96.29 MHz, $CDCl_3$) δ: -6.44 (1B), -8.22 (1B), -10.66 (6B), -13.27 (2B). *m/z* (EI): m/z calcd.: 640.41. Found: 639.82 ($M^{+\cdot}$, 100). Anal. Calcd. for $C_{32}H_{41}B_{10}N_3O_4$: C, 60.07; H, 6.46; N, 6.57. Found: C, 60.20; H, 6.51, N, 6.50.

Synthesis and characterization of compound 4-{3-{1-{[(1',2'-dicarba-*closo*-undecaborane)-3',3-cobalt-(-1)(1,2-dicarba-*closo*-undecaborane)]-8-oxy-3-oxa-pentyl}-1*H*-[1,2,3]triazol-4-yl}phenyl}amino-6,7-bis(2-methyloxyethyloxy)quinazoline sodium salt (23).

A 10-mL round-bottom flask equipped with a magnetic stirring bar was charged with Erlotinib (1.1 equiv., 59 mg, 0.15 mmol) dissolved in THF:H_2O (3 mL, 1:1 v/v). Then, sodium ascorbate (4.2 mg, 15 mol %), $CuSO_4.5H_2O$ (3.5 mg, 10 mol %) and **22** (1 equiv., 65 mg, 0.14 mmol) were added. The mixture was left at room temperature for 24 h. After that, the reaction mixture was filtered off and the solvent was removed under vacuum. The orange solid was dissolved in 0.5 mL of EtOH and precipitated as tetramethylammonium salt by adding an aqueous saturated solution of (NMe_4Cl). The suspension was centrifuged and the orange solid was, filtered, rinsed with water and the solid was purified by TLC using CH_2Cl_2:MeOH (97:3) as eluent. Finally, the product was obtained after cation exchange of $^+NMe_4$ by ^+Na in a cation exchange resin, to give an orange solid (96 mg, 79 %), mp: 130-133 °C.

^1H-NMR (300.13 MHz, CD_3COCD_3) δ: 8.60 (bs, 1H, pyrimidine-**H**), 8.39 (s, 1H, -Ar-**H**), 8.30 (s, 1H, -N**H**), 7.89-7.85 (m, 3H, Ar-**H**), 7.66 (d, $J_{H,H}$= 7.6 Hz, 1H, Ar-**H**), 7.32 (t, $J_{H,H}$= 7.9 Hz, 1H, Ar-**H**), 7.27 (bs, 1H, Ar-**H**), 4.66 (t, $J_{H,H}$= 5.1 Hz, 2H, -C**H**$_2$-triazole), 4.32-4.30 (m, 4H; (-C**H**$_2$-OAr)$_2$), 4.21 (bs, 4H, -B-C_c-**H**), 3.96 (t, $J_{H,H}$= 5.0 Hz, 2H, -C**H**$_2$-CH_2-triazole), 3.83-3.80

(m, 4H, (H_3CO-C**H**$_2$-)$_2$), 3.68-3.65 (m, 2H, -C**H**$_2$-CH_2-C_c), 3.62-3.59 (m, 2H, -CH_2-C**H**$_2$-C_c), 3.42-3.42 (m, 6H, (**H**$_3$C-O-)$_2$). $^{13}C\{^1H\}$-NMR (75.47 MHz, CD_3COCD_3) δ: 157.2, 155.0, 151.5, 149.32, 146.5, 143.4, 139.1, 132.0 (2C), 129.1 (2C), 122.0, 121.7, 121.6, 119.6, 103.0, 72.0 (2C), 70.3, 70.3, 69.3, 68.7, 68.6, 58.3 (2C), 53.6 (2C), 50.1, 46.5 (2C). $^{11}B\{^1H\}$-NMR (96.29 MHz, $CDCl_3$) δ: 24.88 (1B), 6.14 (1B), 1.68 (1B), -1.21 (1B), -3.10 (2B), -6.42 (6B), -16.02 (2B), -19.08 (3B), -27.06 (1B). MALDI-TOF-MS: m/z calcd. 846.51. Found: 845.65. Anal. Calcd. for $C_{30}H_{52}B_{18}CoN_6O_6Na$: C, 41.45; H, 6.03; N, 9.67; Na, 2.64. Found: C, 42.29; H, 6.12, N, 9.90; Na, 2.71.

Synthesis and characterization of compound (26)

A 10-mL round-bottom flask equipped with a magnetic stirring bar was charged with Erlotinib (1.1 equiv., 43 mg, 0.11 mmol) dissolved in THF:H_2O (2.5 mL, 1:1 v/v). Then, sodium ascorbate (3.0 mg, 15 mol %), $CuSO_4.5H_2O$ (2.5 mg, 10 mol %) and **25** (1 equiv., 75 mg, 0.10 mmol) were added. The mixture was left at room temperature for 24 h. After that, the reaction mixture was filtered off and the solvent was removed under vacuum. The green solid was dissolved in 10 mL of CH_2Cl_2 and washed with water (2 × 5 mL). The organic layers were dried over $MgSO_4$, filtered, and evaporated in vacuo to dryness. The solid was purified by TLC using CH_2Cl_2:MeOH (99:1) as eluent. The product was obtained following extraction of the silica with CH_2Cl_2 and evaporation under reduced pressure to yield a green solid (81 mg, 71 %), mp: 117-120.

^1H-NMR (300.13 MHz, $CDCl_3$) δ: 9.17 (bs, 1H, pyrimidine-**H**), 8.81 (bs, 1H, -Ar-**H**), 8.65 (bs, 1H, -N**H**), 8.14-8.02 (bs, 2H, Ar-**H**), 7.84 (bs, 1H, Ar-**H**), 7.68 (bs, 1H, Ar-**H**), 7.41-7.20 (m, 2H, Ar-**H**) 4.69 (bs, 2H, (-C**H**$_2$-OAr)$_2$), 4.49 (bs, 2H, (-C**H**$_2$-OAr)$_2$), 4.23 (bs, 2H, H_3CO-C**H**$_2$-), 3.93 (bs, 2H, H_3CO-C**H**$_2$-), 3.93-3.77 (m, 8H, (**H**$_3$C-O-)$_2$-;-C**H**$_2$-triazole), 3.42-3,44 (m, 22H, -C**H**$_2$-O-C**H**$_2$-C**H**$_2$-$B_{12}H_{11}$; $^+$N-C**H**$_2$-), 1.76-1.74 (m, 16H, $^+$N-CH_2C**H**$_2$-), 1.40 (dq, $J_{H,H}$= 14.4, 7.1 Hz, 16H, $^+$N-CH_2CH_2C**H**$_2$-), 0.95 (t, $J_{H,H}$= 7.3 Hz, 24H, $^+$N-$CH_2CH_2CH_2$C**H**$_3$). $^{13}C\{^1H\}$-NMR (75.47 MHz, $CDCl_3$) δ: 157.3, 157.1, 155.0, 149.6, 146.0, 139.4, 138.9, 132.0, 131.8, 129.0, 128.6, 123.6, 122.0, 121.1, 119.7, 103.5, 72.0, 70.7, 70.3, 70.0, 69.5, 69.1, 68.1, 58.6 (4C), 58.3, 55.3, 49.4, 23.6 (4C), 19.5 (4C), 13.0 (4C). $^{11}B\{^1H\}$-NMR (96.29 MHz, $CDCl_3$) δ: 7.55 (1B), -16.03 (10B), -20.68 (1B). MALDI-TOF-MS: m/z calcd. 664.44. Found: 663.54. Anal. Calcd. for $C_{58}H_{114}B_{12}N_8O_6$: C, 60.61; H, 10.00; N, 9.75. Found: C, 60.59; H, 10.12, N, 9.77.

Characterization of 3-azidopropylbenzene (27).[9]

Yellow oil (98 %).
^1H-NMR (300.13 MHz, $CDCl_3$) δ: 7.37-7.31 (m, 2H, Ar-**H**), 7.26-7.21 (m, 3H, -Ar-**H**), 3.32 (t, $J_{H,H}$= 6.8 Hz, 2H, -C**H**$_2$-N_3), 2.74 (t, $J_{H,H}$= 6.7 Hz, 2H, Ph-C**H**$_2$-), 1.95 (dt, , J = 14.0, 6.9 Hz, 2H, -CH_2-C**H**$_2$-CH_2-). $^{13}C\{1H\}$-NMR (75.47 MHz, $CDCl_3$) δ: 140.8, 128.5 (2C), 128.4 (2C), 126.1, 50.7, 32.8, 30.4.

Synthesis and characterization of compound 4-{3-[1-(phenylpropyl)-1*H*-[1,2,3]triazol-4-yl]phenyl}amino-6,7-bis(2-methyloxyethyloxy)quinazoline (28).

A 10-mL round-bottom flask equipped with a magnetic stirring bar was charged with Erlotinib (1.1 equiv., 212 mg, 0.54 mmol) dissolved in THF:H_2O (4 mL, 1:1 v/v). Then, sodium ascorbate (15 mg, 15 mol %), $CuSO_4.5H_2O$ (12 mg, 10 mol %) and **27** (1 equiv., 80 mg, 0.49

mmol) were added. The mixture was left at room temperature for 2 h. After that, a heavy yellow precipitate formed, which it was filtered. The filtrate was poured into CH_2Cl_2 (15 mL) and washed with water (3 × 5 mL). The organic layer was dried over $MgSO_4$ and evaporated *in vacuo* to dryness. The product was purified by preparative TLC and CH_2Cl_2:MeOH (99:1) as eluent. The product was obtained following extraction of the silica with acetone and evaporation under reduced pressure to yield a yellow solid (220 mg, 81 %), mp: 119-123 °C.

^{1}H-NMR (300.13 MHz, $CDCl_3$) 8.64 (s, 1H, pyrimidine-**H**), 8.10 (s, 1H, -Ar-**H**), 8.00 (s, 1H, -N**H**), 7.81 (d, $J_{H,H}$= 8.8 Hz, 1H, Ar-**H**), 7.70 (s, 1H, Ar-**H**), 7.48 (d, $J_{H,H}$= 8.8 Hz, 1H, Ar-**H**), 7.39-7.34 (m, 2H, Ar-**H**), 7.31-7.29 (m, 1H, Ar-**H**), 7.26 (bs, 1H, Ar-**H**), 7.23-7.20 (m, 1H, Ar-**H**), 7.18-7.17 (m, 2H, Ar-**H**), 7.14 (bs, 1H, Ar-**H**), 4.34 (t, $J_{H,H}$= 7.1 Hz, 2H, -C**H**$_2$-triazole), 4.21 (dd, $J_{H,H}$= 9.7, 6.8 Hz, 4H, (-C**H**$_2$-OAr)$_2$), 3.82-3.78 (m, 2H, H_3CO-C**H**$_2$-), 3.77-3.73 (m, 2H, H_3CO-C**H**$_2$-), 3.43 (s, 3H, **H**$_3$C-O-), 3.40 (s, 3H, **H**$_3$C-O-), 2.65 (t, $J_{H,H}$= 7.5 Hz, 2H, -C**H**$_2$-Ar), 2.30-2.19 (m, 2H, -CH_2-C**H**$_2$-CH_2-). ^{13}C{1H}-NMR (75.47 MHz, $CDCl_3$) δ: 156.6, 154.3, 153.6, 148.8, 147.5, 147.4, 140.1, 139.6, 131.2, 129.4, 128.6 (2C), 128.4 (2C), 126.3, 121.7, 121.1, 120.0, 119.0, 109.5, 108.6, 102.6, 70.8, 70.4, 68.9, 68.3, 59.1 (2C), 49.6, 32.5, 31.5. Anal. Calcd. for $C_{31}H_{34}N_6O_4$: C, 67.13; H, 6.18; N, 15.15. Found: C, 67.14; H, 6.16; N, 15.21.

2. Biology

Cell Lines and Culture Conditions

The rat astrocytoma derived cell line C6 (ATCC® CCL-107™) were cultured in Dulbecco's modified Eagle's milieu (DMEM), supplemented with 10 % inactivated foetal bovine serum and 1 % penicillin/streptomycin in 25-cm^2 culture flasks at 37 °C under a 5 % CO_2 humidified environment (normal culture conditions). The medium was changed every 2–3 days and cells were sub-cultured once they reached 90–95 % confluence.

Cytotoxicity assay

Cells were seeded in 96-well plates (20 × 10^3 cells/well) in 100 µL final volume and were allowed to grow 24 h. After that, 100 µL of each concentration of the tested compounds in the culture milieu were added onto the cells and were further incubated for 24 h. Then, cells were fixed with ice-cold trichloroacetic acid for 1 h at 4 °C, the plates were washed five times in distilled water and allowed to dry in the air. Sulphorhodamine B (SRB) solution (50 µL) was added to each well of the dry 96-well plates and allowed staining at room temperature for 30 min. The SRB solution and unbound dye were removed by washing the plates quickly with 1 % v/v acetic acid, five times. The washed plates were dried in the air. The bound SRB was solubilized by adding 100 µL of 10 mM unbuffered Tris Base (pH 10.5) to each well and shaking for 5 min on a shaker platform. The developed colour was read in a 96-well plate reader at 492 nm. The optical density (OD) of SRB in each well is directly proportional to the cell number consequently the OD values were plotted against concentration and the IC_{50} value were determined.

Immunocytochemistry for EGFRr

C6 cells were plated in 35 mm-diameter Petri dishes (350.000 cells/dish) and were maintained in normal culture conditions for 48 h. Cells were fixed with 4 % paraformaldehyde for 20 min at room temperature, followed by three washes with phosphate-buffered saline solution (PBS). Cells were permeated for 20 min by 0.1 % Triton X-100 in PBS and blocked in 5 % bovine serum albumin/PBS for 60 min. The dishes were incubated with rabbit polyclonal anti-EGFRr antibody (1:200 dilution, ab15669) overnight at 4 ºC followed by the incubation with anti-rabbit Alexa Fluor ® 633-conjugated IgG antibody (1:500 dilution, Life technologies,

A-21070) for 90 minutes after 3 washes with PBS. Coverslips were mounted with 50 % glycerol – 1 µg/mL DAPI (4',6-diamidino-2-phenylindole). Fluorescence signal was detected with a LSCM Olympus FV300 microscope.

Primary Cell Cultures

Mixed glial cultures were prepared from 1–2-day-old rat pups according to the procedures of Saneto and De Vellis.[10] Briefly, brain cortexes were dissociated in 0.25 % trypsin for 25 min at 37 °C. Cells were collected by centrifugation, filtered through a 80 µm mesh cell dissociation sieve to get rid of cell debris, and plated at a density of 1.5×10^6 cells per 25 cm^2 flask in DMEM supplemented with 10 % foetal bovine serum, HEPES (3.6 g/L), penicillin (100 IU/mL), and streptomycin (100 g/mL). Milieu was removed after 72 h and then changed each 48 hours, a confluent culture was obtained around a week and half after plating.

3. R_M determination

Reversed-phase TLC experiments were done on precoated TLC plates SIL RP-18W/UV254 and eluted with MeOH:phosphate buffer saline (pH 7.4, 0.01 M) (35:65, v/v). Stock solutions were prepared in pure methanol (Aldrich) prior to use. The plates were developed in a closed chromatographic tank, dried and the spots were located under UV light.

The R_f values were averaged from two to three determinations, and converted to R_M via the relationship:

$$R_M = \log [(1/R_f)-1]$$

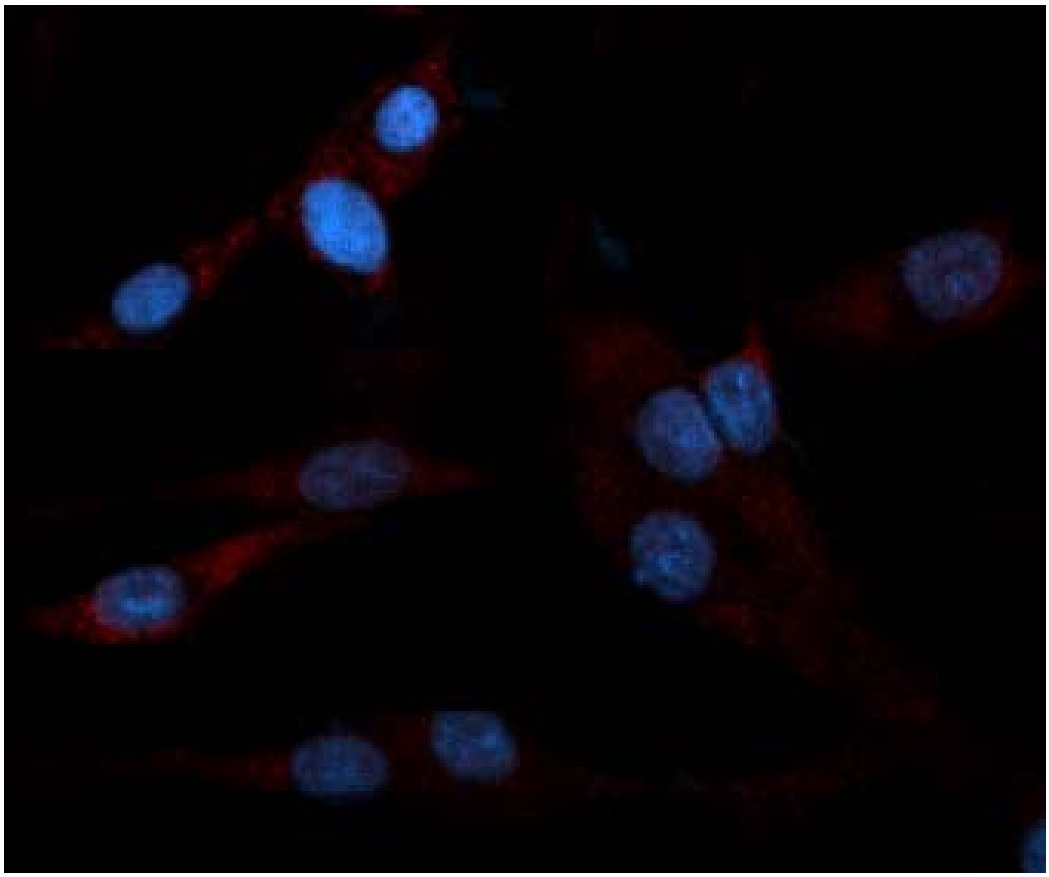


Fig. S1 Immunofluorescence image of the C6 cells stained by anti-EGFR antibodies (red). Nuclei were stained with DAPI (blue). Scale 80x. The staining of the cells demonstrated the EGFR expression in C6 cells.

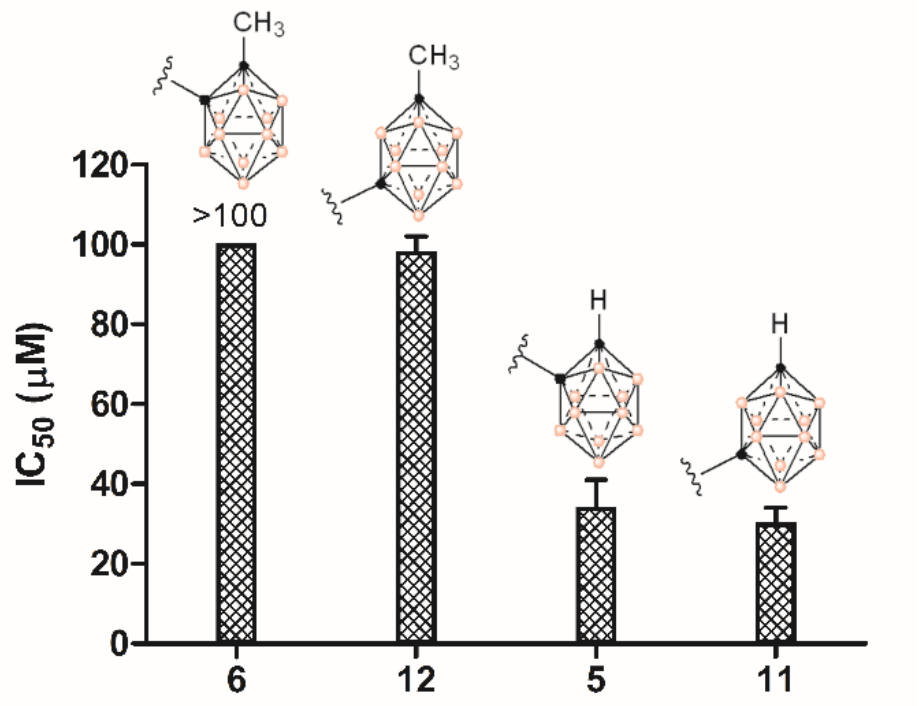


Fig. S2 Structure-activity relationship. IC_{50}s for methyl- and de-methyl-derivatives and *ortho*- and *meta*-isomers belonging to the triazole-linker series.

a)

Compds	Percentage of survival at 100 µM (%)[a]
15	74
16	92
19	72
20	82

[a] The results represent mean of triplicate assays

b)

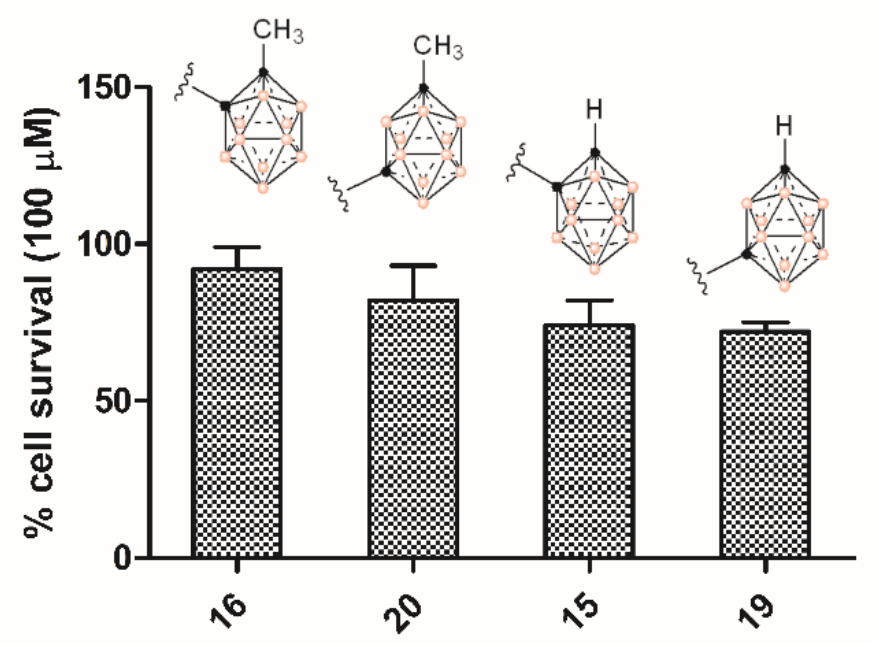
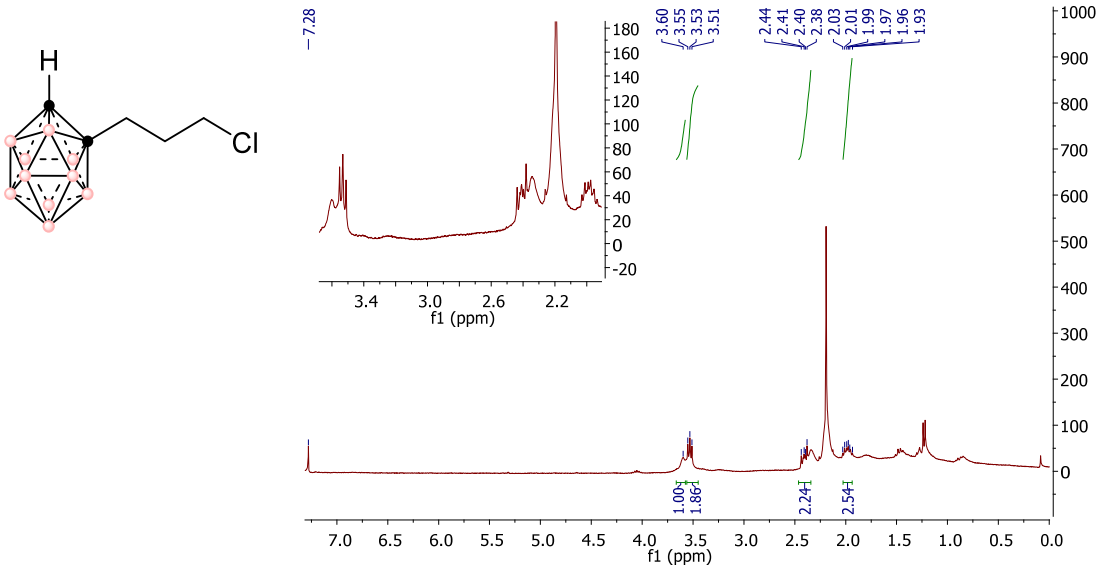
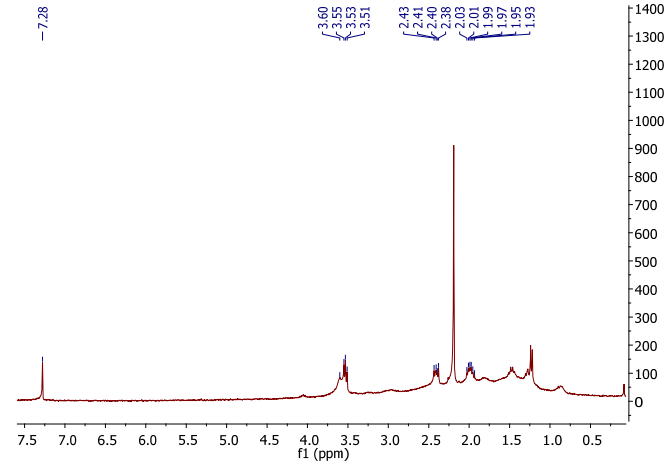


Fig. S3 Structure-activity relationship. (a) *In vitro* C6 percentage of survival of derivatives belonging to ethynylbenzyl-linker series. (b) Relationship of percentage of cell survival and structure of derivatives belonging to the ethynylbenzyl-linker series.

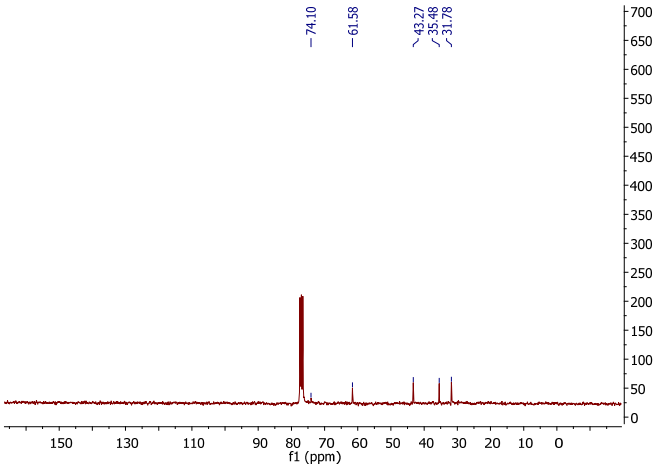
$^{1}H\{^{11}B\}$-NMR



^{1}H-NMR



$^{13}C\{^{1}H\}$-NMR



$^{11}B\{^{1}H\}$-NMR

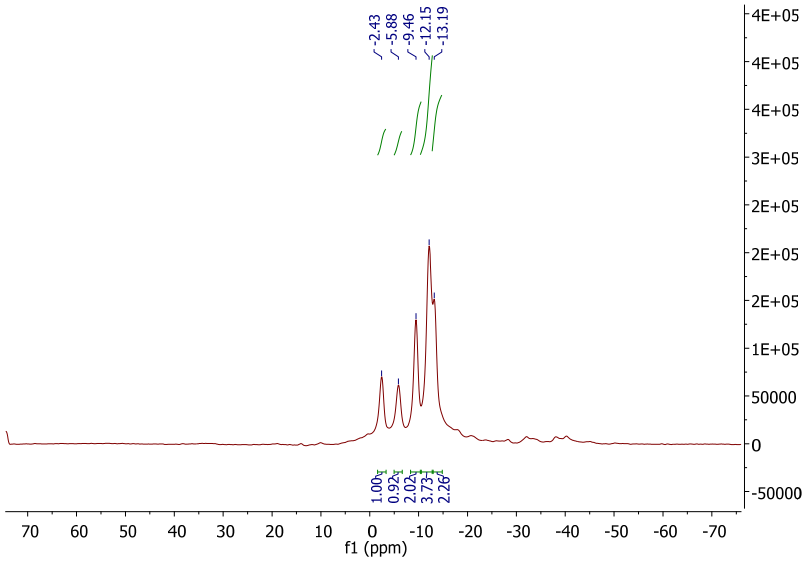
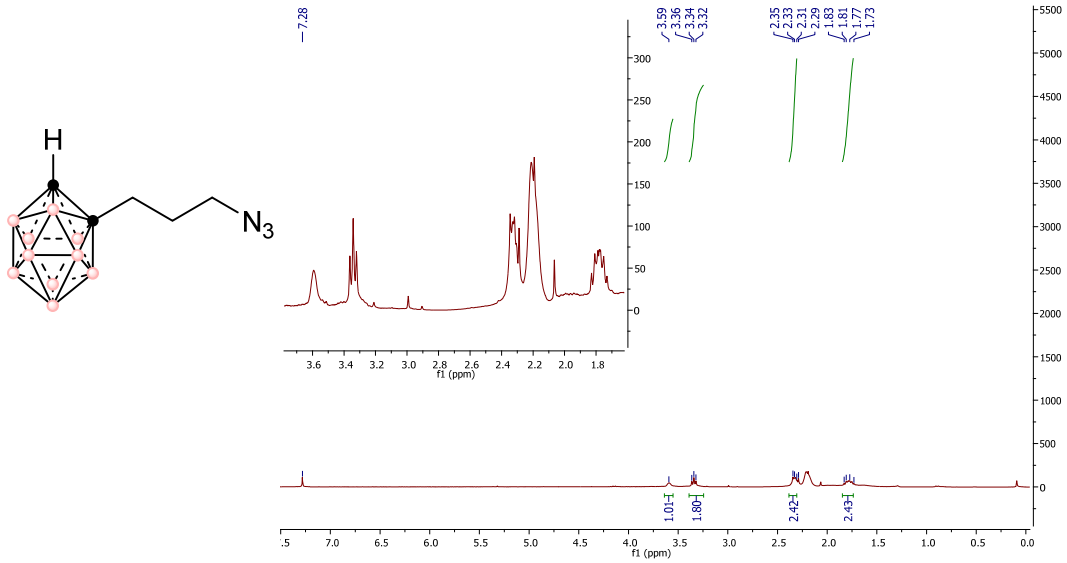
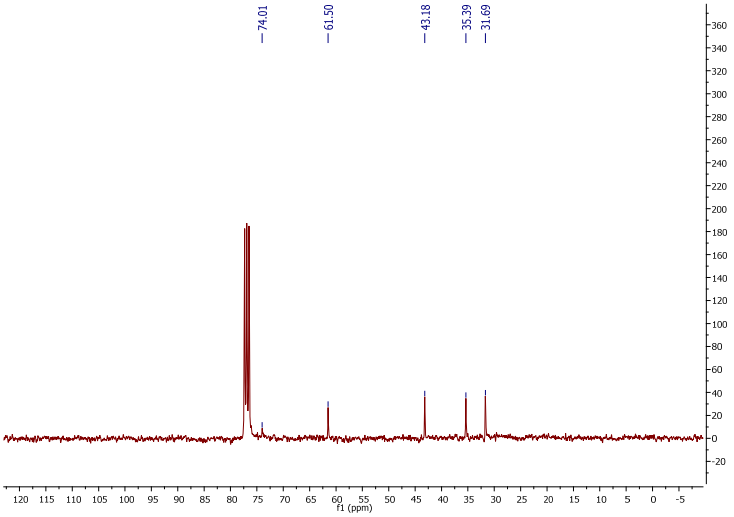


Fig. S4 Spectra of **1**.

$^{1}H\{^{11}B\}$-NMR



$^{13}C\{^{1}H\}$-NMR



$^{11}B\{^{1}H\}$-NMR

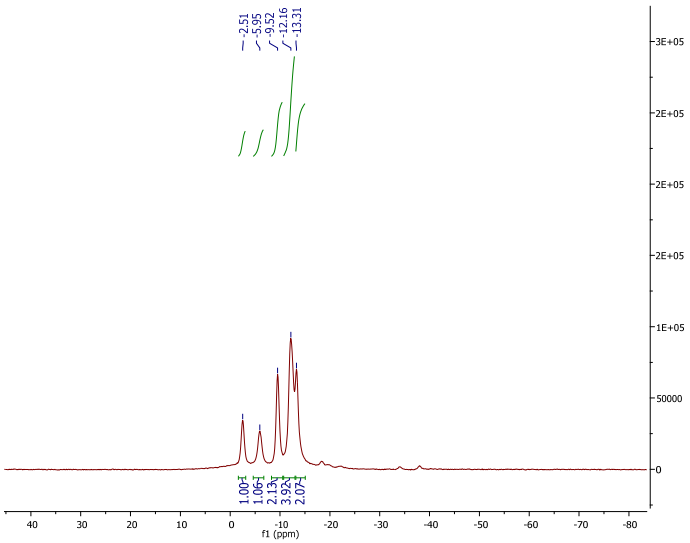
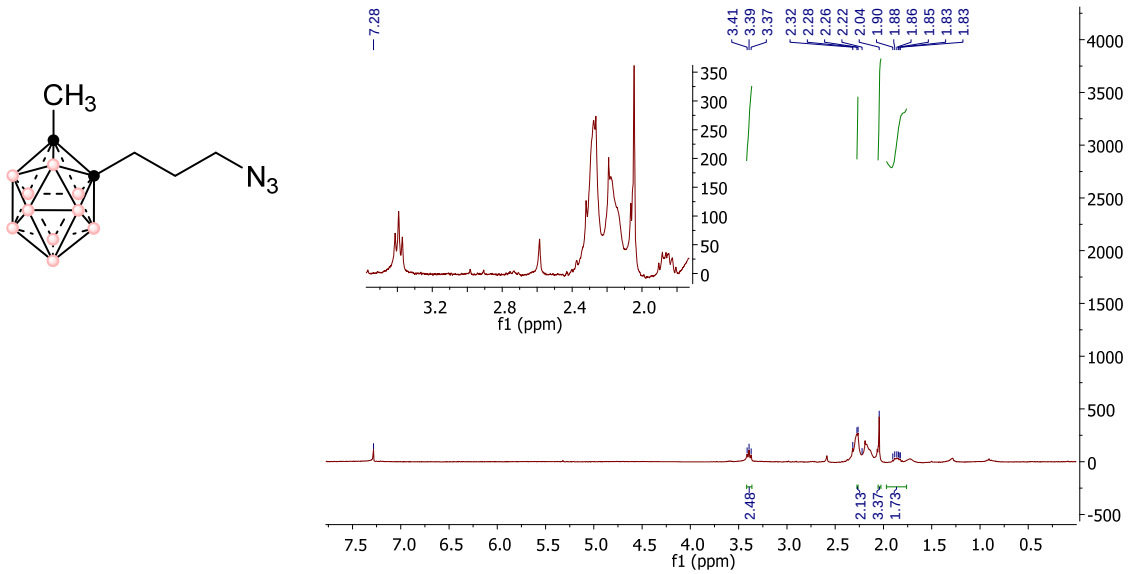
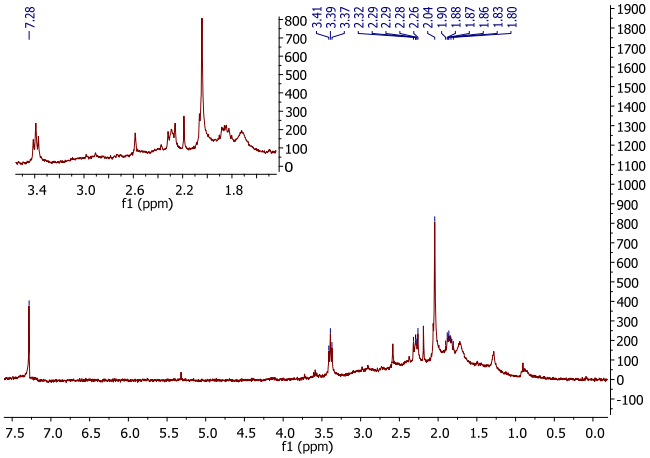


Fig. S5 Spectra of **3**.

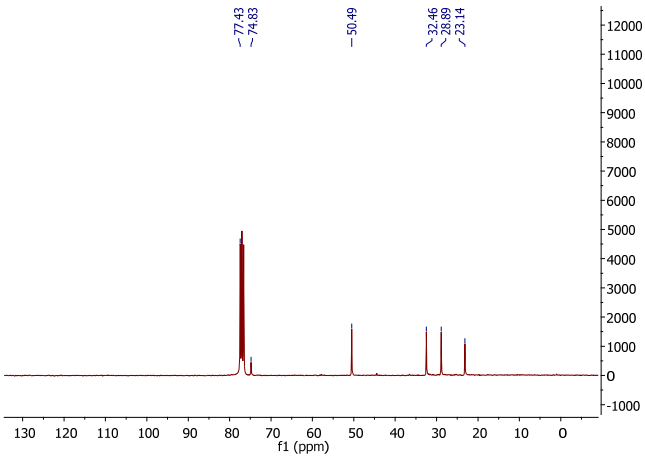
$^{1}H\{^{11}B\}$-NMR



^{1}H-NMR



$^{13}C\{^{1}H\}$-NMR



$^{11}B\{^{1}H\}$-NMR

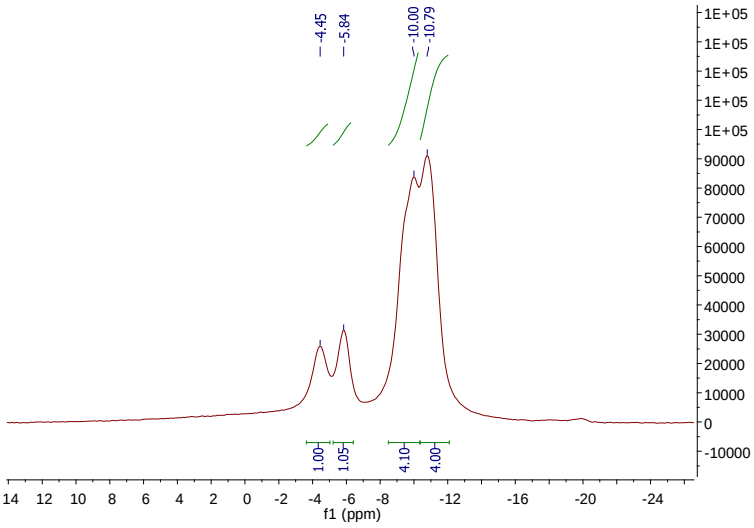
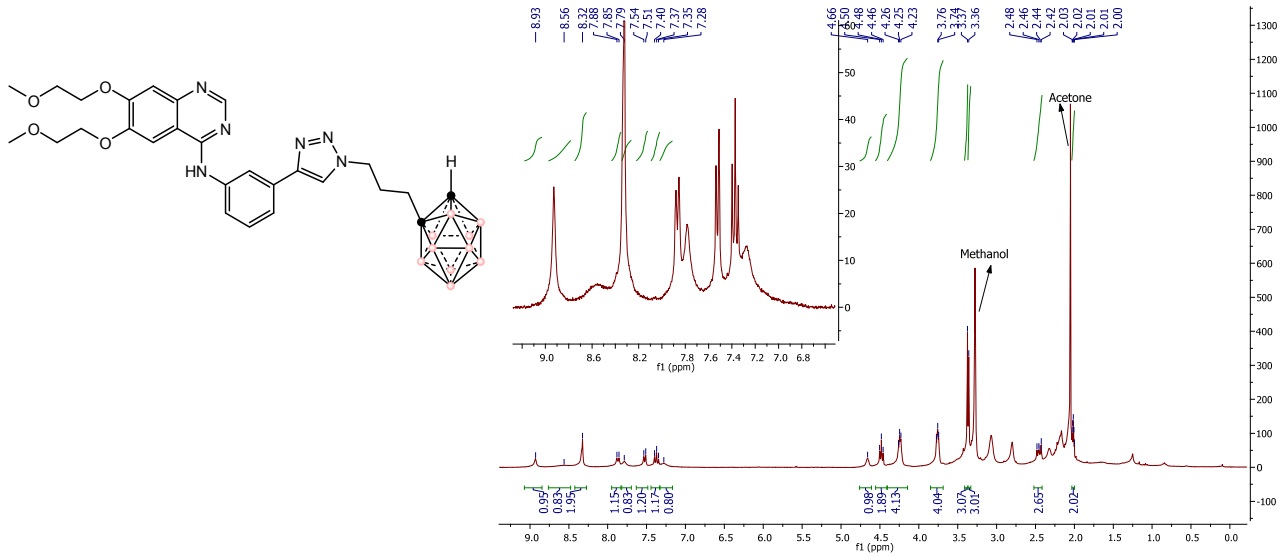
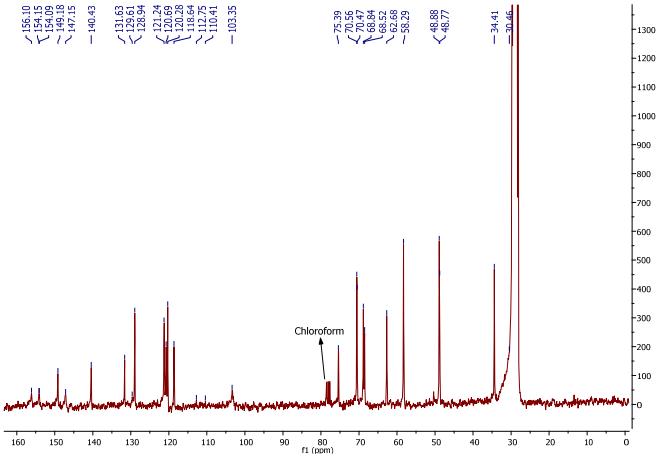


Fig. S6 Spectra of **4**.

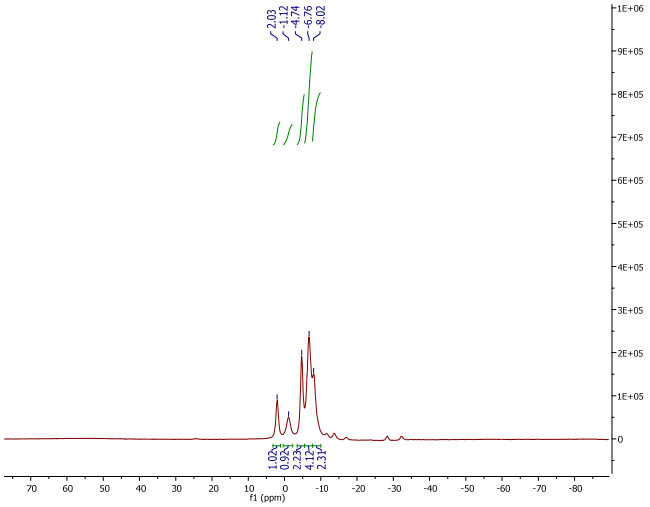
$^{1}H\{^{11}B\}$-NMR



$^{13}C\{^{1}H\}$-NMR



$^{11}B\{^{1}H\}$-NMR



m/z (EI)

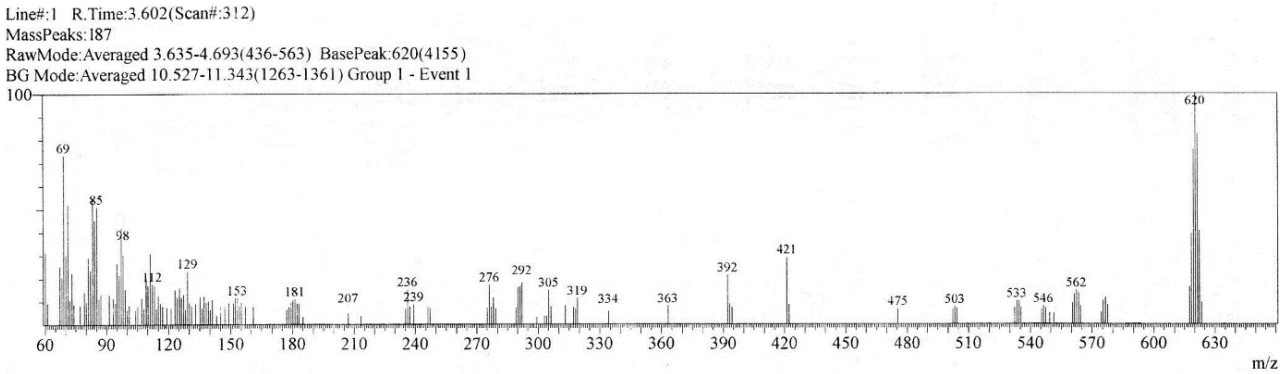
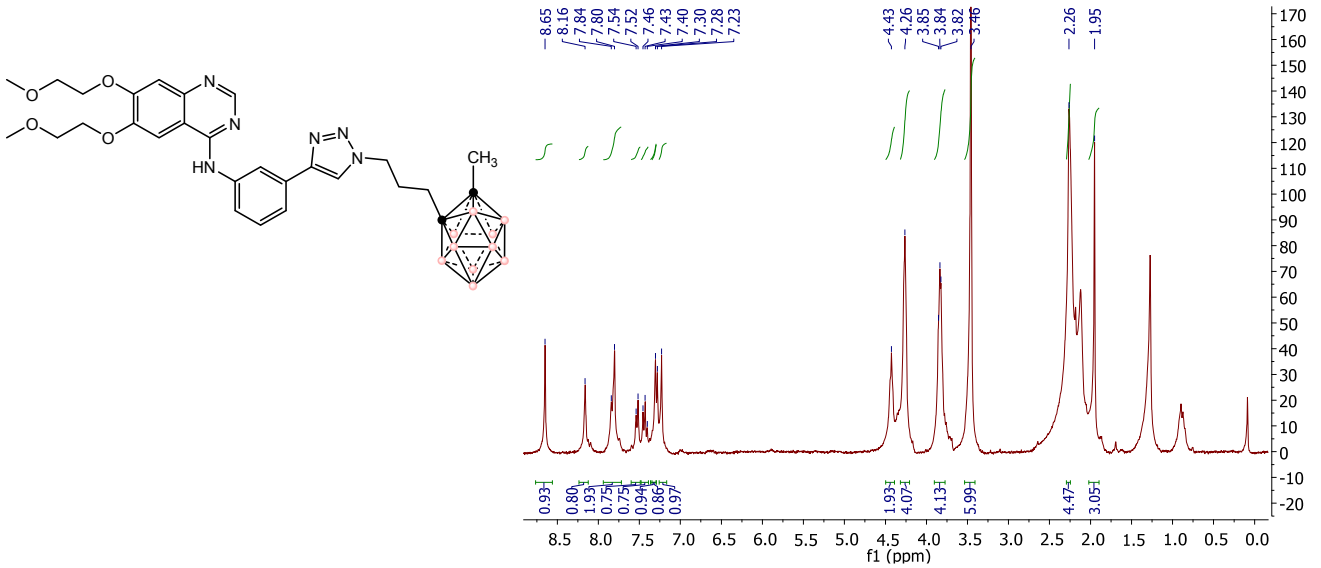
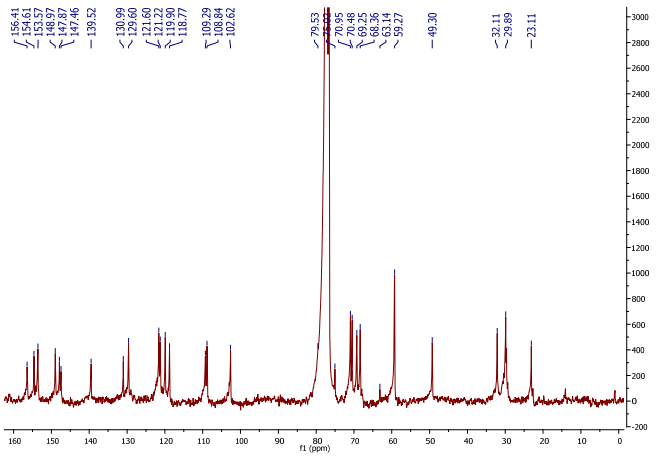


Fig. S7 Spectra of **5**.

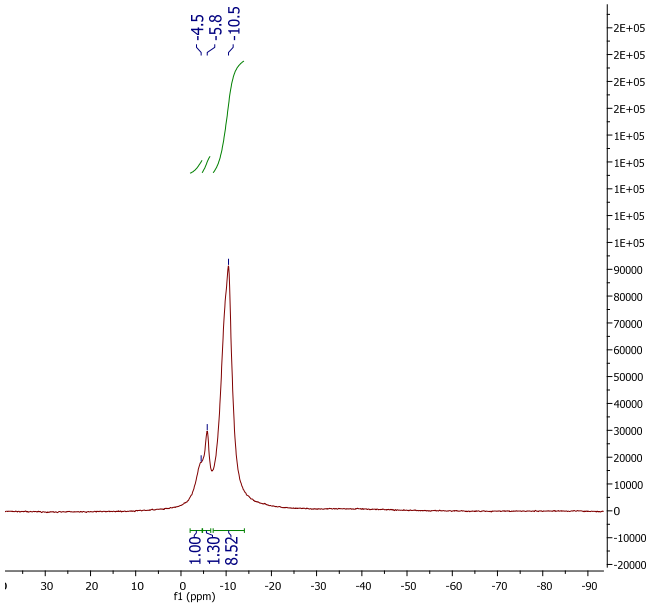
$^{1}H\{^{11}B\}$-NMR



$^{13}C\{^{1}H\}$-NMR



$^{11}B\{^{1}H\}$-NMR



m/z (EI)

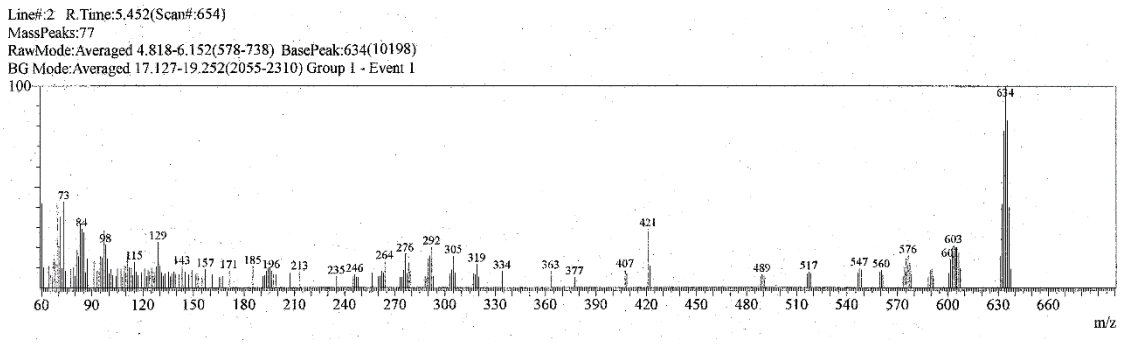
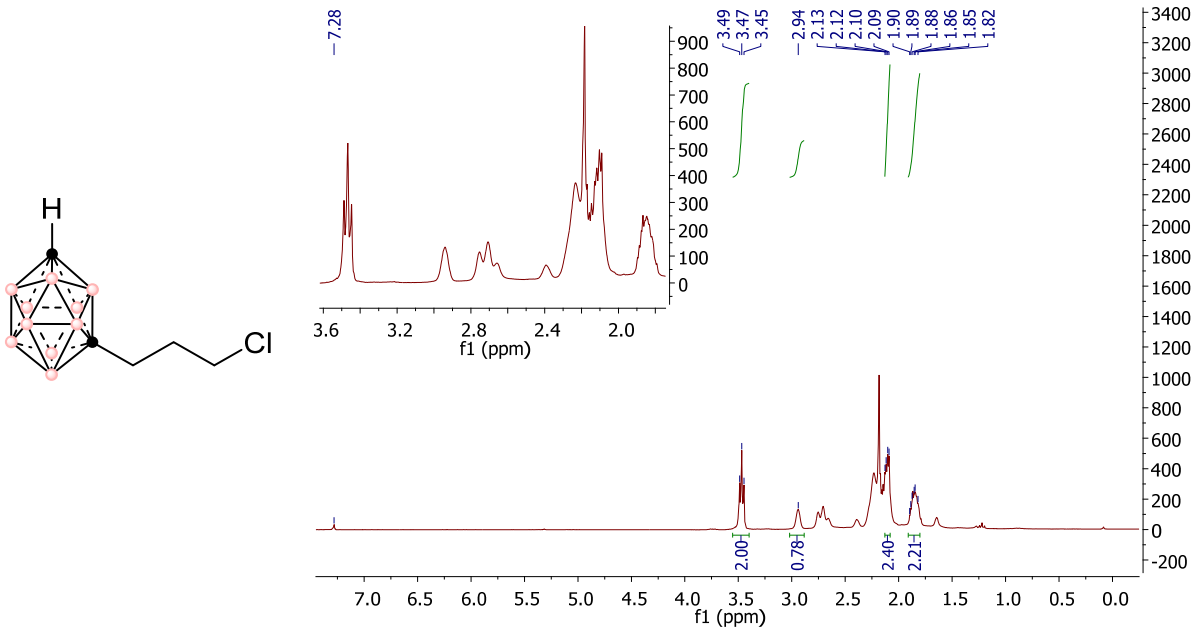
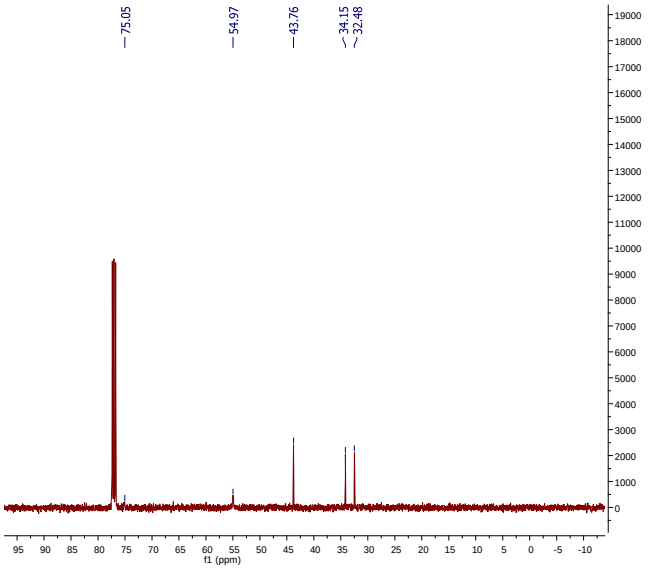


Fig. S8 Spectra of **6**.

$^{1}H\{^{11}B\}$-NMR



$^{13}C\{^{1}H\}$-NMR



$^{11}B\{^{1}H\}$-NMR

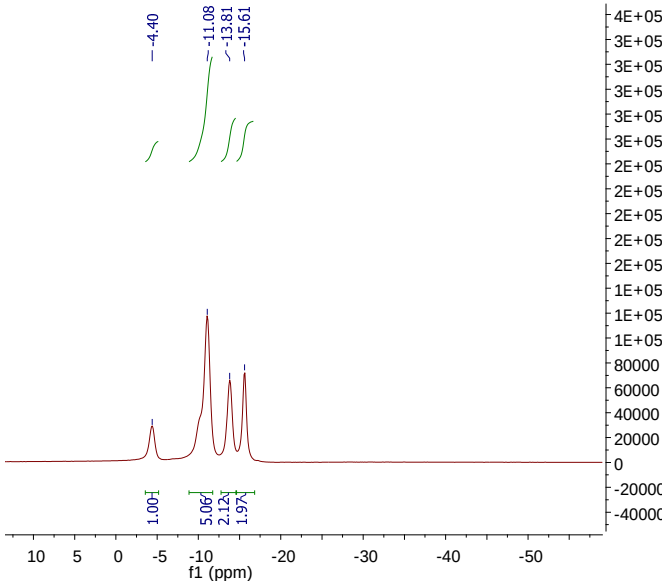
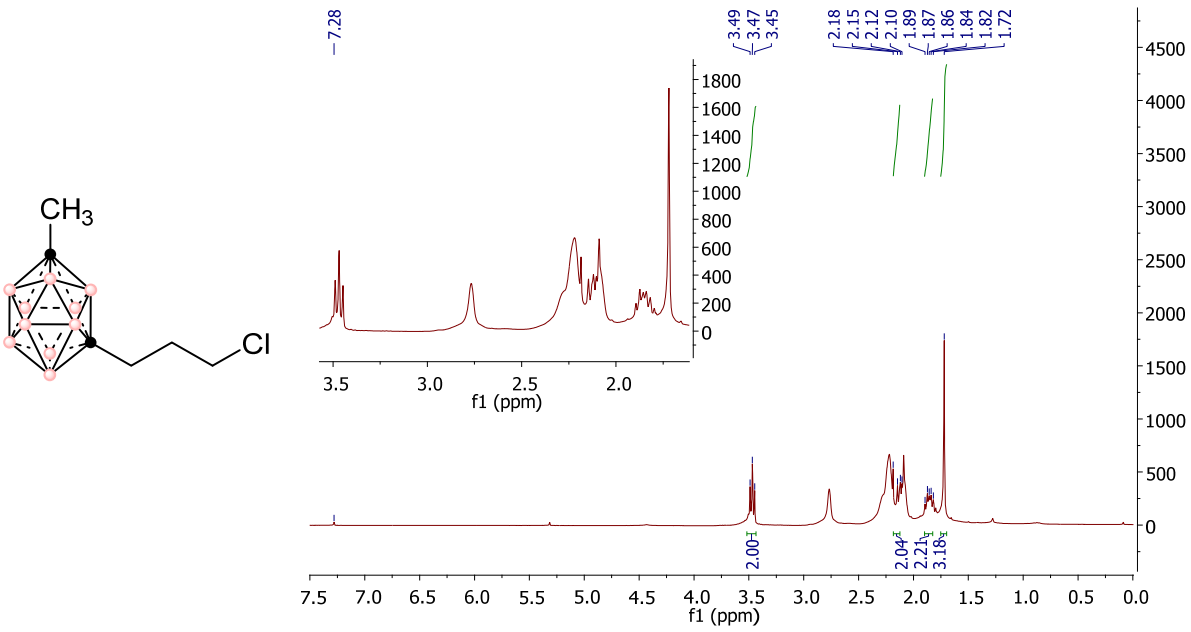
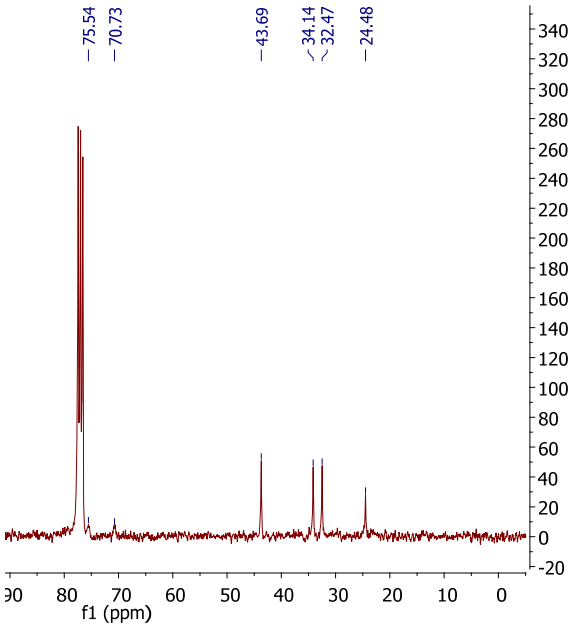


Fig. S9 Spectra of **7**.

$^{1}H\{^{11}B\}$-NMR



$^{13}C\{^{1}H\}$-NMR



$^{11}B\{^{1}H\}$-NMR

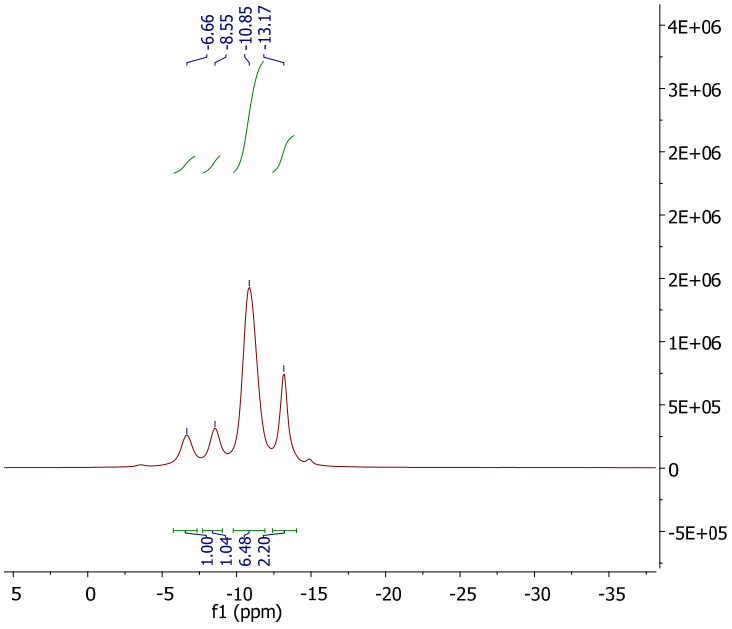
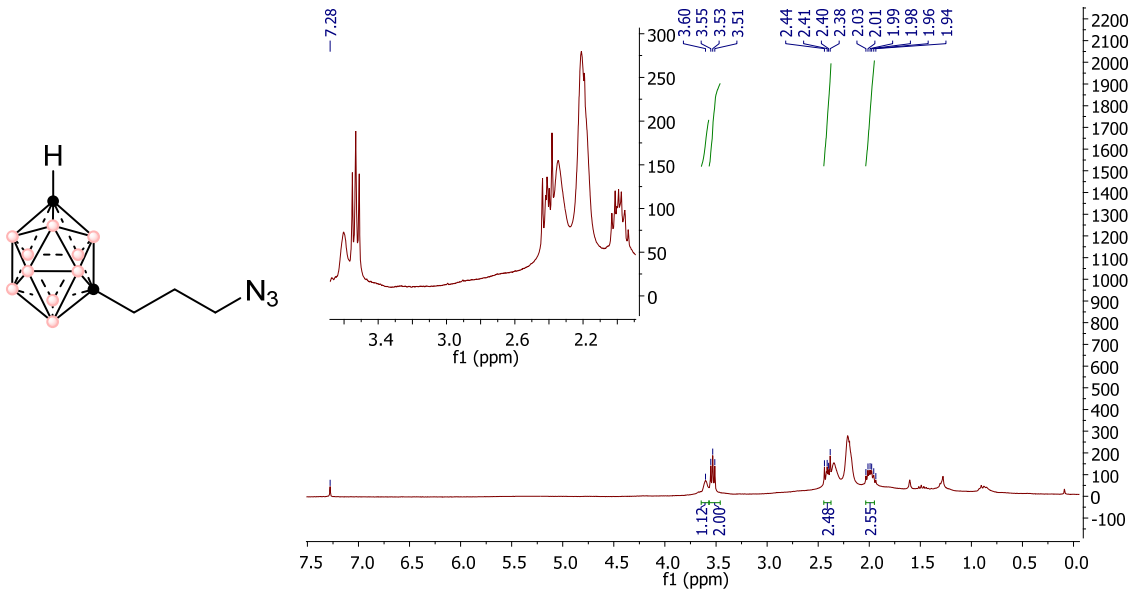
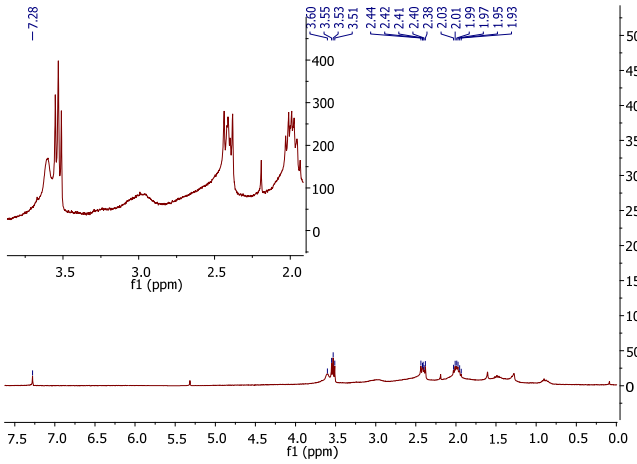


Fig. S10 Spectra of **8**.

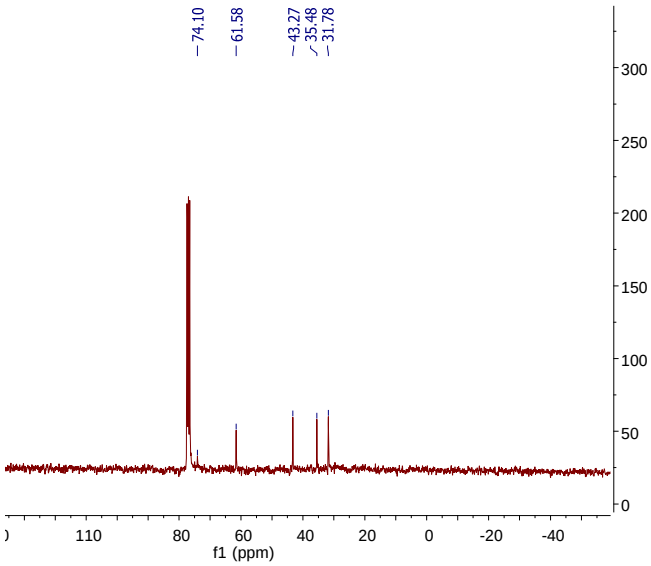
$^{1}H\{^{11}B\}$-NMR



^{1}H-NMR



$^{13}C\{^{1}H\}$-NMR



$^{11}B\{^{1}H\}$-NMR

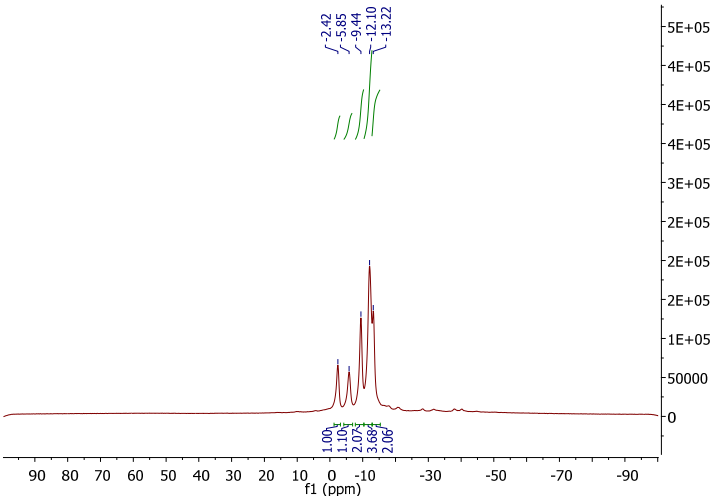
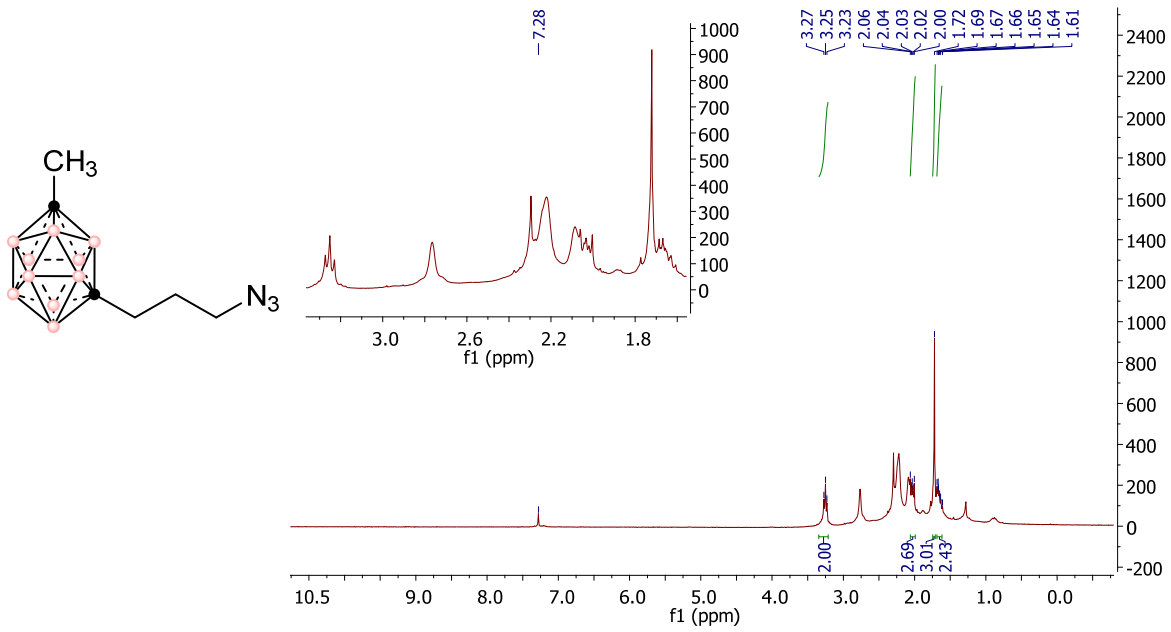
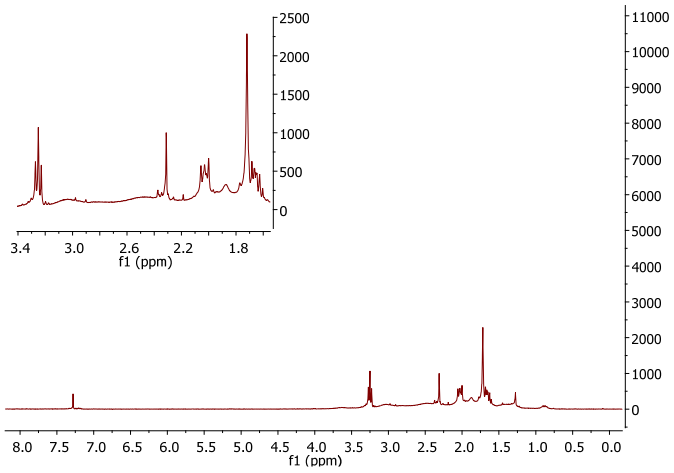


Fig. S11 Spectra of **9**.

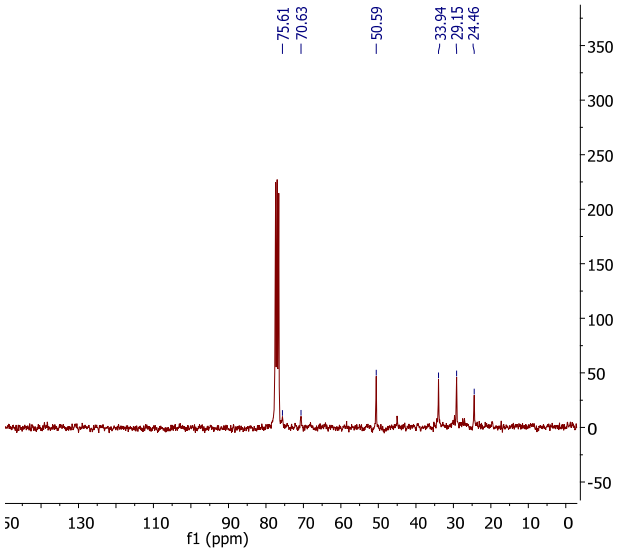
$^{1}H\{^{11}B\}$-NMR



^{1}H-NMR



$^{13}C\{^{1}H\}$-NMR



$^{11}B\{^{1}H\}$-NMR

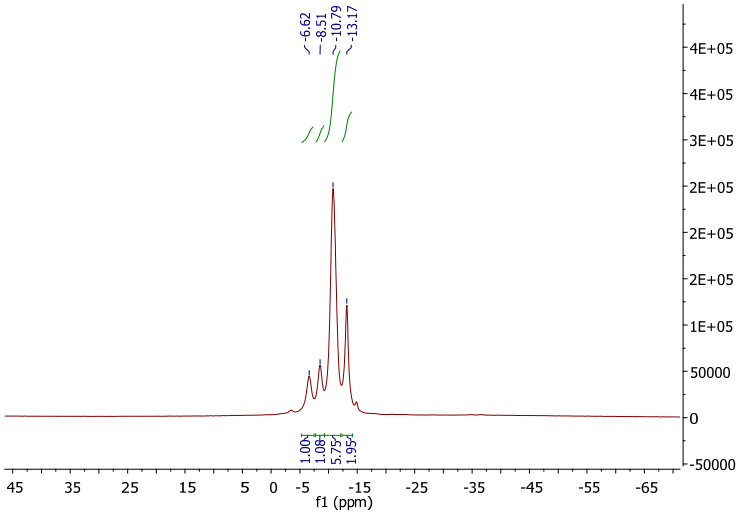
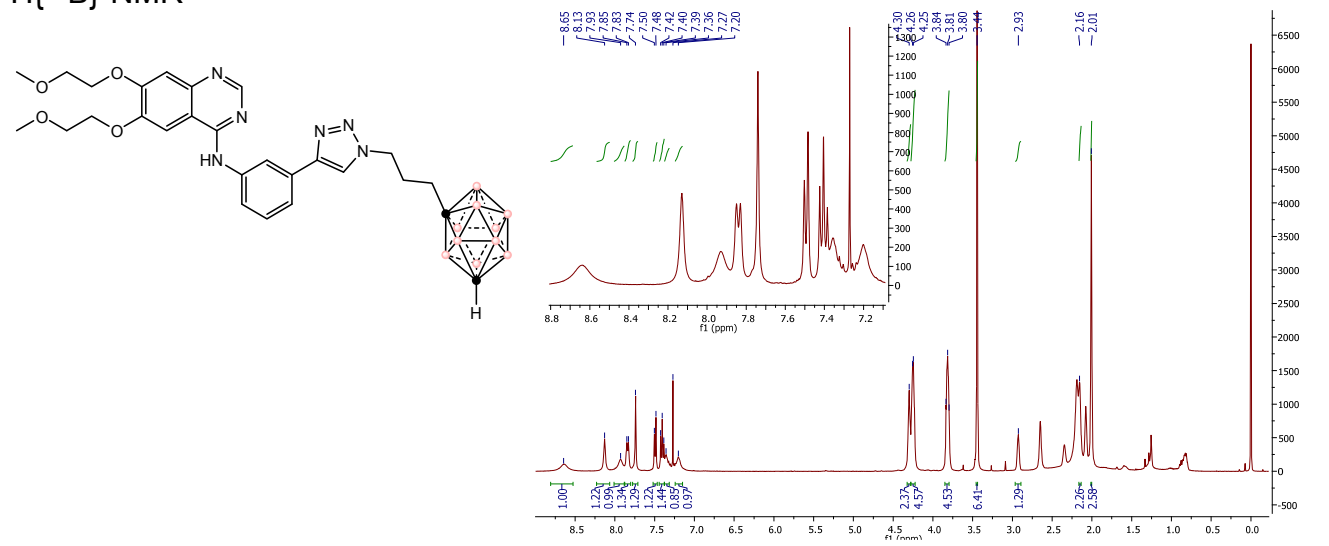
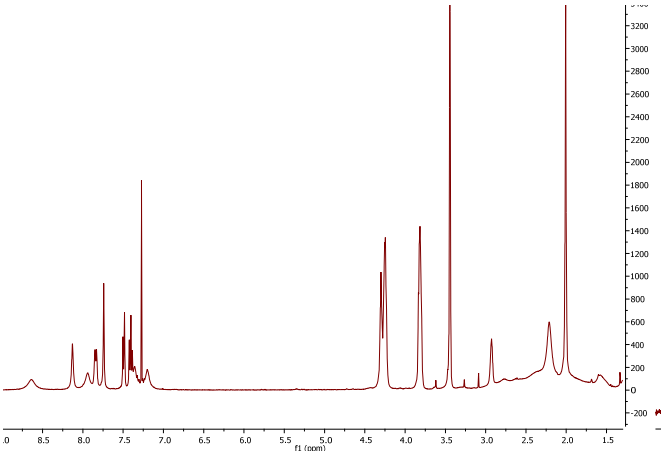


Fig. S12 Spectra of **10**.

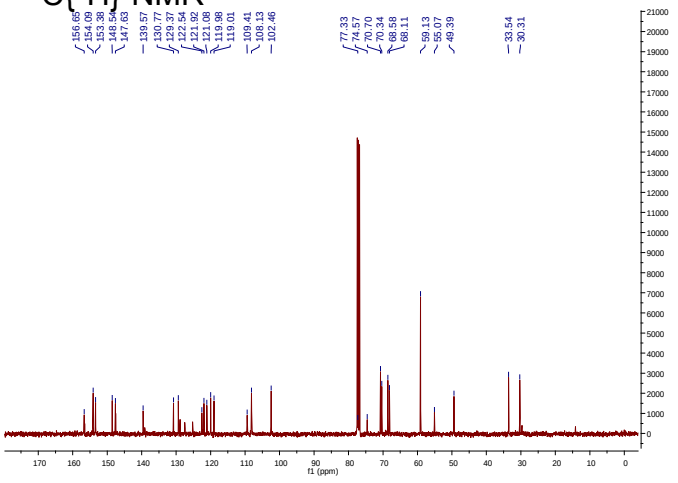
$^{1}H\{^{11}B\}$-NMR



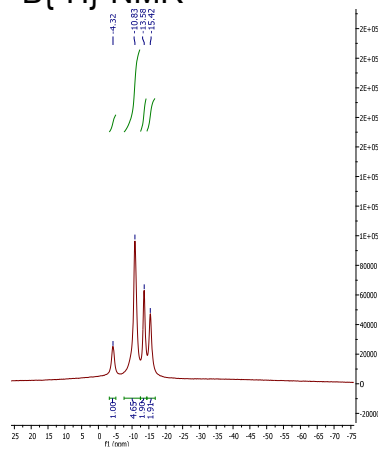
^{1}H-NMR



$^{13}C\{^{1}H\}$-NMR



$^{11}B\{^{1}H\}$-NMR



m/z (EI)

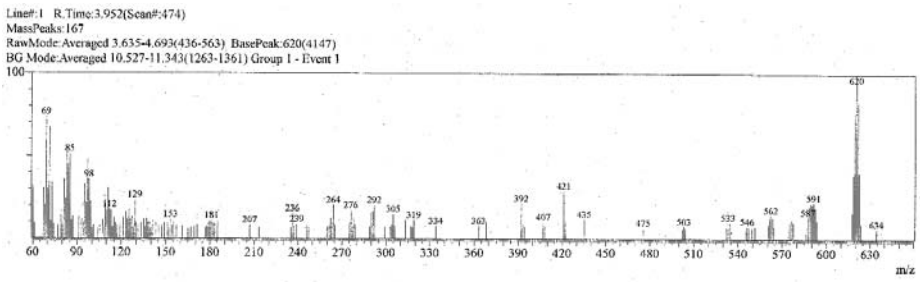
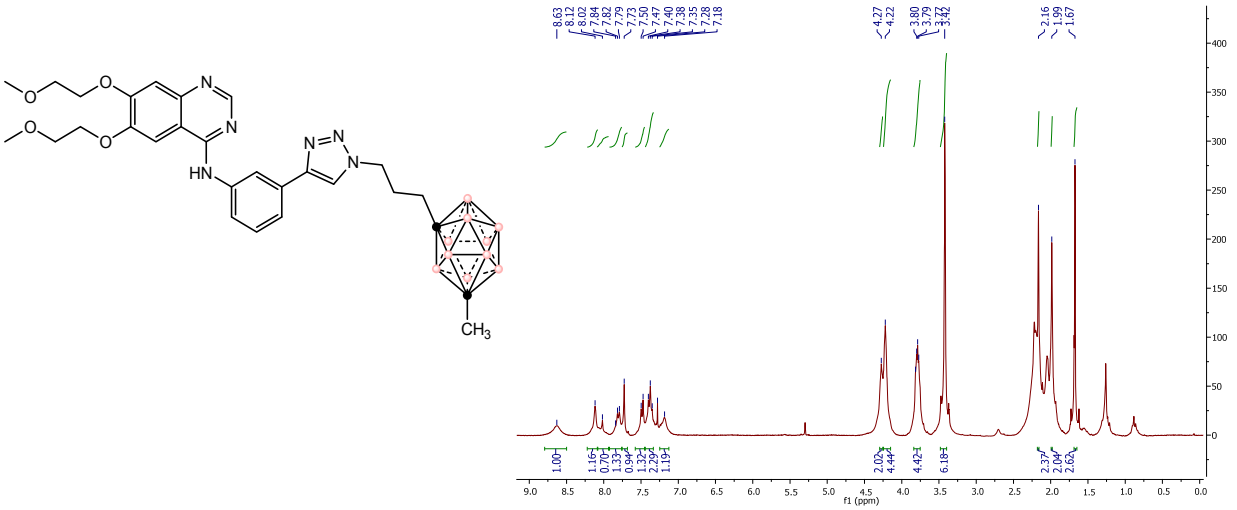
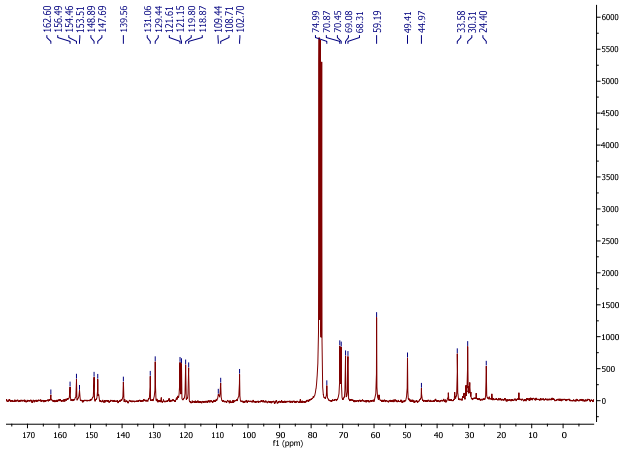


Fig. S13 Spectra of **11**.

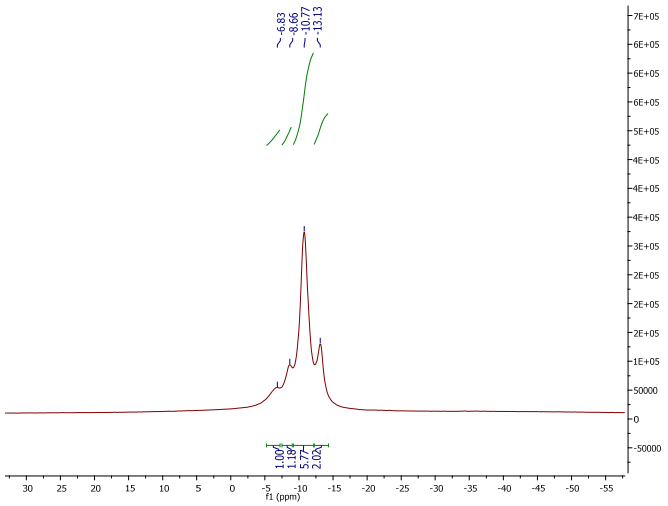
$^{1}H\{^{11}B\}$-NMR



$^{13}C\{^{1}H\}$-NMR



$^{11}B\{^{1}H\}$-NMR



m/z (EI)

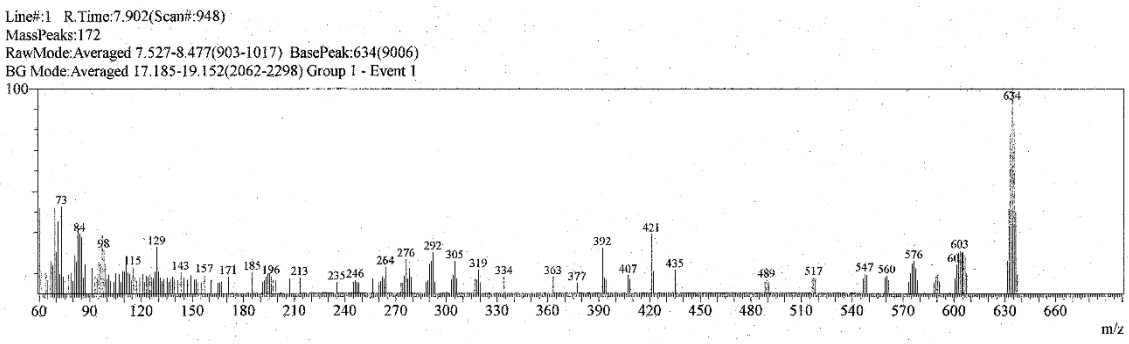
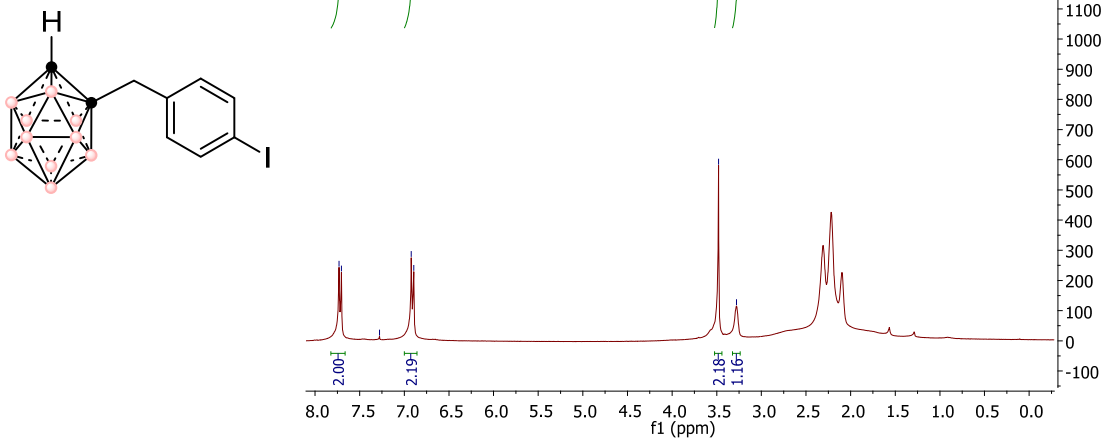
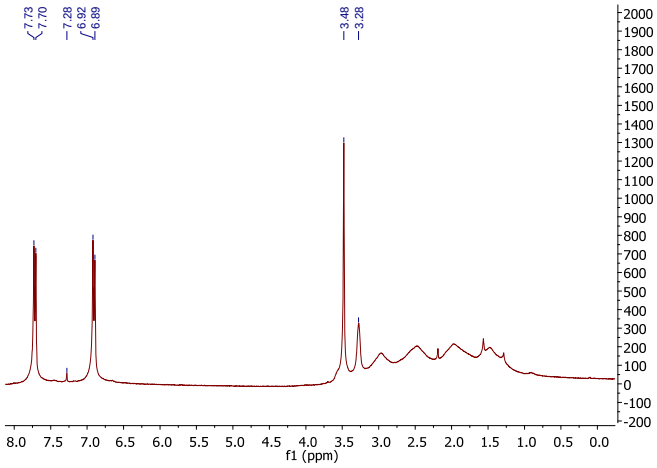


Fig. S14 Spectra of **12**.

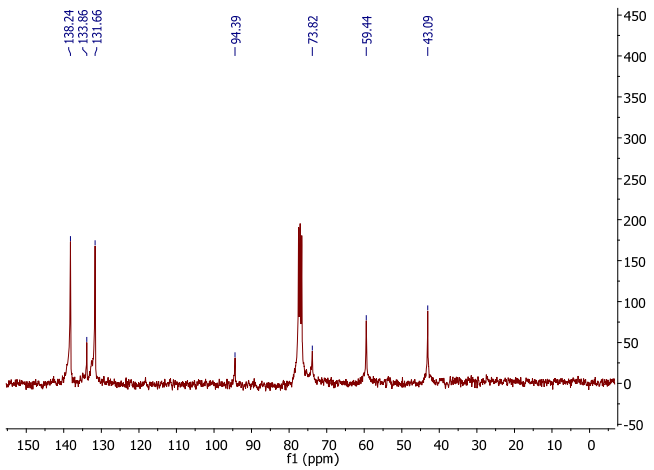
$^{1}H\{^{11}B\}$-NMR



^{1}H-NMR



$^{13}C\{^{1}H\}$-NMR



$^{11}B\{^{1}H\}$-NMR

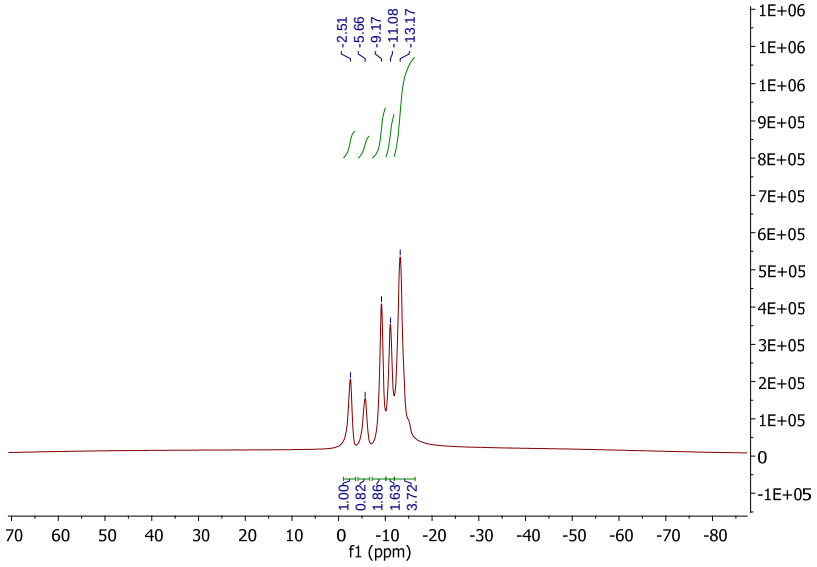
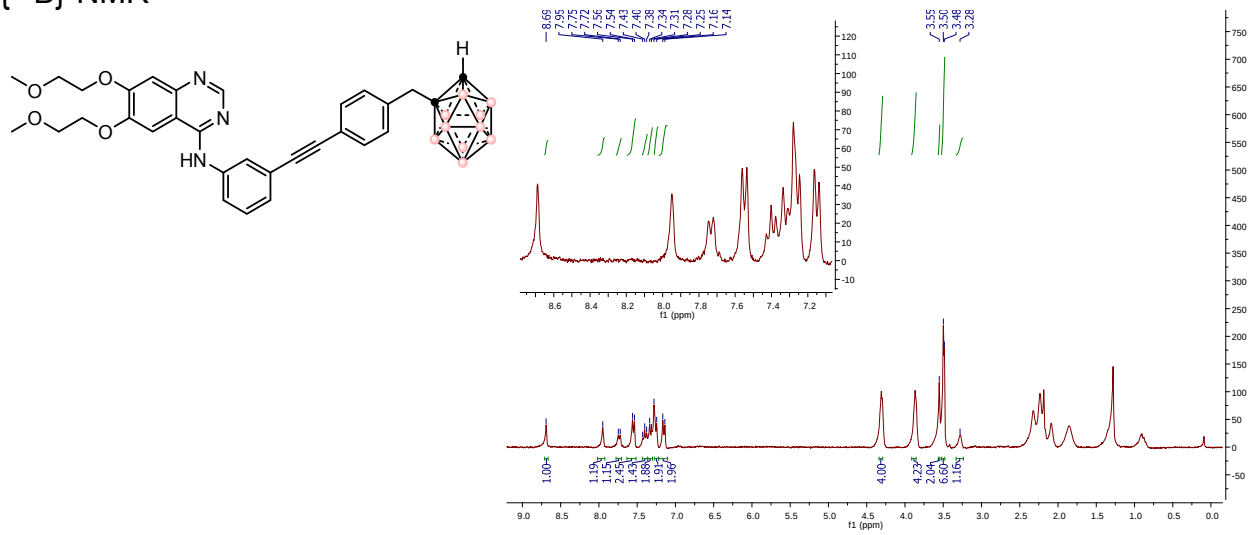
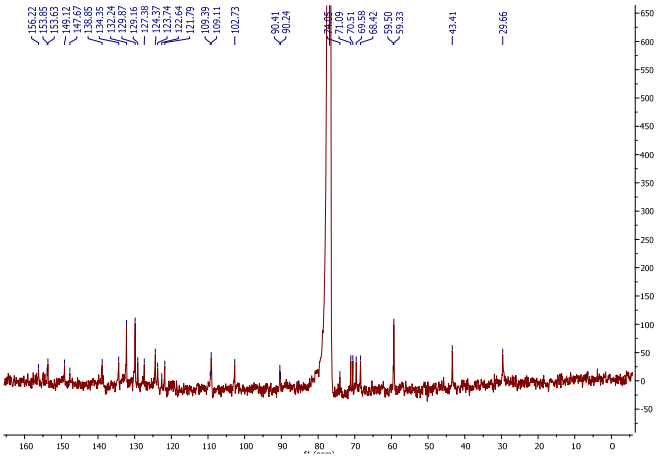


Fig. S15 Spectra of **13**.

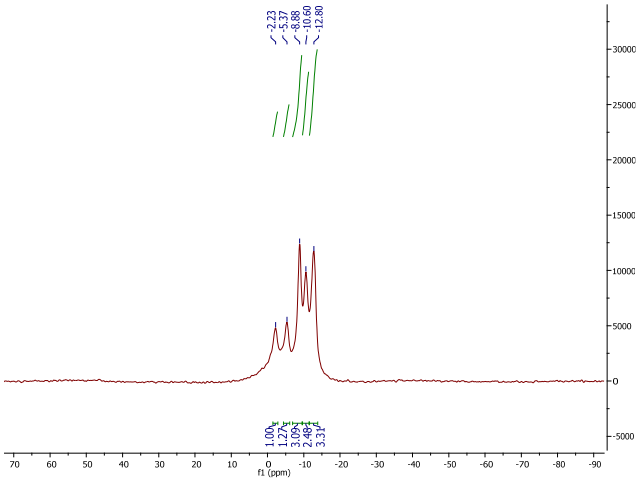
$^{1}H\{^{11}B\}$-NMR



$^{13}C\{^{1}H\}$-NMR



$^{11}B\{^{1}H\}$-NMR



m/z (EI)

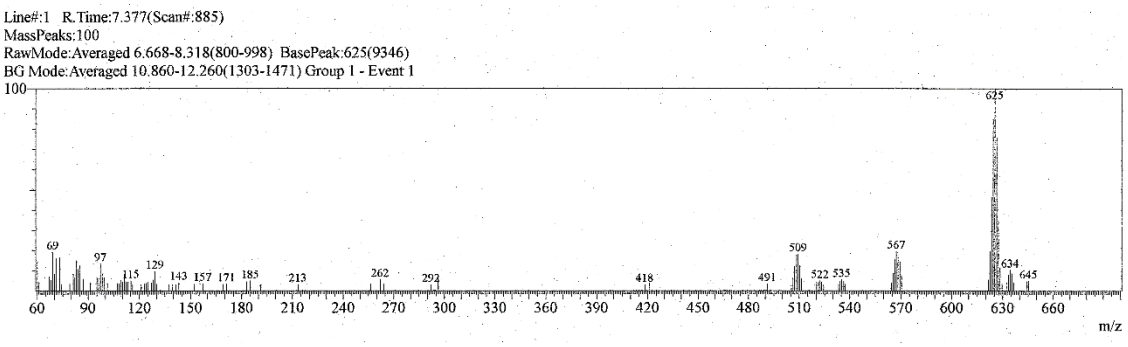
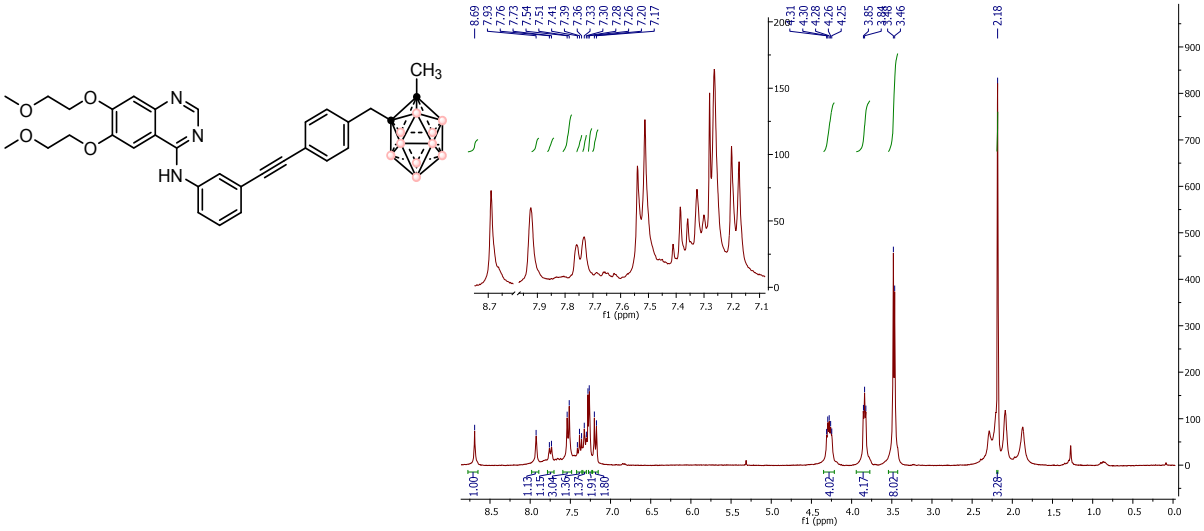
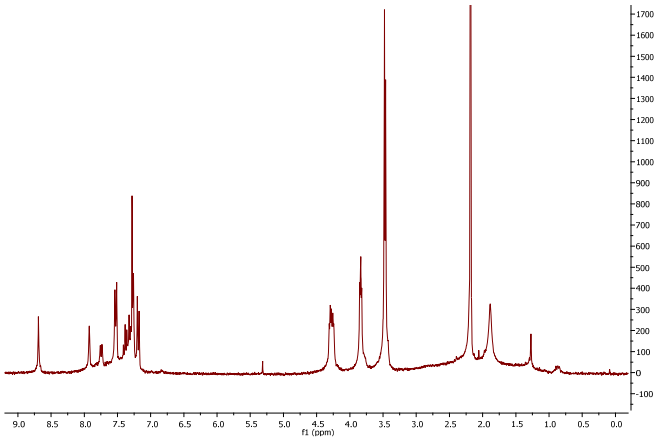


Fig. S16 Spectra of **15**.

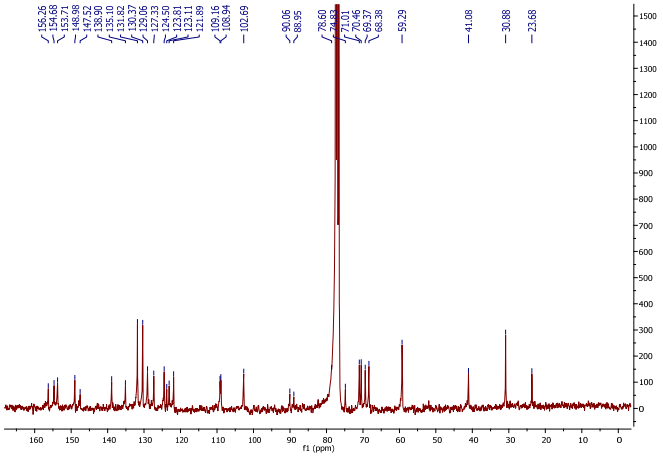
$^{1}H\{^{11}B\}$-NMR



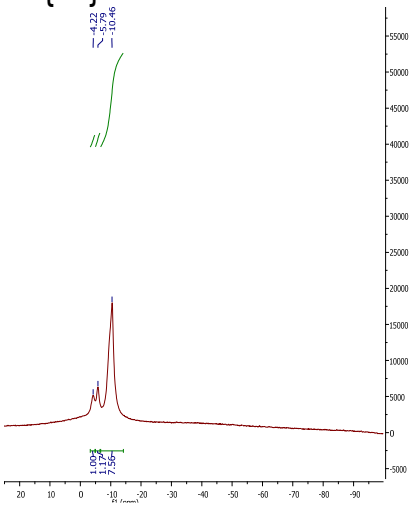
^{1}H-NMR



$^{13}C\{^{1}H\}$-NMR



$^{11}B\{^{1}H\}$-NMR



m/z (EI)

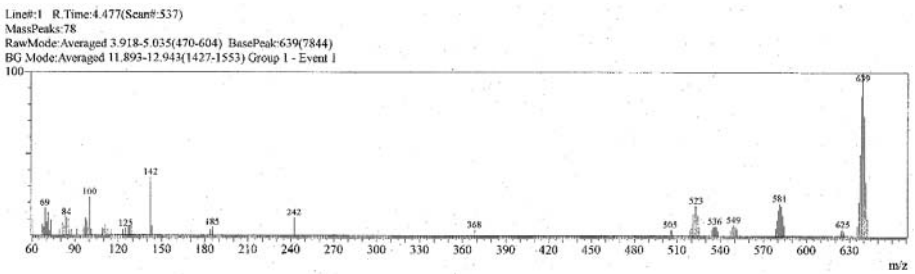
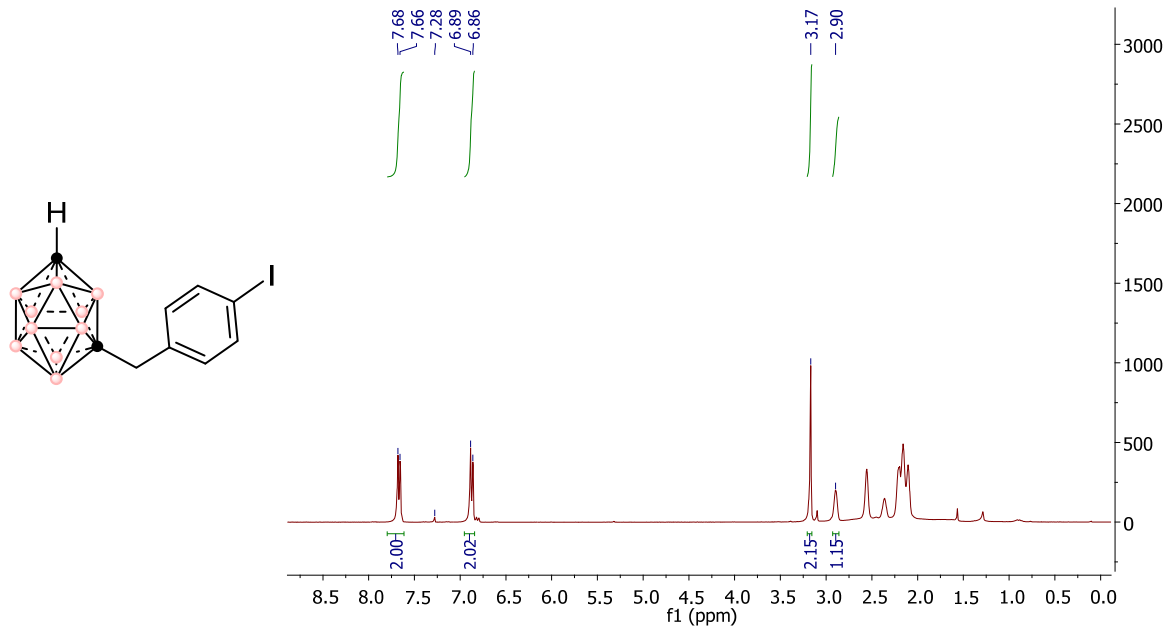
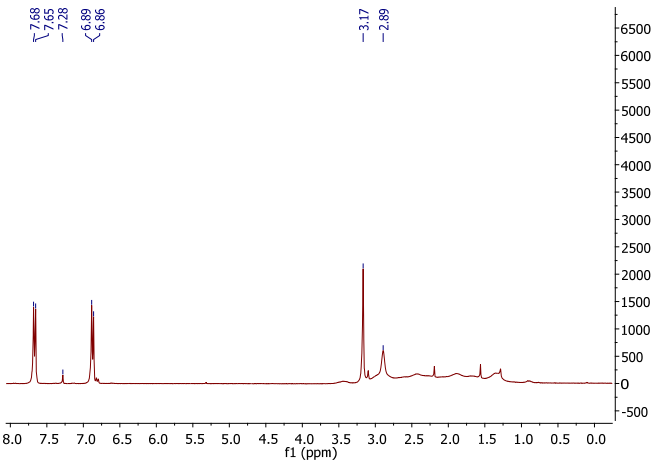


Fig. S17 Spectra of **16**.

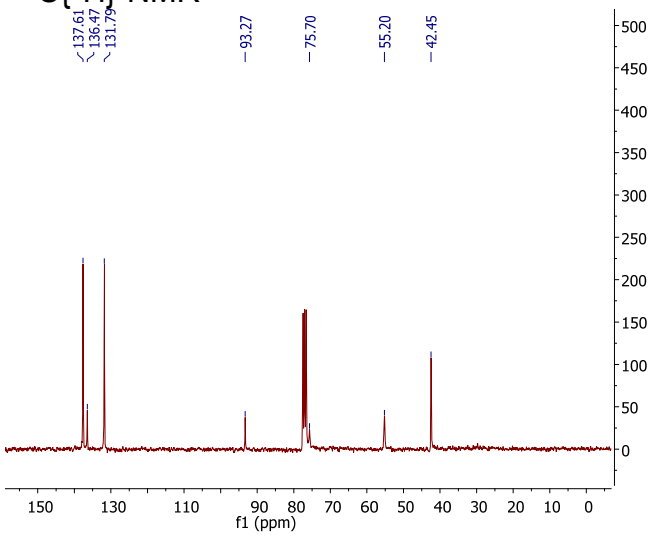
$^{1}H\{^{11}B\}$-NMR



^{1}H-NMR



$^{13}C\{^{1}H\}$-NMR



$^{11}B\{^{1}H\}$-NMR

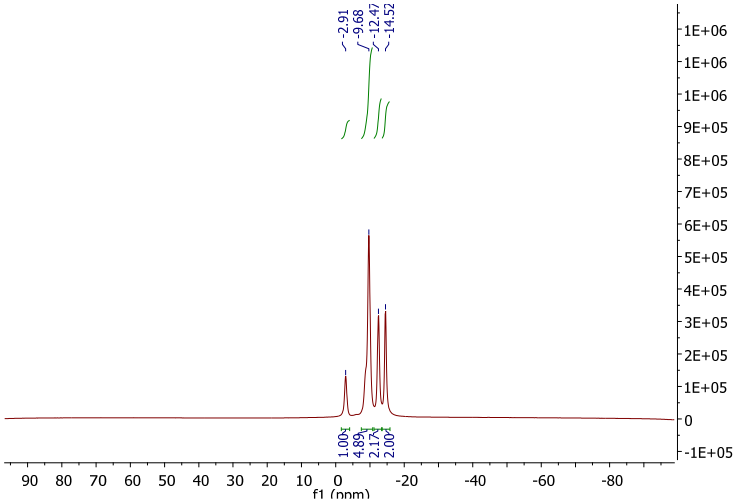
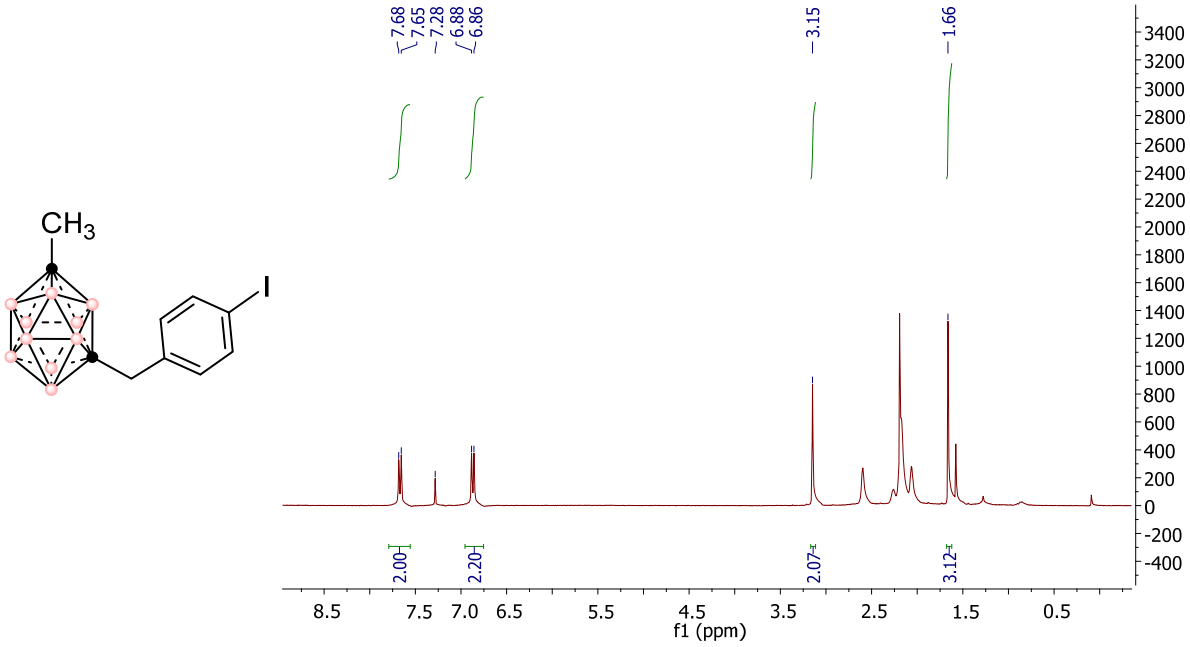
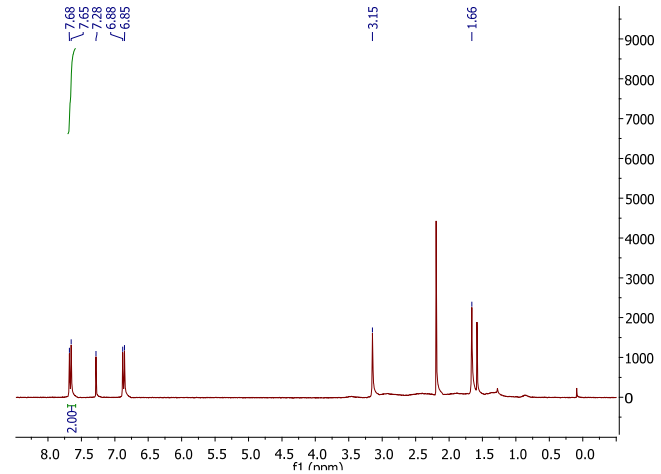


Fig. S18 Spectra of **17**.

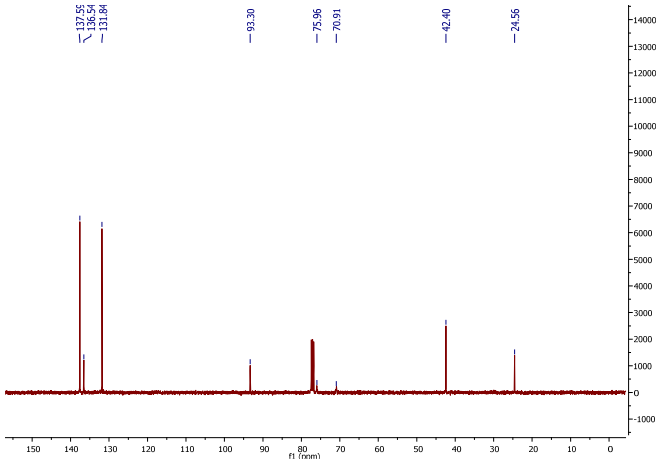
$^{1}H\{^{11}B\}$-NMR



^{1}H-NMR



$^{13}C\{^{1}H\}$-NMR



$^{11}B\{^{1}H\}$-NMR

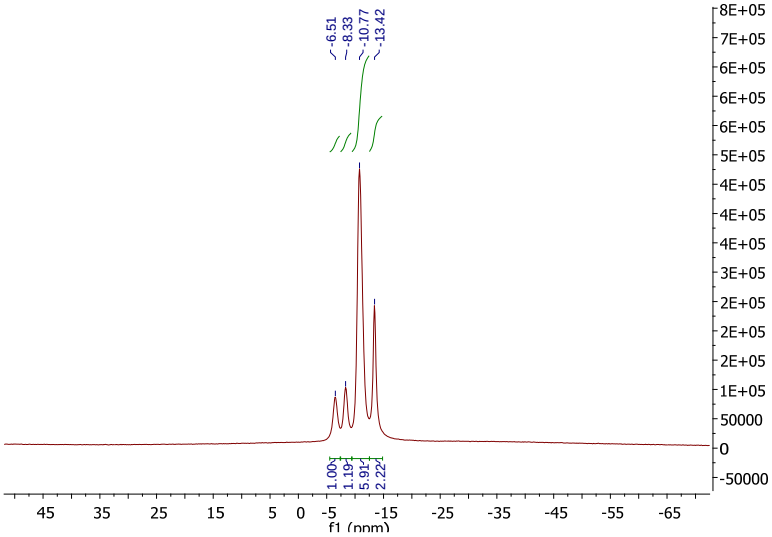
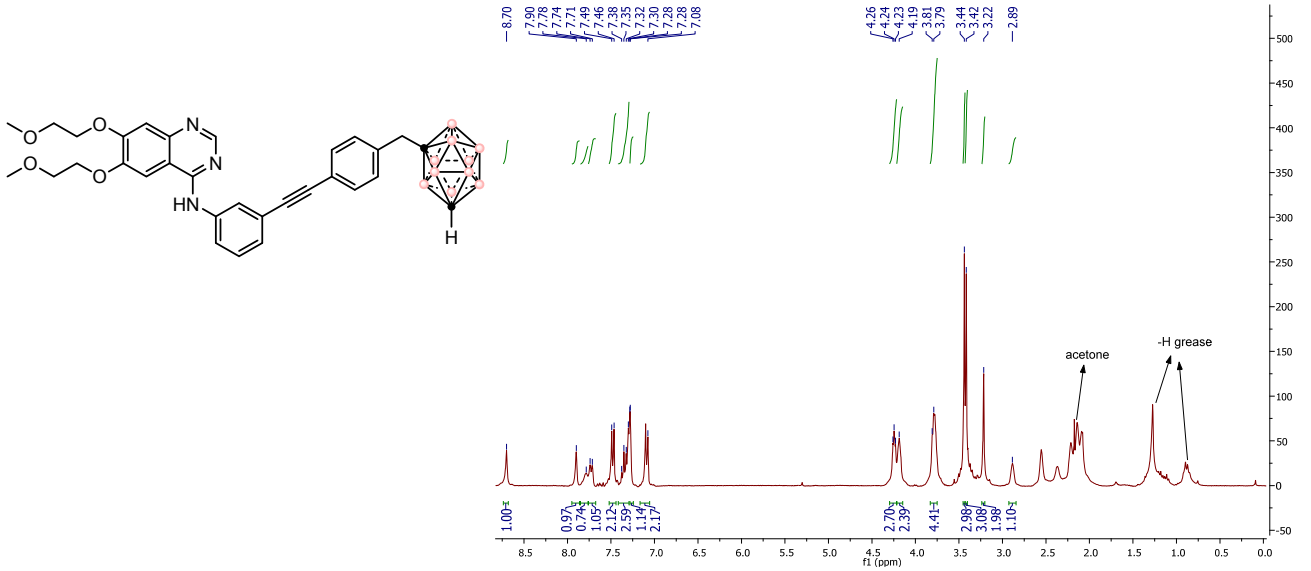
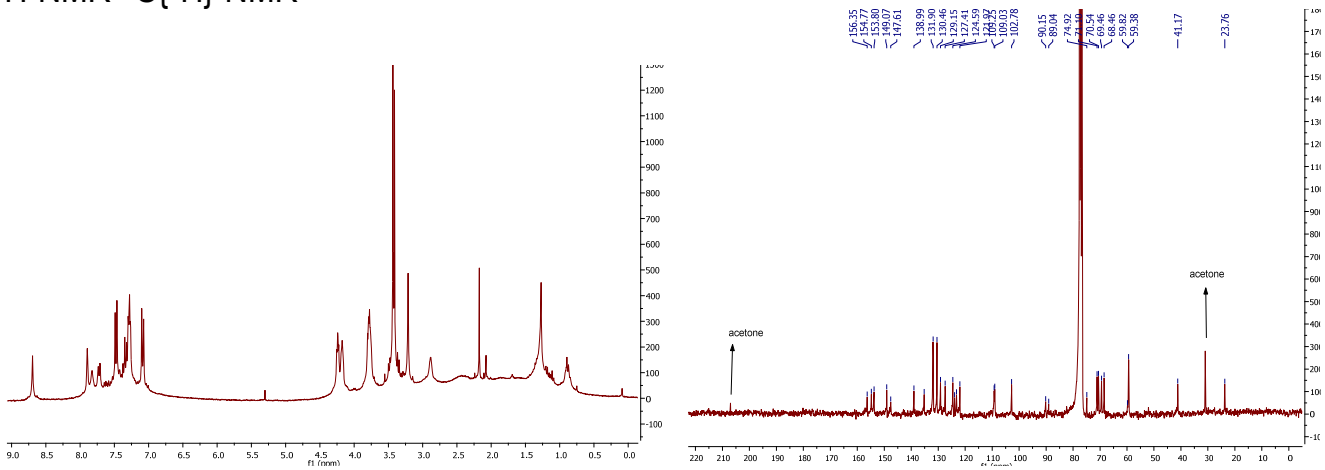


Fig. S19 Spectra of **18**.

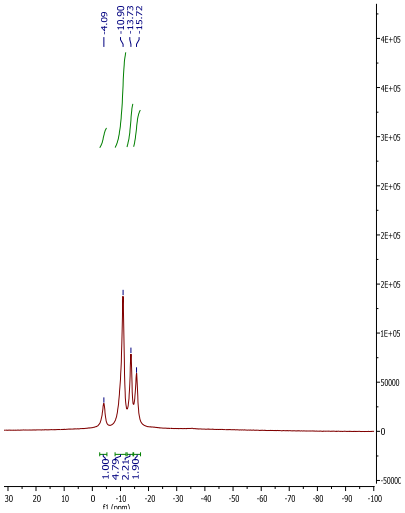
$^{1}H\{^{11}B\}$-NMR



^{1}H-NMR$^{13}C\{^{1}H\}$-NMR



$^{11}B\{^{1}H\}$-NMR



m/z (EI)

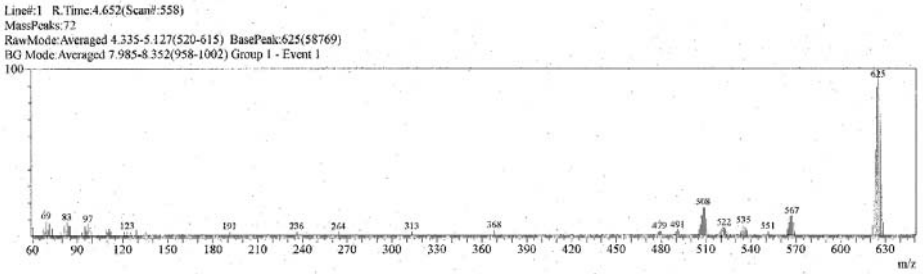
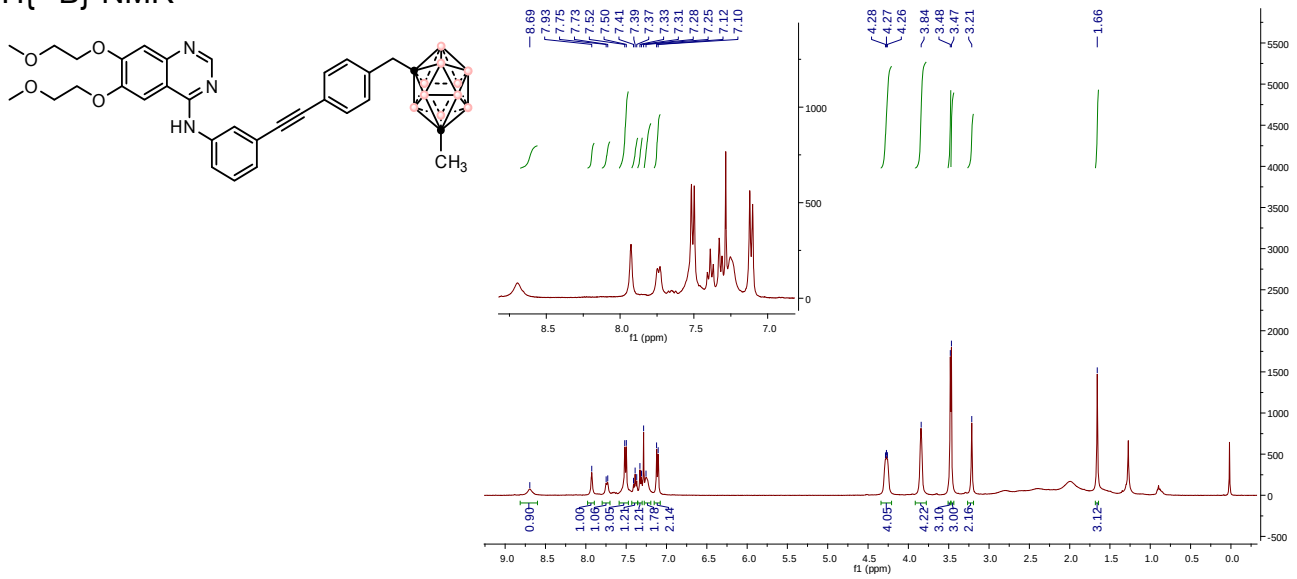
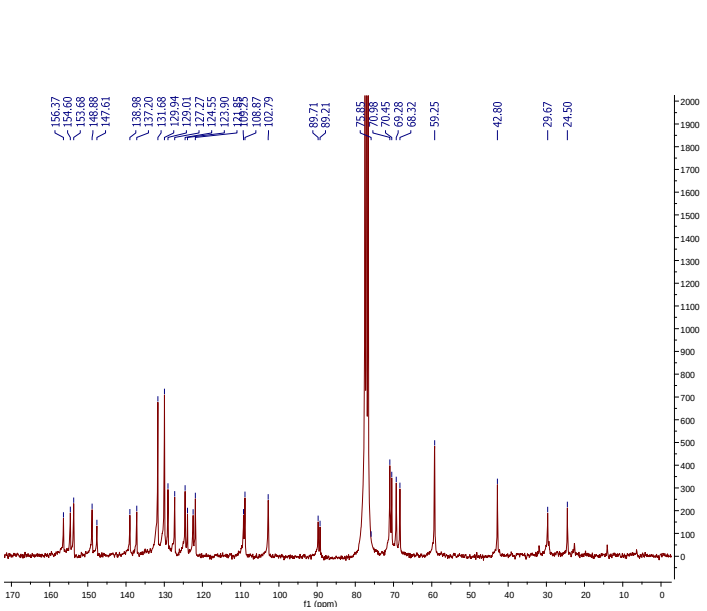


Fig. S20 Spectra of **19**.

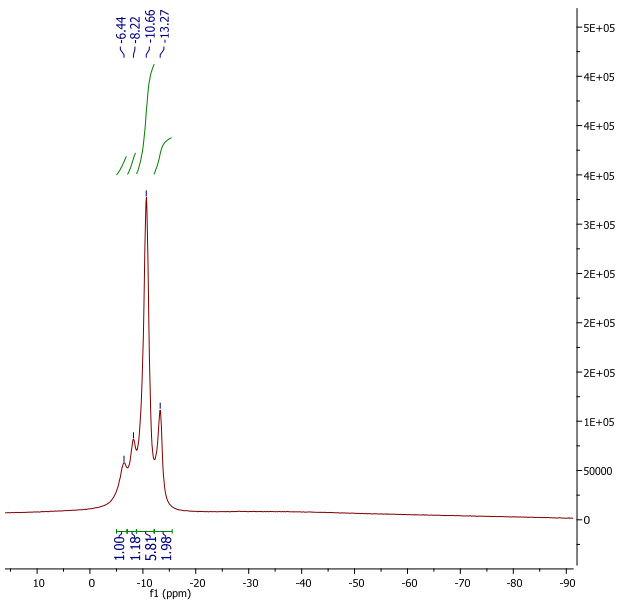
$^{1}H\{^{11}B\}$-NMR



$^{13}C\{^{1}H\}$-NMR



$^{11}B\{^{1}H\}$-NMR



m/z (EI)

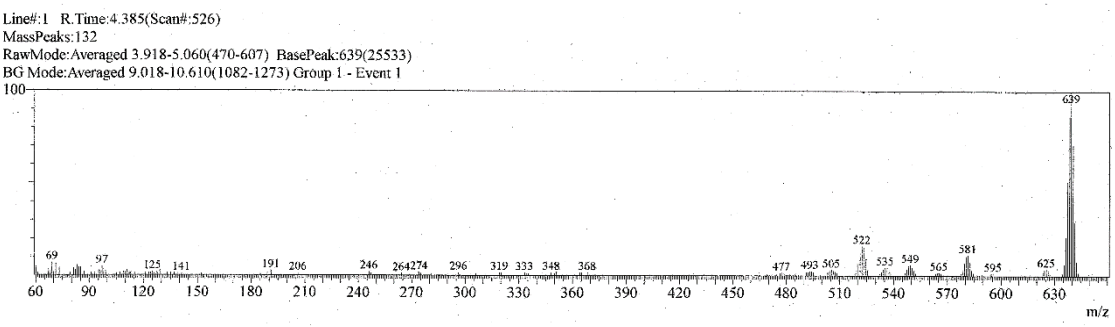
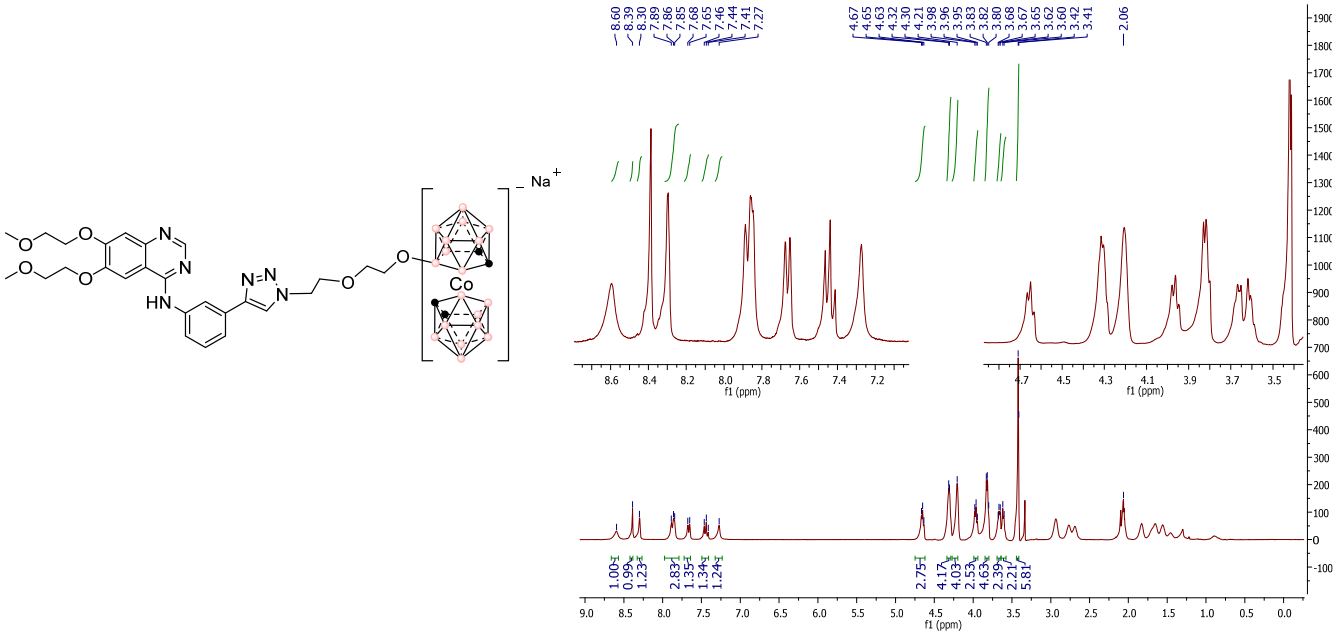
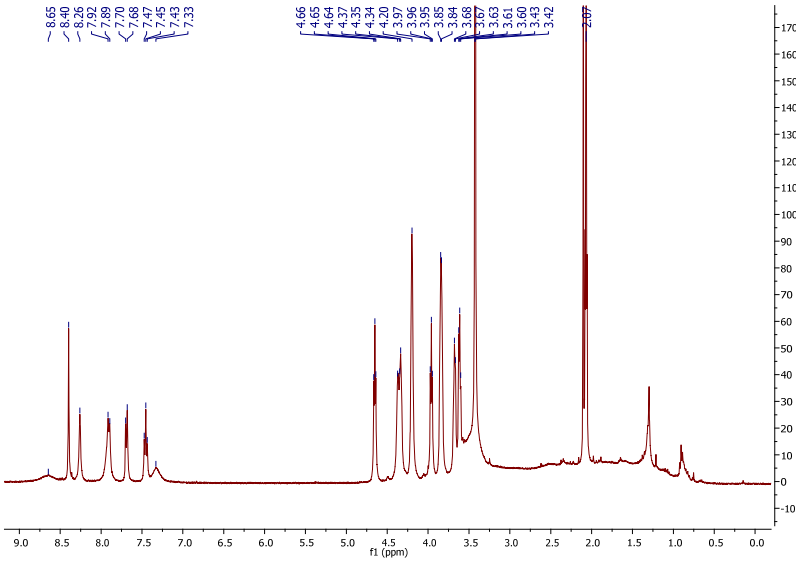


Fig. S21 Spectra of **20**.

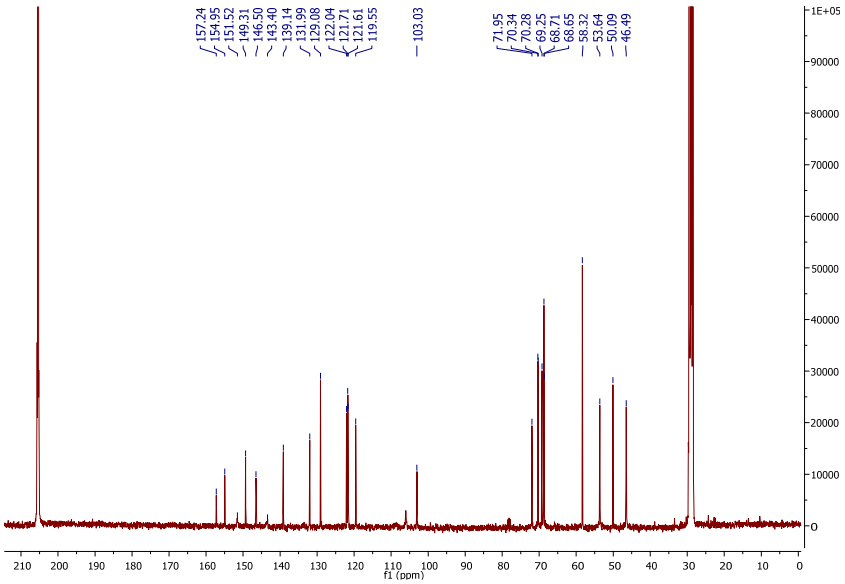
$^{1}H\{^{11}B\}$-NMR



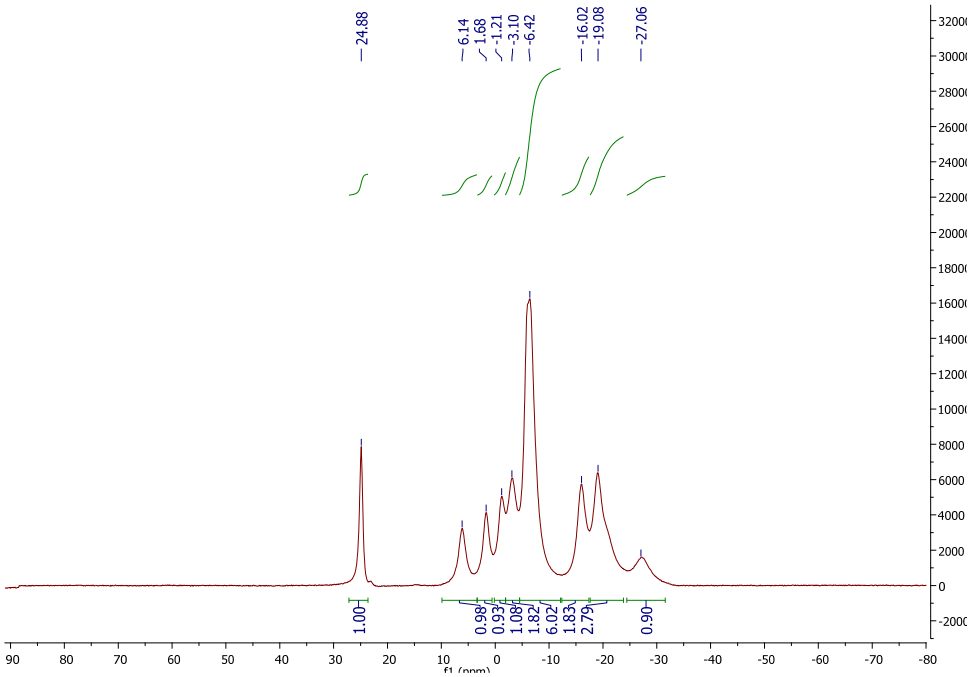
^{1}H-NMR



$^{13}C\{^{1}H\}$-NMR



$^{11}B\{^{1}H\}$-NMR



MALDI-TOF-MS

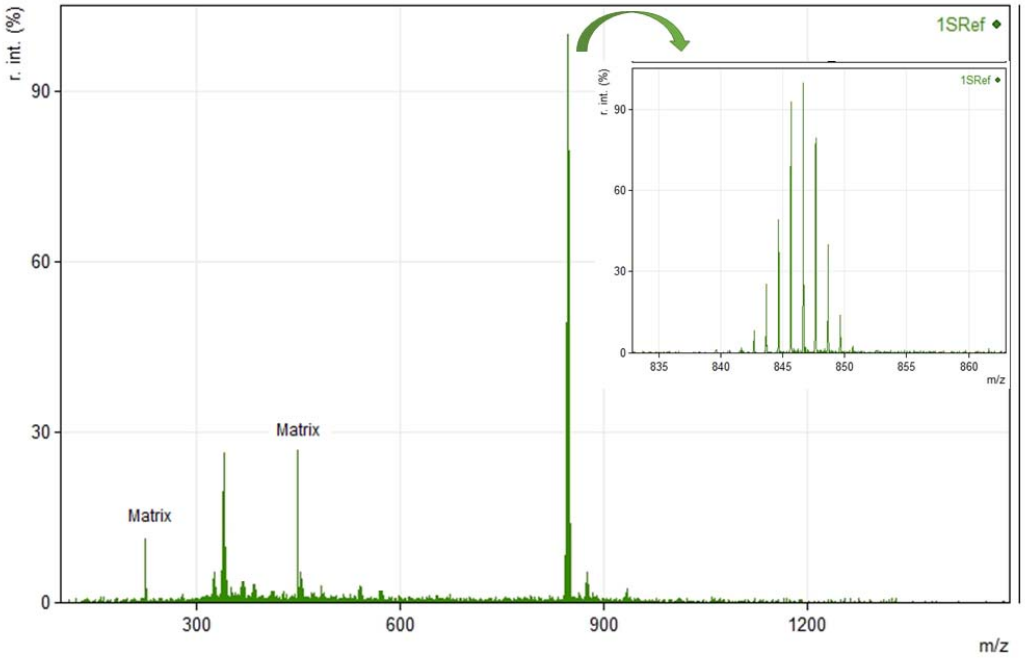
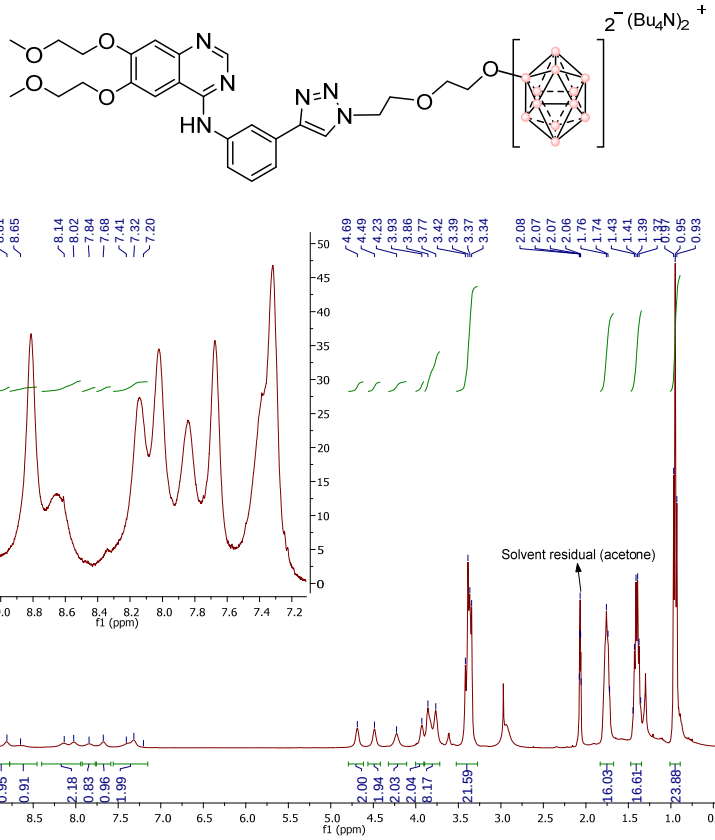
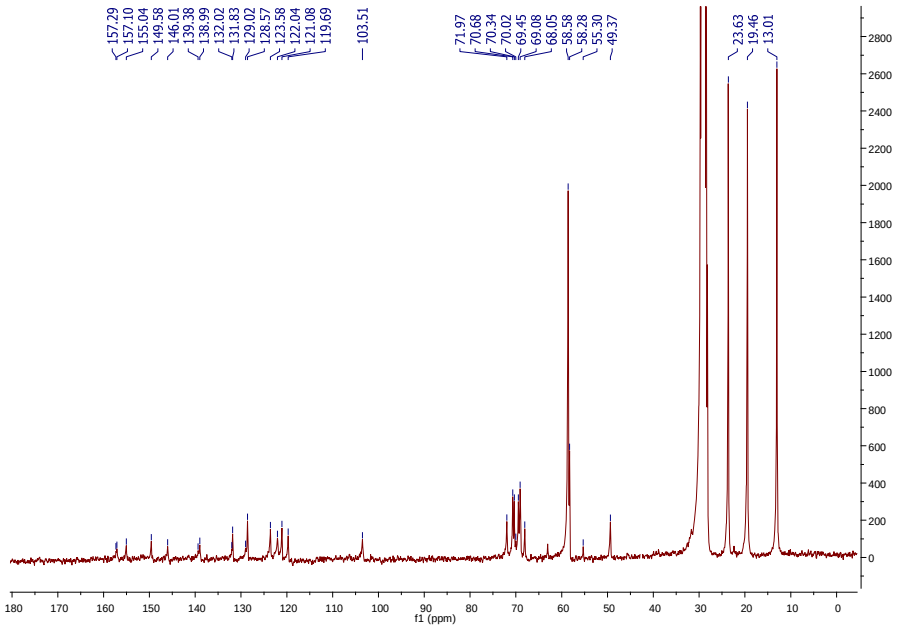


Fig. S22 Spectra of **23**.

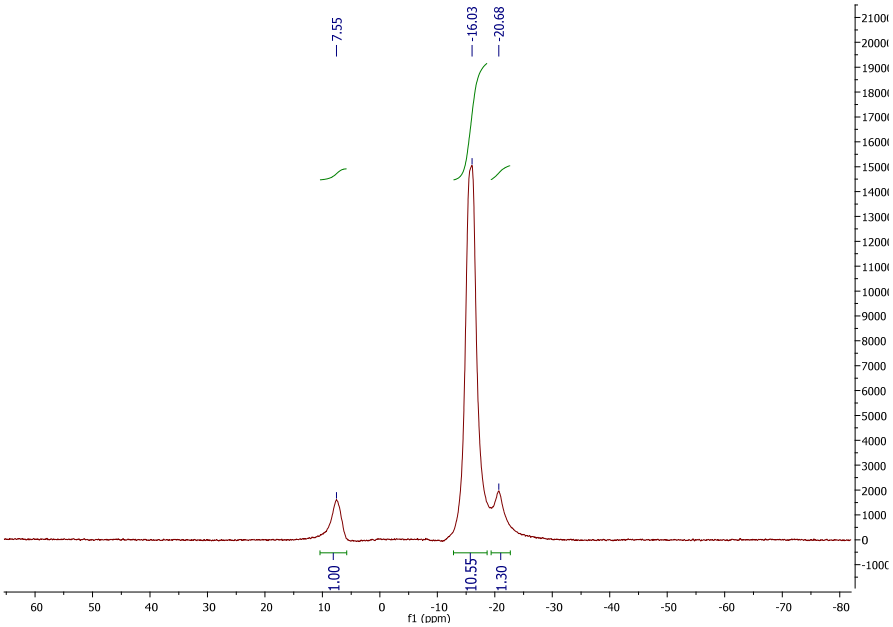
$^{1}H\{^{11}B\}$-NMR



$^{13}C\{^{1}H\}$-NMR



$^{11}B\{^{1}H\}$-NMR



MALDI-TOF-MS

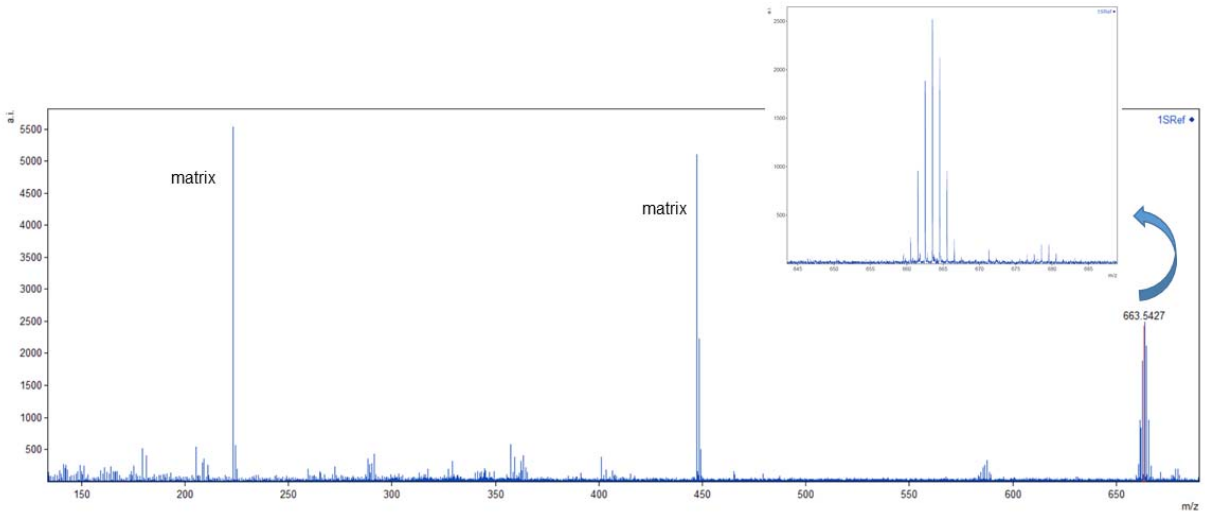
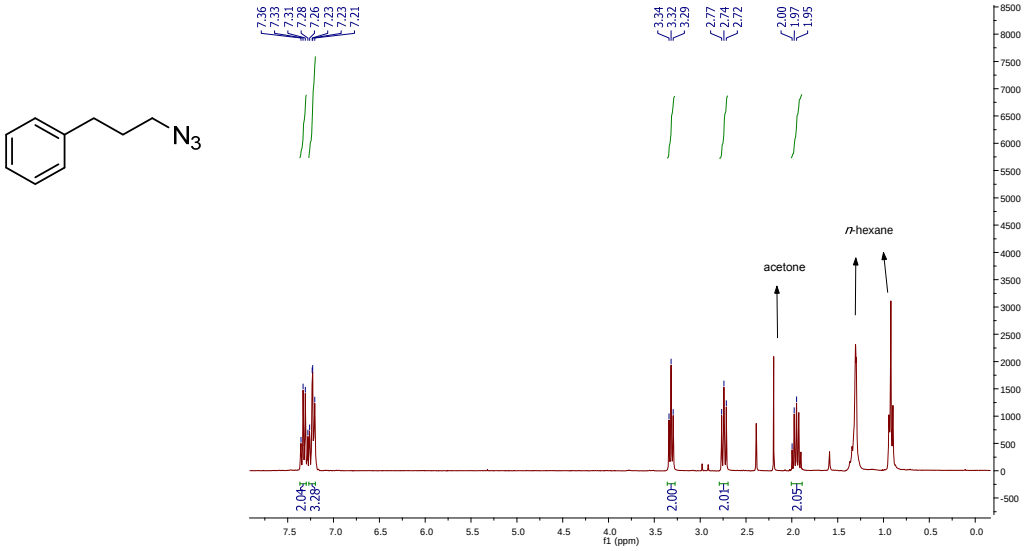


Fig. S23 Spectra of **26**.

^{1}H-NMR



^{13}C{^{1}H}-NMR

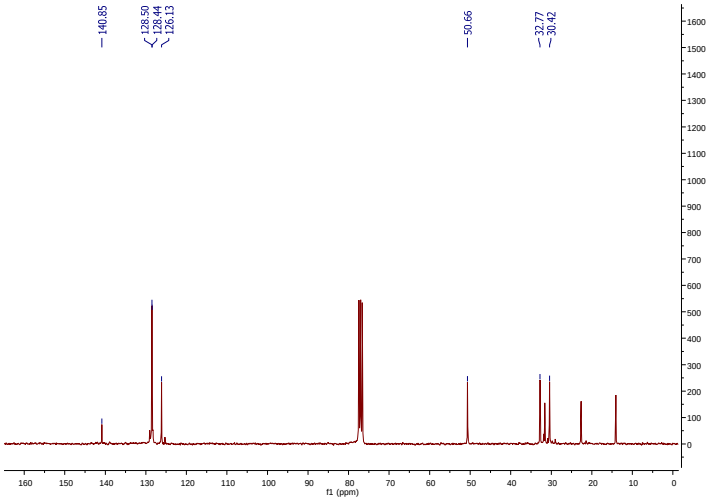
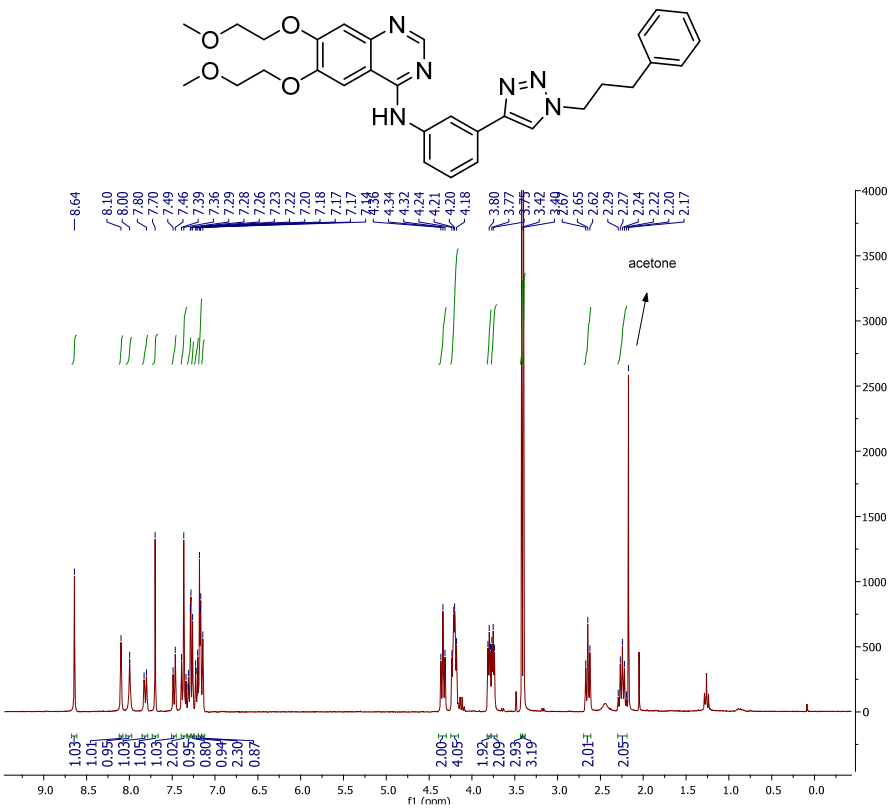


Fig. S24 Spectra of **27**.

^{1}H-NMR



^{13}C{^{1}H}-NMR

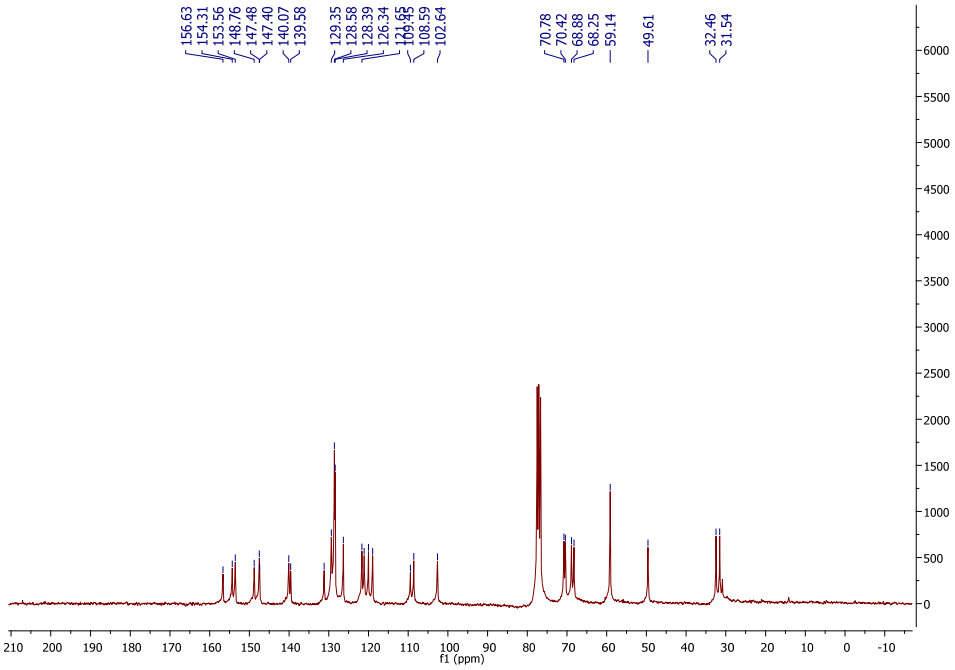


Fig. S25 Spectra of **28**.

References

[1] F. Teixidor, S. Gómez, M. Lamrani and C. Viñas, *Organometallics,* 1997, **16**, 1278-1283.

[2] M. G. H. Vicente, B. F. Edwards, S. J. Shetty, Y. Hou and J. E. Boggan, *Bioorg. Med. Chem.*, 2002, **10**, 481-492.

[3] (a) J. Plesek, S. Hermanek, A. Franken, I. Cisarova and Ch. Nachtigan, *Collect. Czech. Chem. Commun.,* 1997, **62**, 47-56; (b) F. Teixidor, J. Pedrajas, I. Rojo, C. Viñas, R. Kivekäs, R. Sillanpää, I. Sivaev, V. Bregadze and S. Sjöberg, Organometallics, 2003, **22**, 3414-3423.

[4] V. I. Bregadze, A. A. Semioshkin, J. N. Las'kova, M. Ya. Berzina, I. A. Lobanova, I. B. Sivaev, M. A. Grin, R. A. Titeev, D. I. Brittal, O. V. Ulybina, A. V. Chestnova, A. A. Ignatova, A. V. Feofanov and A. F. Mironov, *Appl. Organometal. Chem.,* 2009, **23**, 370-374.

[5] I. B. Sivaev, N. Yu. Kulikova, E. A. Nizhnik, M. V. Vichuzhanin, Z. A. Starikova, A. A. Semioshkin and V. I. Bregadze, *J. Organomet. Chem.,* 2008, **693**, 519-525.

[6] A. V. Orlova, N. N. Kondakov, B. G. Kimel, L. O. Kononov, E. G. Kononova, I. B. Sivaev and V. I. Bregadze, *Appl. Organometal. Chem.,* 2007, **21**, 98-100.

[7] Compound **3** was reported by using another synthetic reaction by M. Matuszewski, A. Kiliszek, W. Rypniewski, Z. J. Lesnikowski and A. B. Olejniczak, *New J. Chem.*, 2015, **39**, 1202-1221.

[8] Compound **4** was reported by using another synthetic reaction by R. Satapathy, B. P. Dash, B. P. Bode, E. A. Byczynski, S. N. Hosmane, S. Buxa and N. S. Hosmane, *Dalton Trans.*, 2012, **41**, 8982-8988.

[9] G. Colombano, C. Travelli, U. Galli, A. Caldarelli, M. G. Chini, P. L. Canonico, G. Sorba, G. Bifulco, G. C. Tron and A. A. Genazzani, *J. Med. Chem.*, 2010, **53**, 616-623.

[10] R. Saneto and J. De Vellis, Neuronal and Glial Cells: Cell Culture of the Central Nervous System, Neurochemistry: A Practical Approach, A. J. Turner and H. S. Brachelard (Eds), IRL, Oxford, 1987, pp 27–63.

Dual-Action Drugs: Hybridized Boron-Rich Clusters

Author: Joseph D. Unsay
Published Date: 10 agosto 2017
Source / Publisher: Chemistry – A European Journal/Wiley-VCH
Copyright: Wiley-VCH Verlag GmbH & Co. KGaA



Related Articles

News: B_{38} Cage: An All-Boron Fullerene Predicted
Magazine: Shedding Light on a Molecular Engine
News: BN Against Cancer
Magazine: Replacing a Ring with a Ball

Related Societies

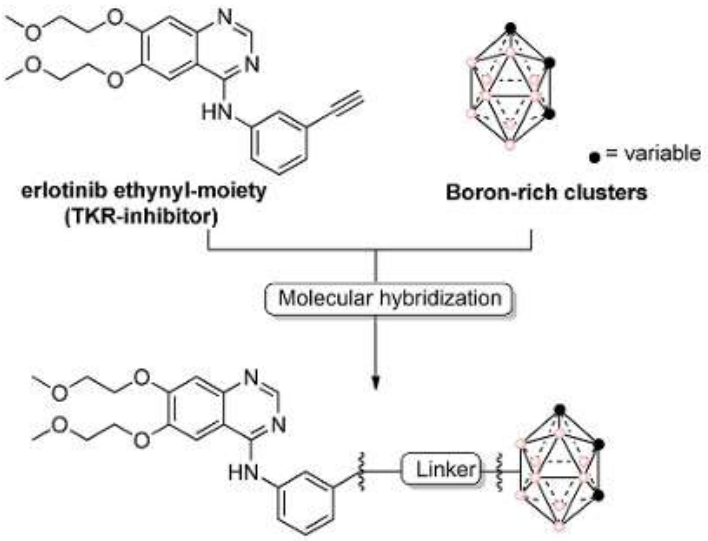
ChemPubSoc Europe

Boron neutron capture therapy (BNCT) is an emerging technique against cancer. It relies on the release of high-energy particles from non-radioactive compounds containing boron-10 upon irradiation with epithermal neutrons (i.e., those with an energy of 0.025–0.4 eV). Because the trajectory of these particles is in the magnitude of a cell's diameter, the BNCT damage is confined within the tumor, as long as the BNCT agents are specifically localized in tumor tissues.

Hugo Cerecetto, Universidad de la República, Montevideo, Uruguay, Clara Viñas, Institut de Ciències dels Materials de Barcelona, Bellaterra, Spain, and colleagues have hybridized boron-rich carboranyl clusters with erlotinib, a tyrosine kinase receptor (TKR) inhibitor to form a series of possible anticancer compounds, varying in the linkage position and linker molecules (example pictured below).

Our site uses cookies to improve your experience. You can find out more about our use of cookies in our "standard cookie policy", including instructions on how to reject and delete cookies if you wish to do so. By continuing to browse this site you agree to us using cookies as described in our "standard cookie policy".

CLOSE



The team then tested the hybrids against C6 glioma cells (brain tumor cells), and found that the hybrids exhibit anticancer activity that is dependent on their lipophilicity. Erlotinib alone did not show significant anticancer activity. It has an IC_{50} value (a measure of the compound's effectiveness) of over 100, compared with 30 μM and 34 μM, respectively, for the two most active hybridized compounds.

The researchers also tested the most active compounds against primary glial cells (healthy brain cells) and showed that the compounds are selective towards cancer cells. This makes them promising anticancer agents with dual action: as TKR inhibitors (based on the erlotinib unit) and as BNCT agents (based on the boron-rich clusters which can capture neutrons).

Small-Molecule Kinase-Inhibitors-Loaded Boron Cluster as Hybrid Agents for Glioma-Cell-Targeting Therapy,
Marcos Couto, Ignacio Mastandrea, Mauricio Cabrera, Pablo Cabral, Francesc Teixidor, Hugo Cerecetto, Clara Viñas,
Chem. Eur. J. **2017**, *23*, 9233–9238.
DOI: 10.1002/chem.201701965

Article Views: 1642

Sign in Area

Please note that to comment on an article you must be registered and logged in.
Registration is for free, you may already be registered to receive, e.g., the newsletter. When you register on this website, please ensure you view our terms and conditions. All comments are subject to moderation.

Article Comments - To add a comment please sign in

If you would like to **reuse any content**, in print or online, from *ChemistryViews.org*, please contact us first for permission. more

CONNECT:

Our site uses cookies to improve your experience. You can find out more about our use of cookies in our "standard cookie policy", including instructions on how to reject and delete cookies if you wish to do so. By continuing to browse this site you agree to us using cookies as described in our "standard cookie policy".

About us ChemPubSoc Europe Editorial Office Contact Us
Advertise Jobs Virtual Events Most Read/Editor's Pick

CLOSE

Awards **Funding** **Just Published & Most Read Research**

Copyright **Masthead/Impressum** **Privacy/Datenschutz** **Terms**

A product of and Wiley-VCH

Our site uses cookies to improve your experience. You can find out more about our use of cookies in our "standard cookie policy", including instructions on how to reject and delete cookies if you wish to do so. By continuing to browse this site you agree to us using cookies as described in our "standard cookie policy".

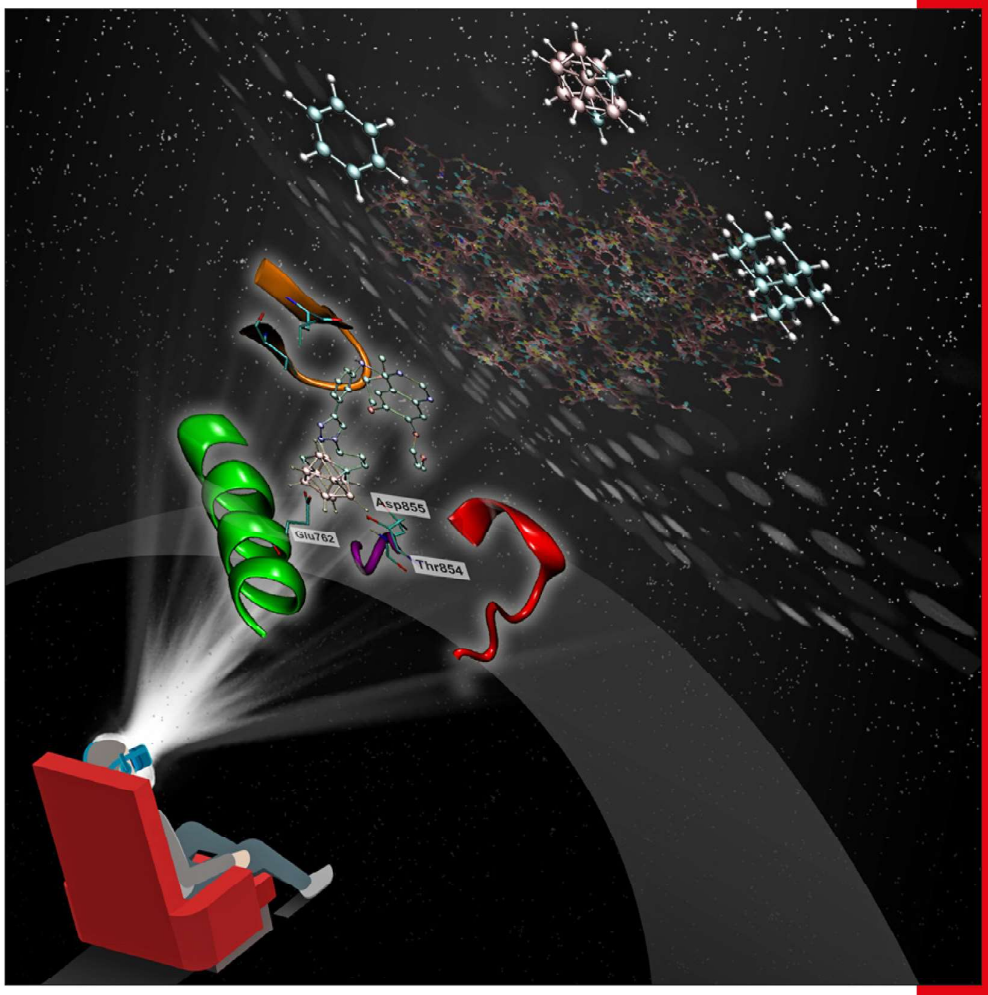
CLOSE

CHEMISTRY
A European Journal

A Journal of ChemPubSoc Europe

www.chemeurj.org

2018-24/00



Cover Feature:
H. Cerecetto, C. Viñas et al.
Discovery of Potent EGFR Inhibitors through the Incorporation of a 3D Aromatic Boron-Rich Cluster into the 4-Anilinoquinazoline Scaffold: Potential Drugs for Glioma Treatment

Supported by ACES Asian Chemical Editorial Society

WILEY-VCH

COVER PICTURE

M. Couto, M. F. García, C. Alamón, M. Cabrera, P. Cabral, A. Merlino, F. Teixidor, H. Cerecetto, C. Viñas**

■■ – ■■

Discovery of Potent EGFR Inhibitors through the Incorporation of a 3D-Aromatic-Boron-Rich-Cluster into the 4-Anilinoquinazoline Scaffold: Potential Drugs for Glioma Treatment



An EGFR inhibitor that incorporates *closo*-carborane has been shown to have higher affinity than erlotinib. The comparative docking analysis with compounds bearing bioisoster substructures demonstrated the relevance of the 3D aromatic boron-rich moiety for interacting into the EGFR ATP binding region. The capability to accumulate in glioma cells, the ability to cross the blood–brain barrier and the stability under simulated biological conditions render these molecules as lead compounds for further structural modifications to obtain dual action drugs to treat glioblastoma. More information can be found in the Communication by H. Cerecetto, C. Viñas et al. (DOI: 10.1002/chem.201705181).

View publication stats

ChemPubSoc Europe

DOI: 10.1002/chem.201705181

CHEMISTRY A European Journal Communication

Biological Chemistry | *Hot Paper*

Discovery of Potent EGFR Inhibitors through the Incorporation of a 3D-Aromatic-Boron-Rich-Cluster into the 4-Anilinoquinazoline Scaffold: Potential Drugs for Glioma Treatment

Marcos Couto,[a, b, c] María Fernanda García,[c] Catalina Alamón,[a] Mauricio Cabrera,[d] Pablo Cabral,[c] Alicia Merlino,[e] Francesc Teixidor,[b] Hugo Cerecetto,*[a, c] and Clara Viñas*[b]

Abstract: New 1,7-*closo*-carboranylanilinoquinazoline hybrids have been identified as EGFR inhibitors, one of them with higher affinity than the parent compound erlotinib. The comparative docking analysis with compounds bearing bioisoster-substructures, demonstrated the relevance of the 3D aromatic-boron-rich moiety for interacting into the EGFR ATP binding region. The capability to accumulate in glioma cells, the ability to cross the blood–brain barrier and the stability on simulated biological conditions, render these molecules as lead compounds for further structural modifications to obtain dual action drugs to treat glioblastoma.

The epidermal growth factor receptor (EGFR, ErbB1), a member of the ErbB protein family of tyrosine kinases receptors, is a transmembrane glycoprotein that consists of an extracellular binding domain, a single hydrophobic transmembrane segment, and an intracellular protein tyrosine kinase domain.[1] Upon ligand binding to EGFR, epidermal growth factor (EGF) causes downstream signals to stimulate cell growth, proliferation, and differentiation. Therefore, the signalling pathways governed by the EGF–EGFR plays key roles in essential cellular functions including regulation of cell proliferation, survival, differentiation and migration.[2,3] Besides, overexpression of EGFR has been frequently detected in a wide range of solid tumour types: lung, pancreatic, head and neck, colorectal, breast, renal, glioma, prostate, ovarian and bladder.[4] According to this, several cancers therapeutic strategies have been based on EGFR inhibition to interfere with EGFR mediated cellular effects.[5] The most extensively used agents in clinical research are both monoclonal antibodies directed against the extracellular receptor domain, such as cetuximab,[6] and small molecules that bind reversible or irreversible into the catalytic pocket of EGFR, commonly known as tyrosine kinase inhibitors (TKIs).[5,7] Among those, molecules bearing the 4-anilinoquinazoline core scaffold, such as gefitinib[8,9] and erlotinib (Figure 1),[10,11] were found to be highly selective EGFR inhibitors and effective anticancer drugs. A broad spectrum of modifications of the 4-anilinoquinazoline pharmacophore have been studied on the last decade in order to find more potent and selective TKIs.[12,13] Nonetheless, the icosahedral boron cluster has been an underexplored moiety in the development of EGFR kinase inhibitors. These boron-rich motifs including polyhedral boranes, carboranes and metallacarboranes, have emerged as interesting alternatives and promising scaffolds to be used in pharmaceutical drug design.[14] It might be expected, then, that the use of neutral dicarba-*closo*-dodecarborane moieties (1,2-*closo*-$C_2B_{10}H_{11}$, 1,7-*closo*-$C_2B_{10}H_{11}$, 1,12-*closo*-$C_2B_{10}H_{11}$) may offer extraordinary advantages in medicinal chemistry, such as kinetic inertness to reagents, resistance to catabolism, strong hydrophobicity, fascinating globular architecture and well-established chemistry that afford the opportunity to exploit them as novel pharmacophores.[15] Specifically, carborane has roughly the same molecular volume as adamantane (148 vs. 136 Å^3) but is more hydrophobic.[14] As a consequence of their electronic structure, carboranes are aromatic[14] and are therefore used as bioisosteres for phenyl groups. However, the medicinal chemistry of carboranes has traditionally focused on their use in boron neutron capture therapy (BNCT).[16] BNCT is a cancer treatment that involves the irradiation of non-radioactive ^{10}B-enriched tumour with low energy thermal neutrons, to yield high linear energy particles ($^4He^{2+}$ and $^7Li^{3+}$). Because these particles have a linear path trajectory similar to the diameter of a cell, the BNCT damage is selectively confined within the tumour when the drug is delivered into the

[a] *M. Couto, C. Alamón, Prof. H. Cerecetto*
Grupo de Química Medicinal, Laboratorio de Química Orgánica
Facultad de Ciencias, Universidad de la República
Iguá 4225, 11400 Montevideo (Uruguay)
E-mail: hcerecetto@cin.edu.uy

[b] *M. Couto, Prof. F. Teixidor, Prof. C. Viñas*
Institut de Ciències dels Materials de Barcelona-CSIC
Campus UAB, 08193 Bellaterra (Spain)
E-mail: clara@icmab.es

[c] *M. Couto, M. F. García, Prof. P. Cabral, Prof. H. Cerecetto*
Área de Radiofarmacia, Centro de Investigaciones Nucleares
Facultad de Ciencias, Universidad de la República
Mataojo 2055, 11400 Montevideo (Uruguay)

[d] *Prof. M. Cabrera*
Laboratorio de I + D de Moléculas Bioactivas
Centro Universitario Paysandú
CenUR Litoral Norte, Universidad de la República
60000 Paysandú (Uruguay)

[e] *Prof. A. Merlino*
Laboratorio de Química TeóricayComputacional
Facultad de Ciencias, Universidad de la República
Iguá 4225, 11400 Montevideo (Uruguay)

Supporting information and the ORCID identification number(s) for the author(s) of this article can be found under https://doi.org/10.1002/chem.201705181.

© 2017 Wiley-VCH Verlag GmbH & Co. KGaA, Weinheim

These are not the final page numbers! ↗↗

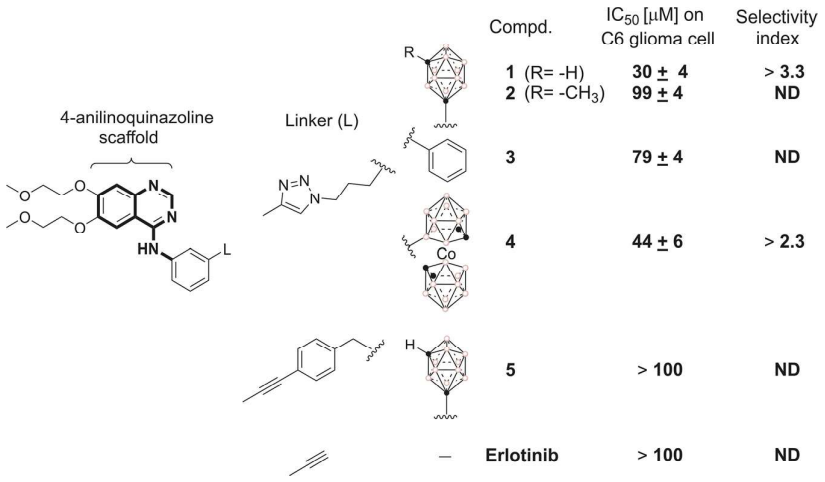
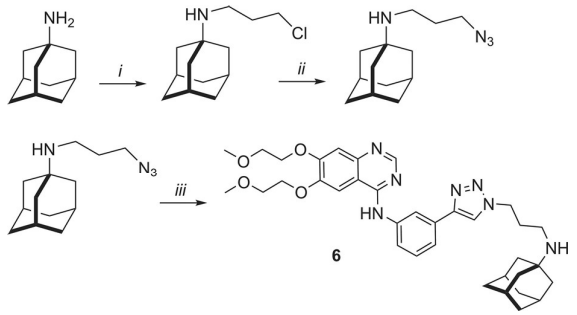


Figure 1. Previous in vitro result on EGFR-overexpressing C6 glioma cells and selectivity indexes, defined as $IC_{50,mix\ of\ primary\ glial\ cells}/IC_{50,C6\ cells}$, of our developed hybrids.[18].

target cells.[17] Regarding this, we recently described the synthesis of hybrid agents derived from erlotinib and containing icosahedral boron clusters. Some of these hybrids displayed the ability to be active against EGFR-overexpressing C6 glioma cells (Figure 1).[18] Following this concept and as a continuation of our previous work, we have undergone efforts to identify the mechanism of action of these novel hybrid compounds. To this end, we investigated their kinase inhibitory activities on wild type EGFR and its erlotinib-resistant variant, T790M.[5,19] Additionally, through molecular docking we gained further insight into the interaction of the most relevant derivatives with EGFR. Thinking of these compounds as agents for glioma treatment, we performed the following studies attempting to surpass the "hit-to-lead" stage in the drug development pipeline: i) ^{10}B accumulation in cells treated with the studied compounds; ii) studied compounds ability to cross blood–brain barrier (BBB); iii) solution and metabolic stabilities.

With these goals in mind, we focused on the synthesis of an erlotinib derivative containing an adamantyl moiety as 3D non-aromatic isostere of the icosahedral boron cluster (Scheme 1). This derivate allowed the comparison between the



Scheme 1. Synthesis of hybrid **6**. Reaction conditions: i) 1-bromo-3-chloropropane, Cs_2CO_3, $CHCl_3$, reflux, 72 h, 33%; ii) NaN_3, DMF, room temperature, 24 h, 100% conversion; iii) erlotinib, $CuSO_4{\cdot}5H_2O$, sodium ascorbate, THF/H_2O (1:1), RT, 5 h, 61%.

previously synthesized analogues with 3D-aromatic substituents (**1**, **2** and **5**) and the 2D-aromatic derivative (**3**). As shown in Scheme 1, in the first synthetic step the 1-adamantylamine was functionalized by nucleophilic substitution with 1-bromo-3-chloropropane to give the N-alkylated product in moderate yield (33% after column chromatography purification). Subsequently, the azidopropyl intermediate was prepared by the reaction of the chloropropyl derivative with sodium azide at room temperature to give an almost quantitative yield of the desired compound. Finally, erlotinib was functionalized with azidopropyladamantylamine by using Cu^I-catalyzed azide–alkyne cycloaddition giving hybrid **6** as a yellow solid in good yield (61% after purification). The structures were confirmed by multinuclear (^1H and $^{13}C\{^1H\}$) NMR spectroscopy and elemental analysis (see Supporting Information).

The activity against EGFR was measured through cell-free biochemical kinase inhibition using ADP-Glo™ Kinase Assay and EGFR Kinase Enzyme System[20] (see Supporting Information, Figures S1 and S2). The introduction of *closo*-caboranyl (derivatives **1**, **2** and **5**) and cobaltabisdicarbollide (derivative **4**) frameworks into the 4-anilinoquinazoline scaffold led to IC_{50} values in the nanomolar range against wild type EGFR ($EGFR_{WT}$) as shown in Table 1. For the carboranylanilinoquinazoline hybrids the inhibition of $EGFR_{WT}$ showed the same trend as the previously observed cytotoxicity on EGFR-overexpressing C6 glioma cells (Figure 1).[18] Again, derivative **1** was the most powerful inhibitor with an IC_{50} value of 2.3 nM against $EGFR_{WT}$, 10-fold higher than the parent compound erlotinib. Among the *closo*-carboranyl derivatives (**1**, **2**, and **5**), the presence of a rigidized ethynylbenzyl-connector in derivative **5** resulted in 224 times lower activity than derivative **1**, with a [1,2,3]triazolyl-connector. Likewise, the incorporation of a methyl group in the cluster, in derivative **2**, led to an inhibitory activity 136 times lower than derivative **1**. By combining in derivative **1**, into the 4-anilinoquinazoline scaffold, the properties of a 2D-aromatic core moiety (like in **3**) with a hydrophobic 3D-non-aromatic group (like in **6**) we obtained a very potent EGFR inhib-

© 2017 Wiley-VCH Verlag GmbH & Co. KGaA, Weinheim

Table 1. Performance of hybrid entities and erlotinib on tyrosine kinase activity of $EGFR_{WT}$.

Compds.[a]	IC_{50} (nM) $EGFR_{WT}$[b]	Confidence Interval (95%)
1	2.3	(0.9 to 6.2)
4	296.3	(155.7 to 564.2)
2	312.2	(200.3 to 487.6)
5	517.2	(320.0 to 836.0)
3	2340.0	(1215.0xtox4506.0)
6	974.4	(600.7 to 1581.0)
Erlotinib	22.9	(14.1 to 37.2)

[a] Carboranes are ordered according to their in vitro C6-activities (Figure 1). [b] The agent concentrations are those required to inhibit the phosphorylation of the poly(Glu:Tyr) substrate by 50% (IC_{50}). They were determined from dose-response curves, and represent the mean ± s.d. All experiments were repeated at least three times.

itor (compare activity of derivative **1** to those of derivative **3** or **6**).

EGFR resistance to TKIs has been described for a great number of cancers.[21] One of the resistant variants has been the result of replacing the gatekeeper residue threonine 790 with methionine (T790M mutation) in the catalytic domain of the EGFR. This mutation is detected in approximately 50% of the non-small cell lung cancer patients with acquired resistance after treatment with erlotinib.[5,21b] In the search for new agents able to circumvent this problem we also studied the ability of the most active derivative, **1**, to inhibit EGFR harbouring the T790M mutation. As expected, erlotinib was ineffective against the isolated T790M mutant form but, on the contrary, derivative **1** displayed a good activity with an IC_{50} value of 1125 nM on EGFR T790M showing the therapeutic potential of this new compound in other kind of neoplasias (see Supporting Information, Figure S2).

These experimental results could be explained through the incorporation of the carboranyl moiety into the 4-anilinoquinazoline scaffold. The carborane motif may interact through non-classical dihydrogen bonds such as, B–H···H–X (X = N, C, O and S), also called proton-hydride bonds due to the electropositivity of boron atoms in the carborane cage. Besides, B-bridging interactions, and B–H···π and C–H···π hydrogen bonds could be established.[22–24] To better understand the EGFR-inhibitory profile shown by hybrids **1**, **2**, **3**, and **6** we explored in silico the binding mode of these compounds by means of molecular docking, employing AutoDock4.2 and Gaussian 09 suite of programs (see Supporting Information for experimental details), and using as initial template the structure of wild type EGFR in complex with erlotinib (PDB ID: 1M17,[25] Figure S3 in Supporting Information). The most active derivative, compound **1**, fits perfectly into the catalytic cleft (Figure 2A and Figure S4 in Supporting Information). The 3-[1,2,3]triazolyl-4-phenyl moiety establishes hydrophobic interactions with Leu718 and Val726 of the ATP binding loop while the carborane cluster forms hydrogen bonds with Glu762 of the α-helix C and Asp855 of the DFG-motif. Also, dihydrogen bond interactions are established with Thr854 and Asp855 (Table S2 in Supporting Information). Compound **2**, exhibiting a 135-fold higher IC_{50} value than **1**, adopts a different binding mode with the 4-anilinoquinazoline scaffold located outside the catalytic cleft (see superimposition of **1–3**, **6** and erlotinib in Figure S4, Supporting Information). However, the moderate activity of this compound may be due to hydrogen and dihydrogen bond interactions established be-

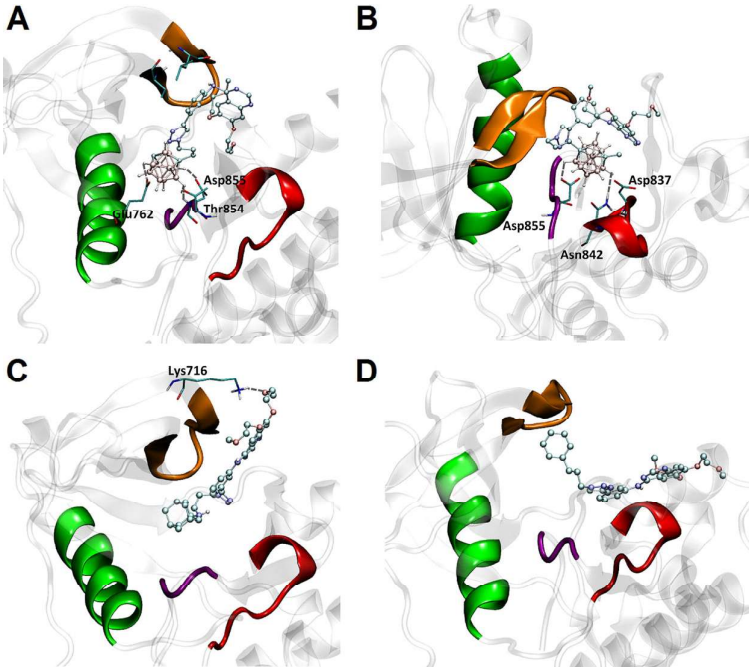


Figure 2. Binding mode of hybrids **1** (**A**), **2** (**B**), **6** (**C**), and **3** (**D**) predicted by ligand-protein molecular docking. The hybrids are shown in ball and stick representations and relevant amino acids in stick representations. Orange: ATP-binding loop, green: α-helix C, purple: DFG-motif, red: catalytic loop.

© 2017 Wiley-VCH Verlag GmbH & Co. KGaA, Weinheim

tween the cluster and Asp837 and Asn842 of the catalytic loop and a hydrogen bond with Asp855 of the DFG-motif (Figure 2B).

As reported in the literature, those H···H bonds with a contact distance shorter than 2.4 Å qualify as dihydrogen bonds. Clearly, dihydrogen bond lengths observed in our ligand-protein complexes fulfil that criterion. Compound **6** with an adamantyl moiety substituting the carborane cluster adopts a binding mode similar to compound **1**, lying along the catalytic cleft (Figure 2C and superimposition of **1–3**, **6** and erlotinib in Figure S4, Supporting Information). However, compound **6** shows a 400-fold higher IC_{50} value, pointing out the importance of the carborane for enhancing the inhibitory activity. It is observed that unlike compound **1**. Derivative **6** fails to make contact with important residues involved in catalysis. In fact, it is hold to the enzyme by only one hydrogen bond interaction between one oxygen present in the ethyloxy fragment and Lys716. The less active molecule, compound **3**, binds on the surface of the catalytic cleft being weakly attached to the enzyme (Figure 2D and Figure S4 in Supporting Information). Although its phenyl moiety locates between the catalytic loop and the ATP binding loop, this molecule does not establish hydrogen bond or hydrophobic interactions with any residue lining the catalytic cleft. This might explains its low inhibitory power and demonstrates that substitution of the phenyl group on the 4-anilinoquinazoline scaffold for a 3D-aromatic system has proved to be an effective strategy in the search for better inhibitors of EGFR.

To unambiguously prove the presence of the *m*-carboranyl cluster hybrid agent derived from erlotinib, **1**, into the C6 glioma cells after 24 h incubation at 37 °C, high resolution XPS spectrum of C6 dried-cells sample was done. The peak at 189 eV in the XPS analysis, which is characteristic of B–B bonding,[26] was observed clearly confirming the presence of *m*-carboranyl (Figure S8, Supporting Information). Although in high-grade gliomas the presence of high-resistance tight junctions between the cerebral capillary endothelial cells that form the barrier is highly altered, experimental[27] and theoretical[28] BBB-cross ability" studies were made for derivatives **1**, **4**, erlotinib and diazepam (Table 2). Erlotinib was included as structural parent compound in order to know the effect of the hybridization process in the BBB capability of the new compounds and diazepam was included as positive BBB penetrant agent.[29] Clearly, for both methodologies, the results indicated that derivative **1** could be able to reach the target organ, the brain. Furthermore, we analysed the solution and metabolic stability of selected derivatives, **1**, **4**, and erlotinib, on aqueous solution at different pHs and on simulated physiological conditions, presence of hepatic rat cytosolic and microsomal fractions[30] (Table 2). Derivative **1** was stable in all the studied conditions while derivative **4**, like erlotinib, was instable on liver fractions (Figures S9–S13, Supporting Information). No attempt to isolate and characterize the metabolic products was made.

In conclusion, we demonstrated that the most active hybrid developed, derivative **1**, acts as EGFR-inhibitor becoming a lead antitumor agent with dual action, targeting EGFR and for BNCT application. The physicochemical studied properties also showed that hybrid **1** could be a template for further structural modifications in order to generate new drugs for glioma treatment. Future studies, like use of carriers to improve compounds water solubility or interaction with serum albumin, to advance in the drug development process will be conducted.

Table 2. BBB cross penetration data and physicochemical properties for **1**, **4**, and erlotinib.

Compds.	Ability to cross BBB		Stability				
	$\Delta\log P$[a]	theor.[b]	2.0[c]	7.4[c]	8.6[c]	cf[d]	mf[d]
1	1.49 ± 0.15	+ BBB	S	S	S	NM	NM
4	4.05 ± 0.30	− BBB	S	S	S	M	M
Erlotinib	3.32 ± 0.30	+ BBB	S	S	S	PM	PM
Diazepam[e]	0.008 ± 0.002	–	–	–	–	–	–

[a] The LogP values were determined by HPLCs. $\Delta\log P = \log P$(octanol/PBS) − $\log P$ (cyclohexane/PBS). Optimal $\Delta\log P$ for brain uptake is < 2. [b] Calculated according to http://lmmd.ecust.edu.cn:8000/predict/. [c] In aqueous-buffer solutions at the indicated pH. S: stable over a period of 24 h incubation, @ 37 °C. [d] cf: hepatic cytosolic fraction; mf: hepatic microsomal fraction. NM: non-metabolized over a period of 30 min incubation, @ 37 °C. M: complete metabolism over a period of 30 min incubation, @ 37 °C. PM: partial metabolism over a period of 30 min incubation, @ 37 °C. [e] Positive control.

Acknowledgements

We thank the Comisión Sectorial de Investigación Científica-Universidad de la República (UdelaR, Uruguay), the "Convenio CSIC (Spain)-UdelaR (Uruguay)", the Spanish Ministerio de Economía *y* Competitividad (CTQ2016-75150-R) and the Generalitat de Catalunya (2014/SGR/149) for financial support and the Agencia Nacional de Investigación e Innovación (ANII, Uruguay) for providing M.C. with a fellowship (POS_NAC_2015_1_110068).

Conflict of interest

The authors declare no conflict of interest.

Keywords: biological chemistry · boron · carborane · drug development · glioma

[1] E. M. Bublil, Y. Yarden, *Curr. Opin. Cell Biol.* **2007**, *19*, 124–134.
[2] R. S. Herbst, *Int. J. Radiat. Oncol. Biol. Phys.* **2004**, *59*, S21–26.
[3] Y. Yarden, M. Sliwkowski, *Nat. Rev. Mol. Cell. Biol.* **2001**, *2*, 127–137.
[4] F. X. Real, W. J. Rettig, P. G. Chesa, M. R. Melamed, L. J. Old, J. Mendelsohn, *Cancer Res.* **1986**, *46*, 4726–4731.
[5] L. V. Sequist, B. A. Waltman, D. Dias-Santagata, S. Digumarthy, A. B. Turke, P. Fidias, K. Bergethon, A. T. Shaw, S. Gettinger, A. K. Cosper, S. Akhavanfard, R. S. Heist, J. Temel, J. G. Christensen, J. C. Wain, T. J. Lynch, K. Vernovsky, E. J. Mark, M. Lanuti, A. J. Iafrate, M. Mino-Kenudson, J. A. Engelman, *Sci. Transl. Med.* **2011**, *3*, 75ra26.
[6] J. Graham, M. Muhsin, P. Kirkpatrick, *Nat. Rev. Drug Discovery* **2004**, *3*, 11.
[7] W. Blaszczak, W. Barczak, A. Wegner, W. Golusinski, W. M. Suchorska, *Med. Oncol. (N. Y., NY, U. S.)* **2017**, *34*, 60.
[8] Y. J. Liu, C. M. Zhang, Z. P. Liu, *Anticancer Agents. Med. Chem.* **2012**, *12*, 391–406.

© 2017 Wiley-VCH Verlag GmbH & Co. KGaA, Weinheim

[9] A. E. Wakeling, S. P. Guy, J. R. Woodburn, S. E. Ashton, B. J. Curry, A. J. Barker, K. H. Gibson, *Cancer Res.* **2002**, *62*, 5749–5754.
[10] D. R. Duckett, M. D. Cameron, *Expert Opin. Drug Metab. Toxicol.* **2010**, *6*, 1175–1193.
[11] F. A. Shepherd, J. Rodrigues Pereira, T. Ciuleanu, E. H. Tan, V. Hirsh, S. Thongprasert, D. Campos, S. Maoleekoonpiroj, M. Smylie, R. Martins, M. van Kooten, M. Dediu, B. Findlay, D. Tu, D. Johnston, A. Bezjak, G. Clark, P. Santabarbara, L. Seymour, *N. Engl. J. Med.* **2005**, *353*, 123–132.
[12] R. S. M. Ismail, N. S. M. Ismail, S. Abuserii, D. A. A. El Ella, *J. Fut. J. Pharm. Sci.* **2016**, *2*, 9–19.
[13] H. S. Ban, H. Nakamura, *Chem. Rec.* **2015**, *15*, 616–635.
[14] a) M. Scholz, E. Hey-Hawkins, *Chem. Rev.* **2011**, *111*, 7035–7062; b) Z. J. Leśnikowski, *J. Med. Chem.* **2016**, *59*, 7738–7758; c) C. Viñas, *Fut. Med. Chem.* **2013**, *5*, 617–619; d) J. Poater, M. Solà, C. Viñas, F. Teixidor, *Angew. Chem. Int. Ed.* **2014**, *53*, 12191–12195; *Angew. Chem.* **2014**, *126*, 12387–12391.
[15] a) W. N. Lipscomb, *Angew. Chem.* **1977**, *89*, 685–696; b) A. F. Armstrong, J. F. Valliant, *Dalton Trans.* **2007**, 4240–4251; c) M. Kassiou, L. M. Rendina, *Chem. Rev.* **2011**, *111*, 5701–5722; d) G. Calabrese, J. J. Nesnas, E. Barbu, D. Fatouros, J. Tsibouklis, *Drug Discovery Today* **2012**, *17*, 153–159.
[16] W. Sauerwein, A. Wittig, R. Moss, Y. Nakagawa, Neutron Capture Therapy. Principles and Applications, Springer-Verlag Berlin Heidelberg, **2012**.
[17] M. F. Hawthorne, M. W. Lee, *J. Neuro-Oncol.* **2003**, *62*, 33–45.
[18] M. Couto, I. Mastandrea, M. Cabrera, P. Cabral, F. Teixidor, H. Cerecetto, C. Viñas, *Chem. Eur. J.* **2017**, *23*, 9233–9238.
[19] G. Qu, C. Liu, B. Sun, C. Zhou, Z. Zhang, P. Wang, *Oncol. Rep.* **2014**, *32*, 341–347.
[20] H. Zegzouti, M. Zdanovskaia, K. Hsiao, S. A. Goueli, *Assay Drug Dev. Technol.* **2009**, *7*, 560–572.
[21] a) A. Prahallad, C. Sun, S. D. Huang, F. Di Nicolantonio, R. Salazar, D. Zecchin, R. L. Beijersbergen, A. Bardelli, R. Bernards, *Nature* **2012**, *483*, 100–103; b) S. Kobayashi, T. J. Boggon, T. Dayaram, P. A. Janne, O. Kocher, M. Meyerson, B. E. Johnson, M. J. Eck, D. G. Tenen, B. Halmos, *N. Engl. J. Med.* **2005**, *352*, 786–792.
[22] M.-B. Sárosi, W. Neumann, T. P. Lybrand, E. Hey-Hawkins, *J. Chem. Inf. Model.* **2017**, *57*, 2056–2067.
[23] X. Zhang, H. Dai, H. Yan, W. Zou, D. Cremer, *J. Am. Chem. Soc.* **2016**, *138*, 4334–4337.
[24] J. Fanfrlík, M. Lepšík, D. Horinek, Z, Havlas, P. Hobza, *ChemPhysChem* **2006**, *7*, 1100–1105.
[25] J. Stamos, M. X. Sliwkowski, C. Eigenbrot, *J. Biol. Chem.* **2002**, *277*, 46265–46272.
[26] X. Lu, W. Liu, J. Ouyang, Y. Tian, *Appl. Surf. Sci.* **2014**, *311*, 749–752.
[27] a) R. C. Young, R. C. Mitchell, T. H. Brown, C. R. Ganellin, R. Griffiths, M. Jones, K. K. Rana, D. Saunders, I. R. Smith, N. E. Sore, T. J. Wilks, *J. Med. Chem.* **1988**, *31*, 656–671; b) L. Di, E. Kerns, *Drug-like Properties: Concepts, Structure Design and Methods from ADME to Toxicity Optimization*, 1st Ed., Academic Press, **2008**.
[28] a) http://lmmd.ecust.edu.cn/admetsar1/predict/; b) J. Shen, F. Cheng, Y. Xu, W. Li, Y. Tang, *J. Chem. Inf. Model.* **2010**, *50*, 1034–1041.
[29] Y. Yang, W. Ang, H. Long, Y. Chang, Z. Li, L. Zhou, T. Yang, Y. Deng, Y. Luo, *Sci. Rep.* **2016**, *6*, 34711.
[30] M. Couto, S. de Ovalle, M. Cabrera, H. Cerecetto, M. González, *Future Med. Chem.* **2015**, *7*, 857–871.

Manuscript received: November 1, 2017
Accepted manuscript online: November 30, 2017
Version of record online: ■■ ■■, 0000

© 2017 Wiley-VCH Verlag GmbH & Co. KGaA, Weinheim

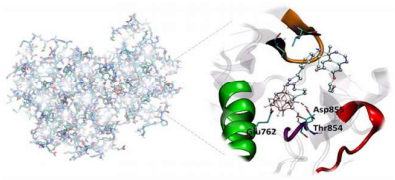
COMMUNICATION

Biological Chemistry

M. Couto, M. F. García, C. Alamón, M. Cabrera, P. Cabral, A. Merlino, F. Teixidor, H. Cerecetto, C. Viñas**

■■ – ■■

Discovery of Potent EGFR Inhibitors through the Incorporation of a 3D-Aromatic-Boron-Rich-Cluster into the 4-Anilinoquinazoline Scaffold: Potential Drugs for Glioma Treatment



A most active hybrid derivative 1 has been developed, which acts as an EGFR-inhibitor thus with great potentional as a lead antitumor agent with dual action, targeting EGFR and for BNCT application. The physicochemical studied properties also showed that hybrid **1** (with IC_{50} value of 2.3 nM, 10-fold higher than the parent compound) could be a template for further structural modifications in order to generate new drugs for glioma treatment.

© 2017 Wiley-VCH Verlag GmbH & Co. KGaA, Weinheim

View publication stats

CHEMISTRY
A European Journal

Supporting Information

Discovery of Potent EGFR Inhibitors through the Incorporation of a 3D-Aromatic-Boron-Rich-Cluster into the 4-Anilinoquinazoline Scaffold: Potential Drugs for Glioma Treatment

Marcos Couto,[a, b, c] María Fernanda García,[c] Catalina Alamón,[a] Mauricio Cabrera,[d] Pablo Cabral,[c] Alicia Merlino,[e] Francesc Teixidor,[b] Hugo Cerecetto,*[a, c] and Clara Viñas*[b]

chem_201705181_sm_miscellaneous_information.pdf

Experimental section

1. Synthesis

1.1 Instrumentation

1.2 Materials and methods

2. Biology

2.1 Kinase enzymatic assays

2.2 Docking studies

2.3 X-Ray photoelectron spectroscopy studies

2.4 Ability to cross the BBB studies

2.5 Stability studies

2.5.1 On aqueous solution at different pHs

2.5.2 On rat microsomal and cytosolic fractions

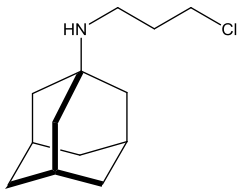
Experimental Section

1. Synthesis

1.1 Instrumentation: Melting points were measured on an Electrothermal 9100 apparatus and are uncorrected. Elemental analyses were performed using a Carlo Erba Model EA1108 elemental analyzer instrument. ^{1}H and ^{13}C NMR spectra were recorded on a Bruker DPX-400 spectrometer at 400.13 and 100.77 MHz, respectively, with $CDCl_3$ as solvent and calibrated using residual undeuterated solvent as an internal reference. Chemical shifts are reported in units of parts per million (ppm) downfield from the reference, and all coupling constants are reported in Hertz (Hz). Multiplicity is abbreviated as: s is the singlet, d is the doublet, dd is the doublet of doublet, dt is doublet of triplets, dq is doublet of quartets, t is the triplet, m is the multiplet, and bs is the broad singlet. High resolution X-ray photoelectron spectroscopy (HRXPS) was performed with a Phoibos 150 analyzer (SPECS GmbH, Berlin, Germany) in ultra-high vacuum conditions (base pressure 4E-10 mbar) with a monochromatic aluminium K alpha X-ray source (1486.74 eV). The energy resolution as measured by the FWHM of the Ag 3d5/2 peak for a sputtered silver foil was 0.8 eV.

1.2 Materials and methods: All the reactions were performed under an atmosphere of dinitrogen by employing standard Schlenk techniques. Analytical thin-layer chromatography (TLC) was carried out on pre-coated plates with silica gel 60 on aluminium foil F254 (Merck). Compounds were visualized by use of UV light (254 nm). All chemical reagents were obtained from Merck, Fluka or Acros and were used without further purification unless otherwise noted.

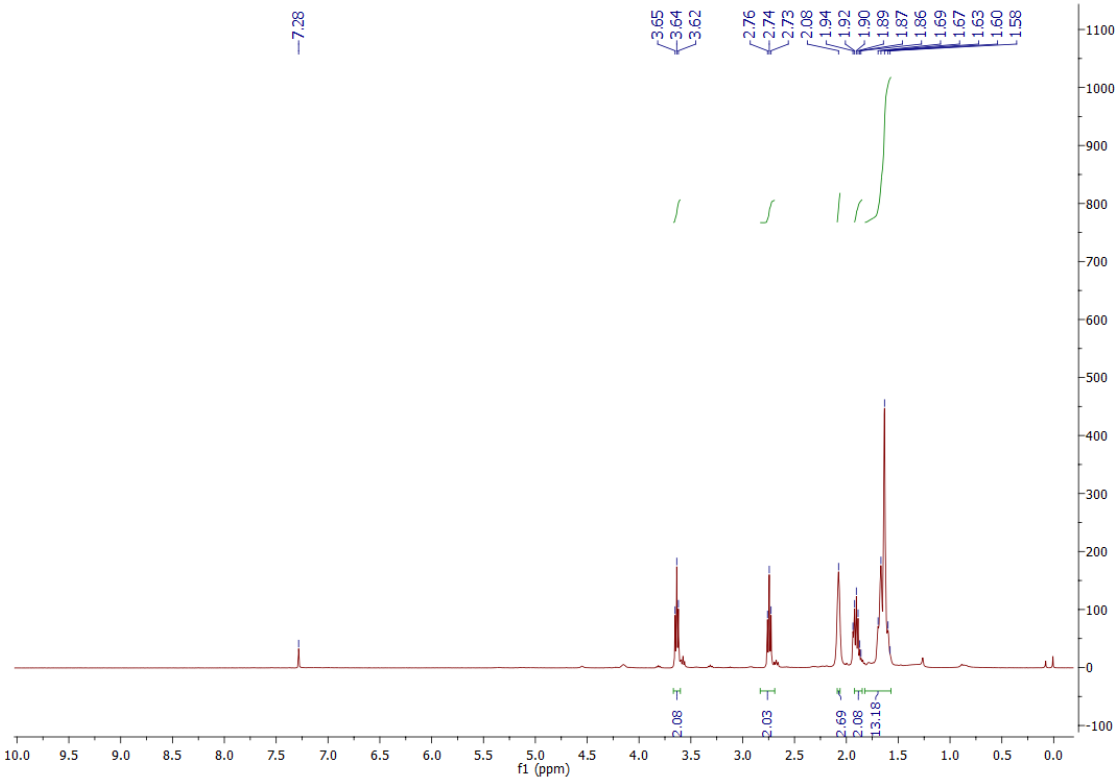
Synthesis and characterization of compound 1-(3-chloropropyl)-1-adamantinylamine.

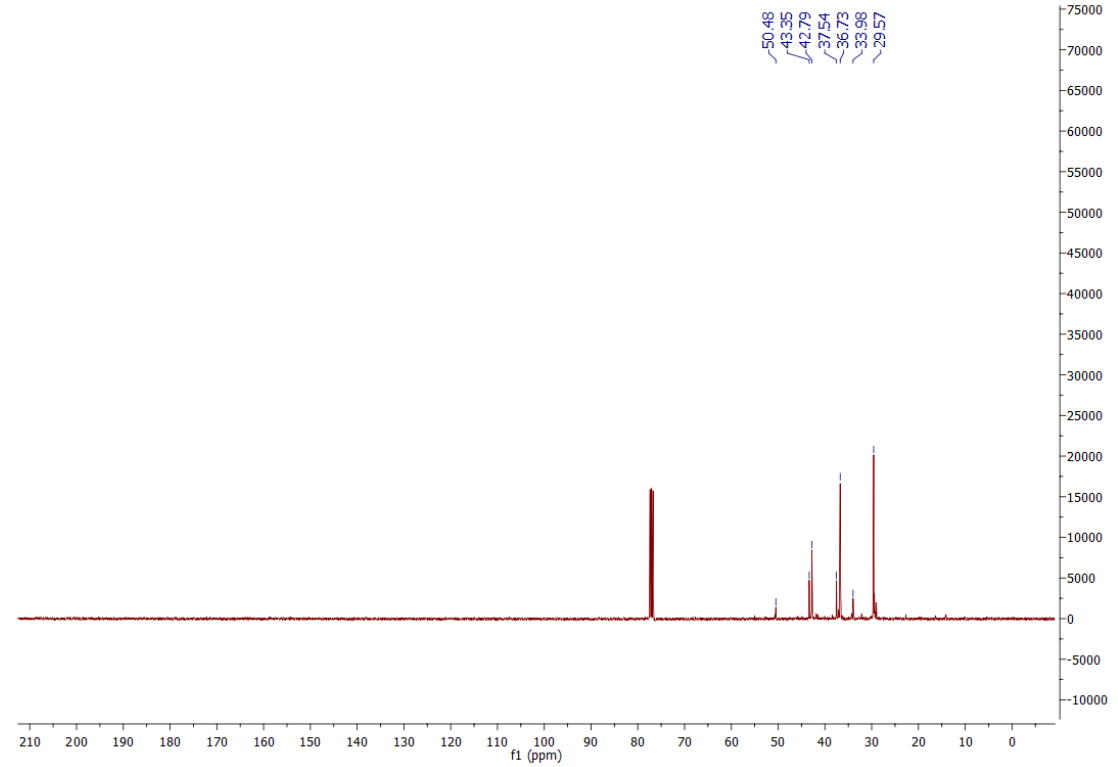


1-Bromo-3-chloropropane (5 equiv., 1.58 mL) was added dropwise to a white suspension containing anhydrous DMF (6 mL), 1-adamantinylamine hydrochloride (1 equiv., 0.6 g) and cesium carbonate (2.2 equiv., 2.29 g) previously stirred for 30 min. After that, the reaction was allowed to proceed at room temperature for 72 h. The reaction mixture was filtered to remove undissolved solids and washed several times with cooled ethyl acetate. The filtrate was concentrated, and the residue was taken up in aqueous solution of NaOH (1 N), and extracted with ethyl acetate (6 × 20 mL). The product was

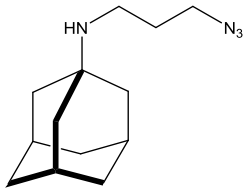
purified by column chromatography and ethyl acetate:EtOH (90:10) as eluent. The product was obtained after removal the solvent under reduced pressure to yield a light yellow oil (0.24 g, 33 %).

^{1}H-NMR (400.13 MHz, $CDCl_3$) δ: 3.64 (t, $J_{H,H}$= 6.4 Hz, 2H, -C**H**$_2$Cl), 2.74 (t, $J_{H,H}$= 6.9 Hz, 2H, -C**H**$_2$NH), 2.08 (bs, 2H, -C**H**$_2$-adamantyl), 1.94-1.89 (m, 2H, -HNCH$_2$-C**H**$_2$-CH$_2$Cl), 1.69-1.60 (m, 13H, C**H** and C**H**$_2$-adamantyl). ^{13}C{^{1}H}-NMR (100.77 MHz, $CDCl_3$) δ: 50.5, 43.4, 42.8 (3C), 37.5, 36.7 (3C), 34.0, 29.6 (3C).



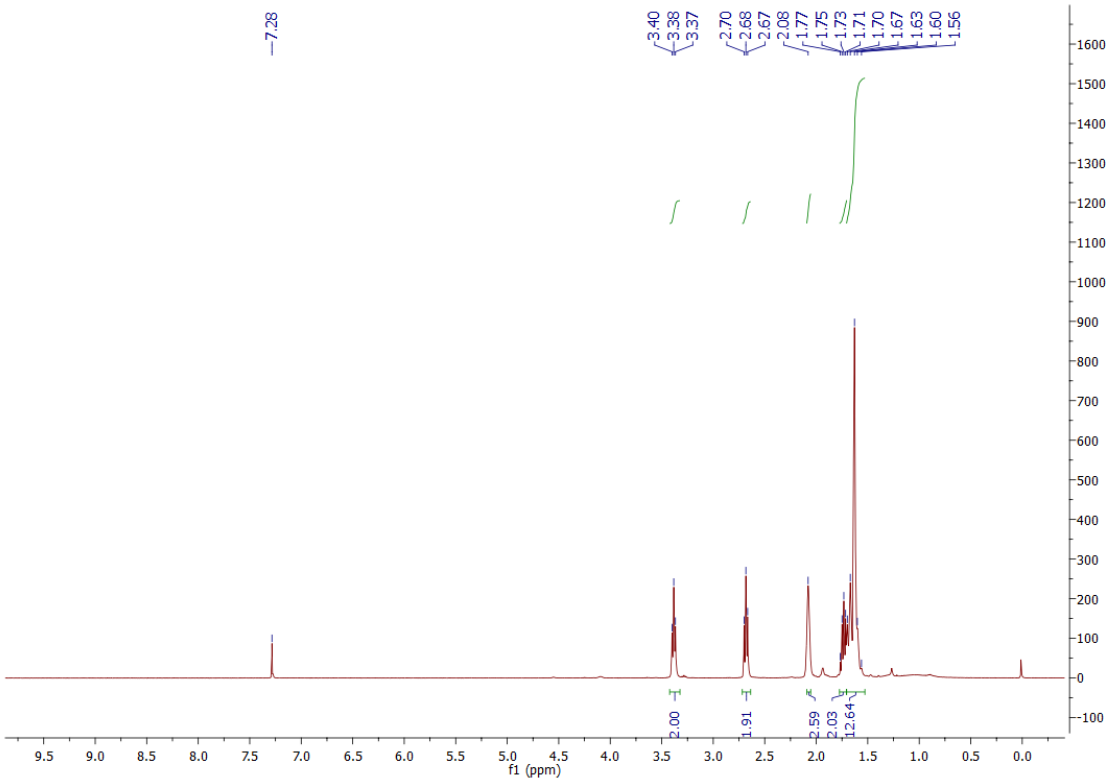


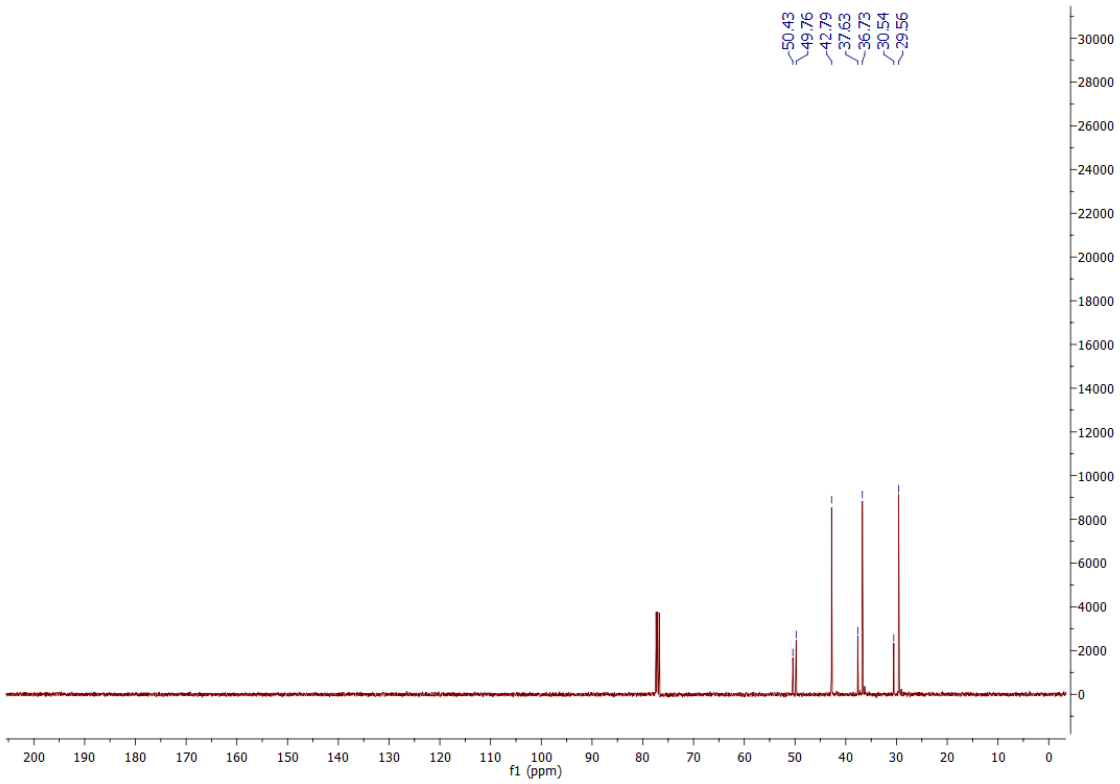
Synthesis and characterization of compound 1-(3-azidopropyl)-1-adamantinylamine.



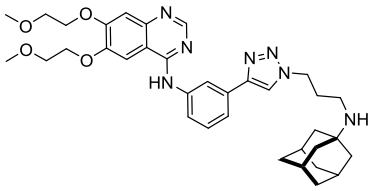
A 10-mL round-bottom flask equipped with a condenser and a magnetic stirring bar was charged with 1-(3-chloropropyl)-1-adamantinylamine (200 mg, 0.88 mmol) and sodium azide (458 mg, 7.0 mmol) and was heated at reflux in dry DMF (4 mL) for 14 h. The light yellow solution was evaporated under reduced pressure to dryness and the residue was suspended in toluene (8 mL) and washed with 6 mL of water. Two extractions of the water were performed with CH_2Cl_2 (2 × 10 mL).The organic layers were dried over Na_2SO_4, filtered, and evaporated under reduced pressure to dryness. The product was purified by preparative TLC and 100 % *n*-hexane as eluent. The product was obtained following extraction of the silica with acetone and evaporation under reduced pressure to yield a light yellow oil (206 mg, conversion of 100 %).

^{1}H-NMR (400.13 MHz, $CDCl_3$) δ: 3.38 (t, $J_{H,H}$= 6.6 Hz, 2H, -C**H**$_2$N$_3$), 2.68 (t, $J_{H,H}$= 7.1 Hz, 2H, -C**H**$_2$NH), 2.08 (bs, 2H, -C**H**$_2$-adamantyl), 1.73 (dt, $J_{H,H}$= 13.6 Hz, $J_{H,H}$= 6.8 Hz, 2H,-HNCH$_2$-C**H**$_2$-CH$_2$Cl), 1.69-1.58 (m, 13H, C**H** and C**H**$_2$-adamantyl). ^{13}C{^{1}H}-NMR (100.77 MHz, $CDCl_3$) δ: 50.4, 49.8, 42.8 (3C), 37.6, 36.7 (3C), 30.5, 29.6 (3C).





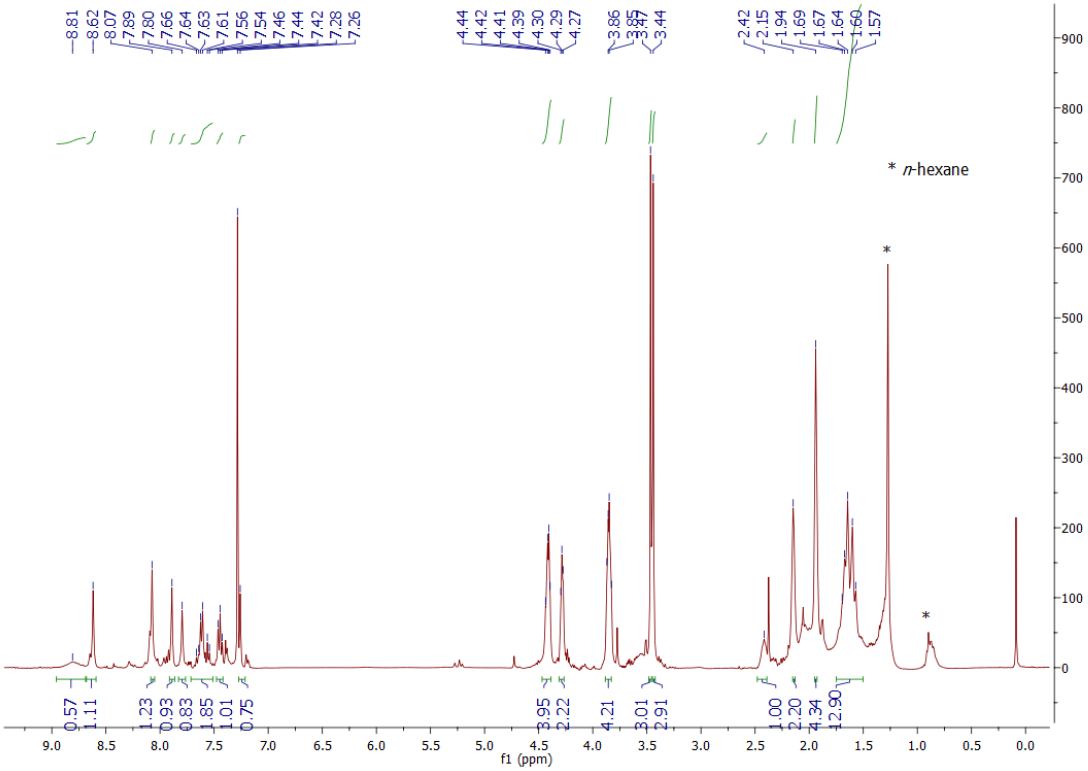
Synthesis and characterization of compound 4-{3-[1-(3-adamantinylaminopropyl]-1*H*-[1,2,3]triazol-4-yl}phenylamino-6,7-bis(2-methyloxyethyloxy)quinazoline

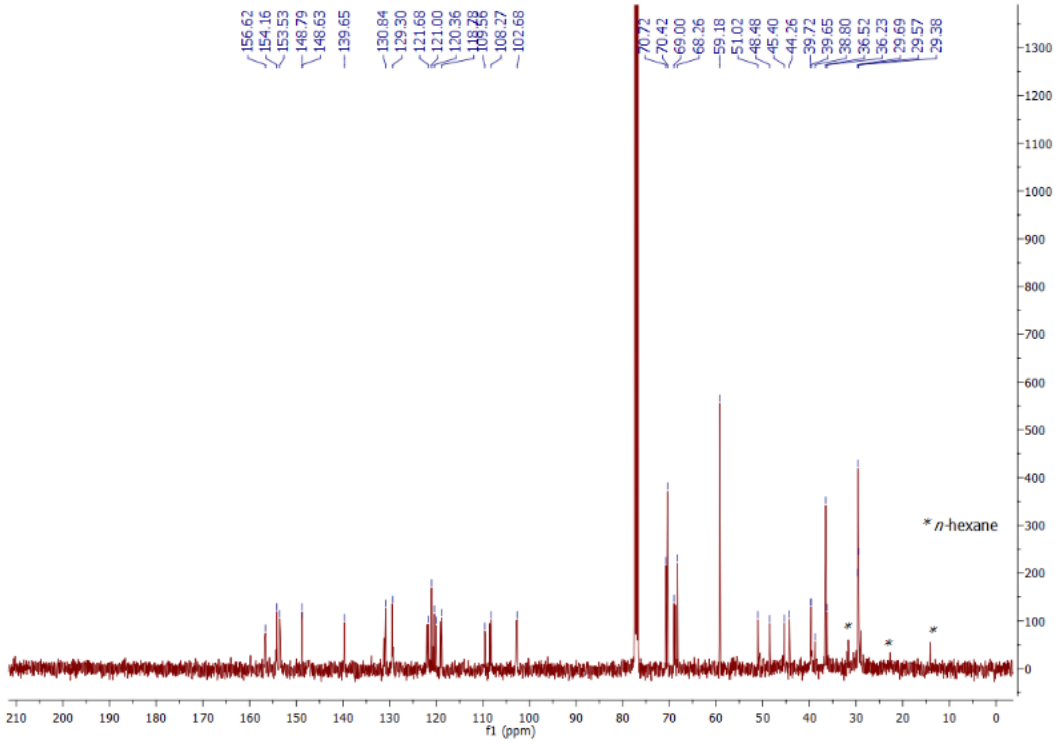


A 10-mL round-bottom flask equipped with a magnetic stirring bar was charged with erlotinib (1.1 equiv., 100 mg, 0.25 mmol) dissolved in THF:H_2O (3 mL, 1:1 v/v). Then, sodium ascorbate (7.4 mg, 15 mol %), $CuSO_4{\cdot}5H_2O$ (6.3 mg, 10 mol %) and 1-(3-azidopropyl)-1-adamantinylamine (1 equiv., 142 mg, 0.23 mmol) were added. The mixture was left at room temperature for 24 h. After that, a heavy white precipitate was formed, which it was filtered. The filtrate was poured into CH_2Cl_2 (15 mL) and washed with water (3 × 5 mL). The organic layer was dried over $MgSO_4$ and evaporated under reduced pressure to dryness. The product was purified by preparative TLC and CH_2Cl_2:MeOH (97:3) as eluent. The product was obtained following extraction of the silica with CH_2Cl_2:MeOH and evaporation under reduced pressure to yield a white solid (88 mg, 61 %). mp: 106.0 - 109.0 °C.

^{1}H-NMR (400.13 MHz, $CDCl_3$) δ: 8.81 (bs, 1H, -N**H**), 8.62, (s, 1H, pyrimidine-**H**), 8.07 (s, 1H, triazole-**H**), 7.89 (s, 1H, Ar-**H**), 7.80 (s, 1H, Ar-**H**), 7.66-7.54 (m, 2H, Ar-**H**), 7.44 (t, $J_{H,H}$= 7.9, 1H, Ar-**H**), 7.26 (s, 1H, Ar-**H**), 4.41 (dd, $J_{H,H}$= 10.7 Hz, $J_{H,H}$= 6.2 Hz, 4H, (-C**H**$_2$-OAr)$_2$), 4.34-4.25 (m, 2H, -C**H**$_2$-triazole), 3.85 (dd, $J_{H,H}$= 10.3 Hz, $J_{H,H}$= 6.7 Hz, 4H, (H_3CO-C**H**$_2$-)$_2$), 3.47 (s, 3H, **H**$_3$C-O-), 3.44 (s, 3H,

H$_3$C-O-), 2.42 (bs, 1H, -N**H**-adamantyl), 2.15 (bs, 2H,-HNCH$_2$-C**H**$_2$-CH$_2$-triazole) 1.94 (bs, 4H, -C**H**$_2$-adamantyl and -CH$_2$-C**H**$_2$-NH-adamantyl), 1.69-1.57 (m, 13H, C**H** and C**H**$_2$-adamantyl). ^{13}C{^{1}H}-NMR (100.77 MHz, $CDCl_3$) δ: 156.6, 154.2, 153.5, 148.8, 148.6, 139.7, 130.8, 129.3, 121.7, 121.0, 120.4, 120.1, 118.8, 109.6, 108.3, 102.7, 70.7, 70.4, 69.0, 68.3, 59.2 (2C), 51.0, 48.5, 45.4, 44.3, 39.72, 39.65, 38.8, 36.5 (2C), 36.2, 29.7, 29.6, 29.4. Anal. Calcd. for $C_{35}H_{45}N_7O_4$: C, 66.96; H, 7.23; N, 15.62. Found: C, 66.63; H, 7.36, N, 15.50.




156.62
154.16
153.53
148.79
148.63
139.65
130.84
129.30
121.68
121.00
120.36
108.27
102.68
70.72
70.42
69.00
68.26
59.18
51.02
48.48
45.40
44.26
39.72
39.65
38.80
36.52
36.23
29.69
29.57
29.38
* n-hexane
f1 (ppm)

2. Biology

2.1 Kinase enzymatic assays

The wild-type EGFR kinase enzyme system (Catalog. V3831) and the T790M-mutated EGFR kinase enzyme (Catalog. V4507) were purchased from Promega Corporation (Fitchburg, WI, USA). The experiments were performed according to the manufacturer instructions. For more detailed and complete protocols, see the ADP-Glo™ kinase Assay Technical Manual and the active kinase datasheet available at: http://www.promega.com/KESProtocol. Briefly, for the kinase reaction step serial dilutions of the compounds on a range of 100, 25, 5, 2.5, 0.5, 0.1, 0.02, 0.004, and 0.0008 µM were prepared. A 10 µL enzyme reaction mixture was performed containing 2 µL of the compound dilution, 3 µL of the enzyme dilution and 5 µL of the ATP/substrate solution to get a final concentration of 50 µM ATP, 0.2 g/mL of Poly(Glu, Tyr) substrate and 5 mg/mL of enzyme. Each reaction was performed by triplicate on a 384-well plate and incubated during 1 h at room temperature. The kinase reaction was stopped with 5 µL of ADP-Glo™ during 40 min, followed by the addition of 10 µL of Kinase Detection Reagent. Luminiscenence was measured after 30 min on a BioTek® FLx800 Multi-Detection Microplate Reader (Integration time 0.5–1 s). Curve fitting and data presentations were performed using GraphPad Prism version 5.0 (GraphPad Software, Inc.).

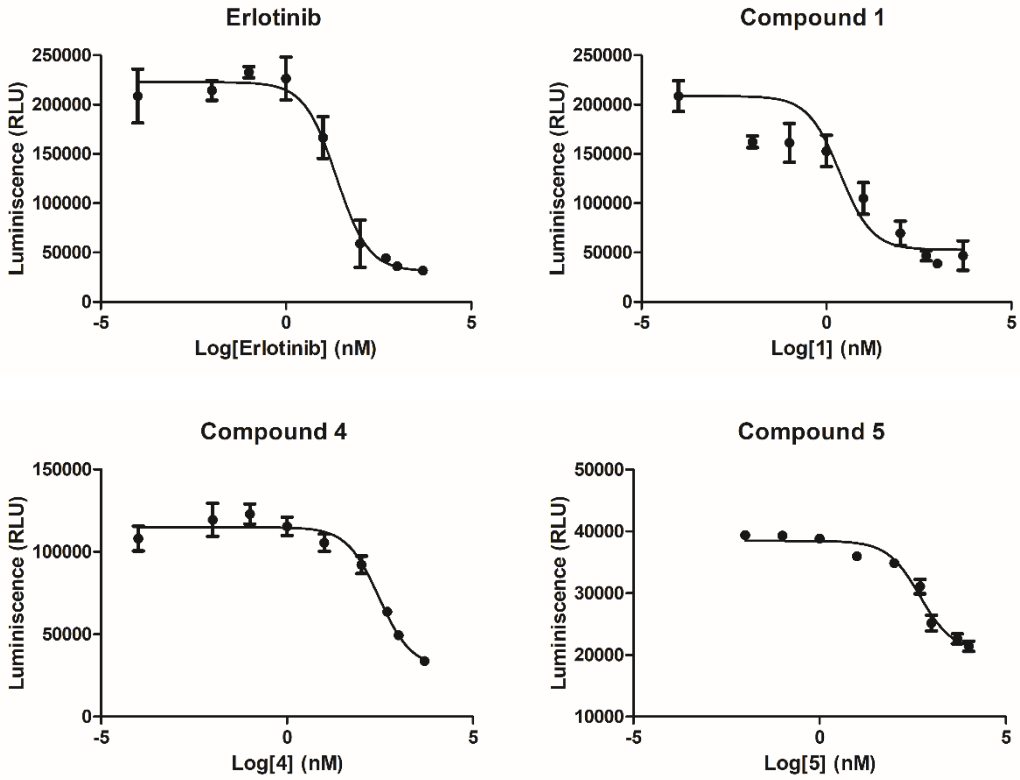


Figure S1. Inhibition studies of $EGFR_{WT}$ kinase. Dose-response curves for parent compound and hybrids **1**, **4**, and **5**.

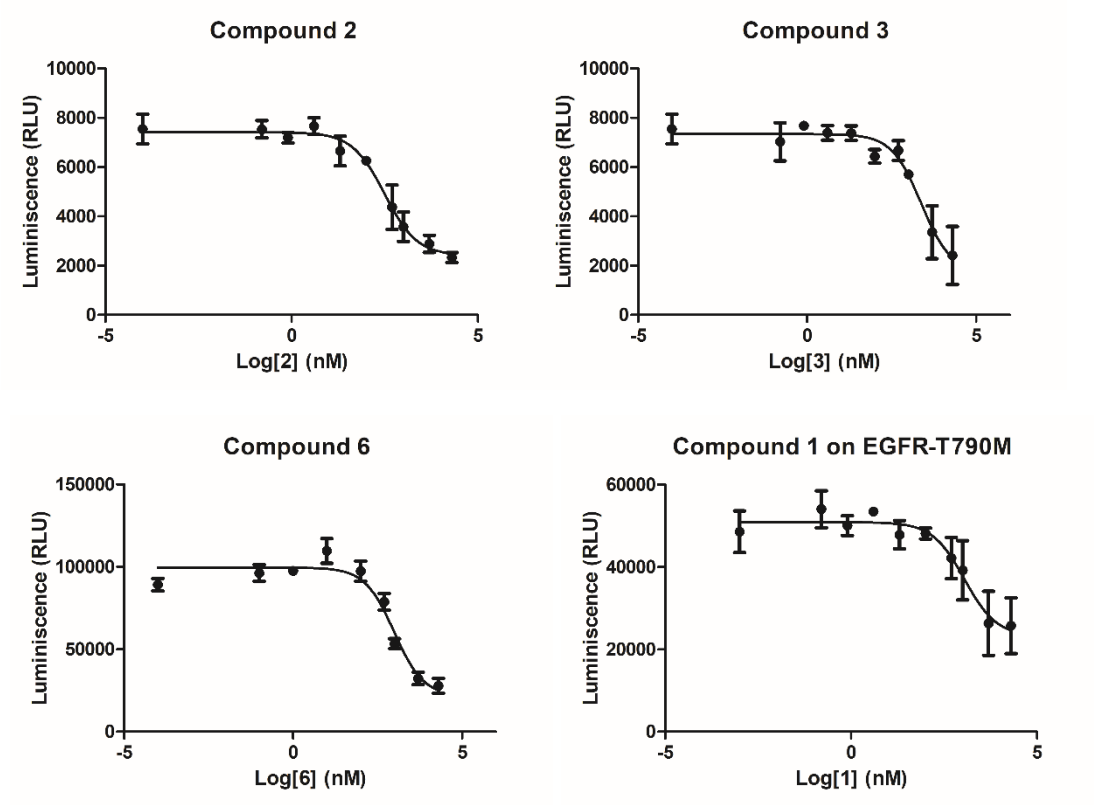


Figure S2. Inhibition studies of EGFR kinases. Dose-response curves for parent hybrids **2**, **3**, and **6** against wild type and hybrid **1** against mutant one (T790M).

2.2 Docking studies

Ligands preparation

Before docking, compounds (**1**, **2**, **3**, and **6**) were optimized in water using the IEF-PCM continuum model with Bondi radii at the wb97XD/6-31+G(d,p) level of theory[1]. All calculations were performed with the Gaussian 09[2] suite of programs.

Biosystem preparation

The crystal structure of the EFGR kinase domain in its active conformation in complex with AMP-PNP inhibitor (PDB ID: 2ITX) was retrieved from the Protein Data Bank. Crystallographic water molecules and the inhibitor were removed.

Docking procedure

AutoDock4.2 was used for conducting protein-ligand docking studies[3]. Input files were prepared with AutoDockTools[4] using Gasteiger-Marsili charges for both the ligands and the protein. The van der Waals radius (R) and the associated van der Waals well-depth (ε) for boron, carbon and hydrogen atoms in the carborane cluster were taken from Oda et. al.[5] and are shown in Table S1. All torsion angles within the carborane clusters were set to non-rotatable. A grid box of 126 × 126 × 126 points with a spacing of 0.375 Å between points was employed in order to cover the entire protein surface. The box was centered on the macromolecule. For each ligand, a population size of 150 individuals and $2.5x10^6$ energy evaluations were used for 300 independent search runs. Conformations differing by less than 2.0 Å in root-square deviation were clustered together. The conformation with the lowest binding energy was chosen from the most populated cluster and the corresponding ligand-protein complex was used for further analyses.

Table S1. Parameters for atoms in the carborane cluster

	R	ε
B	2.285	0.1786
Cb	1.908	0.1317
Hb	1.019	0.015
Hc	1.019	0.015

Hb: hydrogen boded to boron in carborane

Hc: hydrogen bonded to carbon in carborane

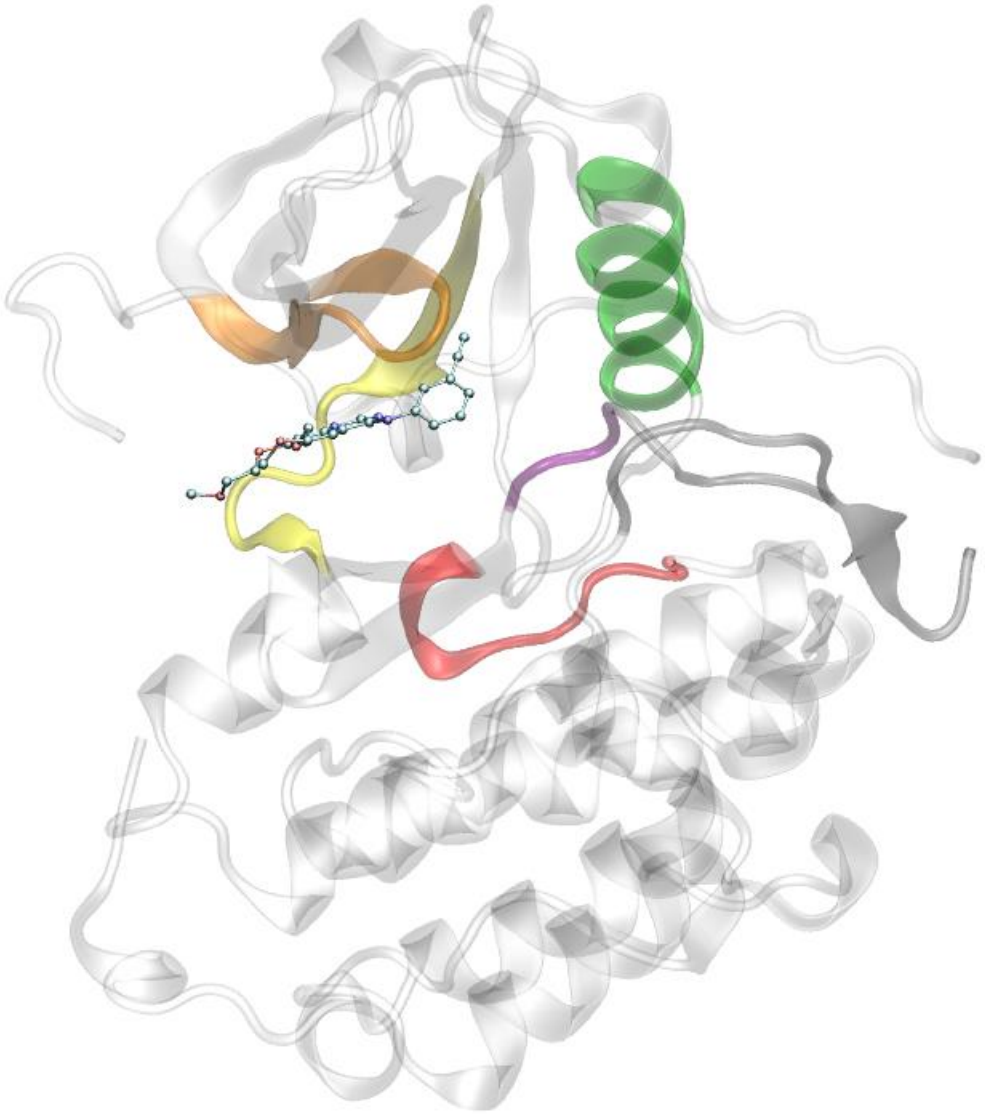


Figure S3. Crystal structure of erlotinib (ball and sticks) bound to active EGFR-TKD (PDB ID: 1M17)[6]. Structural elements are highlighted as follows, orange: ATP binding loop (residues 718 to 726), green: α-helix C (residues 756 to 768), yellow: hinge region (residues 788 to 797), red: catalytic loop (residues 836 to 842), purple: DFG-motif (residues 855 to 857), gray: activation loop (residues 855 to 876).

Table S1. Hydrogen and dihydrogen bonds distances in hybrid-EGFR complexes

Compds.	Hydrogen bonds	Dihydrogen bonds	Distance (Å)
1	B-H···Glu762@OE2	-	2.07
	B-H···Asp855@OD2	-	1.89
	-	B-H···Thr854@OH	0.92
	-	B-H···Asp855@NH	1.34
2	B-H···Asp837@OD2	-	2.05
	B-H···Asp855@OD2	-	1.95
	-	B-H···Asn842@HD2	2.04
6	H3CO···Lys716@NZ	-	1.85

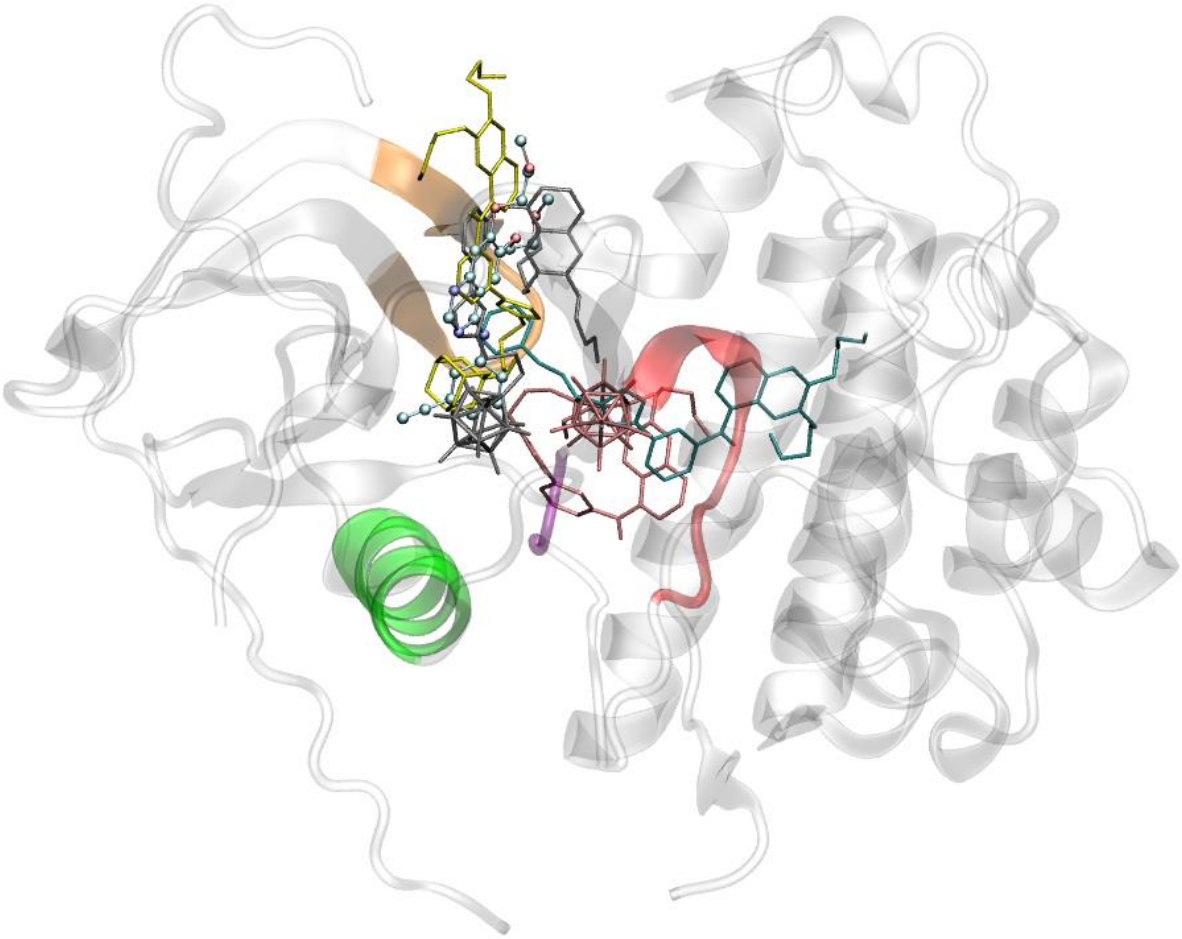


Figure S4. Comparative binding mode into active EGFR-TDK of hybrid **1** (gray), compound **2** (pink), compound **3** (cyan), compound **6** (yellow) and erlotinib (ball and sticks). EGFR-selected structural elements are colored as indicated in Fig. S3.

2.3 X-Ray photoelectron spectroscopy studies

2.3.1 Cell uptake studies

A 100 mM stock solution in DMSO of compound **1** was prepared. Warm culture milieu (37 °C) was treated with stock compound solution to final concentration of 30 μM (IC_{50}). The C6 cells (ATCC® CCL-107™) were cultured as a monolayer in 75 cm^2 flasks to 70-80 % confluence and then incubated with the boron-containing culture milieu for 24 h at 37 °C in a humidified 5 % CO_2 atmosphere. The milieu was removed and the cells were washed with PBS, and then trypsinized. The cell suspension was sedimented by centrifugation at 2000 x g for 3 min, then the supernatant was removed and the cell pellet was lyophilizated and analysed by X-Ray photoelectron spectroscopy (XPS) for boron content.

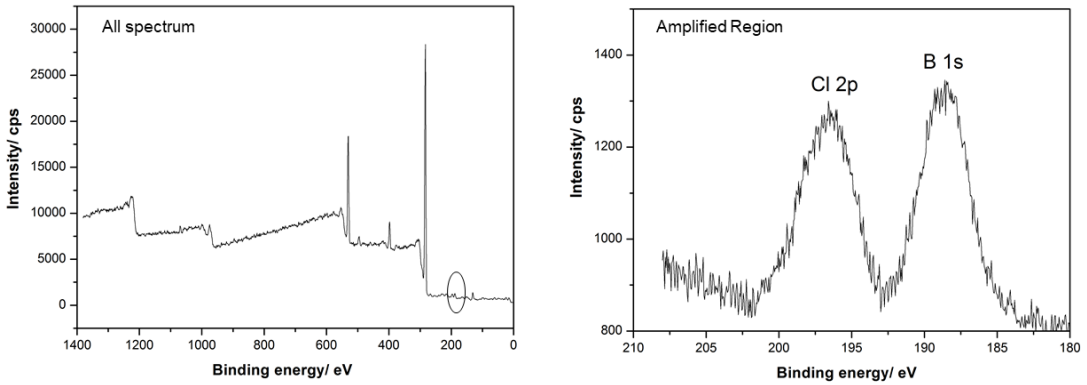


Figure S8. X-Ray photoelectron spectra for studied conditions observing the presence of boron into C6 cells.

2.4 Ability to cross the BBB studies

To determine the Δlog *P* values we used the method commonly known as *Shake Flas*[7]. In both cases (log $P_{(octanol/PBS)}$ and log $P_{(cyclohexane/PBS)}$) 5 µL of the stock solution of each derivative (2.5 mM in DMSO) were incubated, in an Eppendorf tube, in 500 µL of Dulbecco's Phosphate Buffered, pH 7.4, 0.01 M and 500 µL of the corresponding organic phase. After that, the Eppendorf was vortexed for 1 minute and then incubated 24 h at 25 °C with orbital shaking. Subsequently it was centrifuged for 5 minute at 5000 rpm and 50 µL of each phase was taken with syringe to analyse by RP-HPLC. All experiments were performed at least two times. Standards calibration curves: mAu/min were plotted against variable concentration of each derivative to obtain calibration curves.

Diazepam				
phase	**mAu/min**	**C (M)**	**Organic phase/PBS phase**	**log**
Octanol	2820	5,71E-05	109,4771	2,039323
PBS	10	5,22E-07		
Octanol	2759	6,25E-07	89,50185	1,951832
PBS	15	6,25E-07		
Octanol	3293	6,67E-05	106,7249	2,028266
PBS	15	6,25E-07		
Cyclohexane	4176	8,452E-05	95,26202	1,97892
PBS	28	8,87E-07		
Cyclohexane	4566	9,23E-05	83,30161	1,920653
PBS	39	1,11E-06		
Cyclohexane	4456	9,01E-05	73,30555	1,865137
PBS	45	1,23E-06		

Diazepam	**Average**
log *P* (octanol/PBS)	2.006473
log *P* (cyclohexane/PBS)	1,921570
Δlog *P*	**0,008490**

Erlotinib				
phase	**mAu/min**	**C (M)**	**Organic phase/PBS phase**	**log**
Octanol	1581,642	2,259E-05	332,4621	2,521742
PBS	4,762046	6,796E-08		
Octanol	1758,499	2,512E-05	234,9264	2,370932
PBS	7,49	1,069E-07		
Cyclohexane	33,34117	4,762E-07	0,141338	-0,84974
PBS	235,8684	3,369E-06		
Cyclohexane	34,85928	4,979E-07	0,123965	-0,9067
PBS	281,1688	4,017E-06		

Erlotinib	**Average**
log *P* (octanol/PBS)	2,446337
log *P*(cyclohexane/PBS)	-0,87822
Δlog *P*	**3,324558**

Hybrid 4				
phase	**mAu/min**	**C (M)**	**Organic phase/PBS phase**	**log**
Octanol	1662.924	2,86E-05	285,2179	2,455177
PBS	7,030471	1E-07		
PBS	3,583511	5,11E-08	478,5347	2,679913
Octanol	1712,59	2,45E-05		
Cyclohexane	9,1788	1,31E-07	0,023075	-1,636854
PBS	397,5778	5,68E-06		
Cyclohexane	19,95104	2,85E-07	0,043417	-1,362339
PBS	459,4167	6,56E-06		
Cyclohexane	12,68644	1,81E-07	0,023999	-1,61981
PBS	528,4363	7,55E-06		
Octanol	1541,89	2,2E-05	253,7337	2,404378
PBS	6,081486	8,68E-08		

Hybrid 4	**Average**
log *P*(octanol/PBS)	2,513156143
log *P*(cyclohexane/PBS)	-1,539667525
Δlog *P*	**4,052823668**

Hybrid 1				
phase	**mAu/min**	**C (M)**	**Organic phase/PBS phase**	**log**
Octanol	11091	0,000113	3192,137	3,504082
PBS	2,491411	3,55E-08		
Octanol	12700	0,000181	319,3618	2,504283
PBS	39,77149	5,68E-07		
Octanol	12873	0,000184	1972,468	3,29501
PBS	6,53104	9,32E-08		
Cyclohexane	1804,469	2,58E-05	47,17349	1,673698
PBS	38,25636	5,46E-07		
Cyclohexane	2068,104	2,95E-05	28,63651	1,45692
PBS	72,22366	1,03E-06		
Cyclohexane	2231,125	3,19E-05	50,46154	1,702961
PBS	44,21897	6,32E-07		

Hybrid 1	**Average**
log *P* (octanol/PBS)	3,101125
log *P* (cyclohexane/PBS)	1,611193
Δlog *P*	**1,489932**

2.5 Stability studies

2.5.1 On aqueous solution at different pHs

For pH stability studies, we utilized the following aqueous solution: KCl·HCl buffer, pH 2; phosphate buffer, pH 7.4; and Tris·HCl buffer, pH 8.6. The stock solutions of derivatives were prepared in DMSO and the final concentration in the aqueous milieu was variable. The solutions were further homogenized and incubated at 37 °C for 24 h. Each experiment was performed in triplicate.

Reverse phase-high performance liquid chromatography (RP-HPLC) was performed on an Agilent 1200 Series Infinity Star equipped with GABI detector, a UV detector and a ThermoScientific Hypersil ODS reverse phase C18 column (300 mm × 4.6 × 10 microns). We used an isocratic mode (flow rate 1 mL/min) and mobile phase consisted of a mixture of phosphate buffer 0.05 M, pH 5.1 (40 %) and acetonitrile (60 %). The injection volume was 30 µL and the detection was performed at a wavelength of 340 nm (Figures S9, S10, and S11).

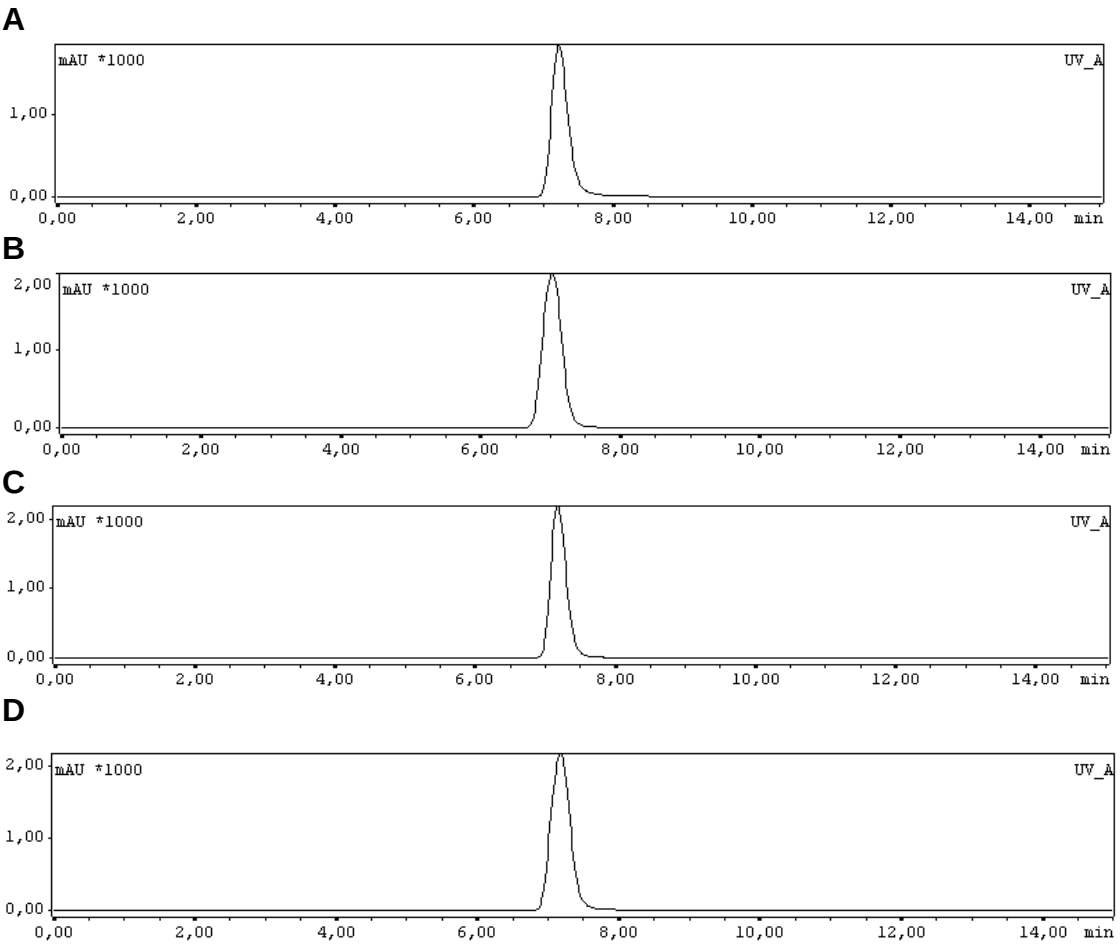


Figure S9. RP-HPLC profiles of erlotinib incubated on aqueous solutions according to Experimental (UV-detection, λ= 340 nm). **A**, without incubation; **B**, incubated at pH= 7.4; **C**, incubated at pH= 8.6; **D**, incubated at pH= 2.0.

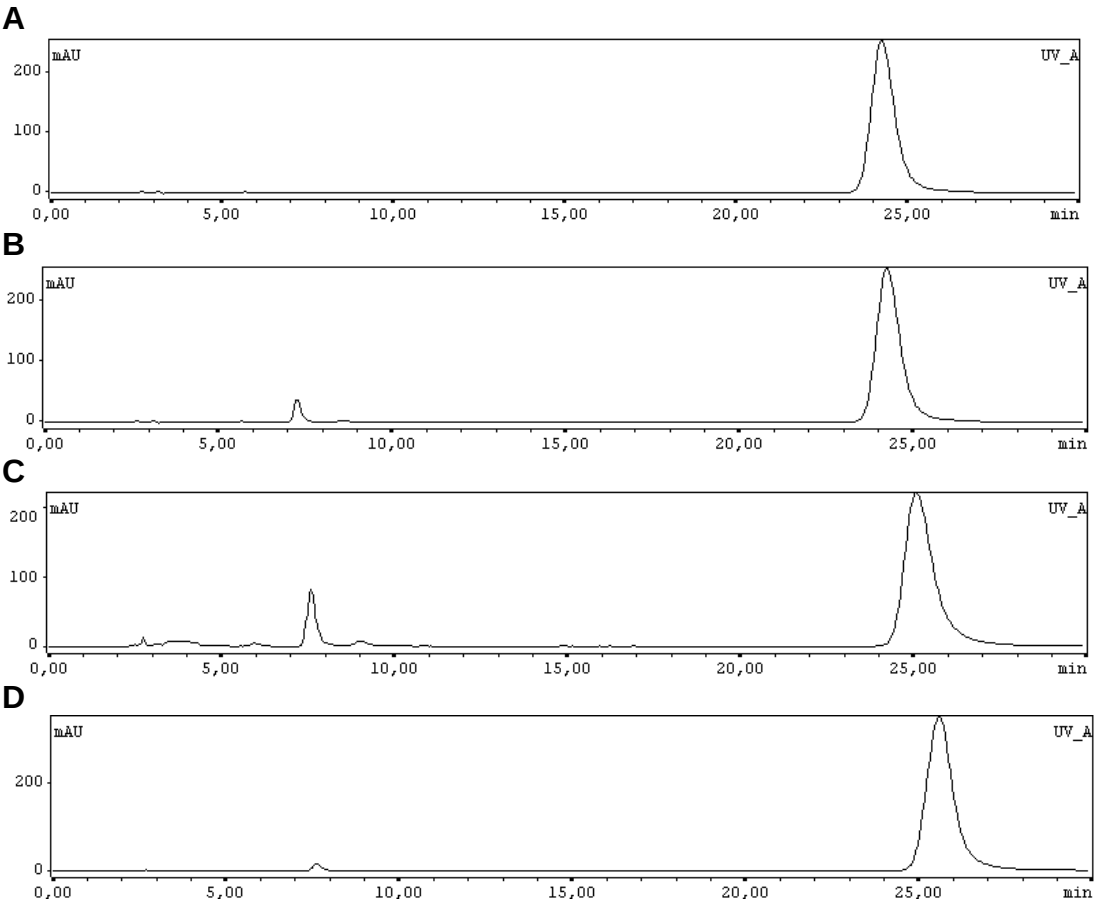


Figure S10. RP-HPLC profiles of the hybrid **1** incubated on aqueous solutions according to Experimental (UV-detection, λ= 340 nm). **A**, without incubation; **B**, incubated at pH= 7.4; **C**, incubated at pH= 8.6; **D**, incubated at pH= 2.0.

2.3 Incubation conditions for rat microsomal and cytosolic fractions

The standard incubation mixture contains $MgCl_2$ (1.3 mM), $NADP^+$ (0.4 mM), glucose 6-phosphate (3.5 mM), 0.5U ml^{-1} glucose 6-phosphate dehydrogenase in a phosphate buffer (0.1 M, pH 7.4) containing EDTA (1.5 mM) and the corresponding derivative (40 mM, from stock solutions in DMSO) with 1 mL of final volume. The final concentration of the DMSO in the incubation mixture was below 1.0 %. After pre-equilibration of the mixture at 37 °C, appropriate volumes of microsomal or cytosolic fraction were added to give a final protein concentration of 1 $mg.mL^{-1}$. The mixtures were incubated for 0.5 h, in 24-well plates open to the air, at 37 °C. The experiments were performed by triplicate. At the end of the incubation, 400 µL of methanol were added and the mixture was kept at 4 °C for protein precipitation. After centrifugation, the incubated mixtures were extracted with EtOAc (3 × 400 µL) and the organic layer was evaporated to dryness under reduced pressure. HPLC were done with the extracts in order to confirm or discard metabolism product presence. For this, we used isocratic mode (flow rate 1 mL/min) and mobile phase consisted of a

mixture of: phosphate buffer 0.01 M, pH 5.1 (40 %) and acetonitrile (60 %). The injection volume was 50 µL and the detection was performed at a wavelength of 340 nm (Figures S12, and S13).

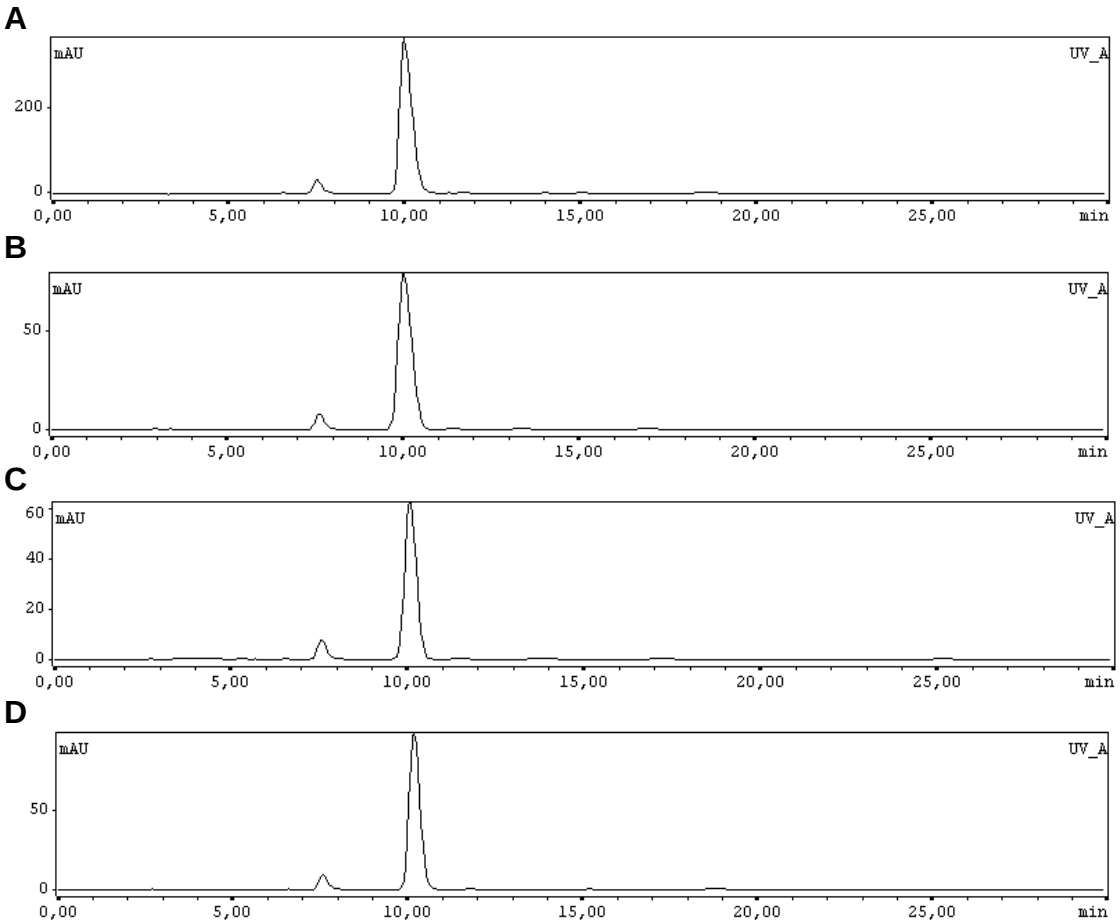


Figure S11. RP-HPLC profiles of the hybrid **4** incubated on aqueous solutions according to Experimental (UV-detection, λ= 340 nm). **A**, without incubation; **B**, incubated at pH= 7.4; **C**, incubated at pH= 8.6; **D**, incubated at pH= 2.0.

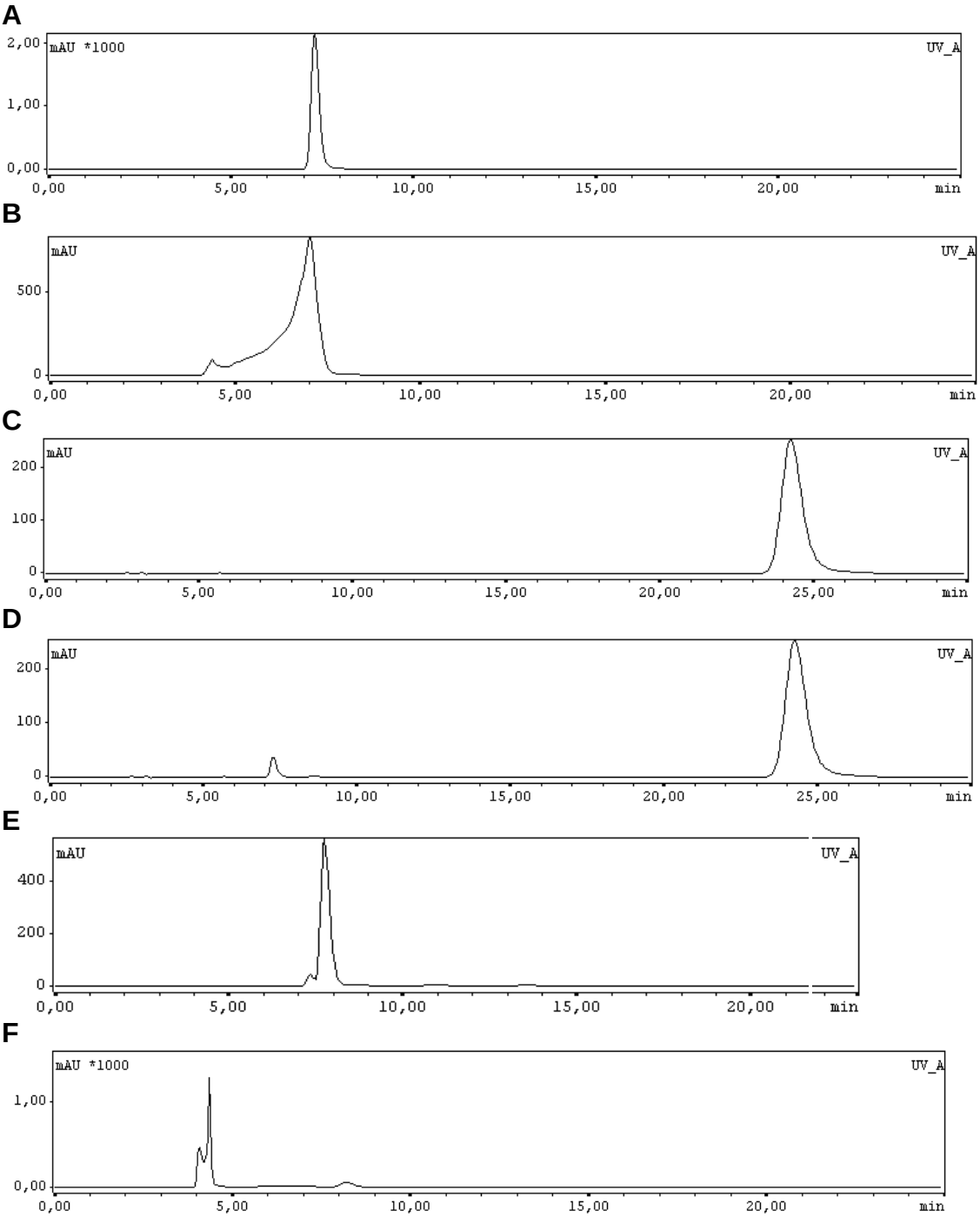


Figure S12. RP-HPLC profiles of the studied compounds incubated on rat hepatic cytosolic fraction according Experimental (UV-detection, λ= 340 nm). **A**, and **B**, erlotinib without and with incubation; **C**, and **D**, hybrid **1** without and with incubation; **E**, and **F**, hybrid **4** without and with incubation.

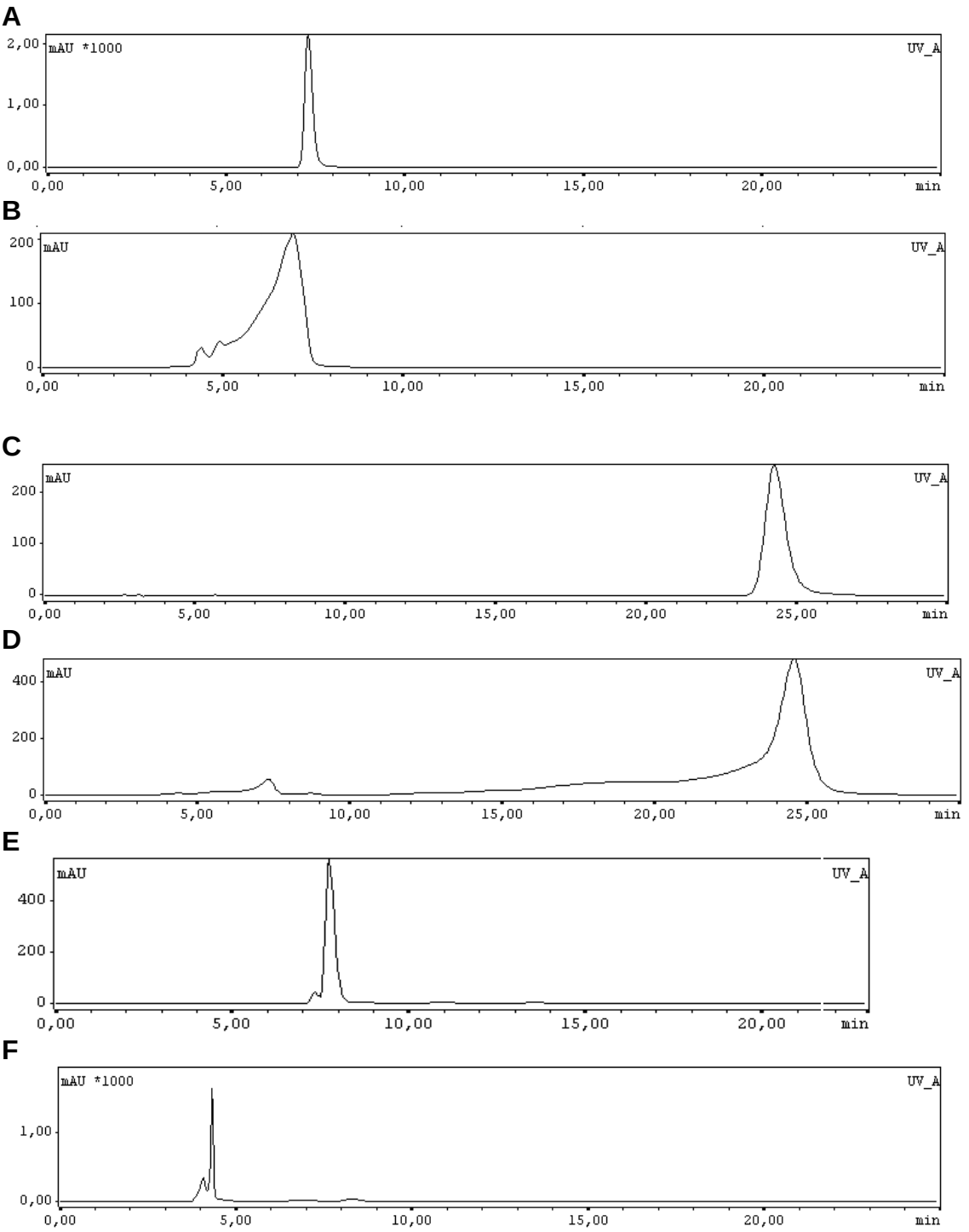


Figure S13. RP-HPLC profiles of the studied compounds incubated on rat hepatic microsomal fraction according Experimental (UV-detection, λ= 340 nm). **A**, and **B**, erlotinib without and with incubation; **C**, and **D**, hybrid **1** without and with incubation; **E**, and **F**, hybrid **4** without and with incubation.

References

1- S. Grimme, *J. Comput. Chem*. 2006, **27**, 1787.

2- M.J. Frisch, G.W. Trucks, H.B. Schlegel, G.E. Scuseria, M.A. Robb, J.R. Cheeseman, G. Scalmani, V. Barone, B. Mennucci, G.A. Petersson, H. Nakatsuji, M. Caricato, X. Li, H.P. Hratchian, A.F. Izmaylov, J. Bloino, G. Zheng, J.L. Sonnenberg, M. Hada, M. Ehara, K. Toyota, R. Fukuda, J. Hasegawa, M. Ishida, T. Nakajima, Y. Honda, O. Kitao, H. Nakai, T. Vreven, J.A. Montgomery, Jr., J.E. Peralta, F. Ogliaro, M. Bearpark, J.J. Heyd, E. Brothers, K.N. Kudin, V.N. Staroverov, R. Kobayashi, J. Normand, K. Raghavachari, A. Rendell, J.C. Burant, S.S. Iyengar, J. Tomasi, M. Cossi, N. Rega, J.M. Millam, M. Klene, J.E. Knox, J.B. Cross, V. Bakken, C. Adamo, J. Jaramillo, R. Gomperts, R.E. Stratmann, O. Yazyev, A.J. Austin, R. Cammi, C. Pomelli, J.W. Ochterski, R.L. Martin, K. Morokuma, V.G. Zakrzewski, G.A. Voth, P. Salvador, J.J. Dannenberg, S. Dapprich, A.D. Daniels, Ö. Farkas, J.B. Foresman, J.V. Ortiz, J. Cioslowski, and D.J. Fox, Gaussian 09, Revision E.01, Gaussian, Inc., Wallingford CT, 2009.

3- (*a*) G.M. Morris, R. Huey, W. Lindstrom, M.F. Sanner, R.K. Belew, D.S. Goodsell and A.J. Olson, *J. Comput. Chem*. 2009, **30**, 2785. (*b*) R. Tiwari, K. Mahasenan, R. Pavlovicz, C. Li and Werner Tjarks, *J. Chem. Inf. Model*. 2009, **49**, 1581.

4- M.F. Sanner, *J. Mol. Graph. Mod*. 1999, **17**, 57.

5- A. Oda, K. Ohta, Y. Endo, S. Fukuyoshi, Proceedings of the 37th Symposium on Chemical Information and Computer Science, 2014, Japan, doi: 10.11545/ciqs.2014.0_P02.

6- J. Stamos, M.X. Sliwkowski and C. Eigenbrot, *J. Biol. Chem*. 2002, 277, 46265.

7- OECD Guideline for the Testing of Chemicals, Adopted by the Council on 27th July 1995, Partition Coefficient (*n*-octanol/water): “Shake Flask Method.” 1995.

Research Article

For reprint orders, please contact: reprints@future-science.com

Future Medicinal Chemistry

Carboranylanilinoquinazoline EGFR-inhibitors: toward 'lead-to-candidate' stage in the drug-development pipeline

Marcos Couto[1], Catalina Alamón[1], Carina Sánchez[1], Belén Dávila[1], Marcelo Fernández[2], Nicole Lecot[1,3], Pablo Cabral[4], Francesc Teixidor[5], Clara Viñas[5] & Hugo Cerecetto*[,1,4]

[1]Laboratorio de Química Orgánica Medicinal, Instituto de Química Biológica

[2]Laboratorio de Experimentación Animal, Centro de Investigaciones Nucleares

[3]Laboratorio de Técnicas Nucleares Aplicadas a Bioquímica y Biotecnología, Centro de Investigaciones Nucleares

[4]Área de Radiofarmacia, Centro de Investigaciones Nucleares, Facultad de Ciencias, Universidad de la República, Montevideo (Uruguay)

[5]Institut de Ciències dels Materials de Barcelona-CSIC Campus, Bellaterra (Spain)

*Author for correspondence: Tel.: +598 25250800, hcerecetto@cin.edu.uy

Background: Carboranylanilinoquinazoline-hybrids, developed for boron neutron capture therapy, have demonstrated cytotoxicity against murine-glioma cells with EGFR-inhibition ability. In addition, their adequate aqueous/metabolic stabilities and ability to cross blood–brain barrier make them good leads as to become antiglioma drugs. **Aim:** Analyze drug-like properties of representative carboranylanilinoquinazolines. **Materials & methods:** To expand carboranylanilinoquinazolines therapeutic spectrum, we studied their ability to act against glioma-mammal cells, U-87 MG and other tyrosine kinase-overexpress cells, HT-29. Additionally, we predicted theoretically and studied experimentally drug-like properties, in other words, organisation for economic cooperation and development-recommended toxicity-studies and, due to some aqueous-solubility problems, and vehicularization for oral and intravenous administrations. **Conclusion:** We have identified a promising drug-candidate with broad activity spectrum, appropriate drug-like properties, adequate toxicological behavior and able ability to be loaded in suitable vehicles.

First draft submitted: 4 March 2019; Accepted for publication: 22 May 2019; Published online: TBC

Keywords: acute oral toxicity • Ames test • carboranylanilinoquinazoline • HT-29 cytotoxicity • nanovehicles • U-87 MG cytotoxicity

Glioblastoma multiforme (GBM) is a malignant tumor from glial cells with the highest frequency among brain tumors, with a very low survival rate and a limited prognosis, despite the variety of modern therapies and diagnostic advances [1]. According to WHO more than 50 % of diagnosed gliomas are the most malignant form of the glioblastoma, in other words, grade IV type [2]. Despite the GBM heterogeneity some common molecular characteristics could be stated [3], like the amplification of EGFR [3]. This receptor, EGFR, is a member of transmembrane tyrosine kinase receptor ErbB family that its activation promotes tumoral growth and progression, via angiogenesis, invasion and metastasis, and additionally resistance to drugs and inhibition of apoptosis is involved [4]. For that reason, the anilinoquinazolines erlotinib, gefitinib, vandetanib, lapatinib and CUDC-101 have been studied in GBM as small-drugs, which target the tyrosine kinase receptors. Specifically, the tyrosine kinase inhibitor erlotinib (erl, Figure 1) prevents the intracellular autophosphorylation of the EGFR tyrosine kinase domain. Erlotinib has been used in glioblastoma, for example, in combination with temozolomide, a classical methylating agent for GBM, resulting well-tolerated and improving patients survival [5]. Other assayed GBM-therapy has been boron neutron capture therapy (BNCT). BNCT is a noninvasive chemotherapy modality for treating locally invasive malignancies. The mode of action of BNCT is based on the production of harmful ions by nuclear reaction, $^{10}B(n,\alpha)^{7}Li$, between nonradioactive nuclide ^{10}B (20 % of natural abundance) and thermal neutrons [6]. Initially, the nuclear reaction produces excited ^{11}B that after a fast nuclear fission yields both reactive α-particle ($^{4}He^{2+}$) and ^{7}Li nucleus ($^{7}Li^{3+}$). Because of the short trajectory of these cations, near to 10 μm, the radiation damage is confined to the tumoral cells loaded with ^{10}B-containing compound [7]. Although BNCT has

newlands press

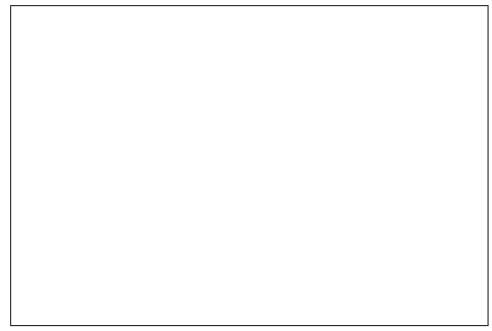


Figure 1. Tyrosine kinase receptor inhibitor erlotinib, boron neutron capture therapy-agent BSH and general structure of carboranylanilinoquinazoline developed as hybrids (X: variable) [11]. .

also been used in the treatment of melanoma, liver and colon tumors [8,9], most studies to date have focused on the treatment of GBM. Regarding to clinical agents used in BNCT the BSH (disodium ^{10}B-mercaptoundecahydro-*closo*-dodecaborate, Figure 1) is one of the most relevant. Nevertheless, it is not selectively accumulated into tumor cells, which results in cytotoxicity and limits its application [10].

Recently, combining both concepts, TK inhibitors incorporating boron-rich moieties have been exploited as bifunctional hybrid boron-containing drug targeting within glioma cells (Figure 1) [11–13]. However, the developed boronic-acid derivatives [12] could have limited application in BNCT due to the low concentration of boron in the cells. But, on the other hand, carboranyl derivatives [11,13] have high boron content, which is optimal for BNCT use, and also have favorable drug-like properties. In this sense, carboranyl-erlotinib derivatives, in other words, **1–10** (Table 1), have been studied as cytotoxic agents for glioma cells with potential applicability in BNCT [11]. Some of these derivatives, in other words, **1–3** and **9**, were more cytotoxic against murine-cells C6 than erl and selective for the glioma-system (Table 1). In regards to their mechanism of action, EGFR-inhibition ability could be, at least in part, responsible for their bioactivity (Table 1) [13]. Additionally, the most interesting hybrid, in other words, **1**: was able to inhibit one of the EGFR mutated form (EGFR T790M), with an IC_{50} of 1.125 μM, were erlotinib was ineffective [13]; displayed aqueous/metabolic stability; and showed ability to cross blood–brain barrier (BBB, Table 1).

These studies [11,13] have arisen lead-compounds for BNCT-glioma treatment, in other words, derivatives **1–3** and **9**. However, in order to fully assess the safety profile so as to turn them into drug-candidates further studies are needed. In this study, we analyze some relevant features necessary to propose these compounds as drug candidates. On the one hand, we confirmed their ability to act against glioma-mammal system, using U-87 MG cells, and expanded their therapeutic spectrum evaluating them against another tumoral model, HT-29 colon-cells which express high contents of EGFR. Second, we predicted some drug-like descriptors theoretically and others experimentally studying the *in vitro* mutagenic potential and *in vivo* oral LD_{50} value for derivative with the best performances in the previous studies, in other words, **1**. And finally, in order to avoid some aqueous-solubility and potential low-bioavailability problems, different vehicles for oral and intravenous administrations were studied.

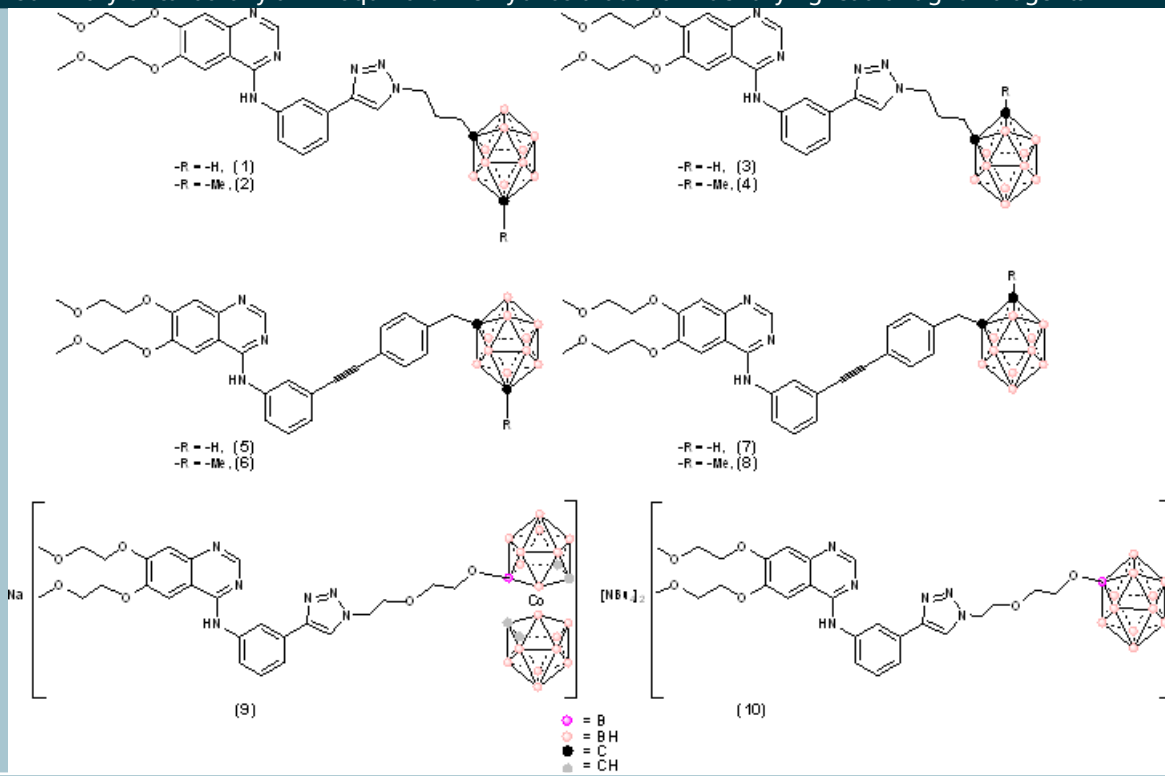
Materials & methods

General

Chemicals & reagents

Hybrids **1–10** were prepared according to literature [11,13] and erl was purchased from Hong Kong Guokang Bio-Technology Co. (Baoji, China); Pluronic® F127 (F127), Pluronic® L121 (L121) and Tetronic® T1307 (T1307) were gifted by BASF Corporation (NJ, USA). Fetal bovine serum, penicillin, streptomycin, phosphate-buffered saline (PBS), DMSO, trichloroacetic acid, sulphorhodamine B (SRB), unbuffered Tris Base, sodium chloride, polysorbate 80 (Tween 80™), and cholesterol were obtained from Sigma–Aldrich Co. (MO, USA). Dulbecco's modified Eagle's milieu high glucose with stable glutamine with sodium pyruvate milieu was obtained from Capricorn Scientific GmbH (Ebsdorfergrund, Germany). Phosphatidylcholine was obtained from Avanti Polar Lipids Inc. (AL, USA). Difco Bacto® agar milieu was obtained from Werner Lab (Montevideo, Uruguay). In all the experiments, MilliQ ultrapure water was used.

Table 1. Summary of carboranylanilinoquinozaline-hybrids that allow identifying lead antiglioma agents.



Cpd	$IC_{50,C6}$ †	$IC_{50,EGFR}$ ‡	Stabilities		BBB#	Cpd	$IC_{50,C6}$ †	Cpd	$IC_{50,C6}$ †	$IC_{50,EGFR}$ ‡	Stabilities		BBB#
			aq§	hep¶							aq§	hep¶	
1	30††,‡‡	2.3	S§§	S	(+)¶¶	**5**	>100	**9**	44‡‡,##	296.3	S	NS†††	(-)‡‡‡
2	99	312.2				**6**	>100	**10**	>100				
3	34‡‡,§§§					**7**	>100						
4	>100					**8**	>100	**erl**	>100‡‡,¶¶¶	22.9	S	PS###	(±)††††

†Concentrations, in μM, required to inhibit the C6 growth by 50 %. C6 cells consist on a rat glioma cell line that overexpress of EGFR21f [11].
‡Concentrations, in nM, required to inhibit the phosphorylation of the poly(Glu:Tyr) substrate by 50 % [13].
§In aqueous-buffer solutions at 2.0, 7.4 and 8.6 pH [13].
¶In hepatic cytosolic and microsomal fractions [13].
#Ability to cross BBB [13].
††Selectivity index ($IC_{50,mix\ of\ primary\ glial\ cells}$ / $IC_{50,C6\ cells}$) = 3.3.
‡‡From [11].
§§S over a period of 24 h incubation for aqueous solutions or over a period of 30 min for hepatic fractions, @ 37°C.
¶¶Able to cross BBB;
##Selectivity index ($IC_{50,mix\ of\ primary\ glial\ cells}$ / $IC_{50,C6\ cells}$) = 2.3.
†††NS over a period of 30 min incubation, @ 37°C.
‡‡‡Unable to cross BBB.
§§§Selectivity index ($IC_{50,mix\ of\ primary\ glial\ cells}$ / $IC_{50,C6\ cells}$) = 2.9.
¶¶¶Higher doses than 100 μM could not be evaluated due to solubility problems.
###SP over a period of 30 min incubation, @ 37°C.
†††Medium ability to cross BBB.
BBB: Blood-brain barrier; NS: Nonstable; S: Stable SP: Partial metabolism.

Cell lines & culture conditions

The cells, in other words, mammal malignant glioblastoma cell line U-87 MG (HTB-14™, ATCC®), mammal colon adenocarcinoma cell line HT-29 (HTB-38™, ATCC®) and rat astrocytoma derived cell line C6 (CCL-107™, ATCC®), were cultured in Dulbecco's modified Eagle's milieu high glucose (4.5 g/l), with stable glutamine, with sodium pyruvate milieu supplemented with 10 % inactivated fetal bovine serum and penicillim/streptomycin (1 %). The cells were cultured at 37°C under a 5 % CO_2 humidified environment, the milieu was changed every 2–3 days, and cells were subcultured once they reached 90–95% confluence.

10.4155/fmc-2019-0060

Animals

All protocols for animal experimentation were carried out in accordance with procedures authorized by the University's Ethical Committee for Animal Experimentation, Uruguay, to whom this project was previously submitted. The authors state that they followed the principles outlined in the Declaration of Helsinki for all animal experimental investigations. Animals were housed in wire mesh cages at 20 ± 2°C with 12 h light-dark cycles. The animals were fed *ad libitum* to standard pellet diet and water, and were used after a minimum of 3 days acclimation to the housing conditions.

In vitro cytotoxicity assays

Cells were seeded in 96-well plates (7000–10000 cells/well) in 100 µl final volume and allowed to grow 24 h. After that, 125 µl of fresh culture milieu was added and the cells were allowed to grow again for additional 24 h. Then, 25 µl of a solution of desired dose of the tested compounds in the culture milieu and 1 % DMSO were added onto the cells and further incubated for 24 h. Afterward, culture milieu was removed and cells were washed twice with 200 µl of PBS. Then, they were fixed with trichloroacetic acid (50 µl) for 60 min at 4°C. After that the plates were washed with distilled water (×5) and dried in the air. About 50 µl of SRB solution was added to each well and allowed staining for 30 min at room temperature. The plates were washed quickly with acetic acid (1% v/v) until excess dye was fully removed (at least five-times) and dried in the air. The bound SRB was solubilized by adding unbuffered Tris Base (10 mM, pH 10.5) (100 µl), and the resulting solution was shook for 5 min on a shaker platform and the optical density (OD) was read at 540 nm. Cell viability percentage (CV%) was calculated according to the following equation: CV% = $(A_{540} - B)/(C - B)$, where A_{540} is the OD of the studied wells, B is the OD of untreated wells (without cells) and C is the OD of control wells (cells treated with 1 % of DMSO). CV% values were plotted against studied compound doses and the IC_{50} values were determined.

Drug-like properties prediction

Drug-like properties were calculated using admetQSAR tool kit (http://lmmd.ecust.edu.cn/admetsar1/predict/) from the molecule SMILE code generated with ChemDraw Standard 14.0 software.

In vitro genetic-toxicity

Salmonella typhimurium TA 98 strain was incubated in agar minimum glucose milieu solution (Difco Bacto® agar) and aqueous glucose solution (40 %). First of all, the direct toxicity of the hybrid **1** against *S. typhimurium* TA 98 strain was studied. From these data, the mutagenic assay was performed. Briefly, **1** in phosphate buffer (0.1 M, pH 7.4) and DMSO (10 % v/v) at seven doses, 1000.0, 333.0 166.0, 111.0, 83.0, 66.7 and 55.0 µg/plate, starting at the highest doses without toxic effects (1000.0 µg/plate), were studied in triplicate. When the influence of metabolic activation was analyzed, **1**, at the same seven doses, was mixture with S9 fraction of mouse liver (Moltox, Inc., MD, USA) (500 ml) instead of phosphate buffer. Controls: positive control in the assay without S9 activation: 4-nitro-*o*-phenylendiamine (NPD, 20.0 mg/plate); positive control in the assay with S9 activation: 2-aminofluorene (2AF, 10.0 mg/plate); negative control: phosphate buffer and DMSO (10 % v/v) (no effect on cells growth was observed by this mixture of solvents). The revertant numbers were counted and the studied system was considered mutagenic if the colonies number was at least doubled the natural revertants (negative control) for two or more consecutive doses.

In vivo oral acute-toxicity

Formulation of **1** for *in vivo* trial: compound **1** was suspended in a mixture of sterile physiological saline/Tween 80 (4:1) solution (96 %) and DMSO (4 %) (vehicle solution), immediately prior to oral administration. This preparation was made under aseptic conditions.

Animals: the experiments were carried out on 7- to 8-week-old Balb/c female mice (17.6–18.0 g of body weight [bw]) bred under specific pathogen-free conditions. At the end of experiments, they were anesthetized with isoflurane and sacrificed by cervical dislocation.

'Limit test' treatment: each animal, n = 3, was dosed with **1**, at 2000 mg/kg bw (0.5 ml of suspension), orally using an intragastric syringe. Animals were observed individually, submitting them to Irwin test, after dosing during the first 0.5, 1.5, 3, 5, 12, 24, 48 and 72 h, and daily until day 14. The observations were recorded individually for each animal. According to OECD recommendations changes in skin and fur, changes in eyes and mucous membranes, respiratory-, circulatory-, autonomic-, CNS- and somatomotor activity-changes and behavior pattern,

presence of tremors, convulsions, salivation, diarrhea, lethargy, sleep and coma, were recorded. Daily individual weight of each animal was determined. Weight changes were systematically recorded. At day 14, surviving animals were weighed and humanely killed. Then each animal was subjected to gross necropsy. All gross pathological changes were recorded for each animal. A new cycle with three animals was repeated using 2000 mg/kg bw of 1 orally administered. The observations were repeated for this group of animals during 14 days.

Formulations

Preparation of compounds-loaded polymeric micelles

Polymeric micelles (PM) encapsulated compounds systems were fabricated by direct hydration method. For 1 mg of compound 1 used 270 mg of mixture composed of Pluronics F127 and L121 or 150 mg of mixture composed of Pluronic F127 and Tetronic T1307. The hydration of all the copolymers was performed by the addition of water (2.5 ml). The preparation was left overnight at 4°C. Then, water was added up to 3.0 ml, final volume, at room temperature. Finally, compound **1** was added (1 mg/ml) and the preparation was stirred for about 3 h to obtain a solid compound/copolymer matrix.

Preparation of compounds-loaded liposome

Compounds-containing liposomes were fabricated by thin-film hydration method. About 3 mg of compound 1, 165.4 mg of phosphatidylcholine and 50 mg of cholesterol were dissolved in 12.5 ml of chloroform in a round-bottom flask. The solvent was evaporated by rotary evaporation at 50°C for about 1 h to obtain a thin film that was hydrated with 3 ml of PBS (50 mM, pH 7.01). The mixture was stirred at 700 rpm for 30 min and at 50°C to obtain a micelle solution. Immediately, the liposomes were formed by pressure extrusion using an Avanti Mini Extruder. The resulting multilamellar liposomes were subjected to 11 passages through Whatman polycarbonate filters having pore diameters of 400, 200 and 100 nm.

Determination of particle size & ζ potential

The average size of the formulations and their polydispersity index (size distribution) were determined by dynamic light scattering method (Zetasizer Nano-ZS, Malvern Instruments, UK) with a dispersion instrument equipped with a laser He-Ne (633 nm) and a digital correlator, model ZEN3600. Measurements, after adequate dilution with water at 25°C, were made in triplicate at an angle of dispersion of 173° and a fixed laser light of 4.65 mm. The measurements were taken immediately prior to cytotoxicity tests. The same conditions and equipment were used to measure ζ potential. The data are represented as mean ± SD.

Results & discussion

In vitro activity against other overexpressing EGFR-cells

To confirm the potential use as drug of hybrid carboranylanilinoquinazolines (Table 1), cytotoxicity assays were performed using different kind of human cells. On the one hand, U-87 MG (HTB-14™, ATCC®) cell line was employed, which are cells derived from *Homo sapiens* malignant gliomas that overexpresses EGFR [14]. On the other hand, HT-29 (HTB-38™, ATCC®), derived cells from *H. sapiens* colorectal adenocarcinoma EGFR-overexpressing [15], was also included as manner to potentially expand BNCT-strategy in other tumoral pathology [8].

The studied hybrids **1–10** were active, displaying different level of cytotoxicities against both mammal cells (Table 2). For both cellular systems, the hybrids with an ethynylbenzyl linker, **5–8**, were the least active while the hybrids with a [1,2,3]triazolylpropyl linker, **1–4** and **9**, were among the most active. This effect is in concordance with those shown in C6 cell line [11]. Additionally, we observed that carboranyl isomer type or carbon cluster pattern substitution plays a key role in the bioactivity. Against HT-29 cells, compounds **1** and **2**, *meta*-carboranyl-isomers, were more active than the corresponding *ortho*-isomers **3** and **4** (Table 2). This could be partially explained by the difference of the dipole moments and hydrophobicity of *closo*-carboranyl moiety, which is strongly dependent on the position of the carbon atoms in the carboranyl cage. The hydrophobicity of *closo*-carboranyl isomers increases in the following order: *ortho* < *meta* < *para*. On the other hand, the methyl-substitution, in the *ortho* or *meta* position, in other words, hybrids **2** and **4**, produced a decrease of the cytotoxicity on colon tumoral cells compared with the unsubstituted analogs, in other words, **1** and **3**. These effects of the structural-features that decorate the anilinoquinazoline system were also observed previously in C6-glioma cell line [11].

Table 2. *In vitro* activity of carboranylanilinoquinozaline-hybrids and erl against *Homo sapiens* glioma- and *Homo sapiens* colorectal adenocarcinoma cells.

Cpd	$IC_{50,U\text{-}87\ MG}$ †	$I_{C50,HT\text{-}29}$ †	Cpd	$IC_{50,U\text{-}87\ MG}$ †	$I_{C50,HT\text{-}29}$ †	Cpd	$IC_{50,U\text{-}87\ MG}$ †	$I_{C50,HT\text{-}29}$ †
1	70.0	25.0	**5**	NS‡	100.0	**9**	23.0	25.0
2	NS	45.0	**6**	NS	100.0	**10**	NS	100.0
3	49.0	100.0	**7**	NS	100.0			
4	NS	>100.0	**8**	>100.0§	100.0	**erl**	63	>100.0§

†Concentrations, in μM, required to inhibit the cellular growth by 50 %. They were determined from dose-response curves and represent the mean ± SD. All experiments were repeated at least three-times.
‡Not studied.
§Higher doses than 100 μM could not be evaluated due to solubility problems.

Among the ionic derivatives, compound **9** was the most active in both EGFR-overexpressing cells. However, in spite of the activity displayed and the fact that it could deliver two-times more boron atoms per molecule, no further assays were performed due to the unfavorable stability and the BBB parameters observed.

Some aqueous solubility problems, mainly with the parent EGFR-inhibitor erl (Supplementary Material), was evidenced in these *in vitro* assays.

Hybrids **1–3**, and **9** displayed similar or better biological activities against U-87 MG and/or HT-29 than erl.

Drug-like properties

Predictions

In early stage of drug development, the knowledge of absorption, distribution, metabolism, excretion and toxicity (ADMET) properties are relevant for the selection of potential drug candidates. In addition, the theoretical predictions could provide clear and compelling advantages in decision-making for drug candidates.

In this study, we determined some drug-like predictors for selected carboranylanilinoquinazoline derivatives using the admetQSAR tool kit [16] (Table 3). Specifically, we focused in human intestinal absorption, Caco-2 permeability, P-glycoprotein (P-gp) inhibition, renal organic cation transporter (OCT2) inhibition, ability to be substrate of CYP450s, human ether-a-go-go-related gene (hERG) inhibition and carcinogen effects. Compounds **1-4**, **8** and **9**, were compared against the parent compound erl. On the other hand, we predicted the aqueous solubility (LogS) for 8 and erl due to the solubility problems observed in the *in vitro* assays. Finally, using the previously described LogD [13], we analyzed the fitting on Lipinski's 'rule of five' and the binding affinity to EGFR through the lipophilic ligand efficiency descriptor (LLE = pIC_{50} - LogD) for the most relevant compound, in other words, **1**, **9** and erl.

One of the most important challenges in the oral process is the absorption of the drug across the intestinal epithelial barrier. Herein, the predicted HIA parameter showed that most of the derivatives were positive, indicating that they could be absorbed to the bloodstream. However, Caco-2 permeability [21,22] was less than 8×10^{-6} cm/s for all the analyzed hybrids, no finding differences according to the type of substructures. This aspect should be considered at the moment to select the administration route of the drug. Transport of drugs by P-gp is another widely studied parameter in the early stage of the drug design process. P-gp, a member of the ATP-binding cassette family, extensively distributed and expressed in many human organs working as an efflux pumps in different tissues, in other words, intestinal epithelium, hepatocytes, renal proximal tubular cells, adrenal gland and endothelial capillaries of the brain [19,20]. Additionally, overexpression of P-gp has been demonstrated to generate resistant phenotypes in various tumors [19,20]. According to prediction, all the studied hybrids were potential substrate of P-glycoprotein (data not shown) and non-P-gp-inhibitors. However, derivatives **2** and **4**, methyl-substituted belonging to [1,2,3]triazolylpropyl derivatives like erl**,** were predicted as inhibitors with one of the methods and could be taken into account, in further synthetic developments, as an efficient way of sensitizing drug resistance in cancer chemotherapy.

In reference to the drug elimination processes, kidneys have a key role in the elimination of cationic drugs among others [28]. The organic cation transporter 2 (OCT2) is involved in the initial step of renal secretion at the proximal tubule in the kidney [23]. Several drugs have been classified as substrate or inhibitor of OCT2 leading to potential drug–drug interactions. Due to the presence of a system susceptible to protonation, such as the amino-quinazoline feature in the studied compounds, we evaluated the potential inhibition of OCT2. All the studied hybrids and erl were predicted as noninhibitor of OCT2 indicating the potential absence of renal drug–drug interactions problems.

Table 3. Drug-like properties of the carboranylanilinoquinazolines studied herein and erl.

	Absorption				Metabolism	Toxicity		LogS[§§]	$LogD_{7.4}$[¶¶]	Rule 5	LLE[†††]
Cpd	HIA[†]	Caco-2[‡]	P-gp inh[§]	OCT2 inh[¶]	CYP-subs[#]	hERG[††]	Carc[‡‡]			n viol[##]	
1	(+)	(-)	(-)	(-)	CYP450 3A4	w-inh [17] inh [18]	(-)	−3.13	3.10	1[‡‡‡]	5.54
2	(+)	(-)	(+) [19] (-) [20]	(-)	CYP450 3A4	w-inh [17] inh [18]	(-)	−3.23	-	1[‡‡‡]	-
3	(+)	(-)	(-)	(-)	CYP450 3A4	w-inh [17] inh [18]	(-)	−3.13	-	1[‡‡‡]	-
4	(+)	(-)	(+) [19] (-) [20]	(-)	CYP450 3A4	w-inh [17] inh [18]	(-)	−3.23	-	1[‡‡‡]	-
8	(-)	(-)	(-)	(-)	CYP450 3A4	w-inh [17] inh [18]	(-)	−3.29	-	1[‡‡‡]	-
9	(+)	(-)	(-)	(-)	CYP450 3A4	w-inh [17] inh [18]	(-)	−3.20	2.51	2[§§§]	4.02
erl	(+)	(+)	(+) [19] (-) [20]	(-)	CYP450 3A4	w-inh [17] non [18]	(-)	−3.16	2.45	0	5.19

[†]Human intestinal absorption: if the compound has the HIA% less than 30 %, it is labeled as (-), otherwise it is labeled as (+) [21].
[‡]Caco-2 permeability. If the compound has the Caco-2 permeability value $\geq 8 \times 10^{-6}$ cm/s, it is labeled as high Caco-2 permeability (+) otherwise it is labeled as moderate-poor permeability (-) [22].
[§]P-glycoprotein inhibition [19,20]. Noninhibition is labeled as (-) otherwise it is labeled as (+).
[¶]Renal organic cation transporter (OCT2) inhibition [23]. Noninhibition is labeled as (-) otherwise it is labeled as (+).
[#]Ability to be substrate of three cytochrome P450 isoenzymes (CYP450 2C9, CYP450 2D6 and CYP450 3A4) [24]. It is shown the predicted isoform-CYP that the compound potentially acts as substrate.
[††]Human ether-a-go-go-related gene inhibition [17,18]. Noninhibition is labeled as 'non', weak-inhibition is labeled 'w-inh' and inhibition is labeled 'inh'.
[‡‡]Potential as carcinogens [25]. Noncarcinogen is labeled as (-).
[§§]Aqueous solubility [26].
[¶¶]Distribution coefficient at pH 7.4, from [13].
[##]Number of violations of 'rule of five'.
[†††]Lipophilic ligand efficiency (pIC_{50} - $LogD_{7.4}$) [27].
[‡‡‡]MW higher than 500 Da.
[§§§]MW higher than 500 Da and hydrogen bond acceptors higher than 10.
HIA: Human intestinal absorption; LLE: Lipophilic ligand efficiency.

Regarding to metabolism predictors, we analyzed the hybrids as substrate of Cytochrome P450 isoenzymes (CYPs). Nowadays, metabolization by CYP superfamily, together with P-gp, are the main cause of adverse drug reactions that lead to withdraw products from the market [29]. CYP3A4, one of the analyzed CYPs, is located in small bowel and liver and responsible for the oral drug administered metabolism [30]. Hybrids **1–4**, **8** and **9**, like erl were classified to be substrate of CYP450 3A4; consequently, this aspect should be considered when the administration route is selected.

In order to inquire about cytotoxicity, we estimated the ability of hybrids to inhibit hERG and to act as carcinogens. In reference to hERG inhibition, the hybrids were classified as weak inhibitors or inhibitors, according to the prediction-methods, while erl was predicted as noninhibitor in the method described by Wang *et al.* [18]. However, experimentally erl was identified as hERG-weak inhibitor [31] compared with other tyrosine kinase inhibitors. On the other hand, carcinogen effects were discarded according to Lagunin *et al.* classification [25]. Absence of mutagenicity against *S. typhimurium* [32], and LD_{50}, rat acute toxicity by oral exposure [33], higher than 2000 mg/kg of body weight were also predicted for all the hybrids, and erl, (data not shown). Additionally, both properties were also experimentally studied for hybrid **1** and the classifications confirmed, leading this derivative as a potential candidate for further studies (see next section).

Aqueous solubility and Lipinski's 'rule of five' are among the most common drug-properties filters. For that reason, LogS was predicted for all derivatives finding values in an adequate range for a drug candidate (LogS higher than -5 [26]). Specifically, hybrids **1** and **3** are more soluble in water than erl suggesting that they could be administrated orally or intravenously. As expected, LogS variations were observed due to different structural features, such as methyl-substituent or ethynylbenzyl linker decreasing both the water solubility of compounds bearing these moieties (Table 2) and it could be taken into account in further synthetic efforts. Surprisingly, the ionic hybrid **9** was predicted with lower solubility than erl. In reference to the 'rule of five', unlike erl the hybrids **1–4**, **8** and **9** possess molecular weight greater than 500 Da. Additionally, hybrid **9** has a number of hydrogen bond acceptor, according to Lipinski definition, higher than 10.

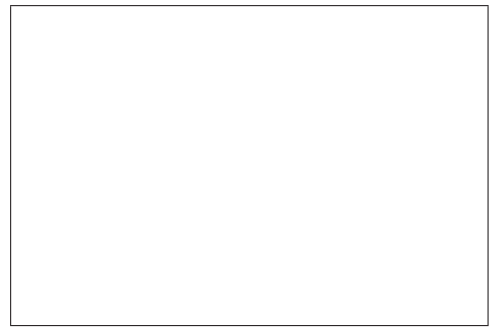


Figure 2. Number of revertant of *Salmonella typhimurium* strain TA98, in the absence (-S9) and presence (+S9) of metabolic activation, incubated with hybrid 1 at different doses. Cutoff is defined as twice of the natural revertants produced by the vehicle control (DMSO) treatments. Number of revertants for NPD (positive control, -S9): 317; number of revertants for 2AF (positive control, +S9): 80.

Table 4. Summary of *in vivo* oral acute-toxicity for hybrid 1.

Administration via	Vehicle	LD_{50} (mg/kg bw)	Irwin test[†,‡]	Necropsies observation[§]
Oral	Saline:Tween 80 (4:1)[¶]	>2000	(+)	(-)

[†]According to [37].
[‡]The test was performed at 0.5, 1.5, 3, 5, 12, 24, 48 and 72 h postoral administration. If all the analyzed parameters were similar than saline treatment, it is labeled as (+) otherwise it is labeled as (-).
[§](-) Denotes absence of organs alterations or organs adherences.
[¶]DMSO (4 %) was added to allow the complete solubilization of **1**.

Finally, the LLEs were determined using $LogD_{7.4}$ values reported previously for derivatives **1**, **9** and erl [13]. LLE is a simple but relevant index (LLE = pIC_{50} - $LogD_{7.4}$) that combines *in vitro* potency and lipophilicity estimating the effectiveness of a drug-biomolecule interaction with respect to the physicochemical properties of the drug. The LLE ideal value for an drug candidate is ranged between 5 and 7 units [34], showing near to 10^6-fold higher affinity to the biotarget compared with *n*-octanol. Derivative **1** stood out among the studied compounds having better behavior than erl and hybrid **9**.

Estimating the efficiency of a binding interaction with respect to the magnitude of the physical properties of the ligand.

In these predictions hybrid **1** displayed similar or better drug-like properties than the parent EGFR-inhibitor erl.

In vitro genetic- & in vivo oral acute-toxicity

In order to gain further information about the potentiality of hybrid **1** as drug candidate, supplementary studies related to toxicity were experimentally conducted. We centered our attention in some of the OECD recommendations, specifically *in vitro* genetic toxicity, in other words, mutagenicity, and *in vivo* median lethal oral dose, in other words, LD_{50}, were explored [35,36].

In the *in vitro* genetic toxicity, in other words, Ames test, we classified hybrid **1** as nonmutagenic, without and with metabolic activation (Figure 2), as no dose-response was observed, working with a wide range of dose of **1**, and in all the cases the number of revertants were lower than twice-values of vehicle control (cut-off lines, Figure 2).

In reference to the *in vivo* oral toxicity, we applied 'limit test' recommended by OECD [36] due to the admetQSAR prediction of **1**-no toxicity (see previous section). Table 4 summarizes the results of the analyses performed showing the safety profile of hybrid **1**.

Formulations

Due to the aqueous solubility problems observed in some hybrids, in other words, derivative **8**, and erl (Table 2 and Table 4 footnotes), we analyzed different alternative formulations for solubilization, including polymeric micelles and liposomes.

As first formulation, we used PMs systems, combining Pluronic® block copolymers F127 (hydrophilic) and L121 (hydrophobic) or the hydrophilics Pluronic® F127 and Tetronic® T1307 [38,39]. First, to study these PMs,

Table 5. Example of characterization of some hybrids-formulations developed herein.

Nanovehicle	Loaded with†	T (K)	Peak 1		Peak 2		PDI§
			D_h (nm)‡	%	D_h (nm)‡	%	
F127/L121	-	298	442.3 ± 18.7	100	-	-	0.252 ± 0.029
		310	340.3 ± 6.3		-	-	0.172 ± 0.012
	8	298	359.5 ± 14.2		-	-	0.234 ± 0.020
		310	322.1 ± 4.0		-	-	0.207 ± 0.006
F127/T1307	-	298	57.38 ± 1.83	70.3 ± 0.9	1537 ± 263	29.7 ± 2.3	0.530 ± 0.028
	1		57.10 ± 1.83	14.8 ± 2.6	1346 ± 253	86.2 ± 9.3	0.865 ± 0.292
Liposome	-	298	261.8 ± 14.1	100	-	-	0.490 ± 0.034
	1	298	321.6 ± 0.3		-	-	0.280 ± 0.009
		310	323.4 ± 4.5		-	-	0.269 ± 0.002

†In a concentration of 1 mg/ml.
‡Particle size.
§Polydispersity index.
PDI: Polydispersity index.

Table 6. *In vitro* activity of 1, 8 and erl alone and vehiculizated with F127/T1307 or liposome.

	Without vehicularization		F127/T1307		Liposome	
Cpd	$IC_{50,C6}$†,‡	$IC_{50,U\text{-}87\ MG}$†,§	$IC_{50,C6}$†	$IC_{50,U\text{-}87\ MG}$†	$IC_{50,C6}$†	$IC_{50,U\text{-}87\ MG}$†
1	30.0	70.0	>100.0¶	>100.0¶	14.0	6.25
8	>100.0¶	>100.0#	>100.0¶	NS††	NS	NS
erl	>100.0#	63	>100.0¶	>100.0¶	>100.0¶	17.0

†Concentrations, in μM, required to inhibit the cellular growth by 50 %. They were determined from dose-response curves and represented the mean ± SD. All experiments were repeated at least three-times.
‡From Table 1 [11].
§From Table 2.
¶Maximum evaluated doses.
#Higher doses than 100 μM could not be evaluated due to solubility problems.
††Not studied.
NS: Not studied

we selected the insoluble hybrid **8** and it was loaded in the F127/L121 system generating a formulation with homogeneous and adequate particle size (Table 5). However, similarly to what it was described for other cells [40], the observed C6-glioma cytotoxicity of unloaded F127/L121 micelles (data not shown) prevent further assays with this system. Therefore, hybrid **8** was loaded in PMs F127/T1307 system. The result confirmed that the lack of cytotoxicity of hybrid **8** is not related to aqueous solubility (Table 6). For hybrid **1** and erl, we directly assayed the mixture of F127 and T1307 as vehicle. This formulation did not improve erl activity (Table 6). The nanovehiculization of **1** produced two populations of particle resulting in some degree of polydispersion (Table 5) with ζ potentials slightly negatives (data not shown). The formulation of **1** in the mixture of F127/T1307 promoted lack of bioactivity (Table 6).

When liposomes were used as vehicle, formulation obtained for hybrid **1** and erl presented low polydispersion (Table 5). This formulation improved the activity of **1** in both cell lines and, as in the case of the assayed PMs, the activity of erl against U-87 MG glioblastoma cells increased (Table 6).

Interestingly, for all the vehicled compounds, the formulations resulted less active when the concentration of loaded compound increases. This relevant aspect is currently studied.

Conclusion

The carboranylanilinoquinazoline **1**, with ability to inhibit EGFR in the low nanomolar range [11,13], exhibits desirable *in vitro* antitumor activities against EGFR-overexpressing mammal cells opening the possibility of new targets for BNCT applications. Moreover hybrid **1** meets many drug-like properties highlighting the absence of toxicity, adequate water-solubility and lipophilic ligand efficiency, being among the studied compounds and other EGFR-inhibitors described in the literature [41], the most efficient ligand. Nevertheless, certain absorption problems can occur when **1** is administered orally due to the modest Caco-2 permeability predicted values. Besides eventual

multidrug resistance could be expected because of the lack of P-gp inhibition, something that could be minimized with the assayed formulations [42,43]. Additionally, hybrid **1** fulfills the initial requirements of the OECD in reference to mutagenicity and acute oral toxicity. Currently, we are working in a murine glioblastoma model with hybrid **1** as a way of completing this drug-discovery stage.

Future perspective

Great efforts are being made nowadays toward the development of multifunctional hybrid compounds which could be applied in multimodal treatments to obtain more efficient drugs with diminishing secondary effects. BNCT, which exhibits great potential for the treatment of various cancers, has still limited clinical application. To improve this, efforts should be devoted to the developments of new multimodal drugs that accumulate selectively in the tumoral tissues for diagnosis and therapy. It is expected that this treatment would speed up the effects while diminishing secondary effects. On the one hand, EGFR results an attractive target due to its overexpression in a variety of cancers. On the other hand, the stability of the 3D rigid carborane scaffold might be amalgamated with the capacity to functionalize the different vertexes with different moieties with ending branches (fluorescent dyes, radiopharmaceuticals, anionic or neutral boron clusters, etc.) to provide multimodal treatments besides performing as drug delivery nanocarriers. Therefore, in the future, the following aspects should be considered in the design and synthesis of BNCT drugs: high tumor targeting; high boron-accumulation; desirable drug-like properties to satisfy the requirements in further clinical application.

Summary points

- Drug-like properties of a series of hybrid carboranylanilinoquinazoline EGFR-inhibitors were analyzed.
- Some of these compounds were active against other tyrosine kinase-overexpress mammal cellular systems.
- Predicted theoretic drug-like properties allowed to identify 4-{3-{1-[3-(1,7-dicarba-*closo*dodecaboran-1-yl)propyl]-1*H*-[1,2,3]triazol-4-yl}phenyl}amino-6,7-bis(2-methyloxyethyloxy)quinazoline as one of the best derivatives among the studied.
- 4-{3-{1-[3-(1,7-Dicarba-*closo*dodecaboran-1-yl)propyl]-1*H*-[1,2,3]triazol-4-yl}phenyl}amino-6,7-bis(2-methyloxyethyloxy)quinazoline was nonmutagenic, without and with metabolic activation, in the Ames test.
- 4-{3-{1-[3-(1,7-Dicarba-*closo*dodecaboran-1-yl)propyl]-1*H*-[1,2,3]triazol-4-yl}phenyl}amino-6,7-bis(2-methyloxyethyloxy)quinazoline has a LD_{50} in the oral administration higher than 2000 mg/kg body weight.
- 4-{3-{1-[3-(1,7-Dicarba-*closo*dodecaboran-1-yl)propyl]-1*H*-[1,2,3]triazol-4-yl}phenyl}amino-6,7-bis(2-methyloxyethyloxy)quinazoline could be formulated using liposomes.

Financial & competing interests disclosure

Funding from Agencia Nacional de Investigación e Innovación (Uruguay), POS_NAC_2015_1_110068, is acknowledged. The authors have no other relevant affiliations or financial involvement with any organization or entity with a financial interest in or financial conflict with the subject matter or materials discussed in the manuscript apart from those disclosed.

No writing assistance was utilized in the production of this manuscript.

Ethical conduct of research

The authors state that they have obtained appropriate institutional review board approval or have followed the principles outlined in the Declaration of Helsinki for all human or animal experimental investigations.

References

Papers of special note have been highlighted as: • of interest; •• of considerable interest

1. Alphandéry E. Glioblastoma treatments: an account of recent industrial developments. *Front. Pharmacol.* 9, 879 (2018).
2. Messaoudi K, Clavreul A, Lagarce F. Toward an effective strategy in glioblastoma treatment. Part I: resistance mechanisms and strategies to overcome resistance of glioblastoma to temozolomide. *Drug Discov. Today* 20, 899–905 (2015).
3. Crespo I, Vital AL, Gonzalez-Tablas M *et al.* Molecular and genomic alterations in glioblastoma multiforme. *Am. J. Pathol.* 185, 1820–1833 (2015).

4. Tuncel G, Kalkan R. Receptor tyrosine kinase-Ras-PI 3 kinase-Akt signaling network in glioblastoma multiforme. *Med. Oncol.* 35, 122 (2018).
5. Prados MD, Chang SM, Butowski N *et al.* Phase II study of erlotinib plus temozolomide during and after radiation therapy in patients with newly diagnosed glioblastoma multiforme or gliosarcoma. *J. Clin. Oncol.* 27, 579–84 (2009).

• **A typical example of clinical study with combination of drugs for glioblastoma multiforme treatment.**

6. Conger AD, Giles NH. The cytogenetic effect of slow neutrons. *Genetics* 35, 397–419 (1950).
7. Calabrese G, Daou A, Barbu E, Tsibouklis J. Towards carborane-functionalised structures for the treatment of brain cancer. *Drug Discov. Today* 23, 63–75 (2018).

•• **An excellent review that describes the carborane potential use in brain cancer.**

8. Hiratsuka J, Kamitani N, Tanaka R *et al.* Boron neutron capture therapy for vulvar melanoma and genital extramammary Paget's disease with curative responses. *Cancer Commun.* 38, 38 (2018).
9. Trivillin VA, Pozzi ECC, Colombo LL *et al.* Abscopal effect of boron neutron capture therapy (BNCT): proof of principle in an experimental model of colon cancer. *Radiat. Environ. Biophys.* 56, 365–375 (2017).

• **An important investigation on the use of boron neutron capture therapy in colon cancer.**

10. Hey-Hawkins E, Viñas C. *Boron-Based Compounds: Potential and Emerging Applications in Medicine*. John Wiley & Sons Incorporated, Newark, NJ, USA (2018).

•• **Offers a summary of the present status and highlights the range and capacity of new boron-containing compounds in medical applications.**

11. Couto M, Mastandrea I, Cabrera M *et al.* Small-molecule kinase-inhibitors-loaded boron cluster as hybrid agents for glioma-cell-targeting therapy. *Chem. Eur. J.* 23, 9233–9238 (2017).

•• **An important investigation on the development of novel boron-cluster-containing kinase-inhibitors for glioma treatment.**

12. Nakamura H, Horikoshi R, Usui T, Ban HS. Selective inhibition of EGFR and VEGFR2 tyrosine kinases controlled by a boronic acid substituent on 4-anilinoquinazolines. *MedChemComm* 1, 282–286 (2010).
13. Couto M, García MF, Alamón C *et al.* Discovery of potent EGFR inhibitors through the incorporation of a 3D-aromatic-boron-rich-cluster into the 4-anilinoquinazoline scaffold: potential drugs for glioma treatment. *Chem. Eur. J.* 24, 3122–3126 (2018).

•• **An important investigation on the mechanism of action confirmation of novel antiglioma boron-cluster-containing agents.**

14. Mamot C, Drummond DC, Greiser U *et al.* Epidermal growth factor receptor (EGFR)-targeted immunoliposomes mediate specific and efficient drug delivery to EGFR- and EGFRvIII-overexpressing tumor cells. *Cancer Res.* 63, 3154–3161 (2003).
15. Cheng CC, Liao PN, Ho AS *et al.* STAT3 exacerbates survival of cancer stem-like tumor spheres in EGFR-positive colorectal cancers: RNAseq analysis and therapeutic screening. *J. Biomed. Sci.* 25, 60 (2018).
16. Cheng F, Li W, Zhou Y *et al.* admetSAR: a comprehensive source and free tool for evaluating chemical ADMET properties. *J. Chem. Inf. Model.* 52, 3099–3105 (2012). http://lmmd.ecust.edu.cn/admetsar1/predict/
17. Marchese Robinson RL, Glen RC, Mitchell JBO. Development and comparison of hERG blocker classifiers: assessment on different datasets yields markedly different results. *Mol. Inf.* 30, 443–458 (2011).
18. Wang S, Li Y, Wang J *et al.* ADMET evaluation in drug discovery. 12. Development of binary classification models for prediction of hERG potassium channel blockage. *Mol. Pharm.* 9, 996–1010 (2012).
19. Chen L, Li Y, Zhao Q, Peng H, Hou T. ADME evaluation in drug discovery. 10. Predictions of P-glycoprotein inhibitors using recursive partitioning and naive Bayesian classification techniques. *Mol. Pharm.* 8, 889–900 (2011).
20. Broccatelli F, Carosati E, Neri A *et al.* A novel approach for predicting P-glycoprotein (ABCB1) inhibition using molecular interaction fields. *J. Med. Chem.* 54, 1740–1751 (2011).
21. Shen J, Cheng F, Xu Y, Li W, Tang Y. Estimation of ADME properties with substructure pattern recognition. *J. Chem. Inf. Model* 50, 1034–1041 (2010).
22. Pham-The H, González-Álvarez I, Bermejo M *et al. In Silico* prediction of Caco-2 cell permeability by a classification QSAR approach. *Mol. Inf.* 30, 376–385 (2011).
23. Kido Y, Matsson P, Giacomini KM. Profiling of a prescription drug library for potential renal drug–drug interactions mediated by the organic cation transporter 2. *J. Med. Chem.* 54, 4548–4558 (2011).
24. Carbon-Mangels M, Hutter MC. Selecting relevant descriptors for classification by Bayesian estimates: a comparison with decision trees and support vector machines approaches for disparate datasets. *Mol. Inf.* 30, 885–895 (2011).
25. Lagunin A, Filimonov D, Zakharov A *et al.* Computer-aided prediction of rodent carcinogenicity by PASS and CISOC-PSCT. *QSAR Comb. Sci.* 28, 806–810 (2009).
26. Wang J, Krudy G, Hou T, Zhang W, Holland G, Xu X. Development of reliable aqueous solubility models and their application in druglike analysis. *J. Chem. Inf. Model.* 47, 1395–1404 (2007).
27. Murray CW, Erlanson DA, Hopkins AL *et al.* Validity of ligand efficiency metrics. *ACS Med. Chem. Lett.* 5, 616–618 (2014).

28. Varma MV, Feng B, Obach RS *et al.* Physicochemical determinants of human renal clearance. *J. Med. Chem.* 52, 4844–4852 (2009).
29. Schuster D, Laggner C, Langer T. Antitargets: prediction and prevention of drug side effects. Vaz RJ, Klabunde T (Eds). Wiley-VCH, Weinheim, Germany (2008).
30. Dresser GK, Spence JD, Bailey DG. Pharmacokinetic-pharmacodynamic consequences and clinical relevance of cytochrome P450 3A4 inhibition. *Clin. Pharmacokinet.* 38, 41–57 (2000).
31. Doherty KR, Wappel RL, Talbert DR *et al.* Multiparameter *in vitro* toxicity testing of crizotinib, sunitinib, erlotinib, and nilotinib in human cardiomyocytes. *Toxicol. Appl. Pharmacol.* 272, 245–255 (2013).
32. Hansen K, Mika S, Schroeter T *et al.* Benchmark data set for *in silico* prediction of Ames mutagenicity. *J. Chem. Inf. Model.* 49, 2077–2081 (2009).
33. Zhu H, Martin TM, Ye L, Sedykh A, Young DM, Tropsha A. Quantitative structure-activity relationship modeling of rat acute toxicity by oral exposure. *Chem. Res. Toxicol.* 22, 1913–1921 (2009).
34. Leeson PD, Springthorpe B. The influence of drug-like concepts on decision-making in medicinal chemistry. *Nat. Rev. Drug Discov.* 6, 881–890 (2007).

- **A review that describes and discusses the drug-like concepts on the medicinal chemistry decision-making.**

35. OECD 471, 1997. Organisation for economic co-operation and development (OECD), OECD guidelines for testing of chemicals; guideline no. 471: genetic toxicology: bacterial reverse mutation test. (adopted July 21, 1997).
36. OECD 423, 2001. Organisation for economic co-operation and development (OECD), OECD guidelines for the testing of chemicals, guideline no. 423: acute oral toxicity – acute toxic class method. (adopted December 17, 2001).
37. Irwin S. Comprehensive observational assessment: Ia. A systematic, quantitative procedure for assessing the behavioral and physiologic state of the mouse. *Psychopharmacology* 13, 222–257 (1968).
38. Oh KT, Bronich TK, Kabanov AV. Micellar formulations for drug delivery based on mixtures of hydrophobic and hydrophilic Pluronic® block copolymers. *J. Control. Rel.* 94, 411–422 (2004).
39. Wei Z, Hao J, Yuan S *et al.* Paclitaxel-loaded Pluronic P123/F127 mixed polymeric micelles: formulation, optimization and *in vitro* characterization. *Int. J. Pharm.* 376, 176–185 (2009).
40. Bruce L, Bruce I. Polymer-based anticancer agents. WO 2007/123468 A1 (2007).

- **A description about the ability to reduce cancer cells proliferation rates of some amphiphilic block copolymers.**

41. Hu J, Han Y, Wang J *et al.* Discovery of selective EGFR modulator to inhibit L858R/T790M double mutants bearing a *N*-9-diphenyl-9*H*-purin-2-amine scaffold. *Bioorg. Med. Chem.* 26, 1810–1822 (2018).
42. Guan Y, Huang J, Zuo L *et al.* Effect of pluronic P123 and F127 block copolymer on P-glycoprotein transport and CYP3 A metabolism. *Arch. Pharmacol. Res.* 34, 1719–1728 (2011).
43. Patra A, Satpathy S, Shenoy AK, Bush JA, Kazi M, Hussain MD. Formulation and evaluation of mixed polymeric micelles of quercetin for treatment of breast, ovarian, and multidrug resistant cancers. *Int. J. Nanomed.* 13, 2869–2881 (2018).

Discovery of hybrid sunitinib-carborane with spectacular *in vitro* and *in vivo* anti-glioblastoma behavior

Marcos Couto,[†,‡] Catalina Alamón,[†] María Fernanda García,[§] Carina Sánchez,[†] Mariángeles Kovacs,[∫] Emiliano Trias,[∫] Luis Barbeito,[∫] Martín Gabay,[||] Nidal Zeineh,[||] Moshe Gavish,[||] Francesc Teixidor,[‡] Pablo Cabral,[§] Clara Viñas,[‡] and Hugo Cerecetto[*,†,§]

[†]Laboratorio de Química Orgánica Medicinal, Instituto de Química Biológica, Facultad de Ciencias, Universidad de la República, Montevideo 11400, Uruguay; [‡]Institut de Ciències dels Materials de Barcelona-CSIC Campus, Bellaterra, Spain; [§]Área de Radiofarmacia, Centro de Investigaciones Nucleares, Facultad de Ciencias, Universidad de la República, Montevideo 11400, Uruguay; [∫]Laboratorio de Neurodegeneración, Institut Pasteur de Montevideo, Montevideo 11400, Uruguay; [||] Molecular Pharmacology, Faculty of Medicine, Technion Institute of Technology, Haifa, Israel.

Supporting Information

ABSTRACT: Glioblastoma multiforme is the most aggressive central nervous system tumor, but there are no effective drugs to treat this pathology. Tyrosine kinase receptor inhibitors, on the one hand, and boron neutron capture therapy, on the other, could be, altogether, the future therapeutic strategy. Medicinal chemistry followed by biological screening yielded a series of drug-like compounds with activities in cells expressing tyrosine kinase proteins. One of the best inhibitors was challenged against a panel of 460 tyrosine-kinases resulting a multi-inhibitor. The *in vivo* activity of this, in an immunosuppressed mouse model of human glioblastoma established from U87 MG cells, evidenced significant anti-tumoral behavior.

Glioblastoma multiforme is the most frequent and aggressive adult primary central nervous system tumor, with a scarcely 2-year survival rate for 3 % – 5 % of the patients.[1] The current treatment includes surgery, chemotherapy, angiogenesis inhibition, radiotherapy, boron neutron capture therapy (BNCT), tumor treating fields (TTF) therapy, photodynamic therapy (PDT), or combined therapies. Regarding to chemotherapy, temozolomide (**Tmz**, Chart 1), an oral alkylated and reticulum endoplasmic stress promoter agent, is the first-line chemotherapeutic agent. However, frequently encounters drug resistance in human patients.[2] Since glioblastoma expresses vascular endothelial growth factor (VEGF), its tyrosine kinase receptors VEGFR1 and VEGFR2, and angiogenesis-genes (PDFGR-α and KIT), some tyrosine kinase receptor inhibitors are used as second-line chemotherapeutic treatments.[3-5] Sunitinib (**Sun**, Chart 1), a tyrosine kinase receptor inhibitor, possesses anti-tumoral and anti-angiogenic activities by targeting of VEGFR1, 2 and 3, PDGFR-α and -β, stem-cell growth factor receptor (KIT), fms-related tyrosine kinase 3 (FLT3), rearranged during transfection (RET) proto-oncogene, and colony stimulating factor receptor 1 (CSF1R).[6a] **Sun** is indicated for the treatment of renal carcinoma, gastrointestinal sarcoma and neuroendocrine tumors. In preclinical studies of neuroendocrine tumors, **Sun** produces anti-proliferative, anti-angiogenic and pro-apoptotic effects decreasing the invasive capacity of glioma cells implanted into the brain.[6] However, minimal anti-glioblastoma activity and high toxicity were evidenced in phase II studies.[7] Previously, we have investigated and developed hybrid agents combining substructures derived from erlotinib (**Erl**, Chart 1), inhibitor of the tyrosine kinase domain of the epidermal growth factor receptor, and icosahedral boron-clusters with potential use in BNCT[8]. We demonstrated that the incorporation of boron cluster resulted in hybrid compounds with enhanced *in vitro* activity, like compound **A** (Chart 1).[9,10] Traditionally, boron clusters has been used for BNCT applications. However, due to their particular chemical properties, there is growing interest in exploring their use as pharmacophore.[11] The electron-deficient nature of the boron atoms, the globular architecture and convenient molecular size make B-cluster able to establish hydrophobic interactions in a tridimensional way.[12] Moreover, boron clusters offer an instance for improvement of drug-like properties like hydrophilicity and lipophilicity, permeability, and catabolism among others.

The substituent at the C-3-indol system of **Sun** plays relevant role in the protein binding and especially in the compound solubility because the pyrrole ring is close to the opening of the binding target-pocket exposing to solvent,[13] while, the indolin-2-one motive plays a key role in the proteins-binding processes.[14] Additionally, boron-clusters can establish hydrogen and dihydrogen bonds, such as C-H···X and BH ···H-X (X = N, C, O and S), as well as BH ···π and C-H···π hydrogen bonds,[15] which could provide extra beneficial interactions with the targets through these special non-classical interactions. Herein, **Sun** is used as structural scaffold to prepare new boron-cluster bearing hybrid compounds with anti-glioblastoma activities. The new compounds were synthesized and *in vitro* evaluated. **Sun** was selectively propargylated in the indolin-2-one nitrogen in order to subsequently apply "click" and Sonogashira cross-

couplings reactions with adequate functionalized boron-clusters (Scheme S1). Thus, modifications at the pyrrole nitrogen could be detrimental in the expected biological/pharmaceutical behaviors.

Synthesized compounds were evaluated *in vitro* in the murine C6 and human U87 MG glioma cell lines. Derivatives **1**, **2** and **4**, bearing the triazolylpropyl system as a linker, were identified as novel *in vitro* anti-glioblastoma agents (Table 1). Additionally, compounds **1**, **2** and **4** also showed to be potent growth inhibitors of the HT-29 cell lines (Table S1), an overexpressing EGFR tumoral cell line derived from *Homo sapiens* colorectal adenocarcinoma.[16] As we previously observed for **Erl**-carborane hybrids,[9] the best biological results for the current family of compounds are observed when the linker is the triazolylpropyl system. On the other hand, those derivatives with the ethynylbenzyl-linker showed null or lower activity. This behavior could be the result of their different lipophilicities having compound **1** the best value for the studied compounds (expressed as R_M, Figure S1). Within the triazolylpropyl-derivatives, as our previous results with **Erl**-hybrids,[9] the 1,7-dicarba-*closo*dodecarboran-1-yl one, i.e. **1**, resulted the best cellular-inhibitor in the three studied tumoral-cells. However, unlike our previous results,[9] the cosane-derivative **5** was not active in the current assayed conditions. Moreover, compound **1**, besides being better cell-growth inhibitor than the tyrosine kinase receptor inhibitors **Erl** and lapatinib (**Lap**, see Chart 1), was at least 4-times more active against glioblastoma cells than the parent compound **Sun** (Table 1) and 12-times more active against U87 MG than the classical therapeutic **Tmz**. Additionally, compound **1** was evaluated against normal glial cells (Table S2), in order to determine if this compound selectively killed tumor cells, while having no cytotoxic effects on normal glial cells. The results showed that compound **1**, regardless of displaying no selectivity between tumors on normal astrocytes, did account for the same or better selectivity index compared to the parent compound **Sun** and to **Lap**, respectively (Table S2). Moreover, unlike **Lap** compound **1**, and **Sun**, displayed similar IC_{50} in both astrocytes and tumoral cells.

In order to inquire about the tyrosine-kinases inhibition ability of compound **1**, it was extensively profiled in a high-throughput competition binding assay against a panel of 460 kinases (KINOMEscan®) at 10 μM. It demonstrated highly activity against 33 out of the 460 analyzed bio-targets (Figure 1, Table S3), with a final selectivity score, or "S", of 0.04. Like **Sun**, hybrid **1** displays the inhibition properties against FLT3, PDGFR-α and -β, KIT, CSF1R and VEGFR2. Compound **1** was identified as a multi-tyrosine-kinase inhibitor but unlike **Sun** (Figure S2) it is selective against some specific bio-systems. Specifically, the best inhibition ability of compound **1** was against the FLT3 internal tandem duplication mutation of the gatekeeper residue F691 (FLT3-ITD, F691L) involved, among others, in acute myeloid leukemia.[17] Secondly, **1** inhibited in good level PDGFR-β and the mutations that occur in the exon 11 of KIT gene which encodes the juxtamembrane domain (V559D and L576P) involved, among others, in gastrointestinal stromal tumors.[18]

To resemble the cellular environment of a developing brain tumor, U87 MG cells, stained with PKH26 dye, were co-cultured together with astrocytes. These co-cultured cells were incubated with **1** and **Sun**, or DMSO (control) at the corresponding $IC_{50,\ U87\ MG}$ doses during 24 h. Confocal microscopy revealed a very different behaviors among the studied compounds and the control (Figure 2). As expected, PKH26 dye showed the decrease of U87 MG population upon treatment comparing to control untreated cells. Similarly, according to astrocytic markers M2 and GFAP,[19,20] the population of tumor-associated astrocytes, potentially present in control and mainly in **Sun**-incubated system, was not present in the co-culture treated with compound **1**. Moreover, when comparing GFAP staining of **Sun**-treated cells and control cells it was possible to observe that **Sun** made astrocytes become reactive, as indicated by increased GFAP expression. These results highlighted the particular **1** biological behavior against astrocyte-systems open the possibility of new bio-target to new drugs. Finally, DAPI nuclei staining showed on both, **Sun**- and compound **1**-treatment chromatin condensation, which is associated with the onset of apoptosis. Consequently, in order to confirm the kind of death promoted by compound **1** in U87 MG cells flow cytometry assays and mitochondrial membrane potential change studies were performed. The results showed that compound **1**, like **Sun**, produced cellular death of U87 MG tumoral-cells by apoptosis mechanisms (Figures S3 and S4).

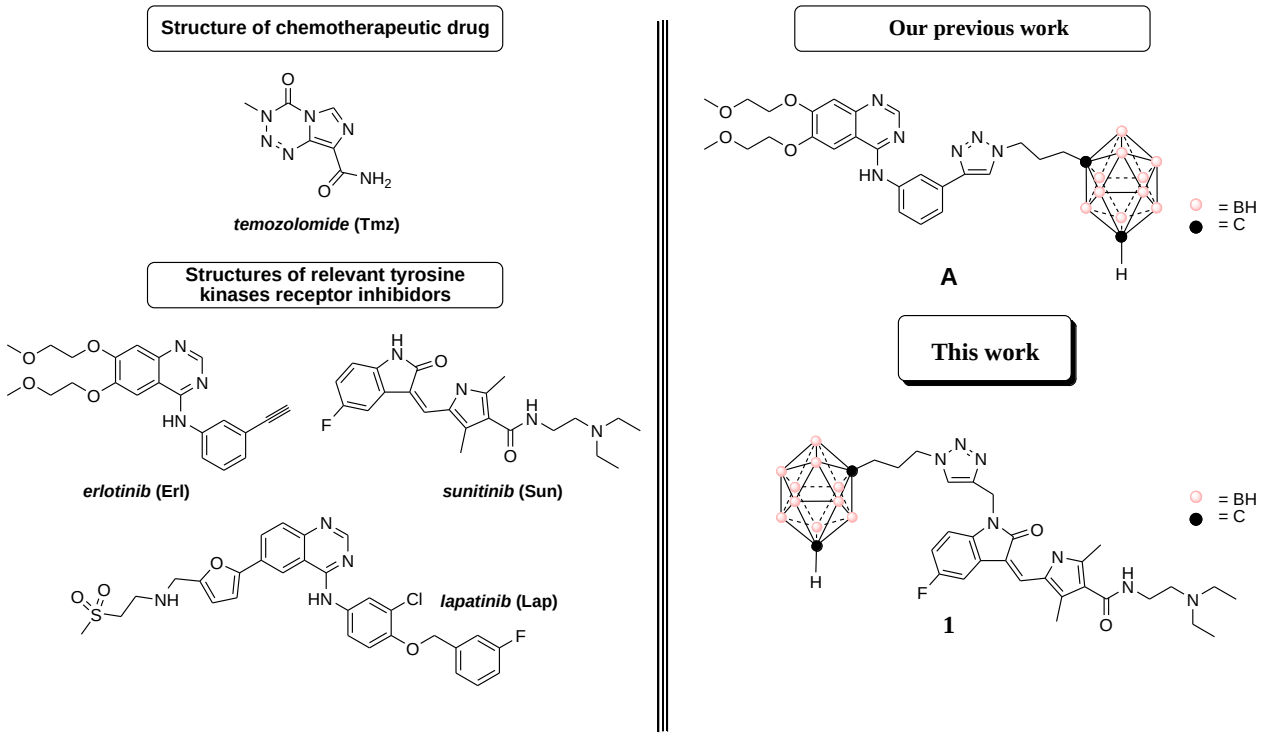
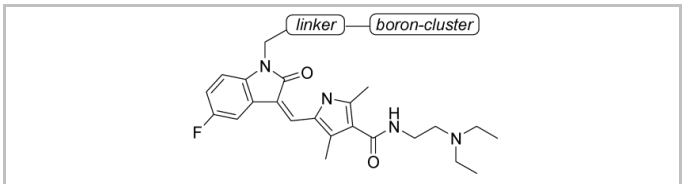
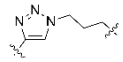
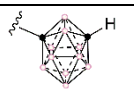
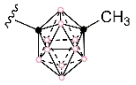
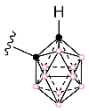
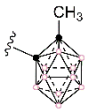
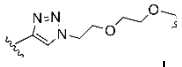
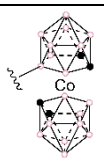
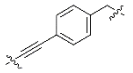
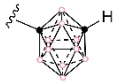
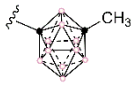
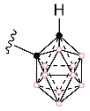
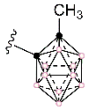


Chart 1. Chemical structures of glioblastoma multiforme drug, *temozolomide* (**Tmz**), some relevant tyrosine kinase receptor inhibitors, *erlotinib* (**Erl**), *sunitinib* (**Sun**), and *lapatinib* (**Lap**), previous hybrid erlotinib-boron cluster developed by us, **A**, and the best hybrid sunitinib-boron cluster described herein, **1**.

Table 1. Structures and *in vitro* Activity of Compounds 1-9 as IC_{50} (μM) or the percentage of cells survival at 100 μM on C6 and U87 MG cells.



Cpd	linker	boron-cluster	$IC_{50,C6}$ (μM)[a]	$IC_{50,U87MG}$ (μM)[a]
1			6.9 ± 0.5	8.0 ± 0.3
2			5.2 ± 0.5	8.0 ± 0.4
3			78.3 ± 0.8	> 100 (95 ± 5 %)
4			4.4 ± 0.5	8.0 ± 0.5
5[a]			> 100 (100 ± 5 %)	> 100 (100 ± 4 %)
6			> 100 (65 ± 5 %)	> 100 (100 ± 5 %)
7			> 100 (100 ± 5 %)	> 100 (64 ± 4 %)
8			80 ± 4	> 100 (100 ± 5 %)
9			30 ± 5	> 100 (94 ± 6 %)
Sun	-	-	36 ± 10	32 ± 4
A	-	-	30 ± 5	70 ± 5
Erl	-	-	> 100	63 ± 5
Lap	-	-	54 ± 14	> 100 (89 ± 5 %)
Tmz	-	-	*ns*[b]	> 100

[a] Values in parenthesis are the percent of cells survival at 100 μM. [b] As sodium salt. [b] *ns*: not studied.

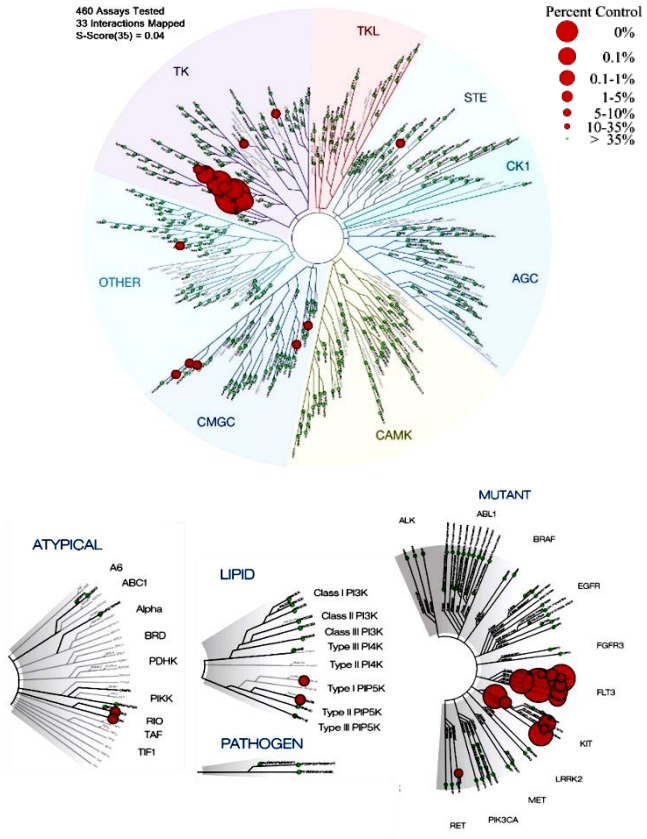


Figure 1. Selectivity profile of compound **1** against 460 protein kinases. Relative binding affinities are indicted by red circles in a phylogenetic kinome tree for wild-type enzymes (left) and atypical/mutant/lipo/pathogen variants (right). The size of the red cycles are proportional to the strength of the binding, the larger circles indicates higher affinity. A total of 33 best interactions with binding levels of less than 35% of control (red circles) at a fixed concentration of test compound of 10 μM were mapped. Selectivity factor, S35 = 0.04. Image generated using TREEspot™ Software Tool and reprinted with permission from KINOMEscan®, a division of DiscoveRx Corporation, © DISCOVERX CORPORATION 2010.

This particular *in vitro* biological-behavior of compound **1**, not sharing with its parent compound **Sun**, led us to study deeply into its *in vivo* behavior. Previously, some drug-like properties of **1** were theoretical and experimentally analyzed. On the one hand, theoretical predictions of drug-like properties,[21] showed that compound **1** shared drug-like properties with **Sun**, mainly absence of toxicities and adequate water solubility (Table S4). On the other hand, compound **1** has proven not to be mutagenic, another desirable characteristic that would act in favor of this compound (Table S5).[22] Thirdly, we determined if compound **1** could pass through the brain blood barrier (BBB) using an artificial endothelial-cells model.[23] Near to 3-times more compound **1** was observed on the other side of the artificial-BBB than before (Table S5).

In vivo anti-glioblastoma activity of **1** was evaluated in immunosupressed mice bearing human U87 MG-tumor.[24] Compound **1** was intraperitoneally administered at 1 mg/kg/day and three times a week. In this assay, **Tmz** was used as positive used therapy-drug administered in the same conditions at 4 mg/kg/day. We found that treatment with compound **1** slowed down GBM growth when it was compared to untreated animals (Figure 3A-C). Additionally, compound **1**, at a dose four times lower than the dose of **Tmz** and in the same conditions, significantly prolonged (2- and 1.8-times) the survival of unhealthy-mice, with a median survival time of 45 days (Figure 3D), having the **Tmz**-treated and untreated control values of 23 and 25 days, respectively. Additionally, **1** provoked an increase of 70 and 89 % of mice' survival time, from 30 and 27 to 51 days, and an increase of 32 and 43 % of time no mice deaths, from 25 and 23 to 33 days, respectively. These results clearly showed the significantly spectacular *in vivo* anti-glioblastoma behavior of compound **1**.

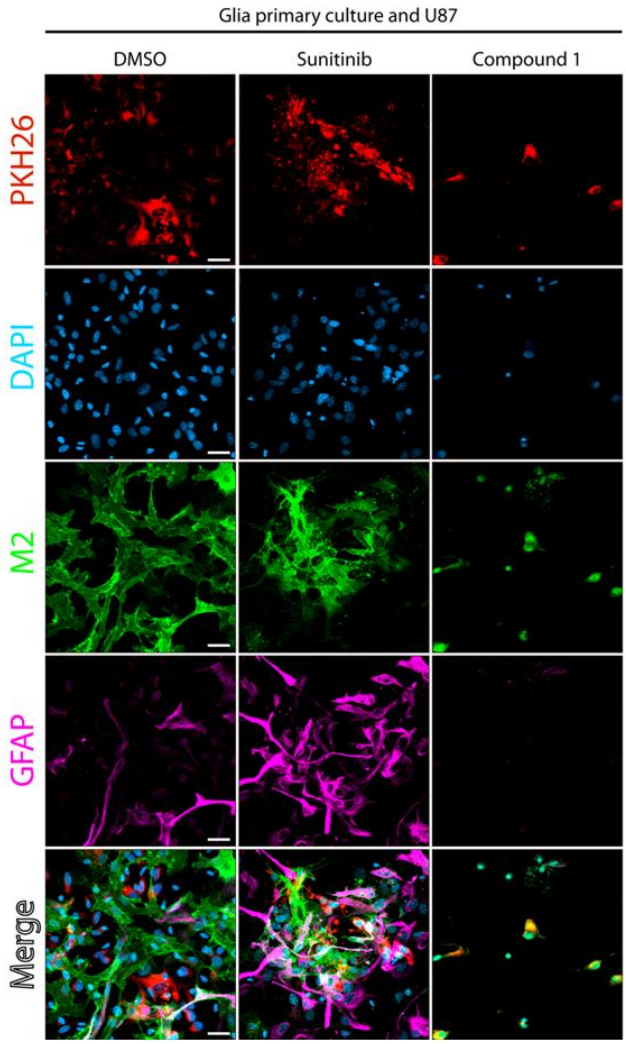


Figure 2. Fluorescence microscopies of astrocytes co-cultured with U87 MG and treated with **Sun**, **1** or with DMSO as control during 24 h. Probes (PKH26 marker for U87-MG cell membrane, DAPI marker for nucleus, M2 and GFAP markers for astrocytes and astrocyte activation, respectively) show the differential behavior of **1** comparing to **Sun** and control.

Nowadays, bearing in mind a polytherapeutic strategy, using drugs with different mode of action/cellular death,

we are currently analyzing the *in vitro* efficiency, against U87 MG cells, of the **1**+**Tmz** combination, working with each compound at the corresponding IC_{25} (Figure S5). We found that this combination displayed excellent biological behavior and it should be further analyzed *in vivo*.

In summary, compound **1** is a broadly active inhibitor of kinases and exhibits significant cellular and *in vivo* activities against EGFR-cellular systems. Rational inhibitor development based on this pharmacological leader and structural platform could lead to compounds with improved potency and potentially combined with other therapeutic tool like BNCT.

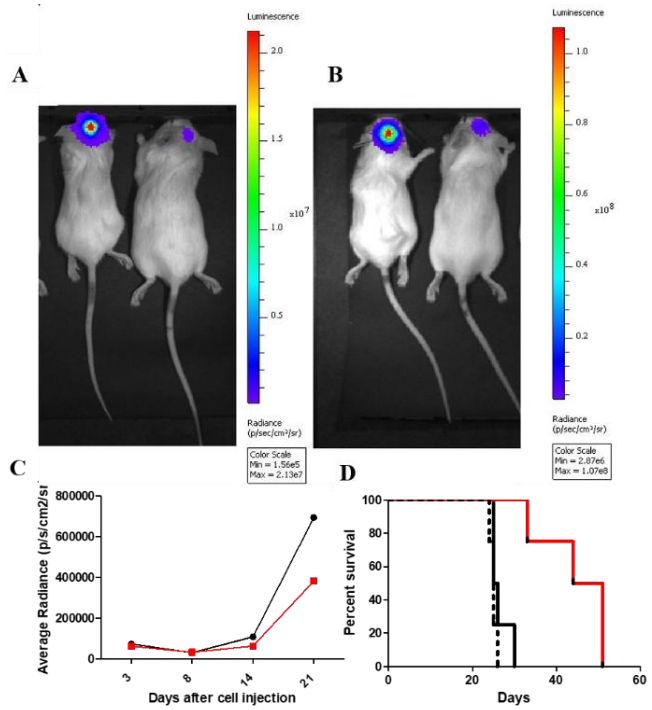


Figure 3. (A & B) Selected images of evolution of GBM sizes (for details see Supplementary Material). (A) corresponds to 14 days and (B) to 21 days after cell injection, in each case left mouse was untreated-control and the right one, treated with compound **1**. (C) Weekly evolution of GBM sizes. In the fourth week the study was ended because all the untreated animals died. (D) Kaplan-Meier survival curves of mice bearing GBMs. Black: untreated animals; dotted: **Tmz**-treated animals; red: **1**-treated animals.

ASSOCIATED CONTENT

Supporting Information

The Supporting Information is available free of charge on the ACS Publications website.

Chemical and biological experimental procedures, and supporting figures and tables (PDF)

AUTHOR INFORMATION

Corresponding Author

* hcerecetto@cin.edu.uy

ORCID

Hugo Cerecetto: 0000-0003-1256-3786

Notes

The authors declare no competing financial interests.

ACKNOWLEDGMENT

This work was supported in part by grants by FCE-ANII (FCE_3_2018_1_148288), Institut Pasteur de Montevideo – FOCEM. M.C., M.F.G., E.T., L.B., P.C., and H.C. are Sistema Nacional de Investigadores- Agencia Nacional de Investigación e Innovación (ANII) researchers. M.C. thanks CSIC-Universidad de la República (UdelaR) (Grupo I+D, CSIC-421) for his scholarships, and C.A. also thanks CSIC-UdelaR (MIA Program) for her scholarship. M.C. thanks funding from ANII for his doctoral-scholarship (POS_NAC_2015_1_110068).

REFERENCES

(1) Fitzmaurice, C.; Dicker, D.; Pain, A.; *et al. JAMA Oncol.* **2015**, *1*, 505-527.

(2) Stupp, R.; Mason, W. P.; van den Bent, M. J.; *et al. N. Engl. J. Med.* **2005**, *352*, 987-996.

(3) Batchelor, T. T.; Mulholland, P.; Neyns, B.; *et al. J. Clin. Oncol.* **2013**, *31*, 3212-3218.

(4) Lombardi, G.; Pambuku, A.; Bellu, L.; Farina, M.; Della Puppa, A.; Denaro, L.; Zagonel, V. Crit. *Rev. Oncol. Hematol.* **2017**, *111*, 94-102.

(5) Goodwin, C. R.; Rath, P.; Oyinlade, O.; Lopez, H.; Mughal, S.; Xia, S.; Li, Y.; Kaur, H.; Zhou, X.; Ahmed, A. K.; Ho, S.; Olivi, A.; Lal, B. *Clin. Neurol. Neurosurg.* **2018**, *171*, 26-33.

(6) (a) Papaetis, G.S.; Syrigos, K.N. *BioDrugs* **2009**, *23*, 377-389. (b) Giannopoulou, E.; Dimitropoulos, K.; Argyriou, A. A.; Koutras, A. K.; Dimitrakopoulos, F.; Kalofonos, H. P. *Invest. New Drugs* **2010**, *28*, 554-560. (c) de Bouard, S.; Herlin, P.; Christensen, J. G.; Lemoisson, E.; Gauduchon, P.; Raymond, E.; Guillamo, J. S. *Neuro Oncol.* **2007**, *9*, 412-423.

(7) Hutterer, M.; Nowosielski, M.; Haybaeck, J.; Embacher, S.; Stockhammer, F.; Gotwald, T.; *et al. Neuro Oncol.* **2014**, *16*, 92-102.

(8) Barth, R. F.; Vicente, M. H.; Harling, O. K.; Kiger, W. S.; Riley, K. J.; Binns, P. J.; Wagner, F. M.; Suzuki, M.; Aihara, T.; Kato, I.; Kawabata, S. *Radiat. Oncol.* **2012**, *7*, 1–21.

(9) (a) Couto, M.; García, M. F.; Alamón, C.; Cabrera, M.; Cabral, P.; Merlino, A.; Teixidor, F.; Cerecetto, H.; Viñas, C. *Chem. Eur. J.* **2018**, *24*, 3122-3126. (b) Couto, M.; Mastandrea, I.; Cabrera, M.; Cabral, P.; Teixidor, F.; Cerecetto, H.; Viñas, C. *Chem. Eur. J.* **2017**, *23*, 9233-9238.

(10) Couto, M.; Alamón, C.; Sánchez, C.; Dávila, B.; Fernández, M.; Lecot, N.; Cabral, P.; Teixidor, F.; Viñas, C.; Cerecetto, H. *Fut. Med. Chem.* **2019**, *in press*.

(11) (a) Cerecetto, H.; Couto, M. *Medicinal Chemistry of Boron-Bearing Compounds for BNCT-Glioma Treatment: Current Challenges and Perspectives* in *Glioma. Contemporary Diagnostic and Therapeutic Approaches*; Omerhodzic, I.; Arnautovic, K., Eds; IntechOpen Ltd., United Kingdom, 2018. (b) Hey-Hawkins, E.; Viñas, C. *Boron-Based Compounds. Potential and Emerging Applications in Medicine*. John Wiley & Sons Incorporated, Newark, 2018.

(12) (a) Fujii, S. *Yakugaku Zasshi.* **2017**, *137*, 31-41. (b) Leśnikowski, Z. J. *Expert Opin. Drug Discov.* **2016**, *11*, 569-578.

(13) (a) Laird, A. D.; Vajkoczy, P.; Shawver, L. K.; *et al. Cancer Res.* **2000**, *60*, 4152-4160. (b) Sun, L.; Liang, C.; Shirazian, S.; *et al. J. Med. Chem*. **2003**, *46*, 1116-1119.

(14) Balana, C.; Gil, M. J.; Perez, P.; Reynes, G.; Gallego, O.; Ribalta, T.; Capellades, J.; Gonzalez, S.; Verger, E. *Target. Oncol.* **2014**, *9*, 321-329.

(15) (a) Zhang, X.; Dai, H.; Yan, H.; Zou, W.; Cremer, D. *J. Am. Chem. Soc.* **2016**, *138*, 4334-4337. (b) Fox, M. A.; Hughes, A. K. *Coord. Chem. Rev.* **2004**, *248*, 457-476.

(16) Cheng, C. C.; Liao, P. N.; Ho, A. S.; Lim, K. H.; Chang, J.; Su, Y. W.; Chen, C. G.; Chiang, Y. W.; Yang, B. L.; Lin, H. C.; Chang, Y. C.; Chang, C. C.; Chang, Y. F. *J. Biomed. Sci.* **2018**, *25*, 60.

(17) Gilliland, D. G.; Griffin, J. D. *Blood*. **2002**, *100*, 1532-1542.

(18) Heinrich, M. C.; Corless, C. L.; Demetri, G. D.; *et al. J. Clin. Oncol.* **2003**, *21*, 4342-4349.

(19) Chen, Z.; Zhong, D.; Li, G. *J. Neuroinflammation.* **2019**, *16*, 76.

(20) Brandao, M.; Simon, T.; Critchley, G.; Giamas, G. *Glia*. **2018**, 1–12.

(21) Cheng, F.; Li, W.; Zhou, Y.; Shen, J.; Wu, Z.; Liu, G.; Lee, P. W.; Tang, Y. *J. Chem. Inf. Model.* **2012**, *52*, 3099-3105. http://lmmd.ecust.edu.cn/admetsar1/predict/.

(22) OECD 423, 2001. Organisation for Economic Co-operation and Development (OECD), OECD Guidelines for the Testing of Chemicals, Guideline No. 423: Acute Oral Toxicity – Acute Toxic Class Method (adopted December 17, 2001).

(23) Malina, K. C. K.; Cooper, I.; Teichberg, V. I. *Brain Res.* **2009**, *1284*, 12-21.

(24) Vainshtein, A.; Veenman, L.; Shterenberg, A.; Singh, S.; Masarwa, A.; Dutta, B.; Island, B.; Tsoglin, E.; Levin, E.; Leschiner, S.; Maniv, I.; Pe'er, L.; Otradnov, I.; Zubedat, S.; Aga-Mizrachi, S.; Weizman, A.; Avital, A.; Marek, I.; Gavish, M. *Cell Death Discov.* **2015**, *1*, 15027.

SUPPORTING INFORMATION

Discovery of hybrid sunitinib-carborane with spectacular *in vitro* and *in vivo* anti-glioblastoma behavior

Marcos Couto,[†,‡] Catalina Alamón,[†] María Fernanda García,[§] Carina Sánchez,[†] Mariángeles Kovacs,[∫] Emiliano Trias,[∫] Luis Barbeito,[∫] Martín Gabay,[‖] Nidal Zeineh,[‖] Moshe Gavish,[‖] Francesc Teixidor,[‡] Pablo Cabral,[§] Clara Viñas,[‡] and Hugo Cerecetto[*,†,§]

Correspondence to: hcerecetto@cin.edu.uy

[†]*Laboratorio de Química Orgánica Medicinal, Instituto de Química Biológica, Facultad de Ciencias, Universidad de la República, Montevideo 11400, Uruguay;* [‡]*Institut de Ciències dels Materials de Barcelona-CSIC Campus, Bellaterra, Spain;* [§]*Área de Radiofarmacia, Centro de Investigaciones Nucleares, Facultad de Ciencias, Universidad de la República, Montevideo 11400, Uruguay;* [∫]*Laboratorio de Neurodegeneración, Institut Pasteur de Montevideo, Montevideo 11400, Uruguay;* [‖] *Molecular Pharmacology, Faculty of Medicine, Technion Institute of Technology, Haifa, Israel.*

Table of contents

I) Chemical Experimental Section Page S3

1.- Materials Page S3

2.- Methods Page S3

3.- Scheme S1.- Synthetic procedures for preparation of compounds **1-9** Page S4

4.- Synthesis and Characterization of compounds 1-9

Sunitinib derivative Page S5

Compound **1** Page S6

Compound **2** Page S8

Compound **3** Page S10

Compound **4** Page S12

Compound **5** Page S14

Compound **6** Page S16

Compound **7** Page S19

Compound **8** Page S21

Compound **9** Page S23

II) Biological Experimental Section Page S25

5.- *In vitro* cytotoxicity assays Page S25

Cytotoxicity assay on normal brain cells Page S25

Immunofluorescence staining of treated co-cultures of U87 MG and astrocytes Page S25

Cytotoxicity assays of the **1+Tmz** combination Page S26

6.- Other *in vitro* studies Page S26

Assessment of cell death mechanism by flow cytometry Page S26

Collapse of the mitochondrial membrane potential ($\Delta\Psi m$) Page S26

Ames Test Page S27

BBB *in vitro* passage assay Page S27

R_M determination Page S27

7.- *In vivo* studies Page S27

Figures S1-S5 Page S29

Tables S1-S5 Page S34

References Page S47

I) Chemical Experimental Section

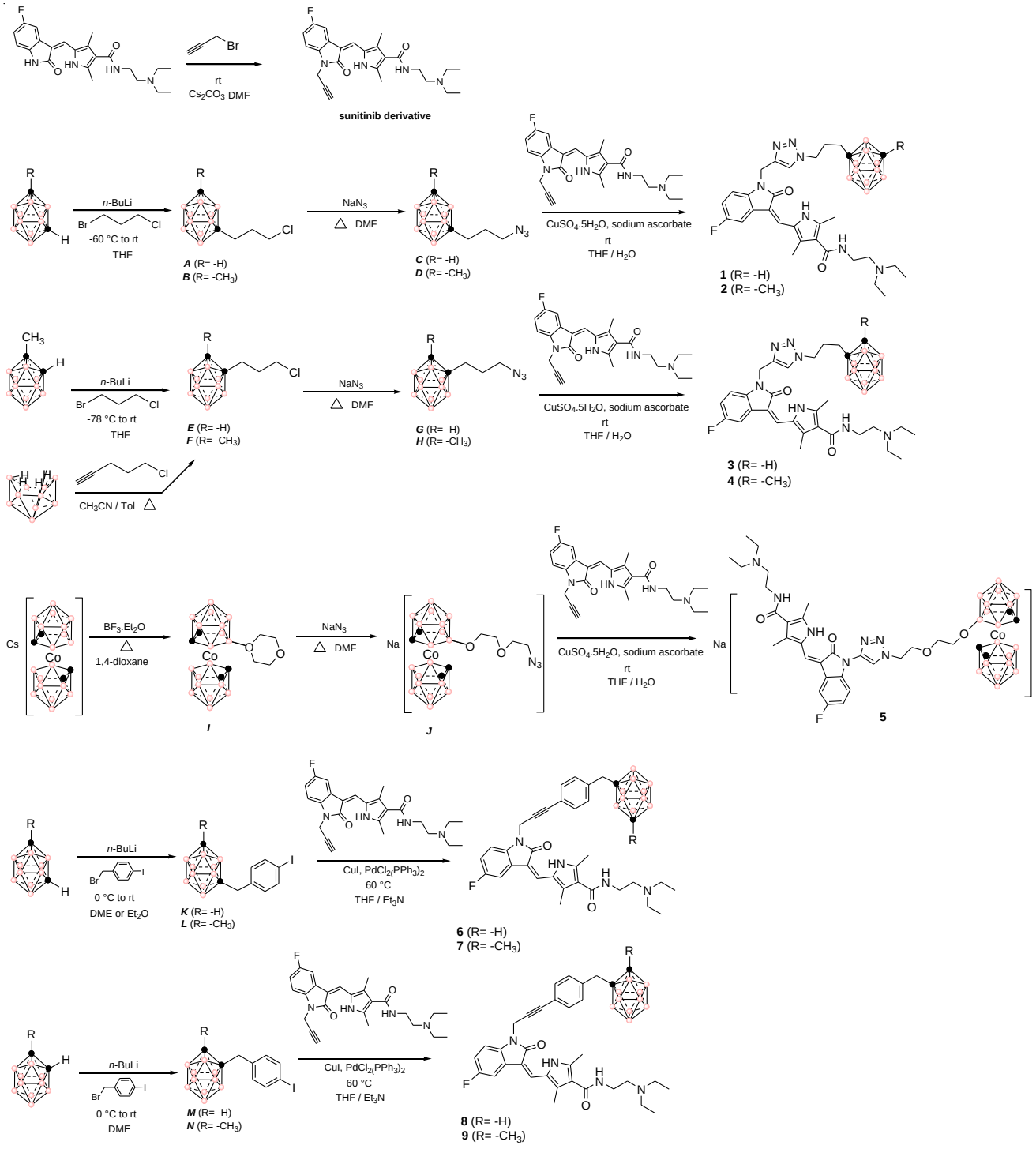
1.- Materials

Most reactions were performed under an atmosphere of dinitrogen by employing standard Schlenk techniques. Analytical thin-layer chromatography (TLC) was carried out on pre-coated plates with silica gel 60 on aluminium foil F254 (Merck). Compounds were visualized by use of UV light (254 nm) or by a 0.5 % acidic solution of $PdCl_2$ in HCl/Methanol by heat gun for boron containing derivatives. Chemicals were reagent grade and were used as received from commercial suppliers. 1,2-*closo*-$C_2B_{10}H_{12}$, and 1,7-*closo*-$C_2B_{10}H_{12}$, were obtained from Katchem. Compounds ***A***-***E***[1], ***G***-***H***[1], ***K***-***M***[1], ***F***[2], ***I***[3], ***J***[4], and ***N***[5] (Scheme S1) were synthesized as reported at the literature.

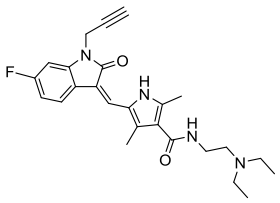
2.- Methods

Instrumentation: Elemental analyses were performed using a Carlo Erba Model EA1108 elemental analyzer instrument. All NMR spectra were recorded on Bruker ARX-300 or on Bruker DPX-400 spectrometers equipped with the appropriate decoupling accessories. The ^{1}H (300.13 MHz or at 400.13 MHz); $^{11}B\{^{1}H\}$ (96.29 MHz); and $^{13}C\{^{1}H\}$ (75.47 MHz or at 100.77 MHz) NMR spectra were recorded in $CDCl_3$, CD_3COCD_3 or $(CD_3)_2SO$ at 298 K. Chemical shifts are reported in units of parts per million (ppm) downfield from the reference, and all coupling constants are reported in Hertz (Hz). Multiplicity is abbreviated as: s is the singlet, d is the doublet, dd is the doublet of doublet, dt is doublet of triplets, dq is doublet of quartets, t is the triplet, m is the multiplet, and bs is the broad singlet. MS were performed at a Shimadzu QP-2010 spectrometer at 70 eV ionizing voltage. Mass spectra are presented as *m*/*z* (% rel int.). MALDI-TOF mass spectra were recorded in the negative-ion mode using a Bruker Biflex MALDI-TOF (N_2 laser; λ_{exc}= 337 nm; 0.5 ns pulses); voltage ion source 20.00 KV (Uis1) and 17.50 KV (Uis2)). UV measurements were performed on spectrofluorometer Varioskan flash, Thermo ® at 298 K and using 1.0 cm cuvettes.

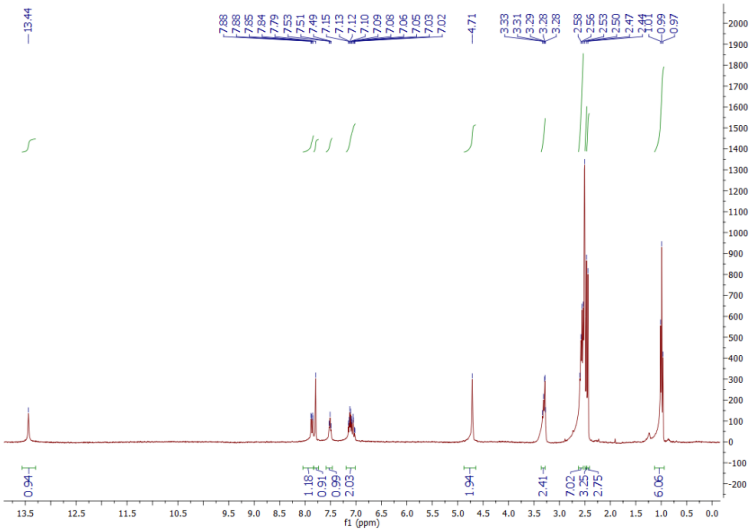
3.- Scheme S1.- Synthetic procedures for preparation of compounds **1-9**.



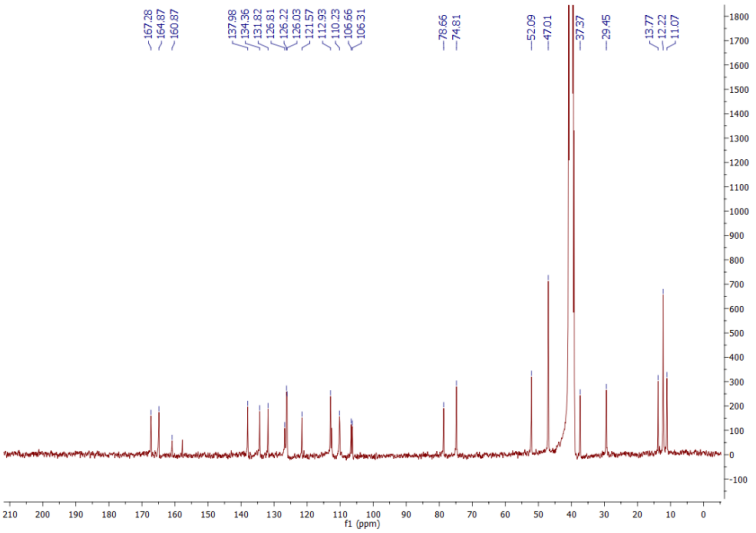
4.- Synthesis and Characterization of compounds 1-9
Sunitinib derivative



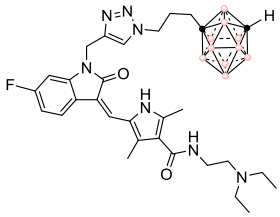
Cesium carbonate (2.5 equiv., 610 mg, 1.87 mmol) was added to a stirred suspension of Sunitinib (1 equiv., 300 mg, 0.75 mmol) in DMF (10 mL). The mixture was stirred for 25 min at room temperature. After that, 3-bromo-1-propyne solution (80 % in toluene, 1.66 equiv., 0.13 mL, 1.25 mmol) was added over a period of 20 min. The mixture was stirred overnight at room temperature, then it was quenched with an aqueous saturated solution of NH_4Cl (15 mL), and extracted with CH_2Cl_2 (3 × 20 mL). The organic layer was dried over $MgSO_4$ and evaporated *in vacuo* to dryness. The orange residue was purified by SiO_2 column chromatography (CH_2Cl_2:MeOH, 99:1) to give the desired compound as orange solid (193 mg, 59 %).
^{1}H-NMR (300.13 MHz, $(CD_3)_2SO$) δ: 13.44 (s, 1H, pyrrole-N**H**), 7.86 (dd, $J_{H,H}$= 9.4 Hz; 2.2 Hz, 1H, Ar-**H**), 7.79 (s, 1H, -C=C-**H**), 7.51 (t, $J_{H,H}$= 5.5 Hz, 1H, Ar-**H**), 7.20-6.98 (m, 2H, Ar-**H** and -N**H**CO-), 4.71 (s, 2H, -N-C**H**$_2$-C≡CH), 3.33-3.28 (m, 2H, -NHCO-C**H**$_2$-CH$_2$-), 2.59-2.52 (m, 7H, -N(C**H**$_2$)$_3$- and -C≡C-**H**), 0.99 (t, 6H, $J_{H,H}$= 7.1 Hz, -N-(CH$_2$)$_2$-(C**H**$_3$)$_2$). ^{13}C{^{1}H}-NMR (75.47 MHz, $(CD_3)_2SO$) δ: 167.3, 164.9, 160.9, 138.0, 134.5, 132.8, 126.8, 126.2, 126.0, 121.6, 112.9, 110.2, 106.7, 106.3, 78.7, 74.8, 52.1, 47.0 (2C), 37.4, 29.5, 13.8, 12.2 (2C), 11.1. Calcd. for $C_{25}H_{29}FN_4O_2$: C, 68.79; H, 6.70; N, 12.83. Found: C, 68.90; H, 6.72, N, 12.81.
^{1}H-NMR



^{13}C{^{1}H}-NMR

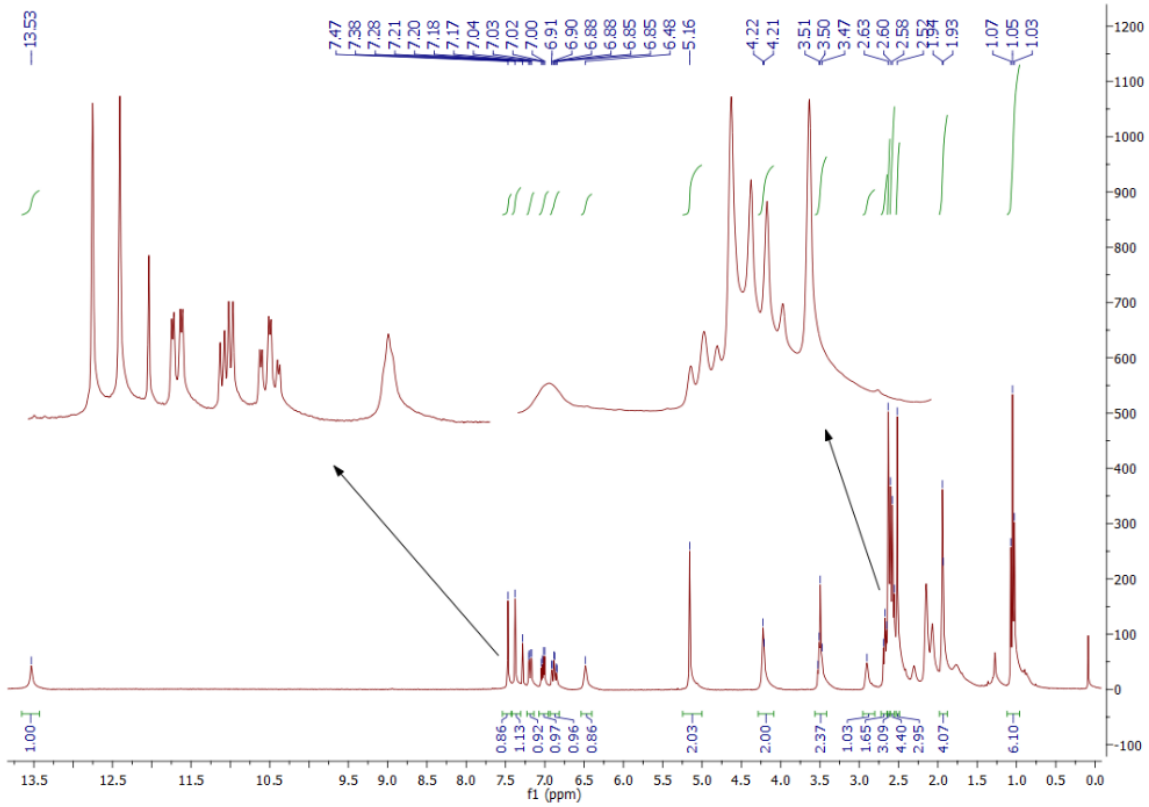


Compound 1

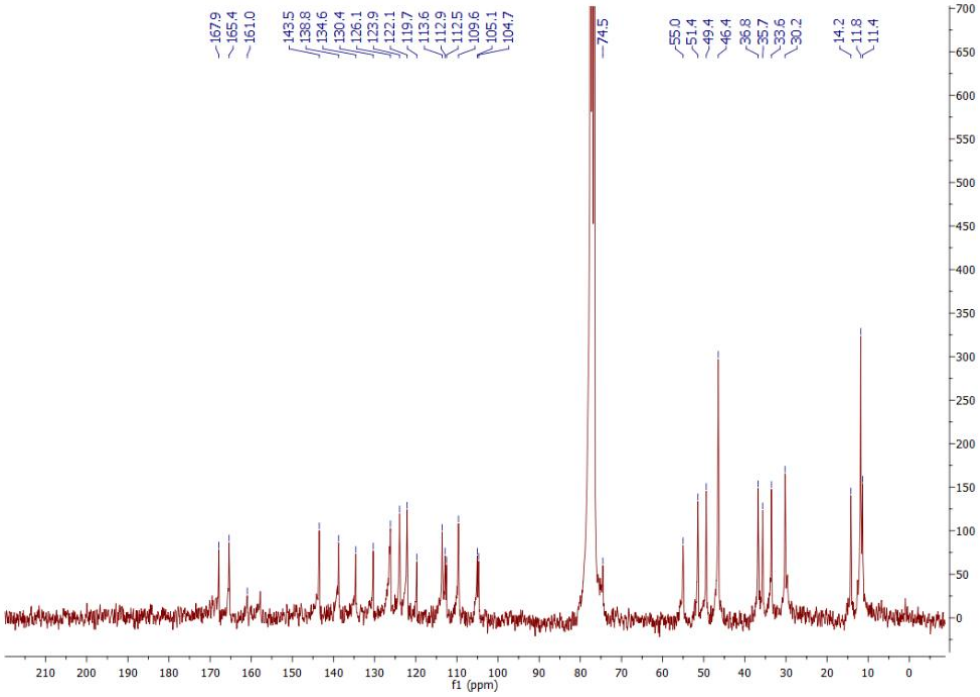


A 10-mL round-bottom flask equipped with a magnetic stirring bar was charged with Sunitinib derivative (1 equiv., 77 mg, 0.18 mmol) dissolved in THF:H_2O (3 mL, 1:1 v/v). Then, sodium ascorbate (5.3 mg, 15 mol %), $CuSO_4 \cdot 5H_2O$ (4.5 mg, 10 mol %) and ***C*** (1.1 equiv., 45 mg, 0.20 mmol) were added. The mixture was left at room temperature overnight. After that, the mixture was quenched by evaporation of the solvent. The crude was dissolved in CH_2Cl_2 (15 mL) and washed with brine (3 × 5 mL). The organic layer was dried over $MgSO_4$ and evaporated *in vacuo* to dryness. The product was purified by preparative SiO_2-TLC and CH_2Cl_2:MeOH (96:4) as eluent. The product was obtained following extraction of the silica with CH_2Cl_2 and evaporation under reduced pressure to yield a yellow solid (98 mg, 82 %).
$^1H\{^{11}B\}$-NMR (300.13 MHz, $CDCl_3$) δ: 13.53 (s, 1H, pyrrole-N**H**), 7.47 (s, 1H, -C=C-**H**), 7.38 (s, 1H, triazole-**H**), 7.19 (dd, 1H, $J_{H,H}$= 8.6 Hz; 2.3 Hz, Ar-**H**), 7.02 (dd, 1H, $J_{H,H}$= 8.5 Hz; 4.2 Hz, Ar-**H**), 6.88 (td, 1H, $J_{H,H}$= 8.9 Hz; 2.3 Hz, Ar-**H**) 6.52-6.43 (bs, 1H, -N**H**CO-), 5.16 (s, 2H, -N-C**H**$_2$-triazole), 4.25-4.18 (bs, 2H, -C**H**$_2$-triazole), 3.53-3.47 (m, 2H, -NHCO-C**H**$_2$-CH_2-), 2.90 (s, 1H, -B-$C_{cluster}$-**H**), 2.69-2.65 (m, 2H, -NHCO-CH_2-C**H**$_2$-), 2.63 (s, 3H, pyrrole-C**H**$_3$), 2.60-2.55 (m, 4H, -N-(C**H**$_2$)$_2$-(CH_3)$_2$), 2.52 (s, 3H, pyrrole-C**H**$_3$), 1.94-1.93 (bs, 4H, triazole-CH_2-C**H**$_2$-C**H**$_2$-$C_{cluster}$-), 1.05 (t, 6H, $J_{H,H}$= 7.1 Hz, -N-(CH_2)$_2$-(C**H**$_3$)$_2$). $^{13}C\{^1H\}$-NMR (75.47 MHz, $CDCl_3$) δ: 167.9, 165.4, 161.0, 143.5, 138.8, 134.6, 130.4, 126.1, 123.9, 122.1, 119.7, 113.6, 112.9, 112.6, 109.6, 105.1, 104.7, 74.5, 55.02, 51.4, 49.4, 46.5, 36.8, 35.7, 33.6, 30.2, 14.2, 11.8 (2C), 11.4. $^{11}B\{^1H\}$-NMR (96.29 MHz, $CDCl_3$) δ: -4.6 (1B), -11.1 (5B), -13.9 (2B), -15.8 (2B). Calcd. for $C_{30}H_{46}B_{10}FN_7O_2$: C, 54.28; H, 6.98; N, 14.77. Found: C, 54.49; H, 6.71, N, 14.61.

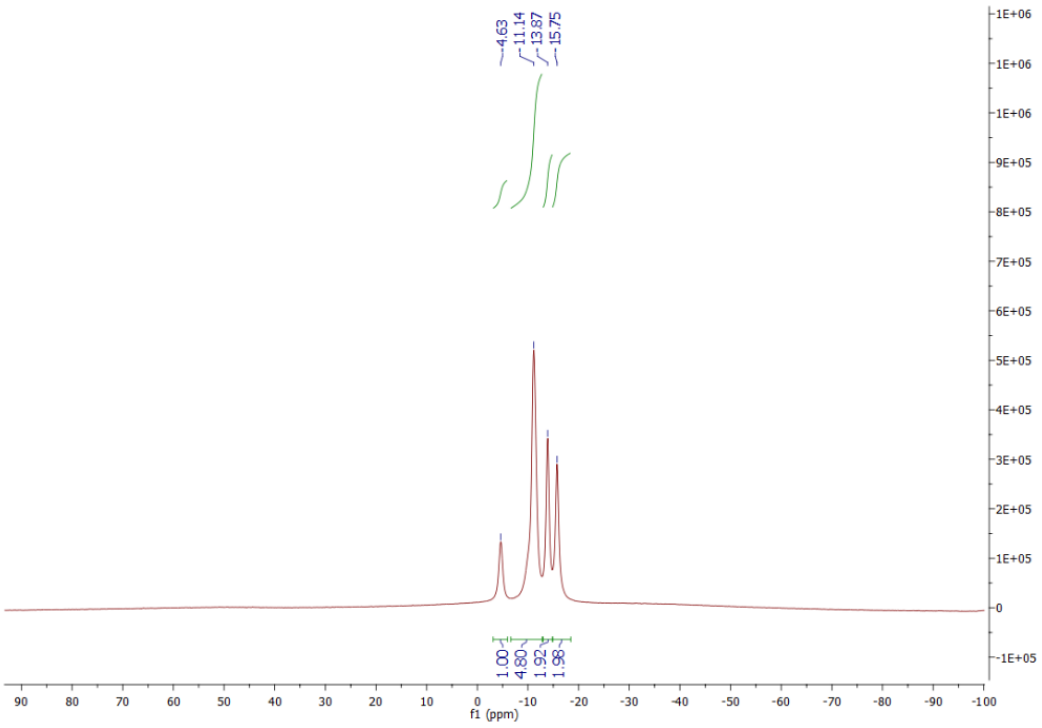
$^1H\{^{11}B\}$-NMR



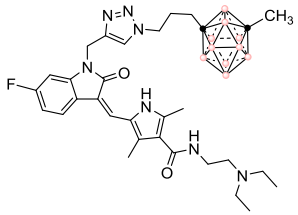
$^{13}C\{^{1}H\}$-NMR



$^{11}B\{^{1}H\}$-NMR



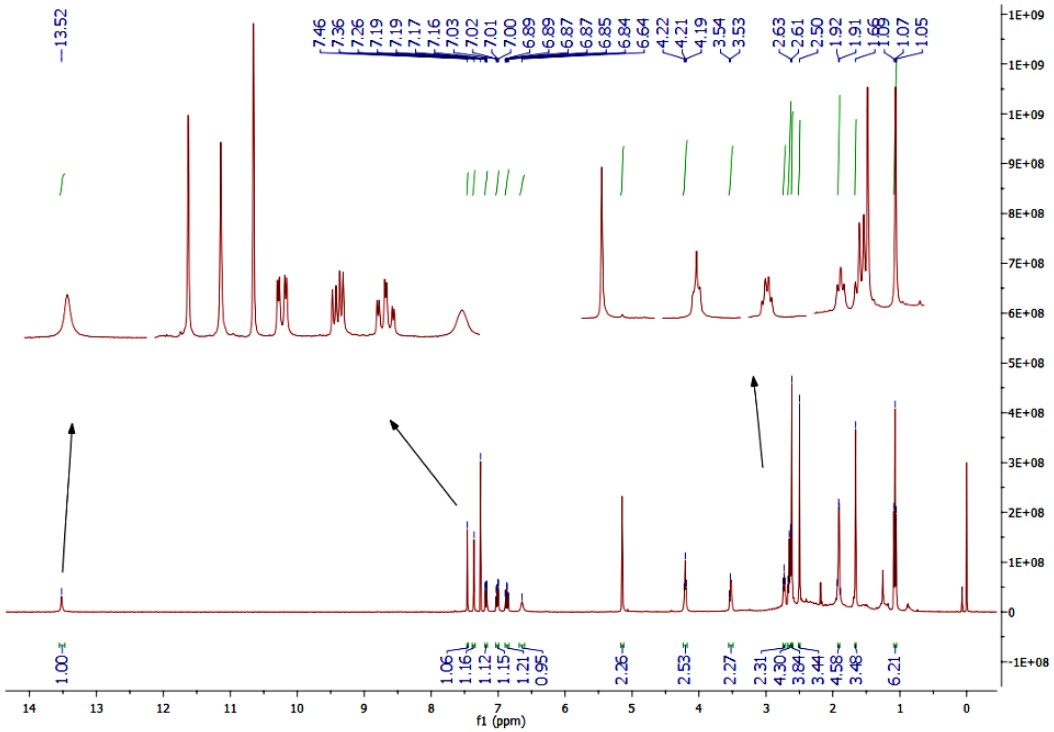
Compound 2



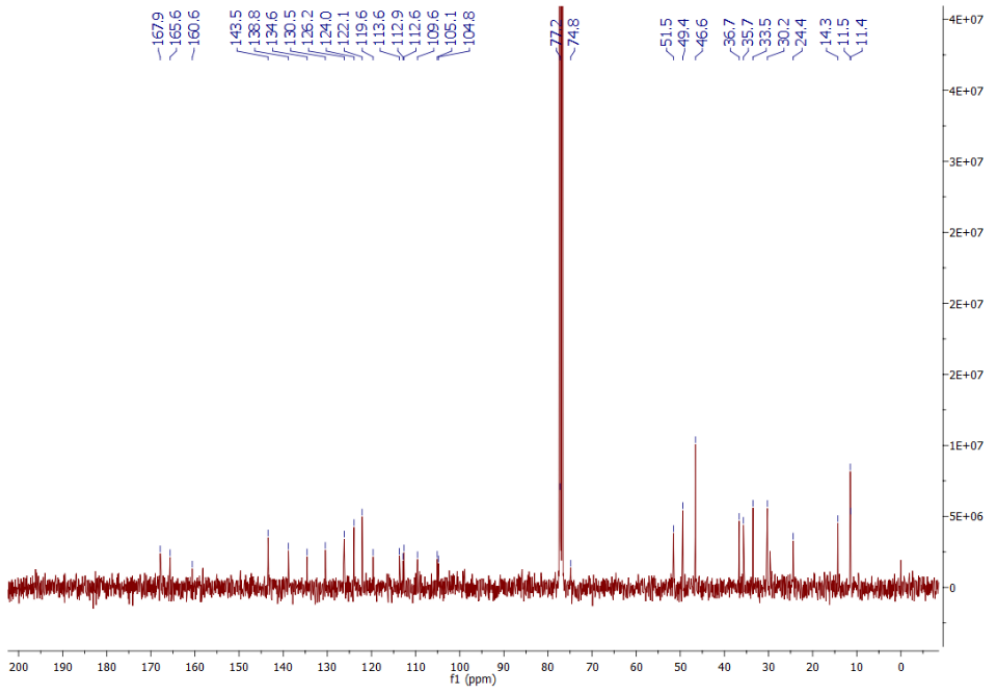
A 10-mL round-bottom flask equipped with a magnetic stirring bar was charged with Sunitinib derivative (1 equiv., 50 mg, 0.12 mmol) dissolved in THF:H_2O (3 mL, 1:1 v/v). Then, sodium ascorbate (3.6 mg, 15 mol %), $CuSO_4 \cdot 5H_2O$ (2.9 mg, 10 mol %) and ***D*** (1.1 equiv., 30 mg, 0.13 mmol) were added. The mixture was left at room temperature for 10 h. After that, the mixture was quenched by evaporation of the solvent. The crude was dissolved in CH_2Cl_2 (15 mL) and washed with brine (3 × 5 mL). The organic layer was dried over $MgSO_4$ and evaporated *in vacuo* to dryness. The product was purified by preparative SiO_2-TLC and CH_2Cl_2:MeOH (96:4) as eluent. The product was obtained following extraction of the silica with CH_2Cl_2 and evaporation under reduced pressure to yield a yellow solid (61 mg, 78 %).

^{1}H-NMR (400.13 MHz, $CDCl_3$) δ: 13.53 (s, 1H, pyrrole-N**H**), 7.46 (s, 1H, -C=C-**H**), 7.36 (s, 1H, triazole-**H**), 7.18 (dd, 1H, $J_{H,H}$= 8.6 Hz; 2.1 Hz, Ar-**H**), 7.02 (dd, 1H, $J_{H,H}$= 8.5 Hz; 4.2 Hz, Ar-**H**), 6.88 (td, 1H, $J_{H,H}$= 9.0 Hz; 2.1 Hz, Ar-**H**) 6.64 (bs, 1H, -N**H**CO-), 5.15 (s, 2H, -N-C**H**$_2$-triazole), 4.22 (t, 2H, $J_{H,H}$= 6.1 Hz, -C**H**$_2$-triazole), 3.52 (dd, 2H, $J_{H,H}$= 10.9 Hz; 5.2 Hz, -NHCO-C**H**$_2$-CH_2-), 2.73 (t, 2H, $J_{H,H}$= 5.7 Hz, -NHCO-CH_2-C**H**$_2$-), 2.67-2.63 (m, 4H, -N-(C**H**$_2$)$_2$-(CH_3)$_2$), 2.61 (s, 3H, pyrrole-C**H**$_3$), 2.50 (s, 3H, pyrrole-C**H**$_3$), 1.93-1.89 (bs, 4H, triazole-CH_2-C**H**$_2$-C**H**$_2$-$C_{cluster}$-), 1.66 (s, 3H, -$C_{cluster}$-C**H**$_3$) 1.07 (t, 6H, $J_{H,H}$= 7.1 Hz, -N-(CH_2)$_2$-(C**H**$_3$)$_2$). ^{13}C{^{1}H}-NMR (100.77 MHz, $CDCl_3$) δ: 167.9, 165.6, 160.6, 143.5, 138.8, 134.6, 130.5, 126.2, 124.0, 122.1, 119.6, 113.6, 112.9, 112.6, 109.6, 105.1, 104.8, 77.2, 74.8, 51.5, 49.4, 46.6, 36.7, 35.7, 33.5, 30.2, 24.4, 14.3, 11.5 (2C), 11.4. ^{11}B{^{1}H}-NMR (96.29 MHz, $CDCl_3$) δ: -6.6 (1B), -5.8 (1B), -8.7 (1B), -10.8 (6B), -13.2 (2B). Calcd. for $C_{31}H_{48}B_{10}FN_7O_2$: C, 54.93; H, 7.14; N, 14.46. Found: C, 54.96; H, 7.17, N, 14.43.

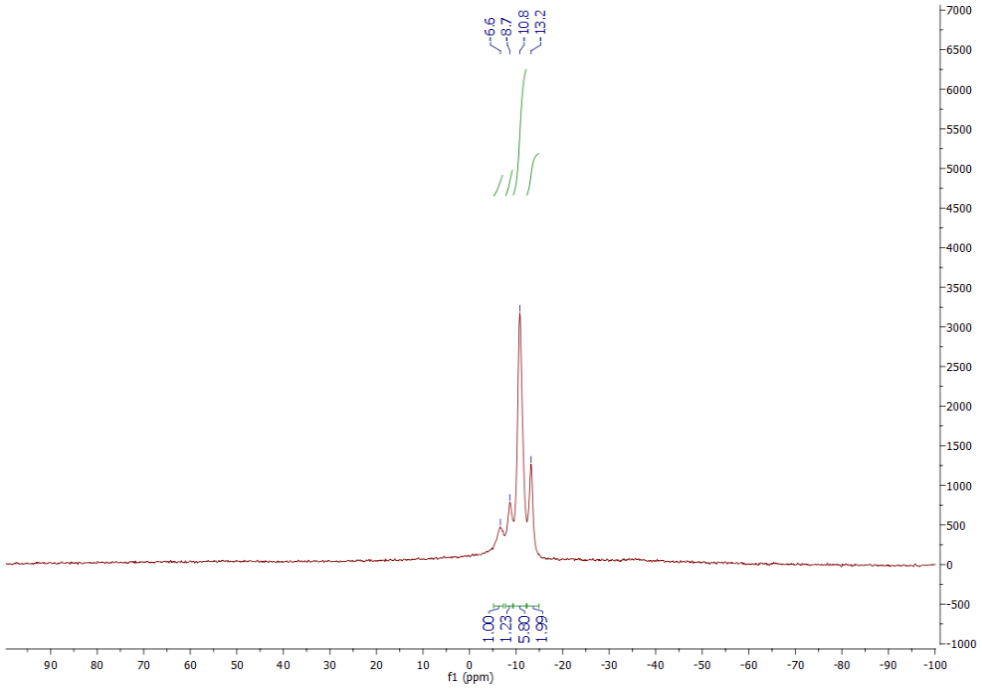
^{1}H-NMR



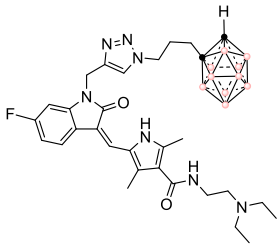
$^{13}C\{^{1}H\}$-NMR



$^{11}B\{^{1}H\}$-NMR

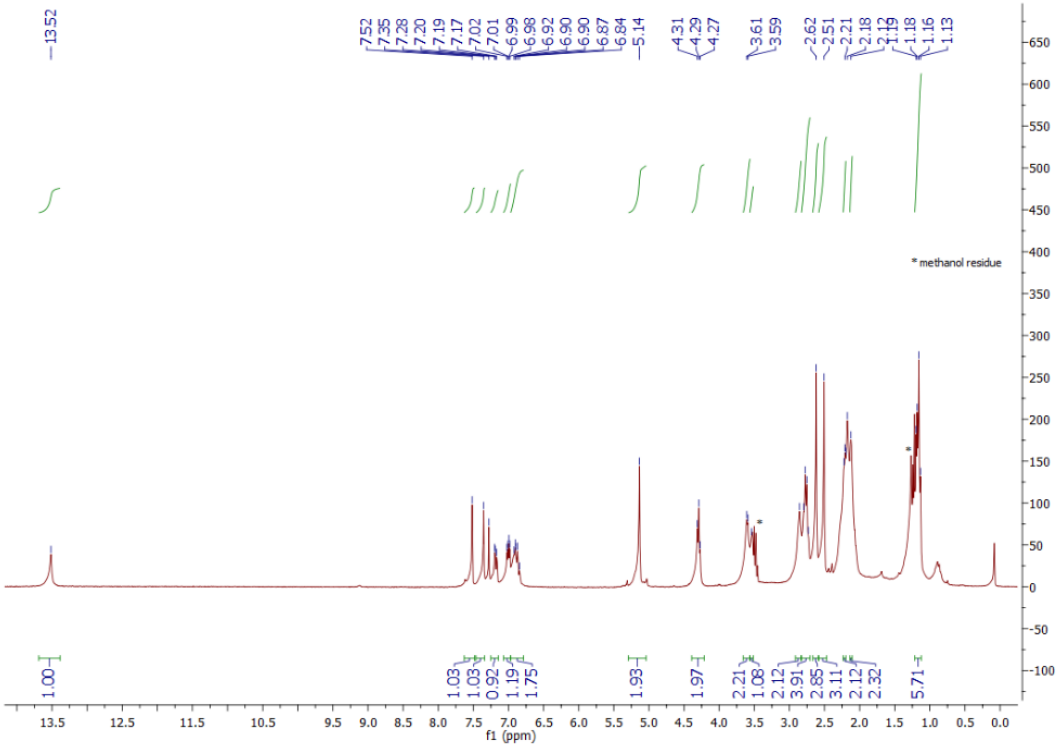


Compound 3

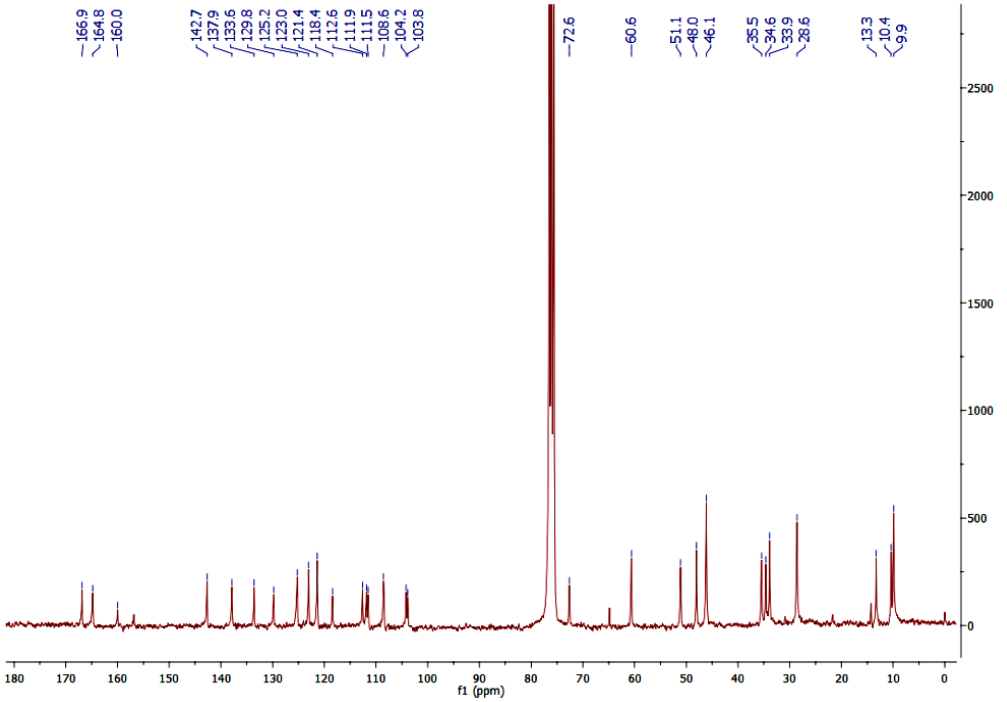


A 10-mL round-bottom flask equipped with a magnetic stirring bar was charged with Sunitinib derivative (1 equiv., 62 mg, 0.14 mmol) dissolved in THF:H_2O (3 mL, 1:1 v/v). Then, sodium ascorbate (4.2 mg, 15 mol %), $CuSO_4 \cdot 5H_2O$ (3.5 mg, 10 mol %) and ***G*** (1.1 equiv., 35 mg, 0.15 mmol) were added. The mixture was stirred overnight at room temperature. After that, the mixture was quenched by evaporation of the solvent. The crude was dissolved in CH_2Cl_2 (15 mL) and washed with brine (3 × 5 mL). The organic layer was dried over $MgSO_4$ and evaporated *in vacuo* to dryness. The product was purified by preparative SiO_2-TLC and CH_2Cl_2:MeOH (97:3) as eluent. The product was obtained following extraction of the silica with CH_2Cl_2 and evaporation under reduced pressure to yield a orange solid (80 mg, 86 %).
$^1H\{^{11}B\}$-NMR (300.13 MHz, $CDCl_3$) δ: 13.52 (s, 1H, pyrrole-N**H**), 7.52 (s, 1H, -C=C-**H**), 7.35 (s, 1H, triazole-**H**), 7.22-7.15 (m, 1H, Ar-**H**), 7.00 (dd, 1H, $J_{H,H}$= 8.5 Hz; 4.2 Hz, Ar-**H**), 6.97-6.80 (m, 2H, Ar-**H** and -N**H**CO-), 5.14 (s, 2H, -N-C**H**$_2$-triazole), 4.29 (t, $J_{H,H}$= 6.1, 2H, -C**H**$_2$-triazole), 3.63-3.58 (m, 2H, -NHCO-C**H**$_2$-CH_2-), 3.59 (s, 1H, -B-Cc-**H**), 2.86 (m, 2H, -NHCO-CH_2-C**H**$_2$-), 2.76 (dd, $J_{H,H}$= 13.4 Hz; 6.5 Hz, 4H, -N-(C**H**$_2$)$_2$-$(CH_3)_2$), 2.62 (s, 3H, pyrrole-C**H**$_3$), 2.51 (s, 3H, pyrrole-C**H**$_3$), 2.22-2.12 (bs, 4H, triazole-CH_2-C**H**$_2$-C**H**$_2$-Ccluster-), 1.16 (t, 6H, $J_{H,H}$= 6.9 Hz, -N-$(CH_2)_2$-(C**H**$_3$)$_2$).
$^{13}C\{^1H\}$-NMR (75.47 MHz, $CDCl_3$) δ: 166.9, 164.8, 160.0, 142.7, 137.9, 133.6, 129.8, 125.2, 123.0, 121.4, 118.4, 112.6, 111.9, 111.5, 108.6, 104.2, 103.8, 72.6, 64.8, 51.1, 48.0, 46.1, 35.5, 34.6, 33.9, 28.6, 13.3, 10.4, 9.90 (2C). $^{11}B\{^1H\}$-NMR (96.29 MHz, $CDCl_3$) δ: -2.5 (1B), -5.8 (1B), -9.5 (2B), -12.2 (6B). Calcd. for $C_{30}H_{46}B_{10}FN_7O_2$: C, 54.28; H, 6.98; N, 14.77. Found: C, 54.29; H, 6.65, N, 14.53.

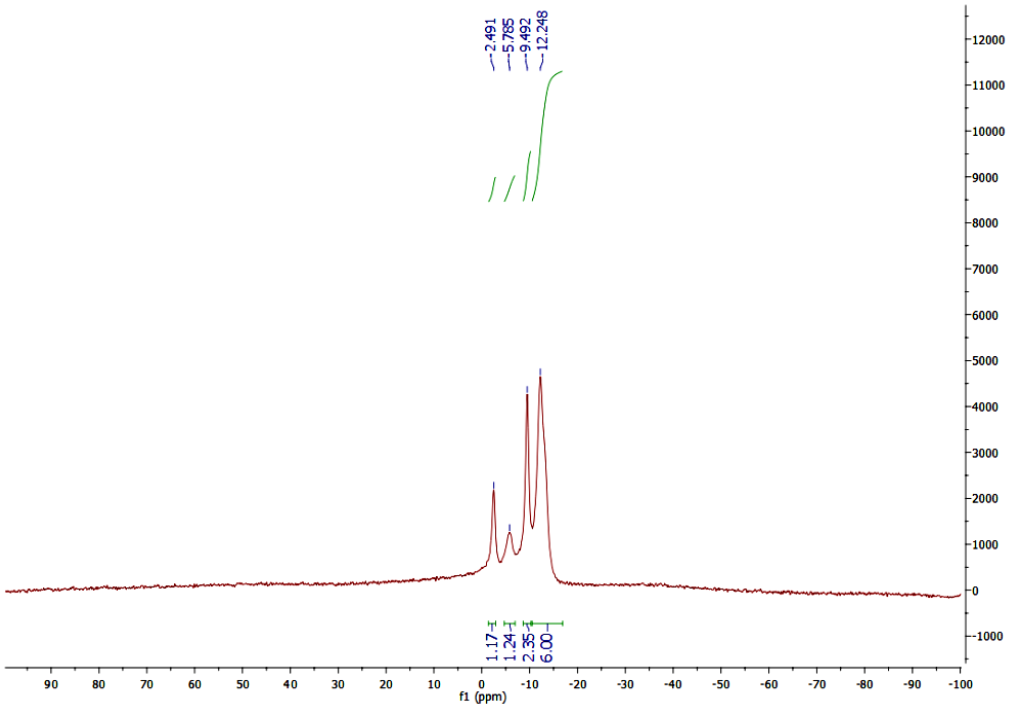
^1H-NMR



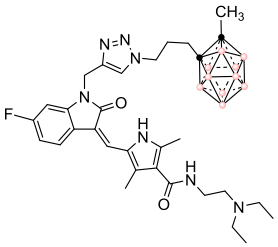
$^{13}C\{^{1}H\}$-NMR



$^{11}B\{^{1}H\}$-NMR

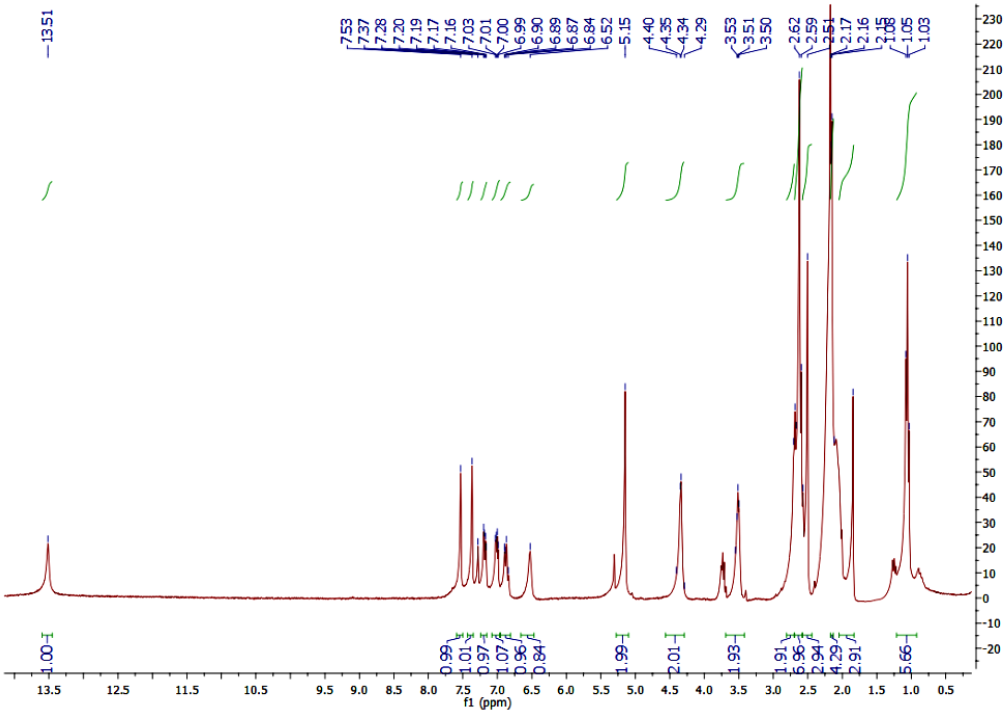


Compound 4

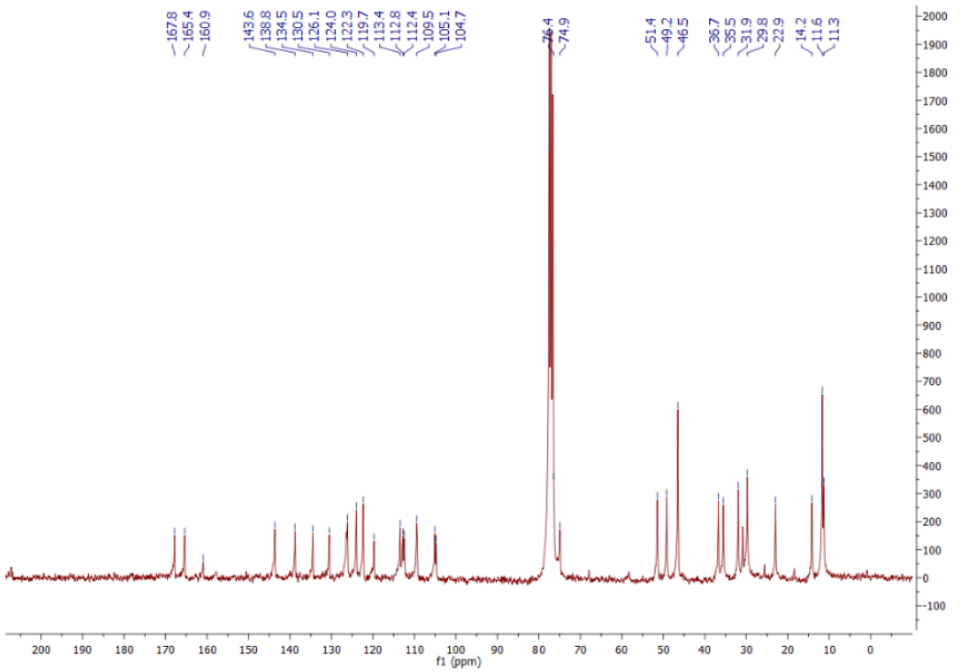


A 10-mL round-bottom flask equipped with a magnetic stirring bar was charged with sunitinib derivative (1 equiv., 40 mg, 0.09 mmol) dissolved in THF:H_2O (3 mL, 1:1 v/v). Then, sodium ascorbate (2.7 mg, 15 mol %), $CuSO_4 \cdot 5H_2O$ (2.3 mg, 10 mol %) and ***H*** (1.1 equiv., 26 mg, 0.1 mmol) were added. The mixture was left at room temperature for 8 h. After that, the mixture was quenched by evaporation of the solvent. The crude was dissolved in CH_2Cl_2 (15 mL) and washed with brine (3 × 5 mL). The organic layer was dried over $MgSO_4$ and evaporated *in vacuo* to dryness. The product was purified by preparative SiO_2-TLC and CH_2Cl_2:MeOH (96:4) as eluent. The product was obtained following extraction of the silica with CH_2Cl_2 and evaporation under reduced pressure to yield a yellow solid (48 mg, 79 %).
$^1H\{^{11}B\}$-NMR (300.13 MHz, $CDCl_3$) δ: 13.51 (s, 1H, pyrrole-N**H**), 7.53 (s, 1H, -C=C-**H**), 7.37 (s, 1H, triazole-**H**), 7.18 (dd, 1H, $J_{H,H}$= 8.4 Hz; 2.0 Hz, Ar-**H**), 7.01 (dd, $J_{H,H}$= 8.4 Hz; 4.2 Hz, 1H, Ar-**H**), 6.87 (dd, 1H, $J_{H,H}$= 12.2 Hz; 5.4 Hz, Ar-**H**), 6.52 (bs, 1H, -N**H**CO-), 5.15 (s, 2H, -N-C**H**$_2$-triazole), 4.40-4.29 (m, 2H, -C**H**$_2$-triazole), 3.55-3.50 (m, 2H, -NHCO-C**H**$_2$-CH_2-), 2.70-2.67 (m, 2H, -NHCO-CH_2-C**H**$_2$-), 2.67-2.57 (m, 7H, pyrrole-C**H**$_3$ and -N-(C**H**$_2$)$_2$-$(CH_3)_2$), 2.51 (s, 3H, pyrrole-C**H**$_3$), 2.16-2.12 (bs, 4H, triazole-CH_2-C**H**$_2$-C**H**$_2$-$C_{cluster}$-), 1.85 (s, 3H, -$C_{cluster}$-C**H**$_3$), 1.05 (t, 6H, $J_{H,H}$= 7 Hz, -N-$(CH_2)_2$-$(CH_3)_2$). $^{13}C\{^1H\}$-NMR (75.47 MHz, $CDCl_3$) δ: 167.8, 165.4, 160.9, 143.6, 138.8, 134.5, 130.5, 126.1, 124.0, 122.3, 119.7, 113.4, 112.8, 112.4, 109.5, 105.1, 104.8, 76.4, 74.9, 51.4, 49.2, 46.5, 36.7, 35.5, 31.9, 29.8, 22.9, 14.2, 11.6 (2C), 11.3. $^{11}B\{^1H\}$-NMR (96.29 MHz, $CDCl_3$) δ: -4.4 (1B), -5.8 (1B), -10.5 (8B). Calcd. for $C_{31}H_{48}B_{10}FN_7O_2$: C, 54.93; H, 7.14; N, 14.46. Found: C, 54.90; H, 7.15, N, 14.61.

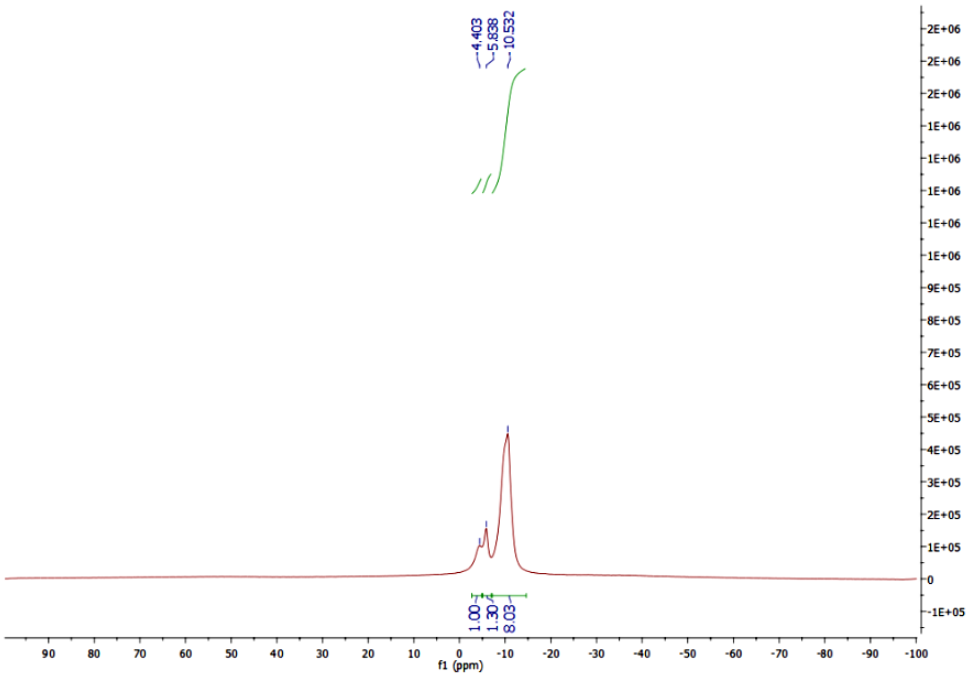
^{1}H-NMR



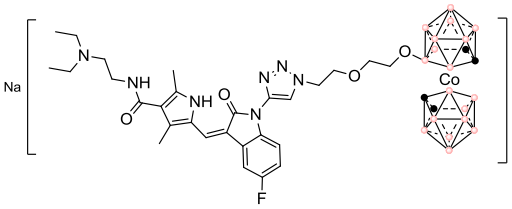
$^{13}C\{^{1}H\}$-NMR



$^{11}B\{^{1}H\}$-NMR

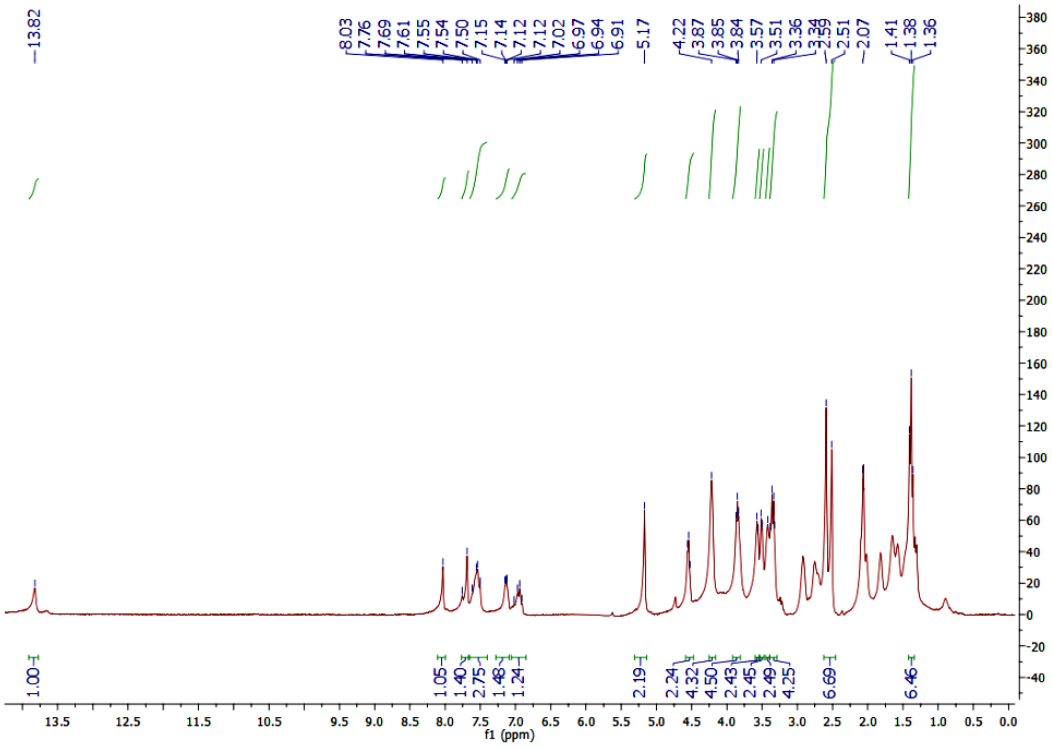


Compound 5

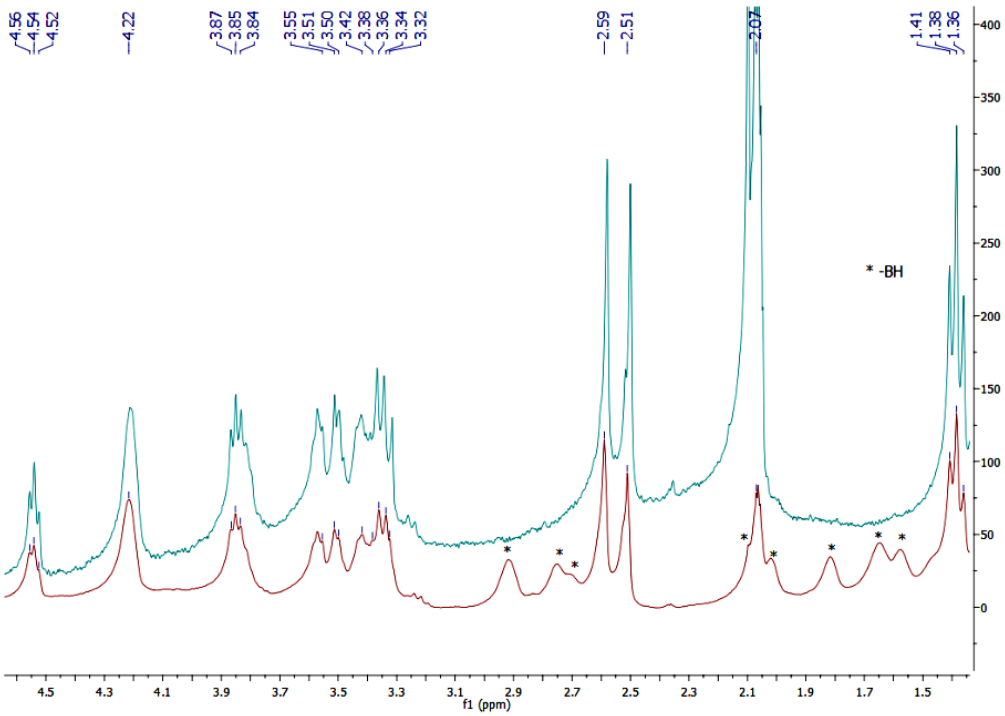


A 25-mL round-bottom flask equipped with a magnetic stirring bar was charged with Sunitinib derivative (1 equiv., 64 mg, 0.15 mmol) dissolved in THF:H_2O (4 mL, 1:1 v/v). Consecutively, sodium ascorbate (4.5 mg, 15 mol %), $CuSO_4{\cdot}5H_2O$ (3.8 mg, 10 mol %) and ***J*** (1.1 equiv., 79 mg, 0.17 mmol) were added. The mixture was left at room temperature for 8 h. After that, the reaction mixture was filtered off and the solvent was removed under vacuum. The orange solid was dissolved in 0.5 mL of EtOH and precipitated as tetramethylammonium salt by adding an aqueous saturated solution of NMe_4Cl. The suspension was centrifuged and the orange solid was filtered, rinsed with water and the solid was purified by SiO_2-TLC using CH_2Cl_2:MeOH (98:2) as eluent. Finally, the product was obtained after cation exchange of $^{+}NMe_4$ by ^{+}Na in a cation exchange resin, to give an orange solid (97 mg, 71 %).
$^1H\{^{11}B\}$-NMR (300.13 MHz, CD_3COCD_3) δ: 13.82 (s, 1H, pyrrole-N**H**), 8.03 (s, 1H, triazole-**H**), 7.72 (bs, 1H, -C=C-**H**), 7.55 (bs, 3H, Ar-**H** and -N**H**CO-), 7.13 (dd, 1H, $J_{H,H}$= 6.3 Hz, 2.0 Hz, Ar-**H**), 7.02-6.91 (m, 1H, Ar-**H**), 5.17 (s, 2H, -N-C**H**$_2$-triazole), 4.54 (t, 2H, $J_{H,H}$= 5.1 Hz, -C**H**$_2$-triazole), 4.22 (bs, 4H, -B-C_c-**H**), 3.87.3.82 (m, 4H, -OC**H**$_2$-CH_2-triazole and -NHCO-C**H**$_2$-CH_2-), 3.57-3.54 (m, 2H, -OC**H**$_2$-CH_2OB-), 3.52-3.50 (m, 2H, -OCH_2-C**H**$_2$OB-), 3.42-3.32 (m, 6H, N-(C**H**$_2$)$_3$), 2.59 (3H, pyrrole-C**H**$_3$), 2.51 (3H, pyrrole-C**H**$_3$), 1.38 (t, 6H, $J_{H,H}$= 7.1 Hz, -N-$(CH_2)_2$-(C**H**$_3$)$_2$). $^{13}C\{^1H\}$-NMR (75.47 MHz, CD_3COCD_3) δ: 168.4, 167.7, 142.3, 138.4, 135.4, 130.5, 126.5, 124.1, 123.8, 117.9, 114.9, 112.8, 112.4, 109.9, 105.7,105.3, 71.9, 69.1, 68.5, 54.9, 54.4, 53.9, 50.1 (2C), 48.3 (2C), 46.5, 36.9, 35.2, 13.4, 10.4, 9.7, 9.4. $^{11}B\{^1H\}$-NMR (96.29 MHz, $CDCl_3$) δ:24.73 (1B), 6.04 (1B), 1.76 (1B), -1.31 (1B), -3.07 (2B), -5.96 (6B), -15.92 (2B), -18.89 (3B), -26.94 (1B). MALDI-TOF-MS: *m/z* calcd. 889.49. Found: 889.62.Calcd. for $C_{33}H_{59}B_{18}CoFN_7O_4$: C, 44.51; H, 6.68; N, 11.01. Found: C, 44.22; H, 6.94, N, 10.79.

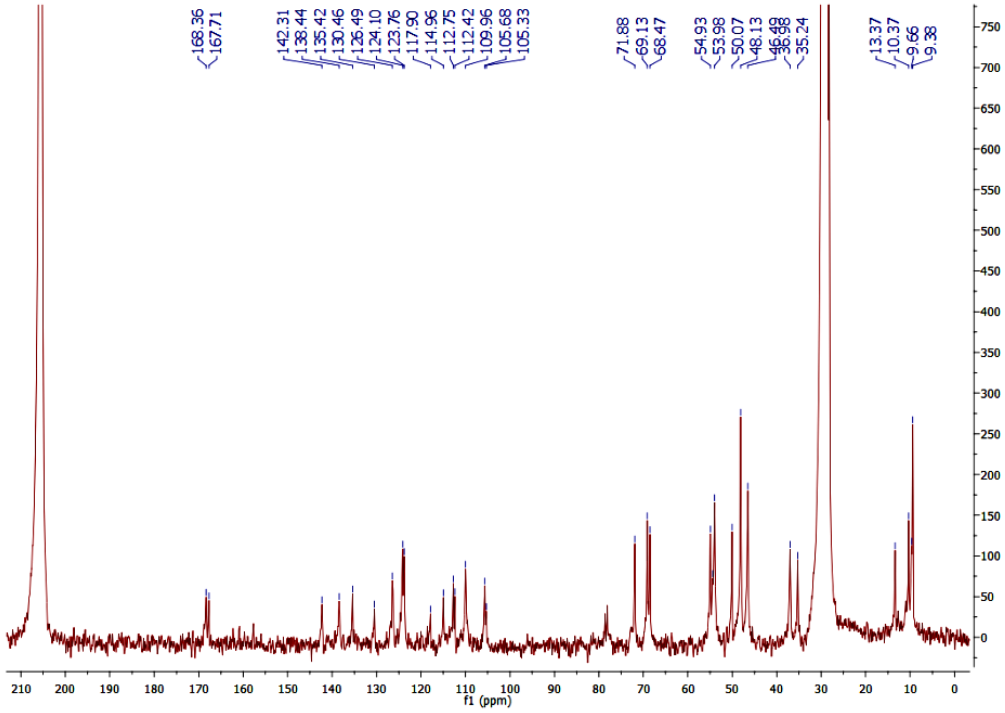
$^1H\{^{11}B\}$-NMR



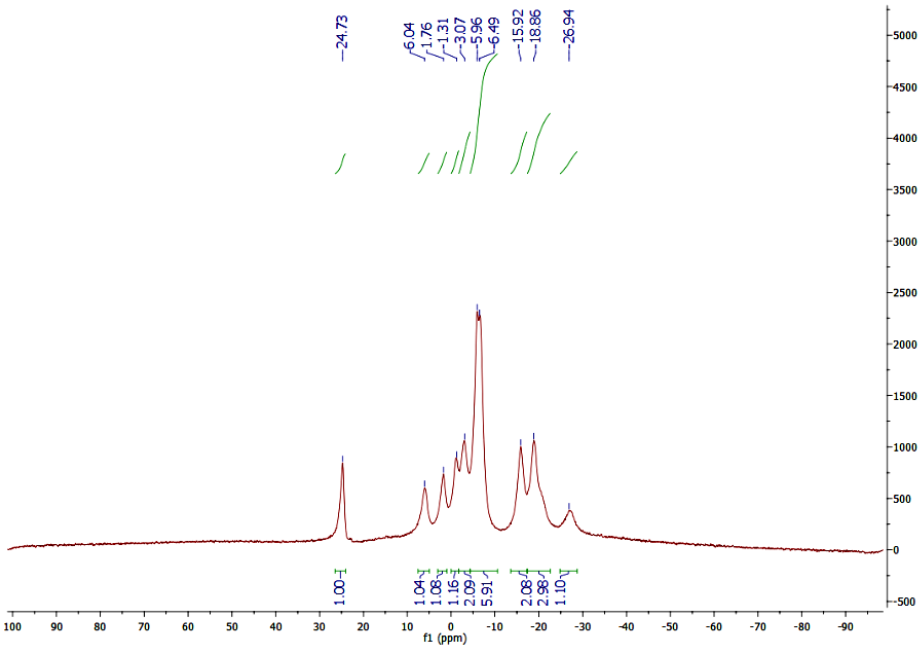
Coupled spectra $^{1}H\{^{11}B\}$-NMR (red) and ^{1}H-NMR (green).



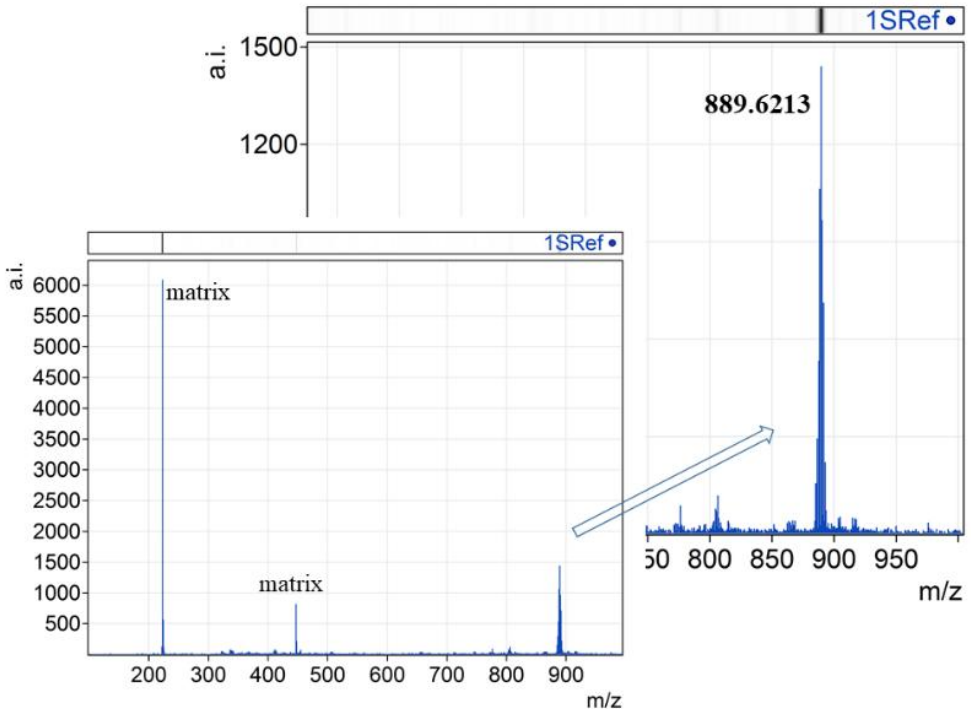
$^{13}C\{^{1}H\}$-NMR



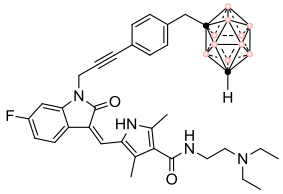
$^{11}B\{^{1}H\}$-NMR



MALDI-TOF-MS

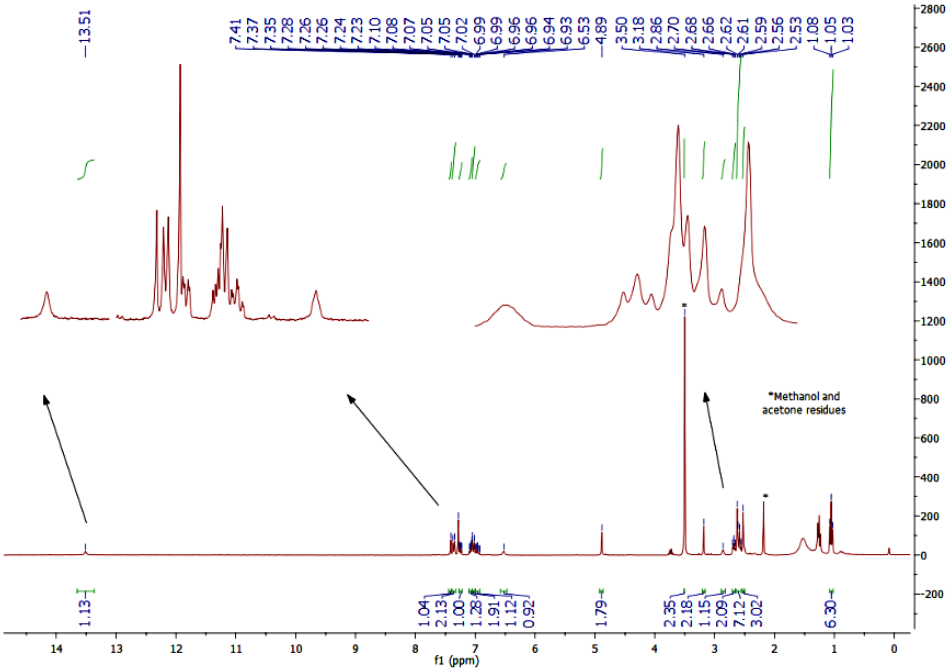


Compound 6

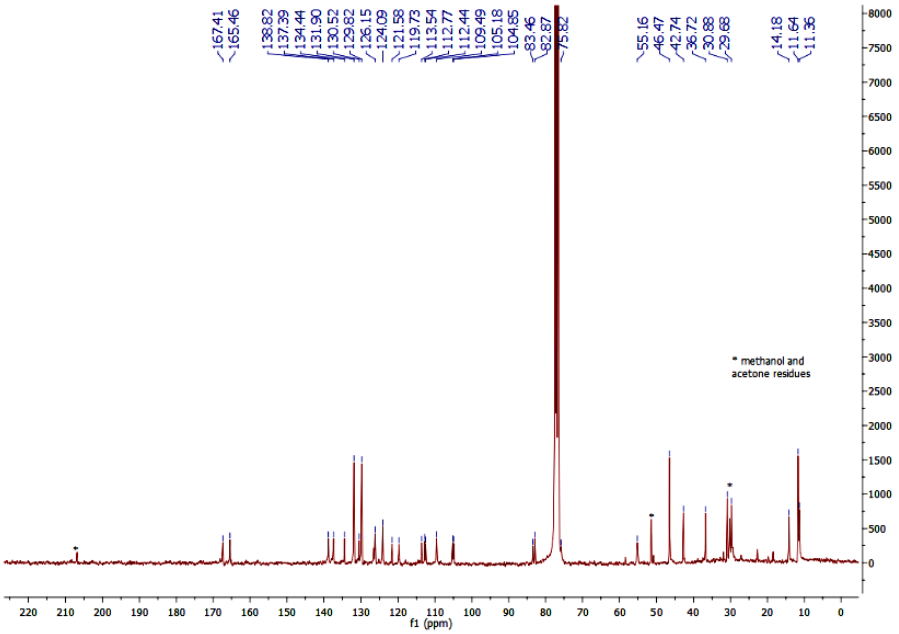


To a 10-mL oven-dried round bottom flask equipped with a magnetic stirring bar was charged under nitrogen with ***K*** (1 equiv., 50 mg, 0.14 mmol), CuI (2.6 mg, 10 mol %), $PdCl_2(PPh_3)_2$ (7.8 mg, 8 mol %) and Sunitinib derivative (1 equiv. 60 mg, 0.14 mmol). A dry solvent system of THF:Et_3N (4 mL, 3:1, v/v) was well-degassed under nitrogen for 45 min prior to addition to the reaction mixture. After heating at 60 °C for 10 h, the solution was filtered through a small pad of celite and washed with methanol (10 mL). The solution was concentrated *in vacuo* and the crude was dissolved in CH_2Cl_2 (10 mL) and washed with brine (4 × 5 mL). The organic layer was dried over $MgSO_4$ and evaporated *in vacuo* to dryness. The product was purified by preparative SiO_2-TLC and CH_2Cl_2:MeOH (95:5) as eluent. The product was obtained following extraction of the silica with CH_2Cl_2:MeOH and evaporation under reduced pressure to yield a yellow solid (21 mg, 22 %).
$^1H\{^{11}B\}$-NMR (300.13 MHz, $CDCl_3$) δ: 13.51 (s, 1H, pyrrole-N**H**), 7.41 (s, 1H, -C=C-**H**), 7.36 (d, 2H, $J_{H,H}$= 8.0 Hz, Ar-**H**), 7.25 (dd, 1H, $J_{H,H}$= 8.6 Hz, 2.3 Hz, Ar-**H**), 7.08 (dd, 1H, $J_{H,H}$= 8.6 Hz; 4.4 Hz, Ar-**H**), 7.03 (d, 2H, $J_{H,H}$= 8.1 Hz, Ar-**H**), 6.96 (td, 1H, $J_{H,H}$= 8.8 Hz; 2.3 Hz, Ar-**H**), 6.53 (bs, 1H, -N**H**CO-), 4.89 (s, 2H, -N-C**H**$_2$-C≡C-), 3.52-3.49 (m, 2H, -NHCO-C**H**$_2$-CH_2-), 3.18 (s, 2H, -Ph-C**H**$_2$-$C_{cluster}$-), 2.86 (bs, 1H, -B-$C_{cluster}$-**H**), 2.68 (t, 2H, $J_{H,H}$= 5.8 Hz, -NHCO-CH_2-C**H**$_2$-), 2.65-2.55 (m, 7H, pyrrole-C**H**$_3$ and -N-(C**H**$_2$)$_2$-$(CH_3)_2$), 2.60-2.65 (m, 4H -N-(C**H**$_2$)$_2$-$(CH_3)_2$), 2.53 (s, 3H, pyrrole-C**H**$_3$), 1.05 (t, 6H, $J_{H,H}$= 7.1 Hz, -N-$(CH_2)_2$-(C**H**$_3$)$_2$). $^{13}C\{^1H\}$-NMR (75.47 MHz, $CDCl_3$) δ: 167.4, 165.5, 138.8, 137.4, 134.4, 131.9 (2C), 130.5, 129.8 (2C), 128.5, 126.2, 124.1, 121.6, 119.7, 113.5, 112.8, 112.4, 109.5, 105.2, 104.9, 83.5, 82.9, 75.8, 55.2, 46.5 (2C), 42.7, 36.7, 30.9, 29.7, 14.2, 11.6, 11.4. $^{11}B\{^1H\}$-NMR (96.29 MHz, $CDCl_3$) δ: -4.20 (1B), -10.97 (5B), -13.78 (2B), -15.81 (2B). Calcd. for $C_{34}H_{45}B_{10}FN_4O_2$: C, 61.05; H, 6.78; N, 8.38. Found: C, 61.34; H, 6.96, N, 8.17.

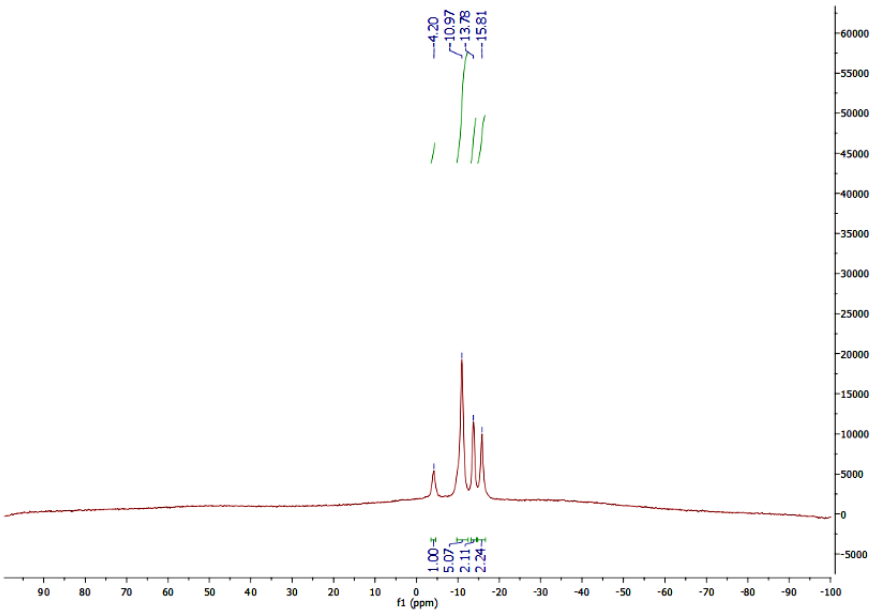
$^1H\{^{11}B\}$-NMR



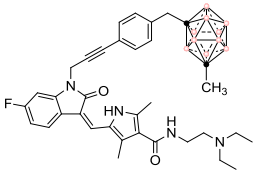
$^{13}C\{^{1}H\}$-NMR



$^{11}B\{^{1}H\}$-NMR

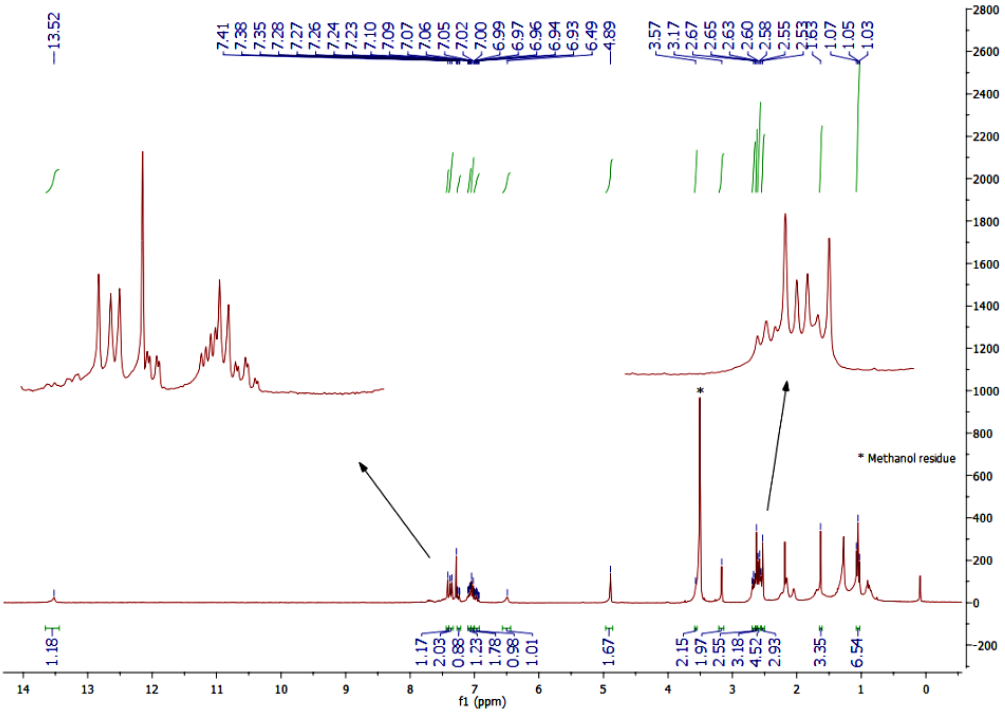


Compound 7

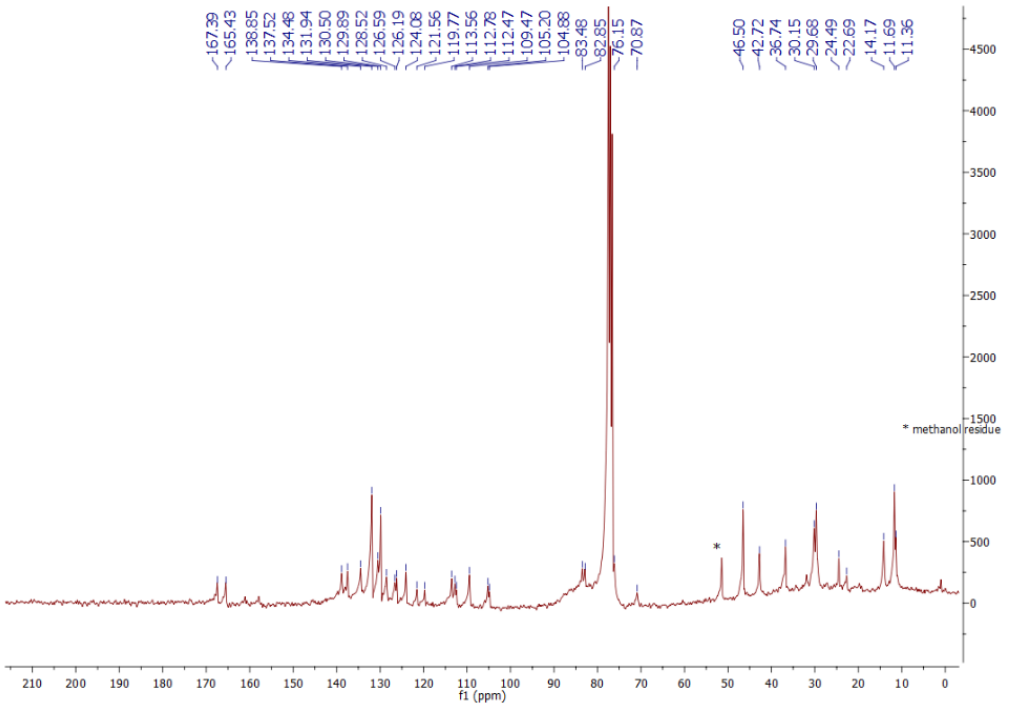


To a 10-mL oven-dried round bottom flask equipped with a magnetic stirring bar was charged under nitrogen with ***L*** (1 equiv., 85 mg, 0.22 mmol), CuI (3.8 mg, 10 mol %), $PdCl_2(PPh_3)_2$ (11.2 mg, 8 mol %) and Sunitinib derivative (1 equiv. 95 mg, 0.22 mmol). A dry solvent system of THF:Et_3N (4 mL, 3:1, v/v) was well-degassed under nitrogen for 45 min prior to addition to the reaction mixture. After heating at 60 °C for 10 h, the solution was filtered through a small pad of celite and washed with methanol (10 mL). The solution was concentrated *in vacuo* and the crude was dissolved in CH_2Cl_2 (10 mL) and washed with brine (4 × 5 mL). The organic layer was dried over $MgSO_4$ and evaporated *in vacuo* to dryness. The product was purified by preparative SiO_2-TLC and CH_2Cl_2:MeOH (97:3) as eluent. The product was obtained following extraction of the silica with CH_2Cl_2:MeOH and evaporation under reduced pressure to yield an orange-red solid (44 mg, 29 %).
$^1H\{^{11}B\}$-NMR (300.13 MHz, $CDCl_3$) δ: 13.52 (s, 1H, pyrrole-N**H**), 7.41 (s, 1H, -C=C-**H**), 7.36 (d, 2H, $J_{H,H}$= 8.1 Hz, Ar-**H**), 7.25 (dd, 1H, $J_{H,H}$= 8.6 Hz, 2.4 Hz, Ar-**H**), 7.08 (dd, 1H, $J_{H,H}$= 8.5 Hz; 4.3 Hz, Ar-**H**), 7.03 (d, 2H, $J_{H,H}$= 8.1 Hz, Ar-**H**), 7.01-6.93 (m, 1H, Ar-**H**), 6.49 (bs, 1H, -N**H**CO-), 4.89 (s, 2H, -N-C**H**$_2$-C≡C-), 3.57-3.50 (m, 2H, -NHCO-C**H**$_2$-CH_2-), 3.17 (s, 2H, -Ph-C**H**$_2$-$C_{cluster}$-), 2.69-2.65 (m, 2H, -NHCO-CH_2-C**H**$_2$-), 2.63 (s, 3H, pyrrole-C**H**$_3$), 2.60-2.65 (m, 4H -N-(C**H**$_2$)$_2$-(CH_3)$_2$), 2.53 (s, 3H, pyrrole-C**H**$_3$), 1.63 (s, 3H, -$C_{cluster}$-C**H**$_3$), 1.05 (t, 6H, $J_{H,H}$= 7.1 Hz, -N-(CH_2)$_2$-(C**H**$_3$)$_2$).
$^{13}C\{^1H\}$-NMR (75.47 MHz, $CDCl_3$) δ: 167.4, 165.4, 138.9, 135.5, 134.5, 131.9, 130.5, 129.9, 128.5, 126.6, 126.2, 124.1, 121.6, 119.8, 113.6, 112.8, 112.5, 109.5, 105.2, 104.9, 83.5, 82.9, 76.2, 70.9, 46.5, 42.7, 36.7, 30.2, 29.7, 24.5, 22.7, 14.2, 11.7 (2C), 11.4. $^{11}B\{^1H\}$-NMR (96.29 MHz, $CDCl_3$) δ: -6.46 (1B), -8.32 (1B), -10.76 (6B), -13.40 (2B). Calcd. For $C_{35}H_{47}B_{10}FN_4O_2$: C, 61.56; H, 6.94; N, 8.20. Found: C, 61.89; H, 6.77, N, 8.53.

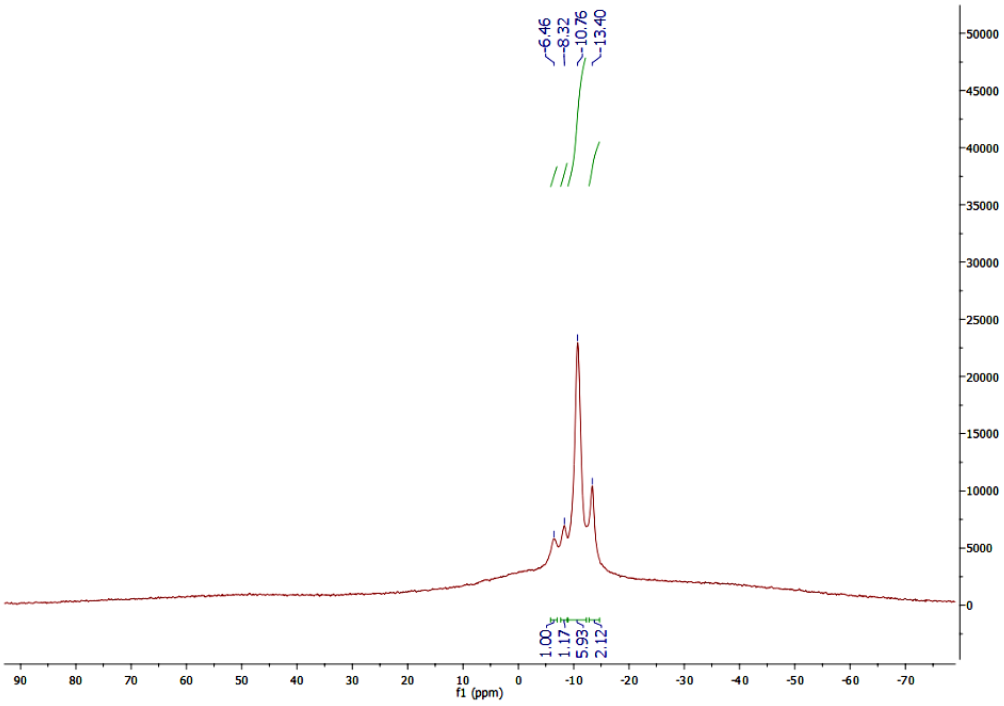
$^1H\{^{11}B\}$-NMR



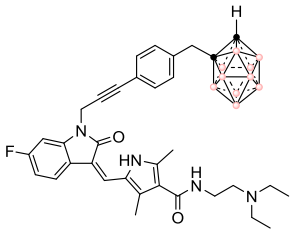
$^{13}C\{^{1}H\}$-NMR



$^{11}B\{^{1}H\}$-NMR

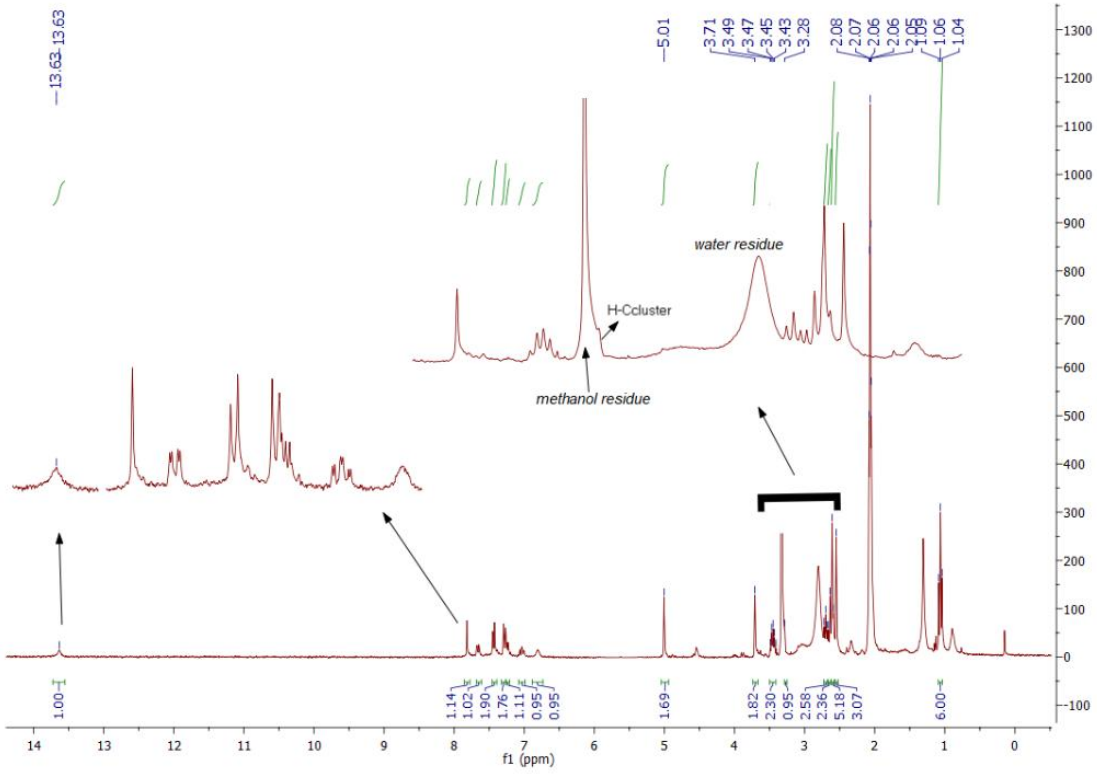


Compound 8

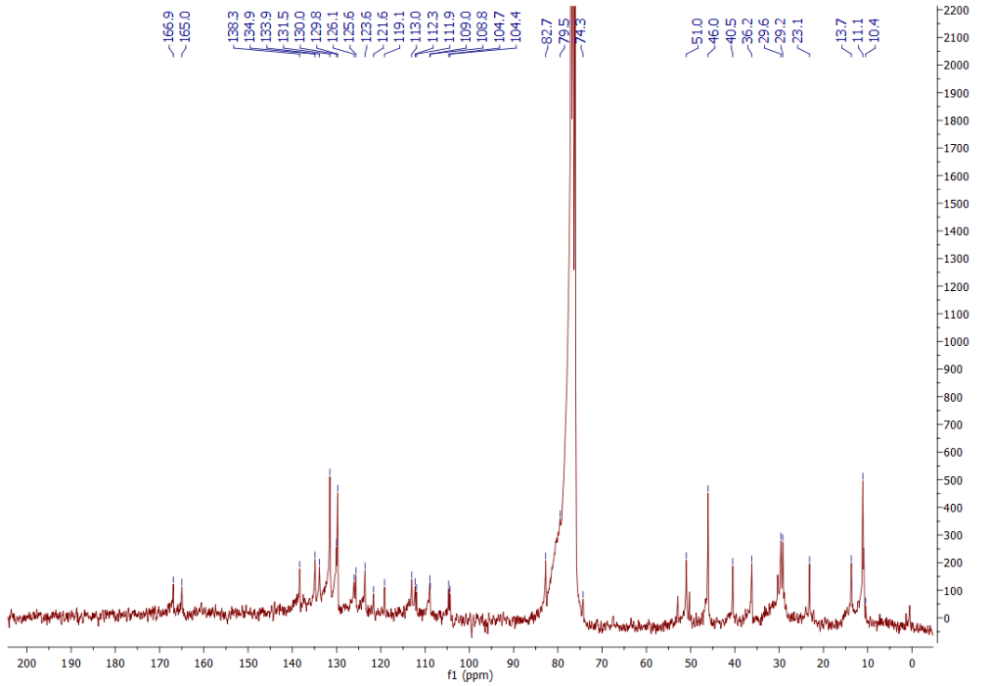


To a 10-mL oven-dried round bottom flask equipped with a magnetic stirring bar was charged under nitrogen with ***M*** (1 equiv., 75 mg, 0.21 mmol), CuI (3.9 mg, 10 mol %), $PdCl_2(PPh_3)_2$ (12 mg, 8 mol %) and Sunitinib derivative (1 equiv. 91 mg, 0.21 mmol). A dry solvent system of THF:Et_3N (2 mL, 3:1, v/v) was well-degassed under nitrogen for 45 min prior to addition to the reaction mixture. After heating at 60 °C for 10 h, the solution was filtered through a small pad of celite and washed with methanol (10 mL). The solution was concentrated *in vacuo* and the crude was dissolved in CH_2Cl_2 (10 mL) and washed with brine (4 × 5 mL). The organic layer was dried over $MgSO_4$ and evaporated *in vacuo* to dryness. The product was purified by preparative SiO_2-TLC and CH_2Cl_2:MeOH (96:4) as eluent. The product was obtained following extraction of the silica with CH_2Cl_2:MeOH and evaporation under reduced pressure to yield an orange solid (30 mg, 22 %).
$^1H\{^{11}B\}$-NMR (300.13 MHz, CD_3COCD_3) δ: 13.63 (s, 1H, pyrrole-N**H**), 7.82 (s, 1H, -C=C-**H**), 7.66 (dd, 1H, $J_{H,H}$= 9.1 Hz; 2.3 Hz, Ar-**H**), 7.44 (d, 2H, $J_{H,H}$= 8.1 Hz, Ar-**H**), 7.28 (d, 2H, $J_{H,H}$= 8.61 Hz, Ar-**H**), 7.24 (dd, 1H, $J_{H,H}$= 7.6 Hz; 3.2 Hz, Ar-**H**), 7.08-6.98 (m, 1H, Ar-**H**), 6.8 (bs, 1H, -N**H**CO-), 5.01 (s, 2H, -N-C**H**$_2$-C≡C-), 3.71 (s, 2H, -Ph-CH_2-$C_{cluster}$), 3.45 (m, 2H, -NHCO-C**H**$_2$-CH_2-), 3.28 (s, 1H, -B-$C_{cluster}$-**H**), 2.72-2.59 (m, 6H, -NHCO-CH_2-C**H**$_2$- and -N-(C**H**$_2$)$_2$-(CH_3)$_2$), 2.61 (s, pyrrole-C**H**$_3$), 2.55 (s, pyrrole-C**H**$_3$), 1.06 (t, 6H, $J_{H,H}$= 7.1 Hz, -N-(CH_2)$_2$-(C**H**$_3$)$_2$). $^{13}C\{^1H\}$-NMR (75.47 MHz, $CDCl_3$) δ: 169.9, 165.5, 138.3, 134.9, 133.9, 131.5, 130.0, 129.8, 126.1, 125.6, 123.6, 121.6, 119.1, 113.0, 112.3, 111.9, 109.0, 108.8, 104.7, 104.4, 82.7, 79.5, 74.3, 51.0, 46.0 (2C), 40.5, 36.2, 29.6, 29.2, 23.1, 13.7, 11.1, 10.4. $^{11}B\{^1H\}$-NMR (96.29 MHz, $CDCl_3$) δ: -2.27 (1B), -5.41 (1B), -8.91 (2B), -10.64 (2B), -12.85 (4B). Calcd. for $C_{34}H_{45}B_{10}FN_4O_2$: C, 61.05; H, 6.78; N, 8.38. Found: C, 60.97; H, 6.87, N, 8.42.

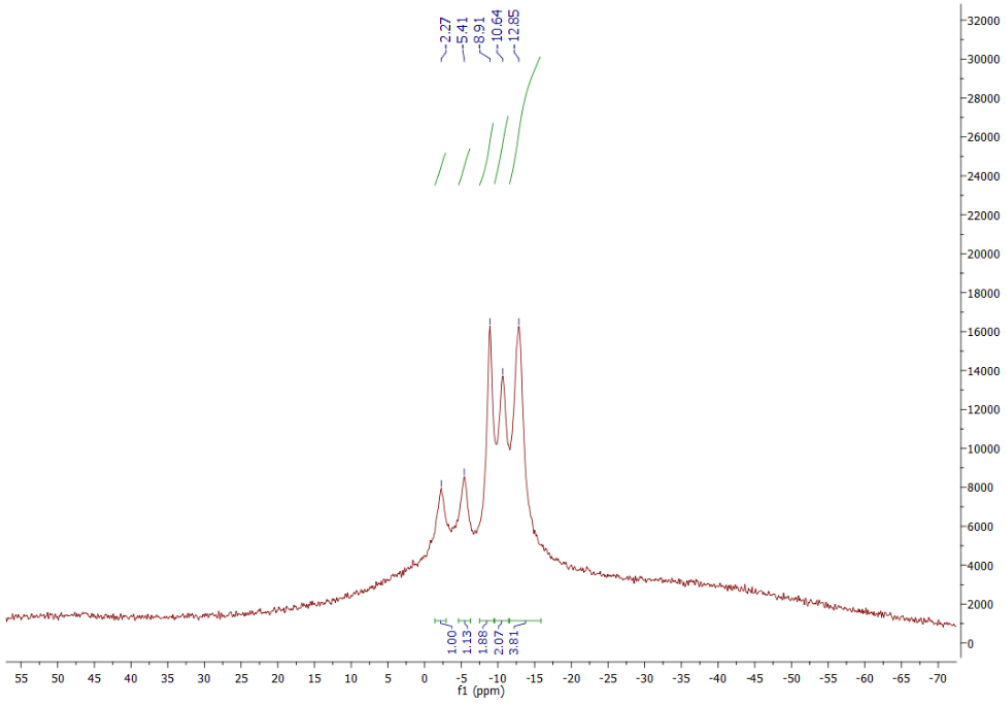
^{1}H-NMR



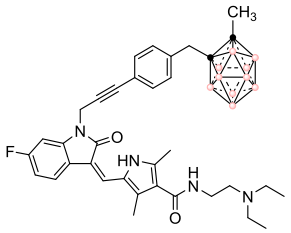
$^{13}C\{^{1}H\}$-NMR



$^{11}B\{^{1}H\}$-NMR

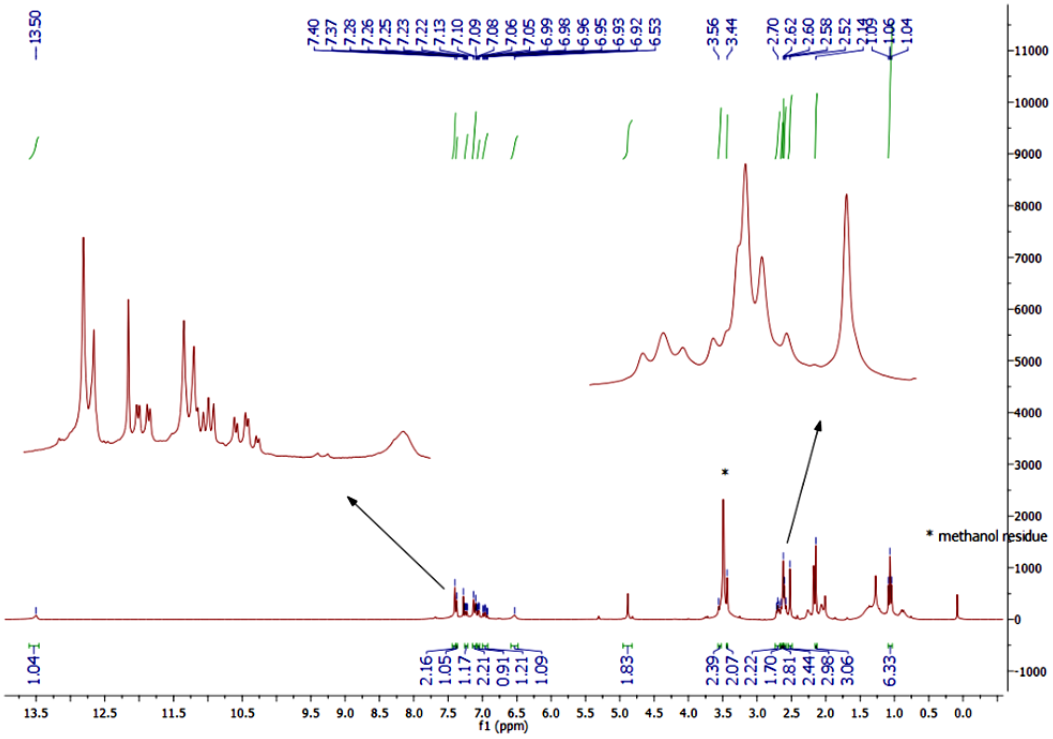


Compound 9

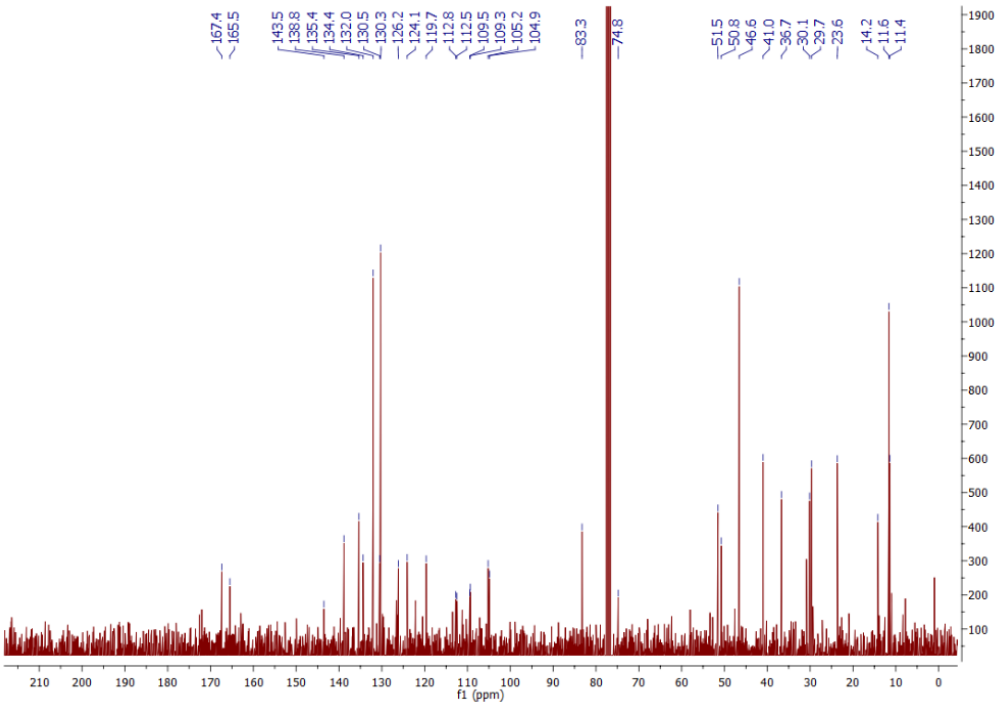


To a 10-mL oven-dried round bottom flask equipped with a magnetic stirring bar was charged under nitrogen with ***N*** (1 equiv., 34 mg, 0.09 mmol), CuI (1.7 mg, 10 mol %), $PdCl_2(PPh_3)_2$ (5.2 mg, 8 mol %) and Sunitinib derivative (1 equiv. 40 mg, 0.09 mmol). A dry solvent system of THF:Et_3N (2 mL, 3:1, v/v) was well-degassed under nitrogen for 45 min prior to addition to the reaction mixture. After heating at 60 °C for 10 h, the solution was filtered through a small pad of celite and washed with methanol (10 mL). The solution was concentrated *in vacuo* and the crude was dissolved in CH_2Cl_2 (10 mL) and washed with brine (4 × 5 mL). The organic layer was dried over $MgSO_4$ and evaporated *in vacuo* to dryness. The product was purified by preparative SiO_2-TLC and CH_2Cl_2:MeOH (96:4) as eluent. The product was obtained following extraction of the silica with CH_2Cl_2:MeOH and evaporation under reduced pressure to yield an orange solid (17 mg, 27 %).
$^1H\{^{11}B\}$-NMR (300.13 MHz, $CDCl_3$) δ: 13.50 (s, 1H, pyrrole-N**H**), 7.40-7.37 (d, 2H, $J_{H,H}$= 8.4 Hz, Ar-**H** and 1H, -C=C-**H**), 7.24 (dd, 1H, $J_{H,H}$= 8.6 Hz; 2.4 Hz , Ar-**H**), 7.11 (d, 2H, $J_{H,H}$= 8.4 Hz, Ar-**H**), 7.07 (dd, 1H, $J_{H,H}$= 8.6 Hz; 4.3 Hz, Ar-**H**), 7.01-6.92 (m, 1H, Ar-**H**), 6.53 (bs, 1H, -N**H**CO-), 4.88 (s, 2H, -N-C**H**$_2$-C≡C-), 3.56-3.51 (m, 2H, -NHCO-C**H**$_2$-CH_2-), 3.44 (s, 2H, -Ph-C**H**$_2$-$C_{cluster}$-), 2.73-2.68 (m, 2H, -NHCO-CH_2-C**H**$_2$-), 2.65-2.58 (m, 7H, pyrrole-C**H**$_3$ and -N-(C**H**$_2$)$_2$-(CH_3)$_2$), 2.52 (s, 3H, pyrrole-C**H**$_3$), 2.14 (s, 3H, -$C_{cluster}$-C**H**$_3$), 1.06 (t, 6H, $J_{H,H}$= 7.1 Hz, -N-(CH_2)$_2$-(C**H**$_3$)$_2$). $^{13}C\{^1H\}$-NMR (75.47 MHz, $CDCl_3$) δ: 167.4, 165.5, 143.5, 138.8, 135.4, 134.4, 132.0 (2C), 130.5, 130.3 (2C), 126.2, 124.1, 119.7, 112.8, 112.5, 109.5, 109.4, 105.2, 104.9, 83.3, 74.8, 51.5, 50.8, 46.6 (2C), 40.9, 36.7, 30.1, 29.7, 23.6, 14.2, 11.6 (2C), 11.4. $^{11}B\{^1H\}$-NMR (96.29 MHz, $CDCl_3$) δ: -4.17 (1B), -5.79 (1B), -10.43 (8B). Calcd. For $C_{35}H_{47}B_{10}FN_4O_2$: C, 61.56; H, 6.94; N, 8.20. Found: C, 61.27; H, 6.77, N, 8.43.

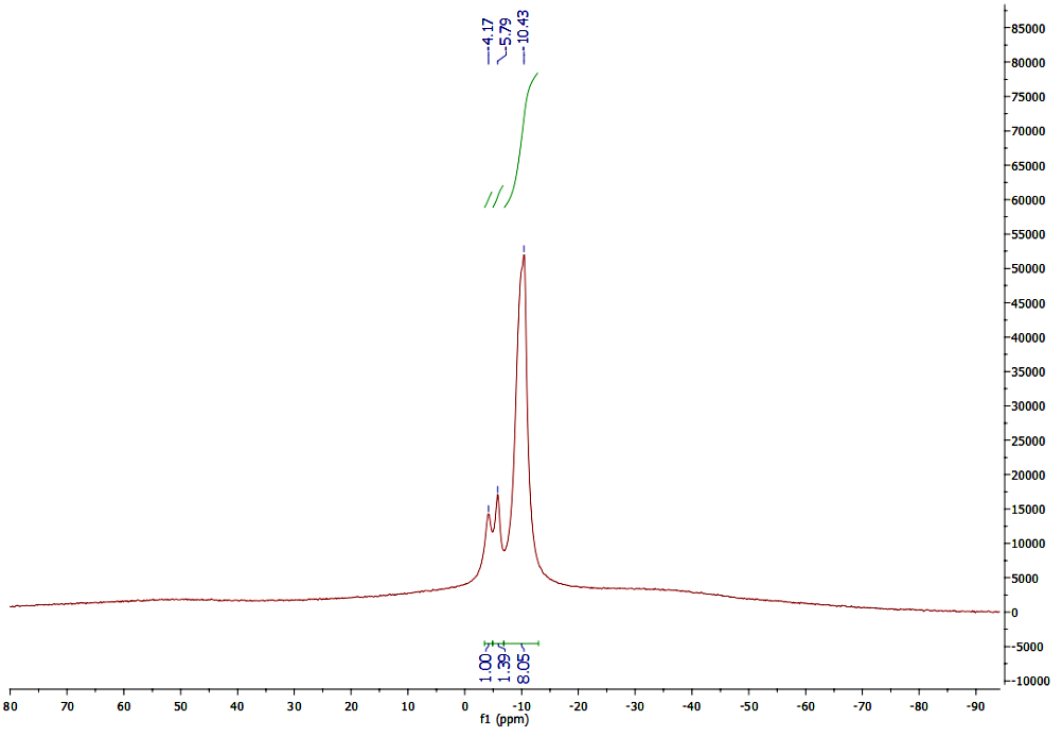
$^1H\{^{11}B\}$-NMR



$^{13}C\{^{1}H\}$-NMR



$^{11}B\{^{1}H\}$-NMR



II) Biological Experimental Section

5.- *In vitro* cytotoxicity assays

Cells (C6, U87 MG or HT-29) were seeded in 96-well plates (7000 - 10000 cells/well depending on the cell line) in 100 μL final volume of growing milieu and were allowed to grow for 24 h. After that, 125 μL of fresh culture milieu was added and the cells were allowed to grow again for additional 24 h. Then, 25 μL of a solution 10× of desired final concentration of the tested compounds in culture milieu was added onto the cells and were further incubated for 24 h. Afterwards, culture milieu was removed and cells were washed twice with 200 μL of PBS. Cells were then fixed with 50 μL of ice-cold trichloroacetic acid for 1 h at 4 °C, the plates were washed five times in distilled water and allowed to dry in the air. Sulphorhodamine B (SRB) solution (50 μL) was added to each well of the dry 96-well plates and allowed staining at room temperature for 30 min. The SRB solution and unbound dye were removed by washing the plates quickly with 1 % v/v acetic acid, at least five times (until excess dye was fully removed). The washed plates were allowed to dry in the air for 24 h. The bound SRB was solubilized by adding 100 μL of 10 mM Tris Base buffer (pH 10) to each well and the resulting solution was shook for 5 min on a shaker platform. The optical density (OD) of each well solution was read in a 96-well plate reader at 540 nm. The OD of SRB solution in each well is directly proportional to the cell number. Cell viability percentage was calculated according to the following equation:

$$\mathbf{C.V.\% = A_{540\ nm} - BC - B}$$

where C.V. % stands for Cell Viability Percentage, $A_{540\ nm}$ corresponds to OD of a particular well, B is the OD of untreated wells with no cells seeded onto them, and C is the OD of control wells treated only with 1 % of dimethylsulfoxide (DMSO). C.V. % values were plotted against compound concentration and the IC_{50} values were determined.

Cytotoxicity assay on normal brain cells

Isolation and culture of glial cells from newborn rats.

Confocal microscopy of treated co-cultures of U87 MG and astrocytes

3×10^4 astrocytes cells were seeded into p35 dishes and were allowed to grow until 80 % confluence. Next, 5×10^4 U87 MG stained cells with PKH26 dye were seeded onto a p35 dish containing a growing primary cell culture of astrocytes. After a 48 h-incubation in fresh growing milieu, the p60 dishes were treated with the IC_{50} doses of compound **1** or **Sun**. A p60 dish treated with 1 % DMSO served as a negative control. Treated cells were incubated for further 24 h. After that, treated co-cultures were fixed for 20 min at 4 ^{o}C with PFA and washed 2 times with PBS. Then, samples were permeabilized for 10 min at room temperature with 0.1 % Triton X-100 in PBS, passed through washing PBS, blocked with 5 % BSA:PBS for 1 h at room temperature, and incubated overnight in a solution of 1 % BSA:PBS containing the primary antibodies and DAPI at 4 ^{o}C. After washing, treated cells were incubated in 1:500-diluted secondary antibodies during 2 h at room temperature. The following antibodies were used for immunofluorescence staining: primary antibodies 1:400 mouse monoclonal anti-GFAP (Sigma) and 1:50 rat monoclonal anti M2, and secondary antibodies conjugated to AlexaFluor 633 (Invitrogen) o AlexaFluor 488 (Invitrogen) respectively. DAPI was used at a 1:1000 dilution. Antibodies were detected by confocal microscopy using a confocal Olympus FV300 microscope.

Cytotoxicity assays of the **1+Tmz** combination

Each compound was incubated at the corresponding IC_{25} with U87 MG cells (see above) and the cytotoxicity was measured as follow:

2,3-Bis[2-methoxy-4-nitro-5-sulphophenyl]-2*H*-tetrazolium-5carboxylanilide inner salt (XTT) based colorimetric assay: Cellular metabolism was measured using XTT cell viability assay kit (Abcam, Cambridge, UK), according to the manufacturer's protocol (absorbance at 492 nm wavelength with reference wavelength of 620 nm). The assay is based on reduction of XTT by mitochondrial dehydrogenases in viable cells. This reduction reaction results in an orange formazan product. The measurements of optic density were made with a spectrophotometer Zenyth 200 (Anthos, Eugendorf, Austria).

Cellular cytotoxicity measurement by lactate dehydrogenase (LDH) activity:[7] Briefly, cytotoxicity detection Kit (LDH) (Roche pharmaceuticals, Basel, Switzerland) was applied according to the manufacturer's protocol (absorbance at 492 nm wavelength with reference wavelength of 620 nm). Measurements were performed with a spectrophotometer Zenyth 200 (Anthos, Eugendorf, Austria) and the results were calculated and normalized according to the formula given by the manufacturer.

6.- Other *in vitro* studies

Assessment of cell death mechanism by flow cytometry

6×10^4 astrocytes cells were seeded into p60 dishes and were allowed to grow until 80 % confluence. Next, 1×10^5 U87 MG stained cells with PKH26 dye were seeded onto a p60 dish containing a growing primary cell culture of astrocytes. After a 48 h-incubation in fresh growing milieu, the p60 dishes were treated with the IC_{50} doses of compound **1** or **Sun**. A p60 dish treated with 1 % DMSO served as a negative control. Treated cells were incubated for further 24 h. Then, cells were harvested with trypsin, and centrifuged at 250 g speed. The resulting pellet was resuspended in an appropriate volume of Annexin binding buffer (0.01M Hepes pH 7.4, 0.14 M NaCl, and 2.5 mM $CaCl_2$) as to get a cell suspension of 1×10^6 cells per mL. After cell counts, samples were divided and cells alone and isotype-matched control samples were generated to control for nonspecific binding of antibodies and for autofluorescence. An Annexin V- FITC antibody solution (catalog number: A13199) was used at a 1:20 concentration. After 30 min of incubation with the aforementioned antibody at 4 ^oC, samples were incubated with DAPI at a 1:5000 concentration and immediately after were submitted to flow cytometry analysis. To perform the analysis, cells were first gated for PKH26 in order to tell apart U87 MG cells from astrocytes. In each type of cells, the following markers were used to define four different populations: for living cells DAPI low, Annexin V low; for necrotic cells DAPI high, Annexin V low; for early apoptotic cells DAPI low, Annexin V high; and finally for late apoptotic cells DAPI high, Annexin V high.

Collapse of the mitochondrial membrane potential (ΔΨm)

Collapse of the ΔΨm can lead to the initiation of the mitochondrial apoptosis cascade. The cationic lipophilic 5,5′,6,6′-tetrachloro-1,1′,3,3′-tetraethylbenzimidazolylcarbocyanine-chloride (JC-1) dye was utilized as an indicator of changes in ΔΨm, as previously described.[6] In intact cells with high ΔΨm, JC-1 can enter the mitochondria and reversibly form aggregates with intense red fluorescence (emission at 590 nm; orange-red fluorescence). In case of mitochondrial membrane potential collapse, JC-1 remains in the cytosol as monomers and emits at 527 nm (green fluorescence). After, 4 h of U87 MG incubation with compound **1**, the cells were trypsinized, centrifuged (660 × g, 5 min, 4 ^oC), and collected. Cells were resuspended and incubated with 400 µL of JC-1 dye (1/500 dilution) for 30 min. Then, the cells were centrifuged, resuspended in 500 µL of PBS and transferred into FACS tubes. The mean fluorescence intensity of JC-1 labeling was measured by FACS. The results were calculated using FlowJo (FlowJo LLC, Ashland, Oregon).

Ames Test

Salmonella typhimurium TA98 and TA100 strains were incubated in agar minimum glucose milieu solution (Difco Bacto® agar) and aqueous glucose solution (40 %). First of all, the direct toxicity of

the hybrid **1** against *S. typhimurium* TA 98 strain was studied. From these data, the mutagenic assay was performed. Briefly, **1** in phosphate buffer (0.1 M, pH 7.4) and DMSO (10 %, v/v) at five doses, 0.450, 0.150, 0.050, 0.016, and 0.005 μg/plate, starting at the highest doses without toxic effects (0.450 μg/plate), were studied in triplicate. Controls: positive control in the assay: 4-nitro-*o*-phenylendiamine (NPD, 20.0 mg/plate for TA98 strain and 2.0 mg/plate for TA100 strain); negative control: phosphate buffer and DMSO (10 % v/v) (no effect on cells growth was observed by this mixture of solvents). The revertant numbers were counted and the studied system was considered mutagenic if the colonies number was at least doubled the natural revertants (negative control) for two or more consecutive doses.

BBB *in vitro* passage assay

BBB artificial model

Isolation and culture of porcine brain microvessel endothelial cells. Pig brains were obtained fresh from the abattoir, washed in ethanol 70 % and transported on ice in PBS (with Ca^{++}/Mg^{++}). The hemispheres of three brains were washed, the cerebellum removed, and meninges peeled off and discarded. White matter was carefully removed. The grey matter was collected in milieu M-199 Earle's salts (Biological industries, Beit Ha'emek, Israel) with added penicillin (100 U/mL) and streptomycin (100 μg/mL) and forced through a 20 mL syringe. The homogenized, was centrifuged and filtered successively through 160 and 80 μm nylon meshes. The resulting microvessels were seeded in T75 culture flasks, previously coated over night with calf skin collagen (Sigma cat. C-8919), in M-199 milieu with 10 % newborn calf serum, penicillin (100 U/mL), streptomycin (100 μg/mL), glutamine (2 mM) and puromycin (2 μg/mL) and cultured until 80 % confluency.

Endothelial cells were detached by brief trypsinisation and seeded into rat tail collagen coated Transwell filter inserts 2.5×10^5 cells/filter (0.5 mL). Trans-endothelial electrical resistance (TEER) was measured as indication of membrane stability with EVOM2 epithelial voltohmmeter (World precision instruments, Inc.). After 3 days, filters with endothelial cells were transferred to 12-well plates containing primary glial cells, and the milieu was changed to serum-free milieu DMEM:F12 supplemented with penicillin (100 U/mL), streptomycin (100 μg/mL), glutamine (2 mM) and hydrocortisone (550 nM).

After 3 days of co-culture, TEER was measured and treated given to the cells (epithelial side) for 24 h. When ending the experiment, TEER was measured again in order to check the stability of membrane after treatment, and media from both sides of membrane were collected.

Incubation protocol

Compound **1** (400 μM) was incubated in the upper layer for 24 h at room temperature in the dark and without stirring.

Determination assay

In order to quantify the amount of compound **1** that passes through the BBB, reverse phase-high performance liquid chromatography (RP-HPLC) studies were performed. RP-HPLC was done on an Agilent 1200 Series Infinity Star equipped with GABI detector, a UV detector and a ThermoScientific Hypersil ODS reverse phase C18 column (300 mm × 4.6 × 10 microns). A gradient mode (flow rate 1 mL/min), beginning with a mobile phase consisting of an aqueous solution of TFA 0.1 % (A) that gradually was converted to acetonitrile (B) (0 to 100 % in 20 min) was used. The injection volume was 50 μL and the detection was performed at a wavelength of 220 nm.

RM determination

Reversed-phase TLC experiments were done on precoated TLC plates SIL RP-18W/UV254 and eluted with MeOH:acetone:PBS (pH 7.4, 0.01 M) (60:10:30, v/v). Stock solutions were prepared in pure methanol (Aldrich) prior to use. The plates were developed in a closed chromatographic tank,

dried and the spots were located under UV light. The R_f values were averaged from two to three determinations, and converted to R_M via the relationship:

$$R_M = \log [(1/R_f)-1]$$

7.- *In vivo* studies

Animals. All protocols for animal experimentation were carried out in accordance with experimentation procedures approved by Technion Institute of Technology Ethical Commission in the Use of Animal, Israel (Protocol number IL-143-10-17 Technion). All animal experimental protocols followed the principles outlined in the Declaration of Helsinki. Animals were housed in wire mesh cages at 20 ± 2 ^{o}C with 12 h artificial light-dark cycles. The animals were fed *ad libitum* to standard pellet diet and water and were used after a minimum of 5 days acclimation to the housing conditions.

In vitro glioblastoma U87 MG cell growing. Glioblastoma U87 MG cells are grown in full milieu, MEM-Eagle with Fetal Cow Serum (9 %), glutamine (2 %) and Gentamycin (0.05 %) (Biological Industries, Beit Ha'emek, Israel). The cells are thawed and grown. After three days the cells are split and grown for additional 4 more days until the injection. The culture milieu is changed every two days. To prepare the cells for injection into the mouse brain, they are counted and suspended in PBS.

Stereotactic surgery – cell injection in brain. The mice are anesthetized either by inhalation of isoflurane or injection of ketamine-xylazine mixture in physiological saline (ketamine 1 mg/mL: xylazine 20 mg/mL). Eye ointment should be applied to maintain adequate moisture during the procedure. Using a sterile scalpel, a sagittal incision is preformed over the parieto-occipital bone, approximately 1 cm long. The exposed skull surface is then cleaned. With stereotactic surgery, coordinates where the cells were injected are marked (1.5 mm right and 1.5 mm backward bregma). A volume of 3 μL containing 2.5-3.0 × 10^5 U87 MG cells is injected into a depth of 2.5 mm skull. After the cell injection wait 4 minutes until taking the syringe out.

Treatments - The experiments were carried out on 7-8 weak-old BALB/c female mice (17.6-18.0 g of body weight, bw) bred under specific pathogen-free conditions. At the end of experiments they were anaesthetized with isoflurane and sacrificed by cervical dislocation.
When tumors begin to develop, according to bioluminescence imaging, six mice were located in one cage and the treatments began. Three groups of treatment were defined: i) compound **1**, dissolved in sterile physiological saline:Tween 80 (4:1, v/v), administered at 1 mg/kg bw ip; ii) **Tmz**, dissolved in sterile physiological saline:Tween 80 (4:1, v/v), administered at 4 mg/kg bw ip; iii) negative control (vehicle, sterile physiological saline:Tween 80 (4:1, v/v)). Days of treatments: 5^{th}, 7^{th}, 9^{th}, 12^{th}, 14^{th}, and 16^{th}. Tumoral volumes were determined by bioluminescence imaging weekly.
Bioluminescence imaging with LUMINA X5 imaging system - Bioluminescence imaging is based on the oxidation of luciferin [*d*-(-)-2-(6-hydroxy-2-benzothiazolyl)-thiazole-4-carboxylic acid] in the presence of oxygen and adenosine triphosphate. This reaction is catalyzed by the enzyme luciferase, which converts chemical energy into photons with resultant emission of light. Luciferase is present only in the injected cancer cells (that were pre transfected with plasmid encoding for the enzyme). Bioluminescence monitoring is done once a week beginning two days after cell injection until mice death. After the administration of luciferin (*d*-luciferin potassium salt, 150 mg/kg) via intraperitoneal injection, mice are anesthetized with isoflurane. Measurements are taken every minute until 24 min after luciferin injection. Regions of interest encompassing the intracranial area of signal are defined using Living Image software, and the total photons/s/sr/cm^2 (photons per second per radian per square cm) was recorded.

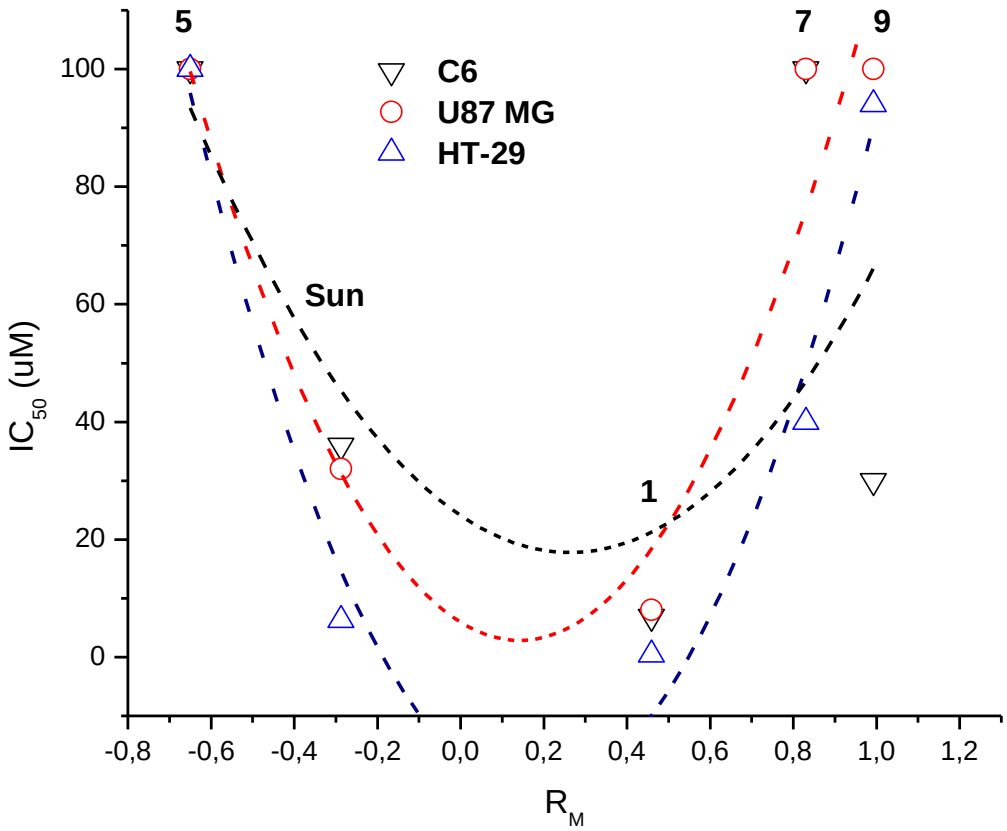


Figure S1. Relationship between IC_{50} and lipophilicity (expressed as R_M). The number and name of the studied compounds are shown inset the graphic.

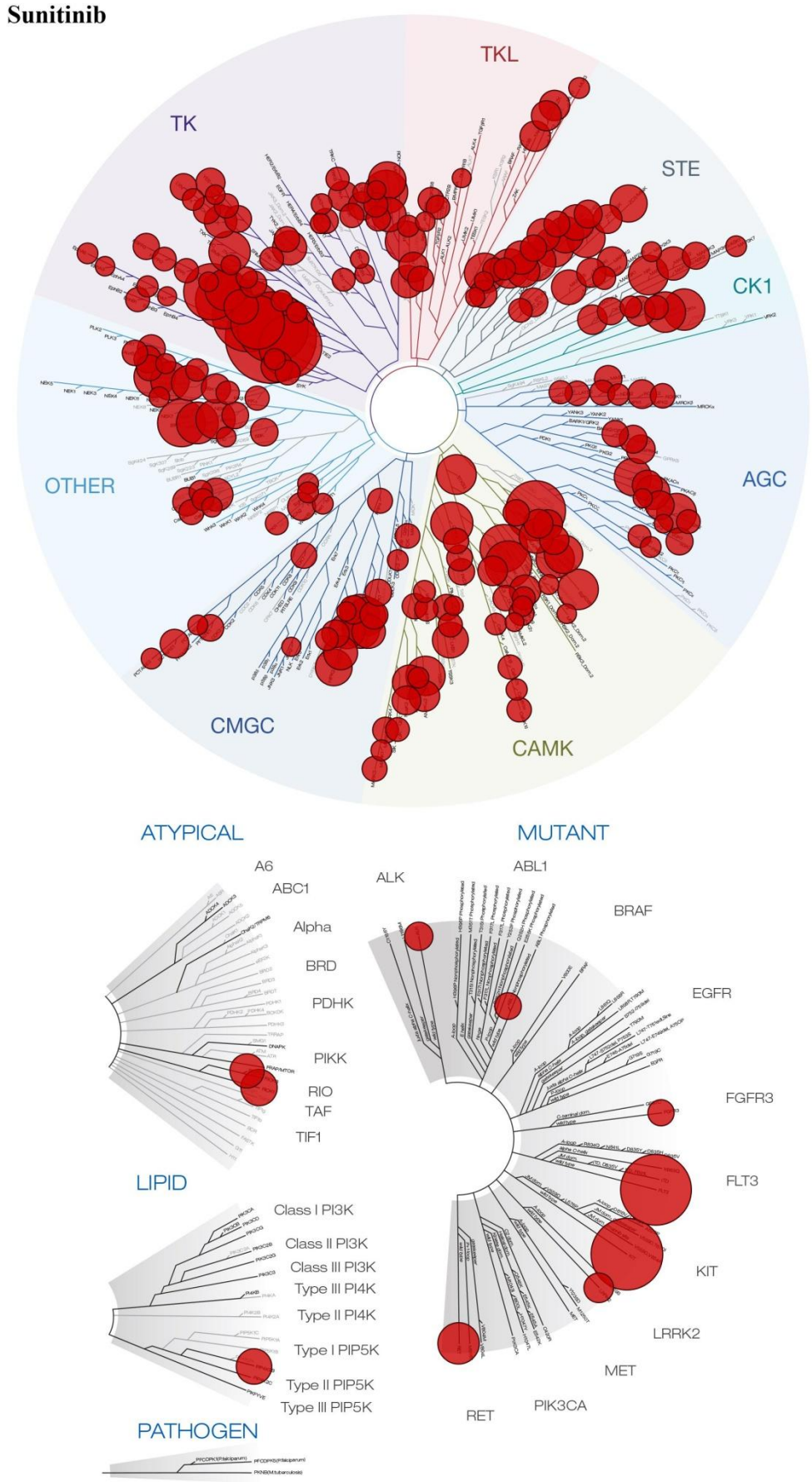


Figure S2. Profile of **Sun** against 460 protein kinases. Relative binding affinities are indicted by red circles in a phylogenetic kinome tree for wild-type enzymes and atypical/mutant/lipo/pathogen variants (right). Image generated using TREEspot™ Software Tool (KINOMEscan®, a division of DiscoveRx Corporation,© DISCOVERX CORPORATION 2010).

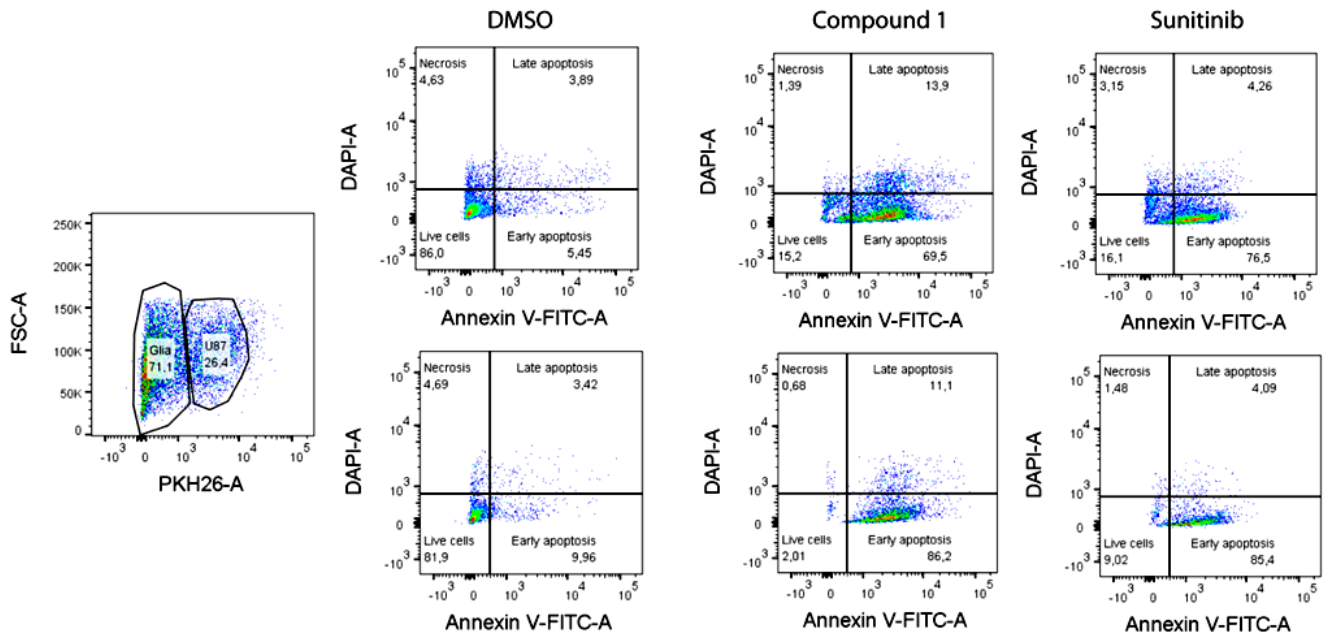


Figure S3. Flow cytometry results.

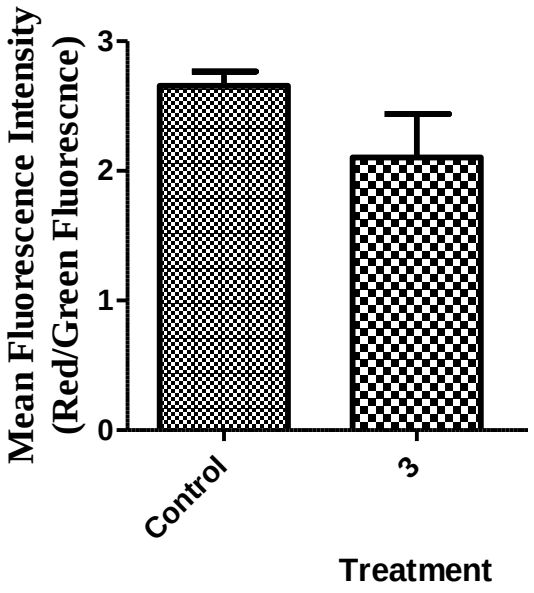
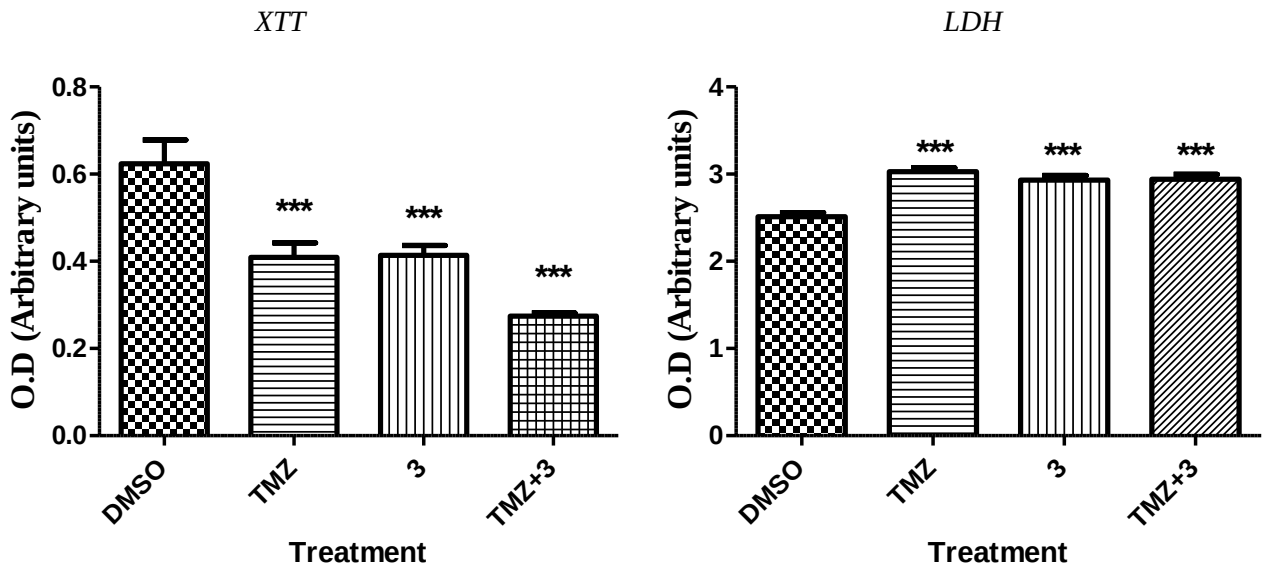


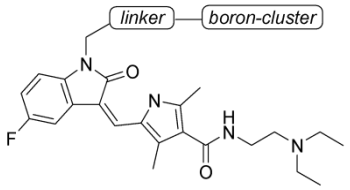
Figure S4. Collapse of the mitochondrial membrane potential results for compound **1**.

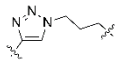
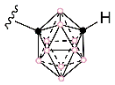
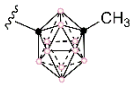
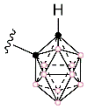
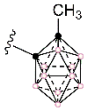
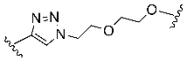
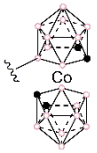
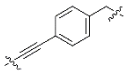
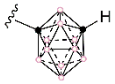
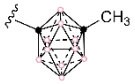
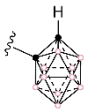
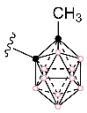


One-way Anova compared with DMSO (*** $p < 0.0001$)

Figure S5. *In vitro* assays of combined treatments on U87 MG cells. When combined, each agent was assayed at its IC_{25} doses, and when alone, each drug was assayed at its IC_{50} doses.

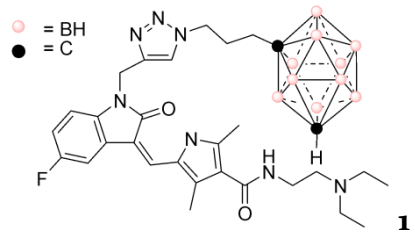
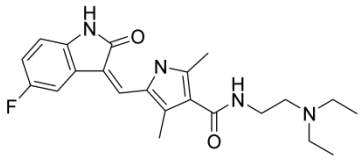
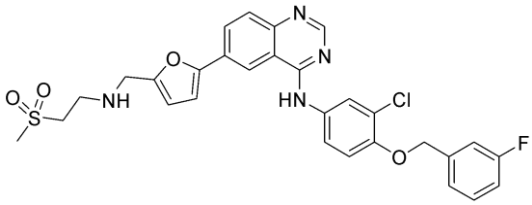
Table S1. *In vitro* activity of studied compounds against *H. sapiens* colorectal adenocarcinoma-cells.



Cpd	linker	boron-cluster	$IC_{50,HT\text{-}29}$ (μM)[a,b]
1			**< 6.25 (0.45 ± 0.04 %)**
2			**< 6.25 (0.79 ± 0.01 %)**
3			**> 100 (34 ± 5 %)**
4			**< 6.25 (0.63 ± 0.03 %)**
5[c]			**100 ± 5**
6			**45 ± 4**
7			**40 ± 6**
8			**> 100 (40 ± 5 %)**
9			**94 ± 7**
Sun	-	-	**6.25 ± 0.04**
A	-	-	**25.0 ± 5.0**
Erl	-	-	**> 100**[d]
Lap	-	-	**6.25 ± 0.05**

[a] Concentrations, in μM, required to inhibit the cellular growth by 50 %. They were determined from dose-response curves, and represent the mean ± s.d. All experiments were repeated at least three times. [b] Values in parenthesis are the percent of cells survival at 100 μM. [c] As sodium salt. [d] Higher doses than 100 μM could not be evaluated due to solubility problems.

Table S2. *In vitro* activity of studied compounds against astrocytes.

Cpd	$IC_{50,astrocytes}$ (μM)[a]	Selectivity indexes	
		C6	U87 MG
 **1**	4.7 ± 0.6	0.7	0.6
 **Sun**	20 ± 4	0.6	0.6
 **Lap**	8 ± 3	0.15	< 0.08

[a] Concentrations, in μM, required to inhibit the cellular growth by 50 %. They were determined from dose-response curves, and represent the mean ± s.d. All experiments were repeated at least three times.

Table S3. Complete list of kinases and primary screening results[a] of KINOMEScan assay for compound **1.**

DiscoveRx Gene Symbol	Entrez Gene Symbol	Percent Control	Compound Concentration (nM)
AAK1	AAK1	100	10000
ABL1(E255K)-phosphorylated	ABL1	78	10000
ABL1(F317I)-nonphosphorylated	ABL1	85	10000
ABL1(F317I)-phosphorylated	ABL1	69	10000
ABL1(F317L)-nonphosphorylated	ABL1	95	10000
ABL1(F317L)-phosphorylated	ABL1	71	10000
ABL1(H396P)-nonphosphorylated	ABL1	74	10000
ABL1(H396P)-phosphorylated	ABL1	80	10000
ABL1(M351T)-phosphorylated	ABL1	82	10000
ABL1(Q252H)-nonphosphorylated	ABL1	84	10000
ABL1(Q252H)-phosphorylated	ABL1	88	10000
ABL1(T315I)-nonphosphorylated	ABL1	87	10000
ABL1(T315I)-phosphorylated	ABL1	74	10000
ABL1(Y253F)-phosphorylated	ABL1	72	10000
ABL1-nonphosphorylated	ABL1	82	10000
ABL1-phosphorylated	ABL1	83	10000
ABL2	ABL2	93	10000
ACVR1	ACVR1	95	10000
ACVR1B	ACVR1B	77	10000
ACVR2A	ACVR2A	89	10000
ACVR2B	ACVR2B	93	10000
ACVRL1	ACVRL1	83	10000
ADCK3	CABC1	95	10000
ADCK4	ADCK4	79	10000
AKT1	AKT1	100	10000
AKT2	AKT2	91	10000
AKT3	AKT3	100	10000
ALK	ALK	58	10000
ALK(C1156Y)	ALK	75	10000
ALK(L1196M)	ALK	93	10000
AMPK-alpha1	PRKAA1	87	10000
AMPK-alpha2	PRKAA2	86	10000
ANKK1	ANKK1	63	10000
ARK5	NUAK1	59	10000
ASK1	MAP3K5	99	10000
ASK2	MAP3K6	100	10000
AURKA	AURKA	96	10000
AURKB	AURKB	65	10000
AURKC	AURKC	40	10000
AXL	AXL	66	10000
BIKE	BMP2K	28	10000
BLK	BLK	89	10000
BMPR1A	BMPR1A	80	10000
BMPR1B	BMPR1B	81	10000

BMPR2	BMPR2	70	10000
BMX	BMX	90	10000
BRAF	BRAF	75	10000
BRAF(V600E)	BRAF	94	10000
BRK	PTK6	77	10000
BRSK1	BRSK1	84	10000
BRSK2	BRSK2	89	10000
BTK	BTK	89	10000
BUB1	BUB1	58	10000
CAMK1	CAMK1	100	10000
CAMK1B	PNCK	90	10000
CAMK1D	CAMK1D	97	10000
CAMK1G	CAMK1G	100	10000
CAMK2A	CAMK2A	100	10000
CAMK2B	CAMK2B	100	10000
CAMK2D	CAMK2D	100	10000
CAMK2G	CAMK2G	100	10000
CAMK4	CAMK4	83	10000
CAMKK1	CAMKK1	100	10000
CAMKK2	CAMKK2	100	10000
CASK	CASK	98	10000
CDC2L1	CDK11B	96	10000
CDC2L2	CDC2L2	97	10000
CDC2L5	CDK13	42	10000
CDK11	CDK19	39	10000
CDK2	CDK2	51	10000
CDK3	CDK3	68	10000
CDK4	CDK4	68	10000
CDK4-cyclinD1	CDK4	63	10000
CDK4-cyclinD3	CDK4	82	10000
CDK5	CDK5	88	10000
CDK7	CDK7	70	10000
CDK9	CDK9	99	10000
CDKL1	CDKL1	69	10000
CDKL2	CDKL2	29	10000
CDKL3	CDKL3	99	10000
CDKL5	CDKL5	79	10000
CHEK1	CHEK1	97	10000
CHEK2	CHEK2	80	10000
CIT	CIT	100	10000
CLK1	CLK1	73	10000
CLK2	CLK2	100	10000
CLK3	CLK3	94	10000
CLK4	CLK4	63	10000
CSF1R	CSF1R	5.9	10000
CSF1R-autoinhibited	CSF1R	5.6	10000
CSK	CSK	98	10000
CSNK1A1	CSNK1A1	93	10000
CSNK1A1L	CSNK1A1L	92	10000
CSNK1D	CSNK1D	74	10000
CSNK1E	CSNK1E	85	10000
CSNK1G1	CSNK1G1	100	10000
CSNK1G2	CSNK1G2	79	10000

CSNK1G3	CSNK1G3	89	10000
CSNK2A1	CSNK2A1	85	10000
CSNK2A2	CSNK2A2	87	10000
CTK	MATK	52	10000
DAPK1	DAPK1	100	10000
DAPK2	DAPK2	100	10000
DAPK3	DAPK3	99	10000
DCAMKL1	DCLK1	70	10000
DCAMKL2	DCLK2	85	10000
DCAMKL3	DCLK3	67	10000
DDR1	DDR1	87	10000
DDR2	DDR2	65	10000
DLK	MAP3K12	54	10000
DMPK	DMPK	98	10000
DMPK2	CDC42BPG	94	10000
DRAK1	STK17A	44	10000
DRAK2	STK17B	92	10000
DYRK1A	DYRK1A	71	10000
DYRK1B	DYRK1B	74	10000
DYRK2	DYRK2	80	10000
EGFR	EGFR	73	10000
EGFR(E746-A750del)	EGFR	65	10000
EGFR(G719C)	EGFR	70	10000
EGFR(G719S)	EGFR	66	10000
EGFR(L747-E749del, A750P)	EGFR	73	10000
EGFR(L747-T751del,Sins)	EGFR	56	10000
EGFR(L858R)	EGFR	70	10000
EGFR(L858R,T790M)	EGFR	76	10000
EGFR(L861Q)	EGFR	82	10000
EGFR(T790M)	EGFR	88	10000
EIF2AK1	EIF2AK1	100	10000
EPHA1	EPHA1	84	10000
EPHA2	EPHA2	88	10000
EPHA3	EPHA3	100	10000
EPHA4	EPHA4	97	10000
EPHA5	EPHA5	91	10000
EPHA6	EPHA6	90	10000
EPHA7	EPHA7	92	10000
EPHA8	EPHA8	97	10000
EPHB1	EPHB1	96	10000
EPHB2	EPHB2	90	10000
EPHB3	EPHB3	90	10000
EPHB4	EPHB4	99	10000
EPHB6	EPHB6	96	10000
ERBB2	ERBB2	100	10000
ERBB3	ERBB3	99	10000
ERBB4	ERBB4	100	10000
ERK1	MAPK3	97	10000
ERK2	MAPK1	88	10000
ERK3	MAPK6	98	10000
ERK4	MAPK4	95	10000
ERK5	MAPK7	97	10000
ERK8	MAPK15	91	10000

ERN1	ERN1	92	10000
FAK	PTK2	92	10000
FER	FER	100	10000
FES	FES	86	10000
FGFR1	FGFR1	87	10000
FGFR2	FGFR2	97	10000
FGFR3	FGFR3	94	10000
FGFR3(G697C)	FGFR3	84	10000
FGFR4	FGFR4	88	10000
FGR	FGR	95	10000
FLT1	FLT1	14	10000
FLT3	FLT3	2.1	10000
FLT3(D835H)	FLT3	26	10000
FLT3(D835V)	FLT3	0.1	10000
FLT3(D835Y)	FLT3	5.2	10000
FLT3(ITD)	FLT3	2.3	10000
FLT3(ITD,D835V)	FLT3	0.55	10000
FLT3(ITD,F691L)	FLT3	0	10000
FLT3(K663Q)	FLT3	5.3	10000
FLT3(N841I)	FLT3	10	10000
FLT3(R834Q)	FLT3	59	10000
FLT3-autoinhibited	FLT3	6	10000
FLT4	FLT4	63	10000
FRK	FRK	74	10000
FYN	FYN	66	10000
GAK	GAK	100	10000
GCN2(Kin.Dom.2,S808G)	EIF2AK4	100	10000
GRK1	GRK1	81	10000
GRK2	ADRBK1	54	10000
GRK3	ADRBK2	96	10000
GRK4	GRK4	55	10000
GRK7	GRK7	100	10000
GSK3A	GSK3A	59	10000
GSK3B	GSK3B	88	10000
HASPIN	GSG2	60	10000
HCK	HCK	97	10000
HIPK1	HIPK1	78	10000
HIPK2	HIPK2	67	10000
HIPK3	HIPK3	69	10000
HIPK4	HIPK4	81	10000
HPK1	MAP4K1	32	10000
HUNK	HUNK	100	10000
ICK	ICK	74	10000
IGF1R	IGF1R	98	10000
IKK-alpha	CHUK	59	10000
IKK-beta	IKBKB	49	10000
IKK-epsilon	IKBKE	95	10000
INSR	INSR	83	10000
INSRR	INSRR	99	10000
IRAK1	IRAK1	54	10000
IRAK3	IRAK3	82	10000
IRAK4	IRAK4	100	10000
ITK	ITK	90	10000

JAK1(JH1domain-catalytic)	JAK1	97	10000
JAK1(JH2domain-pseudokinase)	JAK1	13	10000
JAK2(JH1domain-catalytic)	JAK2	100	10000
JAK3(JH1domain-catalytic)	JAK3	52	10000
JNK1	MAPK8	61	10000
JNK2	MAPK9	90	10000
JNK3	MAPK10	76	10000
KIT	KIT	0.25	10000
KIT(A829P)	KIT	52	10000
KIT(D816H)	KIT	98	10000
KIT(D816V)	KIT	84	10000
KIT(L576P)	KIT	7.4	10000
KIT(V559D)	KIT	0.45	10000
KIT(V559D,T670I)	KIT	1.4	10000
KIT(V559D,V654A)	KIT	15	10000
KIT-autoinhibited	KIT	12	10000
LATS1	LATS1	100	10000
LATS2	LATS2	93	10000
LCK	LCK	100	10000
LIMK1	LIMK1	100	10000
LIMK2	LIMK2	91	10000
LKB1	STK11	100	10000
LOK	STK10	100	10000
LRRK2	LRRK2	68	10000
LRRK2(G2019S)	LRRK2	56	10000
LTK	LTK	97	10000
LYN	LYN	94	10000
LZK	MAP3K13	86	10000
MAK	MAK	82	10000
MAP3K1	MAP3K1	76	10000
MAP3K15	MAP3K15	68	10000
MAP3K2	MAP3K2	73	10000
MAP3K3	MAP3K3	81	10000
MAP3K4	MAP3K4	81	10000
MAP4K2	MAP4K2	86	10000
MAP4K3	MAP4K3	79	10000
MAP4K4	MAP4K4	75	10000
MAP4K5	MAP4K5	67	10000
MAPKAPK2	MAPKAPK2	91	10000
MAPKAPK5	MAPKAPK5	84	10000
MARK1	MARK1	93	10000
MARK2	MARK2	81	10000
MARK4	MARK4	85	10000
MEK1	MAP2K1	71	10000
MEK2	MAP2K2	55	10000
MEK3	MAP2K3	64	10000
MEK4	MAP2K4	83	10000
MEK5	MAP2K5	40	10000
MEK6	MAP2K6	76	10000
MELK	MELK	86	10000
MERTK	MERTK	91	10000
MET	MET	91	10000
MET(M1250T)	MET	74	10000

MET(Y1235D)	MET	100	10000
MINK	MINK1	65	10000
MKK7	MAP2K7	67	10000
MKNK1	MKNK1	82	10000
MKNK2	MKNK2	76	10000
MLCK	MYLK3	79	10000
MLK1	MAP3K9	93	10000
MLK2	MAP3K10	92	10000
MLK3	MAP3K11	100	10000
MRCKA	CDC42BPA	91	10000
MRCKB	CDC42BPB	98	10000
MST1	STK4	90	10000
MST1R	MST1R	100	10000
MST2	STK3	98	10000
MST3	STK24	100	10000
MST4	MST4	100	10000
MTOR	MTOR	100	10000
MUSK	MUSK	50	10000
MYLK	MYLK	87	10000
MYLK2	MYLK2	76	10000
MYLK4	MYLK4	57	10000
MYO3A	MYO3A	100	10000
MYO3B	MYO3B	100	10000
NDR1	STK38	75	10000
NDR2	STK38L	57	10000
NEK1	NEK1	53	10000
NEK10	NEK10	47	10000
NEK11	NEK11	92	10000
NEK2	NEK2	100	10000
NEK3	NEK3	100	10000
NEK4	NEK4	94	10000
NEK5	NEK5	100	10000
NEK6	NEK6	84	10000
NEK7	NEK7	86	10000
NEK9	NEK9	100	10000
NIK	MAP3K14	82	10000
NIM1	MGC42105	72	10000
NLK	NLK	100	10000
OSR1	OXSR1	96	10000
p38-alpha	MAPK14	100	10000
p38-beta	MAPK11	97	10000
p38-delta	MAPK13	100	10000
p38-gamma	MAPK12	100	10000
PAK1	PAK1	97	10000
PAK2	PAK2	90	10000
PAK3	PAK3	91	10000
PAK4	PAK4	100	10000
PAK6	PAK6	100	10000
PAK7	PAK7	99	10000
PCTK1	CDK16	28	10000
PCTK2	CDK17	37	10000
PCTK3	CDK18	25	10000
PDGFRA	PDGFRA	2.6	10000

PDGFRB	PDGFRB	0.05	10000
PDPK1	PDPK1	99	10000
PFCDPK1(P.falciparum)	CDPK1	94	10000
PFPK5(P.falciparum)	MAL13P1.279	100	10000
PFTAIRE2	CDK15	51	10000
PFTK1	CDK14	26	10000
PHKG1	PHKG1	61	10000
PHKG2	PHKG2	100	10000
PIK3C2B	PIK3C2B	94	10000
PIK3C2G	PIK3C2G	100	10000
PIK3CA	PIK3CA	85	10000
PIK3CA(C420R)	PIK3CA	96	10000
PIK3CA(E542K)	PIK3CA	83	10000
PIK3CA(E545A)	PIK3CA	95	10000
PIK3CA(E545K)	PIK3CA	98	10000
PIK3CA(H1047L)	PIK3CA	79	10000
PIK3CA(H1047Y)	PIK3CA	54	10000
PIK3CA(I800L)	PIK3CA	86	10000
PIK3CA(M1043I)	PIK3CA	90	10000
PIK3CA(Q546K)	PIK3CA	74	10000
PIK3CD	PIK3CD	77	10000
PIK3CG	PIK3CG	74	10000
PIK4CB	PI4KB	80	10000
PIKFYVE	PIKFYVE	75	10000
PIM1	PIM1	100	10000
PIM2	PIM2	98	10000
PIM3	PIM3	100	10000
PIP5K1A	PIP5K1A	33	10000
PIP5K2B	PIP4K2B	35	10000
PIP5K2C	PIP4K2C	100	10000
PKAC-alpha	PRKACA	100	10000
PKAC-beta	PRKACB	100	10000
PKMYT1	PKMYT1	96	10000
PKN1	PKN1	99	10000
PKN2	PKN2	100	10000
PKNB(M.tuberculosis)	pknB	84	10000
PLK1	PLK1	88	10000
PLK2	PLK2	71	10000
PLK3	PLK3	74	10000
PLK4	PLK4	80	10000
PRKCD	PRKCD	91	10000
PRKCE	PRKCE	100	10000
PRKCH	PRKCH	100	10000
PRKCI	PRKCI	100	10000
PRKCQ	PRKCQ	88	10000
PRKD1	PRKD1	79	10000
PRKD2	PRKD2	87	10000
PRKD3	PRKD3	97	10000
PRKG1	PRKG1	94	10000
PRKG2	PRKG2	91	10000
PRKR	EIF2AK2	51	10000
PRKX	PRKX	91	10000
PRP4	PRPF4B	67	10000

PYK2	PTK2B	98	10000
QSK	KIAA0999	100	10000
RET	RET	54	10000
RET(M918T)	RET	59	10000
RET(V804L)	RET	50	10000
RET(V804M)	RET	27	10000
RIOK1	RIOK1	11	10000
RIOK2	RIOK2	97	10000
RIOK3	RIOK3	19	10000
RIPK1	RIPK1	91	10000
RIPK2	RIPK2	59	10000
RIPK4	RIPK4	84	10000
RIPK5	DSTYK	78	10000
ROCK1	ROCK1	56	10000
ROCK2	ROCK2	70	10000
ROS1	ROS1	100	10000
RPS6KA4(Kin.Dom.1-N-terminal)	RPS6KA4	79	10000
RPS6KA4(Kin.Dom.2-C-terminal)	RPS6KA4	80	10000
RPS6KA5(Kin.Dom.1-N-terminal)	RPS6KA5	100	10000
RPS6KA5(Kin.Dom.2-C-terminal)	RPS6KA5	100	10000
RSK1(Kin.Dom.1-N-terminal)	RPS6KA1	83	10000
RSK1(Kin.Dom.2-C-terminal)	RPS6KA1	99	10000
RSK2(Kin.Dom.1-N-terminal)	RPS6KA3	59	10000
RSK2(Kin.Dom.2-C-terminal)	RPS6KA3	78	10000
RSK3(Kin.Dom.1-N-terminal)	RPS6KA2	74	10000
RSK3(Kin.Dom.2-C-terminal)	RPS6KA2	99	10000
RSK4(Kin.Dom.1-N-terminal)	RPS6KA6	54	10000
RSK4(Kin.Dom.2-C-terminal)	RPS6KA6	100	10000
S6K1	RPS6KB1	73	10000
SBK1	SBK1	95	10000
SGK	SGK1	73	10000
SgK110	SgK110	100	10000
SGK2	SGK2	40	10000
SGK3	SGK3	76	10000
SIK	SIK1	81	10000
SIK2	SIK2	100	10000
SLK	SLK	100	10000
SNARK	NUAK2	67	10000
SNRK	SNRK	92	10000
SRC	SRC	95	10000
SRMS	SRMS	84	10000
SRPK1	SRPK1	30	10000
SRPK2	SRPK2	100	10000
SRPK3	SRPK3	60	10000
STK16	STK16	100	10000
STK33	STK33	67	10000
STK35	STK35	100	10000
STK36	STK36	90	10000
STK39	STK39	97	10000
SYK	SYK	100	10000
TAK1	MAP3K7	82	10000
TAOK1	TAOK1	76	10000
TAOK2	TAOK2	89	10000

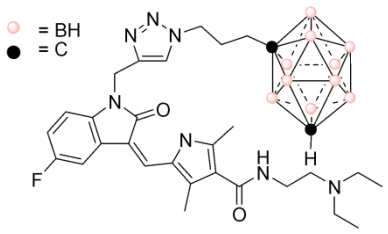
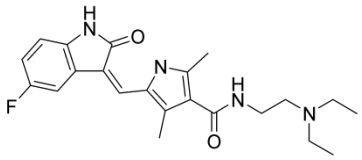
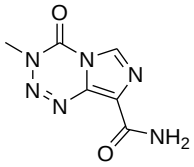
TAOK3	TAOK3	81	10000
TBK1	TBK1	94	10000
TEC	TEC	98	10000
TESK1	TESK1	71	10000
TGFBR1	TGFBR1	88	10000
TGFBR2	TGFBR2	82	10000
TIE1	TIE1	91	10000
TIE2	TEK	70	10000
TLK1	TLK1	100	10000
TLK2	TLK2	93	10000
TNIK	TNIK	91	10000
TNK1	TNK1	93	10000
TNK2	TNK2	100	10000
TNNI3K	TNNI3K	50	10000
TRKA	NTRK1	14	10000
TRKB	NTRK2	57	10000
TRKC	NTRK3	52	10000
TRPM6	TRPM6	95	10000
TSSK1B	TSSK1B	99	10000
TSSK3	TSSK3	76	10000
TTK	TTK	92	10000
TXK	TXK	85	10000
TYK2(JH1domain-catalytic)	TYK2	64	10000
TYK2(JH2domain-pseudokinase)	TYK2	62	10000
TYRO3	TYRO3	55	10000
ULK1	ULK1	67	10000
ULK2	ULK2	58	10000
ULK3	ULK3	91	10000
VEGFR2	KDR	1.3	10000
VPS34	PIK3C3	52	10000
VRK2	VRK2	69	10000
WEE1	WEE1	88	10000
WEE2	WEE2	96	10000
WNK1	WNK1	97	10000
WNK2	WNK2	69	10000
WNK3	WNK3	95	10000
WNK4	WNK4	56	10000
YANK1	STK32A	100	10000
YANK2	STK32B	97	10000
YANK3	STK32C	92	10000
YES	YES1	100	10000
YSK1	STK25	90	10000
YSK4	MAP3K19	54	10000
ZAK	ZAK	81	10000
ZAP70	ZAP70	49	10000

[a] Assay performed by DiscoveRx in 460 selected kinases. The 33 best mapped targets are highlighted in in blue scale.

% Ctrl. Legend

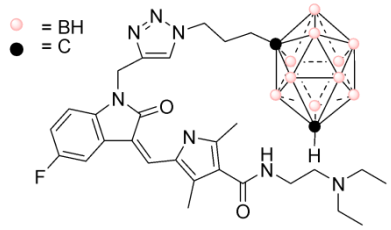
0≤X<0.1	0.1≤X<1	1≤X<10	10≤X<35	X≥35

Table S4. Predicted drug-like properties of compound **1**, **Sun** and **Tmz**.[8]

Cpd	HIA[a]	Subcellular localization	CYP-subs[b]	hERG[c]	Carc[d]	LD_{50}[e]	LogS[f]	Viol, rule 5[g]
 **1**	(+)	Mit[h]	3A4	w	(-)	2.69	-3.48	1[i]
 **Sun**	(+)	Mit	3A4	w	(-)	2.66	-3.24	0
 **Tmz**	(+)	Mit	-	w	(-)	2.53	-1.63	0

[a] Human intestinal absorption: If the compound has the HIA% less than 30 %, it is labeled as (-), otherwise it is labeled as (+);[9] [b] Ability to be substrate of three Cytochrome P450 isoenzymes (CYP450 2C9, CYP450 2D6, and CYP450 3A4).[10] It is shown the predicted isoform-CYP that the compound potentially acts as substrate; [c] Human ether-a-go-go-related gene (hERG) inhibition.[11,12] Weak-inhibition is labeled as "w"; [d] Potential as carcinogens.[13] Non-carcinogen is labeled as (-);[e] Rat acute toxicity by oral exposure,[14] expressed as mol/kg; [f] Aqueous solubility;[15] [g] number of violations of Lipinski "Rule of five"; [h] Mit: mitochondria; [i] MW higher than 500 Da.

Table S5. Summary of Ames and BBB permeability tests.

<table>
<tr><th rowspan="2">Cpd</th><th rowspan="2">Ames test</th><th colspan="2">TA98 / TA100</th><th colspan="2" rowspan="2">BBB</th></tr>
<tr><th>TA98</th><th>TA100</th></tr>
<tr><td rowspan="10"> 

1</td><td>Dose (μg/plate)</td><td colspan="2">Number of revertants</td><td colspan="2" rowspan="6">The concentration of compound 1 in the assay milieu before and after the BBB were measured by HPLC (see Experimental). According to the HPLC results, the compound has the ability to pass the BBB.
Example of results for one selected experiment:</td></tr>
<tr><td>0.45</td><td>12 ± 1</td><td>67±3</td></tr>
<tr><td>0.15</td><td>9 ±1</td><td>56±3</td></tr>
<tr><td>0.05</td><td>7.5 ± 1.5</td><td>46.5±1.5</td></tr>
<tr><td>0.016</td><td>6 ±1</td><td>37±6</td></tr>
<tr><td>0.005</td><td>8± 1</td><td>29.5±0.5</td></tr>
<tr><td>0</td><td>11.6 ± 2.05</td><td>95.6±5.7</td><td>Before BBB</td><td>[1] = 15 μM</td></tr>
<tr><td>Positive control</td><td>294.6 ± 11.1</td><td>704.3±6.3</td><td>After BBB</td><td>[1] = 48 μM</td></tr>
<tr><td>Mutagenic</td><td>(-)</td><td>(-)</td><td colspan="2"></td></tr>
</table>

References

[1] Couto M, Mastandrea I, Cabrera M, Cabral P, Teixidor F, Cerecetto H, Viñas C. Chem. Eur. J. 2017, 23, 9233-9238.
[2] Teixidor F, Gómez S, Lamrani M, Viñas C. Organometal. 1997, 16, 1278-1283.
[3] (a) Plesek J, Hermanek S, Franken A, Cisarova I, Nachtigan Ch. Collect. Czech. Chem. Commun., 1997, 62, 47-56. (b) Teixidor F, Pedrajas J, Rojo I, Viñas C, Kivekäs R, Sillanpää R, Sivaev I, Bregadze V, Sjöberg S. Organometal. 2003, 22, 3414-3423.
[4] Bregadze VI, Semioshkin AA, Las'kova JN, Berzina NY, Lobanova IA, Sivaev IB, Grin MA, Titeev RA, Brittal DI, Ulybina OV, Chestnova AV, Ignatova AA, Feofanov AV, Mironov AF. Appl. Organometal. Chem. 2009, 23, 370-374.
[5] Vicente MGH, Edwards BF, Shetty SJ, Hou Y, Boggan JE. Bioorg. Med. Chem. 2002, 10, 481-492.
[6] Zeno S, Zaaroor M, Leschiner S, Veenman L, Gavish M. Biochem. 2009, 48, 4652-4661.
[7] Weiner D, Levy Y, Khankin EV, Reznick AZ. J. Physiol. Pharmacol. 2008, 59 (Suppl 6), 727-737.
[8] Cheng F, Li W, Zhou Y, *et al*. J. Chem. Inf. Model. 2012, 52, 3099-3105. http://lmmd.ecust.edu.cn/admetsar1/predict/.
[9] Shen J, Cheng F, Xu Y, Li W, Tang Y. J. Chem. Inf. Model. 2010, 50, 1034-1041.
[10] Carbon-Mangels M, Hutter MC. Mol. Inf. 2011, 30, 885-895.
[11] Marchese Robinson RL, Glen RC, Mitchell JBO. Mol. Inf. 2011, 30, 443-458.
[12] Wang S, Li Y, Wang J, *et al*. Mol. Pharm. 2012, 9, 996-1010.
[13] Lagunin A, Filimonov D, Zakharov A, *et al*. QSAR Comb. Sci. 2009, 28, 806-810.
[14] Zhu H, Martin TM, Ye L, Sedykh A, Young DM, Tropsha A. Chem. Res. Toxicol. 2009, 22, 1913-1921.
[15] Wang J, Krudy G, Hou T, Zhang W, Holland G, Xu X. J. Chem. Inf. Model. 2007, 47, 1395-1404.

We are IntechOpen, the world's leading publisher of Open Access books Built by scientists, for scientists

3,900
Open access books available

116,000
International authors and editors

120M
Downloads

Our authors are among the

154
Countries delivered to

TOP 1%
most cited scientists

12.2%
Contributors from top 500 universities

CLARIVATE ANALYTICS
BOOK CITATION INDEX
INDEXED

WEB OF SCIENCE™

Selection of our books indexed in the Book Citation Index in Web of Science™ Core Collection (BKCI)

Interested in publishing with us?
Contact book.department@intechopen.com

Numbers displayed above are based on latest data collected.
For more information visit www.intechopen.com

Provisional chapter

Medicinal Chemistry of Boron-Bearing Compounds for BNCT-Glioma Treatment: Current Challenges and Perspectives

Hugo Cerecetto and Marcos Couto

Additional information is available at the end of the chapter

Abstract

Since its first description, boron neutron capture therapy (BNCT) was a special type of radiotherapy for treatment of cancer and with focus mainly on glioma therapeutic. This procedure requires the selective accumulation of boron into the tumoral cells, and due to this requirement, different boron-enriched compounds have been designed and developed. Efforts to circumvent the selectivity-uptake challenge and other problems, such as solubility, stability, and toxicity, have been to driving force behind the medicinal chemistry field in boron-based compounds. In this regard, a wide diversity of medicinal chemistry hypothesis has been used to obtain new and efficient potential BNCT-glioma drugs. In this chapter, these ideas are analyzed focusing on their medicinal chemistry characteristics.

Keywords: glioma, glioblastoma, drug discovery, boron neutron capture therapy, boron-bearing compounds

1. Introduction

1.1. Boron neutron capture therapy: historical account

In 1932 in the UK, Chadwick discovered neutrons, and for his contribution, he was awarded in 1935 with the Nobel Prize in Physics [1]. One year later in the USA, Gordon Locher introduced the concept of boron neutron capture therapy (BNCT) [2]. He hypothesized that if boron could be selectively concentrated in a tumoral tissue and then exposed to a neutrons

IntechOpen

© 2018 The Author(s). Licensee IntechOpen. This chapter is distributed under the terms of the Creative Commons Attribution License (http://creativecommons.org/licenses/by/3.0), which permits unrestricted use, distribution, and reproduction in any medium, provided the original work is properly cited. CC BY

beam, a higher radiation dose to the tumor relative to surrounding normal cells would result. A mere 2 years later, Goldhaber, Hall, and Kruger performed the first radiobiological studies using boric acid and slow neutrons in a murine tumoral model [3]. However, the first clinical trials against human brain tumors (glioblastoma multiforme (GBM)) that used BNCT could not be initiated until 1951 at the Brookhaven National Laboratory in collaboration with the Massachusetts General Hospital and the Massachusetts Institute of Technology (MIT) [4, 5]. In this case, ten patients were treated with borax (disodium tetraborate decahydrate, $Na_2B_4O_7{\cdot}10H_2O$; **Figure 1**) and thermal neutrons without much success. While there were no serious side effects of BNCT in the patients, the large doses of borax (^{10}B-enriched) infused 200 mg/kg, inducing slight toxicity symptoms. In order to improve this, a second approach was developed comprising nine glioma patients but now with a less toxic compound, sodium pentaborate (NaB_5O_8; **Figure 1**) in combination with D-glucose. Unlike the first one, a higher dose of ^{10}B was used, and a higher fluency of incident thermal neutron was applied [6]. Unfortunately, again, serious side effects such as radio-dermatoses of the scalp and deep ulcerations were observed [6, 7]. Simultaneously, in 1963, Sweet and co-workers, from the MIT, treated 18 patients using boron-rich disodium decahydrodecaborate ($Na_2B_{10}H_{10}$; **Figure 1**) [8], which was considered to be less toxic and with the ability to deposit more boron atoms per cell. Symptoms of brain necrosis in patients undergoing BNCT were again observed [9]. Due to these disappointing events, the USA halted the progress of research on BNCT in 1961.

On the other hand, in 1968 at Hitachi training reactor, the Japanese neurosurgeon Hiroshi Hatanaka, who in previous years had worked with Sweet in Boston, began treating patients with high-grade malignant gliomas using disodium mercaptoundecahydro-*closo*-dodecaborate ($Na_2B_{12}H_{11}SH$, named as BSH; **Figure 1**) which originally had been synthesized by Soloway in 1967 [10]. The results reported by Hatanaka and co-workers were extraordinary with a 5-year survival rate of 58% [11–13].

From the 1990s to the present day with the development of new boron compounds and the improvement in radiation source, the boron neutron capture therapy has been expanded to several centers worldwide, among them in the USA at Brookhaven and Cambridge, in the Netherlands at high flux reactor in collaboration with the Department of Radiotherapy of the University of Essen in Germany, in Finland at FiR-1 Otaniemi reactor, in Sweden at R2–R0 reactor, in the Czech Republic at LVR-15 reactor, in Italy at TRIGA reactor, in Japan at Kyoto University Research Reactor Institute, in Argentina at RA-6 and RA-3 reactors, and in Taiwan at THOR reactor, just to name a few [14].

1.2. Boron neutron capture therapy: principles and general requirements

BNCT is considered as a rationale and promising binary therapy modality for treatment of several cancers in particular malignant gliomas. The cell-killing effect of BNCT is based on the nuclear reaction $^{10}B(n,\alpha)^7Li$ (**Figure 2**) that occurs when the nuclide ^{10}B, which is a nonradioactive constituent of natural elemental boron (approximately 20% abundance), is irradiated with neutrons of the appropriate energy, thermal neutrons. The nuclear reaction yields excited boron-11 (^{11}B*) that after instantaneous nuclear fission produces two high-linear energy transfer entities, i.e., α-particle ($^4He^{2+}$) and recoiling lithium-7 nucleus ($^7Li^{3+}$). Because of the very short track length of these heavy particles (<10 μm; roughly one cell diameter), radiation damage is confined to those cells loaded with ^{10}B.

The probability that a nuclide captures a neutron is measured by the neutron capture cross section, σ_{th}, having ^{10}B a value of σ_{th} = 3838 barns [15]. However, other abundant endogenous nuclei present in the healthy tissue, such as ^{1}H and ^{14}N, could also capture neutrons yielding after nuclear reactions of a gamma ray in the first case, $^{1}H(n,\gamma)^{2}H$, and a proton in the second one, $^{14}N(n,p)^{14}C$. However, the σ_{th} of these nuclei is smaller than the value for ^{10}B, i.e., $\sigma_{th,1H}$ = 0.332 and $\sigma_{th,14N}$ = 1.82 barns, and the amount of radiation produced by these nuclear reactions is lesser than the produced by the particle and recoiling nucleus in the case of boron [15].

On the other hand, for brain tumor such as GBM, usually higher energy epithermal neutron beams which have a greater depth penetration being thermal neutrons unable to act on tumors located below the tissue surface because of scattering effects have been used. Epithermal neutrons do not suffer from the disadvantages of H-recoil processes and, consequently, allow capture reactions to occur at some distance within the tissue; then, epithermal neutrons are progressively slowed into thermal neutrons through heat-releasing interactions with the hydrogen atom and constituents of biological system, that do not cause damage to the tissue [16].

In order for BNCT to be successful, the ^{10}B-loaded agent must completely fulfill some overriding conditions, namely, (a) selective uptake by tumor tissue relative to normal tissue (preferably accumulating within specific tumoral cell substructure) with ideal tumor:normal tissues and tumor:blood ratios of 3:1 and 5:1, respectively, and (b) appropriate amount of ^{10}B delivered to the tumor tissue, i.e., at least 20 μg ^{10}B/g tumor, corresponding to about 10^{9} atoms of ^{10}B/cell.

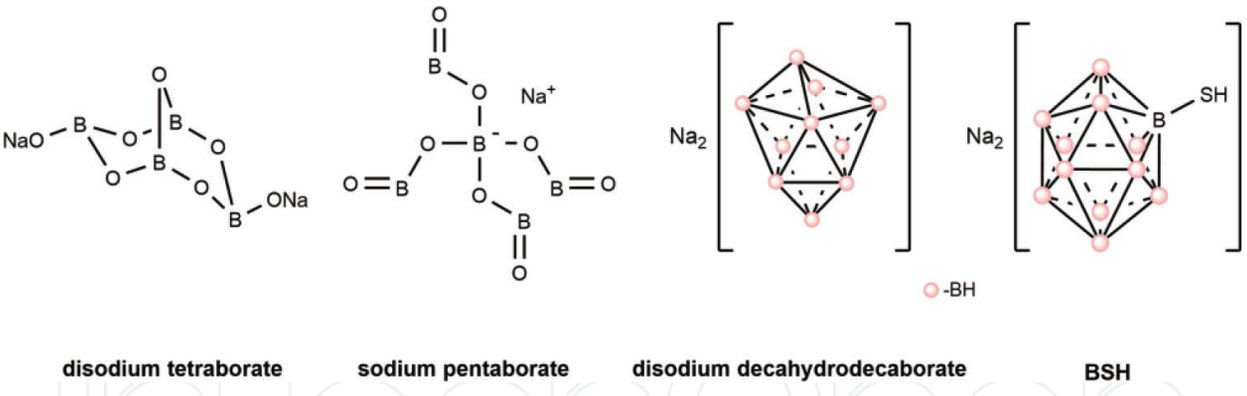


Figure 1. First and current available boron-based drugs for BNCT.

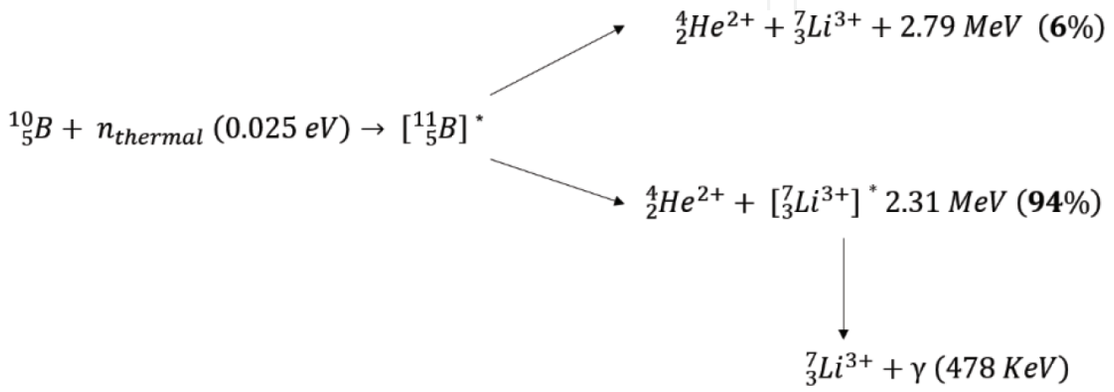


Figure 2. The two parallel nuclear fission reactions that occur upon capture of a slow (thermal) neutron by a ^{10}B nucleus.

However, this amount could be lower if the boron delivery system is concentrated in or near the cell nucleus; (c) retention of ^{10}B in tumor during the BNCT process; (d) rapid clearance from blood and healthy tissues; (e) and adequate lipophilicity especially for glioma treatment where the drug should be able to cross blood-brain barrier (BBB) [17]. Furthermore, like any drug in medicinal chemistry, the ^{10}B-loaded agent must meet the following requirements: (f) absence of systemic toxicity, (g) chemical and metabolic stability, and (h) appropriate water solubility.

1.3. Boron neutron capture therapy: current therapeutic agents

After the first efforts, during the 1940s and 1950s (see Section 1.1.), the lack of selectivity and low boron tumor accumulation observed for the simplest boron salts (**Figure 1**) used until the moment prevented their application in BNCT clinical trials. However, around the 1960s, the first studies of the two compounds currently in clinical began, both ^{10}B-enriched, the polyhedral borane BSH (**Figure 1**) and L-4-dihydroxyborylphenylalanine, known as L-boronophenylalanine (L-BPA; **Figure 3**) [18], which could be accumulated into desired tissues for its structural analogy to some biomolecules.

Due to BSH is a small hydrophilic molecule (**Figure 1**), it does not cross the intact BBB. It only penetrates into the brain passively when the BBB is disrupted [10], as it is observed in the GBM. Although BSH has been applied for the treatment of GBM in infusions with no toxic effects, the efficacy has been limited due to low observed tumor:brain (3:1) and tumor:blood (0.9–2.5:1) ratios [19]. The main structural advantage of BSH compared to L-BPA is that BSH contains 12 times more B per molecule yielding a higher number of events after neutron capture than in L-BPA. BSH has been studied in different therapeutic schedules, combined or not with other small molecules, like L-BPA, or vehicles looking for the improvement of the

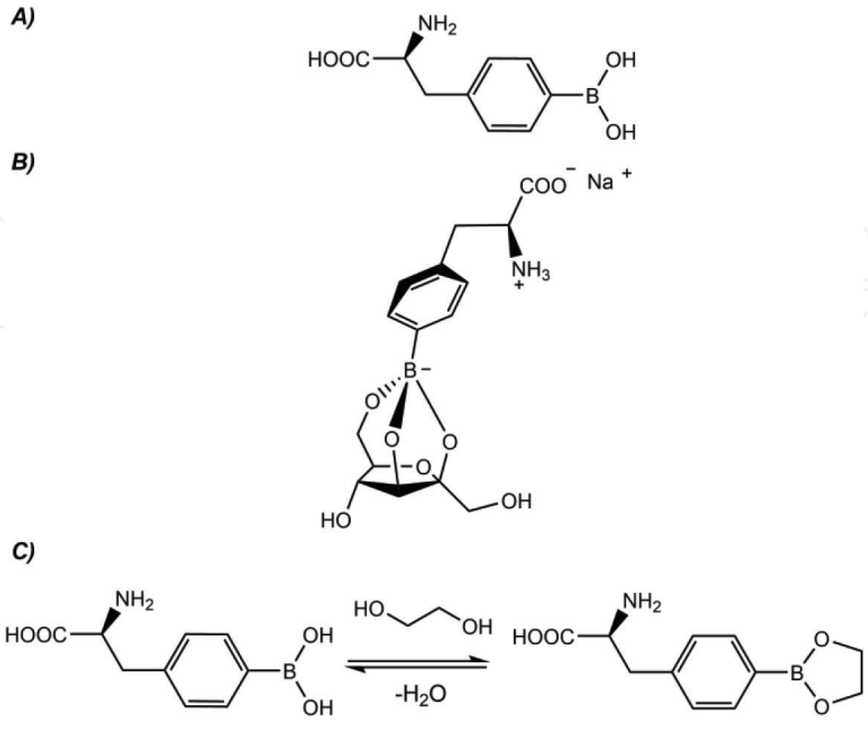


Figure 3. (A) Currently, available boronic acid for treatment of GBM trough BNCT. (B) L-BPA-F complex. (C) Esterification of L-BPA with ethylene glycol.

efficacy and the delivery into the glioma [20]. Medicinal chemistry on BSH, structural modifications, has also been done (see below) seeking better biological behavior.

Nowadays, L-BPA (**Figure 3**) is the standard therapeutic drug used in BNCT [21–23]. Since the L-amino acid transport system is highly expressed in tumor cells compared with normal cells in most organs including the brain, some natural amino acid boron derivatives have been studied [24]. L-BPA has very limited water solubility (1.6 g/L), and searching to circumvent this problem, the standard strategy used for clinical BNCT treatment, it is as a soluble fructose complex, known as L-BPA-F (**Figure 3**), which leads to a pharmaceutical product with favorable biodistribution in human GBM, ratios tumor:blood of 3–4:1 [25], low toxicity, and good capability to cross BBB. Other two strategies include (a) the transformation into the corresponding hydrochloride salt and (b) the esterification of the boronic acid moiety with 1,2- and 1,3-diol producing 1,3,2-dioxaborolanes or 1,3,2-dioxaborinanes, respectively, which is then easily hydrolysable in an aqueous environment (**Figure 3**) [26, 27]. On the other hand, L-BPA is actively transported across the tumor cell membrane, by the L-amino acid transporter system. It is highly expressed in tumor cells, including the brain, compared with normal tissues and can be stimulated by the previous accumulation of the L-DOPA resulting in a substrate-coupled antiport (exchange) mechanism [28]. At this point, L-BPA is considered to be a better B delivery agent than BSH.

2. Medicinal chemistry of boron-bearing compounds for BNCT

2.1. General

From a medicinal chemistry point of view, different strategies have been studied in order to identify new and more selective molecules to glioma cells, with adequate ability to cross the BBB, with higher tumor concentration in the path of the neutron beam and drug-like properties. The third-generation products, which potentially may accumulate into glioma for its structural analogy to some biomolecules, could be classified [15] in (a) macromolecular species and (b) low molecular weight molecules. In reference to the first group, we could mention monoclonal and bispecific antibodies, epidermal growth factor, and encapsulating agents such as boron-containing nanovehicles (liposomes). Here, we will discuss compounds belonging to the second group, like polyhedral boron cluster derivatives, boronic acid derivatives, and other boron-containing small molecules (e.g., oxaborolanes, dioxaborolanes, and azaboro-heterocycles, among others).

2.2. Polyhedral boron clusters

2.2.1. Implications for drug discovery: structural features of closo-carboranes and metallacarboranes. How do they influence on the drug-like properties?

The most known and commonly used class of polyhedral boron compounds in the medicinal chemistry field are the icosahedral dicarba-*closo*-dodecaborane ($C_2B_{10}H_{12}$) commonly referred to as carboranes which exist in three isomeric forms named with respect to the positioning of the two CH vertices (**Figure 4**): 1,2- or *ortho*- (**1**); 1,7- or *meta*- (**2**); and 1,12- or *para*-carborane (**3**); to a lesser extent, their mono-anionic derivatives resulting from the loss of a B vertex, commonly

known as *nido*-carborane (**4** $[C_2B_9H_{12}]^-$); and their metal complexes known as metallacarborane (**5** $[M(C_2B_9H_{11})_2]^-$, where M is a metal) that are generated after removal of the bridge hydrogen from the *nido*-carborane (**Figure 4**) [29, 30].

Among the outstanding and widely explored properties of carboranes and metallacarboranes for medicinal chemistry research are (a) the geometry and the electron-deficient nature of the boron atoms, which generate a strong hydride character in the BH shell, which are some of the main features that determine the intermolecular interactions with the biological targets because they make the B-clusters extremely hydrophobic; (b) both the pharmacokinetics and the bioavailability can be modulated according to the chemotype of boron cluster selected, so the hydrophilicity and lipophilicity, or both, could be tuned; (c) the globular architecture and rigid geometry allow for molecular construction in three dimensions improving the docking, or not, with bio-targets; (d) high boron content per molecule and stability to catabolism are important criteria for the development of agent for BNCT; and (e) the well-established chemistry that makes boron clusters attractive synthons to construct novel pharmaceuticals [31].

Nevertheless, some problems persist today that delay the application of boron clusters in the development of new drugs: (a) the relatively high cost of carboranes and their derivatives even more if they will be used in BNCT because ^{10}B-enriched compound will be needed; (b) the difficulty of in silico drug design and screening of boron cluster drugs, due to the lack of appropriate descriptors for the interaction potentials of boron and the attached hydrogen atoms; and (c) the lack of libraries of boron cluster compounds for high-throughput screening.

2.2.2. Closo-carboranes and metallacarboranes designed and studied for BNCT-glioma treatment

In the past decade, saccharides have been widely studied due to their low toxicities, generally having high water solubility, high expression of specific receptor on the tumor cell surface (specifically in the brain capillary endothelial cells that form the brain barriers, resulting in optimal BBB penetration), and an increased rate of glycolysis in cancer cells. According to this and in order to improve boron uptake, carbohydrates such as ribose, mannose, maltose, and galactose have been chosen to generate carbohydrate-based boron delivery platforms for successful BNCT approach [32, 33]. Since the first description by Hawthorne's group [34], there have been numerous works on the synthesis and biological evaluation of carboranyl-carbohydrate conjugates. Later, Tietze and co-workers developed and evaluated both in vitro and in vivo, against rat glioma cells (C6) and melanoma cell line (B16), a series of carboranyl glycosides including glucoside, lactoside, and maltoside conjugates (**6–8**; **Figure 5**) [35–37]. Although in the in vitro assays significant killing effect was observed because the three derivatives showed an optimum cellular uptake in the C6 glioma cell line, with maltoside **8** being the derivative that exhibited the highest uptake (65.7 ppm at 12 h), the in vivo performance in rat model bearing brain tumor revealed that the concentration of all carboranyl-appended carbohydrate in blood was maintained at levels that were unacceptably high for meaningful use in BNCT. In order to overcome this drawback, Tietze and Yamamoto designed a new type of mixed carboranyl bisglicoside derivatives as prodrugs (**9–12**; **Figure 5**) [38]. Initially, selective uptake of these compounds was not expected due to the hydrophilic sugar moieties at both ends of the carborane preventing cell internalization. The authors demonstrated that the activation of the prodrug could be performed using monoclonal antibodies conjugated

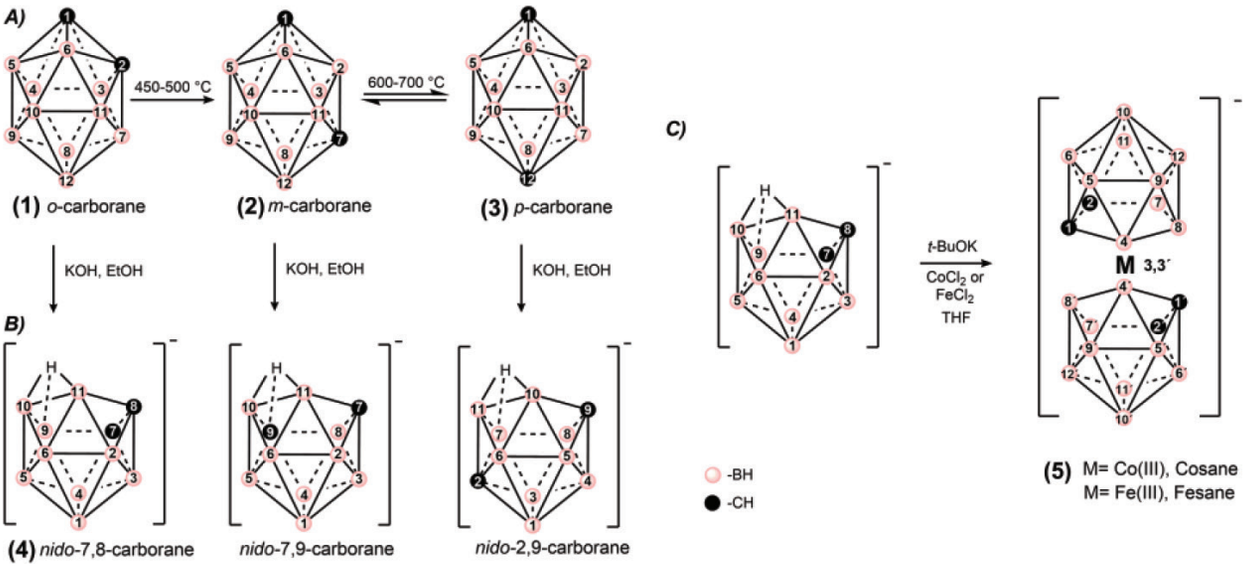


Figure 4. (A) Numbering and nomenclature of the *closo*-carborane systems. Synthesis of *meta* and *para*-carborane derivatives from the *ortho*-carborane isomer through thermal isomerization. (B) Partial degradation of *ortho-*, *meta-*, and *para*-carborane and numbering of nido-carborane system according to IUPAC. (C) Synthesis of metallacarborane from *nido*-carborane.

to glycohydrolases, which bind to tumor-associated antigens, through the glucosidic bond cleavage and concomitant release of carboranyl moiety in the tumor cell surface.

On the other hand, in the last few years, boron-bearing purines, pyrimidines, thymidines, nucleosides, and nucleotides have been widely explored as a novel approach to improve boron uptake in glioma tumor cells. This strategy is based on the fact that tumor cells have higher metabolic activity and an increased requirement for DNA and RNA precursors [39, 40]. Although in recent years several strategies have been addressed, the main focus has been on thymidine analogs substituted with *ortho*-carbonyl cluster at the *N*-3 positions (**13** and **14**, named as 3CTAs; **Figure 6**). Both analogs are potential substrates for human thymidine kinase 1 (hTK1), a cytosolic deoxynucleoside kinase of the DNA synthesis salvage pathway that is predominantly found in proliferating cancer cells. The selective accumulation and retention of 3CTAs in tumor cells via a mechanism known as kinase-mediated trapping (KMT) render these molecules as potential BNCT delivery agents against high-grade brain glioma, such as GBM [41–43]. Another considerable attention has also been to metallacarborane, mainly the bis-(dicarbollyl)-cobalt and bis-(dicarbollyl)-iron derivatives (**15–17**, **Figure 6**). They can also be selectively accumulated in rapidly multiplying neoplastic cells; following their conversion to the corresponding nucleotides, trapped within the cell; or, ideally, incorporated into nuclear DNA of tumors [44]. Despite this, these compounds still have not studied in gliomas.

Barth and co-workers evaluated ^{10}B-enriched derivative **14**, using the RG2 model as in vivo brain tumor model [45]. First, they demonstrated that derivative **14** efficiently delivers boron atoms in cancer cell, which allowed tumor reduction after BNCT in nude mice bearing tumor induced with TK1 positive cell. In addition, based on these favorable results, BNCT studies carried out in the RG2 rat model lead to an increased in life span (ILS) 2.4× in comparison with L-BPA as control therapy. Nevertheless, the greatest percent ILS (122%) was seen in RG2 glioma-bearing rats that received the combination of derivative **14** and

L-BPA, and this correlated with the fact that the tumor in these animals received the highest physical radiation doses. These biological studies clearly revealed the therapeutic potential of derivative **14** although some problems and limitation appeared. Among these, derivative **14** showed clear solubility problems under physiological conditions, possibly due to the presence of the carboranyl hydrophobic core and the absence of any functional groups that can be ionized.

Since the first description by Haushalter and Rudolph in 1978 (**18** and **19**; **Figure 7**) [46, 47], the potential for medical application of several boron cluster-containing fluorescent dyes, including porphyrins and related macrocyclic, have been highly explored and scrutinized for several reasons, among them: (a) well-known ability to selective accumulate into tumor cells in high amounts, (b) subsequent persistence within tumors, (c) general low dark cytotoxicity, (d) capability to bind to DNA due to their plane aromatic structure, and (e) highly fluorescence, thus enabling tumor diagnosis and facilitating treatment planning. Nonetheless, without any doubt, the most exploited feature of these molecules is the ability to act in photodynamic therapy (PDT). PDT combines a photosensitizer (porphyrin), light, and tissue oxygen, to generate reactive oxygen species, including singlet oxygen, triggering subsequently cell death mechanisms by necrosis and/or apoptosis. The combination of this therapy with BNCT has been of particular interest to control local recurrence of high-grade gliomas such as GBM, because they target different mechanisms of tumor cell death and, thus, increase the

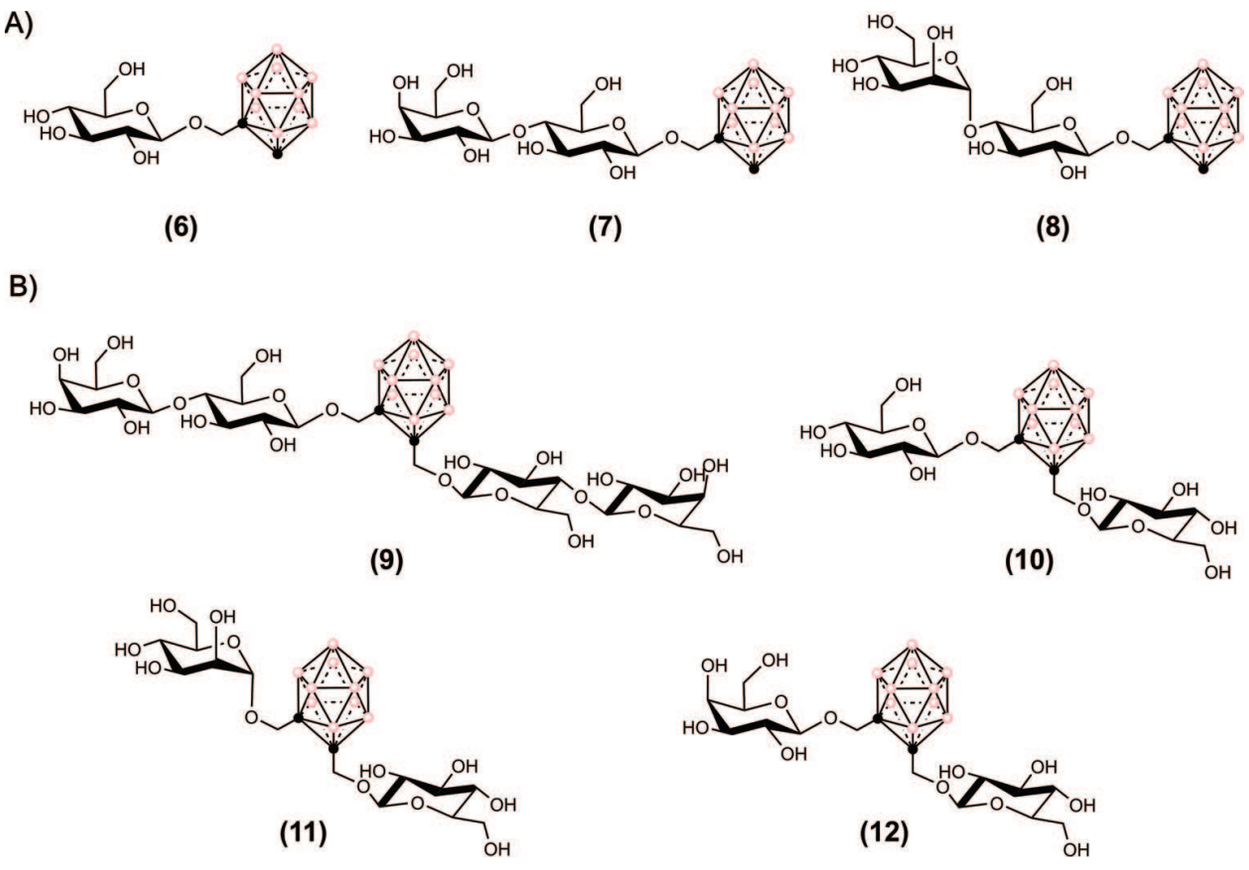


Figure 5. (A) Compound **6** corresponds to carboranyl derivative of D-glucose, and compounds **7** and **8** are derivatives of lactose and maltose, respectively. (B) *Ortho*-carboranyl bisglycosides **9–12** containing lactose, glucose, mannose, and galactose in their structures.

therapeutic effect. Both are bimodal therapies, the individual components of which are non-toxic in isolation, but which are tumoricidal in combination.

In the last few years, a large number of boron-containing natural porphyrins have been synthesized and evaluated both in cellular and animal models (**20–23**; **Figure 8**) [48]. To date, the tetrakis-carborane carboxylate ester of 2,4-bis(α,β-dihydroxyethyl)deuteroporphyrin IX (**22**, known as BOPP) was the only compound to be employed in a phase I clinical study against GBM [49, 50]. Pharmacological studies showed its ability to selectively incorporate in tumor cells, in xenograft models of glioma, relative to the surrounding normal brain cells (tumor:brain ratio as high as 400) and situated preferentially in tumor cell mitochondria. Nevertheless, these results could not be replicated in humans.

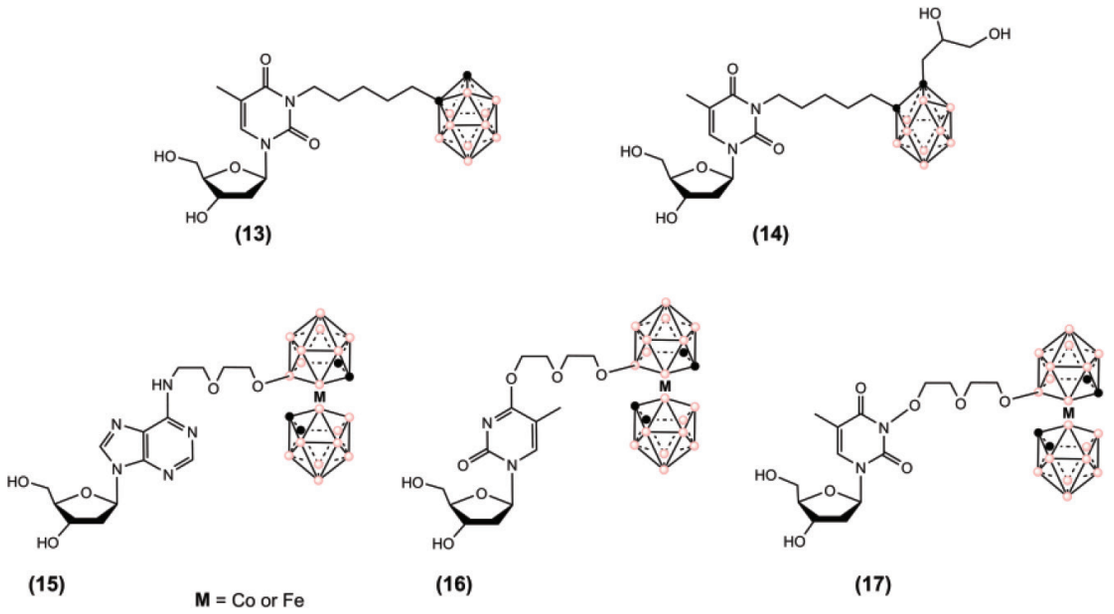


Figure 6. Chemical structure of the main carborane-bearing nucleoside delivery agents.

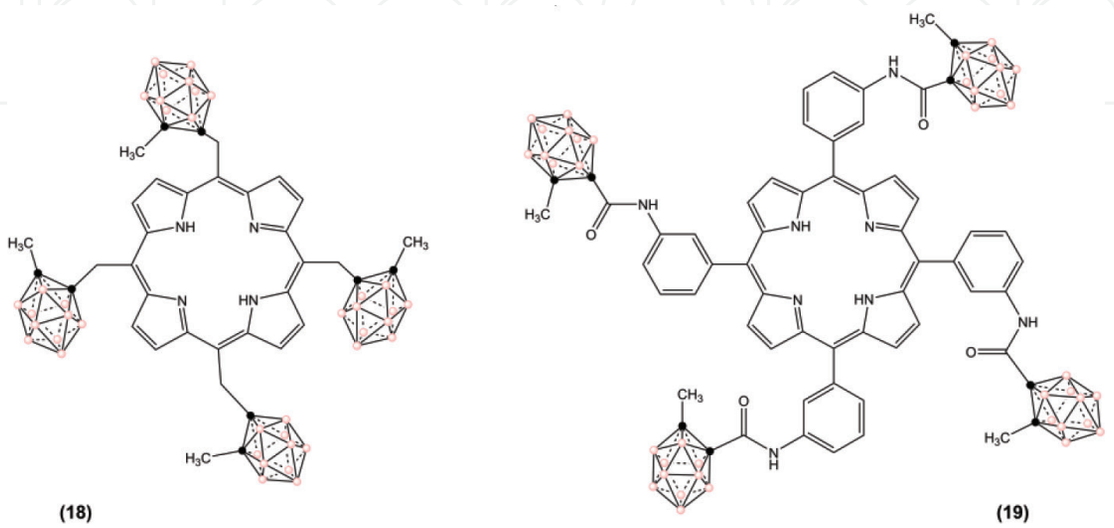


Figure 7. First boron-containing porphyrins developed by Haushalter and Rudolph for catalysis application.

The success of derivative **22** was interrupted in a phase I clinical trial for several reasons: (a) it could not deliver to the tumor a therapeutic amount of boron in patients with GBM; (b) thrombocytopenia was observed in patients due to the direct toxic effect of derivative **22** or its metabolites (probably of carboxylic carborane) on platelets; and (c) the pharmacokinetic behavior of derivative **22** in humans was characterized by a prolonged clearance phase, giving rise to potentially toxic metabolites and cutaneous photosensitivity [51].

In order to overcome this drawback, several researchers designed and synthesized a highly boron water-soluble porphyrins as a possible BNCT agents. In this sense, Vicente and co-workers described *nido*-carborane cluster-linked porphyrins via aromatic linkage (e.g., **24**; **Figure 8**). These amphiphilic derivatives showed very low toxicity, were taken up by 9 L and U-373MG cells in both time- and concentration-dependent manners, and were localized preferentially in cell lysosomes [52]. On the other hand, Deen and co-workers developed the polyboronated ionic porphyrin **25**, known as TABP-1, which was administrated by convection-enhanced delivery (CED) to nude rats bearing intracerebral implant of human glioblastoma cell line U-87MG [53]. In contrast to diffusion, CED uses a pressure gradient established at the tip of an infusion catheter to establish bulk flow and distribute drug and solvent throughout the extracellular space. This demonstrated high tumor and low blood boron concentration through intracerebral administration by CED related to systemic administration.

Carborane-containing nucleosides and analogues as the means to concentrate boron within the tumor cell nucleus were described. However, another class of derivatives, which could interact directly to chromosomal DNA, has been developed and widely explored for boron neutron capture therapy. Among this the following could be mentioned (**Figure 9**): (a) alkylating agents (i.e., **26** and **27**), (b) DNA intercalators (i.e., **28** and **29**), (c) minor groove binders (i.e., **30** and **31**), and (d) cationic polyamines (i.e., **32** and **33**) [54]. Regarding the last group of compounds, it should be stated that natural polyamines such as spermidine, spermine, and putrescine, found in both prokaryotic and eukaryotic cell types, are a class of biologically active compounds known to be essential for every cell to support their function such as growth and differentiation. In addition, because they have a specific transportation system, they have been found in high concentration in rapidly proliferating tumor cells. This characteristic was used by Zhuo and co-workers, synthesizing and evaluating derivatives **32** and **33** [55]. These compounds proved to be highly water-soluble, in vitro they have the ability to interact to calf thymus DNA, and they are rapidly taken up by F98 rat glioma cells at levels which match that of clinically used agents. Unfortunately, in vivo biodistribution studies of these derivatives, performed in mice-bearing intracerebral implants of the GL21 glioma and subcutaneous implants of the B16 melanoma, suggested that they were unable to deliver adequate amounts of boron to tumor.

More recently, Vicente's group proposed other interesting strategies that involved the use of porphyrins bearing *p*-carboranylmethylthiol moiety conjugated to polyamines (**34**–**41**; **Figure 10**) [56]. In vitro, the polyamines displayed low dark cytotoxicity, low phototoxicity, preferential localization in the endoplasmic reticulum, Golgi and the lysosomes, and, except derivative **34**, higher uptake into human glioma T89G cells (up to 12-fold for spermine derivative **39**) than the tri-ethyleneoxy conjugate **41**. All these results suggested that spermine derivative could serve as an effective carrier of boronated porphyrins for the BNCT of tumor.

2.2.3. BSH structural modifications

As it is indicated above, BSH inadequate drug-like properties, i.e., lack tumor selectivity and poor BBB crossing ability, have conducted to develop BSH hybrid compounds containing other pharmacophoric moieties seeking improvement biological behavior.

In this sense, some approaches were based on the particular tumoral amino acid requirement and the special ability of some peptides to interact with receptors that, via endocytosis, are internalized into tumoral cells. In the first strategy, hybrid **42** (**Figure 11**), carrying a fragment derived from an unnatural amino acid that demonstrated a particular uptake by glioblastoma cells [57], was prepared and in vivo evaluated in F98 glioma-bearing animals [58].

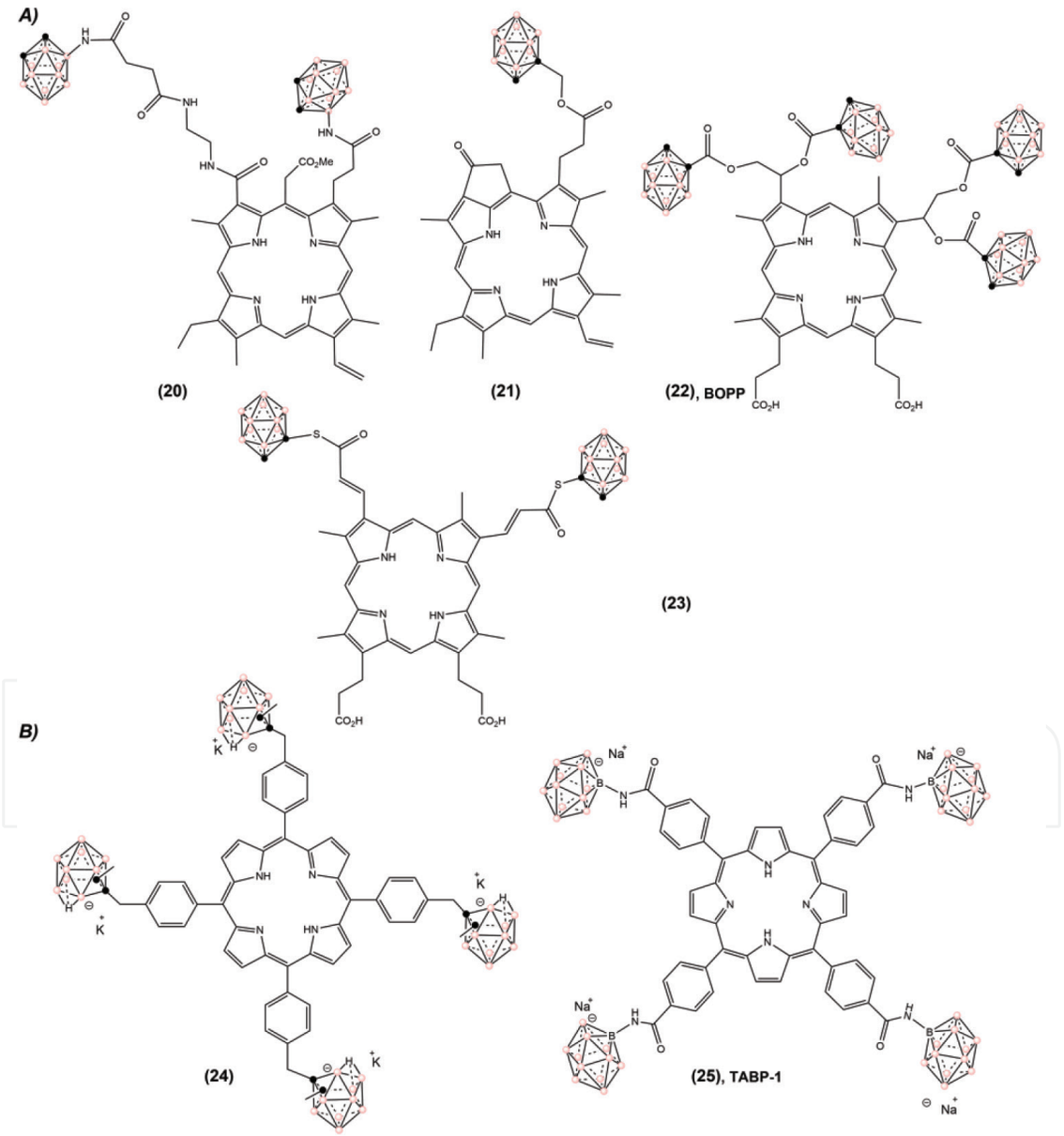


Figure 8. (A) Structures of some relevant boron-containing porphyrins. (B) Some relevant polyhedron boron cluster water-soluble porphyrins.

The biodistribution studies showed higher tumor boron concentrations for derivative **42** than for BSH but lower than for L-BPA-F i.v. treatments. The CED intracerebral administration of derivative **42** was assayed combined with BNCT reaching better animals' survival rates than the treatment with L-BPA-F/i.v. On the other hand, in the use of peptides as carrier strategy, the hybrid **43** (**Figure 11**), derived from Tyr^3-octreotate peptide that interacts to somatostatin receptor, was synthesized [59]. This BSH octapeptide still has not study biologically.

As it was already mentioned, the biochemical peculiarities of the porphyrin system also allowed the delivery of BSH within the tumor. In this sense, hybrid BSH porphyrin **44** (**Figure 11**) was prepared and evaluated in a 9 L glioma-bearing rat model [60]. Compound **44** displayed higher boron tumor:blood ratio in comparison to BSH 24 h after i.v. treatment and in an in vitro BNCT colony-forming assay higher cytotoxicity than BSH. Another series of BSH porphyrin hybrids consists of compounds like **45** and **46** (**Figure 11**) that still has not been biologically studied on gliomas [61].

GBM contains areas with different oxygenation levels, and consequently different metabolic patterns, which make difficult the therapeutic strategies [62]. Highly oxygenated regions are close to blood vessels, present high proliferation rate and oxidative metabolism and are susceptible to metabolism-active drugs and radiotherapy. While hypoxic regions present low proliferation rate, reductive metabolism and are resistant to chemo- and radiotherapy. The hypoxic condition in GBM tumors, which induces metastasis and promotes angiogenesis and resistance, has been attributed to contribute to tumor regrowth and, therefore, in a relapse. The troublesome characteristics of hypoxic regions have been exploited to generate cancer therapeutics known as hypoxia-selective bioreductive prodrugs which are compounds able

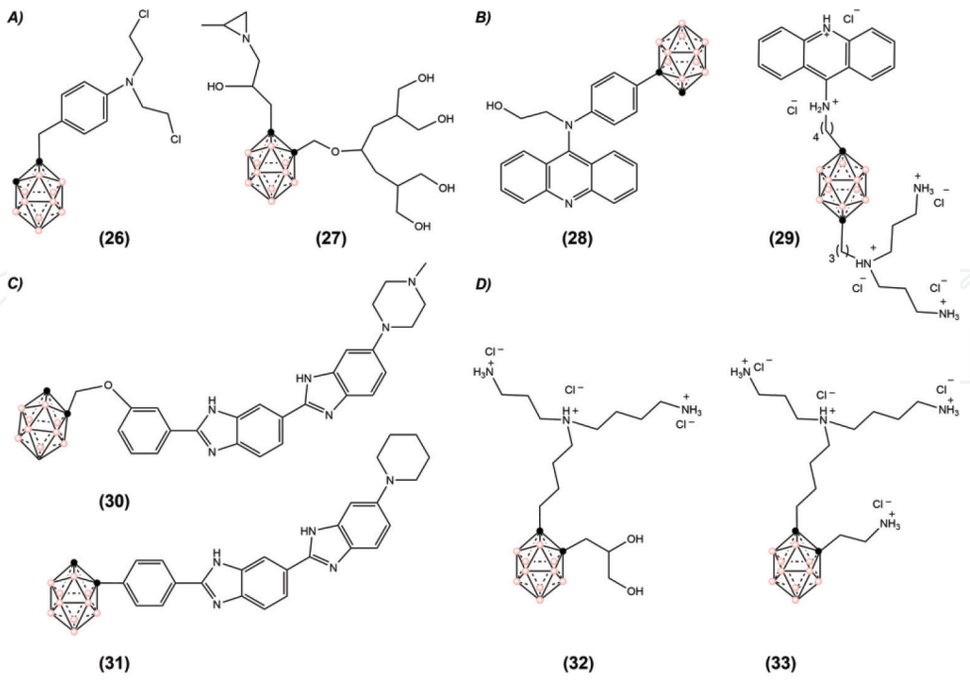


Figure 9. Carborane-containing DNA-interacting agents. (A) Alkylators. (B) Intercalators. (C) Minor-groove binders. (D) Polyamines.

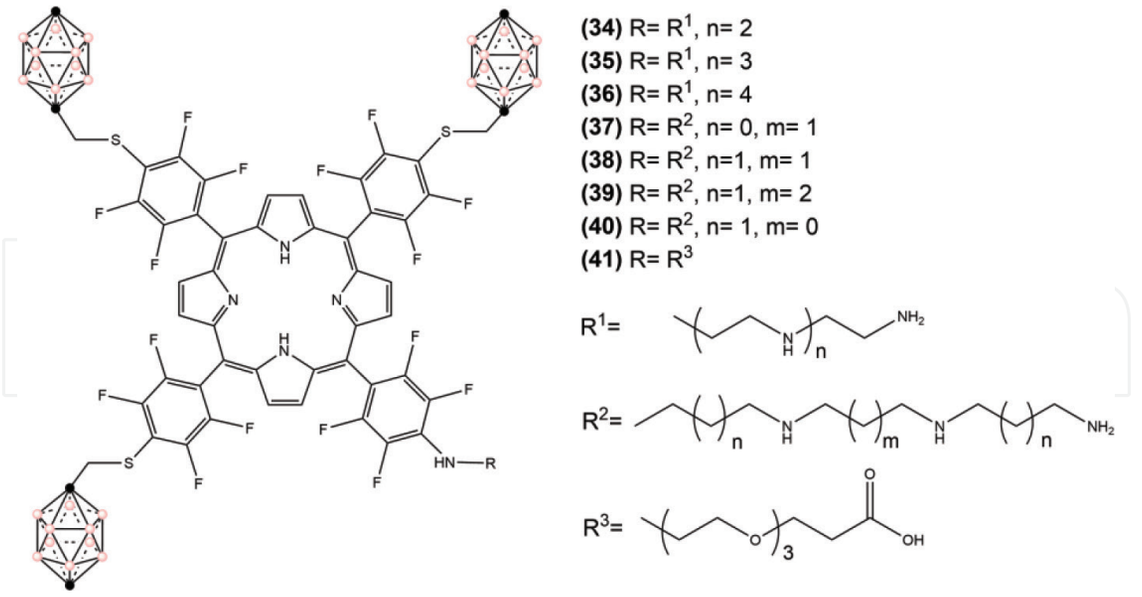


Figure 10. Carborane-containing porphyrins porting polyamine framework.

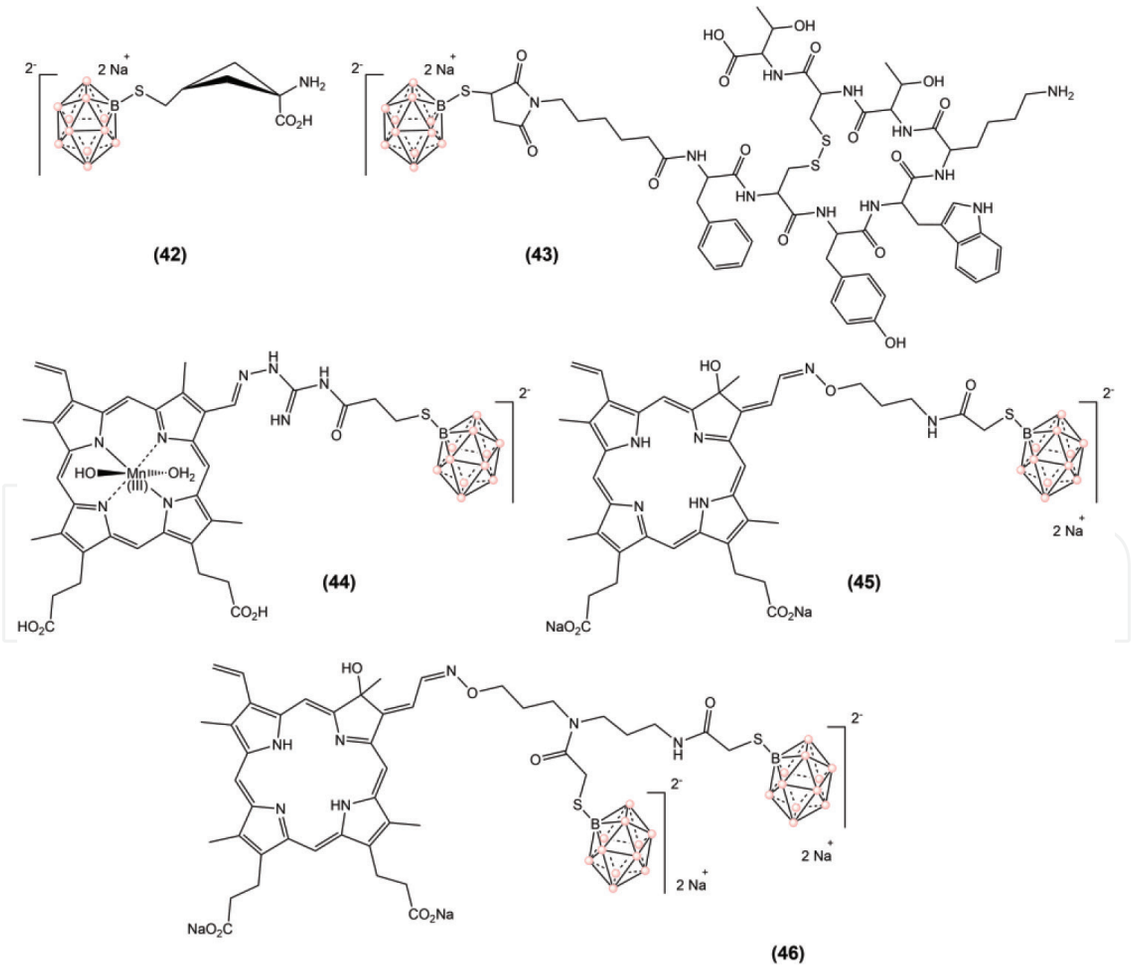


Figure 11. Some BSH hybrids attempting to improve BSH biological behavior.

to undergo reduction producing cytotoxic events. Some of the well-known bioreductive pharmacophores, nitroimidazoles, and *N*-oxide containing heterocycles were used to prepare BSH hybrids for potential use in hypoxia. Thereby, 2-nitroimidazoles **47** and **48** or quinoxaline dioxides **49** and **50** (**Figure 12**) were prepared and evaluated against some tumoral models using BNCT, but unfortunately they have not yet been studied on glioma models [63–65].

2.3. Boronic acids and their esters

Boronic acid (R-$B(OH)_2$) has been utilized as a pharmacophore in the searching of new agents to be employed in BNCT. This functional group has some relevant drug-like properties turning it into a useful moiety for biological applications, for example [66–68], (a) the sp^2-hybridized boron atom possesses a vacant *p*-orbital which, after biomolecule donor atom attacks, allows the interconversion of boron hybridization, from sp^2 to sp^3, to generate a new stable anionic compound; (b) the enhanced ability of $–B(OH)_2$ system to interact with biomolecule via (b1) hydrogen bonds, as acceptor and donor through OH groups, and (b2) strong boron Lewis acidity that allows boron-nitrogen, boron-oxygen, or boron-sulfur bonds; (c) the apparent pK_a of $–B(OH)_2$ ranging 4.5–8.8, for arylboronic, that allows large acid-base behavior finding the protonated and deprotonated form of the acid according to physiological pH conditions; and (d) apart from the reactivity mentioned above (section a) the particular ability to react with diol-containing compounds, like sugars and sugar-containing biomolecules, yielding the corresponding stable cyclic ester 1,3,2-dioxaborolane. Additionally, the $–B(OH)_2$ group has weak electronic effects being electron donor for induction and electron withdrawing for mesomerism. In reference to the lipophilicity of the $–B(OH)_2$ moiety, it is as lipophilic as –CN group, lesser lipophilic than $–CO_2CH_3$ and neutral $–CO_2H$ moieties, and more lipophilic than $–CONH_2$, $–CH_2OH$, and –CHO groups (π Hansch constants which are −0.55, −0.57, −0.01, −0.32, −1.49, −1.03, and −0.65, respectively [69]). In vitro boronic acids degrade leading deboronation via hydrolysis/oxidation yielding boric acid (H_3BO_3). For example, degradation of bortezomib, known as Velcade™ the first boronic acid-containing drug on the market and approved by the US Food and Drug Administration, under acidic and basic conditions seems to be mediated by an initial oxidation producing boric acid and having a plasma half-life of 9–15 h in humans. The end product, boric acid, is not considered especially toxic to humans. For this, it is not expected that boronic acids possess intrinsic toxicity.

The success of the L-BPA in preliminary studies in patients with GBM, followed by PET studies with 1-aminocyclobutane-1-[^{11}C]-carboxylic acid, revealing that cyclic amino acids were located preferentially in this tumor [57], led to the development of series of these cycloalkane-boronic acids (**51**–**54**; **Figure 13**) [70, 71]. They are water-soluble, cross the BBB, and are not metabolized by tumor cells, and while all accumulate into tumor similarly, the *cis*-isomers (**51** and **53**) biodistributed four times higher in tumor than in blood that of the *trans*-ones (**52** and **54**) and that of L-BPA-F [72–74]. By secondary ion mass spectrometry, it was proven that nearly 70% of the boron pool from derivative **51** was in the nucleus and cytoplasm of T98G GBM cells [75]. Until now there have been no studies of BNCT with these compounds, and further studies should be done prior to clinical trials.

As it is mentioned above, polyamines are essential for differentiation and growth of mammalian cell, and their depletion has growth inhibitory effects on tumors. Furthermore, a polyamine-facilitated transport system is present and allows the uptake by malignant cells [76].

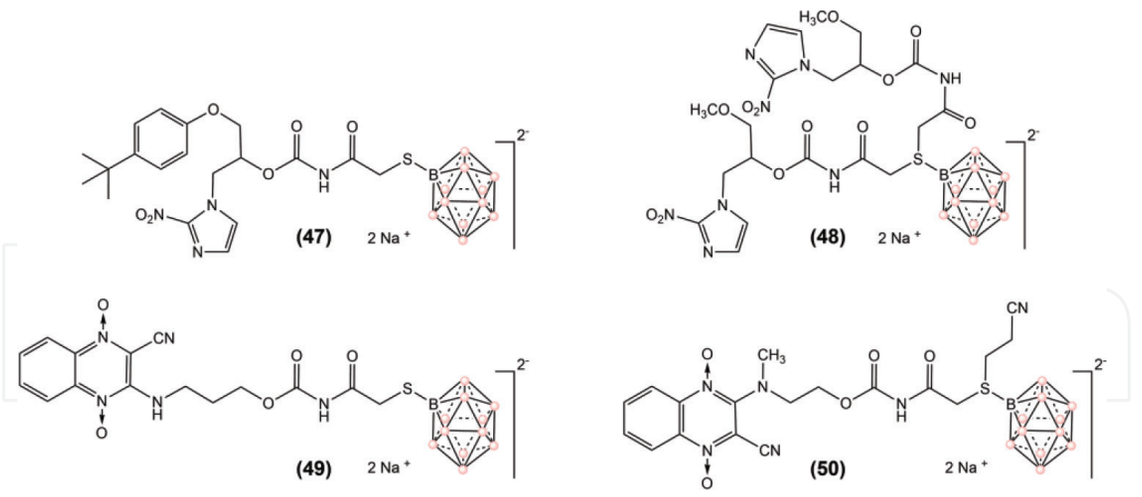


Figure 12. BSH hybrids with potential use in hypoxic glioma.

For that, boronic acid-containing polyamines have been also studied as potential BNCT agents [77]. Compound **55** (**Figure 13**) with higher hydrophilicity that of carboranyls **32** and **33** (**Figure 9**) was designed in order to minimize the carboranyl's nonspecific binding to biolipids that limits the tumor specificity. This boronic acid derivative was able to bind to calf thymus DNA and rapidly was taken up in vitro by F98 rat glioma cells, but the in vivo biodistribution showed unmeasurable levels of boron in tumor, and for this reason, the authors have considered that derivative **55** is not appropriate for BNCT [55].

Thinking about DNA as target to metabolically incorporate boron atoms to the tumoral cell, boronic acid-containing nucleic acids have been studied. One of the first described compounds was the uracil derivative **56** (**Figure 13**) [78] which demonstrated unfavorable tumor:blood and brain:blood biodistribution ratios being in all studied times in favor to blood. After that some boronic acid-containing nucleosides, such as **57** (**Figure 13**), were prepared and studied as potential agents for BNCT; however, no studies with glioma were performed [79]. However, recently nucleoside **58**, a boronic cyclic ester (a dioxaborolane derivative; **Figure 13**), was prepared and evaluated as cytotoxic agent against some tumoral cells [80, 81] including U-118 MG glioblastoma cells [82]. Additionally, the ability of ester **58** to be incorporated into cellular DNA and its selectivity for tumoral cells become its potential usefulness tool in glioma BNCT.

The combination of PDT and BNCT has been also proposed using boronic acid-containing porphyrins, i.e., **59** and **60** (**Figure 14**) [83]. However, it still has not been conducted studies with these compounds in gliomas.

As previously stated the particular hypoxic condition of some GBM regions was used as strategy to produce boronic acid derivatives that could be selectively accumulated in this tissue. For example, the well-known 2-nitroimidazolyl hypoxia pharmacophore was employed as structural guide to boron-enriched tumoral cells generating the boronic acid ester **61** (**Figure 14**) [84]. This dioxaborolane was selectively accumulated in D54 glioma when it was injected intratumorally in a xenograft mouse model reaching 9.5 times the levels of boron into the tumor of L-BPA in the same conditions. However, the pharmacokinetic behavior of derivative **61** should be solved in order to improve the use of this agent in BNCT.

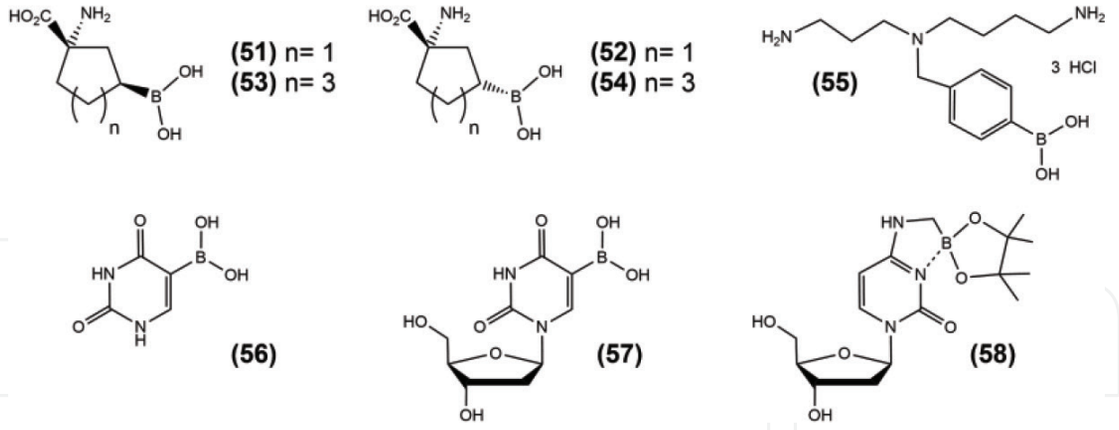


Figure 13. Some boronic acid derivatives developed as potential BNCT agents. Amino acids **51–54** were studied as a mixture of enantiomers.

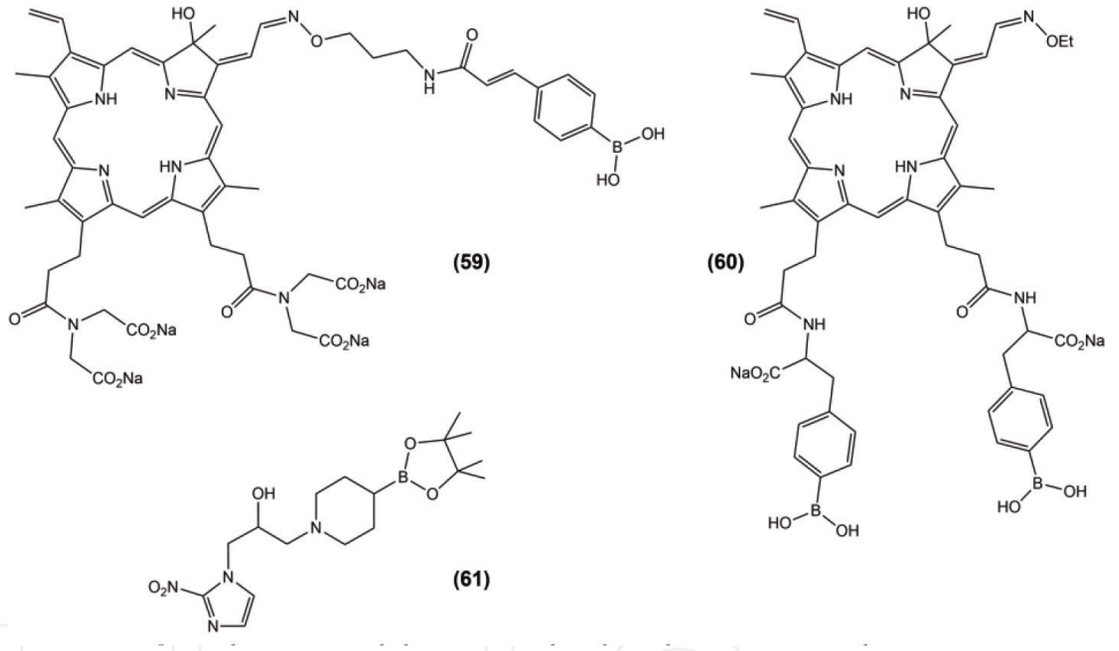


Figure 14. Some boronic acid derivatives developed as two-target drugs.

2.4. Miscellaneous compounds

Other boron-containing moieties have been described for BNCT, for example, in compounds **62–68** (**Figure 15**) [85–90]. However, in spite of their attractive features as pharmacophores, they have not been applied for glioma treatment. Additionally, they contribute with low number of boron atom per molecule which, as mentioned above, which is a disadvantage respect to boron clusters. However, this could be overcome with a high selective accumulation into the tumor cells. For example, the betaine **68**, a boron-containing dipeptide analogue, showed selective accumulation in rat C6 gliosarcomas with ^{10}B tumor:blood and tumor:normal brain ratios of 8.9 and 3.0, respectively [91].

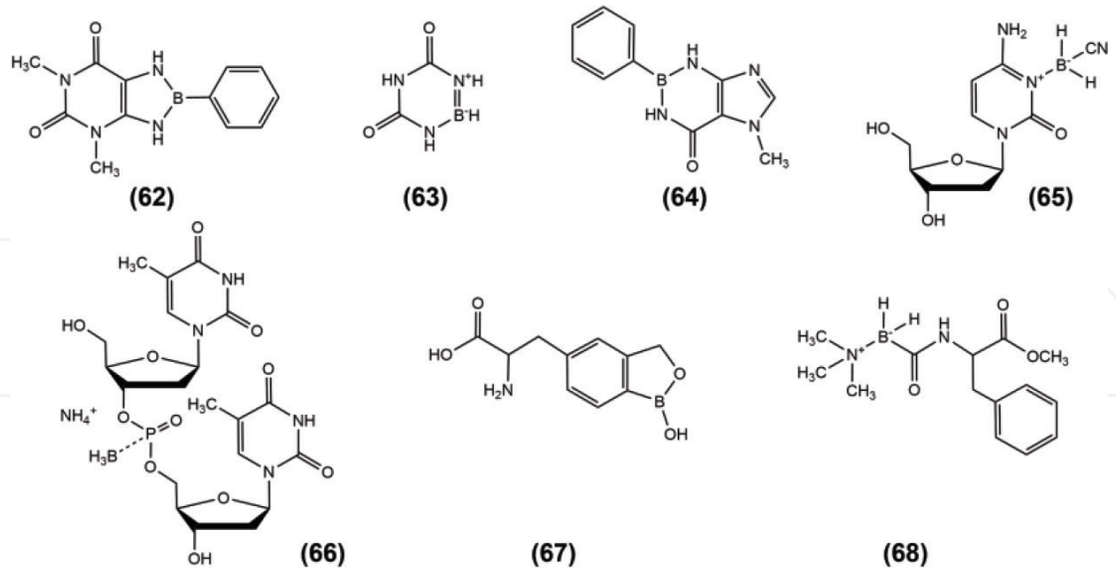


Figure 15. Some other potential boron pharmacophores for glioma BNCT, i.e., boradiazoles, aza-borauracils, 2-boradihydropurines, cyanoboranes, boranophosphates, benzoxaboroles, and trialkylamine-carboxyboranes.

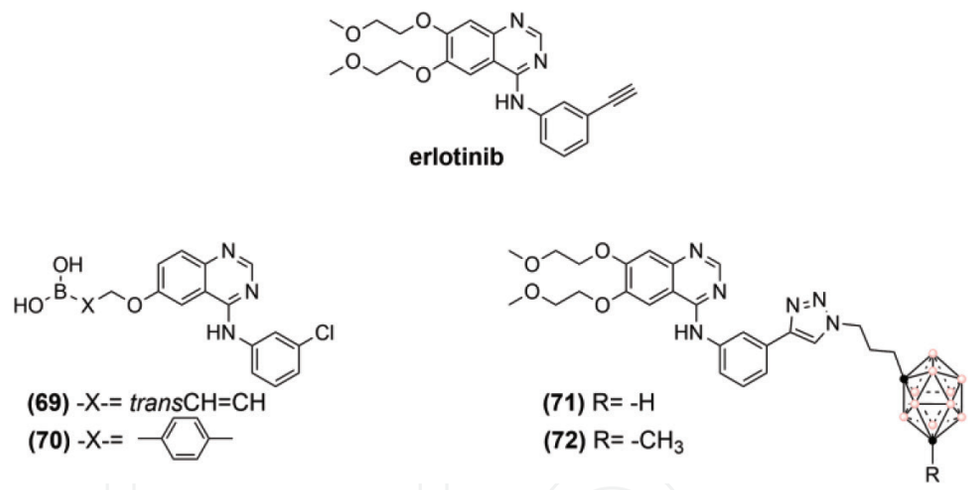


Figure 16. Structure of the well-known PTK inhibitor erlotinib and boron-containing compounds derived from 4-anilinoquinazolinyl pharmacophore.

2.5. Other approaches: site-specific delivery

Beyond the strategies of therapy combination mentioned above, such as phototherapy or hypoxia, another hypothesis has been choosing a bio-system overexpressed in tumoral cells, but not in healthy cells, as a way to selectively accumulate boron drugs in the desired tissue to further BNCT. In this sense, Nakamura and colleagues have described the use of protein tyrosine kinases (PTKs), that its uncontrolled activation is often associated with uncontrolled cell growth and tumor progression, to generate boronic acid and esters hybridized with PTK pharmacophores as new drugs (i.e., **69** and **70**; **Figure 16**) [92]. However, they did not bear

in mind the glioma treatment nor BNCT with this strategy. Nevertheless, we considered the GBM-PTKs [93] as the target to accumulate a boron-enriched drug to further BNCT procedure. Thereby, we hybridized the 4-anilinoquinazolinyl PTKs and the carboranes as boron delivery pharmacophores, i.e., **71** and **72** (**Figure 16**) [94]. Especially, hybrid **71** demonstrated 3.3 times higher activity against C6 glioma cells than the parent drug erlotinib (**Figure 16**), lower cytotoxic effects on normal glia cells, excellent PTK inhibition, capability to accumulate in glioma cells, ability to cross BBB, and stability on simulated biological conditions [94, 95].

3. Conclusion

The development of boron-bearing compound for BNCT has been a vast field of research within medicinal chemistry. New and interesting pharmacophores have been described in order to fulfill the BNCT requirements. Despite this, very few reached the stage of clinical studies, being currently L-BPA and BSH, the only two potential therapeutic agents. However, due to the multidisciplinary approach of the BNCT and the emerging novel structures, we expect with optimism the new developments in the years to come.

Acknowledgements

The authors are SNI-ANII researchers and PEDECIBA members.

Conflict of interest

The authors declare no conflict of interest.

Author details

Hugo Cerecetto[1]* and Marcos Couto[2]

*Address all correspondence to: hcerecetto@cin.edu.uy

1 Área de Radiofarmacia, Centro de Investigaciones Nucleares Facultad de Ciencias, Universidad de la República, Uruguay

2 Grupo de Química Orgánica Medicinal, Facultad de Ciencias, Universidad de la República, Uruguay

References

[1] Chadwick J. The existence of a neutron. Proceedings of the Royal Society of London A. 1932;**136**:692-708. DOI: 10.1098/rspa.1932.0112

[2] Locher GL. Biological effects and therapeutic possibilities of neutrons. The American Journal of Roentgenology and Radium Therapy. 1936;**36**:1-13

[3] Kruger PG. Some biological effects of nuclear disintegration products on neoplastic tissue. Proceedings of the National Academy of Sciences of the United States of America. 1940;**26**:181-192

[4] Sweet WH. The uses of nuclear disintegration in the diagnosis and treatment of brain tumor. The New England Journal of Medicine. 1951;**245**:875-878. DOI: 10.1056/NEJM195112062452301

[5] Javid M, Brownell GL, Sweet WH. The possible use of neutron-capturing isotopes such as boron10 in the treatment of neoplasms. II. Computation of the radiation energies and estimates of effects in normal and neoplastic brain. The Journal of Clinical Investigation. 1952;**31**:604-610. DOI: 10.1172/JCI102647

[6] Farr LE, Robertson JS, Stickley EE, Bagnall HJ, Easterday OD, Kahle W. Recent advances in neutron capture therapy. In: Proceedings of the Second United Nations International Conference on the Peaceful Uses of Atomic Energy. Vol. 26. Geneva: United Nations; 1958. pp. 451-456

[7] Archambeau JO. The effect of increasing exposures of the $^{10}B(n,\alpha)^{7}Li$ reaction on the skin of man. Radiology. 1970;**94**:178-187. DOI: 10.1148/10.1148/94.1.179

[8] Sweet WH, Soloway AH, Brownell GL. Boron-slow neutron capture therapy of gliomas. Acta Radiologica: Therapy, Physics, Biology. 1963;**1**:114-121. DOI: 10.3109/028418663091350 70

[9] Asbury AK, Ojeman RG, Nielsen SL, Sweet WH. Neuropathological study of fourteen cases of malignant brain tumor treated by boron-10 slow neutron capture radiation. Journal of Neuropathology and Experimental Neurology. 1972;**31**:278-303. DOI: 10.1097/00005072-197204000-00005

[10] Soloway AH, Hatanaka H, Davis MA. Penetration of brain and brain tumor. VII. Tumor-binding sulfhydryl boron compounds. Journal of Medicinal Chemistry. 1967;**10**:714-717. DOI: 10.1021/jm00316a042

[11] Hatanaka H. Boron-neutron capture therapy for tumors: Preface. In: Boron-Neutron Capture Therapy for Tumors. Niigata: Nishimura Co. Ltd.; 1986

[12] Hatanaka H. Clinical results of boron neutron capture therapy. Basic Life Sciences. 1990;**54**:15-21

[13] Hatanaka H, Sweet WH, Sano K, Ellis F. The present status of boron-neutron capture therapy for tumors. Pure and Applied Chemistry. 1991;**63**:373-374. DOI: 10.1351/pac199163030373

[14] Sauerwein W, Moss RL, editors. Requirements for Boron Neutron Capture Therapy (BNCT) at a Nuclear Research Reactor. Luxembourg: Office for Official Publications of the European Communities; 2009. 125 p. DOI: 10.2790/11743

[15] Barth RF, Soloway AH, Brugger RM. Boron neutron capture therapy of brain tumours: Past history, current status, and future potential. Cancer Investigation. 1996;**14**:534-550. DOI: 10.3109/07357909609076899

[16] Calabrese G, Daou A, Barbu E, Tsibouklis J. Towards carborane-functionalised structures for the treatment of brain cancer. Drug Discovery Today. 2017;**23**:63-75. DOI: 10.1016/j.drudis.2017.08.009

[17] Sauerwein W, Rassow J, Mijnheer B. Considerations about specification and reporting of dose in BNCT. In: Larsson B, Crawford J, editors. Advances in Neutron Capture Therapy: Medicine and Physics. New York: Plenum Press; 1997. pp. 531-534

[18] Studenov A, Ding Y-S, Ferrieri R, Miura M, Coderre J, Fowler JS. Synthesis and PET studies of [^{11}C]D- and [^{11}C]L-boronophenylalanine for improving BNCT in brain tumors. Journal of Labelled Compounds and Radiopharmaceuticals. 2001;**44**:S345-S347. DOI: 10.1002/jlcr.25804401121

[19] Kageji T, Nakagawa Y, Kitamura K, Matsumoto K, Hatanaka H. Pharmacokinetics and boron uptake of BSH ($Na_2B_{12}H_{11}SH$) in patients with intracranial tumors. Journal of Neuro-Oncology. 1997;**33**:117-130. DOI: 10.1023/A:1005785718533

[20] Barth RF, Vicente MG, Harling OK, Kiger WS, Riley KJ, Binns PJ, Wagner FM, Suzuki M, Aihara T, Kato I, Kawabata S. Current status of boron neutron capture therapy of high grade gliomas and recurrent head and neck cancer. Radiation Oncology. 2012;**7**:146. DOI: 10.1186/1748-717X-7-146

[21] Kawabata S, Miyatake S, Kuroiwa T, Yokoyama K, Doi A, Iida K, Miyata S, Nonoguchi N, Michiue H, Takahashi M, Inomata T, Imahori Y, Kirihata M, Sakurai Y, Maruhashi A, Kumada H, Ono K. Boron neutron capture therapy for newly diagnosed glioblastoma. Journal of Radiation Research. 2009;**50**:51-60. DOI: 10.1269/jrr.08043

[22] Kawabata S, Miyatake S, Hiramatsu R, Hirota Y, Miyata S, Takekita Y, Kuroiwa T, Kirihata M, Sakurai Y, Maruhashi A, Ono K. Phase II clinical study of boron neutron capture therapy combined with X-ray radiotherapy/temozolomide in patients with newly diagnosed glioblastoma multiforme-study design and current status report. Applied Radiation and Isotopes. 2011;**69**:1796-1799. DOI: 10.1016/j.apradiso.2011.03.014

[23] Miyatake S, Kawabata S, Hiramatsu R, Kuroiwa T, Suzuki M, Kondo N, Ono K. Boron neutron capture therapy for malignant brain tumors. Neurologia Medico-Chirurgica (Tokyo). 2016;**56**:361-371. DOI: 10.2176/nmc.ra.2015-0297

[24] Spielvogel BF, Sood A, Hall IH, Fairchild RG, Micca PL. Synthesis, antineoplastic activity and biodistribution of boron analogues of amino acids and related compounds. Strahlentherapie und Onkologie. 1989;**165**:123-125

[25] Coderre JA, Elowitz EH, Chadha M, Bergland R, Capala J, Joel DD, Liu HB, Slatkin DN, Chanana AD. Boron neutron capture therapy for glioblastoma multiforme using *p*-boronophenylalanine and epithermal neutrons: Trial design and early clinical results. Journal of Neuro-Oncology. 1997;**33**:141-152. DOI: 10.1023/A:1005741919442

[26] Ichihashi M, Nakanishi T, Mishima Y. Specific killing effect of ^{10}B-*para*-boronophenylalanine in thermal neutron capture therapy of malignant melanoma: *In vitro* radiobiological evaluation. Journal of Investigative Dermatology. 1982;**78**:215-218. DOI: 0022-202X/82/7803-02 15$02.00/0

[27] Lorand JP, Edwards JO. Polyol complexes and structure of the benzeneboronate ion. The Journal of Organic Chemistry. 1959;**24**:769-774. DOI: 10.1021/jo01088a011

[28] Wittig A, Sauerwein WA, Coderre JA. Mechanisms of transport of *p*-borono-phenylalanine through the cell membrane *in vitro*. Radiation Research. 2000;**153**:173-180

[29] Scholz M, Hey-Hawkins E. Carbaboranes as pharmacophores: Properties, synthesis, and application strategies. Chemical Reviews. 2011;**111**:7035-7062. DOI: 10.1021/cr200038x

[30] Viñas C. The uniqueness of boron as a novel challenging element for drugs in pharmacology, medicine and for smart biomaterials. Future Medicinal Chemistry. 2013;**5**:617-619. DOI: 10.4155/fmc.13.41

[31] Leśnikowski ZJ. Recent developments with boron as a platform for novel drug design. Expert Opinion on Drug Discovery. 2016;**11**:569-578. DOI: 10.1080/17460441.2016.1174687

[32] Satapathy R, Dash BP, Mahanta CS, Swain BR, Jena BB, Hosmane NS. Glycoconjugates of polyhedral boron clusters. Journal of Organometallic Chemistry. 2015;**798**:13-23. DOI: 10.1016/j.jorganchem.2015.06.027

[33] Calabrese G, Daou A, Barbu E, Tsibouklis J. Towards carborane functionalised structures for the treatment of brain cancer. Drug Discovery Today. 2017;**23**:63-75. DOI: 10.1016/j.drudis.2017.08.009

[34] Maurer JL, Serino AJ, Hawthorne MF. Hydrophilically augmented glycosyl carborane derivatives for incorporation in antibody conjugation reagents. Organometallics. 1988;**7**:2519-2524. DOI: 10.1021/om00102a015

[35] Tietze LF, Bothe U. *Ortho*-carboranyl glycosides of glucose, mannose, maltose and lactose for cancer treatment by boron neutron-capture therapy. Chemistry – A European Journal. 1998;**4**:1179-1183. DOI: 10.1002/(SICI)1521-3765(19980710)4:7<1179::AID-CHEM1179>3.0.CO;2-F

[36] Tietze LF, Bothe U, Schuberth I. Preparation of a new carboranyl lactoside for the treatment of cancer by boron neutron capture therapy: Synthesis and toxicity of fluoro carboranyl glycosides for *in vivo* ^{19}F-NMR spectroscopy. Chemistry – A European Journal. 2000;**6**:836-842. DOI: 10.1002/(SICI)1521-3765(20000303)6:5<836::AID-CHEM836>3.0.CO;2-8

[37] Tietze LF, Bothe U, Griesbach U, Nakaichi M, Hasegawa T, Nakamura H, Yamamoto Y. *Ortho*-carboranyl glycosides for the treatment of cancer by boron neutron capture therapy. Bioorganic & Medicinal Chemistry. 2001;**9**:1747-1752. DOI: 10.1016/S0968-0896(01)00061-X

[38] Tietze LF, Bothe U, Griesbach U, Nakaichi M, Hasegawa T, Nakamura H, Yamamoto Y. Carboranyl bisglycosides for the treatment of cancer by boron neutron capture therapy. Chembiochem. 2001;**2**:326-334. DOI: 10.1002/1439-7633(20010504)2:5<326::AID-CBIC326>3.0.CO;2-Y

[39] Bregadze VI, Sivaev IB. Polyhedral boron compounds for BNCT. In: Hosmane N, editor. Boron Science: New Technologies and Applications. Boca Raton, Florida, USA: CRC Press; 2012. pp. 181-208

[40] Tjarks W. The use of boron clusters in the rational design of boronated nucleosides for neutron capture therapy of cancer. Journal of Organometallic Chemistry. 2000;**614-615**:37-47. DOI: 10.1016/S0022-328X(00)00574-X

[41] Byun Y, Thirumamagal BTS, Yang W, Eriksson S, Barth R, Tjarks W. Preparation and biological evaluation of ^{10}B-enriched 3-[5-{2-(2,3-dihydroxyprop-1-yl)-*o*-carboran-1-yl} pentan-1-yl]thymidine (N5-2OH), a new boron delivery agent for boron neutron capture therapy of brain tumors. Journal of Medicinal Chemistry. 2006;**49**:5513-5523. DOI: 10.1021/jm060413w

[42] Barth R, Yang W, Al-Madhoun AS, Johnsamuel J, Byun Y, Chandra S, Smith DR, Tjarks W, Eriksson S. Boron-containing nucleosides as potential delivery agents for neutron capture therapy of brain tumors. Cancer Research. 2004;**64**:6287-6295. DOI: 10.1158/0008-5472.CAN-04-0437

[43] Al-Madhoun AS, Johnsamuel J, Barth R, Tjarks W, Eriksson S. Evaluation of human thymidine kinase 1 substrates as new candidates for boron neutron capture therapy. Cancer Research. 2004;**64**:6280-6286. DOI: 10.1158/0008-5472.CAN-04-0197

[44] Leśnikowski Z, Paradowska E, Olejniczak AB, Studzińska M, Seekamp P, Schüßler U, Gabel D, Schinazi RF, Plešek J. Towards new boron carriers for boron neutron capture therapy: Metallacarboranes and their nucleoside conjugates. Bioorganic & Medicinal Chemistry. 2005;**13**:4168-4175. DOI: 10.1016/j.bmc.2005.04.042

[45] Barth R, Yang W, Wu G, Swindall M, Byun Y, Narayanasamy S, Tjarks W, Tordoff K, Moeschberger ML, Eriksson S, Binns PJ, Riley KJ. Thymidine kinase 1 as a molecular target for boron neutron capture therapy of brain tumors. Proceedings of the National Academy of Sciences of the United States of America. 2008;**105**:17493-17497. DOI: 10.1073/pnas.0809569105

[46] Haushalter RC, Rudolph RW. *meso*-Tetracarboranylporphyrins. Journal of the American Chemical Society. 1978;**100**:4628-4629. DOI: 10.1021/ja00482a068

[47] Haushalter RC, Butler WM, Rudolph RW. The preparation and characterization of several *meso*-tetracarboranylporphyrins. Journal of the American Chemical Society. 1981;**103**:2620-2627. DOI: 10.1021/ja00400a023

[48] Renner MW, Miura M, Easson MW, Vicente MGH. Recent progress in the syntheses and biological evaluation of boronated porphyrins for boron neutron-capture therapy. Anti-Cancer Agents in Medicinal Chemistry. 2006;**6**:145-157. DOI: 10.2174/187152006776119135

[49] Kahl SB, Koo MS. Synthesis of tetrakis-carborane-carboxylate esters of 2,4-bis-(α,β-dihydroxyethyl)-deuteroporphyrin IX. Journal of the Chemical Society, Chemical Communications. 1990;**0**:1769-1771. DOI: 10.1039/C39900001769

[50] Hill JS, Kahl SB, Kaye AH, Stylli SS, Koo MS, Gonzales MF, Vardaxis NJ, Johnson CI. Selective tumor uptake of a boronated porphyrin in an animal model of cerebral glioma. Proceedings of the National Academy of Sciences of the United States of America. 1992;**89**:1785-1789. DOI: 10.1073/pnas.89.5.1785

[51] Rosenthal MA, Kavar B, Hill JS, Morgan DJ, Nation RL, Stylli SS, Basser RL, Uren S, Geldard H, Green MD, Kahl SB, Kaye AH. Phase I and pharmacokinetic study of photodynamic therapy for high grade gliomas using a novel boronated porphyrin (BOPP). Journal of Clinical Oncology. 2001;**19**:519-524. DOI: 10.1200/JCO.2001.19.2.519

[52] Vicente MGH, Edwards BF, Shetty SJ, Hou Y, Boggan JE. Syntheses and preliminary biological studies of four *meso*-tetra[(*nido*-carboranylmethyl)phenyl]porphyrins. Bioorganic & Medicinal Chemistry. 2002;**10**:481-492. DOI: 10.1016/S0968-0896(01)00300-5

[53] Ozawa T, Santos RA, Lamborn KR, Bauer WF, Koo MS, Khal SB, Deen DF. *In vivo* evaluation of the boronated porphyrin TABP-1 in U-87 MG intracerebral human glioblastoma xenografts. Molecular Pharmaceutics. 2004;**1**:368-374. DOI: 10.1021/mp049933

[54] Crossley EL, Ziolkowski EJ, Coderre JA, Rendina LM. Boronated DNA-binding compounds as potential agents for boron neutron capture therapy. Mini-Reviews in Medicinal Chemistry. 2007;**7**:303-313. DOI: 10.2174/138955707780059808

[55] Zhuo JC, Cai J, Soloway AH, Barth RF, Admas DM, Ji W, Tjarks W. Synthesis and biological evaluation of boron-containing polyamines as potential agents for neutron capture therapy of brain tumors. Journal of Medicinal Chemistry. 1999;**42**:1282-1292. DOI: 10.1021/jm980703f

[56] Bhupathiraju NV, Vicente MGH. Synthesis and cellular studies of polyamine conjugates of a mercaptomethyl–carboranylporphyrin. Bioorganic & Medicinal Chemistry. 2013;**21**:485-495. DOI: 10.1016/j.bmc.2012.11.007

[57] Hubner KF, Thie JA, Smith GT, Kabalka GW, Keller IB, Kliefoth AB, Campbell SK, Buonocore E. Positron emission tomography (PET) with 1-aminocyclobutane-1-[(11)C] carboxylic acid (1-[(11)C]-ACBC) for detecting recurrent brain tumors. Clinical Positron Imaging. 1998;**1**:165-173

[58] Futamura G, Kawabata S, Nonoguchi N, Hiramatsu R, Toho T, Tanaka H, Masunaga S-I, Hattori Y, Kirihata M, Ono K, Kuroiwa T, Miyatake S-I. Evaluation of a novel sodium borocaptate containing unnatural amino acid as a boron delivery agent for neutron capture therapy of the F98 rat glioma. Radiation Oncology. 2017;**12**:26. DOI: 10.1186/s13014-017-0765-4

[59] Mier W, Gabel D, Haberkorn U, Eisenhut M. Conjugation of the *closo*-borane mercaptoundecahydrododecaborate (BSH) to a tumour selective peptide. Zeitschrift für Anorganische und Allgemeine Chemie. 2004;**630**:1258-1262. DOI: 10.1002/zaac.200400064

[60] Matsumura A, Shibata Y, Yamamoto T, Yoshida F, Isobe T, Nakai K, Hayakawa Y, Kiriya M, Shimojo N, Ono K, Sakata I, Nakajima S, Okumura M, Nose T. A new boronated porphyrin (STA-BX909) for neutron capture therapy: An *in vitro* survival assay and *in vivo* tissue uptake study. Cancer Letters. 1999;**141**:203-209. DOI: 10.1016/S0304-3835(99)00105-6

[61] Asano R, Nagami A, Fukumoto Y, Miura K, Yazama F, Ito H, Sakata I, Tai A. Synthesis and biological evaluation of new BSH-conjugated chlorine derivatives as agents for both photodynamic therapy and boron neutron capture therapy of cancer. Journal

of Photochemistry and Photobiology B: Biology. 2014;**140**:140-149. DOI: 10.1016/j.jphotobiol.2014.07.008

[62] Brat DJ, Mapstone TB. Malignant glioma physiology: Cellular response to hypoxia and its role in tumor progression. Annals of Internal Medicine. 2003;**138**:659-668. DOI: 10.7326/0003-4819-138-8-200304150-00014

[63] Masunaga S, Nagasawa H, Hiraoka M, Sakurai Y, Uto Y, Hori H, Nagata K, Suzuki M, Maruhashi A, Kinashia Y, Ono K. The usefulness of 2-nitroimidazole-sodium borocaptate-^{10}B conjugates as ^{10}B-carriers in boron neutron capture therapy. Applied Radiation and Isotopes. 2004;**61**:953-958. DOI: 10.1016/j.apradiso.2004.05.018

[64] Masunaga S, Nagasawa H, Hiraoka M, Sakurai Y, Uto Y, Hori H, Nagata K, Suzuki M, Maruhashi A, Kinashia Y, Ono K. Applicability of the 2-nitroimidazole-sodium borocaptate-^{10}B conjugate, TX-2060, as a ^{10}B-carrier in boron neutron capture therapy. Anticancer Research. 2004;**24**:2975-2984

[65] Masunaga S, Nagasawa H, Gotoh K, Uto Y, Hori H, Sakurai Y, Nagata K, Suzuki M, Maruhashi A, Kinashi Y, Ono K. Evaluation of hypoxia-specific cytotoxic bioreductive agent sodium borocaptate-^{10}B conjugates, as ^{10}B-carriers in boron neutron capture therapy. Radiation Medicine. 2006;**24**:98-107. DOI: 10.1007/BF02493275

[66] Yang W, Gao X, Wang, B. Biological and medicinal applications of boronic acids. In: Hall DG, editor. Boronic Acids: Preparation and Applications in Organic Synthesis and Medicine. Weinheim: Wiley-VCH Verlag GmbH & Co.; 2005. pp. 481-512. DOI: 10.1002/3527606548.ch13

[67] Hall DG. Structure, properties, and preparation of boronic acid derivatives. Overview of their reactions and applications. In: Hall DG, editor. Boronic Acids: Preparation and Applications in Organic Synthesis and Medicine. Weinheim: Wiley-VCH Verlag GmbH & Co.; 2005. pp. 1-99. DOI: 10.1002/3527606548.ch1

[68] Yang W, Gao X, Wang B. Boronic acid compounds as potential pharmaceutical agents. Medicinal Research Reviews. 2003;**23**:346-368. DOI: 10.1002/med.10043

[69] Hansch C, Leo A, Unger SH, Kim KH, Nikaitani D, Lien EJ. Aromatic substituent constants for structure-activity correlations. Journal of Medicinal Chemistry. 1973;**16**:1207-1216. DOI: 10.1021/jm00269a003

[70] Kabalka GW, Das BC, Das S. Synthesis of novel boron containing unnatural cyclic amino acids as potential therapeutic agents. Tetrahedron Letters. 2001;**42**:7145-7146. DOI: 10.1016/S0040-4039(01)01486-1

[71] Akedo H, Christensen HN. Transfer of amino acids across the intestine: A new model amino acid. The Journal of Biological Chemistry. 1962;**237**:113-117

[72] Aoyagi M, Agranoff BW, Washburn LC, Smith QR. Blood-brain barrier transport of 1-aminocyclohexanecarboxylic acid, a nonmetabolizable amino acid for *in vivo* studies of brain transport. Journal of Neurochemistry. 1988;**50**:1220-1226. DOI: 10.1111/j.1471-4159.1988.tb10596.x

[73] Christensen HN, Jones JC. Amino acid transport models: Renal resorption and resistance to metabolic attack. The Journal of Biological Chemistry. 1962;**237**:1203-1206

[74] Barth RH, Kabalka GW, Yang W, Huo T, Nakkula RJ, Shaikh AL, Haider SY, Chandra S. Evaluation of unnatural cyclic amino acids as boron delivery agents for treatment of melanomas and gliomas. Applied Radiation and Isotopes. 2014;**88**:38-42. DOI: 10.1016/j.apradiso.2013.11.133

[75] Chandra S, Ahmad T, Barth RF, Kabalka GW. Quantitative evaluation of boron neutron capture therapy (BNCT) drugs for boron delivery and retention at subcellular scale resolution in human glioblastoma cells with imaging secondary ion mass spectrometry (SIMS). Journal of Microscopy. 2014;**254**:146-156. DOI: 10.1111/jmi.12126

[76] Seiler N, Delcros JG, Moulinoux JP. Polyamine transport in mammalian cells. An update. The International Journal of Biochemistry & Cell Biology. 1996;**28**:843-861. DOI: 10.1016/1357-2725(96)00021-0

[77] Martin B, Possémé F, Le Barbier C, Carreaux F, Carboni B, Seiler N, Moulinoux J-P, Delcros J-G. *N*-Benzylpolyamines as vectors of boron and fluorine for cancer therapy and imaging: Synthesis and biological evaluation. Journal of Medicinal Chemistry. 2001;**44**:3653-3664. DOI: 10.1021/jm010897q

[78] Hatanaka H, Soloway AH, Sweet WH. Incorporation of pyrimidines and boron analogues into brain tumour and brain tissue of mice. An approach to boron-neutron capture therapy. Neurochirurgia. 1967;**10**:87-95. DOI: 10.1055/s-0028-1095340

[79] Goudgaon NM, El-Kattan GF, Schinazi RF. Boron containing pyrimidines, nucleosides, and oligonucleotides for neutron capture therapy. Nucleosides & Nucleotides. 1994;**13**:849-880. DOI: 10.1080/15257779408013283

[80] Nizioł J, Zieliński Z, Leś A, Dąbrowska M, Rode W, Ruman T. Synthesis, reactivity and biological activity of *N*(4)-boronated derivatives of 2′-deoxycytidine. Bioorganic & Medicinal Chemistry. 2014;**22**:3906-3912. DOI: 10.1016/j.bmc.2014.06.014

[81] Nizioł J, Uram Ł, Szuster M, Sekuła J, Ruman T. Biological activity of *N*(4)-boronated derivatives of 2′-deoxycytidine, potential agents for boron-neutron capture therapy. Bioorganic & Medicinal Chemistry. 2015;**23**:6297-6304. DOI: 10.1016/j.bmc.2015.08.026

[82] Uram Ł, Nizioł J, Maj P, Sobich J, Rode W, Ruman T. *N*(4)-[*B*-(4,4,5,5-tetramethyl-1,3,2-dioxaborolan)methyl]-2′-deoxycytidine as a potential boron delivery agent with respect to glioblastoma. Biomedicine & Pharmacotherapy. 2017;**95**:749-755. DOI: 10.1016/j.biopha.2017.08.134

[83] Asano R, Nagami A, Fukumoto Y, Miura K, Yazama F, Ito H, Sakata I, Tai A. Synthesis and biological evaluation of new boron-containing chlorine derivatives as agents for both photodynamic therapy and boron neutron capture therapy of cancer. Bioorganic & Medicinal Chemistry Letters. 2014;**24**:1339-1343. DOI: 10.1016/j.bmcl.2014.01.054

[84] Luderer MJ, Muz B, de la Puente P, Chavalmane S, Kapoor V, Marcelo R, Biswas P, Thotala D, Rogers B, Azab AK. A hypoxia-targeted boron neutron capture therapy agent

for the treatment of glioma. Pharmaceutical Research. 2016;**33**:2530-2539. DOI: 10.1007/s11095-016-1977-2

[85] Zimmer H, Sill AD, Andrews ER. Functional organoboron compounds. Naturwissenschaften. 1960;**47**:378. DOI: 10.1007/BF00631386

[86] Maitra A. Boron analogue of uracil. Indian Journal of Chemistry. 1978;**16B**:85-86

[87] Chissick SS, Dewar MJS, Maitlis PM. New heteroaromatic compounds. XIV. Boron-containing analogs of purine, quinazoline and perimidine. Journal of the American Chemical Society. 1961;**83**:2708-2711. DOI: 10.1021/ja01473a025

[88] Sood A, Shaw BR, Spielvogel BF. Boron-containing nucleic acids. Synthesis of cyanoborane adducts of 2′-deoxynucleosides. Journal of the American Chemical Society. 1989;**111**:9234-9235. DOI: 10.1021/ja00208a019

[89] Sood A, Shaw BR, Spielvogel BF. Boron-containing nucleic acids. 2. Synthesis of oligodeoxynucleoside boranophosphates. Journal of the American Chemical Society. 1990;**112**:9000-9001. DOI: 10.1021/ja00180a066

[90] Li X, Plattner JJ, Hernandez V, Ding CZ, Wu W, Yang Y, Xu M. Synthesis of novel benzoxaborole-containing phenylalanine analogues. Tetrahedron Letters. 2011;**52**:4924-4926. DOI: 10.1016/j.tetlet.2011.07.053

[91] Takagaki M, Powell W, Sood A, Spielvogel BF, Hosmane NS, Kirihata M, Ono K, Masunaga SI, Kinashi Y, Miyatake SI, Hashimoto N. Boronated dipeptide borotrimethylglycylphenylalanine as a potential boron carrier in boron neutron capture therapy for malignant brain tumors. Radiation Research. 2001;**156**:118-122. DOI: 10.1667/0033-7587(2001)156[0118:BDBAAP]2.0.CO;2

[92] Ban HS, Usui T, Nabeyama W, Morita H, Fukuzawa K, Nakamura H. Discovery of boron-conjugated 4-anilinoquinazoline as a prolonged inhibitor of EGFR tyrosine kinase. Organic & Biomolecular Chemistry. 2009;**7**:4415-4427. DOI: 10.1039/b909504g

[93] Kwatra MM. A rational approach to target the epidermal growth factor receptor in glioblastoma. Current Cancer Drug Targets. 2017;**17**:290-296. DOI: 10.2174/1568009616666161227091522

[94] Couto M, Mastandrea I, Cabrera M, Cabral P, Teixidor F, Cerecetto H, Viñas C. Small-molecule kinase-inhibitors-loaded boron cluster as hybrid agents for glioma-cell-targeting therapy. Chemistry. 2017;**23**:9233-9238. DOI: 10.1002/chem.201701965

[95] Couto M, García MF, Alamón C, Cabrera M, Cabral P, Merlino A, Teixidor F, Cerecetto H, Viñas C. Discovery of potent EGFR inhibitors through the incorporation of a 3D-aromatic-boron-rich-cluster into the 4-anilinoquinazoline scaffold: Potential drugs for glioma treatment. Chemistry. 2018;**24**:3122-3126. DOI: 10.1002/chem.201705181